Identification, preparation and UHPLC determination of process-related impurity in zolmitriptan

Michal Douša*, Petr Gibala, Stanislav Rádl, Ondřej Klecán, Zuzana Mandelová, Jiří Břicháč, Tomáš Pekárek

Zentiva, a.s. Praha, U Kabelovny 130, 102 37 Praha 10, Czech Republic

ARTICLE INFO

ABSTRACT

A new impurity was detected and determined using gradient ion-pair UHPLC method with UV detection in zolmitriptan (ZOL). Using MS, NMR and IR study the impurity was identified as (4S,4′S)-4,4′-(2,2′-(4-(dimethylamino)butane-1,1-diyl)bis(3-(2-(dimethylamino) ethyl)-1H-indole-5,2-diyl))bis(methylene)di(oxazolidin-2-one) (ZOL-dimer). The standard of ZOL-dimer was consequently prepared via organic synthesis followed by semipreparative HPLC purification. The UHPLC method was optimized in order to selectively detect and quantify other known and unknown process-related impurities and degradation products of ZOL as well. The presented method which was validated with respect to linearity, accuracy, precision and selectivity has an advantage of a very quick UHPLC chromatographic separation (less than 7 min including re-equilibration time) and therefore is highly suitable for routine analysis of related substances and stability studies of ZOL.

1. Introduction

Zolmitriptan, 4(S)-4-[3-(2-dimethylaminoethyl)-1H-5-indolyl-methyl]-1,3-oxazolan-2-one belongs to a group of medicines known as Serotonin 5-HT1D receptor agonist [1,2]. In liver, zolmitriptan (ZOL) is well absorbed and undergoes extensive metabolism. Its major metabolites are 4(S)-4-[3-(2-methylamino-ethyl)-1H-5-indolyl-methyl]-1,3-oxazolan-2-one (N-desmethyl-zolmitriptan; impurity A in USP draft 2011) and (4S)-4-[3-[2-(dimethyloxidoamino)ethyl]-1H-indol-5-yl]methyl-2-oxazolidi-non (zolmitriptan N-oxide) [3] and several HPLC methods for their determination have been reported. Quantification of ZOL in human plasma using mass [4], coulometric [5] or fluorescence detection [6] was described as well.

LC methods were developed and reported for the determination of ZOL and its related substances known as (S)-4-(4-aminobenzyl)-1,3-oxazolidin-2-one (ZOL1), (2S)-2-amino-3-[3-(2-dimethylaminoethyl)-1H-5-indolyl]-propan-1-ol (ZOL2; impurity B in USP draft 2011), (S)-4-(4-hydrazinobenzyl)-1,3-oxazolidin-2-one (ZOL-hydrazine) and (4S)-4-[3-(2-aminoethyl)-1H-indol-5-yl methyl]-1,3-oxazolidon-2-one (ZOL-amine) (Fig. 1) [7,8]. Unfortunately the long analysis time (>20 min) and low separation efficiency are ones of the disadvantages of reported methods [8]. The other unknown related impurity of ZOL in tablets

was isolated using preparative chromatography and characterized as 4-4-[3-[2-(dimethyloxidoamino) ethyl]-1H-indol-5-yl] methyl-2-oxazolidinone by mass spectroscopy and NMR [9].

This paper describes identification, preparation and determination of new impurity of ZOL ((4S,4′S)-4,4′-(2,2′-(4-(dimethyl-amino)butane-1,1-diyl)bis(3-(2-(dimethylamino) ethyl)-1H-indole-5,2-diyl))bis(methylene)di(oxazolidin-2-one); ZOL-dimer) which was found in the drug substance using gradient ion-pair UHPLC method with UV detection at 220 nm. The applicability of the UHPLC method was successfully verified by analysis of several batches of ZOL.

2. Experimental

2.1. Reagents and chemicals

Acetonitrile of HPLC gradient grade (J.T. Baker, USA) and water purified on Milli-Q system (Millipore, USA) were used for preparation of sample and reference solutions and mobile phases. All other chemicals used were of analytical grade or pure grade quality (Sigma–Aldrich, Czech Republic). Three different batches of ZOL were obtained from Zentiva (Turkey). The standards of impurities N-desmethylzolmitriptan, zolmitriptan N-oxide and ZOL-amine were obtained from Matrix Laboratories Limited (India), ZOL1 and ZOL2 were supplied by Dr. Reddy's Laboratories Limited (India).

* Corresponding author.
 *E-mail addresses:* hplc@hplc.cz, michal.dousa@seznam.cz (M. Douša).
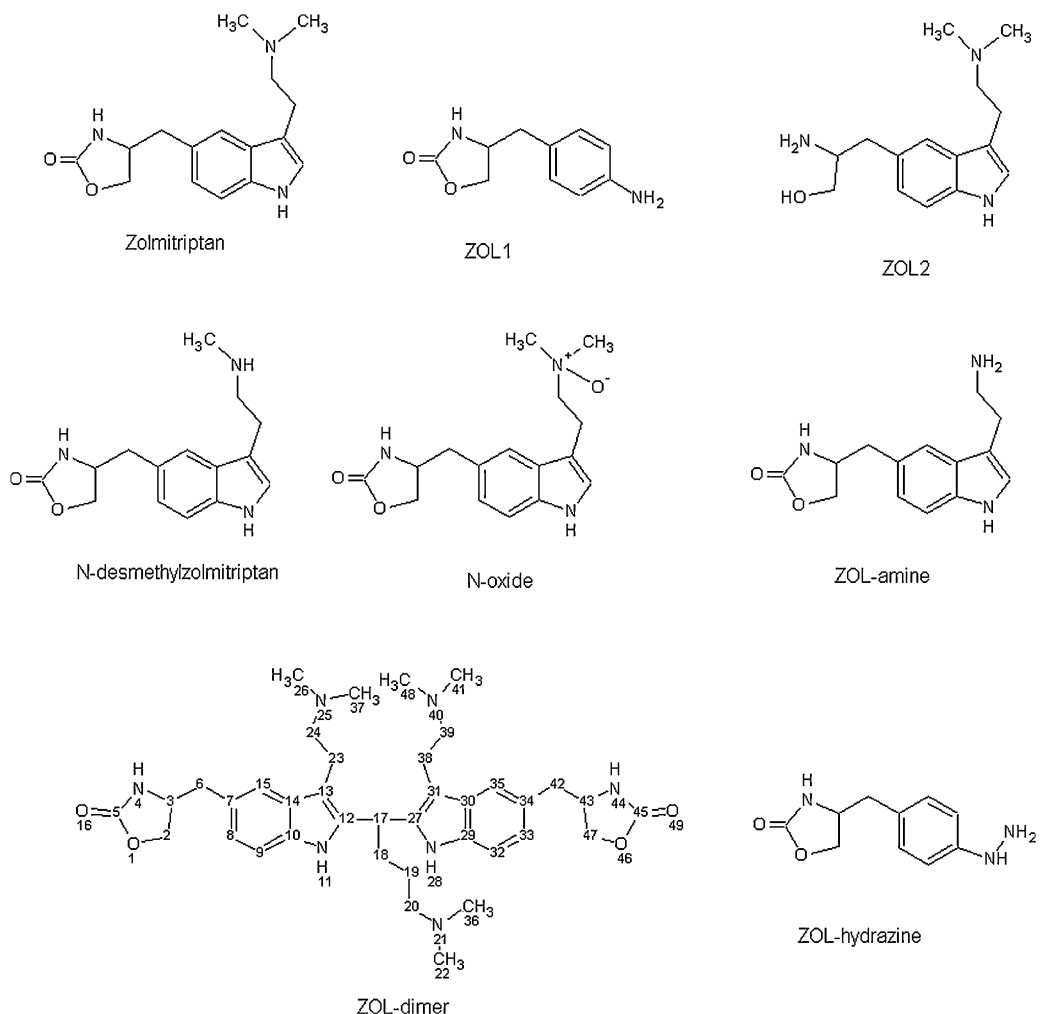
Fig. 1. Chemical structures of zolmitriptan and related substances.

2.2. Sample and standard preparation

The standard of ZOL (in house standard, purity 99.8%) was dissolved in sample solvent consisting of a mixture of mobile phase A and B in ratio 9:1 (v/v) to obtain the standard stock solution (concentration of 1.0 mg/ml). The system suitability test solution was prepared by spiking of ZOL standard stock solution by N-desmethylzolmitriptan to obtain concentration of 0.15% with respect to ZOL. The reference solution was prepared by diluting ZOL standard stock solution to obtain concentration of 1.5 μg/ml (concentration of 0.15% with respect to ZOL preparation solution). Preparation of ZOL-dimer impurity is described in Section 3.

10 mg of ZOL sample was weighed into a 10 ml volumetric flask. Sample solvent (about 8 ml) was added and sample was dissolved by sonication for 2 min in an ultrasonic bath UCC4 (TESON, Slovakia) to obtain ZOL preparation solution. After cooling to the laboratory temperature, the flask was filled to the mark by sample solvent.

2.3. Chromatographic apparatus and conditions

All chromatographic experiments were carried out on an Acquity UPLC system with a photodiode array detector (all Waters,

USA). The system was controlled and acquired data processed by the Empower software (Waters, USA).

Chromatographic separations were performed on an Ascentis Express Phenyl-Hexyl column (100 mm × 3.0 mm, 2.7 μm; Supelco, USA). The gradient elution employed solutions A and B as mobile phase components. The solution A contained a mixture of 20 mM potassium dihydrogenphophate and 5 mM sodium 1-hexansulfonate, pH adjusted to 2.0 using 5 M phosphoric acid, solution B was acetonitrile. The flow rate of the mobile phase was 0.8 ml/min and column temperature was maintained at 20 °C. The gradient program was set as follows: time/% solution B: 0/10, 0.5/10, 4/20, 5/20, 5.5/10 with an equilibration time of 2 min. The injection volume was 0.8 μl and analytes were monitored at a wavelength of 220 nm.

2.4. LC–MS apparatus and conditions

High-resolution MS experiments were performed on a LTQ Orbi-trap Hybrid Mass Spectrometer (Fisher Scientific, Waltham, USA) coupled to an HPLC HTS PAL system (CTC Analytics, Switzerland). LC separation was performed an a Kinetex C18, 150 mm × 4.60 mm, 2.6 μm (Phenomenex, USA) column using 0.3 ml/min flow rate, consisting mobile phase 0.1% formic acid and acetonitrile (gradient acetonitrile ranging from 10 to 100% for 20 min). For ionisation of
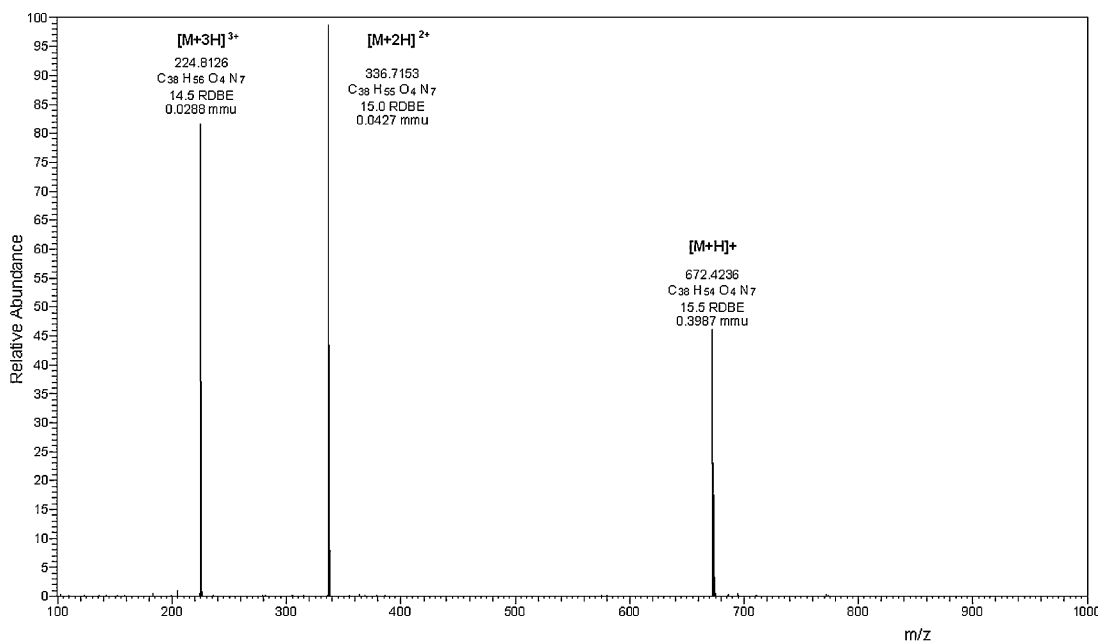
Fig. 2. Positive ion mode ESI full scan mass spectra of ZOL-dimer.

eluted analytes ESI ion source operated in the positive mode (capillary temperature 300 °C, source voltage 4 kV and tube lens voltage 110 V) was employed.

2.5. Semipreparative apparatus and conditions

A semipreparative XBridge Prep C18 OBD column (100 mm × 19 mm, 5 µm; Waters, USA) was used for preparative purposes using a mobile phase consisting of aqueous solution of 1.5% triethylamine–acetonitrile (67:33, v/v). Preparative HPLC separation and fraction collection was carried out on a Waters Autopurification system (System fluidics organiser, 2545 binary gradient module, 2767 sample manager, 515 HPLC pump and 2487 dual-wavelength absorbance detector; Waters, USA). The flow rate 20 ml/min was employed throughout the preparation. The volume of solution injected into the semipreparative column was 900 µl. In order to monitor UV signal of the effluent from the semipreparative column the effluent was splitted in ratio 1:1000 into the methanol flow from 515 HPLC pump which was directed to UV detector. The fraction collection was triggered by setting a minimal intensity threshold (MIT = 5000 µV for isolation of unknown impurity from ZOL and MIT = 500,000 µV for ZOL-dimer standard purification) of the UV signal at 300 nm.

2.6. NMR, IR and other apparatus and conditions

Nuclear magnetic resonance (NMR) spectra were obtained using a Bruker Avance 500 (Bruker Biospin, Germany) at 500.13 MHz (^{1}H). All NMR experiments were performed in dimethylsulfoxide at 298 K. At 500 MHz, standard 5 mm TBI (triple-broadband inverse) probehead equipped with z-gradient coils was employed for all measurements.

IR spectra were measured with the single-reflection ATR (ZnSe) FTIR spectrometer Nicolet Nexus (Thermo, USA). The spectra were acquired by accumulation of 64 scans with 2 cm^{-1} resolution.

The other apparatus are described in text.

3. Results and discussion

3.1. Identification of ZOL-dimer

An unknown impurity with relative retention time (RRT) 1.23 with respect to ZOL was detected in several batches of ZOL using gradient ion-pair UHPLC method with UV detection. ZOL sample with the highest concentration (0.21%) of the impurity was dissolved in water–acetonitrile mixture (1:1, v/v) to obtain concentration of 100 mg/ml and the unknown impurity was isolated from the solution by semipreparative HPLC. Fractions of the unknown impurity from multiple semipreparative HPLC separations were collected, combined and evaporated to dryness under vacuum at 50 °C. About 5 mg of relatively pure unknown impurity (chromatographic purity of 95%) was obtained and used for its identification by LC–MS and NMR studies.

LC–MS measurement revealed ions corresponding to the unknown impurity, including protonated molecular ion [M+H]$^+$ at $m/z = 672.4236$, double charged ion [M+2H]$^{2+}$ at m/z 336.7153 and triple charged ion [M+3H]$^{3+}$ at $m/z = 224.8126$ (Fig. 2). Use of the high resolution MS in this measurement allowed determination of accurate monoisotopic mass 671.4159 and corresponding elemental composition $C_{38}H_{53}N_7O_4$ of the unknown impurity.

Knowledge of ZOL synthesis served as another clue to molecular structure of the unknown impurity. The last step of the ZOL synthesis could be the Fischer indole synthesis (Fig. 3) of (S)-4-(4-hydrazinylbenzyl)oxazolidin-2-one (II), obtained by in situ reduction of the corresponding amine I, with 4-(dimethylamino)butanal diethyl acetal (III) under acidic conditions [10]. It is well documented that 3-substituted indoles with no substitution at position 2 can react under various conditions with both aromatic [11] and aliphatic aldehydes [12,13] providing the corresponding 2,2′-bis(indolyl) methanes. Since the Fischer indole synthesis is done under acidic condition, 4-(dimethylamino)butanal is formed in situ and can further react with ZOL to provide (4S,4′S)-4,4′-(2,2′-(4-(dimethylamino)butane-1,1-diyl)bis(3-(2-(dimethylamino)ethyl)-1H-indole-5,2-diyl))bis(methylene)di(oxazolidin-2-one) (ZOL-dimer; Fig. 1). Analogous impurity of rizatriptan has already been described [14]. The
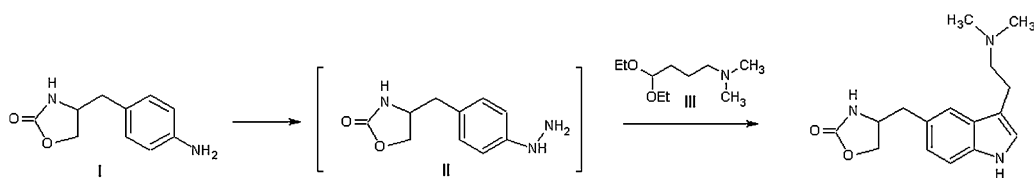
Fig. 3. Scheme of synthesis of zolmitriptan.

rationalisation given above clearly indicates that the ZOL-dimer would be a process related impurity, according to the Q3A classification [15]. The structure of ZOL-dimer impurity is in agreement with measured accurate mass of unknown impurity RRT 1.23 and its MS spectra.

Identification of unknown impurity was verified by NMR study of the isolated impurity. The assignment of NMR signals was performed for ZOL-dimer and the given structure was unambiguously confirmed: ^{1}H NMR (500 MHz, DMSO) d (ppm): 10.63 (bs, 2H, *11, 28*), 7.74 (bd, *J* = 7.9 Hz, 2H, *4, 44*), 7.26–7.24 (m, 2H, *15, 35*), 7.22 (d, *J* = 8.2 Hz, 2H, *9, 32*), 6.88 (dd, *J* = 8.2, 1.3 Hz, 2H, *8, 33*), 4.45 (t, *J* = 7.3 Hz, 1H, *17*), 4.23–4.12 (m, 2H, *2a, 47a*), 4.06–3.95 (m, 4H, *2b, 3, 43, 47b*), 2.93–2.67 (m, 8H, *6a, 42a, 23, 38, 6b, 42b*), 2.40–2.25 (m, 4H, *24, 39*), 2.25–2.17 (m, 2H, *20*), 2.21 (s, 12H, *26, 37, 41, 48*), 2.17–2.09 (m, 2H, *18*), 2.06 (s, 6H, *22, 36*), 1.35 (pent, *J* = 7.3 Hz, 2H, *17*); ^{13}C NMR (500 MHz, DMSO) d (ppm): 158.62(*5, 45*), 136.68(*12, 27*), 134.39(*10, 29*), 128.04(*14* or *30*), 128.02(*14* or *30*), 125.98(*7* or *34*), 125.97(*7* or *34*), 122.09(*8* or *33*), 122.03(*8* or *33*), 118.28(*15, 35*), 110.76(*9* or *32*), 110.74(*9* or *32*), 108.21(*13* or *31*), 108.20(*13* or *31*), 67.97(*2, 47*), 60.28(*24, 39*), 58.52(*20*), 53.18(*3, 43*), 45.14(*26, 37, 41, 48*), 45.11(*22, 36*), 40.59(*6* or *42*), 40.56(*6* or *42*), 33.82(*17*), 31.34(*18*), 25.55(*19*), 22.26(*23, 38*).

3.2. ZOL-dimer reference standard preparation and characterization

The procedure of preparation of ZOL-dimer was following: 4-(dimethylamino)butanal diethyl acetal (1.0 g, 5.3 mM) was added to a stirred solution obtained by addition of concentrated hydrochloric acid (10 ml) to a stirred slurry of ZOL (4.0 g, 13.9 mM) in water (50 ml). The mixture was then heated to 70 °C for 48 h, cooled to room temperature and diluted with water (100 ml). The pH of the mixture was adjusted with a 20% aqueous solution of sodium hydroxide to 5 and the mixture was extracted with dichloromethane (2 × 50 ml). The combined extracts were washed with water, dried with anhydrous magnesium sulfate and evaporated to dryness. The residue was then pre-purified by column chromatography (silica gel, ethyl acetate–ethanol–25% aqueous ammonia 6:3:1) and the combined fractions containing the required product were evaporated to dryness, dissolved in water–acetonitrile mixture (1:1, v/v) to obtain concentration of 100 mg/ml and purified by semipreparative HPLC. The collection parameters of the semipreparative HPLC method were optimized with respect to high concentration of ZOL-dimer in the injected solution. The solution of crude sample was injected into the semipreparative column and the fractions of ZOL-dimer were repeatedly collected and combined. The combined fractions were evaporated under vacuum at 50 °C to dryness to obtain pure solid ZOL-dimer impurity reference standard (reddish substance, consistence of honey).

The structure of ZOL-dimer reference standard was once again verified by MS and NMR studies under the conditions mentioned above and obtained data were in agreement with the data measured for impurity isolated from ZOL sample. The qualitative characterization of ZOL-dimer impurity reference standard was also performed using IR and UV measurements (Fig. 4). Finally,

ZOL dimer impurity reference standard was quantitatively characterized for pharmaceutical use. The potency of the standard was calculated based on the values obtained from determination of impurities (organic, inorganic, water and residual solvents) by applying the principle of mass balance. The potency of ZOL dimer impurity was >98%.

3.3. Optimization of UHPLC method

The composition and gradient profile of the mobile phase was optimized to achieve the retention factor of ZOL $k \geq 3.0$, symmetry factor $A_S \leq 1.5$ and resolution between N-desmethylzolmitriptan and ZOL $R_S \geq 2.0$. The dead volume of column used was determined using injection of sodium nitrate. These chromatographic data were calculated in agreement with European Pharmacopoeia (*Ph. Eur.*) [16]. Separation of ZOL and its impurities was tested by varying proportions of acetonitrile or methanol and ion-pair buffer type (sodium 1-octanesulfonate and sodium 1-decanesuflonate) in the mobile phase. All the experiments were performed with 20 mM phosphate buffer and pH mobile phase adjusted to 2.0 as these values found to be optimal. Acceptable resolution was achieved with gradient elution and acetonitrile as the organic modifier using flow rate 0.8 ml/min at temperature of 20 °C. The chromatogram of separation of ZOL and impurities measured by the optimized UHPLC method is shown in Fig. 5.

3.4. Validation of UHPLC method

The method was partially validated according to ICH Q2(R1) guideline [17].

3.4.1. System suitability

The system suitability test was performed before each run to assure that the analytical method can be used within the employed UHPLC system with a satisfactory performance. Repeatability of injections expressed as relative standard deviation (RSD %) of peak area of N-desmethylzolmitriptan and resolution between N-desmethylzolmitriptan and ZOL for the five consecutive injections of a system suitability test solution were limited to ≤1.0% and $R_S \geq 2.0$ respectively. For all the measurements performed during the validation, the resolution more than 3.0 and RSD of peak areas ≤0.4% was achieved.

3.4.2. Limit of detection (LOD), limit of quantification (LOQ) and linearity

LOD and LOQ were calculated for ZOL-dimer based on signal-to-noise ratio (S/N). The baseline noise was measured in a blank experiment in the region of retention time of ZOL-dimer using chromatographic software. The LOD ($S/N = 3$) and LOQ ($S/N = 10$) were found to be 0.057 μg/ml and 0.173 μg/ml, respectively.

A set of six ZOL-dimer and ZOL solutions at the concentration range from LOQ to 200% of the general specification limit (LOQ – 3.0 μg/ml) was prepared. The calibration curves were constructed by plotting the peak area of the given analyte against its concentration and the calibration equations were calculated using linear regression analysis. It showed slope 71,154, *y*-intercept 83.5
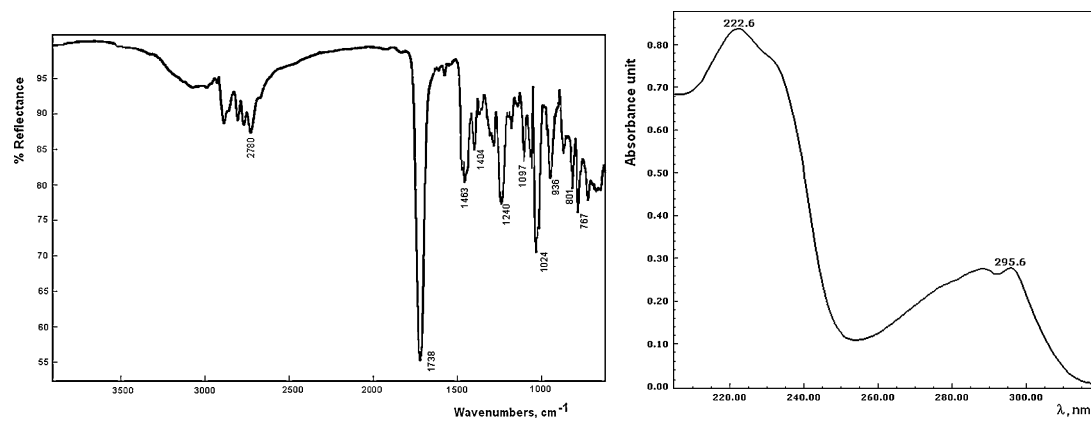
Fig. 4. IR and UV spectra of ZOL-dimer (UV spectra were obtained from ACQUITY UPLC photodiode array detector).

and correlation coefficient (R) of 0.9991 for ZOL-dimer and slope 122,272, y-intercept 590.65 and $R = 0.9994$ for ZOL. The calculated parameters of calibration curves indicate a satisfactory linearity. The linearity of the calibration curves was investigated using other statistical test like the quality coefficient QC [18]. The linearity of calibration model considered as valid if the quality coefficient QC fulfils the criterion QC < 5%. The calculated value of QC was 2.0% for ZOL-dimer and 1.9 for ZOL.

The correction response factor (CRF) of ZOL-dimer with respect to ZOL at 220 nm was obtained from slope ratio of the appropriate calibration curves. CRF of ZOL-dimer was 1.72.

3.4.3. Precision, accuracy and determination in commercial preparations

The precision of ZOL-dimer was evaluated by analysis of six independent preparations of the same homogenous sample under the prescribed conditions. Table 1 shows the results of content of ZOL-dimer in four batches of API.

Accuracy of the ZOL-dimer was evaluated in triplicate at three concentration levels (0.5, 1.5 and 3.0 μg/ml) in ZOL. The average total recovery of ZOL-dimer was 103.9% with RSD of 3.4%. The determined contents (c_d) were compared with the expected ones (c_e)

Table 1
The content of ZOL-dimer impurity in different API batches.

Samples (Zentiva, Turkey)	Content (%)	Relative standard deviation (%)
Batch 01	0.09	1.4
Batch 02	0.06	1.1
Batch 03	0.09	0.8
Batch 04	0.08	1.5

using linear regression. The regression equation (significance level $P = 0.95$) was $c_d = (0.034 \pm 0.284) + (1.012 \pm 0.163)c_e$ and $R = 0.9998$. The first and second constants were not statistically different from zero and one, respectively. It can be concluded that the analytical method gives accurate results for determination of ZOL-dimer impurity in ZOL API.

3.4.4. Selectivity

The method selectivity was established using UHPLC analysis of blank (sample solvent) and samples spiked with impurities. No interfering coeluting peaks in sample solvent were observed (Fig. 5) which demonstrated the selectivity of UHPLC method.

4. Conclusion

The new related compound of ZOL was detected using highly selective UHPLC method and identified by means of LC–MS and NMR studies. The impurity is generated in the last step of the ZOL synthesis by the Fischer indole synthesis and was identified as (4*S*,4′*S*)-4,4′-(2,2′-(4-(dimethylamino)butane-1,1-diyl)bis(3-(2-(dimethylamino) ethyl)-1*H*-indole-5,2-diyl)) bis(methylene)di(oxazolidin-2-one) (ZOL-dimer). The analytical standard of ZOL-dimer was prepared and fully characterized. The quick and efficient UHPLC method for the measurement of ZOL and related impurities has been described. The method has obvious advantages over those previously reported such as very short analysis time and high separation efficiency.

Fig. 5. (A) The separation of spiked related substances of ZOL under method conditions on an Ascentis Express Phenyl-Hexyl column (100 mm × 3.0 mm, 2.7 μm; Supelco, USA). The retention factor of ZOL was $k = 4.54$, symmetry factor $A_S = 1.36$ and resolution between ZOL and N-desmethylzolmitriptan $R_S = 4.56$. (B) UHPLC analysis of blank (sample solvent).

References

[1] K.W. Johnson, J.M. Schaus, M.M. Durkin, J.E. Audia, S.W. Kaldor, M.E. Flaugh, N. Adham, J.M. Zgombick, M.L. Cohen, T.A. Branchek, L.A. Phebus, 5-HT1F receptor agonists inhibit neurogenic dural inflammation in guinea pigs, Neuroreport 8 (1997) 2237–2240.
[2] R. Whale, Z.A. Bhagwagar, P.J. Cowen, Zolmitriptan induced growth hormone release in humans mediated by 5-HT1D receptors? Psychopharmacology 145 (1999) 223–226.
[3] R. Dixon, A. Warrander, The clinical pharmacokinetics of zolmitriptan, Cephalalgia 17 (Suppl. 18) (1997) 15–20.

[4] Z. Zhang, F. Xu, J.Y. Tian, W. Li, G. Mao, Quantification of zolmitriptan in plasma by high-performance liquid chromatography–electrospray ionization mass spectrometry, J. Chromatogr. B 813 (2004) 227–233.

[5] E.M. Clement, M. Franklin, Simultaneous measurement of zolmitriptan and its major metabolites N-desmethylzolmitriptan and zolmitriptan N-oxide in human plasma by high-performance liquid chromatography with coulometric detection, J. Chromatogr. B 766 (2002) 339–343.

[6] J. Chen, X.G. Jiang, W.M. Jiang, N. Mei, X.L. Gao, Q.Z. Zhang, High-performance liquid chromatographic analysis of zolmitriptan in human plasma using fluorescence detection, J. Pharm. Biomed. Anal. 35 (2004) 639–645.

[7] E.K.S. Vijayakumar, M.A. Samel, S.B. Bhalekar, S.M. Pakhale, A new stability indicating HPLC method for related substances in zolmitriptan, Ind. J. Pharm. Sci. 72 (2010) 119–122.

[8] B.M. Rao, M.K. Srinivasu, G. Sridhar, P.R. Kumar, L.B. Chandrasekhar, A. Islam, A stability indicating LC method for zolmitriptan, J. Pharm. Biomed. Anal. 39 (2005) 503–509.

[9] A. Miglani, P. Kumar, B. Negi, H.D. Gautam, Isolation and characterization of the zolmitriptan unknown impurity by chromatographic and mass spectroscopy, Anal. Chem. 9 (2010) 12–16.

[10] A.D. Robertson, A.P. Hill, R.C. Glen, G.R. Martin, US Patent 5,466,699 (1995).

[11] K. Dittmann, U. Pindur, Darstellung und NMR-spektroskopie Charakterisierung von 2,2′-Bis(methylindolyl)-aryl-methanen, Arch. Pharm. 318 (1985) 340–350.

[12] B.P. Bandgar, S.V. Bettigeri, N.S. Joshi, Hexamethylenetetraamine-bromine catalyzed rapid and efficient synthesis of bis(indolyl)methanes, Monatsh. Chem. 135 (2004) 1265–1273.

[13] M. Chakrabarty, N. Ghosh, R. Basak, Y. Harigaya, A facile and efficient synthesis of 2,2-bis(3′/2′-indolyl)ethylamines and three bisindolic natural products, Synth. Commun. 34 (2004) 421–434.

[14] T.J. Sunder Raj, C. Bharathi, M.S. Kumar, J. Prabahar, P.N. Kumar, H.K. Sharma, K. Parikh, Identification, isolation and characterization of process-related impurities in Rizatriptan benzoate, J. Pharm. Biomed. Anal. 49 (2009) 156–162.

[15] ICH Harmonised Tripartite Guidelines Q3A(R2) Impurities in New Drug Substances, 2006.

[16] European Pharmacopoeia, 6th ed., Council of Europe, Strasbourg, 2009, pp. 4407–4413.

[17] ICH Q2(R1), Validation of Analytical Procedures, Step 4 version, 2005.

[18] J. Van Loco, M. Elskens, Ch. Croux, H. Beernaert, Linearity of calibration curves: use and misuse of the correlation coefficient, Accredit. Qual. Assur. 7 (2002) 281–285.

Fingerprinting of sildenafil citrate and tadalafil tablets in pharmaceutical formulations via X-ray fluorescence (XRF) spectrometry

Rafael S. Ortiz [a,b], Kristiane C. Mariotti [b], Nicolas V. Schwab [c], Guilherme P. Sabin [c], Werickson F.C. Rocha [d], Eustáquio V.R. de Castro [e], Renata P. Limberger [b], Paulo Mayorga [b], Maria Izabel M.S. Bueno [c], Wanderson Romão [e,*]

[a] Rio Grande do Sul Technical and Scientific Division, Brazilian Federal Police, 90160-093 Porto Alegre, RS, Brazil
[b] Department of Pharmacy, Federal University of Rio Grande do Sul, 90610-000 Porto Alegre, RS, Brazil
[c] Institute of Chemistry, State University of Campinas, 13084-971 Campinas, SP, Brazil
[d] National Institute of Metrology, Standardization and Industrial Quality, Directorate of Industrial and Scientific Metrology, Division of Chemical Metrology, 25250-020 Duque de Caxias, Rio de Janeiro, RJ, Brazil
[e] Department of Chemistry, Federal University of Espírito Santo, 29075-910 Vitória, ES, Brazil

ARTICLE INFO

ABSTRACT

The production of counterfeited drugs is a criminal problem that carries serious risks to public health in the worldwide. In Brazil, Viagra® and Cialis® are the most counterfeit medicines, being used to inhibit the phosphodiesterase type 5 (PDE-5), treating thus, problems related to erectile dysfunction. X-ray fluorescence (XRF) is a suitable technique to control the quality of new pharmaceutical formulations and distinguish between authentic and counterfeit tablets. XRF has advantageous features like multielemental capability, good detectivity, high precision, short analysis times, and is nondestructive, which makes it suitable to be extended to a great variety of samples. In this work, the inorganic fingerprinting chemical of forty-one commercial samples (Viagra®, Cialis®, Lazar®, Libiden®, Maxfil®, Plenovit®, Potent 75®, Rigix®, V-50®, Vimax® and Pramil®) and fifty-six counterfeit samples (Viagra and Cialis) were obtained from XRF data. XRF presented an excellent analytical methodology for semi-quantitative determination of active ingredient (in case of sildenafil citrate that presents S in its structure) and excipients such as calcium phosphate, titanium oxide and iron oxide (P, Ca, Ti and Fe). The matrix data were allied to chemometric methods (Principal Component Analysis and Hierarchical Cluster Analysis) to classify the tablets investigated between authentic and counterfeit, grouping the samples into of seven groups: **A**, **B**, **C**, **D** and **E** (counterfeit group) and **F** and **G** (authentic group).

Crown Copyright © 2011 Published by Elsevier B.V. All rights reserved.

1. Introduction

The production of counterfeit drugs is a criminal problem that carries serious risks to public health in the worldwide. Recent studies suggest that a significant growth of counterfeiting processes in the last decade may be associated with easier access, by the counterfeiters, the technologies needed to copy pharmaceutical products genuine [1]. Moreover, the marketing supplied by the Internet allows the buying of any drug without prescription, easily and anonymously, in fraudulent sites [2,3]. In an attempt to combat this phenomenon, the WHO created in 2006 a global coalition of stakeholders called IMPACT (International Medical Products Anti-Counterfeiting Taskforce). The IMPACT has been active in forging international collaboration, finding global solutions to combat this challenge and in raising awareness of the dangers of counterfeit medical products [4].

By definition, counterfeit medicines are drugs that have "*been deliberately and fraudulently mislabeled with respect to identity and/or source*" [5]. All kinds of medicines are counterfeited [6–9], but the illegal market of most successful is related to three approved phosphodiesterase type 5 (PDE-5) inhibitors for treating erectile dysfunction, sildenafil citrate (Viagra®,[1] Pfizer), tadalafil (Cialis®, Eli Lilly), and vardenafil (Levitra®, Bayer). These medicines have led to an explosion in counterfeit versions of these drugs [10]. PDE-5 inhibitors are prime target for counterfeiting due to the high cost and the embarrassment associated with the underlying condition leading people and becoming the Internet as main source in buying these medicines [10].

---

* Corresponding author. Tel.: +55 27 3335 2043.
E-mail address: wandersonromao@gmail.com (W. Romão).

---

[1] The symbol ® will be used only in reference to the original medicines.

Table 1
Description of numbers of samples and register of seizures for authentic and counterfeit samples and elemental concentrations of S, Ca, Ti and Fe obtained from XRF data.

	Number of samples	Register of seizure	S (μg g^{-1})	Ca (μg g^{-1})	Ti (μg g^{-1})	Fe (μg g^{-1})
Authentic Viagra®	4	–	7555 ± 222	$18,703 \pm 1165$	1020 ± 1896	10 ± 20
	6	I	5300 ± 925	$16,908 \pm 2138$	1032 ± 1220	110 ± 7
Counterfeit Viagra	10	II	$28,806 \pm 1064$	$26,186 \pm 1375$	189 ± 232	99 ± 69
	1	III	–	–	–	–
	1	IV	–	–	–	–
Authentic Cialis®	4	–	–	–	1512 ± 510	1003 ± 148
	10	V	$31,767 \pm 8787$	$31,295 \pm 5373$	1459 ± 1138	75 ± 79
Counterfeit Cialis	10	VI	$10,693 \pm 11,500$	$40,820 \pm 3039$	834 ± 588	107 ± 40
	18	I	$26,073 \pm 6622$	$41,126 \pm 12,390$	253 ± 533	99 ± 93
Lazar®	3	–	3663 ± 2619	$12,457 \pm 10,817$	2736 ± 2707	–
Potent 75®	2	–	7120 ± 57	7365 ± 1009	3875 ± 1873	–
Vimax®	3	–	7793 ± 1545	$17,030 \pm 2313$	2813 ± 1344	–
Maxfil®	3	–	7717 ± 457	$15,697 \pm 361$	933 ± 846	57 ± 6
Rigix®	2	–	6540 ± 382	$16,360 \pm 1032$	170 ± 240	20 ± 28
Plenovit®	6	–	8702 ± 4787	$18,128 \pm 13,449$	1577 ± 818	30 ± 48
Pramil®	10	–	$15,384 \pm 3853$	4890 ± 1438	2569 ± 1897	69 ± 47
V-50®	3	–	$11,840 \pm 151$	337 ± 83	2990 ± 784	27 ± 23
Libiden®	1	–	9630	460	3670	–

In Brazil, Viagra® and Cialis® are the most counterfeited medicines [11]. Routinely, seizures of suspected counterfeit drugs are forwarded to the Brazilian Federal Police (PF) for forensic analysis. The database of the PF shows that from January 2007 to September 2010 371 reports were issued involving counterfeit drugs and of these, 295 (80%) included counterfeit Cialis® and Viagra® samples.

To control the quality of new pharmaceutical formulations and distinguish between authentic and counterfeit tablets, the development of powerful analytical tools is necessary. Analytical methods have been reported in Viagra® and Cialis® tablets analyses such as chromatography [12–15] and voltammetry [16,17]. For forensic analyzes, these methods are disadvantage, requiring a high time-consuming and extensive sample preparation.

X-ray fluorescence (XRF) is a suitable technique for characterization of the presence of metals [18,19]. This technique has advantageous features like multielemental capability, good detectivity, high precision, short analysis times, and is nondestructive, which makes it suitable to be extended to a great variety of samples. Thus, XRF presents an excellent analytical methodology for determination of active ingredient (in case of sildenafil citrate that presents sulfur, S, in its structure), excipients and covering agents as calcium phosphate, titanium oxide and iron oxide (P, Ca, Ti and Fe) that can be detected directly by XRF on the surface of pharmaceutical formulations.

XRF allied to chemometrics has been applied to the study of complex samples [18]. In this article, the inorganic fingerprinting chemical of several commercial samples (Viagra®, Cialis®, Lazar®, Libiden®, Maxfil®, Plenovit®, Potent 75®, Rigix®, V-50®, Vimax® and Pramil®) and counterfeit samples (Viagra® and Cialis®) were obtained from XRF data and allied to chemometric methods PCA (Principal Component Analysis) and HCA (Hierarchical Cluster Analysis) to classify the tablets investigated between authentic and counterfeit.

2. Multivariate analysis

Multivariate methods consider the correlation among many variables simultaneously, allowing the extraction and visualization of a much larger amount of information [19]. In PCA [20–22], the dataset (matrix **X**) composed by samples (rows) and variables (columns) is decomposed in two new sets, named scores and loadings. Scores and loadings have information about samples and variables, respectively, and analyzing both information together, the matrix **X** is visualized in a smaller dimension (named principal

components). The purpose of PCA is data reduction, facilitating an exploratory analysis.

Cluster analysis is a method for dividing a group of objects into classes so that similar objects are in the same class. As in PCA, the groups are not known prior to the mathematical analysis and no assumptions are made about the distribution of the variables. Cluster analysis searches for objects which are close to each other in the variable space. The distance, d, between two points in n-dimensional space with coordinates $(x_1, x_2, \ldots, x_n)$ and $(y_1, y_2, \ldots, y_n)$ is usually taken as the Euclidean distance defined by Eq. (1):

$$d = \sqrt{(x_1 - y_1)^2 + (x_2 - y_2)^2 + (x_3 - y_3)^2 + \cdots + (x_n - y_n)^2} \qquad (1)$$

As in PCA, a decision has to be made as to whether or not the data are standardized. Standardizing the data will mean that all the variables are measured on a common scale so that one variable does not dominate the other.

There are a number of methods for searching clusters. One method starts by considering each object as forming a 'cluster' of size one, and compares the distances between these clusters. The two points which are closest to each other are joined to form a new cluster. The distances between the clusters are again compared and the two nearest clusters combined. This procedure is repeated and, if continued indefinitely, will group all the points together. There are a variety of ways of computing the distance between two clusters which contain more than one member. The simplest concept is to take the distance between two clusters as the distance between nearest neighbors. This is called the single linkage method and was used in this work.

3. Methods and materials

Eight authentic samples of Viagra® and Cialis® containing 50 mg of sildenafil (4) and 20 mg of tadalafil (4), respectively, were supplied by Pfizer Ltda and Eil Lilly do Brasil Ltda Laboratories. Thirty-three tablets containing sildenafil citrate and/or tadalafil as active ingredient of several trademarks and fifty-six counterfeit samples were provided by the PF and analyzed via XRF. Information about numbers of samples analyzed, register of seizures (for counterfeit samples) and elemental concentrations of S, Ca, Ti and Fe are shown in Table 1.

3.1. X-ray fluorescence

The ED-XRF experiments were performed using an X-ray spectrometer Shimadzu®, model EDX 700 (Kyoto, Japan). The
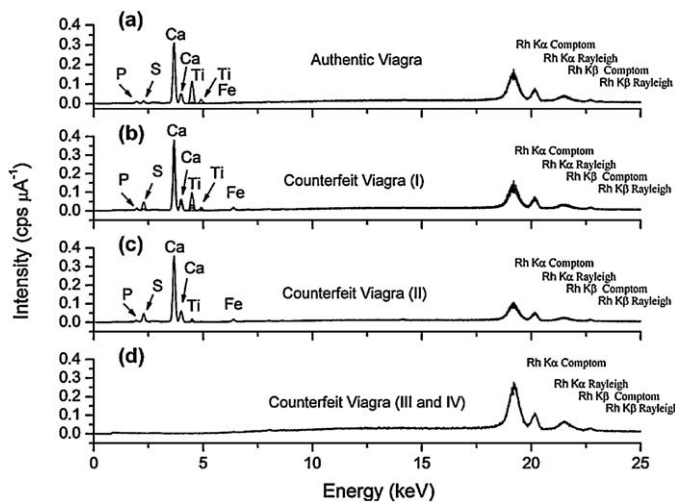
Fig. 1. ED-XRF spectra of (a) authentic Viagra®, and counterfeit Viagra samples with different register of seizures: (b) **I**, (c) **II**, (d) **III** and **IV**.

Fig. 2. ED-XRF spectra of (a) authentic Cialis®, and counterfeit Cialis samples with different register of seizures: (b) **V**, (c) **VI**, and (d) **I**.

measurements were performed under air, with a beam collimation of 3 mm, 25% of detector dead time, with the current automatically adjusted during spectrum acquisition to keep the detector dead time of 25%. The Shimadzu EDX 700 also presents the following characteristics: (1) a Rh X-ray generator, with tube voltage ranging from 5 to 50 kV, and tube current from 1 to 1000 μA; (2) a semiconductor detector, Si(Li), with detection area of 10 mm^2 and resolution of <155 eV.

For spectral acquisition, sildenafil and tadalafil tablets were crushed using a mortar and placed into XRF cells on Mylar^{TM} film (3 μm thickness). The measurement time was 250 s. In all cases the spectra were recorded from 0 to 40 keV, with an energy step of 0.02 keV, resulting in 2048 points for each spectrum.

3.2. Chemometric analysis

For XRF, the spectral data were mean centered. Then, to classify the tablets between authentic and counterfeit after XRF fingerprinting, PCA and HCA were applied to the XRF data using the software Pirouette v. 3.11 and Matlab using PLS Toolbox, version 4.21 from Eigenvector Technologies. The entire spectra were used in PCA and HCA analysis (0–40 keV), resulting in 2048 points (variables) and 97 samples.

4. Results

A set of 22 samples of Viagra® classified between authentic (4) and counterfeit (18, corresponding to seizures termed of **I**, **II**, **III** and **IV**, Table 1) were selected by PF and analyzed via ED-XRF. Fig. 1a shows the combined ED-XRF spectra for the 4 authentic Viagra® samples. All spectra show the presence of Kα characteristic lines for P (1.98 keV), S (3.30 keV), Ca (3.62 keV), Ti (4.48 keV) and Fe (6.38 keV) and Kβ characteristic lines for Ca (4.00 keV) and Ti (4.90 keV). The S line observed is due the presence of S atom in the structure of active ingredient, sildenafil citrate. Other elements such as P, Ca and Ti correspond to excipients such as calcium phosphate dibasic (CaHPO$_4$) and titanium dioxide (TiO$_2$). The Fe is used as covering agent. The region of a high intensity line is related to the Compton (Rh Kα (19.20 keV), Rh Kβ (21.56 keV) lines) and Rayleigh (Rh Kα (20.16 keV) and Rh Kβ (22.74 keV) lines) effects. These Compton (incoherent scatter) and Rayleigh (coherent scatter) effects contribute significantly to perform quantitative organic ED-XRF analysis, being associated with light elements (C, H, O, among others) [18,19] that are not visualized in ED-XRF spectra
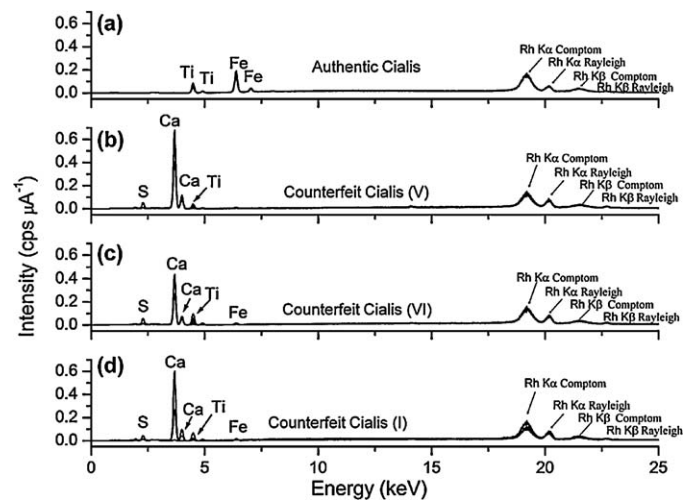
such as excipients organics that are hipromellose, lactose, triacetin and microcrystalline cellulose. This scattering region can provide powerful information for qualitative or even quantitative determinations of light elements when treated with chemometric analysis [18,19].

Fig. 1b and c shows two sets of combined ED-XRF spectra for the counterfeit Viagra® samples (seizures **I** and **II**). Generally, for the seizure **I** (with exception of one sample, Fig. 1b), a lower S concentration (active ingredient) is observed when compared with the authentic Viagra® samples, see Fig. 1b and Table 1. In relation to excipients, the main change is observed for Fe concentration. For the seizure **II**, a much higher S concentration is detected (about 400% higher than the standard). Different to both cases, the seizures **III** and **IV** show no Kα or Kβ characteristic lines, presenting thus, probably an organic composition predominant as mentioned previously.

Authentic and counterfeit Cialis® samples were also analyzed by XRF (Fig. 2a–d). The XRF spectrum obtained for authentic Cialis® samples shows the presence of Kα and Kβ characteristic lines only for Ti (Kα = 4.48 keV and Kβ = 4.90 keV); and Fe (Kα = 6.38 keV and Kβ = 7.02 keV) elements, corresponding to TiO$_2$ and Fe$_2$O$_3$, respectively. This result is specific and completely different to the result observed for Viagra® samples. Therefore, the samples can be easily classified and distinguished between Viagra® and Cialis® using the XRF technique. It is also important to mention that the elemental composition of the tadalafil is formed basically by light elements (CHNO), being therefore, organic composition is directly associated to scattering region (18–25 keV). Counterfeit Cialis samples obtained from different seizures (**V**, **VI** and **I**) were also analyzed, Fig. 2b–d. In contrast to results obtained for authentic Cialis® samples, Fig. 2a, all counterfeit samples show a composition quite similar to XRF results for authentic Viagra® samples, Fig. 1a. Among the set of counterfeit Cialis® samples, the sildenafil citrate concentration in all cases is much higher than the normal levels found for authentic Viagra® (the concentration reaches levels higher than 400%). These values increase in following order: seizure **V** > seizure **I** > seizure **VI** > authentic Viagra®, Fig. 2b–d. For the Ca, Ti and Fe concentrations, the respective order is observed: seizure **I** > seizure **VI** > seizure **V** > authentic Viagra® (for Ca); seizure **V** > authentic Viagra® > seizure **VI** > seizure **I** (for Ti); and seizure **VI** > seizure **I** > seizure **V** > authentic Viagra® (for Fe), see Table 1. Therefore, with the exception of Ti, the elemental concentration referent to counterfeit Cialis samples is always higher in all cases.

Other commercial samples containing sildenafil citrate were also analyzed by ED-XRF: Lazar®, Potent 75®, Vimax®, Maxfil®, Rigix®, Plenovit®, Pramil®, V-50® and Libiden®. All these medicines are not approved by the National Health Surveillance Agency, Anvisa, and cannot be legally commercialized in Brazilian market as typical PDE-5 inhibitors for treating of erectile dysfunction. ED-XRF spectra for these commercial samples are shown in supplementary material.

To clarify the discussion, we compare the XRF results obtained from these commercial samples to the data observed for authentic Viagra® samples. Generally, for the Lazar®, Potent 75® and Vimax® samples, the XRF results show a lower S and Ca concentrations (for S ranges from 3663 ± 2619 to $7793 \pm 1545\,\mu g\,g^{-1}$; and for Ca ranges from 7365 ± 1009 to $17,030 \pm 2313\,\mu g\,g^{-1}$, respectively) and a higher concentration of Ti (ranges from 2736 ± 2707 to $3875 \pm 1873\,\mu g\,g^{-1}$), Table 1. For Maxfil® and Rigix® samples, a lower elemental concentration (with exception of Fe) is observed. For Plenovit® samples, close concentration levels are observed ($[S] = 8702 \pm 4787\,\mu g\,g^{-1}$; $[Ca] = 18,128 \pm 13,449\,\mu g\,g^{-1}$; and $[Ti] = 1577 \pm 818\,\mu g\,g^{-1}$); however, this result shows a high standard deviation, probably due to poor quality control in industrial manufacturing process, Table 1. In contrast with all commercial samples, the Pramil®, V-50® and Libiden® samples show a higher S and Ti concentration, Table 1.

For quantitative analysis of S, Ca, Ti and Fe elements, the fundamental parameter method (FP method) has been used. Because the sample composition is known, the results allow theoretical calculation of intensities of generated fluorescent X-rays using the measuring conditions and physical constants from FP. The FP method utilizes these characteristics in a reverse manner, that is, it tries to obtain the composition from the actually measured intensities [18,23–26]. Also, it is well known that sample preparation is the source of the largest errors of XRF analyzes. Low standard deviations (SD) ($<10\,\mu g\,g^{-1}$, for example) are reached when the particle size is mainly controlled [18,27,28]. Herein, tablets displayed heterogeneous composition, where changes in the weight (100–500 mg), mixture time and particle size contributed to high SD values observed ($<14,000\,\mu g\,g^{-1}$), Table 1. However, the ED-XRF technique requires less effort for sample preparation, providing high composition information, a fast and cheap analysis (in ca. 100 s a spectrum is acquired). These features make ED-XRF as an attractive technique for quality control of pharmaceutical formulations.

4.1. Chemometry

ED-XRF data were subjected to chemometric treatment via PCA and HCA, Figs. 3 and 4. Both were used to statistically evaluate the performance of ED-XRF spectra in classifying of sildenafil citrate and tadalafil samples for quality control purposes. Fig. 3a and b shows PC1 × PC2 scores and loading plots, where the 2 first PCs account for ca. 94% of the total variance. In PC1 × PC2 scores plot, in general, a separation into two large groups is observed corresponding to counterfeit samples (groups **A**, **B**, **C** and **D**, PC1 < 0; and group **E**, PC1 > 0) and commercial samples (groups **F** and **G**; PC1 > 0) according to the PC1 region, Fig. 3a. This separation is mainly due to Ca and Ti variables, where they have a significant influence for PC1 loading, as shown in Fig. 3b. The groups **A**, **B** and **C** are related to counterfeit Cialis samples corresponding to seizures **VI**, **I** and **V**, respectively. Generally, they display a higher Ca and S concentrations observed among all samples analyzed. The groups **D** and **E** are related to counterfeit Viagra samples corresponding to seizures **I** and **II** and **III** and **IV**, respectively. The group **E** (seizures **III** and **IV**) is the uniquely placed in PC1 > 0 region. It is due to the fact of composition being predominantly organic. For other groups (PC1 > 0) related to commercial samples, the group **F** corresponds to authentic Viagra®, Maxfil®, Vimax®, Plenovit® and Rigix® samples and the
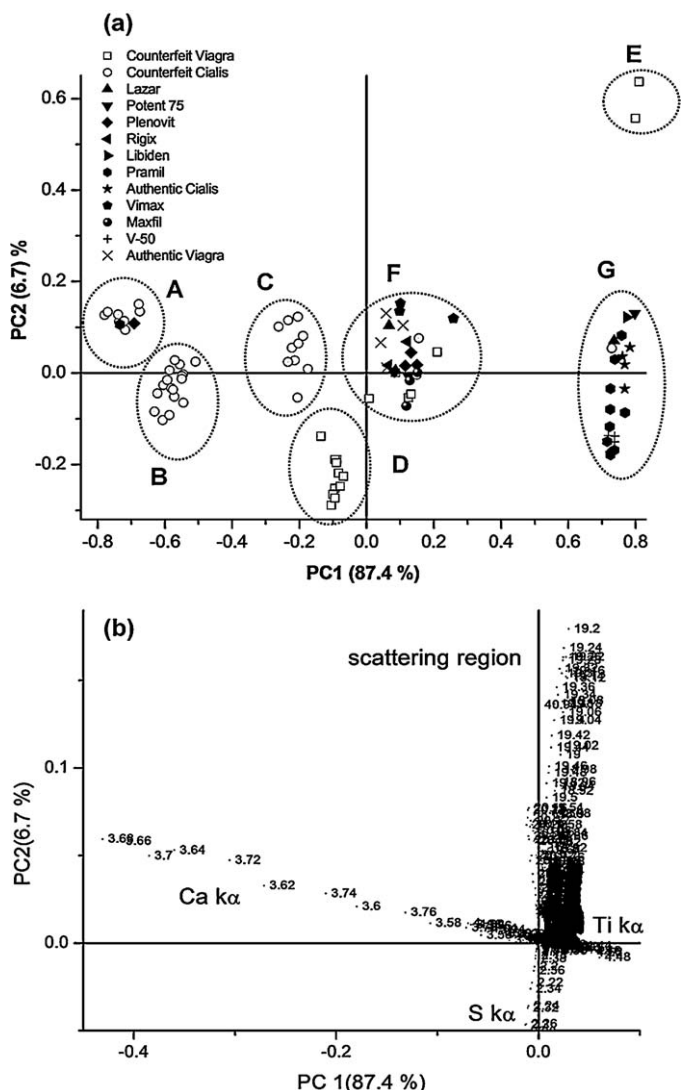

Fig. 3. PC1 × PC2 (a) scores and (b) loading plot for ED-XRF data.

group **G** to authentic Cialis®, Pramil®, Lazar®, V-50®, Libiden® and Potent 75® samples.

The PC1 × PC3 scores plot was also investigated. New subgroups are observed from groups **C**, **F** and **G** according to the PC3 region (responsible for ca. 2.6% of total variance). This separation is mainly
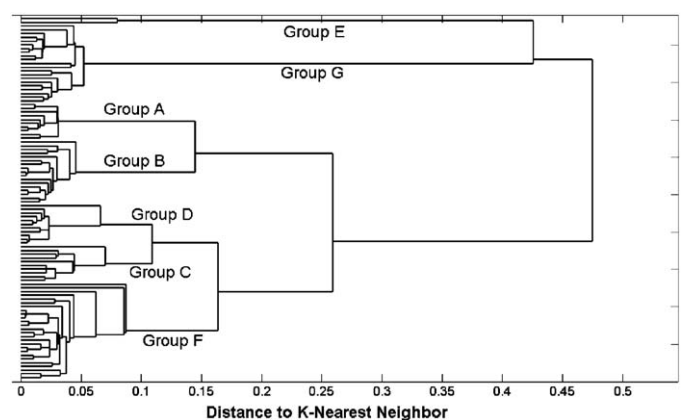

Fig. 4. HCA plot for ED-XRF data.

due to the contribution of another variable, Fe, which has significant influence for PC3 loading (see supplementary material).

Fig. 4 shows the results of the HCA chemometric method for ED-XRF data used. As can be observed, although the HCA was carried out using all the data, the results obtained were similar to those from the PCA: counterfeit samples were classified in groups **A**, **B**, **C**, **D** and **E** and the commercial samples in groups **F** and **G**.

5. Conclusion

ED-XRF data provide relatively simple and fast screening tools in forensic investigations to characterize and classify between authentic samples (formulation commercials of sildenafil citrate and tadalafil) and counterfeit Cialis and Viagra samples. The inorganic fingerprinting chemical of several commercial samples (Viagra®, Cialis®, Lazar®, Libiden®, Maxfil®, Plenovit®, Potent 75®, Rigix®, V-50®, Vimax® and Pramil®) and counterfeit samples (Viagra and Cialis) were obtained from XRF data. Thus, XRF presented an excellent analytical methodology for semi-quantitative determination of active ingredient (in case of sildenafil citrate that presents S in its structure) and excipients such as calcium phosphate, titanium oxide and iron oxide (P, Ca, Ti and Fe). Among the counterfeit samples, the most samples (54) presented sildenafil citrate as an active ingredient. Some counterfeit Viagra samples (seizure **II**) and all counterfeit Cialis samples showed a higher S concentration than normally observed for authentic samples ([S] = $7555 \pm 222\,\mu g\,g^{-1}$). Among the commercial samples investigated, the Lazar® and Pramil® showed a lower and higher S concentration (3663 ± 2619 and $15,384 \pm 3853\,\mu g\,g^{-1}$), respectively.

Generally, Principal Component Analysis and Hierarchical Cluster Analysis applied to XRF data classified samples into seven groups: **A**, **B**, **C**, **D** and **E** (counterfeit) and **F** and **G** (authentic). The variables responsible for separation are mainly related to Ca and Ti elements.

Acknowledgements

Appendix A. Supplementary data

Supplementary data associated with this article can be found, in the online version, at doi:10.1016/j.jpba.2011.09.005.

References

[1] F.M. Fernandez, D. Hostetler, K. Powell, H. Kaur, M. Green, D.C. Mildenhall, P.N. Newton, Poor quality drugs: grand challenges in high throughput detection, countrywide sampling, and forensics in developing countries, Analyst (2010), doi:10.1039/c0an00627k.

[2] P.-Y. Sacré, E. Deconinck, T. de Beer, P. Courselle, R. Vancauwenberghe, P. Chiap, J. Crommen, J.O. de Beer, Impurity fingerprints for the identification of counterfeit medicines—a feasibility study, J. Pharm. Biomed. Anal. 53 (2010) 445–453.

[3] A.L. Rodomonte, M.C. Gaudiano, E. Antoniella, D. Lucente, V. Crusco, M. Bartolomei, P. Bertocchi, L. Manna, L. Valvo, F. Alhaique, N. Muleri, Counterfeit drugs detection by measurement of tablets and secondary packaging colour, J. Pharm. Biomed. Anal. 53 (2010) 215–220.

[4] WHO, International Medical Products Anti-Counterfeiting Taskforce. Available: http://www.who.int/impact/en/, 2011 (accessed 21.02.11).

[5] WHO. Department of Essential Drugs and Other Medicines, Conterfeit Drugs: Guidelines for the Development of Measures to Combat Counterfeit Drugs, World Health Organization, Genebra, 1999.

[6] R. Santamaria-Fernandez, R. Hearn, J.-C. Wolff, Detection of counterfeit antiviral drug Heptodin™ and classification of counterfeits using isotope amount ratio measurements by multicollector inductively coupled plasma mass spectrometry (MC-ICPMS) and isotope ratio mass spectrometry (IRMS), Sci. Justice 49 (2009) 102–106.

[7] M.B. Lopes, J.-C. Wolff, J.M. Bioucas-Dias, M.A. Figueiredo, Determination of the composition of counterfeit Heptodin tablets by near infrared chemical imaging and classical least squares estimation, Anal. Chim. Acta 641 (2009) 46–51.

[8] O.Y. Rodionova, L.P. Houmoller, A.L. Pomerantsev, P. Geladi, J. Burger, V.L. Dorofeyev, A.P. Arzamastsev, NIR spectrometry for counterfeit drug detection—a feasibility study, Anal. Chim. Acta 549 (2005) 151–158.

[9] P. de Peinder, M.J. Vredenbregt, T. Visser, D. de Kaste, Detection of Lipitor® counterfeits: a comparison of NIR and Raman spectroscopy in combination with chemometrics, J. Pharm. Biomed. Anal. 47 (2008) 688–694.

[10] U. Holzgrabe, M. Malet-Martino, NMR techniques in biomedical and pharmaceutical analysis, J. Pharm. Biomed. Anal. 52 (2010) 51–58.

[11] Agência Nacional de Vigilância Sanitária, Ministério da Saúde, Brasil; Medicamentos Falsificados. Available: http://www.anvisa.gov.br/medicamentos/falsificados/index.htm, 2011 (accessed 22.10.08).

[12] Y.J. Yang, D.M. Song, W.M. Jiang, B.R. Xiang, Rapid resolution RP-HPLC-DAD method for simultaneous determination of sildenafil, vardenafil, and tadalafil in pharmaceutical preparations and counterfeit drugs, Anal. Lett. 43 (2010) 373–380.

[13] E. Abourashed, M.S. Abdel-Kader, A.A.M. Habib, HPTLC determination of sildenafil in pharmaceutical products and aphrodisiac herbal preparations, J. Planar Chromatogr. Mod. TLC 18 (2005) 372–376.

[14] Y. Cai, T.G. Cai, Y. Shi, X.L. Cheng, L.Y. Ma, S.C. Ma, R.C. Lin, W. Feng, Simultaneous determination of eight PDE5-IS potentially adulterated in herbal dietary supplements with TLC and HPLC–PDA-MS methods, J. Liq. Chromatogr. Relat. Technol. 33 (2010) 1287–1306.

[15] J.J. Berzas, J. Rodríguez, M.J. Villaseñor, A.M. Contento, M.P. Cabello, Validation of a capillary gas-chromatographic method for the determination of sildenafil citrate in its pharmaceutical formulations (Viagra). Experimental design for evaluating the ruggedness of the method, Chromatographia 55 (2002) 601–606.

[16] K. Tyszczuk, M. Korolczuk, Voltammetric method for the determination of sildenafil citrate (Viagra) in pure form and in pharmaceutical formulations, Bioelectrochemistry 78 (2010) 113–117.

[17] S.-V. Staden, Raluca-Ioana, V. Staden, F. Jacobus, Aboul-Enein, Y. Hassan, Diamond paste-based electrodes for the determination of sildenafil citrate (Viagra), J. Solid State Electrochem. 14 (2010) 997–1000.

[18] W. Romão, M.F. Franco, M.I.M.S. Bueno, M.N. Eberlin, M.-A. De Paoli, Analysing metals in bottle-grade poly(ethylene terephthalate) by X-ray fluorescence spectrometry, J. Appl. Polym. Sci. 117 (2010) 2993–3000.

[19] W. Romão, P.M. Lalli, M.F. Franco, G. Sanvido, N.V. Schwab, R. Lanaro, J.L. Costa, B.D. Sabino, M.I.M.S. Bueno, G. de Sa, R.J. Daroda, V. Souza, M.N. Eberlin, Chemical profile of meta-chlorophenylpiperazine (m-CPP) in ecstasy tablets by easy ambient sonic-spray ionization, X-ray fluorescence, ion mobility mass spectrometry, and NMR, Anal. Bioanal. Chem. 400 (2011) 2685–2686.

[20] M.A. Sharaf, D.L. Illman, B.R. Kowalski, Chemometrics, Wiley-Interscience, New York, 1986.

[21] P. Geladi, Chemometrics in spectroscopy. Part 1. Classical chemometrics, Spectrochim. Acta Part B 58 (2003) 767–782.

[22] K. Miranda, M.I.M.S. Bueno, E.R. Pereira-Filho, Relevant information of concomitants obtained from background signal using thermospray flame furnace atomic absorption spectrometry (TS-FF-AAS) and chemometric tools, J. Anal. Atom. Spectrom. 24 (2009) 304–309.

[23] E. Margu, I. Queralt, M. Hidalgo, Application of X-ray fluorescence spectrometry to determination and quantitation of metals in vegetal material, Trends Anal. Chem. 28 (2009) 362–372.

[24] K. Omote, H. Kohno, K. Toda, X-ray fluorescence analysis utilizing the fundamental parameter method for the determination of the elemental composition in plant samples, Anal. Chim. Acta 307 (1995) 117–126.

[25] J. Sherman, The theoretical derivation of fluorescent X-ray intensities from mixtures, Spectrochim. Acta 7 (1955) 283–306.

[26] T. Shiraiwa, N. Fujino, Theoretical calculation of fluorescent X-ray intensities in fluorescent X-ray spectrochemical analysis, J. Appl. Phys. 5 (1966) 886–899.

[27] F. Demir, G. Budak, E. Baydas, Y. Sahin, Standard deviations of the error effects in preparing pellet samples for WDXRF spectroscopy, Nucl. Instrum. Methods Phys. Res. B 243 (2006) 423–428.

[28] F.L. Melquiadesa, D.D. Ferreirab, C.R. Appolonib, F. Lopesb, A.G. Lonnic, F.M. Oliveirac, J.C. Duartec, Titanium dioxide determination in sunscreen by energy dispersive X-ray fluorescence methodology, Anal. Chim. Acta 613 (2008) 135–143.

A target analogue imprinted polymer for the recognition of antiplatelet active ingredients in *Radix Salviae Miltiorrhizae* by LC/MS/MS

Meixia Huang, Wensheng Pang, Jing Zhang, Siding Lin, Juan Hu*

School of Pharmacy, Fujian University of Traditional Chinese Medicine, Fuzhou 350108, China

ABSTRACT

The purpose of this study was to prepare a propyl gallate (PrG) molecular imprinted polymer as a cartridge stuffing material to isolate antiplatelet active ingredients. A macroporous polymer was synthesized utilizing ethylene glycol dimethacrylate (EDMA) as the crosslinking agent, PrG as the template molecule and 4-vinylpyridine (4-Vpy) as the functional monomer. Subsequently, PrG was removed by washing with methanol–glacial acetic acid (9:1, v/v). The molecular imprinted polymer recognized an active ingredient, protocatechuic acid, from a crude extract of the Chinese herbal medicine, *Radix Salviae Miltiorrhizae* (Danshen), using an on-line column switching solid phase extraction process. Pharmacological experiments showed that protocatechuic acid inhibits arachidonic acid (10 mg/kg) induced aggregation of rat platelets in vivo. This study provides an example of an application of separation-analysis technique for screening potentially bioactive compounds.

© 2011 Elsevier B.V. All rights reserved.

1. Introduction

Historically, traditional Chinese medicines have been used to treat thrombosis with the aim of activating the blood and eliminating stasis. An abnormal increase in the number of platelets within one's blood is associated with many cardiovascular diseases; therefore, many traditional Chinese medicines are selected for their antiplatelet activity to prevent blood clotting [1]. Danshen is one of the most common herbs and has been used to treat coronary heart disease and angina. It can inhibit thrombus formation, prevent platelet aggregation, significantly decrease serum lipid levels, and improve the hemorheological index [2,3]. The extensive clinical use of this herb prompted our selection of it for screening.

Between the 1970s and 1980s, a gallic acid ester derivative was isolated from the herbal medicine *Radix Paeoniae* as well as a modified structure compound named *Radix Paeoniae* 801 (*P. Radix* 801) or propyl gallate (PrG). Chinese State Food and Drug Administration (SFDA) approved *P. Radix* 801 for injection (trade name Beibingzhi) to prevent and treat cerebral thrombosis and coronary heart disease in 2003 [4]. PrG is a commonly used synthetic antioxidant in processed food, cosmetics and food packaging to prevent rancidity and spoilage. It is also approved as a preservative and stabilizer for

medicinal preparations by the US Food and Drug Administration [5] and as an additive by the European Union and many other countries. The PrG daily intake recommended by the Joint FAO/WHO Expert Committee on Food Additives (JECFA) is 0–1.4 mg/kg and the maximum level recommended in foodstuffs is 200 mg/kg [6]. PrG acts to prohibit platelet conglomeration and is a stimulant of platelet granule release, which limits adverse drug reactions that can result in hemorrhage. Unfortunately, PrG has to be given by injection to avoid hepatic first-pass metabolism. Our work focuses on screening for ingredients that display similar antiplatelet activity to PrG and could be given orally.

Molecular imprinting is a technique that is used to introduce molecular recognition sites for a specific analyte into a synthetic polymer, which can then be used for the selective separation or concentration of target molecules [7–9]. Molecular imprinted polymer (MIP) can be used for screening natural products for analogues with similar bioactivities in the hope of finding new drug candidates. This technique has been investigated in other research projects by several scholars [10,11].

The column switching consisted of an extraction module and an analysis module combined in a single automated process [12,13]. A column switching solid phase extraction (CS-SPE) method was used to screen Danshen. The prepared herbal sample was introduced into the SPE cartridge, which was packed with PrG–MIP [14], to pre-concentrate the analytes and remove the sample matrix. The analogues of PrG trapped on the MIP were then eluted with methanol–glacial acetic acid (9:1, v/v), which flows into the analysis module and was identified as protocatechuic acid (PcA) by liquid

* Corresponding author. Tel.: +86 591 83570397; fax: +86 591 22861027.
*E-mail address:* huj@fjtcm.edu.cn (J. Hu).
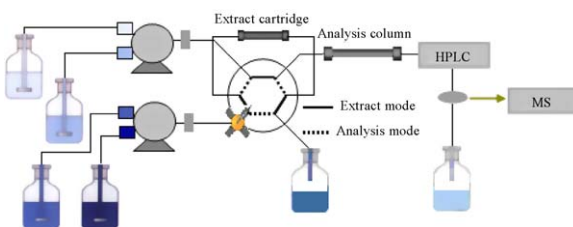
Fig. 1. Schematic diagram of on-line CS-SPE-LC/MS/MS device.

chromatography–tandem mass spectrometry (LC/MS/MS). The rat platelet aggregation induced by arachidonic acid (AA), PcA exhibited obvious activities.

2. Experimental

2.1. Apparatus

A model TU-1800 UV spectrometer was made by Pgeneral Instrument Co., Ltd. (Bejing, China). A model LC-10Atvp high performance liquid chromatography system was made by Shimadzu Corporation (Kyoto, Japan). The empty stainless steel cartridge (i.d. 4.6 mm × 50 mm) was made by Dalian Replete Science and Technology Co., Ltd (Dalian, China). One Diamonsil C_{18} column (i.d. 250 mm × 4.6 mm, 5 μm sizes, 100 A) was made by Dikma Technologies Inc. (Guangzhou, China). Cartridge filled with MIP and C_{18} column were used for coupling on-line with SPE separation and analysis driven by two binary gradient pumps and single six-way valve (Fig. 1). The solutions in all experiments were analyzed using an LC/MS/MS made by Waters Technologies Corp. (Milford, MA, USA). A separation module equipped with a model Alliance 2695 photodiode array detector was used for detection, along with a mass spectrometer equipped with an ESI probe and a model Quattro Micro™ tandem quadrupole analyzer. Data were collected using Masslynx 4.0. Morphological characteristics of the MIP and a non-imprinted polymer (NIP) were observed using a model XL30 ESEM-TMP scanning electron microscope made by Philips Electron Optics (Eindhoven, The Netherlands). A model NS3A-02 nanoscope IIIa atomic force microscope made by Veeco Instruments Inc. (New York, NY, USA) was used to study the ultrastructure. A model CAM-SIZER XT digital imaging particle size and shape analyzer was made by Retsch Technology GmbH (Haan, Germany).

2.2. Materials and chemicals

4-Vinyl pyridine (4-Vpy) and ethylene glycol dimethacrylate (EDMA) were purchased from Fluka Chemical Corp. (Buchs, Switzerland), and azobisisobutyronitrile (AIBN) was purchased from Sigma–Aldrich Corp. (Louis, MO, USA). Before use these chemicals were purified as follows: 4-Vpy was distilled under vacuum, AIBN was recrystallized from ethanol, and activated carbon was used to remove additives from EDMA. PrG was provided by FuJian MinDong Rejuvenation Pharmaceutical Co. Ltd. (Fuzhou, China). Propyl gallate injection was produced by Shandong Weifang Pharmaceutical Co. Ltd. (CH20050720, Weifang, China). Protocatechuic acid (PcA) reference material (99.21% purity) was purchased from the Nanjing TCM Institute of Chinese Materia (Nanjing, China).

Methanol and acetonitrile were HPLC grade purchased from Merck Group (Darmstadt, Germany). Glacial acetic acid, ethyl acetate, chloroform, and acetone were analytical grade purchased from Sinopharm Chemical Reagent Co. Ltd (Shanghai, China). Purified water (18.2 mΩ and TOC ≤50 ppb) used throughout the study was obtained using a Milli-Q® purification system (Bedford, MA, USA).

Danshen slice was produced by Anwei Haixin Chinese Herbal Slices Co. Ltd (Bozhou, China). Crushed Danshen powders (100 mashes) were extracted twice with 85% EtOH under reflux for 30 min. After being filtered, the filtrates combined and then concentrated to 1 g/mL of Danshen and stored in a refrigerator (2–8 °C). The stock solution (1 mL) was diluted in a 100 mL volumetric flask with acetonitrile to 0.01 g/mL. The sample solutions were filtered through a 0.45 μm membrane before being submitted to LC/MS/MS.

2.3. Animals

Male clean grade Wistar rats (200 ± 20 g, Slack Shanghai Laboratory Animal Co. Ltd, Shanghai, China) were used for the animal model experiment. The rats were housed in an environmentally controlled room at a temperature of 22 ± 1 °C, relative humidity 65–70%, air ventilation 12–18 times h, 12-h light/dark cycle of 150–300 lux, and food and water ad libitum. The animal studies were approved by the Fujian Institute of Traditional Chinese Medicine Animal Ethics Committee (Fuzhou, China). The experimental procedures followed the Guidelines for Animal Experimentation of Fujian University of Traditional Chinese Medicine (Fuzhou, China).

2.4. Preparation of the imprinted polymer

The mimic template (PrG, 94.4 mg, 0.46 mmol) was dissolved in 4.72 mL porogenous solvent (ethyl acetate) in a 10 mL tube fitted with a screw cap. The functional monomer (4-Vpy, 192 μL) was added and the mixture sonicated for 5 min. Then the cross-linking agent (EDMA, 2.0 mL) and the initiator (AIBN, 35.46 mg) were added, and the solution degassed with oxygen-free nitrogen for 5 min before sealing. The tube was then placed in a 60 °C water bath for 24 h to complete the polymerization. The MIP was then mechanically ground and sieved using acetone to achieve particle sizes within an appropriate size range for the evaluations. The particulates were dried at 60 °C for 24 h under vacuum and stored in desiccators before use. NIP was prepared in an identical manner to the MIP but without the template.

2.5. Preparation of the MIP cartridges

An aliquot of methanol (2 mL) was added to an empty stainless steel cartridge connected to a vacuum pump. The cartridge was then partially filled with MIP or NIP (0.4 g) and placed under vacuum for 30 s before adding further MIP or NIP, and this procedure was repeated until the cartridge was filled. The templates were then removed from the cartridge by washing with methanol–glacial acetic acid (9:1, v/v) at a flow rate of less than 0.5 mL/min.

2.6. Morphological characterization of polymer

The morphological characteristics of MIP and NIP were observed with a scanning electron microscope (SEM) [15]. A thin slice of MIP or NIP was placed on a 300-mesh Au grid coated with a lacy carbon film and exposed to a beam of electrons. Any blemishes encountered on the surface altered the fraction of electrons diffracted and this was used to identify holes. Atomic force microscopy (AFM) can be used to probe material ultrastructure, and in this project it was used to measure the sizes of holes on the MIP or NIP [16]. A particle size and shape analyzer (PSSA) was used to accurately characterize particle size and shape by image analysis. This provides a better understanding of how the size and shape of polymer particles can affect the various properties of solid phase extraction [17].

2.7. Performance evaluation of the polymers

The binding efficiency of the polymer toward PrG was assessed in the batch rebinding experiments. Briefly, 30 mg of each polymer PrG–MIP and NIP were placed in an eppendorf tube containing a known concentration of PrG (12.6 μg/mL) in 1 mL of porogenous solvent, and the mixture was then mechanically shaken at room temperature for 4 h. Subsequently, the polymers were centrifuged, and the concentration of the substrate remaining in the solution was determined by UV absorption spectrum at 296 nm to calculate the binding efficiency of polymer.

The polymer particles were packed into a MIP cartridge. Acetonitrile was used as the eluent with a flow rate of 0.2 mL/min. PrG, gallic acid, and ferulic acid were applied at a range of concentrations from 100 μg/mL to 300 μg/mL. HPLC was used to determine the retention times that the gallic acid, ferulic acid and PrG were adsorbed onto the MIP and NIP columns in order to calculate the capacity factor (k') and imprinted factor (IF) [18].

2.8. On-line separation and identification of the herbal extract

An aliquot of the Danshen stock solution (100 μL) was introduced into the MIP cartridge. During the extraction, acetonitrile was used as the mobile phase at a flow rate of 0.2 mL/min. The compounds adsorbed on the MIP cartridge were then eluted using methanol–glacial acetic acid (9:1, v/v). The six-way value was then switched to the analysis mode, and any analogues of PrG remaining in the MIP cartridge were identified by LC/MS/MS. These experimental protocols were used to determine whether a compound imprinted on the MIP.

2.9. Inhibition of rat platelet aggregation by PcA in vivo

Eighty Wistar rats were randomly divided into eight groups of 10 rats each, which included the normal control or acute blood stasis model groups [19]. The rats in all groups were intragastrically administered or injected with various drugs through the tail vein for 3 days. On the first day, animals in the positive control groups or drug group received a single injection of 30 mg/kg PrG, aspirin at 10 mg/kg or 10 mg/kg PcA intragastric administration and those in the normal control group received the same volume of a saline solution. On the second day, drug administration to the model group of rats occurred after they had received two intraperitoneal injections, which were four hours apart, of 0.1% epinephrine hydrochloride (0.8 mL/kg). There was a 2-h interval between the two injections of epinephrine hydrochloride, during which time the rats were forced to swim in ice water for 5 min to set up acute blood stasis. Sodium pentobarbital (30 mg/kg) was used to anesthetize the rats after the last injection on the third day and fasting blood samples were collected from their abdominal aorta within 15 min.

Platelet aggregation was determined by turbidimetry [20]. Blood (9.0 mL) was collected into a plastic syringe containing 1.0 mL of 3.8% sodium citrate. The blood was then transferred into a test tube, the tube capped and mixed by gentle inversion. The volume of blood collected can be adjusted depending on the number of tests to be performed, but the blood:anticoagulant ratio must be maintained at 9:1. The anticoagulated blood was centrifuged ($100 \times g$, 10 min) and the platelet rich plasma (PRP) carefully removed using a plastic pipette while avoiding red cell contamination. The PRP was transferred to a plastic container, which was capped and stored at room temperature. The remaining blood sample was centrifuged again ($1500 \times g$, 20 min) and the platelet poor plasma (PPP) transferred to a plastic container with a plastic pipette, and the container capped and stored at room temperature. A platelet count was performed and the PRP adjusted to $200,000 \pm 50,000$ per μL platelets

with the PPP as required. An aliquot of PRP was transferred to a small glass cuvette, which was maintained at body temperature (37 °C). This was constantly stirred for 5 min and an aggregation agent added to clump the platelets together and measure their aggregation ratio.

3. Results and discussion

3.1. Optimization of polymerization conditions

MIP with a high degree of cross-linking is hard and macroporous with a large loading capacity. The effect of imprinted polymers is also strongly dependent on polymerization conditions such as temperature and time as well as the concentrations of the reactants. In this research, a thermopolymerization procedure was employed at 60 °C for 24 h to ensure the formation of highly cross-linked MIP [21]. We investigated how the monomer, cross-linker, initiator and porogenous solvent affected polymerization under different conditions. Because of its polarity, PrG is not soluble in common MIP preparation solvents such as acetonitrile, chloroform, dichloromethane and toluene. It is soluble in ethyl acetate and acetone and in some strong polar or universal solvents such as N,N-dimethylformamide (DMF), tetrahydrofuran (THF) or dimethyl sulfoxide (DMSO).

Methacrylic acid (MAA), acrylic acid (AA), acrylic amide (AM), and 4-Vpy are the most common monomers used in MIP production. In preliminary experiments, the above four were tested for use as the monomer to prepare polymers, P_{MAA}, P_{AA}, P_{AM}, P_{4-Vpy}, at 60 °C for 24 h. P_{MAA} and P_{AA} synthesized in ethyl acetate, were loose, soft or crisp; whereas P_{AM} and P_{4-Vpy} were opaque and hard. During the decantation step, the amount of P_{MAA} and P_{AA} particles lost was considerably more than that of P_{AM} or P_{4-Vpy}, which may have resulted from the greater swelling of P_{MAA} and P_{AA}. 4-Vpy was preferred over AM because it had beneficial electrostatic interactions between the acidic and basic functions of the template molecule and the monomer.

When a strong polar solvent, such as DMF or THF, was used as the porogenous solvent and TRIM was used as the cross-linking agent, it led to a polymer structure that lacked rigidity. A more suitable hardness could be achieved using a medium polar or universal solvent, such as ethyl acetate, acetone, or DMSO. If the PrG was dissolved in acetone or DMSO, the load capacity of the synthesized MIP was smaller.

For this research, ethyl acetate was used as the porogenous solvent, EDMA was used as the cross-linking agent, and 4-Vpy was used as the functional monomer. Under these conditions, the synthetic MIP had excellent hardness, a high degree of cross-linking, and a large binding capacity. The effect of the amount of template on the MIP characteristics was investigated using various proportions of PrG. At low proportions of template, the extraction ability of the resulting polymers was low, and increasing the amount of template molecule increased the efficiency of the prepared MIP. However, the polymer obtained appeared to be nonspecific. The optimal mole ratio of template:functional monomer:cross-linking agent was 1:4:20, and the best ratio of porogenous solvent to the monomer was 3:4 (v/v).

These rebinding experiments were repeated three times for both the imprinted and nonimprinted polymers using different concentrations of PrG (0.3–1 mmol). The NIP was used as a control to determine the nonspecific binding. The amount of PrG bound to the polymers was calculated by subtracting the amount of free substrate from the initial absorbance as $((A_T - A_{MIP})/A_T) \times 100\%$. To compare the imprinting effect, we define the specific adsorption values as $\Delta A = A_{NIP} - A_{MIP}$, where A_{MIP} and A_{NIP} are the absorbance values of bound template on the MIP and NIP, respectively. The

Table 1
The optimization of the synthesis conditions of the imprinted polymer.

Polymer	Templat	Porogenous solvent				Crosslinking agent		Binding efficiency				Mole ratio[a]	Remarks
	PrG mg	DMF ml	Ethyl acetate ml	Acetone ml	DMSO ml	EDMA ml	TRIM ml	A_T	A_{NIP}	A_{MIP}	$\frac{A_T - A_{MIP}}{A_T} \times 100\%$		
MIP1	70.7	1.87				1.26		0.529	0.483	0.472	10.78	1:4:20	Crisp
MIP2	70.7		1.87			1.26		0.529	0.421	0.253	52.17	1:4:20	Optimization[b]
MIP3	70.7			1.87		1.26		0.529	0.512	0.509	3.78	1:4:20	Better rigidity
MIP4	70.7				1.87	1.26		0.529	0.476	0.425	19.66	1:4:20	Better rigidity
MIP5	212.2	1.87					1.92	0.529	0.499	0.490	7.37	1:4:6	Loose soft
MIP6	212.2		1.87				1.92	0.529	0.511	0.502	5.10	1:4:6	Loose soft
MIP7	212.2			1.87			1.92	0.529	0.483	0.477	9.83	1:4:6	Spongy
MIP8	212.2				1.87		1.92	0.529	0.466	0.463	12.48	1:4:6	Loose soft

[a] 4-Vpy as functional monomer, template:functional monomer:cross-linking agent.
[b] Better rigidity and larger load capacity.

amount of PrG bound to the optimum polymers, MIP2 and NIP2, was 17.5 μg/g and 5.2 μg/g, respectively. The imprinting efficiency on MIP was obviously higher than that on NIP. The optimization conditions for the synthesis of the polymer are listed in Table 1.

3.2. Morphological characterization

The surfaces of both MIP and NIP particles were studied by SEM. Compared with NIP, MIP displayed a rougher and more porous surface (Fig. 2). The sectional profile of the polymer was obtained from AFM images. The average holes on NIP were 1.462 μm in diameter with a 1.092 μm horizontal distance, a 27.044 μm vertical distance, and are at an angle of 1.419°. The cavities remaining after the removal of the MIP template were 5.724 μm in diameter. The corresponding cross-sectional data for MIP showed a horizontal distance of 3.343 μm, a vertical distance of 178.04 μm, and an angle of 3.049° (Fig. 3). The cavities were larger on the MIP surface than the ones on the NIP.

The MIP was crushed, mechanically ground, sieved (400 mesh), and dispersed in acetone to deliver polymer particle sizes in the range of 20–60 μm to fill the cartridge. The size and shape of the polymer particles largely affected the column pressure. The ideal particle is approximately 30 μm with a nearly spherical shape (0.95–1.0 sphericity degree). PSSA results showed the PrG MIP particles ranged from 20 to 40 μm in diameter and had an average sphericity degree of 0.869 (Fig. 4). This technique was successfully applied to accurately control the size distribution and shape of the MIP filler.

3.3. Selectivity and recognition performance of PrG MIP

The goal of this study was to prepare a polymer that in the solid phase would retain and resolve the antiplatelet aggregation ingredients from the crude extract of Danshen. The substrate selectivity of the PrG–MIP and NIP was studied with PrG, gallic acid and ferulic acid (200 μg/mL in acetonitrile). All three compounds are inhibitors of platelet aggregation, and their structures are shown in Fig. 5. Their capacity factors (k') and imprinted factors (IF) were utilized to evaluate the molecular selectivity of each polymer.

The choice of the type of eluent is very critical for the binding and recognition of the properties of the MIP. A polar solvent weakens the noncovalent specific interactions between the template and the polymer matrix, and it reduces the affinity and selectivity of the MIP for its template. The cartridge was packed with MIP and NIP (0.35–0.40 g) to prepare the MIP–SPE column. HPLC was used to determine the retention time for the adsorption of gallic acid, ferulic acid and PrG on the column. Using acetonitrile as the eluent at a 0.2 mL/min flow rate, the retention time for PrG was 36 min with the MIP cartridge while changing the cartridge filler to NIP reduced the retention time by only 5 min. Gallic acid and PrG have exactly the same nuclear parent structure (benzoic acid), and the PrG–MIP exhibited a high affinity for gallic acid and its retention time was 45 min. In contrast, the structure of ferulic acid is reasonably different from PrG with regard to its nuclear parent (cinnamic acid) and the number and position of substituent groups attached to the benzene ring. Consequently, the retention time for ferulic acid was only 11 min with the MIP cartridge.

In Table 2, k' values and IF values of the analytes injected on the columns packed with imprinted polymer are listed. The PrG–MIP exhibited a high affinity for PrG itself and its structural analogue, gallic acid. However, it did not retain other structurally unrelated compounds, such as ferulic acid. In addition, all of the examined molecules were retained longer on the MIP than on the NIP, suggesting that the adsorbents of larger imprinted effects could be
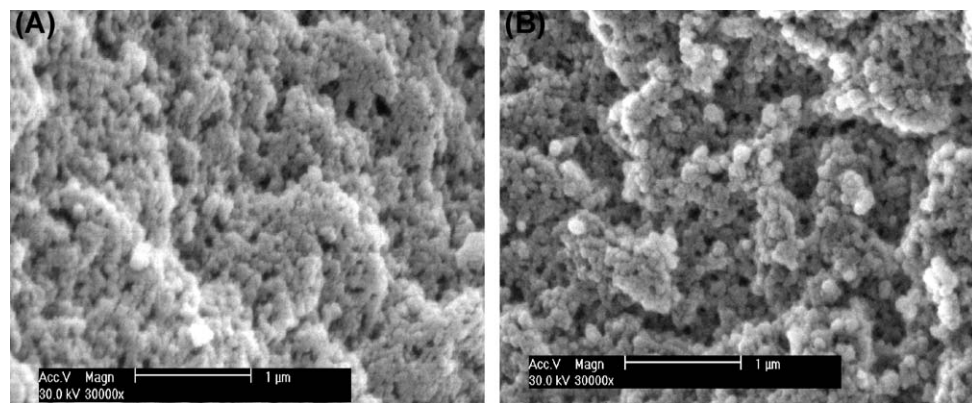


Fig. 2. SEM micrographs ×30,000: (A) NIP and (B) MIP.
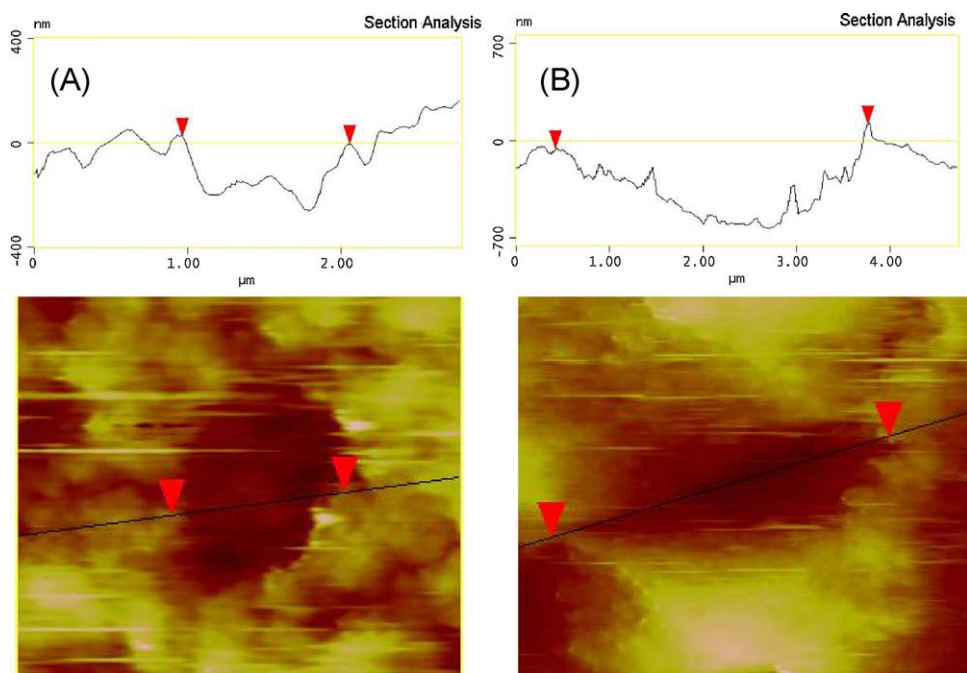
**Fig. 3.** AFM images and section analysis data: (A) NIP and (B) MIP.
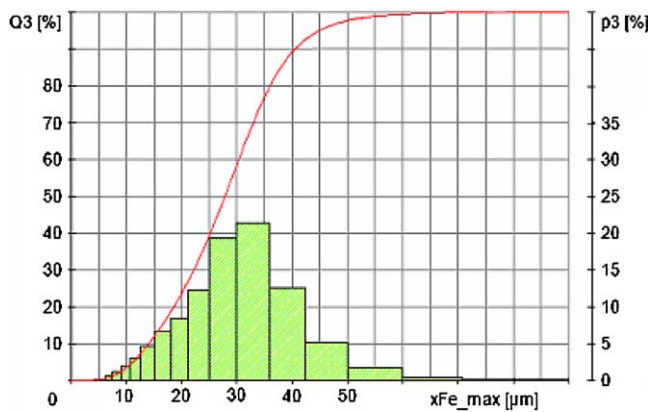
Fig. 4. MIP particle sizes distribute histogram.

Table 2
Retention of substrates on imprinted polymer cartridge.

Compounds	Retention					
	Retention time (min)		Dead time (min)	Capacity factor	Imprinted factor	
	$t_{R, NIP}$	$t_{R, MIP}$	t_0	K_{NIP}'	K_{MIP}'	IF
PrG	5	36	2.0	1.5	17	11.33
Gallic acid	15	45		6.5	21.5	3.31
Ferulic acid	7.5	11		2.75	4.5	1.64

3.4. Separation and identification of the PrG analogues in Danshen extract

In Fig. 6, an aliquot of the prepared Danshen stock solution with an injection sample volume of 20 μL was analyzed by HPLC at 260 nm using a mobile phase of methanol:water:acetic acid (15:84:1, v/v) at a flow rate of 1.0 mL/min (Fig. 6A). Another aliquot of the stock solution (100 μL) was introduced into the MIP–SPE extract cartridge with a mobile phase of acetonitrile at 0.2 mL/min for more than 40 min. The compounds adsorbed on the MIP were then eluted using methanol–glacial acetic acid (9:1, v/v) at 0.2 mL/min for 5 min. At the same time, the six-way value was switched to analysis mode, and the analogue of PrG remaining in

achieved by preparation of imprinted polymers. The k' was calculated from the equation $k' = (t_R - t_0)/t_0$, where t_R is the retention time for a sample and t_0 is the time to elute the void marker acetone [22]. IF was defined as the ratio of the k' value of one molecule on a MIP column to that on its corresponding NIP calculated as follows: IF $= k_{MIP}'/k_{NIP}'$. These compounds were in the following order: $IF_{PrG} > IF_{gallic\ acid} > IF_{ferulic\ acid}$.


PrG   Gallic acid   Ferulic acid

**Fig. 5.** Structures of three compounds of phenolic acids.
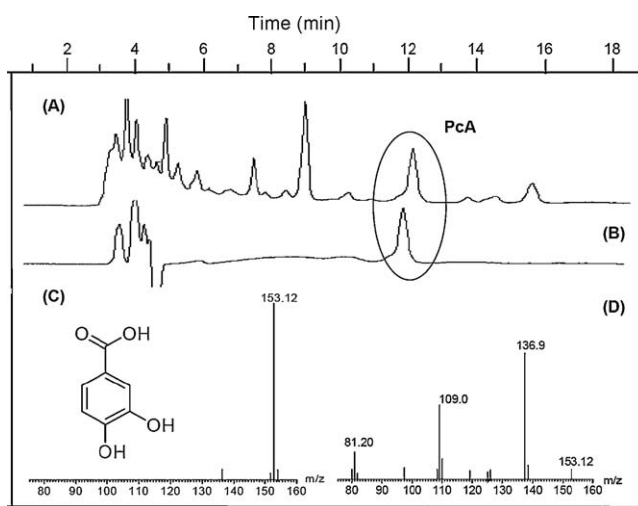
Fig. 6. LC and MS graphs: (A) chromatogram of *Radix Salviae Miltiorrhizae* sample solution, (B) chromatogram of remaining component after MIP-SPE; (C) full scan mass spectra of PcA; (D) daughter scan mass spectra of PcA.

the MIP cartridge was introduced into the LC system. The mobile phase was changed to methanol:water:acetic acid (15:84:1, v/v) at a flow rate of 1.0 mL/min, and the fractions corresponding to the chromatographic peaks were collected (Fig. 6B). They were further identified by MS/MS as the peaks corresponding to the PrG analogue. The MS analysis is shown in Fig. 6C; a deprotonated molecular ion $[M-H]^-$ of m/z 153 was observed. To identify this component, the molecular ion at m/z 153 was selected for a daughter ion scan using collision energy of 30 eV. The sharp signals at m/z 137, 109, and 81 matched the fragmentation pattern of PcA (Fig. 6D) [23].

PcA was found to have a stronger binding capacity to specific sites, and it resided for a longer retention time on the MIP (44 min) than PrG (36 min) or on the NIP (9 min). The affinity for PcA was higher shown by its calculated IF value of 5.3. Their retention characteristics are compared in Fig. 7A and B. To avoid a false positive result, it is necessary to utilize a pharmacology experiment to confirm the compound potency.

3.5. Aggregation test of rat platelet in vivo

Platelet aggregometry is used in routine platelet aggregation studies for evaluating qualitative platelet disorders. It measures the change of light transmission in PRP due to the aggregation of platelets in response to various agonists. PRP is usually cloudy and becomes clearer as platelets clump in response to reagents such as adenosine diphosphate (ADP), arachidonic acid (AA), epinephrine, and collagen. The results are typically reported as percent
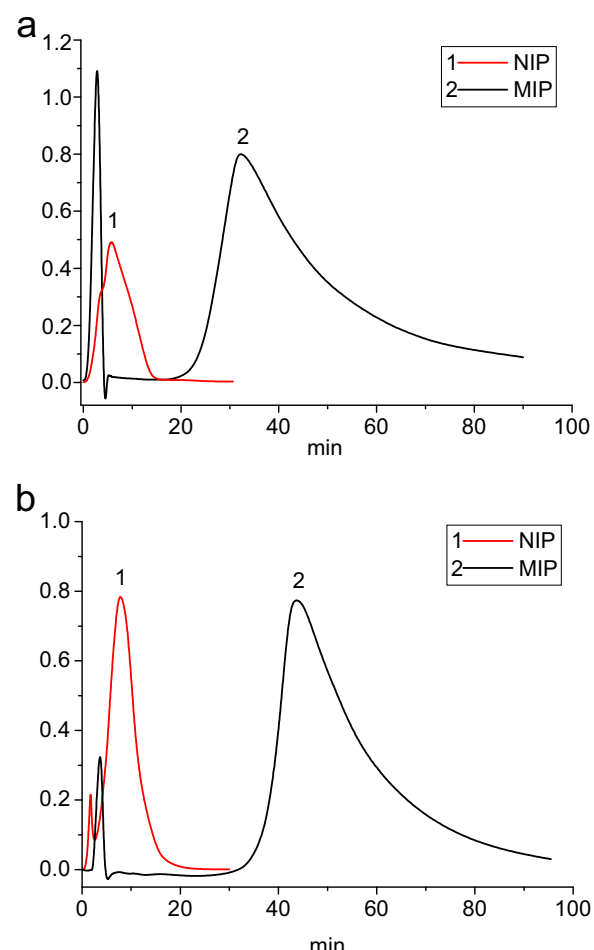

Fig. 7. Retention behavior of PrG (A) and PcA (B) in NIP and MIP cartridge.

aggregation, the 5-min aggregation ratio ($R_{5\,\mathrm{min}}$) and the maximum aggregation ratio (R_{max}).

The rats of normal control and acute blood stasis model groups were tested for anticoagulation activities by a bioassay against AA induced aggregation of platelets in vivo. The statistical analysis of the data confirmed a sharp decline in the maximum aggregation ratio of platelets in rats intragastrically treated with 10 mg/kg of PcA. In comparison with normal control and pharmacological model groups, there were significant differences, but there were no differences in comparison with the positive control (Table 3). The results show that PcA inhibits platelet aggregation and possesses a similar effect to PrG.

Table 3
PcA inhibits on rats platelet aggregation-induced by AA.

Groups	Platelet aggaregation ratio (%)			
	Normal rats		Model rats	
	$R_{(5\,\mathrm{min})}$	R_{max}	$R_{(5\,\mathrm{min})}$	R_{max}
Control	45.43 ± 2.57	47.05 ± 1.65	51.8 ± 3.54	53.77 ± 2.81
Asprin	35.68 ± 3.95▲	40.75 ± 3.65▲	28.83 ± 7.87**	29.75 ± 6.89**
P. Radix 801	11.92 ± 5.06▲▲	0.27 ± 1.43▲▲	16.11 ± 8.12**	30.68 ± 4.42**
PcA	6.96 ± 4.72▲▲	5.03 ± 5.25▲▲	4.78 ± 3.56**	5.58 ± 4.52**

Values are expressed as mean ± SEM, $n = 10$.
▲ $P \leq 0.05$ vs. normal control.
▲▲ $P \leq 0.01$ vs. normal control.
* $P \leq 0.05$ vs. model control.
** $P \leq 0.01$ vs. model control.

Similar to aspirin, PrG is a potent inhibitor of cycloxygenase (COX) and blocks the metabolism of AA to Thromboxane A2 (TXA2) through the COX pathway, which inhibits platelet aggregation [24]. In this paper, compared with two positive controls, aspirin and PrG, PcA was detected as an inhibitor of AA-induced platelet aggregation. H.S. Yun-Choi et al. have also isolated PcA from a different herbal medicine, and its antiplatelet adhesion action was described [25].

PrG is one compound of a class of phenolic acids whose molecules contain benzoic acid nuclear parent. Liu et al. studied nineteen phenolic acid compounds and their structure–activity relationship with anticoagulation activities. They concluded that many phenolic acids exhibit obvious activity. The monohydroxybenzoic acid was the active site of this type of molecule, and o-3-phenolic acids manifested stronger activities than those of o-2-phenolic acids [26]. PcA is an o-2-phenolic acid was identified by PrG–MIP from Danshen. PcA and PrG have the same structural nuclear parent, but differ in the number and position of their substituent groups attached to the benzene ring.

The phytochemical analysis of Danshen has revealed the presence of tanshinones and depside acids [27]. Among these, many compounds may have the inhibitory effect on platelets. Some studies have shown that salvianolic acid B and tanshinone IIA inhibit primary hemostasis and many pathways associated with platelet activation and aggregation [28,29]. The present work showed that PcA could inhibit platelet aggregation induced by AA. This may be one of the mechanisms for the prevention of atherosclerosis because antiplatelet function contributes to cardiovascular disease. These results illustrate that various components in Danshen can inhibit platelet aggregation through different activation pathways, and thus, there is likely not one simple explanation for its biological effects.

4. Conclusion

In this study, an efficient method was developed for screening the target analogues of PrG–MIP in Danshen by using CS–SPE–HPLC–MS–MS. A component was successfully identified based on retention time and MS spectra when compared with the authentic compound and the data in the literature. The pharmacology experiment confirmed that it is effective against platelet aggregation. This method is a straightforward and convenient method that requires only a very simple crude extract preparation procedure; thus, it would be a valuable tool for screening bioactive substances in other herbal medicines.

References

[1] X.D. Li, X.J. Xu, J. Hu, Discovery of inhibitor s for gp IIb/IIIa receptor from Chinese herbal drugs database by pharmacophor e-based virtual searching, Acta Phys. Chim. Sin. 24 (2008) 307–312.

[2] J.V. Levy, Z.f. Xie, Effect of three Chinese herbal medicines (*Ligustrazine, Chrysanthemum indicum, Salviae miltiorrhizae*) on PAF and ADP-induced platelet aggregation in vitro, Prostaglandins 35 (1988) 842–843.

[3] X.F. Lin, Progress in pharmacological research of Chinese medicine *Radix Salviae Miltiorrhizae*, Journal of Tianjin Medical University 10 (2004) 60–62.

[4] Y.R. Jiang, H.J. Yin, K.J. Chen, *Radix paeoniae* 801 research, Chin. J. Int. Trad. West Med. 24 (2004) 760–763.

[5] J.W. Daniel, Metabolic aspects of antioxidants and preservatives, Xenobiotica 16 (1986) 1073–1078.

[6] M.D. Morales, M.C. Gonzaĭlez, A.J. Reviejo, J.M. Pingarroĭn, A composite amperometric tyrosinase biosensor for the determination of the additive propyl gallate in foodstuffs, Microchim. Acta 80 (2005) 71–78.

[7] S.E. Moring, O.S. Wong, J.F. Stobaugh, Target specific sample preparation from aqueous extracts with molecular imprinted polymers, J. Pharm. Biomed. Anal. 27 (2002) 719–728.

[8] H. Sanbe, J. Haginaka, Uniformly sized molecularly imprinted polymers for bisphenol A and β-estradiol: retention and molecular recognition properties in hydro-organic mobile phases, J. Pharm. Biomed. Anal. 30 (2003) 1835–1844.

[9] S.G. Ge, M. Yan, X.L. Cheng, C.C. Zhang, J.H. Yu, P.N. Zhao, W.Q. Gao, Novel On-line molecular imprinted solid-phase extraction flow-injection fluorescence sensor for determination of florfenicol in animal tissues, J. Pharm. Biomed. Anal. 52 (2010) 615–619.

[10] X.J. Xu, L.L. Zhu, L.R. Chen, Separation and screening of compounds of biological origin using molecularly imprinted polymers, J. Chromatogr. B 804 (2004) 61–69.

[11] N.A. O'Connor, D.A. Paisner, D. Huryn, K.J. Shea, Screening of 5-HT1A receptor antagonists using molecularly imprinted polymers, J. Am. Chem. Soc. 129 (2007) 1680–1689.

[12] Y.H. Cheng, J. Hu, HPLC determination of an illicit additive ribavirin in anti-viral oral liquor with column switching, PTCA 44 (2008) 545–547.

[13] E. Anastasios, B. Helen, S. Antoniou, T.J. Despina, Determination of multi-class pesticides in wines by solid-phase extraction and liquid chromatography–tandem mass spectrometry, J. Chromatogr. A 1216 (2009) 5856–5867.

[14] O. Brüggemann, A. Visnjevski, R. Burch, P. Patel, Selective extraction of antioxidants with molecularly imprinted polymers, Anal. Chim. Acta 504 (2004) 81–88.

[15] H.F. Wang, Y. He, T.R. Ji, X.P. Yan, Surface molecular imprinting on Mn-Doped ZnS quantum dots for room-temperature phosphorescence optosensing of pentachlorophenol in water, Anal. Chem. 81 (2009) 1615–1621.

[16] J. Michael, S. Romana, S. Christian, H. Oliver, L. Peter, B. Dieter, P. Guntram, L.D. Franz, Sensing picornaviruses using molecular imprinting techniques on a quartz crystal microbalance, Anal. Chem. 81 (2009) 5320–5326.

[17] S.A. Thyabat, N.J. Miles, An improved estimation of size distribution from particle profile measurements, Powder Technol. 166 (2006) 152–160.

[18] A. Zande, P. Findlay, T. Renne, B. Sellergren, Analysis of nicotine and its oxidation products in nicotine chewing gum by a molecularly imprinted solid phase extraction, Anal. Chem. 70 (1998) 3304–3314.

[19] Y.K. Li, R.M. Jin, Q.M. Wang, Experimental Methodology of TCM Pharmacology, Shanghai Sci. Technol. Press, 2006, p717.

[20] T. Kazuo, J.K. Yu, K. Masahiko, Assessment of antithrombotic agents using platelet aggregation test, Curr. Ther. Res. 61 (2000) 798–800.

[21] B. Sellergren (Ed.), Man-made Mimics of Antibodies and Their Applications in Analytical Chemistry, Elsevier, Amsterdam, 2001, p. p. 40.

[22] J.C. Xie, L.L. Zhu, X.J. Xu, Affinitive separation and on-line identification of anti-tumor components from *Peganum nigellastrum* by coupling a chromatographic column of target analogue imprinted polymer with mass spectrometry, Anal. Chem. 74 (2002) 2352–2360.

[23] S. Shengmin, L. Karen, S.J. Woo, Antioxidative phenolic compounds isolated from almond skins (*Prunus amygdalus* Batsch), J. Agric. Food Chem. 50 (2002) 2459–2463.

[24] Q. Chen, J.D. Huang, H.J. Yin, K.J. Chen, T. Osac, The applications of affinity biosensors: IAsys biosensor and quartz crystal microbalance to the study on interaction between *Paeoniae radix* 801 and endothelin-1, Sens. Actuators B 115 (2006) 116–122.

[25] H.S. Yun-Choi, J.H. Kim, J.R. Lee, Potential inhibitors of platelet aggregation from plant sources III, J. Nat. Prod. 50 (1987) 1059–1064.

[26] D.L. Liu, G.R. Ding, N. Chen, X. Wang, N.L. Wang, J.X. Wang, An inquiry of activities of phenolic acids against the aggregation of rabbit platelet in vitro, J. Shenyang Pharma. Univ. 15 (1998) 25–28.

[27] Y.G. Li, L. Song, M. Liu, Z.B. Hu, Z.T. Wang, Advancement in analysis of *Salviae miltiorrhizae Radix* et *Rhizoma* (Danshen), J. Chromatogr. A 1216 (2009) 1941–1953.

[28] M. Zhou, X.J. Li, X.H. Li, Y.H. Xu, M. Yang, Effects of tanshinone on platelets and coagulation in immune vasculitis, Chin. J. Thromb. Hem. 15 (2009) 8–12.

[29] M.K. Tang, D.C. Ren, J.T. Zhang, G.H. Du, Effect of salvianolic acids from *Radix Salviae miltiorrhizae* on regional cerebral blood flow and platelet aggregation in rats, Phytomedicine 9 (2002) 405–409.

NMR-based metabolic profiling and differentiation of ginseng roots according to cultivation ages

Seung-Ok Yang [a,1], Yoo-Soo Shin [b,1], Sun-Hee Hyun [a], Sayeon Cho [a], Kyong-Hwan Bang [b], Dongho Lee [c], Seung Phill Choi [d], Hyung-Kyoon Choi [a,*]

[a] College of Pharmacy (WCU), Chung-Ang University, Seoul 156-756, Republic of Korea
[b] National Institute of Horticultural and Herbal Science, RDA, Suwon 441-857, Republic of Korea
[c] Division of Biotechnology, College of Life Sciences and Biotechnology, Korea University, Seoul 136-713, Republic of Korea
[d] Department of Chemical and Biological Engineering, College of Engineering, Korea University, Seoul 136-713, Republic of Korea

ARTICLE INFO

ABSTRACT

Ginseng is an important herbal resource worldwide, and the adulteration or falsification of cultivation age has been a serious problem in the commercial market. In this study, ginseng (*Panax ginseng*) roots, which were cultivated for 2–6 years under GAP standard guidelines, were analyzed by NMR-based metabolomic techniques using two solvents. At first, ginseng root samples were extracted with 50% methanol, and analyzed by NMR with D_2O as the NMR dissolution solvent. The 2-, 3-, 4-, and 5/6-year-old ginseng root samples were separated in PLS-DA-derived score plots. However, 5- and 6-year-old ginseng roots were not separated by the solvent system. Therefore, various solvents were tested to differentiate the 5- and 6-year-old ginseng root samples, and 100% methanol-d_4 was chosen as the direct extraction and NMR dissolution solvent. In the PLS model using data from the 100% methanol-d_4 solvent, 5- and 6-year-old ginseng roots were clearly separated, and the model was validated using internal and external data sets. The obtained RMSEE and RMSEP values suggested that the PLS model has strong predictability for discriminating the age of 5- and 6-years-old ginseng roots. The present study suggests that the age of ginseng could be successfully predicted using two solvents, and the developed method in this study can be used as a standard protocol for discriminating and predicting the ages of ginseng root samples.

© 2011 Elsevier B.V. All rights reserved.

1. Introduction

The roots of *Panax ginseng* C.A.Meyer (Araliaceae) have been used as a traditional medicinal herb worldwide. *P. ginseng* roots have been reported to include amino acids, fatty acids, carbohydrates, alkaloids, triterpene saponins, polysaccharides, sesquiterpenes, polyacetlyenes, peptidoglycans, minor elements, vitamins, and phenolic compounds [1,2]. The major biochemical and pharmacological activities of *P. ginseng* have been attributed to triterpene saponins such as ginsenosides [3], and it was reported that the content of ginsenosides in root and root-hair increases with increasing age of *P. ginseng* from one to five years [4]. *P. ginseng* roots exhibit a wide variety of pharmacological effects, such as cardiovascular control of blood pressure [5], increasing learning [6], increasing cognitive performance [7], antiaging [8], antioxidative [9], anticancer [10,11], and immunestimulating activities [12].

In recent years, the adulteration of ginseng cultivation age has been a major problem in ginseng commercial markets, because the 5- and 6-year-old ginseng root price is 30 and 60% higher than that of 4-year-old ginseng root [13], which has encouraged adulteration or falsification practices. However, the differentiation of ginseng according to cultivation age is mainly performed by visual inspection, such as morphological characteristics of the head part of ginseng and the number of branched roots. Therefore such differentiation has been rather subjective and relies on a few experts in the field. Nowadays, metabolomics techniques combining spectrometric methods and multivariate statistical analysis such as principal component analysis (PCA), partial least squares discriminant analysis (PLS-DA), hierarchical cluster analysis (HCA), and partial least squares projections to latent structures (PLS) [14]. Those multivariate statistical analysis techniques coupled with NMR analysis using various extraction protocols were used for metabolic profiling and characterization of various types of plants, foods, and tissues [15–18].

There are a few previous reports regarding fingerprinting or metabolic profiling of ginseng by various analytical methods, such as nuclear magnetic resonance spectroscopy (NMR), 2D *J*-resolved NMR, UPLC-qTOF-MS, and GCxGC-TOF-MS [19–24]. However, there

are no reports regarding the metabolic differentiation and prediction of cultivation age using ginseng samples cultivated under standardized protocols or guidelines. Most of the previous fingerprinting analysis or metabolic profiling studies of ginseng was performed using ginseng roots purchased or obtained from commercial markets [20,21,24,25]. Thus, metabolic profiling and development of a cultivation age prediction model for ginseng cultivated under standard conditions is very crucial for detecting and preventing adulteration or falsification. In this study, we cultivated ginseng root samples in a restricted and controlled area according to standardized cultivation protocols, and then the ginseng samples were analyzed by two-dimensional NMR-based metabolomics techniques using various solvents to develop a differentiation method for ginseng cultivation age.

2. Experimental

2.1. Solvents and chemicals

First-grade methanol, D_2O [99.9%, containing 0.05% 3-(trimethylsilyl)-propionic-2,2,3,3-d_4 acid sodium salt (TSP) as an internal standard], acetone-d_6 [99.9%, containing 0.1% (v/v) tetramethylsilane (TMS)], acetonitrile-d_3 [99.8%, containing 0.05% (v/v) TMS], pyridine-d_5 [99.5%, containing 0.03% (v/v) TMS], and DMSO–d_6 [99.9%, containing 1% (v/v) TMS] were purchased from Sigma (St. Louis, MO). Methanol-d_4 [99.8%], and methanol-d_4 [99.8%, containing 0.05% (v/v) TMS] were obtained from Cambridge Isotope Laboratories (Andover, MA) and NaOD was purchased from Cortec (Paris, France).

2.2. Sample preparation

P. ginseng roots were cultivated in the field of National Institute of Crop Science (Suwon, Republic of Korea) located in latitude 37°15′N, longitude 127°00′E, altitude 24 m, according to the protocol of 'ginseng GAP standard cultivation guide' [26] developed by the Rural Development Administration, Republic of Korea. Two-, three-, four-, five-, and six-year-old ginseng roots were harvested in 2006. Harvested P. ginseng root samples were washed with tap water and then the ginseng root hair (fine root tails) was discarded from the body; only the body parts were prepared for NMR analysis. All parts of the 2-year-old ginseng samples were used for the experiment, because there was no difference between the ginseng root body and hair due to their small size. Voucher specimens were deposited at CAUG (20070521-200705120) at the College of Pharmacy, Chung-Ang University, Republic of Korea. To investigate the individual variability of ginseng samples, 20 different root samples per age of ginseng root were individually freeze-dried (DRC-1000, FDU-2100, EYELA, Tokyo, Japan), ground to a fine powder in a pestle and mortar, and then stored at −70 °C until analysis.

2.3. NMR measurement

For NMR analysis, 100 mg of ground ginseng root sample were transferred into a centrifuge tube. Five milliliters of 50% methanol (water:methanol = 50:50,v/v) were added to the ginseng root samples in test tubes, vortexed for 1 min and sonicated for 1 min, and then the materials were centrifuged at $500 \times g$ for 10 min. The supernatants were transferred separately into a 50-mL round-bottomed flask to dry in a rotary vacuum evaporator. The extraction procedure was repeated twice.

As a buffering agent, KH_2PO_4 was added to D_2O to final concentration of 0.1 M and the pH of the D_2O was adjusted to 6.0 by the addition of 1 N NaOD solution. One milliliter of pH-adjusted D_2O solution was added to the 50-mL round-bottomed flask to

dissolve the dried aqueous extract. The dissolved solutions were transferred to NMR tubes (Norell, Landisville, NJ) for NMR measurements. To select the solvent system for differentiation of 5- and 6-year-old ginseng, various NMR solvent systems were used. For 50% MeOD NMR solvent extraction, 20 mg of 5- and 6-year-old ginseng root samples were transferred into microtubes (Axygen, Inc., MCT-175-C, CA). Three hundred and thirty microliters of KH_2PO_4 buffer in D_2O (with 0.05% TSP) and 330 μL of methanol-d_4 were added to the tube, vortexed for 1 min and sonicated for 15 min. The tubes were centrifuged at $14,000 \times g$ for 10 min. The extract was transferred into microtubes then centrifuged at $14,000 \times g$ for 3 min. The supernatants were transferred to a 5-mm NMR tube. To select suitable NMR solvent among acetone-d_6, acetonitrile-d_3, pyridine-d_5, D_2O-d_4, DMSO-d_6, and 100% methanol-d_4 for direct extraction and NMR measurement, 10 mg of 5- and 6-year-old ginseng root samples were transferred into microtubes. Then 0.65 mL of each of the 6 solvents was added to the ginseng root samples in the microtube, which were then vortexed and sonicated for 1 min. The samples were centrifuged at $500 \times g$ for 15 min and the supernatants were transferred into 5-mm NMR tubes for NMR measurements.

All spectral data were obtained on a Bruker Avance 600 NMR spectrometer (Bruker, Germany). For 1D ^1H NMR spectra, 128 scans were recorded with 65,536 data points over a spectral width of 10,776.9 Hz using the zgcppr pulse sequence employing a relaxation delay of 1.0 s at a temperature of 298 K. TSP (0.05%, w/v) was used as in internal standard for D_2O, while TMS (0.05%, v/v) was used for acetone-d_6, acetonitrile-d_3, pyridine-d_5, D_2O, DMSO-d_6, and methanol-d_4. 2D ^1H–^1H correlation spectroscopy (COSY) spectra were acquired with a 1.4 s relaxation delay, 32 scans, and a 5681.8 Hz spectral width in both dimensions. In addition 2D ^1H–^{13}C heteronuclear single quantum correlation (HSQC) spectra were obtained with a 2.0 s relaxation delay, 32 scans, and 5,896.2 Hz spectral width in F_2 and 30,864.2 Hz in F_1.

Two dimensional J-resolved ^1H NMR spectra were recorded at 298 K on a 600-MHz Varian spectrometer (VnmrJ 2.2, CA). The spectra were collected using the following pulse sequence: [relaxation delay–90°–t_1–180°–t_1–acquire for time t_2] where the relaxation delay was 1.4 sec and t_1 was incremented with increasing delay. Data were acquired in F_2 using 16 FIDs per increment that were collected into 8192 data points, using a spectral width of 6009 Hz in F_2 (chemical shift axis) and 30 Hz in F_1 (spin–spin coupling constant axis). Datasets were zero-filled to 1024 data points in F_1 and the spectra were tilted by 45° to provide orthogonality and subsequently symmetrized about the F_1 axis. Following a magnitude calculation, the spectra were displayed as both contour plots and skyline projections.

2.4. Data analysis

In the aqueous extraction, the spectral ^1H NMR region from $\delta = 0.52$ to $\delta = 10.00$ was segmented into regions with widths of 0.04 ppm (giving 230 integrated regions) using AMIX software (version 3.7, Bruker Biospin Co., MA). The regions from $\delta = 4.60$ to $\delta = 4.90$ were excluded from the analysis due to the presence of the signal from residual water in aqueous extracts. In the case of methanol-d_4 extracts, one-dimensional ^1H NMR spectra were imported into AMIX software (version 3.7, Bruker Biospin Co., MA) for spectral binning. The spectral ^1H NMR region from $\delta = 0.52$ to $\delta = 10.00$ was divided into 0.04 ppm bins (giving 234 integrated regions). The two regions of $\delta = 3.25$–3.33 and 4.80–4.90 ppm were excluded from the analysis because of the residual signals of methanol and water. The remaining regions were normalized to the whole spectrum for principal component analysis (PCA), partial least squares discriminant analysis (PLS-DA), hierarchical

cluster analysis (HCA), and partial least squares projections to latent structures (PLS). PCA, PLS-DA, HCA and PLS were performed with SIMCA-P software (version 12.0, Umetrics, Umeå, Sweden).

For the analysis of PLS-derived relationship between observed and estimated age of the 2–6-year-old ginseng root samples using 50% methanol as an extraction and 100% D_2O as NMR dissolution solvent, ^1H NMR spectral data were collected from 14 samples of ginseng root at each cultivation age (70 total samples). We excluded one outlier based on Hotelling's T^2 in preliminary PCA of 15 samples of ginseng root at each cultivation age, and the PLS-DA was thus performed using 14 samples for each cultivation age group. Among those samples, the training set included randomly selected 11 individual samples, and rests of the 3 samples of 2–6-year-old ginseng root were used as the test set for external validation.

To select suitable NMR solvent among acetone-d_6, acetonitrile-d_3, pyridine-d_5, D_2O-d_4, DMSO-d_6, and 100% methanol-d_4 as direct extraction and NMR measurement solvents for differentiation between 5- and 6-year-old ginseng root samples, 3 individual samples were analyzed in all solvent systems except 50% methanol-d_4 system (19 ginseng root samples). In case of DMSO-d_6 condition, 20 ginseng root samples were further analyzed to confirm the separation.

For further study to differentiate 5- and 6-year-old ginseng samples using 100% methanol-d_4 solvent, 40 ginseng root samples (20 individual samples each of 5- and 6-year-old ginseng), were analyzed. Ten outliers (5 outliers in each cultivation age) were deleted based on Hotelling's T^2 in preliminary PCA from the 5- and 6-year-old ginseng roots, respectively. Thus, 30 samples (15 individual samples each of 5- and 6-year-old ginseng) were analyzed in further studies. Among those, randomly selected 12 samples were used for internal validation, whereas rests of the 3 samples were used for external validation in each cultivation age.

3. Results and discussion

3.1. ^1H NMR spectra and assignment of the peaks in ginseng root samples

The signal overlap was an obstacle to identifying individual metabolites in complex samples from ^1H NMR spectra. This problem could be solved by using 2D J-resolved spectra. Spectral data of J-resolved NMR provided supplementary information and a splitting pattern for each signal with the accurate coupling constant. In addition, the 2D NMR techniques including ^1H–^1H COSY and ^1H–^{13}C HSQC can be useful for peak assignment.

Figs. 1, S1 and S2 showed the representative ^1H NMR spectrum (Fig. 1a), 2D J-resolved spectra (Fig. 1b and c), ^1H–^1H COSY (Fig. S1), and ^1H–^{13}C HSQC (Fig. S2) spectrum of the 50% methanol extract of 6-year-old ginseng root samples measured with D_2O. As described in Table 1, the following signals were assigned based on comparisons with the chemical shifts of standard compounds using the Chenomx NMR suite software (version 5.1, Chenomx, Inc., Edmonton, Canada). 2D J-resolved data, ^1H–^1H COSY and ^1H–^{13}C HSQC signal matches were obtained by referencing ^1H–^{13}C chemical shifts in the Madison Metabolomics Consortium Database (MMCD, http://mmcd.nmrfam.wisc.edu/) and Human Metabolome Database (HMDB, http://www.hmdb.ca/). As shown in Table 1, the amino acids such as valine, threonine, alanine, arginine, proline, glutamate, glutamine, aspartate, asparagine, choline, tyrosine, tryptophan, and phenylalanine were assigned in the ginseng root samples. Organic acids such as acetate, glutarate, pyruvate, malate, 2-oxoglutarate, fumarate, and formate were also identified. In the sugar region (3–6 ppm), glucose, sucrose, and xylose were detected in the ^1H NMR and 2D NMR spectra.

Table 1

Assignments of 1D and 2D NMR spectral peaks obtained from 2- to 6-year-old *P. ginseng* root samples analyzed by D_2O as an NMR dissolution solvent after 50% methanol extraction. s: singlet, d: doublet, t: triplet, m: multiplet, dd: doublet of doublet.

Compound	^1H [a]	^{13}C [b]	Assignment [c]
Amino acids			
Valine	0.98 (d, J = 7.0)	n.d.[d]	H-8
	1.02 (d, J = 7.0)	n.d.	H-7
Threonine[1]	1.34 (d, J = 6.5)	22.50	H-8
Alanine[2]	1.46 (d, J = 7.2)	20.37	H-6
Arginine[3]	1.61–1.76 (m)	26.91	H-7
	1.87–1.96 (m)	30.15	H-6
	3.26 (t, J = 6.9)	43.23	H-8
Proline	1.99–2.09 (m)	n.d.	n.d.
Glutamate[5]	2.10–2.17 (m)	n.d.	H-6
	2.34–2.37 (m)	36.25	H-7
Glutamine	2.45 (m)	33.57	n.d.
Aspartate[9]	2.82 (dd, J = 17.1, 3.7)	39.40	n.d.
Asparagine[10]	2.84–2.88 (m)	37.64	H-6
	2.94–2.97 (m)	37.09	H-6
Choline	3.18 (s)	56.53	H-5, 6, 7
Tyrosine	6.89–6.91 (m)	n.d.	H-2, 6
	7.19–7.20 (m)	n.d.	H-3, 5
Tryptophan	7.21–7.25 (m)	n.d.	H-9
	7.54 (d, J = 8.0)	n.d.	H-6
	7.74 (d, J = 7.9)	n.d.	H-7
Phenylalanine	7.34 (d, J = 7.6)	n.d.	H-2, 6
	7.37–7.40 (m)	n.d.	H-4
	7.41–7.44 (m)	n.d.	H-5, 3
Organic acids			
Acetate[4]	1.90 (s)	n.d.	H-4
Glutarate[6]	2.30 (t, J = 7.4)	n.d.	n.d.
Pyruvate[7]	2.38 (s)	n.d.	H-6
Malate[8]	2.40 (dd, J = 15.5, 9.9)	45.30	H-5
	2.70 (dd, J = 15.5, 3.1)	n.d.	H-5
	4.30 (dd, J = 9.9, 3.1)	n.d.	H-2
2-Oxoglutarate[11]	3.02 (t, J = 7.4)	n.d.	n.d.
Fumarate	6.52 (s)	n.d.	n.d.
Formate	8.42 (s)	n.d.	H-2
Sugars			
Glucose[12]	3.45–3.48 (m)	78.57	H-6
	3.56 (dd, J = 9.9, 3.8)	73.86	H-3
	3.72–3.91 (m)	62.89	H-11, 6
	5.22 (d, J = 3.8)	94.98	H-2
Sucrose[13]	3.47 (t, J = 9.6)	71.97	H-10
	3.56 (dd, J = 10.0, 3.9)	73.65	H-12
	3.66 (s)	64.04	H-13
	3.76 (t, J = 9.5)	75.38	H-11
	3.79–3.91 (m)	63.04	H-17, 19
	4.05 (t, J = 8.6)	76.67	H-4
	4.22 (d, J = 8.8)	78.67	H-3
	5.42 (d, J = 3.9)	95.20	H-7
Xylose	3.38 (t, J = 9.4)	n.d.	H-4
	4.54 (d, J = 8.1)	n.d.	H-2
	5.18 (d, J = 3.9)	n.d.	H-2

[1–13] Compounds confirmed by 2D J-resolved NMR.

[a] ^1H NMR chemical shift (δ), peak multiplicity, and J value (Hz) data from 1H NMR and 2D J-resolved NMR.

[b] ^{13}C chemical shift (δ) data from ^1H–^{13}C HSQC.

[c] Assignment from COSY.

[d] n.d. not detected.

3.2. PLS-DA, HCA, and PLS of ginseng root samples using multiple solvent systems

PLS-DA extends a regression of PCA and uses class information to maximize the separation between groups of observations. This frequently used classification method is categorical (categories described with dummy variables) and expresses the class membership of the statistical units [14,27]. In this study, PLS-DA was performed using the ^1H NMR data of the 50% methanol extract of ginseng root. The data were mean-centered and scaled to unit variance (UV) by the SIMCA-P 12.0 software.

We excluded one outlier in the preliminary PCA of 15 samples of ginseng root at each cultivation age, and the PLS-DA was thus

performed using 14 samples for each cultivation age group. As shown in Fig. 2a, there was a separation of PLS-DA-derived score plots between the 2-, 3-, 4-, 5-, and 6-year-old ginseng root samples, whereas the separation between 5- and 6-year-old samples was not clear in the score plots. In addition, the 2-, 3-, 4-, and 5/6-year-old ginseng root samples were clustered respectively in the HCA-derived dendrogram, whereas 5- and 6-year-old samples did not show separate clustering each other independently (Fig. 2b).
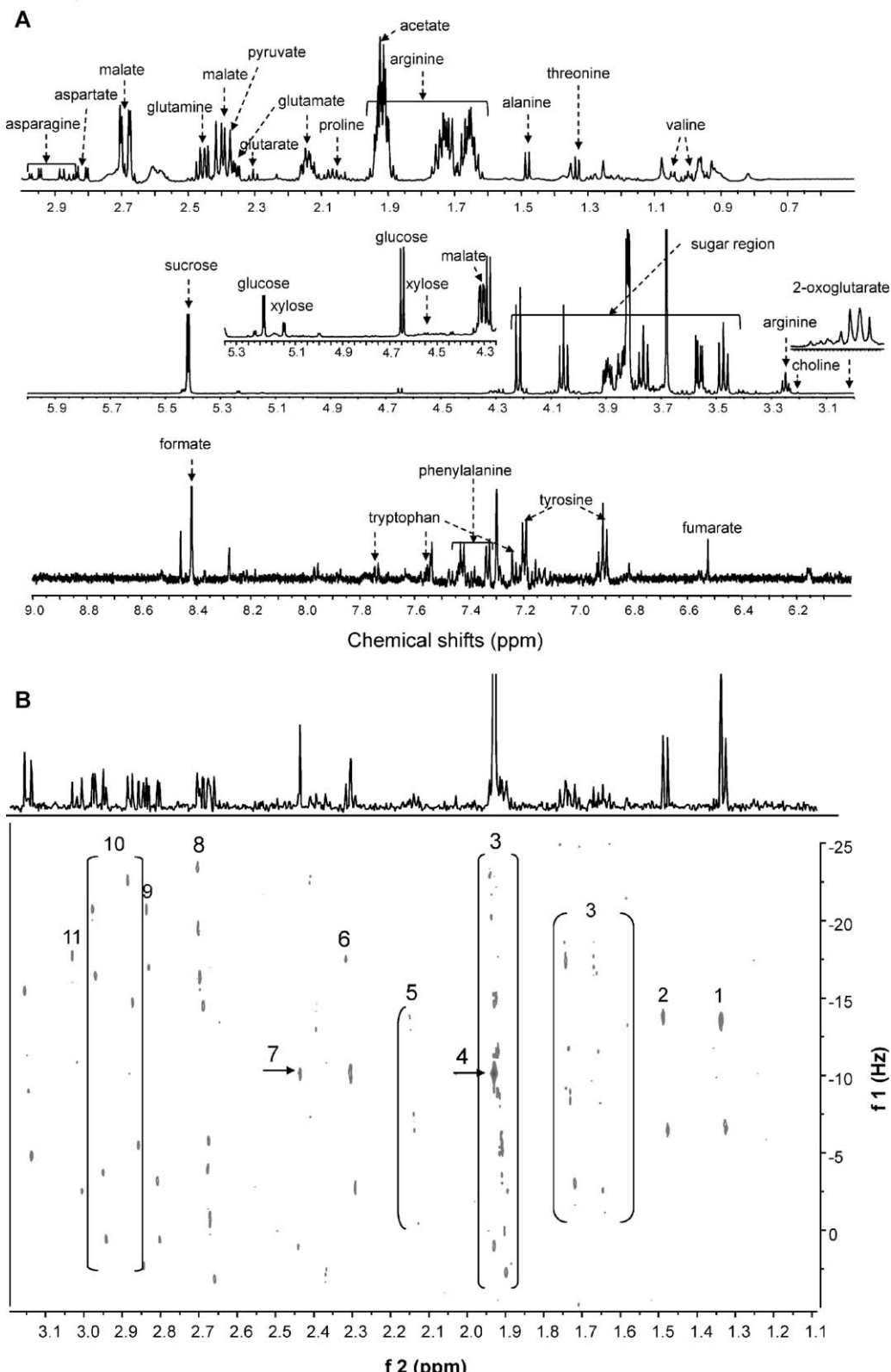

Fig. 1. Representative ^{1}H NMR spectrum (a) and 2D J-resolved NMR spectra of 0–3 ppm (b), 3–6 ppm (c) of 6-year-old ginseng root sample analyzed with D_2O as an NMR dissolution solvent after 50% methanol extraction. 1: threonine, 2: alanine, 3: arginine, 4: acetate, 5: glutamate, 6: glutarate, 7: pyruvate, 8: malate, 9: aspartate, 10: asparagine, 11: oxoglutarate, 12: glucose, 13: sucrose.
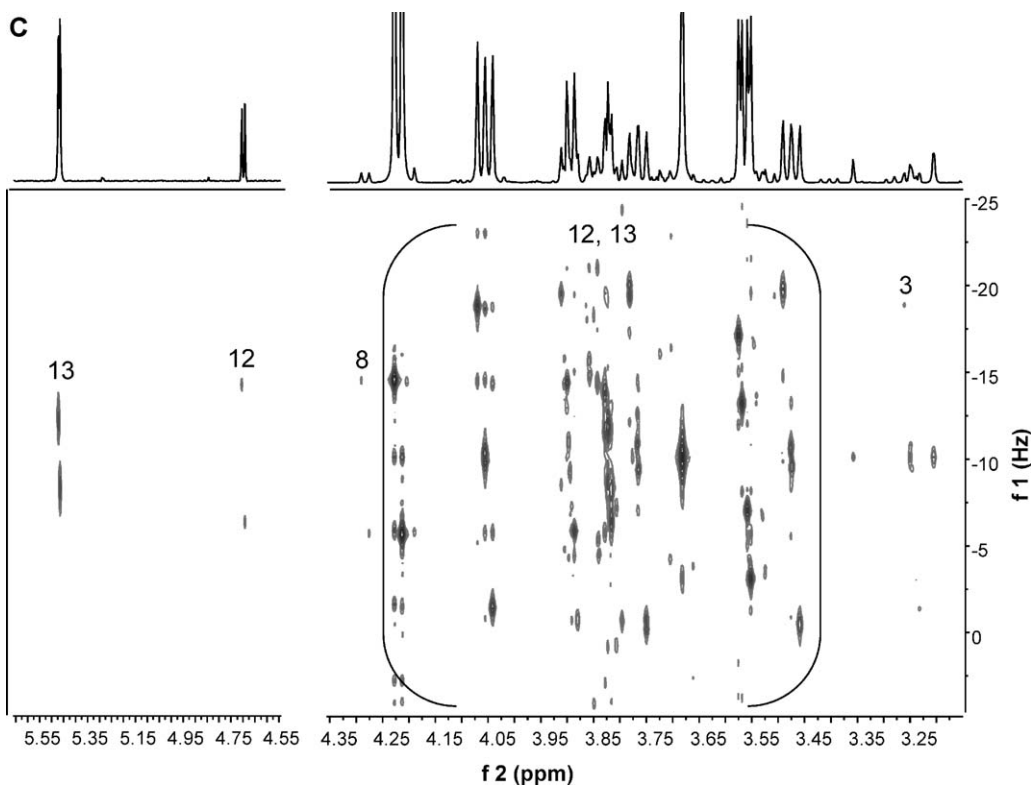
Fig. 1. (*Continued*)

Fig. S3 (supplementary material) shows the PLS-derived relationship between observed and estimated age of the 2- to 6-year-old ginseng root samples using the total ^{1}H NMR spectra of the training set. ^{1}H NMR spectral data were collected from 14 samples of ginseng root at each cultivation age (70 total samples). Among those samples, the training set included 11 individual samples of 2–6-year-old ginseng root, and three random samples were used as the test set for external validation. The differences between actual and predicted ages of ginseng were calculated and expressed as root mean square error of estimation (RMSEE). In the PLS training set model, the RMSEE value of 0.35 corresponded to 4.20 month estimation value in each cultivation age from 2–6-year-old ginseng root. As shown in Fig. S3, there was no clear separation of 5- and 6-year-old ginseng samples (dotted box). Based on this result, a new PLS model was developed using 2-, 3-, 4-, and 5/6-year-old ginseng samples (Fig. 3a). In the model, the 5- and 6-year old ginseng samples were grouped together. The RMSEE was 0.19, corresponding to 2.30 month estimation value for each cultivation age. The RMSEE of the PLS model made with 2- to 6-year-old samples was higher than that made after combining the 5- and 6-year-old samples.

To verify the PLS training set model made with estimation values, the test set model was assessed by choosing three random samples in each cultivation age group from the 2-, 3-, 4-, and 5/6-year-old ginseng root samples. The ability of the model to predict the cultivation ages of ginseng roots was subsequently tested by using the external test set in the resulting PLS model to yield the root mean square error of prediction (RMSEP). The test set was created by importing data set into the training set. RMSEP value of 0.20 corresponded to 2.40 month in each cultivation age (Fig. 3b). Fig. 3a and b showed good PLS model was built in training and test sets and the predictive ability of PLS model was investigated. Therefore, given ginseng samples of ages, these results provided basic information that can be used for separation of ginseng root samples of 2-, 3-, 4, and 5/6 years old by using the PLS model as shown in Fig. 3.

Table 2 shows the PLS-DA-derived VIP values of the major compounds contributing to the separation of each ginseng root sample in the PLS-DA model. The metabolites with VIP values over 0.7, such as valine, threonine, alanine, arginine, acetate, proline, glutamate, glutarate, glutamine, pyruvate, malate, aspartate, asparagine, choline, 2-oxoglutarate, sucrose, glucose, xylose, tyrosine, tryptophan, and formate, were selected for further comparison by ANOVA.

Table 3 shows the relative levels of each metabolite according to the ginseng cultivation age. The levels of aspartate and glutarate were significantly ($p < 0.05$ in all cases) higher in 2- year-old ginseng root, and glutamate, glutamine and glucose were significantly higher in 3-year-old samples. In addition, relatively higher levels of

Table 2
The VIP values of the major metabolites for the separation of 2- to 6-year-old *P. ginseng* root samples in the PLS-DA derived score plots.

| ^{1}H NMR chemical shift (δ)	Compound	VIP value
2.82	Aspartate	1.60
3.18	Choline	1.48
2.70	Malate	1.22
5.18	Xylose	1.21
1.02	Valine	1.19
2.10	Glutamate	1.19
2.46	Glutamine	1.13
2.86	Asparagine	1.12
2.38	Pyruvate	1.11
1.46	Alanine	1.11
2.06	Proline	1.10
7.74	Tryptophan	1.08
5.22	Glucose	1.02
8.42	Formate	0.98
6.90	Tyrosine	0.96
1.34	Threonine	0.95
2.30	Glutarate	0.95
5.42	Sucrose	0.91
1.90	Acetate	0.78
3.02	2-Oxoglutarate	0.72
3.26	Arginine	0.71
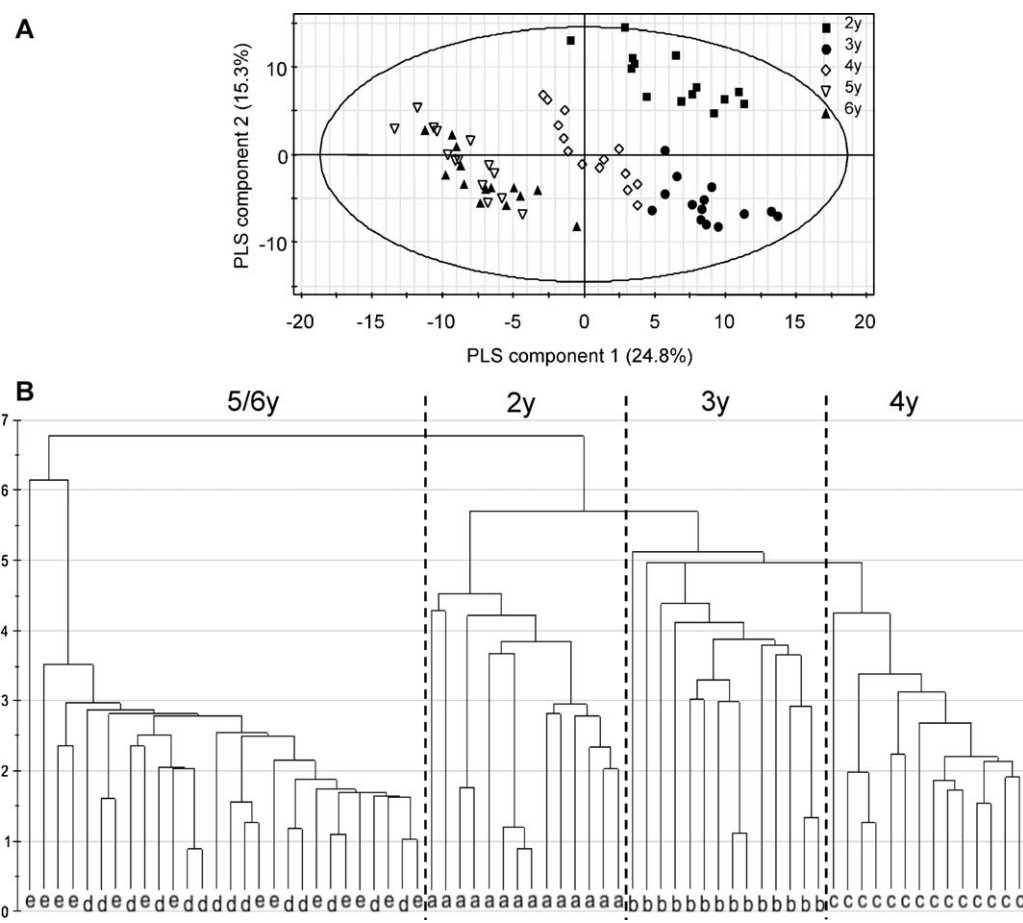
Fig. 2. PLS-DA-derived score plot (a) and HCA dendrogram (b) of 2–6-year-old ginseng root samples analyzed with D_2O as an NMR dissolution solvent after 50% methanol extraction. (a) (■): 2-year-old ginseng, (●): 3-year-old ginseng, (♦): 4-year-old ginseng, (▽): 5-year-old ginseng, (▲): 6-year-old ginseng, (b) a: 2-year-old ginseng, b: 3-year-old ginseng, c: 4-year-old ginseng, d: 5-year-old ginseng, e: 6-year-old ginseng.

acetate, sucrose, tyrosine, tryptophan, and formate were observed in 5- and 6-year-old ginseng samples. On the other hand, levels of acetate in 2-year-old ginseng and of valine, threonine, alanine, proline, pyruvate, malate, and xylose in 3-year-old ginseng samples were relatively lower than those in other samples. The relatively higher level of acetate in 5-year-old ginseng might be related to increased production of ginsenosides in 5- and 6-year-old ginseng roots. On the other hand, the metabolites related to glycolysis and

Table 3
Relative levels of selected metabolites based on VIP values in 2- to 6-year-old *P. ginseng* root samples. ANOVA was performed to compare and assess statistical significance with Duncan's post hoc test ($p < 0.05$). Data are mean values, and the error values represent standard error of mean (SEM) values ($n = 14$). Each superscript letter (a, b, c, and d) in the same row represents significant difference at $p < 0.05$.

| Compound	Cultivation age				
	2	3	4	5	6
Valine	0.38 ± 0.02^a	0.24 ± 0.007^c	0.33 ± 0.02^b	0.39 ± 0.02^a	0.33 ± 0.01^b
Threonine	0.14 ± 0.008^a	0.11 ± 0.005^c	0.15 ± 0.007^{ab}	0.17 ± 0.007^b	0.15 ± 0.005^{ab}
Alanine	0.090 ± 0.004^a	0.061 ± 0.003^c	0.078 ± 0.003^b	0.090 ± 0.004^a	0.084 ± 0.002^{ab}
Arginine	2.59 ± 0.1^a	2.91 ± 0.07^b	2.73 ± 0.08^{ab}	2.88 ± 0.08^b	2.89 ± 0.09^b
Acetate	0.78 ± 0.05^a	0.93 ± 0.03^b	0.93 ± 0.03^b	0.97 ± 0.03^b	0.96 ± 0.03^b
Proline	0.14 ± 0.005^a	0.11 ± 0.002^c	0.13 ± 0.004^a	0.12 ± 0.005^{ab}	0.12 ± 0.002^b
Glutamate	0.41 ± 0.01^a	0.46 ± 0.02^c	0.39 ± 0.01^{ab}	0.37 ± 0.02^b	0.37 ± 0.01^b
Glutarate	0.056 ± 0.003^a	0.031 ± 0.003^c	0.036 ± 0.002^{bc}	0.044 ± 0.007^b	0.030 ± 0.002^c
Pyruvate	0.42 ± 0.03^a	0.29 ± 0.009^d	0.33 ± 0.01^{cd}	0.35 ± 0.007^{bc}	0.38 ± 0.009^{ab}
Malate	1.50 ± 0.3^a	1.12 ± 0.02^c	1.35 ± 0.05^b	1.27 ± 0.02^b	1.47 ± 0.03^a
Choline	0.062 ± 0.003^a	0.034 ± 0.003^c	0.065 ± 0.004^a	0.046 ± 0.003^b	0.042 ± 0.004^{bc}
Aspartate	0.13 ± 0.004^a	0.087 ± 0.005^b	0.073 ± 0.003^c	0.080 ± 0.003^{bc}	0.083 ± 0.003^{bc}
Asparagine	0.045 ± 0.005^a	0.021 ± 0.007^b	0.023 ± 0.005^b	0.027 ± 0.004^b	0.030 ± 0.005^{ab}
2-Oxoglutarate	0.048 ± 0.003^a	0.034 ± 0.004^b	0.031 ± 0.002^b	0.044 ± 0.007^{ab}	0.033 ± 0.003^b
Glutamine	0.18 ± 0.009^a	0.24 ± 0.01^c	0.14 ± 0.008^b	0.15 ± 0.009^{ab}	0.15 ± 0.01^{ab}
Sucrose	18.26 ± 0.3^a	18.21 ± 0.2^a	19.14 ± 0.1^b	19.51 ± 0.2^b	19.26 ± 0.2^b
Glucose	0.15 ± 0.01^a	0.20 ± 0.01^b	0.13 ± 0.01^a	0.13 ± 0.007^a	0.15 ± 0.007^a
Xylose	0.10 ± 0.006^a	0.071 ± 0.003^b	0.094 ± 0.005^a	0.094 ± 0.005^a	0.088 ± 0.003^a
Tyrosine	0.010 ± 0.001^a	0.010 ± 0.002^a	0.010 ± 0.001^a	0.014 ± 0.001^b	0.017 ± 0.002^b
Tryptophan	0.012 ± 0.001^a	0.013 ± 0.002^a	0.012 ± 0.001^a	0.018 ± 0.001^b	0.021 ± 0.001^b
Formate	0.010 ± 0.0002^a	0.010 ± 0.0004^a	0.010 ± 0.001^a	0.011 ± 0.001^b	0.011 ± 0.001^b
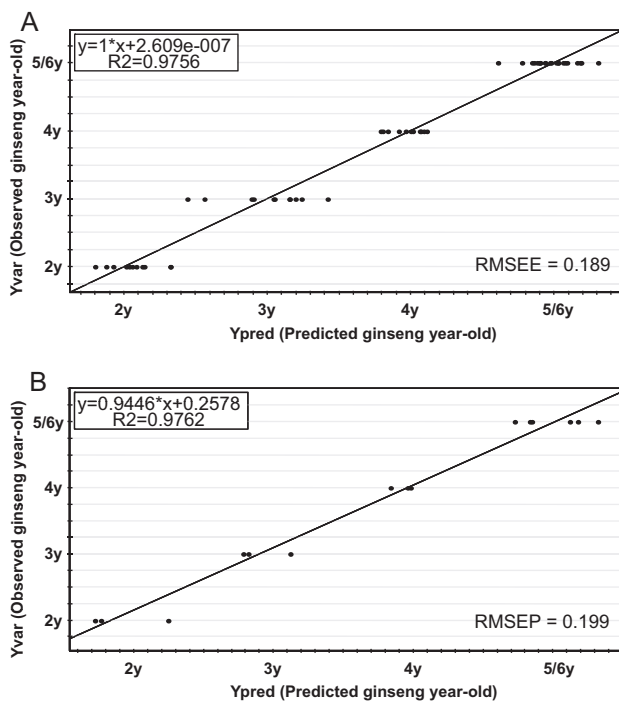
Fig. 3. PLS-derived relationship between observed and estimated age of the 2- to 5/6-year-old ginseng root samples using the total ^{1}H NMR spectra of the training set (a) and test set (b) analyzed with D_2O as an NMR dissolution solvent after 50% methanol extraction.

Fig. 4. PLS-derived score plots of the 100% methanol-d_4 extracts for 5- and 6-year-old ginseng root samples ($\triangledown$): 5-year-old ginseng, ($\blacktriangle$): 6-year-old ginseng).

the tricarboxylic acid cycle, such as pyruvate, 2-oxoglutarate, and malate were found at higher levels in 2-year-old ginseng roots. In addition, the relatively higher levels of tyrosine and tryptophan in 5- and 6-year-old ginseng roots could be related to the production of phenylpropanoid or flavonoids in those samples.

For separation of 5- and 6-year-old ginseng samples, PCA was performed using ^{1}H NMR data obtained with various extraction and NMR measuring solvents such as acetone-d_6, acetonitrile-d_3, pyridine-d_5, D_2O-d_4, DMSO-d_6, 100% methanol-d_4, and 50% methanol-d_4. For analysis, six solvent conditions (acetone-d_6, acetonitrile-d_3, pyridine-d_5, D_2O-d_4, DMSO-d_6, and 100% methanol-d_4) were used as the direct extraction and NMR measuring solvent systems. We performed PCA using 3 individual samples in all solvent systems except 50% methanol-d_4 system. In case of 50% methanol-d_4 system, data from 19 ginseng root samples each from 5- and 6-year-old ginseng roots were used for PCA, since the 50% methanol-d_4 system has been widely used in analysis of natural herbs and plants [15,21,28,29].

Among the solvent conditions, five solvent systems of acetone-d_6, acetonitrile-d_3, pyridine-d_5, D_2O-d_4, and 50% methanol-d_4 could not separate 5- and 6-year-old ginseng root body samples in PCA-derived score plots (Supplementary Fig. S4a–d and g). There was a separation between 5- and 6-year-old ginseng root samples in DMSO-d_6 when 3 samples each from 5- and 6-year-old ginseng roots were analyzed (Fig. S4e), but there was no separation between samples when the increased number of samples (20 samples each from 5- and 6-year-old ginseng roots) were analyzed (Fig. S4h). However, 5- and 6-year-old ginseng root body samples were separated when 100% methanol-d_4 was used for the extraction and as the NMR measuring solvent in the preliminary experiment as shown in Supplementary Fig. S4f. Therefore, further analysis was performed using 40 ginseng root samples (20 samples in each cultivation age), and it was confirmed that there was a clear separation between 5- and 6-year-old ginseng root samples. In the case of 100% methanol-d_4 extraction conditions, PCA was performed to
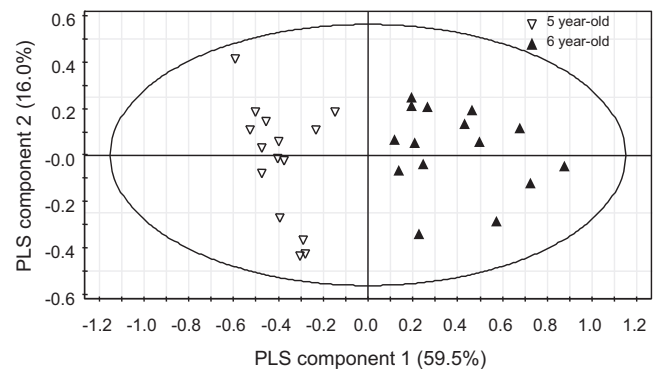
detect and delete outlier samples before PLS model development (data not shown). Ten outliers (5 outliers in each cultivation age) were deleted from the 5- and 6-year-old ginseng roots, respectively. Thus, 30 samples were analyzed in further studies.

PLS models were developed from ^{1}H NMR spectral data of 30 ginseng root samples (15 individual samples each of 5- and 6-year-old ginseng) using 100% methanol-d_4 solvent system. Among those samples, randomly selected 12 samples in each age were used for internal validation, whereas rests of the 3 samples were used as a test set for external validation. The differences between actual and predicted ages of ginseng were calculated and expressed as RMSEE. The ability of the model to predict the cultivation ages of ginseng roots was subsequently tested by using an external test set in the resulting PLS model to yield RMSEP. We used the ^{1}H NMR spectral data as the independent variable and the cultivation ages (5- and 6-year-old) of the ginseng roots as the Y-variable. Prior to PLS modeling, each score vector was *pareto* scaled, because *pareto* scaling showed a better separation of samples than the other scaling methods in preliminary experiment. As shown in Fig. 4, there was a clear separation between 5- and 6-year-old ginseng root samples in the PLS-derived score plots. A permutation test was then performed with 50 permutations as a cross validation to verify the model. Permutation testing has been used to evaluate the statistical significance of the estimated predictive power of models by comparing R^2Y and Q^2Y values from the original model with these values for a reordered model that, was newly created whenever Y-data was permutated at random.

Generally, R^2Y – which describes how well the data in the training set are mathematically reproduced - varies between 0 and 1, where 1 indicates a model with a perfect fit. Q^2Y values of >0.5 and >0.9 are considered indicative of good and excellent predictive abilities, respectively [14]. As shown in Table 4, R^2Y and Q^2Y values were 0.83 and 0.71, respectively, in this PLS model, which meant that the PLS model in this study has good fitness and predictive abilities. The RMSEE value of 0.22 corresponded to 2.60 months, and the RMSEP value of 0.14 was corresponded to 1.71 months. It was known that R^2Y-intercept should not exceed 0.3–0.4 and that

Table 4
PLS model parameters derived from the data of 5- and 6-year-old ginseng root samples analyzed by 100% methanol-d_4 solvent system. The total number of PLS components was three.

PLS parameters	Values
R^2Y	0.83
Q^2Y	0.71
RMSEE	0.22
RMSEP	0.14
R^2Y intercept	0.27
Q^2Y intercept	−0.35

Q^2Y-intercept should not exceed 0.05 [14]. The R^2Y intercept and Q^2Y intercept values were 0.27 and −0.35, respectively, in the PLS model. Thus, the PLS model in this study was validated since the R^2Y-intercept and Q^2Y-intercept values were lower than the above mentioned criteria for validation.

4. Conclusions

In this study, we differentiated ginseng roots of various cultivation ages using 1D and 2D NMR-based metabolomics techniques with two step solvent systems. We used ginseng root samples cultivated according to standard cultivation guidelines, while most of the previous research has been performed using purchased ginseng root samples from commercial markets or farms. Through PLS-DA model obtained by 50% methanol and D_2O as an extraction and dissolution solvent for NMR analysis, 2-, 3-, 4-, and 5/6-year-old ginseng root samples were differentiated, and the relative levels of 23 compounds in each sample were investigated. Then, the 100% methanol-d_4 as a direct extraction and dissolution solvent for NMR analysis was employed and the PLS model built in this study successfully differentiate the 5- and 6-year-old ginseng root samples. In conclusion, we succeeded in discriminating 2–6-year-old ginseng root samples using two step solvents. There seem to be large impacts of the geographical area and ginseng root growing conditions on the final chemical composition of the ginseng extracts. However, we focused on the Korean ginseng roots cultivated by standard cultivation protocols as a basic standard. For the commercial application of the methodology in the study, diverse samples from various origins with different ages should be collected and prediction model should be built using the method in this study. These results suggest that the methods in this study can be used as a standard protocol for the differentiation of ginseng roots according to cultivation age.

Acknowledgments

Appendix A. Supplementary data

Supplementary data associated with this article can be found, in the online version, at doi:10.1016/j.jpba.2011.09.016.

References

[1] Y.Z. Xiang, H.C. Shang, X.M. Gao, B.L. Zhang, A comparison of the ancient use of ginseng in traditional Chinese medicine with modern pharmacological experiments and clinical trials, Phytother. Res. 22 (2008) 851–858.
[2] S.R. Ko, K.J. Choi, K.W. Han, Comparison of proximate composition, mineral nutrient, amino acid and free sugar contents of several Panax species, Korean, J. Ginseng Sci. 20 (1996) 36–41.
[3] Y. Takino, Studies on the pharmacodynamics of ginsenoside-Rg (1), ginsenoside-RB-1 and ginsenoside-RB-2 in rats, Yakugaku Zasshi 114 (1994) 550–564.
[4] W. Shi, Y. Wang, J. Li, H. Zhang, L. Ding, Investigation of ginsenosides in different parts and ages of Panax ginseng, Food Chem. 102 (2007) 664–668.
[5] N.D. Kim, S.Y. Kang, V.B. Schini-Kerth, Ginsenosides evoke endothelium- dependent vascular relaxation in rat aorta, Gen. Pharmacol. 25 (1994) 1071–1077.
[6] J.K. Park, K.Y. Nam, H.C. Hyun, S.H. Jin, S.A. Chepunov, N.E. Chepunov, Effect of red ginseng triol saponin fractions on the spatial memory functions studied with 12-arm radial maze, Korean J. Ginseng Sci. 18 (1994) 32–38.
[7] D.O. Kennedy, A.B. Scholey, Ginseng: potential for the enhancement of cognitive performance and mood, Pharmacol. Biochem. Behav. 75 (2003) 687–700.
[8] K. Metori, The preventive effect of ginseng with Du-Zhong leaf on protein metabolism in aging, Biol. Pharm. Bull. 20 (1997) 237–242.
[9] H.Y. Kim, X. Chen, C.N. Gillis, Ginsenosides protect pulmonary vascular endothelium against free radical-induced injury, Biochem. Biophys. Res. Commun. 189 (1992) 670–676.
[10] T.K. Yun, Experimental and epidemiologic evidence on non-organ specific cancer preventive effect of Korean red ginseng and identification of active compounds, Mutat. Res. 523–524 (2003) 63–74.
[11] K.T. Choi, Botanical characteristics, pharmacological effects and medicinal components of Korean Panax ginseng C.A. Meyer, Acta Pharmacol. Sin. 29 (2008) 1109–1118.
[12] I.B. Keith, N.M. Mark, Immune system effects of echinacea, ginseng, and astragalus: a review, Integr. Cancer Ther. 2 (2003) 247–267.
[13] http://www.geumsan.go.kr/html/kr/info/info_08_06.html?mode=view&idx =2732 &GotoPage=1 (assessed August 7 2010).
[14] L. Eriksson, E. Johansson, N. Kettaneh-Wold, J. Trygg, C. Wikstrom, S. Wold, Multi- and Megavariate Data Analysis, Umetrics Academy, Umea, Sweden, 2006.
[15] H.K. Kim, Y.H. Choi, R. Verpoorte, NMR-based metabolomic analysis of plants, Nat. Protoc. 5 (2010) 536–549.
[16] Y. Sekiyama, E. Chikayama, J. Kikuchi, Profiling polar and semipolar plant metabolites throughout extraction processes using a combined solution-state and high-resolution magic angle spinning NMR approach, Anal. Chem. 82 (2010) 1643–1652.
[17] D.S. Wishart, Metabolomics: applications to food science and nutrition research, Trends Food Sci. Technol. 19 (2008) 482–493.
[18] H. Wu, A.D. Southam, A. Hines, M.R. Viant, High-throughput tissue extraction protocol for NMR- and MS-based metabolomics, Anal. Biochem. 372 (2008) 204–212.
[19] J.H. Kang, M.Y. Choi, S.M. Kang, H.N. Kwon, H. Wen, C.H. Lee, M.S. Park, S. Wiklund, H.J. Kim, S.W. Kwon, S.H. Park, Application of a ^{1}H Nuclear Magnetic Resonance (NMR) metabolomics approach combined with orthogonal projections to latent structure-discriminant analysis as an efficient tool for discriminating between Korean and Chinese herbal medicines, J. Agric. Food Chem. 56 (2008) 11589–11595.
[20] Y.S. Shin, K.H. Bang, D.S. In, O.T. Kim, D.Y. Hyun, I.O. Ahn, B.C. Ku, S.W. Kim, N.S. Seong, S.W. Cha, D.H. Lee, H.K. Choi, Fingerprinting analysis of fresh ginseng roots of different ages using ^{1}H-NMR spectroscopy and principal components analysis, Arch. Pharm. Res. 30 (2007) 1625–1628.
[21] S.Y. Yang, H.K. Kim, A.W. Lefeber, C. Erkelens, N. Angelova, Y.H. Choi, R. Verpoorte, Application of two dimensional nuclear magnetic resonance spectroscopy to quality control of ginseng commercial products, Planta Med. 72 (2006) 364–369.
[22] G. Xie, R. Plumb, M. Su, Z. Xu, A. Zhao, M. Qiu, X. Long, Z. Liu, W. Jia, Ultra-performance LC/TOF MS analysis of medicinal Panax herbs for metabolomic research, J. Sep. Sci. 31 (2008) 1015–1026.
[23] Y.Q. Qiu, X. Lu, T. Pang, C.F. Ma, X. Li, G.W. Xu, Determination of radix ginseng volatile oils at different ages by comprehensive two dimensional gas chromatography/time-of-flight mass spectrometry, J. Sep. Sci. 31 (2008) 3451–3457.
[24] E.J. Lee, R. Shaykhutdinov, A.M. Weljie, H.J. Vogel, P.J. Facchini, S.U. Park, Y.K. Kim, T.J. Yang, Quality assessment of ginseng by ^{1}H NMR metabolite fingerprinting and profiling analysis, J. Agric. Food Chem. 57 (2009) 7513–7522.
[25] I.O. Ahn, S.S. Lee, J.H. Lee, M.J. Lee, B.G. Jo, Comparison of ginsenoside contents and pattern similarity between root parts of new cultivars in Panax ginseng C.A. Meyer, J. Ginseng Res. 32 (2008) 15–18.
[26] Rural Development Administration, Ginseng GAP Standard Cultivation Guideline, National Institute of Crop Science, 2009.
[27] M. Barker, W. Rayens, Partial least squares for discrimination, J. Chemometrics 17 (2003) 166–173.
[28] J.X. Fontaine, R. Molinié, T. Tercé-Laforgue, D. Cailleu, B. Hirel, F. Dubois, F. Mesnard, Use of ^{1}H-NMR metabolomics to precise the function of the third glutamate dehydrogenase gene in Arabidopsis thaliana, Comptes Rendus Chimie 13 (2010) 453–458.
[29] H.K. Kim, S. Saifullah, E.G. Khan, S.D.P. Wilson, A. Kricum, S. Meissner, A.M. Goraler, Y.H. Deelder, R. Choi, Verpoorte, Metabolic classification of south American Ilex species by NMR-base metabolomics, Phytochemisty 71 (2010) 773–784.

A validated CE method for determining dimethylsulfate a carcinogen and chloroacetyl chloride a potential genotoxin at trace levels in drug substances

Muzaffar Khan [a,*], K. Jayasree [a], K.V.S.R. Krishna Reddy [a], P.K. Dubey [b]

[a] Analytical Development, Aptuit Laurus Private Limited, ICICI Knowledge Park, Shameerpet, Hyderabad 500078, India
[b] Department of Chemistry, Jawaharlal Nehru Technological University, Kukatpally, Hyderabad 500072, India

ABSTRACT

A simple and rapid capillary zone electrophoretic method was developed for determining dimethyl sulfate a possible human carcinogen and mutagen and chloroacetyl chloride a potential genotoxic agent at trace levels in pharmaceutical drug substances by indirect photometric detection. A systematic screening of various anionic probes was performed to obtain the best separation conditions and sensitivity. High sensitivities with low quantification and detection levels were achieved for dimethylsulfate and chloroacetyl chloride using a background electrolyte (BGE) containing 5 mM pyridine dicarboxylic acid as the probe ion. The method is specific, precise and accurate for the two genotoxins. The optimized method was validated for specificity, precision, linearity, accuracy and stability in solution. Calibration curves were linear ($R > 0.999$) for both dimethylsulfate and chloroacetyl chloride in the range LOQ – 300% of nominal concentrations. The CE method was effectively implemented for estimating dimethylsulfate and chloroacetyl chloride in two different active pharmaceutical ingredients (APIs).

© 2011 Elsevier B.V. All rights reserved.

1. Introduction

Dimethyl sulfate (DMS) is widely used in the pharmaceutical and chemical industries as a reagent for the methylation of phenols, amines and thiols. Compared to other methylating agents DMS is preferred by the industry because of its low cost and high reactivity. DMS can affect the base-specific cleavage of guanine in DNA by rupturing the imidazole rings present in guanine [1]. This process can be used to determine base sequencing, cleavage on the DNA chain and other applications.

DMS is classified as a Class 2 carcinogen by International Agency for Research on Cancer [2] and is mutagenic, poisonous, corrosive, environmentally hazardous and volatile (presenting an inhalation hazard). DMS is absorbed through the skin, mucous membranes, and gastrointestinal tract. Delayed toxicity allows potentially fatal exposures to occur prior to development of any warning symptoms [3]. DMS has been tested for carcinogenicity in rats by inhalation, subcutaneous and intravenous injection, and following prenatal exposure. It produced local sarcomas and tumours of the nervous system [2]. DMS, in our case is used as a methylating agent in one of the manufacturing steps of an active

pharmaceutical ingredient (API-1). With concerns rising due to the known genotoxicity of DMS, it is necessary to demonstrate that the levels of DMS are within acceptable limits in API-1 through a suitable analytical method. Based on the daily dosage, a limit of 50 ppm of DMS was considered in API-1 applying the threshold of toxicological concern (TTC) concept.

Chloroacetyl chloride (CAC) is bifunctional; the acyl chloride easily forms esters and amides, while the other end of the molecule is able to form other linkages, e.g. with amines. CAC is a known reagent for acylation [4] and as a two carbon building block for cyclization reactions [5]. In our application it has been used for acylation followed by cyclization in an intermediate synthesis of API-2. Although there is limited information available on the carcinogenicity and genotoxicity of CAC, it can be categorized as a structural alert for genotoxic potential (Class 3 category as per Muller classification [10]). CAC decomposes on heating producing toxic and corrosive fumes including phosgene and hydrogen chloride. A suitable analytical method should be developed to demonstrate that CAC is within acceptable limits of not more than 75 ppm in API-2. This limit was arrived at, by considering the maximum daily dosage of API-2 and TTC.

The current ICH guidelines describe a general concept of qualification of impurities in active substances (ICH Q3A (R) [6]) and medicinal products (ICH Q3B (R2) [7]). These guidelines however do not adequately address the concern for genotoxic impurities in drug substances and drug products. A Guideline on the Limits of Genotoxic Impurities [8] was subsequently issued by the

* Corresponding author at: Analytical Development, Aptuit Laurus Private Limited, Turkapally, Shameerpet, Hyderabad, Andhra Pradesh 500078, India.
Tel.: +91 40 230413531; fax: +91 40 23045438.
E-mail address: muzaffarkhan76@rediffmail.com (M. Khan).

Committee for Medicinal Products (CHMP) to overcome the short comings of the ICH Q3A and Q3B guidelines. The CHMP guideline provides a general framework and practical risk based approach to deal with genotoxic impurities in drug substances. As per this guideline, the genotoxic impurities with sufficient evidence for a threshold-related mechanism should be addressed using methods outlined in ICH Q3C (R3) for Class 2 solvents. For genotoxic impurities without sufficient evidence for a threshold-related mechanism, the guideline proposes a policy of controlling levels to "as low as reasonably practicable" (*ALARP principle*). The CHMP guideline and a more recent draft guidance document on limits of genotoxic and carcinogenic impurities [9] issued by the US Food and Drug Administration recommend that an exposure level of 1.5 μg per person per day for each genotoxic impurity can be considered an acceptable qualification threshold. Any impurity found at a level below this threshold generally should not need further safety qualification for genotoxicity and carcinogenicity concerns. The acceptable risk is defined as an additional cancer risk of not greater than 1 in 100,000 based on a lifetime's exposure to a genotoxic impurity. This approach is applied to impurities in the absence of data from carcinogenicity long-term studies or data providing evidence for a threshold mechanism of genotoxicity and is defined by the threshold of toxicological concern (TTC) considering an exposure of 1.5 μg/day lifetime intake of a genotoxic impurity being associated with an acceptable risk [10]. However the CHMP opines that the genotoxic impurity limits can also vary based on differing periods of exposure, while a 10-fold lower values are recommended for high potency carcinogens such as N-nitrosoamines, aflatoxins and azoxy compounds the limits can be relatively relaxed for carcinogens with established dietary exposure and life threatening indication such as cancer. In accordance with this, Muller et al. [11] suggest a staged TTC; whereby the acceptable daily intake values vary between 1.5 μg/day intake for lifetime exposure to 120 μg/day for 28 days (or less) exposure [12]. Dobo et al. have discussed the approach that can be made during drug development to understand potential mutagenic and carcinogenic risks associated with compounds used for synthesis and to understand the capability of synthetic processes to control genotoxic impurities in the API [13]. Snodin provides a qualification strategy based on a review of representative compounds from structurally alerting substances [14]. Even though structurally alerting compounds, particularly highly reactive reagents introduced in the early stages of a multistep synthesis are unlikely to be carried over to the API, regulatory agencies demand that carry over studies are performed to demonstrate the absence of PGIs in the drug substance at TTC levels, considering the potential threat of genotoxins to human health.

GC–FID/MS and HPLC–UV/MS are the most widely applied techniques for determining genotoxic impurities at trace levels owing to their inherent high sensitivity and precision [15–17]. The sample preparation often involves extractions for enhancement of sensitivity and removal of matrix interferences. When the quantification of a genotoxic impurity at trace levels in the API becomes daunting, a higher limit for this impurity can be set in the intermediate step where this genotoxic impurity is introduced. This limit should however be supported with a scientific rationale that the impurity will either be structurally altered so that it is no longer genotoxic or is eliminated through several steps of purification in subsequent stages of synthesis.

Capillary electrophoresis offers simplicity, high separation efficiencies, low reagent consumption and is a cost effective and eco-friendly technique, specifically for the analysis of ionizable species. However the application of CE is not rampant for determining trace analytes due to low sensitivity and poor precision as compared to HPLC and GC. However in CE, the sensitivity of trace analytes can be increased through sample stacking techniques and enrichment of the analytes from the sample matrix using solid phase extractions (SPE) and liquid–liquid extractions (LLE). The use of a MS detector coupled with CE can also enhance the sensitivity of trace analytes. The precision can be improved with the use of an internal standard for quantification purposes.

Alzaga et al. [18] have developed a generic approach for the determination of alkylating agents by derivatisation followed by headspace GC/MS. This method utilizes an in situ derivatisation procedure with pentafluorothiophenol (PFTP) as the derivatisation agent. Methods for determining DMS by Head Space Gas Chromatography (HS-GC) with MS detection [19] and HS-GC with FID detection [20] in intermediates and drug substances have been reported. Hansen and Sheribah [21] have determined five residual alkylating impurities including alkyl chloride and alkyl bromide in bromazepam API using capillary electrophoresis with LOQ of 0.05%. To the best of our knowledge, no CE methods have been reported so far in the literature for the determination of DMS and CAC. In this article, we describe a simple and fast method for determining DMS and CAC in drug substances at trace levels by capillary electrophoresis. This method has been successfully applied to demonstrate that DMS and CAC in two different APIs were within acceptable regulatory limits.

2. Materials and methods

2.1. Chemicals and reagents

Sodium hydroxide (0.1 N, CE grade) and CE grade water were procured from Agilent Technologies (Waldbronn, Germany). Pyridine 2,6-dicarboxilic acid was procured from Merck (Hohenbrunn, Germany), hexadecyl trimethyl ammonium bromide (CTAB), pyromellitic acid and paratoulene sulfonic acid were procured from Sigma–Aldrich (Steinheim, Germany). Benzoic acid and phthalic acid were procured from Rankem (New Delhi, India). DMS and CAC were procured from Spectrochem (Mumbai, India). All reagents were of analytical grade or highest available purity. API-1 and API-2 were synthesized in Aptuit Laurus Private Limited (Hyderabad, India).

2.2. Equipment

The separation was performed on Agilent Technologies Capillary Electrophoresis system with a built-in diode-array detector. The Agilent ChemStation software was used for system control, data acquisition and post-run processing. The separation was performed in a 64.5 cm (56 cm length to detector), 50-μm id, bare fused silica capillary with extended light path having a bubble factor of 3 for enhanced sensitivity (Agilent Technologies, Waldbronn, Germany). An alignment interface, containing an optical slit matched to the internal diameter of 150-μm, was used.

2.3. Preparation of analyte solutions and background electrolyte

About 30 mg each of DMS and CAC standards were accurately weighed into separate 100 mL volumetric flasks. The standards were dissolved in 10 mL methanol by ultra sonication for 10 min. The flasks were cooled to room temperature and the volumes were then made up to 100 mL mark with water. A 1.0 mL aliquot of these stock solutions were further diluted independently to 100 mL each, with the diluent (methanol:water 10:90%, v/v) to obtain the DMS and CAC standard solutions. The standard solutions were filtered through 0.2 μm nylon syringe filters.

About 0.5 g of each API was accurately weighed into a 5 mL volumetric flask. A 0.5 mL aliquot of methanol was added to the flask and sonicated for about 5 min. The flask was cooled to room temperature and volume was made up to 5 mL mark with the diluent and sonicated for 15 min with intermittent shaking. The sample solutions were filtered through 0.2 μm nylon syringe filters.

The background electrolyte (BGE) was prepared by dissolving about 83.0 mg of pyridine carboxylic acid and 14.5 mg of CTAB in 100 mL HPCE grade water followed by ultra sonication for about 10 min to facilitate complete dissolution. The pH of this solution was then adjusted to 5.6 ± 0.1 with 1 N NaOH. The BGE was filtered through 0.2 μm nylon syringe filters.

2.4. Electrophoretic conditions

A 30 kV voltage was applied with negative polarity setting. Samples were injected hydrodynamically by pressure at 50 mbar for 60 s followed by injection of a BGE plug by pressure at 50 mbar for 5 s. The capillary cassette temperature was maintained at 20 °C. The detector signals were monitored at a wavelength of 350 nm (bandwidth 80 nm) with a reference wavelength of 200 nm (bandwidth 20 nm). The migration times for DMS and CAC were about 3.0 min and 3.3 min respectively and the total run time was 5 min. The BGE replenishment was done after every 25 injections.

New bare fused-silica capillaries were flushed with CE grade water for 30 min following by the BGE for 30 min. Prior to every use the capillary was conditioned by flushing for 10 min with water and then with the BGE for 15 min. Between analyses, the capillary was flushed with the BGE for 2 min.

2.5. Method validation

The developed method was validated for determining DMS and CAC with the assessment of specificity, precision, sensitivity, linearity and range, accuracy and stability of analyte solutions. The validation was performed keeping in mind the ICH guidelines for analytical method validation [22].

2.5.1. Specificity

Specificity was evaluated by injecting DMS and CAC individually and spiked to the respective APIs along with all other known process related impurities and solvents at specification levels. The electropherograms were examined for interferences of other analytes with DMS and CAC in the specificity samples.

2.5.2. Precision

The repeatability of the method was evaluated by separately injecting replicate preparations ($n = 6$) of a spiked solution of API-1 containing DMS and spiked solution of API-2 containing CAC at LOQ levels, 50, 100, 150 and 300% of nominal analyte concentrations. To evaluate intermediate precision, six replicate samples of the APIs containing DMS and CAC at these concentrations were prepared and injected every day, on three different days. The %RSD for DMS and CAC and their migration times were evaluated to assess precision of the method.

2.5.3. Sensitivity

Sensitivity of the method was determined by establishing the limit of detection (LOD) and limit of quantitation (LOQ) for DMS and CAC. The detector response was obtained for a series of dilute solutions with known concentrations of DMS and CAC. Concentrations resulting in signal-to-noise ratios of about 3:1 and 10:1 were considered as detection limits and quantitation limits respectively. The precision at LOQ level was assessed in terms of %RSD.

2.5.4. Linearity and range

The linearity solutions were prepared from individual stock solutions of DMS and CAC at nine concentration levels – LOQ, 50, 75, 100, 125, 150, 175, 200 and 300% of analyte concentrations, each in triplicate. The data was subjected to linear regression analysis with the least squares method.

2.5.5. Accuracy

Samples of API-1 and API-2 were spiked with DMS and CAC respectively at LOQ, 50, 100, 150 and 300% of the nominal analyte concentrations. The spiking was performed in triplicate at each level and the spiked samples were analyzed as per the method. Recoveries for DMS and CAC were calculated against freshly prepared standards. The mean percentage recoveries at each level were used as a measure of accuracy of the method. An ANOVA test was performed to confirm that the recoveries were independent of the spiked concentrations.

2.5.6. Stability in analytical solution

Standard solutions of DMS and CAC were prepared in the diluent at analyte concentrations. Each solution was analyzed immediately after preparation and divided into two parts. While one part was stored at 2–8 °C in a refrigerator, the other at bench top in tightly capped volumetric flasks. The stored solutions were reanalyzed after 24 and 48 h and the percentage recoveries of DMS and CAC were calculated against the zero hour samples.

3. Results and discussion

3.1. Method development and optimization

Dimethyl sulfate rapidly decomposes on contact with water to methanol and methyl sulfate [23] as shown in Fig. 1a. Similarly chloroacetyl chloride reacts with water and the end products are chloroacetic acid and hydrochloric acid (Fig. 1b). Both DMS and CAC exist as uni-negative ions at the working pH of 5.6 and tend to migrate towards the anode terminal under the influence of applied electrical field.

In the development and optimization trials, different anionic probes were evaluated at 2, 5 and 10 mM concentrations for obtaining maximum sensitivity, peak symmetry and selectivity for DMS and CAC through indirect photometric detection. A sub-micellar concentration of CTAB (0.4 mM) was used in all BGE systems for EOF reversal and separations were performed by applying potential in negative polarity mode (detector end towards anode terminal). The peaks were found to be fronting in the BGE containing 5 mM pyromellitate + 0.4 mM CTAB (pH 7.7 ± 0.1). While there was poor separation in 5 mM p-toluene sulfonic acid + 0.4 mM CTAB (pH 6.0 ± 0.1), the DMS peak was found to be splitting in 5 mM benzoic acid + 0.4 mM CTAB (pH 6.0 ± 0.1). Peak symmetries were poor and a high level of background noise at the operational wavelength was observed with 5 mM phthalate + 0.4 mM CTAB (pH 6.5 ± 0.1).

In CE, the Kohlraush regulating function determines the probe displacement by the analyte [24] and the probe's mobility and optical properties must be considered. The mobility and concentration of the probe are crucial for the separation performance of the method because they influence peak shapes and efficiency. The mobilities of the probes that were evaluated are in the order: pyromellitate > phthalate > pyridine dicarboxylate > benzoate > p-toluene sulfonate [25]. While the highly mobile pyromellitate probe is suitable for analyzing smaller fast moving anions, the benzoate and p-toluene sulfonate probes are more suitable for analyzing the lower mobility compounds such as short chain (C4–C8) carboxylic acids. Phthalate and pyridine dicarboxylate probes have similar mobilities and are most suitable for analyzing medium mobility species. The absorptivity of the probe at the detection wavelength is a key parameter influencing the method sensitivity. The benzoate and pyridine dicarboxylate probes have higher molar absorptivities when compared to the other probes that were tested [26].
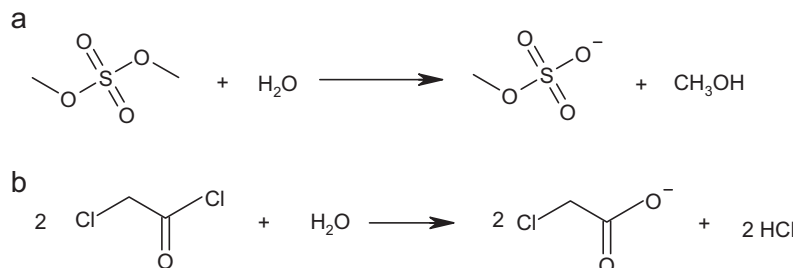
Fig. 1. (a) Reactivity of dimethylsulfate in water. (b) Reactivity of chloroacetyl chloride in water.

The medium mobility and high molar absorptivity of pyridine 2,6-dicarboxylate rendered it as the preferred probe for analyzing the species DMS and CAC. BGEs containing 2–10 mM pyridine 2,6-dicarboxylic acid + 0.4 mM CTAB (pH 5.6 ± 0.1) were evaluated for optimum separation and sensitivity. Lower concentrations of pyridine 2,6-dicarboxylic acid were unfavorable as broad peaks were observed due to electromigration dispersion. On the other hand higher concentrations resulted in higher noise levels, decreased sensitivity and an adverse affect on the linearity of detection [27]. Good peak symmetries, high sensitivity and high resolution between DMS and CAC could be achieved using 5 mM pyridine 2,6-dicarboxylic acid + 0.4 mM CTAB in the BGE system which was eventually finalized.

The separation was evaluated at 20, 25 and 30 kV and the migration times decreased with the increase in the applied voltage. The highest available voltage on the equipment (30 kV) was chosen as it provided higher theoretical plates and resolution since the separation proceeds rapidly minimizing the effects of diffusion and peak broadening. The temperature effects on separation were evaluated at 15, 20, 25, 30 and 35 °C. The migration times decreased with the increase in temperature due to a decrease in BGE viscosity. However the temperature was optimized to 20 °C as the theoretical plates decreased and the noise increased significantly at elevated temperatures. In indirect photometric detection, the transparent analyte species are detected as negative peaks against a high background absorbance of the probe ions. By choosing appropriate sample wavelength (where the sample has minimum absorbance) and reference wavelength (where the probe has maximum absorbance) positive signals can be obtained. Using the capability of the Diode Array Detector (DAD) and with the known knowledge of probe's absorbance, several combinations of the signal (sample wavelength) and reference channels were evaluated. The highest sensitivities (signal-to-noise) ratios were obtained with the signal acquired at 350 nm (bandwidth 80 nm) at a reference wavelength of 200 nm (bandwidth 20 nm).

3.2. Method validation

3.2.1. Specificity
Specificity is the ability of the method to measure the analyte response in the presence of its potential impurities and other interferences. No interferences were observed at the migration times of DMS and CAC in the API samples that were spiked with all other process related impurities and residual solvents. A specimen electropherogram of the DMS and CAC standards is presented in Fig. 2a.

The residual acetic acid, a process related solvent was well separated from DMS (Fig. 2b) in the real time sample analysis of API-1. In API-2, a major peak due to chloride (formed as a byproduct and also introduced from the manufacturing process) was also well resolved from the CAC peak (Fig. 2c). Thus the method was found to be specific for determining DMS and CAC in presence of potential interferences.

3.2.2. Precision
The repeatability and inter-day precision of the method was determined in terms of %RSD for migration times and recoveries of DMS and CAC in the spiked samples. The overall RSD of migration times was not more than 2.2% for DMS and not more than 2.0% for CAC. Similarly the overall RSD of recoveries of DMS and CAC were not more than 6.5% and 6.2% respectively (Table 1).

3.2.3. Sensitivity
The LOD and LOQ were found to be 0.3 μg/mL and 1.0 μg/mL respectively for both DMS and CAC corresponding to 3 ppm and 10 ppm with respect to the sample concentrations. These results emphasize that the method is sensitive enough for determining DMS and CAC at trace levels in real time samples considering the permissible levels of these toxic impurities (Fig. 3).

3.2.4. Linearity and range
The detector response linearity to varying analyte concentrations was established by analyzing standard solutions at nine different concentrations ranging from LOQ to 300% of nominal analyte concentration. Linearity curves (Area vs Conc.) were plotted for DMS and CAC and the data was subjected to regression analysis. Linear relationships confirm that the test results are directly proportional to the concentrations. The linear equation of regression for DMS was $y = 9.9398x - 0.8980$ with a correlation coefficient (R) of 0.9990. Similarly the regression equation for CAC was $y = 15.9874x - 0.9366$ with a correlation coefficient (R) of 0.9992.

The range of a method is the interval in which it has a suitable level of precision, accuracy and linearity. From the results of validation tests that were performed, the range for this method was LOQ to 300% of the nominal analyte concentration.

3.2.5. Accuracy
The accuracy of a method expresses the closeness between the theoretical value and the determined value and was tested in two different ways. The mean recoveries for DMS and CAC at LOQ level were 97.4% and 92.8% respectively. At other concentration levels

Table 1
Precision results.

	DMS (%RSD)		CAC (%RSD)	
	Repeatability[a]	Inter-day precision[b]	Repeatability[a]	Inter-day precision[b]
LOQ	3.8	5.3	2.4	6.2
50%	4.2	6.5	3.7	2.8
100%	2.2	4.2	2.6	3.5
150%	3.7	4.9	4.7	4.1
300%	2.5	3.3	2.9	5.3

[a] $n = 6$ determinations.
[b] $n = 6$ determinations each on three different days.
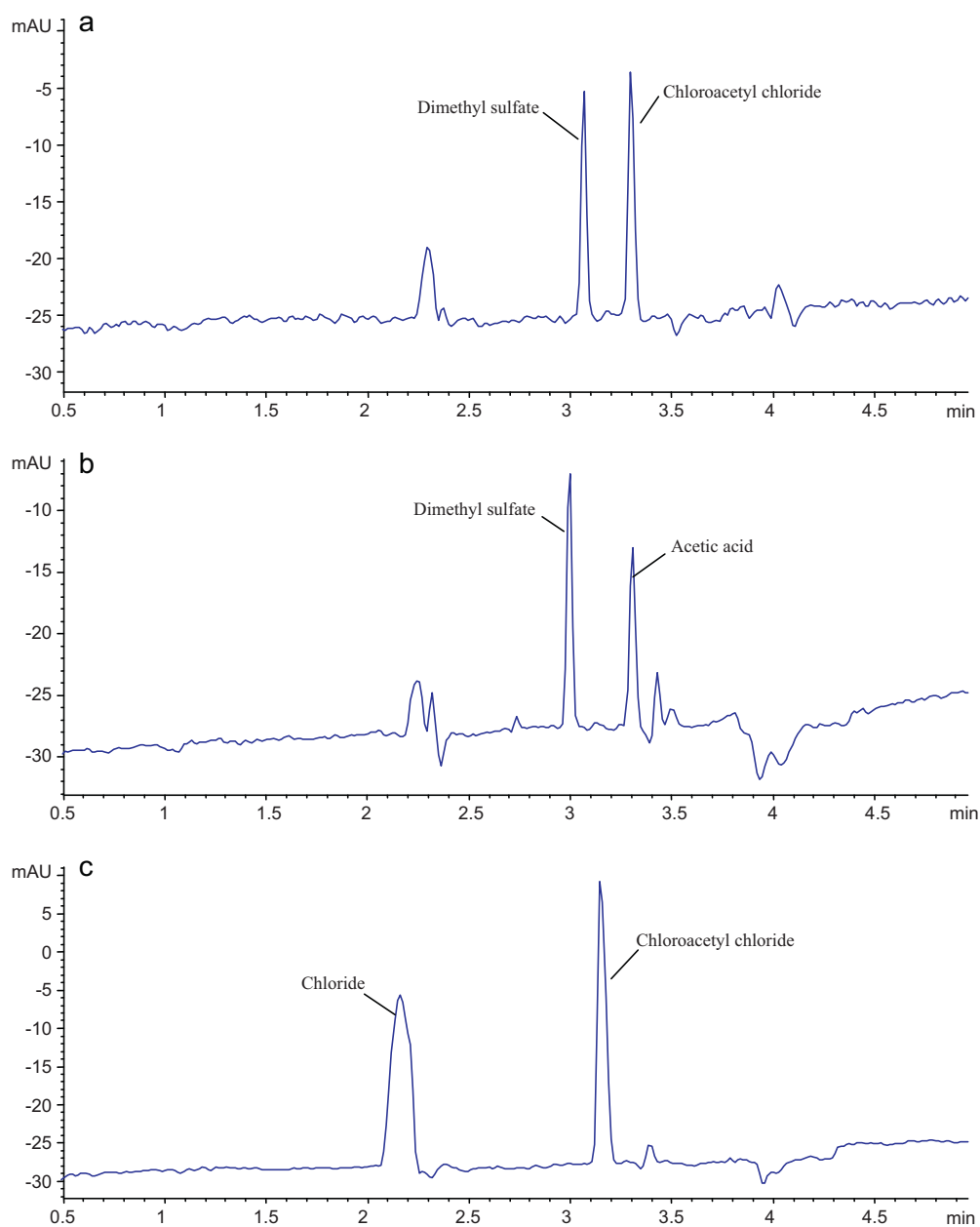
Fig. 2. Specimen electropherograms of (a) DMS and CAC standards, (b) API-1 spiked with dimethylsulfate and (c) API-2 spiked with chloroacetyl chloride.
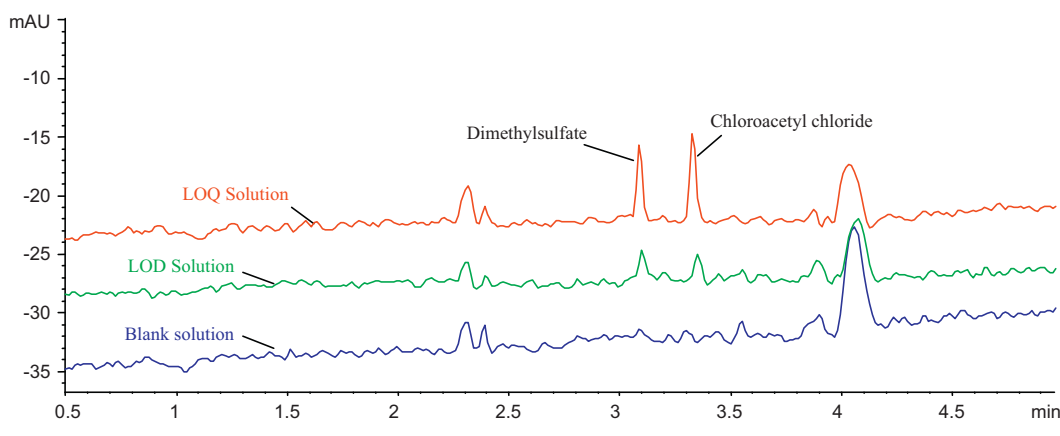

Fig. 3. Overlaid electropherograms of Blank, LOD and LOQ solutions.

Table 2
Accuracy results.

Accuracy level	Dimethyl sulfate spiked to API-1[a]			Chloroacetyl chloride spiked to API-2[a]		
	Amt. spiked (ng)	Amt. recovered (ng)	%Mean recovery ± SD	Amt. spiked (ng)	Amt. recovered (ng)	%Mean recovery ± SD
LOQ	1007.8	981.8	97.4 ± 7.87	981.2	910.9	92.8 ± 2.54
50%	1511.7	1441.1	95.3 ± 7.07	1471.8	1379.9	93.8 ± 2.69
100%	3023.4	2929.2	96.9 ± 6.36	2943.4	2793.4	94.9 ± 3.52
150%	4535.1	4434.3	97.8 ± 2.07	4415.4	4003.0	90.7 ± 1.36
300%	9070.2	8726.8	96.2 ± 3.60	8830.8	8567.4	97.0 ± 1.68

[a] $n = 3$ determinations.

Table 3
Content of DMS in API-1 and CAC in API-2.

Dimethyl sulfate		Chloroacetyl chloride	
Lot # of API-1	DMS content[a] (ppm) (limit = 50 ppm)	Lot # of API-2	CAC content[a] (ppm) (limit = 75 ppm)
001	<10	001	17
002	11	002	ND
003	15	003	ND
004	10	004	13
005	<10	005	ND
006	ND	006	22

ND, not detected.

[a] $n = 3$ determinations.

the recoveries for DMS and CAC ranged between 95.3–97.8% and 90.7–97.0% respectively (Table 2).

The linearity of the method in estimating the recoveries was evaluated by performing a one-way hierarchical analysis of variation (ANOVA) within the range to separate out the systematic variability due to the sample preparation, injection and integration. The recoveries were found to be independent of the spiked concentrations (ANOVA, $p > 0.05$) for both the target analytes. These findings suggest that the described method represents a valuable and accurate tool for the analysis of DMS and CAC in pharmaceutical drug substances.

3.2.6. Stability in analytical solution

No remarkable variations were observed in percentage recoveries of DMS and CAC in the initial samples and samples that were stored at 2–8 °C and at room temperature for 24 and 48 h. Thus the analytes were found to be stable for at least 48 h when stored at either 2–8 °C or at room temperature.

3.2.7. Analysis of real time samples

The developed method was applied for determining DMS in API-1 and CAC in API-2. Six consecutive commercial scale batches of each API were analyzed in triplicate. The results concluded that the content of DMS in API-1 and the content of CAC in API-2 were within the acceptable and safe limits as presented in Table 3.

4. Conclusions

A CE method for determining DMS and CAC, two potentially genotoxic impurities in drug substances by indirect photometric detection was developed and validated. The method is sensitive, offers simplicity and does not include laborious steps of derivatisation as is usually the case for compounds lacking chromophores. The method is very specific, cost effective and eco-friendly; and has been successfully applied for real time sample analyses. This method has been extended for determining other genotoxic impurities such as diethylsulfate and diisopropylsulfate in drug substances, and the validation of this application is under study. Though genotoxins are mostly determined using HPLC–UV/MS and GS–MS techniques for their proven ruggedness and sensitivity, the use of Capillary electrophoresis for estimating genotoxins can complement the existing approach for analysis and also open new horizons.

References

[1] A. Streitwieser, C.H. Heathcock, E.M. Kosower, Introduction to Organic Chemistry, Prentice-Hall Inc., 1992, p. 1169.
[2] IARC monographs, Dimethylsulfate, 71 (1999) 575–588.
[3] J.C.R. Rippey, M.I. Stallwood, Nine cases of accidental exposure to dimethyl sulphate—a potential chemical weapon, Emerg. Med. J. 22 (2005) 878–879.
[4] M.M. Krayushkin, V.N. Yarovenko, S.L. Semenov, I.V. Zavarzin, A.V. Ignatenko, A.Y. Martynkin, B.M. Uzhinov, Synthesis of photochromic 1,2-dihetarylethene using regioselective acylation of thienopyrroles, Org. Lett. 4 (2002) 3879–3881.
[5] G.R. Brown, A.J. Foubister, Unambiguous synthesis of 3-aryloxymethyl- morpholine hydrochlorides without ring enlargement side reactions, J. Chem. Soc., Perkin Trans. 1 (1989) 1401–1403.
[6] ICH Q3A (R), Impurities in New Drug Substances, February 2002, http://www.ICH.org/.
[7] ICH Q3B (R2), Impurities in New Drug Products, July 2006, http://www.ICH.org/.
[8] Guideline on the Limits of Genotoxic Impurities, Committee for Medicinal Products (CHMP), European Medicines Agency, London, 28 June 2006 (CPMP/SWP/5199/02, EMEA/CHMP/QWP/251344/2006).
[9] Guidance for Industry, Genotoxic and Carcinogenic Impurities in Drug Substances and Products: Recommended Approaches, US Department of Health and Human Services, Food and Drug Administration, Centre for Drug Evaluation and Research (CDER), 2008, December.
[10] R. Kroes, A.G. Renwick, M. Cheeseman, J. Kleiner, I. Mangelsdorf, A. Piersma, B. Schilter, J. Sclatter, F. van Schothorst, J.G. Vos, G. Wurtzen, Food Chem. Toxicol. 42 (2004) 65–83.
[11] L. Muller, R.J. Mauthe, C.M. Riley, M.M. Andino, D. de Antonis, C. Beels, J. DeGeorge, A.G.M. De Knaep, D. Ellison, J.A. Fagerland, R. Frank, B. Fritschel, S. Galloway, E. Harpur, C.D.N. Humfrey, A.S. Jacks, N. Jagota, J. Mackinnon, G. Mohan, D.K. Ness, M.R. O'Donovan, M.D. Smith, G. Vudathala, L. Yotti, A rationale for determining, testing, and controlling specific impurities in pharmaceuticals that possess potential for genotoxicity, Regul. Toxicol. Pharmacol. 44 (2006) 198–211.
[12] D.P. Elder, A. Teasdale, A.M. Lipczynski, Control and analysis of alkyl esters of alkyl and aryl sulfonic acids in novel active pharmaceutical ingredients (APIs), J. Pharm. Biomed. Anal. 46 (2008) 1–8.
[13] K.L. Dobo, N. Greene, M.O. Cyr, S. Caron, W.W. Ku, The application of structure-based assessment to support safety and chemistry diligence to manage genotoxic impurities in active pharmaceutical ingredients during drug development, Regul. Toxicol. Pharmacol. 44 (2006) 282–293.
[14] D.J. Snodin, Genotoxic impurities: from structural alerts to qualification, Org. Process Res. Dev. 14 (2010) 960–976.
[15] Q. Yang, B.P. Haney, A. Vaux, D.A. Riley, L. Heidrich, P. He, P. Mason, A. Tehim, L.E. Fisher, H. Maag, N.G. Anderson, Controlling the genotoxins ethyl chloride and methyl chloride formed during the preparation of amine hydrochloride salts from solutions of ethanol and methanol, Org. Process Res. Dev. 13 (2009) 786–791.
[16] D.P. Elder, A.M. Lipczynski, A. Teasdale, Control and analysis of alkyl and benzyl halides and other related reactive organohalides as potential genotoxic impurities in active pharmaceutical ingredients (APIs), J. Pharm. Biomed. Anal. 48 (2008) 497–507.
[17] D.P. Elder, D. Snodin, A. Teasdale, Analytical approaches for the detection of epoxides and hydroperoxides in active pharmaceutical ingredients, drug products and herbals, J. Pharm. Biomed. Anal. 51 (2010) 1015–1023.

[18] R. Alzaga, R.W. Ryan, K. Taylor-Worth, A.M. Lipczynski, R. Szucs, P. Sandra, A generic approach for the determination of residues of alkylating agents in active pharmaceutical ingredients by *in situ* derivatization–headspace-gas chromatography–mass spectrometry, J. Pharm. Biomed. Anal. 45 (2007) 472–479.

[19] J. Zheng, W.A. Pritts, S. Zhang, S. Wittenberger, Determination of low ppm levels of dimethyl sulfate in an aqueous soluble API intermediate using liquid–liquid extraction and GC–MS, J. Pharm. Biomed. Anal. 50 (2009) 1054–1059.

[20] G.F. Deng, T.W. Yao, Determination of dimethyl sulphate residual in granisetron hydrochloride by headspace gas chromatography, Zhejiang Da Xue Xue Bao Yi Xue Ban 37 (2008) 156–158.

[21] S.H. Hansen, Z.A. Sheribah, Comparison of CZE, MEKC, MEEKC and non-aqueous capillary electrophoresis for the determination of impurities in bromazepam, J. Pharm. Biomed. Anal. 39 (2005) 322–327.

[22] ICH Q2R1, Validation of Analytical Procedures: Text and Methodology, 1995, June, http://www.ICH.org/.

[23] B.H. Mathison, M.L. Taylor, M.S. Bogdanffy, Dimethyl sulfate uptake and methylation of DNA in rat respiratory tissues following acute inhalation, Fundam. Appl. Toxicol. 28 (1995) 255–263.

[24] F. Foret, L. Krivánková, P. Bocek, Capillary Zone Electrophoresis, VCH Publishers, New York, 1993, pp. 27–35.

[25] P. Doble, M. Macka, P.R. Haddad, Design of background electrolytes for indirect detection of anions by capillary electrophoresis, Trends Analyt. Chem. 19 (2000) 10–17.

[26] M. Macka, C. Johns, P. Doble, P.R. Haddad, K.D. Altria, Indirect photometric detection in CE using buffered electrolytes. Part I. Principles, LCGC 19 (January) (2001), www.chromatographyonline.com.

[27] X. Xu, Th.W. Kok, H. Poppe, Noise and baseline disturbances in indirect UV detection in capillary electrophoresis, J. Chromatogr. A 786 (1997) 333–345.

Characterization by high-performance liquid chromatography with diode-array detection coupled to time-of-flight mass spectrometry of the phenolic fraction in a cranberry syrup used to prevent urinary tract diseases, together with a study of its antibacterial activity

Ihsan Iswaldi [a,b], Ana María Gómez-Caravaca [a], David Arráez-Román [a,b], José Uberos [c], Marita Lardón [c], Antonio Segura-Carretero [a,b,*], Alberto Fernández-Gutiérrez [a,b]

[a] Department of Analytical Chemistry, Faculty of Sciences, University of Granada, Avenida Fuentenueva s/n, 18071 Granada, Spain
[b] Research and Development Functional Food Centre (CIDAF), Health Science Technological Park, Avenida del Conocimiento 3, 18100 Granada, Spain
[c] UGC Pediatría, Hospital Clínico San Cecilio Granada, 18012 Granada, Spain

ARTICLE INFO

ABSTRACT

The phenolic fraction of a commercial cranberry syrup, which is purported to have good properties for the prevention of urinary diseases, has been thoroughly characterized using HPLC-DAD–TOF-MS. A study of its antibacterial activity has also been carried out. For this purpose a new HPLC-DAD–TOF-MS method using negative and positive ionization modes was developed and it was thus possible to identify 34 different compounds, nine of which have been tentatively characterized for the first time in cranberry syrup. It is also important to highlight that different coumarins in this matrix were also determined, which, to our knowledge, have not been found previously in the cranberry. The phenolic fraction obtained by HPLC-DAD was found to be 5.47 mg/mL. Catechin and procyanidins belonging to flavanols were the family of compounds found at the highest concentrations (2.37 mg/mL); flavonols were at a concentration of 1.91 mg/mL and phenolic-acid derivatives were found at the lowest concentration (0.15 mg/mL). With regard to antibacterial activity, the incubation of *Escherichia coli* with cranberry syrup was found to reduce surface hydrophobicity as a function of the concentration of the extract.

© 2011 Elsevier B.V. All rights reserved.

1. Introduction

In recent years there has been ever increasing interest in the presence of certain compounds in foods that are beneficial to human health. In plant-derived foods these naturally occurring compounds form part of the secondary metabolism of many kinds of fruit and vegetable products and are known as phytochemicals. The antioxidant capacity of phytochemicals, as well as their health-promoting and/or disease-preventing properties, are currently the subject of intense study by the scientific community.

Berries, including raspberries, blueberries, black currants, red currants, and cranberries, are a rich source of these dietary antioxidants [1]. The American cranberry (*Vaccinium macrocarpon*) in particular is a rich source of bioactive compounds with antiproliferative, antioxidant [2], anti-inflammatory and antimicrobial properties, which inhibit the growth of pathogenic bacteria such as *Escherichia coli* and *Helicobacter pylori* for example [3,4]. It has traditionally been used in the treatment and prevention of urinary-tract infections in women and also in digestive-tract ailments. The antitumoral properties of cranberries have made them a popular diet component with an eye to the prevention of neoplastic diseases [5]. The phenolic compounds found in cranberries are believed to be the principal ingredients responsible for these beneficial effects. Cranberries are known for their high concentration of anthocyanins, as well as their significant contents of flavonols, flavan-3-ols, tannins (ellagitannins and proanthocyanidins) and phenolic-acid derivatives [6].

One out of two women experience some sort of urinary tract disorder during their lifetime, which often reoccurs. As has been observed, the consumption of cranberries has a significant influence on lowering the incidence of urinary diseases [7,8]. Nowadays therefore, some dietary supplements containing cranberry extracts are being developed.

The aim of this work was to characterize the phenolic fraction contained in cranberry syrup, made up of glucose, sodium benzoate, potassium sorbate and American cranberry (*V. macrocarpon*),

using HPLC-DAD–TOF-MS, and also to study its antibacterial activity. This study is a preliminary step in our thorough research into the composition of cranberry syrup. The syrup will be then be used for *in vivo* analyses to study the metabolites of these phenolic compounds in urine and evaluate the incidence of urinary disorders in its consumers.

2. Materials and methods

2.1. Materials

Standards of myricetin, *p*-coumaric acid, 7-hydroxycoumarin, and proanthocyanidin A2 were from Extrasynthese (Genay, France). Folin-Ciocalteu phenol reagent was from Fluka, Sigma–Aldrich (Steinheim, Germany). Formic acid and acetonitrile used for preparing mobile phases were from Fluka, Sigma–Aldrich (Steinheim, Germany) and Lab-Scan (Gliwice, Sowinskiego, Poland) respectively. Distilled water with a resistance of 18.2 MΩ was deionized in a Milli-Q system (Millipore, Bedford, MA, USA). Solvents were filtered before use with a Solvent Filtration Apparatus 58061 (Supelco, Bellefonte, PA, USA).

2.2. Sample preparation

200 μL of cranberry syrup, bought in a local pharmacy, was dissolved in 4 mL methanol, vortexed for 2 min in a G560E Vortex-Genie 2 (Scientific Industries, Bohemia, NY, USA), filtered with a polytetrafluoroethylene (PTFE) syringe filter (0.2 μm pore size) and injected directly into the HPLC system.

2.3. Measurement of total polyphenols, proanthocyanidins and anthocyanins

To quantify the total phenolic content in cranberry syrup, the Folin-Ciocalteu method was used [9]. The proanthocyanidin (condensed tannins) and total anthocyanin contents were determined according to the vanillin–HCl method [10] and the methods described by Fuleki and Francis respectively [11].

2.4. Chromatographic separation

HPLC analyses were made with an Agilent 1200 series rapid-resolution LC system (Agilent Technologies, Palo Alto, CA, USA) equipped with a binary pump, an autosampler and a diode-array detector (DAD). Separation was carried out with a Zorbax Eclipse Plus C_{18} analytical column (150 mm × 4.6 mm, 1.8 μm particle size). Gradient elution was conducted using two different programs. Gradient program 1 was used for the MS negative ionization mode consisting of 1% formic acid in water–acetonitrile (90:10, v/v) (phase A) and acetonitrile (phase B) at a constant flow rate of 0.5 mL/min using the following gradient: 0–20 min, linear gradient from 5% B to 20% B; 20–25 min, linear gradient from 20% B to 40% B; 25–30 min, linear gradient from 40% B to 5% B; and 30–35 min, isocratic of 5% B. Subsequently a different chromatographic method (gradient program 2) was used for the MS positive ionization mode. Due to their acid–base equilibrium, anthocyanins need a more acidic pH to be resolved and so the gradient was

modified as follows: water–formic acid (90:10, v/v) (phase A) and acetonitrile (phase B) at a constant flow rate of 0.5 mL/min using the following gradient: 0–13 min, linear gradient from 0% B to 20% B; 13–20 min, linear gradient from 20% B to 30% B; 20–25 min, linear gradient from 30% B to 80% B; 25–30 min, linear gradient from 80% B to 0% B; and 30–35 min, isocratic of 0% B. The addition of formic acid gave better results for the ionization of the compounds in positive mode. The injection volume was 10 μL for both gradient elution programs. The two different methods were chosen as they both afforded short analysis times and good chromatographic separations. UV data were collected using DAD set at 280, 320, 360, and 520 nm.

2.5. ESI-TOF-MS conditions

TOF-MS was conducted using a microTOF™ (Bruker Daltonics, Bremen, Germany) orthogonal-accelerated TOF mass spectrometer equipped with an electrospray ionization (ESI) interface. The parameters for analysis were set using both negative and positive ion modes with spectra acquired over a mass range of 50–1000 *m*/*z*. The other optimum values of the ESI-MS parameters were: capillary voltage, 4500 V; dry gas temperature, 190 °C; dry gas flow, 9.0 L/min; nebulizer pressure, 2.0 bar; and spectra rate 1 Hz. The flow delivered into the MS detector from HPLC was split using a flow splitter (1:2) to achieve stable electrospray ionization and obtain reproducible results. The calibrant was a sodium-formate cluster containing 5 mM sodium hydroxide and 0.2% formic acid in water–isopropanol (1:1, v/v), injected at the beginning of each run with a 74900-00-05 Cole Palmer syringe pump (Vernon Hills, IL, USA) directly connected to the interface. All the spectra were calibrated prior to compound identification. All operations were controlled by DataAnalysis 3.4 software (Bruker Daltonik), which provided a list of possible elemental formulas by using the GenerateMolecularFormula™ Editor.

2.6. Assessment of the method

Quantification was made according to the linear calibration curves of standard compounds. Four calibration curves were prepared using the following standards: myricetin, *p*-coumaric acid, 7-hydroxycoumarin and procyanidin A2. The different parameters of each standard compound are summarized in Table 1. All calibration curves show good linearity between different concentrations depending upon the analytes in question. The calibration plots reveal good correlation between peak areas and analyte concentrations, and the regression coefficients were always higher than 0.995. LOD was found to be within the range 0.053–0.233 μg/mL whilst LOQ was within 0.175–0.679 μg/mL.

Intraday and interday precisions were developed to assess the repeatability of the method. A syrup extract was injected (*n* = 6) during the same day (intraday precision) for 3 consecutive days (interday precision, *n* = 18). The relative standard deviations (RSDs) of analysis time and peak area were determined. The intraday repeatability of the peak area, expressed by the RSD, was 1.2%, whereas interday repeatability was 3.8%.

The accuracy of the assay can be determined by the closeness of the test value to the nominal value and was evaluated with

Table 1
Analytical parameters of the method.

Analyte	RSD	LOD (μg/mL)	LOQ (μg/mL)	Calibration range (μg/mL)	Calibration equations	r^2	Accuracy
Myricetin	0.23	0.053	0.175	LOQ-25	$y = 22.852x + 21.117$	0.996	98.7
p-Coumaric acid	0.31	0.204	0.679	LOQ-250	$y = 127.13x + 7.2384$	0.999	99.2
Procyanidin A2	0.36	0.152	0.287	LOQ-100	$y = 5.8648x + 3.8544$	0.997	101.3
7-Hydroxycoumarin	0.27	0.233	0.656	LOQ-50	$y = 37.724x + 12.555$	0.998	100.8

separately prepared individual primary stock solutions, mixtures and working solutions of all standards. It was calculated over the linear dynamic range at three concentration levels: low (LOQ), medium (intermediate concentration value of the linear calibration range), high (highest concentration value of the linear calibration range) via three assays per concentration on different days. The analyte concentrations were calculated from calibration curves and accuracy was calculated by the ratio of this calculated concentration versus the theoretical (spiked) one.

2.7. Bacteria and cultures

Nine strains of uropathogenic *E. coli* (695, 787, 471, 472, 593, 595, 760, 629 and 607) were obtained from patients with acute pyelonephritis, together with 4 strains of *E. coli* from the Spanish Type Culture Collection (CECT): CECT 424 (F- thr- leu- lacY mtl- thi- ara gal ton 2 malA xyl, resistant to phages T1, T2 and T6.); CECT 4076 (Serovar. O157:H7, originally isolated from haemor-rhagic colitis); CECT 417 (SupE44[am]. mutant tRNA); and CECT 743 (Serovar. O142 K86B:H6, isolated from children with diarrhoea). To enhance the activity of the Type 1 fimbriae [12] the strains were grown in TSB culture medium at 37 °C for 48 h and then centrifuged at 2000 × g for 10 min. The supernatant was then discarded, and the strains resuspended in PBS (pH 7.4). This washing process was performed twice. Finally, the bacterial suspension was adjusted to 10^9 bacteria/mL (OD of 1.0–542 nm). To enhance the activity of the P type fimbriae, the strains were incubated for 16 h on CFA agar [13], extracted from the surface of the agar after washing with 5 mL PBS, and then centrifuged at 2000 × g for 10 min.

2.8. Ammonium sulphate aggregation test

The technique used was that described by Lindahl et al. [14]. Briefly, solutions of ammonium sulphate were prepared, with osmolarities ranging from 0.2 M to 4 M, using sodium phosphate as dilutant. Taking 20 μL of bacterial suspension, an equal volume of ammonium sulphate solution was added and then gently mixed. The presence of aggregation was observed after 30 s gentle manual rotation at room temperature over a glass slide, and the lowest concentration of ammonium sulphate that produced visible aggregation was noted. Aggregation with the 4 M solution was interpreted as a hydrophobicity of 0%, whilst aggregation with the 0.2 M solution was interpreted as 95% hydrophobicity.

3. Results and discussion

3.1. Chromatographic profile and compound identification

The base-peak chromatograms (BPC) of a cranberry syrup, obtained using both negative and positive ionization modes, are set out in Fig. 1(a) and (b). The tentatively identified phenolic compounds are summarized in Tables 2 and 3 (negative and positive ionization modes respectively), including retention times, experimental and calculated m/z, molecular formula, error, sigma values (comparison of theoretical with measured isotope patterns), together with their proposed identities.

Phenolic compounds were successfully separated and identi-fied with a gradient optimized for negative and positive ionization modes. The compounds were identified by interpreting their mass spectra obtained via TOF-MS, taking into account all the data reported in the literature. All these facts were also complemented with the UV spectra provided by DAD, which gave additional information about the family of compounds as far as the absorbance bands are concerned.

3.2. Compounds identified in negative ionization mode

Twenty-seven phenolic compounds were identified in negative ionization mode, including 6 new proposed compounds reported for the first time in the American cranberry (*V. macrocarpon*). Table 2 and Fig 1(a) show the base-peak chromatogram (BPC) in negative mode of an extract of cranberry syrup.

3.2.1. Phenolic-acid derivatives

The first group of peaks migrated between 4.85 and 8.92 min and the compounds were related to the phenolic-acid family. Peak 1 (RT 4.85 min) gave a molecular mass of m/z 325.0929, which was tentatively identified as coumaroyl-hexose according to the molec-ular formula provided for its mass and corroborated by its fragment ion at m/z 163.0406, corresponding to a loss of the sugar moiety (162 Da) [6]. Peak 2 (RT 6.19 min), which showed an ion at m/z 385.1127, gave a fragment at m/z 223.0596, corresponding to a loss of sugar moiety; thus, it was identified as sinapoyl-hexose [15]. The ion at RT 6.44 min corresponds to caffeoyl glucose with the precursor and fragment ions at m/z 341.0888 and 179.0351 respec-tively, indicating the loss of a sugar moiety. Peak 4 (RT 6.89 min) was assigned to chlorogenic acid [16], showing a fragment at m/z 191.0558, corresponding to the quinic-acid moiety previously reported. The presence of another isomeric form of coumaroyl-hexose was tentatively identified in peak 5 (RT 7.16 min). Peak 7 (RT 8.92 min) was tentatively identified as canthoside A [17], this apparently being the first time that this compound has been found in the cranberry.

3.2.2. Flavonoids

The HPLC-DAD–TOF-MS analysis of the cranberry syrup extract revealed a total of 20 flavonoids (summarized in Table 2). For most flavonoids, the negative ionization mode provided the high-est sensitivity and selectivity [18]. The following flavonols already found in cranberry were confirmed in our sample: myricetin 3-O-hexose (peak 9) [19,20], myricetin 3-O-arabinoside (peak 14) [21], quercetin 3-O-hexose (peak 16) [19], quercetin 3-O-xylopyranoside (peak 18) [19], quercetin 3-O-arabinopyranoside (peak 19) [19,21], quercetin 3-O-arabinofuranoside (peak 20) [19,21], quercetin 3-O-rhamnoside (peak 21) [20,21], myricetin (peak 22) [21], methoxyquercetin 3-O-galactoside (peak 23) [19] and quercetin (peak 27) [16,21]. As can be see in Table 2, quercetin and derivates with sugar bonds gave the fragment ion at m/z 301, corresponding to the loss of a sugar moiety.

Three different isomers of A-type procyanidin were identified in cranberry syrup at times 13.35, 14.28, 16.94 min with a m/z of 575.12 (peaks 11, 13 and 17), showing a typical fragment at m/z 423. Two B-type procyanidin isomers with a m/z of 577.13 eluted at 8.00 and 14.15 min (peaks 6 and 12) and their fragments at 425 and 289 were also detected [22]. Peak 8, with a m/z of 289.0714 and a retention time of 9.65 min, was identified as (+)-catechin.

Dihydroferulic acid 4-O-β-D-glucuronide (peak 10), cavi-unin glucoside (peak 15), biochanin A-7-O-glucoside (peak 24), prodelphinidin B4 (peak 25) and kaempferol 3-O-β-D-(6″-p-hydroxybenzoyl)-galactopyranoside (peak 26) were identified using mass spectra, UV spectra and the information provided by the GenerateMolecularFormula^TM Editor. As far as we know, this is the first time that these compounds have been reported in the cranberry.

Dihydroferulic acid 4-O-β-D-glucuronide at m/z 371.0989 pre-sented a fragment at a m/z of 175.0283, which corresponds to the glucuronide moiety after the fragmentation of the dihydroferulic acid. Cavinium glucoside at m/z 535.1482 showed a fragment at m/z 373.0907, indicating the loss of the sugar moiety. Fig. 2 shows the structures of the newly identified compounds in cranberry syrup. Additional unidentified compounds have been included in Table 2
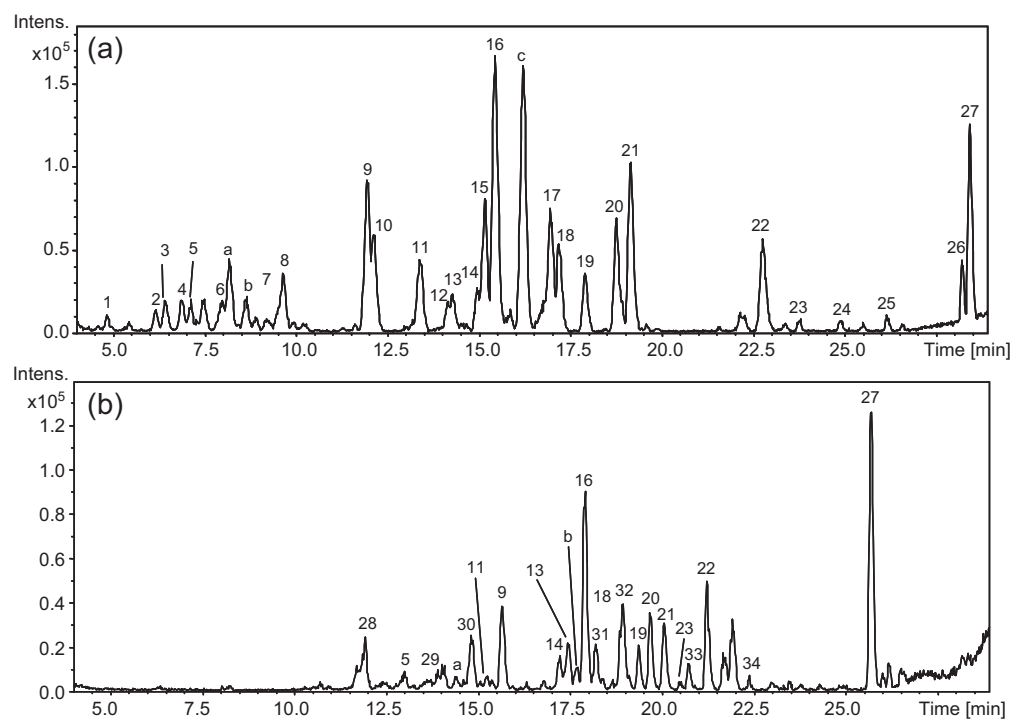
Fig. 1. Chromatographic profiles using the gradient programs: (a) base peak chromatogram (BPC) for the gradient program 1, negative ionization mode; (b) base peak chromatogram (BPC) for the gradient program 2, positive ionization mode.

Table 2
Phenolic compounds in cranberry syrup characterized by HPLC-DAD–TOF-MS in negative ionization mode.

Peak number	Class/phenolic compounds	RT (min)	Selected ion	m/z experimental	m/z calculated	Fragments	Error (ppm)	Sigma	Molecular formula
	Phenolic acid derivatives								
1	Coumaroyl-hexose	4.85	[M−H]$^-$	325.0929	325.0929	163.0406	0.0	0.0213	$C_{15}H_{18}O_8$
2	Sinapoyl-hexose	6.19	[M−H]$^-$	385.1127	385.1140	223.0596	3.3	0.0176	$C_{17}H_{22}O_{10}$
3	Caffeoyl glucose	6.44	[M−H]$^-$	341.0888	341.0878	179.0351	2.9	0.0107	$C_{15}H_{18}O_9$
4	Chlorogenic acid	6.89	[M−H]$^-$	353.0867	353.0878	191.0558	3.0	0.0561	$C_{16}H_{18}O_9$
5	Coumaroyl-hexose	7.16	[M−H]$^-$	325.0918	325.0929	163.0398	3.4	0.0298	$C_{15}H_{18}O_8$
7	Canthoside A	8.92	[M−H]$^-$	445.1355	445.1351		0.8	0.0238	$C_{19}H_{26}O_{12}$
	Flavonols								
9	Myricetin 3-O-hexose	11.94	[M−H]$^-$	479.0835	479.0831	317.0301	0.8	0.0204	$C_{21}H_{20}O_{13}$
10	Dihydroferulic acid 4-O-β-D-glucuronide	12.16	[M−H]$^-$	371.0989	371.0984	175.0283	1.5	0.0131	$C_{16}H_{20}O_{10}$
14	Myricetin 3-O-arabinoside	14.94	[M−H]$^-$	449.0739	449.0725	317.0286	2.9	0.0217	$C_{20}H_{18}O_{12}$
15	Caviunin glucoside	15.15	[M−H]$^-$	535.1482	535.1457	373.0907	4.7	0.0109	$C_{25}H_{28}O_{13}$
16	Quercetin 3-O-hexose	15.44	[M−H]$^-$	463.0894	463.0882	301.0293	2.5	0.0107	$C_{21}H_{20}O_{12}$
18	Quercetin 3-O-xylopyranoside	17.14	[M−H]$^-$	433.0784	433.0776	301.0350	1.9	0.0113	$C_{20}H_{18}O_{11}$
19	Quercetin 3-O-arabinopyranoside	17.88	[M−H]$^-$	433.0797	433.0776	301.0302	4.8	0.0238	$C_{20}H_{18}O_{11}$
20	Quercetin 3-O-arabinofuranoside	18.75	[M−H]$^-$	433.0781	433.0776	301.0332	1.0	0.0132	$C_{20}H_{18}O_{11}$
21	Quercetin 3-O-rhamnoside	19.13	[M−H]$^-$	447.0937	447.0933	301.0325	0.9	0.0021	$C_{21}H_{20}O_{11}$
22	Myricetin	22.73	[M−H]$^-$	317.0292	317.0303		3.6	0.0178	$C_{15}H_{10}O_8$
23	Methoxyquercetin 3-O-galactoside	23.75	[M−H]$^-$	477.1033	477.1038		1.2	0.0271	$C_{22}H_{22}O_{12}$
26	Kaempferol 3-O-β-D-(6''-p-hydroxybenzoyl)-galactopyranoside	28.15	[M−H]$^-$	567.1143	567.1144		0.2	0.0104	$C_{28}H_{24}O_{13}$
27	Quercetin	28.36	[M−H]$^-$	301.0337	301.0354		5.5	0.0196	$C_{15}H_{10}O_7$
	Flavanols								
6	Procyanidin B type isomer 1	8.00	[M−H]$^-$	577.1328	577.1351	289.0687	4.1	0.0405	$C_{30}H_{26}O_{12}$
8	(+)-Catechin	9.65	[M−H]$^-$	289.0714	289.0718		1.3	0.0033	$C_{15}H_{14}O_6$
11	Proacyanidin A2 type isomer 1	13.35	[M−H]$^-$	575.1211	575.1195	423.0631	3.0	0.0156	$C_{30}H_{24}O_{12}$
12	Procyanidin B type isomer 2	14.15	[M−H]$^-$	577.1306	577.1351	425.0761	5.5	0.0263	$C_{30}H_{26}O_{12}$
13	Proacyanidin A2 type isomer 2	14.28	[M−H]$^-$	575.1216	575.1195	423.0631	3.7	0.0476	$C_{30}H_{24}O_{12}$
17	Procyanidin A2 type isomer 3	16.94	[M−H]$^-$	575.1218	575.1195	423.0733	4.0	0.0290	$C_{30}H_{24}O_{12}$
25	Prodelphinidin B4	26.11	[M−H]$^-$	609.1238	609.1250		1.9	0.0355	$C_{30}H_{26}O_{14}$
	Isoflavonoids								
24	Biochanin A-7-O-glucoside	24.82	[M−H]$^-$	445.1156	445.1140		3.5	0.0284	$C_{22}H_{22}O_{10}$
	Unknown compounds								
a		8.20	[M−H]$^-$	431.1554	431.1559		1.1	0.0138	$C_{19}H_{28}O_{11}$
b		8.67	[M−H]$^-$	431.1923	431.1923		0.1	0.0247	$C_{20}H_{32}O_{10}$
c		16.19	[M−H]$^-$	537.1641	537.1614		5.2	0.0109	$C_{25}H_{30}O_{13}$

Table 3
Phenolic compounds in cranberry syrup characterized by HPLC-DAD–TOF-MS in positive ionization mode.

| Peak number	Class/phenolic compounds	RT (min)	Selected ion	m/z experimental	m/z calculated	Fragments	Error (ppm)	Sigma	Molecular formula
	Phenolic acid derivatives								
5	Coumaroyl-hexose	13.01	[M+K]$^+$	365.0575	365.0633	203.0028	15	0.0225	$C_{15}H_{18}O_8$
29	2-Hydroxybenzoic acid	13.90	[M+H]$^+$	139.0401	139.0390		7.8	0.0113	$C_7H_6O_3$
30	Digallic acid	14.82	[M+H]$^+$	323.0438	323.0398	140.9858	12.4	0.0131	$C_{14}H_{10}O_9$
	Flavonols								
9	Myricetin 3-O-hexose	15.66	[M+H]$^+$	481.0973	481.0977	319.0446	0.9	0.0293	$C_{21}H_{20}O_{13}$
14	Mryicetin 3-O-arabinoside	17.19	[M+H]$^+$	451.0872	451.0871	319.0439	0.2	0.0352	$C_{20}H_{18}O_{12}$
16	Quercetin 3-O-hexose	17.91	[M+H]$^+$	465.1023	465.1028	303.0491	1.0	0.0294	$C_{21}H_{20}O_{12}$
18	Quercetin 3-O-xylopiranoside	18.85	[M+H]$^+$	435.0933	435.0922	303. 0485	2.5	0.0351	$C_{20}H_{18}O_{11}$
19	Quercetin 3-O-arabinopyranoside	19.33	[M+H]$^+$	435.0936	435.0922	303.0509	3.4	0.0440	$C_{21}H_{18}O_{11}$
20	Quercetin 3-O-arabinofuranoside	19.67	[M+H]$^+$	435.0934	435.0922	303.0494	2.7	0.0355	$C_{20}H_{18}O_{11}$
21	Quercetin 3-O-rhamnoside	20.04	[M+H]$^+$	449.1063	449.1078	303.0495	3.4	0.0340	$C_{21}H_{20}O_{11}$
23	Methoxyquercetin 3-O-galactoside	20.45	[M+H]$^+$	479.1191	479.1184	317.0663	2.1	0.0773	$C_{22}H_{22}O_{12}$
33	Syringetin (3′,5′-O-Dimethylmyricetin)	20.69	[M+H]$^+$	347.0765	347.0761		1.1	0.0214	$C_{17}H_{14}O_8$
22	Myricetin	21.19	[M+H]$^+$	319.0445	319.0448		1.2	0.0123	$C_{15}H_{10}O_8$
27	Quercetin	25.66	[M+H]$^+$	303.0500	303.0499		0.2	0.0078	$C_{15}H_{10}O_7$
	Flavanols								
11	Procyanidin A2-type isomer 1	15.20	[M+H]$^+$	577.1342	577.1341	425.0875/287.0542	0.2	0.0713	$C_{30}H_{24}O_{12}$
13	Procyanidin A2-type isomer 2	17.41	[M+H]$^+$	577.1336	577.1341	425.0858/287.0532	0.9	0.0127	$C_{30}H_{24}O_{12}$
	Coumarins								
28	7-Hydroxycoumarin	11.94	[M+H]$^+$	163.0395	163.0390		3.1	0.0168	$C_9H_6O_3$
31	Coumarin	18.21	[M+H]$^+$	147.0447	147.0441		4.6	0.0058	$C_9H_6O_2$
32	Scopoletin	18.90	[M+H]$^+$	193.0415	193.0417	177.0538/147.0446	0.4	0.0271	$C_{10}H_8O_4$
	Anthocyanin								
34	Petunidin	22.34	[M+H]$^+$	317.0629	317.0656		8.5	0.0252	$C_{16}H_{14}O_7$
	Unknown compounds								
a		14.37	[M+H]$^+$	441.1104	441.1086		4.1	0.0258	$C_{30}H_{16}O_4$
b		17.68	[M+H]$^+$	397.1375	397.1341		8.7	0.0248	$C_{15}H_{24}O_{12}$
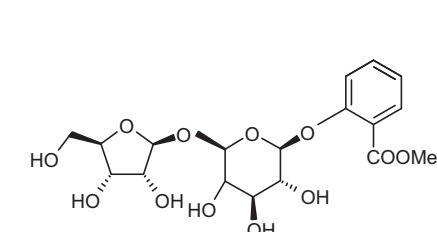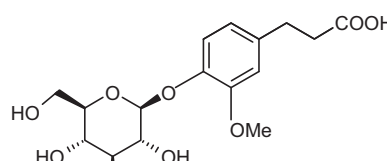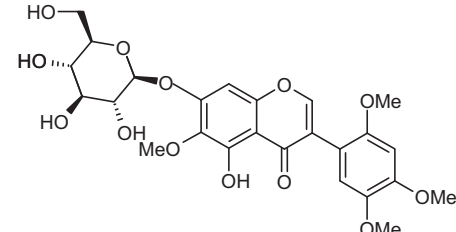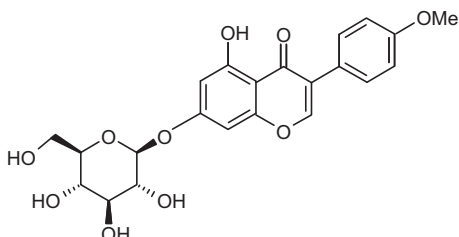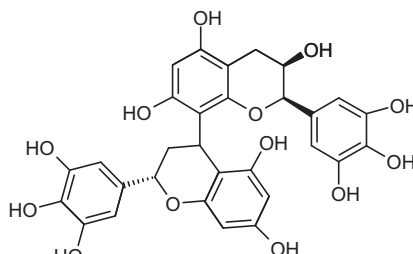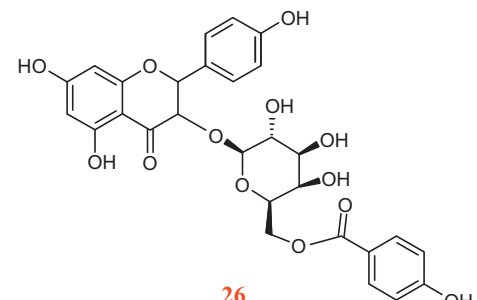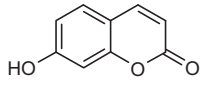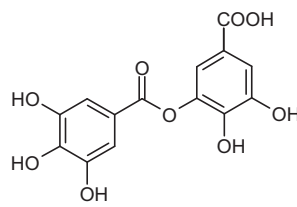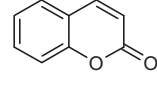
Fig. 2. Structures of new compounds identified in cranberry syrup, (7) canthoside A, (10) dihydroferulic acid 4-O-β-D-glucuronide, (15) caviunin glucoside, (24) biochanin A-7-O-glucoside, (25) prodelphinidin B4, (26) kaempferol 3-O-β-D-(6″-p-hydroxybenzoyl)-galactopyranoside, (28) 7-hydroxycoumarin, (30) digallic acid, and (31) coumarin.

as they form an important part of the polar fraction of cranberry syrup.

3.3. Compounds identified in positive ionization mode

The presence of anthocyanins in cranberries has been reported in the literature, and since anthocyanins have maximum sensitivity in positive mode due to their inherent positive charge [18] the extract was also characterized in positive ionization mode. Fig. 1(b) shows the BPC of an extract of cranberry syrup in positive ionization mode. Thus, by using the proposed method 20 phenolic compounds were identified in positive ionization mode in the cranberry-syrup extract. Despite the fact that several anthocyanidins have been previously described in the cranberry, only petunidin (peak 34) [23] has so far been identified in the syrup.

In addition, several phenolic acids, flavonols, flavanols and hydroxycoumarins were identified in positive ionization mode. It is important to note that some of them were also found in the analysis carried out in negative ionization mode, but most of them could only be identified thanks to this positive ionization mode.

Thus, the phenolic acids identified were: coumaroyl-hexose (peak 5), which had also been identified in the negative mode; 2-hydroxybenzoic acid (peak 29) [24], which presented a m/z of 139.0401 and digallic acid (peak 30) at m/z 323.0438, which showed a fragment at m/z 141, corresponding to the loss of a gallate moiety, thus corroborating its identification [25].

Several flavanols that had already been identified in the negative ionization mode were also detected and identified: myricetin 3-O-hexose (peak 9), myricetin 3-O-arabinoside (peak 14), quercetin 3-O-hexose (peak 16), quercetin 3-O-xylopiranoside (peak 18), quercetin 3-O-arabinopiranoside (peak 19), quercetin 3-O-arabinofuranoside (peak 20), quercetin 3-O-rhamnoside (peak 21), methoxyquercetin 3-O-galactoside (peak 23); myricetin (peak 22) and quercetin (peak 27). Furthermore, syringetin (peak 33), a flavonoid that could not be detected in negative ionization mode, was also identified. All the quercetin and myricetin-sugar conjugates showed a fragment ion at m/z 303 and 319 respectively, corresponding to the aglycone of quercetin and myricetin. Moreover, two isomers of Type A procyanidin (peaks 11 and 13 respectively) were also detected in positive ionization mode.

Finally, several coumarins were tentatively identified only in positive ionization mode. Peak 28 presented a m/z of 163.0395 and was assigned to 7-hydroxycoumarin, as reported in the bibliography [26]. Peak 31, with a m/z of 147.0447, was tentatively identified as coumarin. Another coumarin, at m/z 193.0415 and showing fragments at m/z 177 and 147, was identified as scopoletin, according to Chen et al. [27]. As far as we know, this is the first time that 7-hydroxycoumarin and coumarin have been identified in the cranberry (Fig. 2) by using HPLC-DAD–TOF-MS in the same run.

3.4. Quantification

Quantification was done using the calibration curves shown in Table 1. The calibration curve of myricetin at $\lambda = 280$ nm was used to quantify flavonols, whilst phenolic-acid derivatives were quantified with the calibration curve of p-coumaric acid at $\lambda = 280$ nm. Flavanols were quantified using the curve of procyanidin A2 at $\lambda = 280$ nm and coumarins with the calibration curve of 7-hydroxycoumarin at $\lambda = 280$ nm. The concentrations of the phenolic compounds identified in cranberry syrup are summarized in Table 4. Thus, the overall phenolic content obtained by HPLC-DAD was found to be 5.47 mg/mL. The family of flavanols (catechin and procyanidins) was found at the highest concentration (2.37 mg/mL)

Table 4
Phenolic compounds in cranberry syrup expressed in μg/mL of syrup ($n = 5$).

Class/phenolic compounds	μg/mL cranberry syrup
Phenolic-acid derivatives	
Coumaroyl-hexose	56.70 ± 2.05
Sinapoyl-hexose	10.72 ± 0.37
Caffeoyl glucose	19.63 ± 0.62
Chlorogenic acid	19.35 ± 0.53
Coumaroyl-hexose	40.18 ± 1.15
Canthoside A	1.61 ± 0.04
2-Hydroxybenzoic acid	49.40 ± 1.45
Gallic acid 3-O-gallate	58.36 ± 1.63
Flavonols	
Myricetin 3-O-hexoside	125.87 ± 4.87
Dihydro ferulic acid 4-O-β-D-glucuronide	23.96 ± 1.21
Myricetin 3-O-arabinoside	226.63 ± 8.83
Caviunin glucoside	297.30 ± 13.43
Quercetin 3-O-hexoside	391.13 ± 19.29
Quercetin 3-O-xylopiranoside	68.13 ± 2.37
Quercetin 3-O-arabinopyranoside	66.39 ± 2.17
Quercetin 3-O-arabinofuranoside	120.53 ± 4.31
Quercetin 3-O-rhamnoside	130.51 ± 4.23
Myricetin	114.78 ± 3.79
Methoxyquercetin 3-O-galactoside	nq[a]
Kaempferol 3-O-β-D-(6″-p-hydroxybenzoyl)-galactopyranoside	30.70 ± 1.39
Quercetin	303.27 ± 12.81
Syringetin	24.72 ± 0.83
Flavanols	
Procyanidin B type isomer 1	202.84 ± 7.39
(+)-Catechin	374.31 ± 15.43
Proacyanidin A2 type isomer 1	364.03 ± 14.89
Procyanidin B type isomer 2	215.64 ± 9.10
Proacyanidin A2 type isomer 2	356.99 ± 12.88
Procyanidin A2 type isomer 3	644.37 ± 49.71
Prodelphinidin B4	209.98 ± 7.37
Isoflavonoids	
Biochanin A-7-O-glucoside	nq
Coumarins	
7-Hydroxycoumarin	246.91 ± 8.77
Coumarin	174.90 ± 6.21
Scopoletin	449.99 ± 19.82
Anthocyanin	
Petunidin	9.59 ± 2.90
Total	5469.35 ± 194.81

[a] Not quantified.

followed by flavonols (1.91 mg/mL). Phenolic-acid derivatives were found at the lowest concentration (0.15 mg/mL).

3.5. Total polyphenol, proanthocyanidin and anthocyanin contents

Spectrophotometric methods are normally used to measure phenolic contents so various spectrophotometric assays were made to the syrup extracts. To quantify the total phenolic compounds by the Folin Ciocalteu method, a caffeic acid calibration curve was constructed. The calibration curve showed good linearity between the concentration of caffeic acid and absorbance, as described by the equation $y = 0.0149x - 0.0206$ ($r^2 = 0.995$). The total polyphenol content was 15.26 ± 0.08 mg/mL of cranberry syrup. The total proanthocyanidins expressed as catechin equivalents was 9.9 ± 0.1 mg/mL of cranberry syrup, as described by the equation $y = 0.0098x - 0.0153$ ($r^2 = 0.991$). The anthocyanin content found in cranberry syrup was 1.35 ± 0.04 mg/mL. The results obtained by these spectrophotometric analyses were higher than those obtained by HPLC-DAD. This can be put down to the interference of compounds such as sugars, which can cause an overestimation of the results, and cranberry syrup does in fact, contain a high quantity of glucose.

3.6. Antibacterial activity evaluation

Previous studies [28] have reported the beneficial effect of cranberry syrup in preventing urinary tract infection (UTI) among women, achieving a reduction in the absolute risk of UTI infection compared to placebo treatment. This effect has been explained in terms of the anti-adherent effect of cranberry on *E. coli*. Ferrara et al. [29], in a controlled clinical trial including placebo treatment in children aged over 3 years, showed that cranberry syrup prevents the recurrence of symptomatic UTI.

The first step in the colonisation of the epithelium by *E. coli* is determined by its capacity to adhere to the host cells. Initially, this capacity is determined by the micro-organism's electric surface charge and surface hydrophobicity, and subsequently by other factors such as the formation of diverse types of fimbriae and of specific adhesins. Other authors have shown that fimbriae Types 1, P and S are not essential factors in the adhesion and subsequent colonisation of the urogenital epithelium by *E. coli*. These adhesions may, in general, be considered features of the virulence of extra-intestinal *E. coli*, but they are not essential for *E. coli* to become uropathogenic, all of which accounts for the current research interest in the extent to which cranberry extract may affect the non-specific adherence properties of *E. coli*.

In fact, no differences were observed in the surface hydrophobicity of *E. coli* following its growth in TSB culture medium to enhance the expression of Type 1 fimbriae ($Z = 0.35$; pNS). Nevertheless, the incubation of the bacterial suspension with cranberry syrup at final concentrations of either 1:1000 or 1:100 resulted in significant reductions in surface hydrophobicity, depending upon the concentration of cranberry, both after growth in TSB medium and on CFA agar.

Incubation of *E. coli* with cranberry syrup resulted in a reduction in its surface hydrophobicity and did not depend upon the quantities of Type 1 or Type P fimbriae expressed. In earlier studies [30] it was reported that the incubation of *E. coli* with certain anti-oxidants, such as vitamin E, produced similar reductions in surface hydrophobicity. As far as surface hydrophobicity is concerned, however, the incubation of *E. coli* with 1:1000 dilutions of cranberry extract (which do not affect the haemagglutination mediated by Type P fimbriae) did produce significant reductions in surface hydrophobicity, thus showing that extremely low levels of this extract are capable of modifying the non-specific adherence properties of *E. coli*.

The A-linkage in cranberry procyanidins may represent an important structural feature for anti-adhesive activity in bacteria. It has been demonstrated that Type A cranberry procyanidins hinder the adhesion of P-fimbriated uropathogenic *E. coli* to uroepithelial cells *in vitro* [8] and it has also been found that trimeric proanthocyanidins and Type A dimeric procyanidins are responsible for the anti-adhesive effect of cranberry. The composition of the cranberry syrup used in our study, which was rich in Type A procyanidins, may account for the reductions in surface hydrophobicity.

4. Conclusions

The powerful analytical method HPLC-DAD–TOF-MS was used to characterize a commercial cranberry syrup used to prevent urinary tract diseases. It was possible to identify a total of 34 compounds in the sample in less than 29 min using positive and negative ionization modes. To our knowledge, nine of these compounds are tentatively identified in cranberry for the first time. Different coumarins were also found in cranberry for the first time when analyzing its whole phenolic fraction by HPLC-DAD–TOF-MS. This finding was possible thanks to the mass accuracy and sensitivity provided by TOF-MS. Antibacterial activity was investigated

further and it was possible to prove that very low concentrations of cranberry extract have the capacity to modify the non-specific adherence properties of *E. coli*, producing a reduction in surface hydrophobicity.

This study is of great significance for understanding the beneficial effects of cranberry syrup on health. Further analysis will be required to find out more about the activity leading to the preventative function of these compounds.

References

[1] M.A. Haleem, K.L. Barton, G. Borges, A. Crozier, A.S. Anderson, Increasing antioxidant intake from fruits and vegetables: practical strategies for the Scottish population, J. Hum. Nutr. Diet. 21 (2008) 539–546.

[2] X. He, H.L. Rui, Cranberry phytochemicals: isolation, structure elucidation, and their antiproliferative and antioxidant activities, J. Agric. Food Chem. 54 (2006) 7069–7074.

[3] L.Y. Foo, Y. Lu, A.B. Howell, N. Vorsa, The structure of cranberry proanthocyanidins which inhibit adherence of uropathogenic P-fimbriated *Escherichia coli* in vitro, Phytochemistry 54 (2000) 173–181.

[4] Y.T. Lin, Y.I. Kwon, R.G. Labbe, K. Shetty, Inhibition of *Helicobacter pylori* and associated uruase by oregano and cranberry phytochemical synergies, Appl. Environ. Microbiol. 71 (2005) 8558–8564.

[5] N.P. Seeram, L.S. Adams, Y. Zhang, R. Lee, D. Sand, H.S. Sheuller, D. Heber, Blackberry, black raspberry, blueberry, cranberry, red raspberry, and strawberry extracts inhibit growth and stimulate apoptosis of human cancer cells in vitro, J. Agric. Food Chem. 54 (2006) 9329–9339.

[6] J. Côté, S. Caillet, G. Doyon, J.-F. Sylvain, M. Lacroix, Analyzing cranberry bioactive compounds, Crit. Rev. Food Sci. Nutr. 50 (2010) 872–888.

[7] A.B. Howell, Cranberry proanthocyanidins and the maintenance of urinary tract health, Crit. Rev. Food Sci. Nutr. 42 (2002) 273–278.

[8] A.B. Howell, Bioactive compounds in cranberries and their role in prevention of urinary tract infections, Mol. Nutr. Food Res. 51 (2007) 732–737.

[9] Y.L. Singleton, J.A. Rossi, Colorimetry of total phenolics with phosphomolybdic–phosphotungstic acid reagents, Am. J. Enol. Vitic. 16 (1965) 144–158.

[10] R. Julkunen-Tiitto, Phenolic constituents in the leaves of Northern Willows: methods for the analysis of certain phenolics, J. Agric. Food Chem. 33 (1985) 213–217.

[11] T. Fuleki, F.J. Francis, Quantitative methods for anthocyanins. 1. Extraction and determination of total anthocyanins in cranberries, J. Food Sci. 33 (1968) 72–77.

[12] M. Blanco, J. Blanco, J.E. Blanco, M.P. Alonso, I. Abalia, E. Rodriguez, J.R. Bilbao, A. Umaran, Virulence factors and 0 serogroups of *Escherichia coli* as a cause of community-acquired urinary infections, Enferm. Infecc. Microbiol. Clin. 13 (1995) 236–241.

[13] D.G. Evans, D.J. Evans Jr., W. Tjoa, Hemagglutination of human group A erythrocytes by enterotoxigenic *Escherichia coli* isolated from adults with diarrhea: correlation with colonisation factor, Infect. Immun. 18 (1977) 330–337.

[14] M. Lindahl, A. Faris, T. Wadstrom, S. Hjerten, A new test based on 'salting out' to measure relative surface hydrophobicity of bacterial cells, Biochim. Biophys. Acta 677 (1981) 471–476.

[15] A.G. Marwan, C.W. Nagel, Identification of the hydroxycinnamtic acid derivatives in cranberries, J. Food Sci. 47 (1982) 774–778.

[16] M. Heinonen, Antioxidant activity and antimicrobial effect of berry phenolics – a Finnish perspective, Mol. Nutr. Food Res. 51 (2007) 684–691.

[17] T. Kanchanapoom, R. Kasai, K. Yamasaki, Iridoid and phenolic diglycosides from *Canthium berberidifolium*, Phytochemistry 61 (2002) 461–464.

[18] H. Olsen, K. Aaby, G.I.A. Borge, Characterization, quantification, and yearly variation of the naturally occuring polyphenols in a common red variety of Curly Kale (*Brassica oleracea* L. convar. *acephala* var. *sabellica* cv 'Redbor', J. Agric. Food Chem. 58 (2010) 11346–11354.

[19] I.O. Vvedenskaya, N. Vorsa, Flavonoid composition over fruit development and maturation in American cranberry *Vaccinium macrocarpon* Ait., Plant Sci. 167 (2004) 1043–1054.

[20] A.P. Singh, T. Wilson, A.J. Kalk, J. Cheong, N. Vorsa, Isolation of specific cranberry flavonoids for biological activity assessment, Food Chem. 116 (2009) 963–968.

[21] B.L. White, L.R. Howard, R.L. Prior, Polyphenolic composition and antioxidant capacity of extruded cranberry pomace, J. Agric. Food Chem. 58 (2010) 4037–4042.

[22] K.R. Määttä-Riihinen, M.P. Kähkönen, A.R. Törrönen, I.M. Heinonen, Catechins and procyanidins in berries of *Vaccinium* species and their antioxidant activity, J. Agric. Food Chem. 53 (2005) 8485–8491.

[23] X. Wu, R.L. Prior, Systematic identification and characterization of anthocyanins by HPLC–ESI-MS/MS in common foods in the United States: fruits and berries, J. Agric. Food Chem. 53 (2005) 2589–2599.

[24] Y. Zuo, C. Wang, J. Zhan, Separation, characterization, and quantitation of benzoic and phenolic antioxidants in American cranberry fruit by GC–MS, J. Agric. Food Chem. 50 (2002) 3789–3794.

[25] W. Bhouri, S. Derbel, I. Skandrani, J. Boubaker, I. Bouhlel, M.B. Sghaier, S. Kilani, A.M. Mariotte, M.G. Dijoux-Franca, K. Ghedira, L. Chekir-Ghedira, Study of genotoxic, antigenotoxic and antioxidant activities of the digallic acid isolated from *Pistacia lentiscus* fruits, Toxicol In Vitro 24 (2010) 509–515.

[26] L. Nováková, A. Vildová, J.P. Mateus, T. Gonçalves, P. Solich, Development and application of UHPLC–MS/MS method for the determination of phenolic compounds in Chamomile flowers and Chamomile tea extracts, Talanta 82 (2010) 1271–1280.

[27] S.-N. Chen, A. Turner, B.U. Jaki, D. Nikolic, R.B. van Breemena, J.B. Friesen, G.F. Pauli, An experimental implementation of chemical subtraction, J. Pharm. Biomed. Anal. 46 (2008) 692–698.

[28] T. Kontiokari, K. Sundqvist, M. Nuutinen, T. Pokka, M. Koskela, M. Uhari, Randomised trial of cranberry-lingonberry juice and *Lactobacillus* GG drink for the prevention of urinary tract infections in women, Br. Med. J. 322 (2001) 1571–1573.

[29] P. Ferrara, L. Romaniello, O. Vitelli, A. Gatto, M. Serva, L. Cataldi, Cranberry juice for the prevention of recurrent urinary tract infections: a randomized controlled trial in children, Scand. J. Urol. Nephrol. 43 (2009) 369–372.

[30] J. Uberos, C. Augustin, J. Liébana, A. Molina, A. Muñoz-Hoyos, Comparative study of the influence of melatonin and vitamin E on the surface characteristics of *Escherichia coli*, Lett. Appl. Microbiol. 32 (2001) 303–306.

Homogeneity study of ointment dosage forms by infrared imaging spectroscopy

Renato Lajarim Carneiro[1], Ronei Jesus Poppi*

Institute of Chemistry, University of Campinas—UNICAMP, P.O. Box 6154, Campinas, SP 13083-970, Brazil

ARTICLE INFO

ABSTRACT

Ointment dosage forms are semi-solid preparations intended for local or transdermal delivery of active substances usually for application to the skin and it is important that they present a homogeneous appearance. In this work, a study of the homogeneity of a tacrolimus ointment dosage form was performed using infrared imaging spectroscopy coupled with principal component analysis (PCA) and multivariate curve resolution with alternating least squares (MCR-ALS) to interpret the imaging data. Optical visible microscopy images indicated possible phase separation in the ointment and, based on the results presented by distribution concentration maps from infrared imaging, it was possible to conclude that, in fact, there was phase separation incorporated in the ointment. Thus, infrared imaging spectroscopy associated to PCA and MCR-ALS is demonstrated to be a powerful tool for the development process of ointment dosage forms.

© 2011 Elsevier B.V. All rights reserved.

1. Introduction

Semi-solid dosage forms for cutaneous application are intended for local or transdermal delivery of active pharmaceutical ingredients (API), or for their emollient or protective action. These preparations usually consist of a base material and one or more API dissolved or dispersed in an appropriate solvent, giving the semi-solid a homogeneous appearance. According to its composition, the base material may influence the activity of the preparation [1]. Ointments are semi-solid preparations intended for external application to the skin or mucous membranes. The base materials recognized for use as vehicles belong to four general classes: hydrocarbon bases, absorption bases, water-removable bases, and water-soluble bases. Hydrophobic ointments, containing hydrocarbon bases, can absorb only small amounts of water, protecting API that can undergo hydrolysis reactions. Typical bases used for these formulations are hard, liquid and light liquid paraffins, vegetable oils, animal fats, synthetic glycerides, waxes and liquid polyalkylsiloxanes [1,2].

Tacrolimus (FK506) is a macrocyclic lactone fermented by *Streptomyces tsukubaensis*. It is a potent and effective immunosuppressant that has widespread use in patients with organ transplants [3,4]. The ointment formulation of tacrolimus (Protopic®) was specifically developed for the treatment of atopic dermatitis (AD) and was approved for marketing in the United States in 2000 [5,6].

Imaging spectroscopy, known also as hyperspectroscopy, is an analytical technique that produces spectral images from a sample, the hyperspectrum. These spectral images are formed by a large number of pixels and a spectrum by pixel is obtained. Imaging spectroscopy applications can produce an enormous quantity of data, since an image with 100×100 pixels produces ten thousand spectra for a sample. Chemometric methods are indispensable to work with this amount of data. Principal compound analysis (PCA), partial least squares (PLS) and multivariate curve resolution by alternating least squares (MCR-ALS) are common chemometric methods employed to process hyperspectroscopy data [7–9]. The combination of spectroscopy for compound characterization and imaging for spatial localization in infrared chemical imaging has been demonstrated in pharmaceutical applications such as compound distribution mapping or to detect counterfeits [7–16].

In this work, the infrared imaging technique was used to study a tacrolimus ointment formulation. Optical visible microscopy images indicated possible phase separation in the ointment. An infrared imaging spectrometer was used to verify if optical visible images corresponded to phase separation or to air bubbles incorporated in the ointment. Principal component analysis and multivariate curve resolution methods were performed for exploratory analysis of data set to find scores and concentration maps.

2. Materials and methods

2.1. Imaging system

Chemical images from samples were obtained using a Spotlight 400N NIR imaging system from Perkin-Elmer. Spectra were

---

* Corresponding author. Tel.: +55 19 35213126; fax: +55 19 35213023.
  E-mail address: ronei@iqm.unicamp.br (R.J. Poppi).
  [1] Current address: Federal University of São Carlos, Department of Chemistry, Brazil.

obtained from 2000 cm^{-1} to 7800 cm^{-1} but due high noise level between 2000 cm^{-1} and 2200 cm^{-1} and lack of significant information from 4600 cm^{-1} to 7800 cm^{-1}, it was used in the chemometric treatments the region from 2200 cm^{-1} to 4600 cm^{-1}. Sample analysis was performed using transmittance mode, 25 μm × 25 μm spatial resolution, 16 cm^{-1} spectral resolution and 4 scans per pixel. The sample was placed between two glass slides resulting in a very small optical path. Background was obtained from the glass slides in a position where there was no ointment.

2.2. Chemometric methods

All chemometric procedures were performed in a Matlab 2009b environment. MCR-ALS and the "pure" routine were downloaded from http://www.mcrals.info/. MRC-ALS is an iterative method. The "pure" routine finds the purest spectra in the dataset, i.e., those who present absorbance only due to one chemical specie. Then the MCR-ALS is initialized using these more pure spectra aiding to fast convergence of the model. PCA analyses were performed using a lab-made routine based on a singular value decomposition function from Matlab.

2.2.1. PCA

Principal component analysis [7] is an orthogonal decomposition of **D** matrix, yielding the matrices **T** and **P**, which are scores and loadings matrices, respectively. **D** matrix is related to **T** and **P** matrices by: $\mathbf{D} = \mathbf{T} \times \mathbf{P}^t$, where the superscript "t" indicates a transpose operation. Basically, if samples have similar chemical composition or characteristics, the samples will have similar score values in a **T** matrix. Thus, this matrix can give information about sample homogenization when each sample is a pixel, since each pixel yields a spectrum. Pixels which have similar scores will have similar chemical composition. Instead, if pixels have different score values, their chemical composition will be different.

2.2.2. MCR-ALS

Similar to PCA, the multivariate curve resolution-alternating least squares method [7,8,17] decomposes the data matrix **D** into two matrices, but the objective in this method is recovery pure of the spectra and relative concentration values for compounds presents in the **D** matrix. MCR-ALS can be mathematically written as: $\mathbf{D} = \mathbf{C} \times \mathbf{S}^t + \mathbf{E}$, where **D**, **C**, **S** and **E** are data matrix, relative concentration values of pure compounds, normalized spectra of pure compounds and lack of fit matrix, respectively. Deconvolution process as ALS yield multiple responses due to rotational ambiguity, but deconvolution in **C** and **S** matrices is aided by using constraints such as non-negativity for **C** and **S** values.

2.2.3. PCA and MCR-ALS for hyperspectroscopy data

A hyperspectroscopy image has three dimensions: $x_{\text{spatial-axis}}$, $y_{\text{spatial-axis}}$ and wavenumbers. However, x and y spatial axes only contain the spatial localization of each pixel [18,19]. Then this cube of data can be unfolded without loss of any information about spatial localization of the pixels. Each analyzed pixel can be interpreted as a single sample or a micro sample inside a sample. Fig. 1 shows how this decomposition can be performed in a 3 × 3 pixels hyperspectroscopy image. After the unfolding process, the rows will be the spectra related to the different pixels in the data matrix [7–9]. Fig. 1 also shows how scores maps are obtained by PCA and relative concentration maps are obtained by MCR-ALS. The **W** matrix will be the score matrix (**T**) or relative concentration matrix (**C**) for two components for PCA and MCR-ALS, respectively. **K** matrix will be the loading matrix (**P**) or pure compound spectra matrix (**S**) for PCA and MCR-ALS, respectively, for two components. After PCA or

MCR-ALS is performed, the **W** matrix is refolded, producing score maps or relative concentration maps respectively.

3. Experimental

3.1. Ointment preparation

The ointment preparation was constituted only by an oily phase while the vehicle was a paraffin blend. The production process of these dosage forms is to dissolve the active pharmaceutical ingredient (API) in a flask using an appropriate solvent and to melt the paraffin in another flask by heating. After this, the contents of both flasks are joined and mixed in order to obtain a homogeneous product after the end of the process. Tacrolimus ointment was prepared by using this basic production process, using a semi-solid paraffin and 2-(2-ethoxyethoxy)ethanol as tacrolimus solvent. In the final product, tacrolimus ointment had the following composition: 0.1% tacrolimus, 4% of solvent and 95% of semi-solid paraffin. Other additives, totalizing 0.9%, were used but their composition is strictly confidential. After finishing the process, the product was placed in aluminum tubes for ointments and the tube was sealed.

Two glass slides were used as sample holder. A drop of the lab prepared tacrolimus ointment was placed between the slides, generating a very small optical path. A small area between the two glass slides where there was no sample was used to take background spectra. Analyses were performed in the transmittance mode, scanning a 2 mm^2 area, yielding 80 × 80 (totalizing 6400) pixels. Approximately an hour was spent to scan each sampling area.

Prior analyses realized by optical visible microscopy from an imaging spectrometer showed more than one phase in the ointment structure, but it was not known if this phase separation was between paraffin and solvent or if the other phase was air bubbles incorporated in the ointment structure. The solvent should not separate from the paraffin since homogeneity is a criterion for ointment quality, and such separation could cause problems related to the uniformity of the content inside the tube.

Fig. 2 shows two visible photomontages obtained by imaging spectrometer. "A" to "G" structures were investigated using the imaging spectrometer.

4. Results and discussion

4.1. Visual and univariate analyses

Fig. 2 shows the scanned area of the ointment sample. In this figure there are some structures indicating phase separation. After obtaining the visible image, an infrared hyperspectral image was obtained from the same sampling position.

Fig. 3 shows different spectra, from the scanned area. The major peak around 2960 cm^{-1} comes from high paraffin content, which is responsible for the presence of C–H stretching in the sample. Two overlapping peaks are present around 3300 cm^{-1}. These peaks are due to O–H stretching, present in the API solvent molecule. The peak at 3420 cm^{-1} corresponds to O–H stretching in the presence of hydrogen bonds. The peak shifted a lower wavenumber (3240 cm^{-1}) corresponds to O–H stretching in the absence of hydrogen bonds. Small peaks around 4320 cm^{-1} are in the near infrared range and the absorption corresponds to combination bands of C–H bonds. Fig. 3 presents four major absorption peaks: 4320, 3420, 3240 and 2960 cm^{-1}. In a first direct analysis, the image presented in Fig. 2 can be plotted using absorption intensity in any wavelength. Fig. 4 shows the image plotted using the four major absorption peaks with base line alignment using the
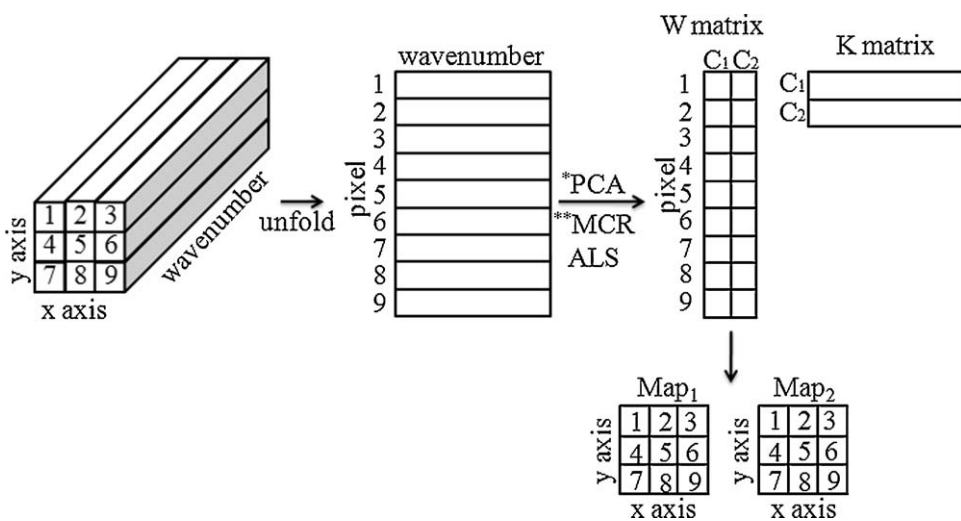
Fig. 1. Illustration of unfolding process for a 3 × 3 pixels hyperspectroscopy image. PCA and MCR-ALS perform analysis on the unfolded matrix, producing score maps/loadings and concentration relative maps/pure spectra, respectively.

average absorption in the range 6000–6200 cm^{-1}. These figures are absorption maps.

Fig. 4 shows that distinct structures have distinct absorptions in some absorption maps. Absorption at 4320 cm^{-1} is intense for B, C and F structures (structure attributions are presented in Fig. 2) indicating the presence of C–H bonds in these positions. This interpretation also can be used for the absorption map at 2960 cm^{-1}, which corresponds to C–H bonds. The same structures presented intense absorption at 4320 cm^{-1} and also at 2960 cm^{-1}, as expected. Absorption maps at 3420 cm^{-1} and 3240 cm^{-1} are very similar, since these bands are broad and overlapped. For these maps, only the B structure presented high absorption, indicating that a large part of the tacrolimus solvent is not incorporated in the paraffin. This conclusion is possible since the only molecule having O–H bonds in the formulation is the API solvent. The B structure presents absorption for C–H bonds, also due the presence of these

bonds in API solvent. Since the API presents high solubility in this solvent, if the solvent has left the paraffin matrix, the product inside the tube can present regions were concentration of API are lower than the specification, which could cause problems for its therapeutic action. A, D, E and G structures did not present any absorption in these four absorption maps, indicating that these structures are only air bubbles inside the ointment. To confirm these facts, PCA and MCR-ALS chemometric methods were used to analyze the data set.

4.2. Principal component analysis

In order to perform the exploratory analyses by PCA and MCR-ALS, the data set was submitted to pretreatments to maximize the difference between the spectra. Pretreatments were performed as follow: selection of specific regions (4600 cm^{-1} up to 2200 cm^{-1}),
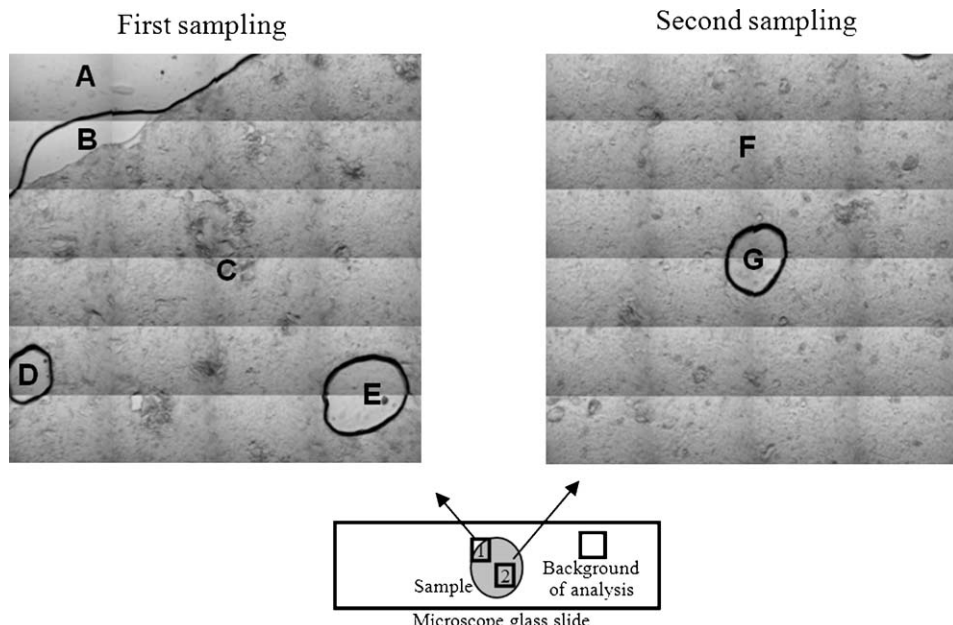

Fig. 2. Photomontage of two sampling of developed tacrolimus ointment. Inferior rectangle shows two microscope glasses slide compressing a drop of ointment; sample is the gray spot in the center of the slides. First sampling was performed in a border of the spot and second sampling was performed in the center of the spot. "A" to "G" represents distinct structures in the ointment, which were investigated.
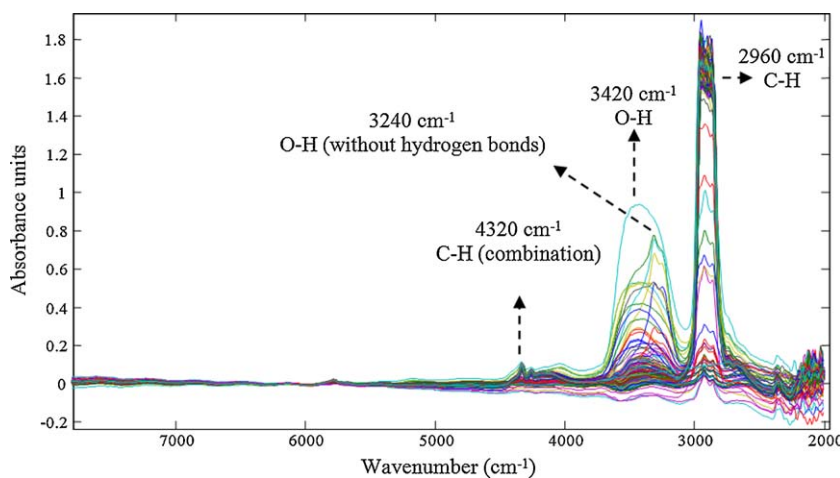
Fig. 3. Some NIR/IR spectra obtained from sample.

move average smoothing ($n = 5$) and first derivative. The first derivative is a pretreatment of samples which is performed on every spectrum (in the rows direction). It was performed in order to increase the performance of PCA and MCR-ALS. The utilization of first derivative decreases the percentage of explained variance on the first principal compound aiding to find the real number of principal compounds in the sample. For MCR-ALS, the first derivative pretreatment aids the algorithm to recovery pure spectra, since the first derivative spectra present more selectivity for overlapped bands. In this case, the mean centering preprocessing (which is performed on every variable, in the columns direction) could not be employed because it is not possible to recovery the true spectra by using of the MCR-ALS. Fig. 5a shows some spectra after all pretreatments and the explained variance percentage of the first ten PCs. Fig. 5b shows that 3 principal components are enough to describe the data variance without including high noise content.

Fig. 6 shows score maps for the first three PCs. Score maps present the chemical similarity between pixels. Pixels that have similar score values will have similar chemical compositions.

The first three score maps for the samplings shows that there are regions where there is not homogeneity, since the pixels have distinct score values. The structures A, D, G and E present score values
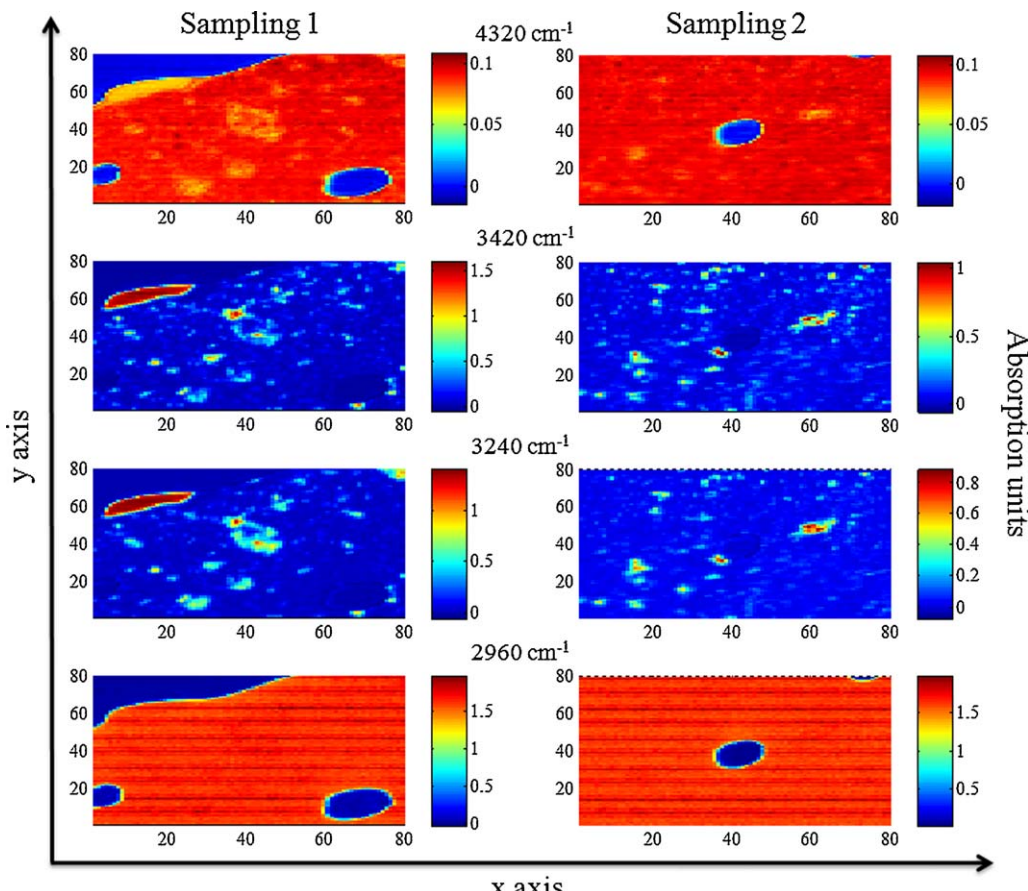

Fig. 4. Absorption maps from the first and second samplings at 4320, 3420, 3240 and 2960 cm^{-1}.
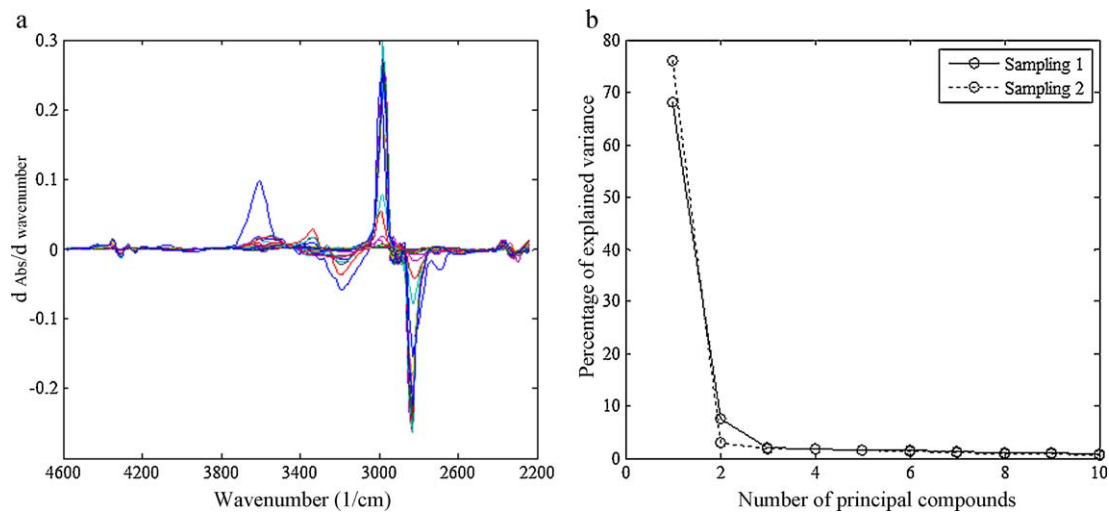
Fig. 5. (a) Some spectra of pixels after pretreatment and (b) percentage of explained variance.

around zero for all PCs. Since PCA analyses employ all wavelengths from 4600 cm^{-1} to 2200 cm^{-1}, it is possible to confirm that these structures do not absorb radiation in any wavelength of this spectral range and that they were only air bubbles. Structure B, present in the first sampling, has distinct score values compared to the other structures for PC1 and PC2 score maps. Small pixel clusters in the center of C and F structures seems have the same composition as B structure, indicating phase separation.

Fig. 7 shows the loadings of score maps from Fig. 6. Due to first derivative pretreatment, it is difficult to interpret the obtained loadings, then, these loads were integrated in order to find which variables are related with which component. Fig. 7 shows that the loading of first PC is basically an absorption peak at 2960 cm^{-1}. Since the intensity of this loading is negative, the presence of this absorption peak is related to negative scores in Fig. 6, i.e., the structures B, C and F, as found earlier by direct analysis of the absorption maps. The same interpretation can be given to the loadings of the second PC, where integrated loadings presented absorption at 3420 cm^{-1} and a small absorption around 2960 cm^{-1}, probably related to the API solvent. It is possible to observe that the loading is negative for the first sampling and positive for the second one. Then, the scores are negative in the PC2 score map in the first sampling and positive in the PC2 score map in the second sampling in regions where there are high contents of API solvent. PC3 loadings are related to API solvent dissolved into the paraffin matrix, since loadings around 3420 cm^{-1} are not so intense compared with loadings around 2960 cm^{-1}, indicating the simultaneous presence of paraffin and API solvent.
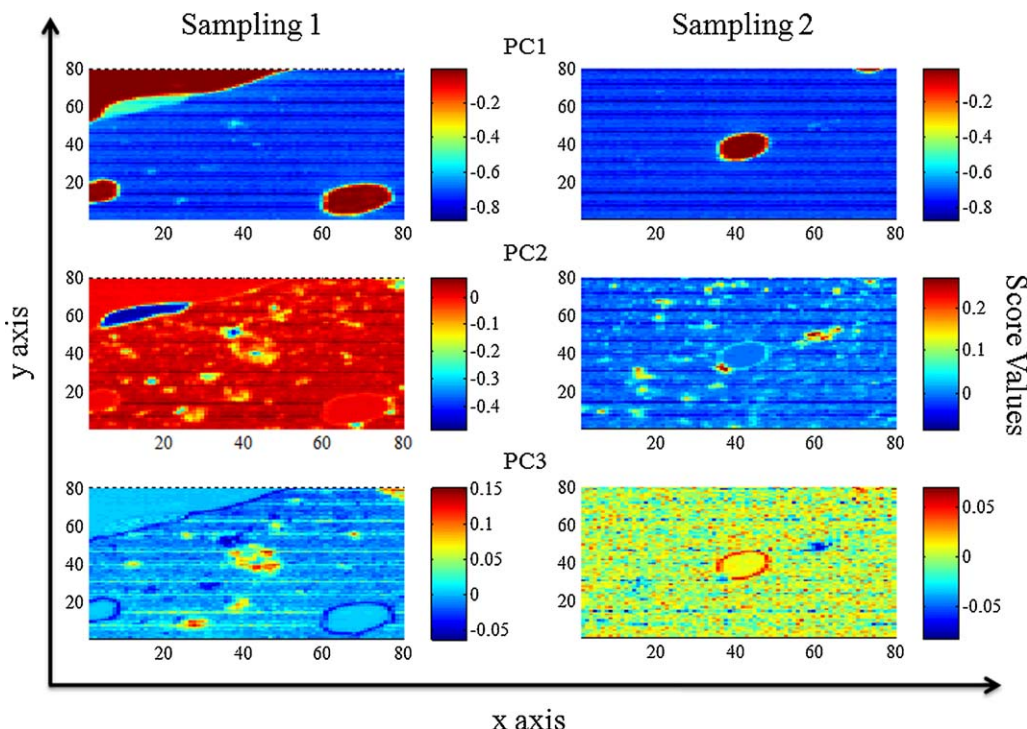


Fig. 6. Score maps for the first three PCs.
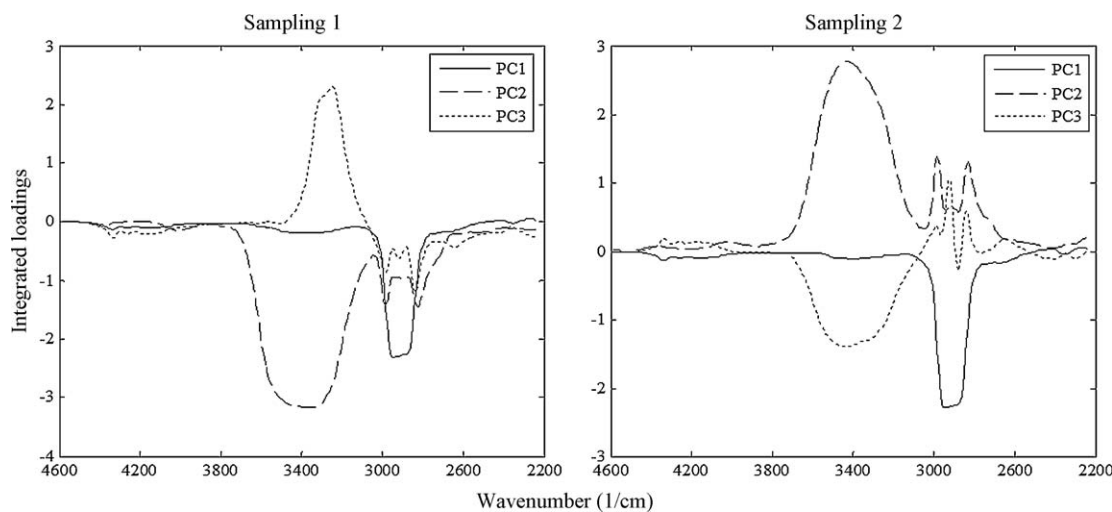
Fig. 7. Integrated PCA loadings from the first three PCs.

4.3. Multivariate curve resolution

In order to initiate the MCR-ALS calculations, a routine was used to find the purest spectra in the data set. Only non-negativity constraint was applied in spectral and concentration profiles in the calculation process. MCR-ALS is a non-supervised chemometric method and recovers pure spectra from data matrices, although these spectra may not be from a pure chemical compound but from a homogenous mixture of pure chemical compounds.

Analysis was performed to find 2, 3 and 4 different pure spectra. Results of lack of fit have shown that it was not possible to find more than 3 different pure spectra in this data set. Fig. 8 presents the recovered spectra by MCR-ALS and the spectra for API solvent and vaseline (tacrolimus molecule has O–H and C–H bounds presenting bands around 3300 cm^{-1} and 2960 cm^{-1}, but its concentration is too low to contribute with total signal of the sample). The first recovered spectrum was from paraffin, due to the high absorption at 2960 cm^{-1}. The second recovered spectrum presents a peak at 2960 cm^{-1} and a smaller peak around 3240 cm^{-1} for first sampling and at 3420 cm^{-1} for second sampling indicate that this spectra is a mixture of paraffin and API solvent. These results can be justified because the absorption at 2960 cm^{-1} is higher than the absorption at 3420/3240 cm^{-1} and the O–H peak is shifted to 3240 cm^{-1}

in the first sampling, indicating that there are no hydrogen bonds between the API solvent molecules. The third recovered spectrum presents a highly intense peak at 3420 cm^{-1} and an intense peak at 2960 cm^{-1}, indicating that this is the spectrum of API solvent, since it has O–H and C–H bonds. A comparison between the recovered spectra and the true spectra shows that paraffin recovered spectrum is identical to the real one. The recovered spectrum for the API solvent presents some differences in the intensities of 3420 cm^{-1} and 2960 cm^{-1} wavenumbers. This occurs due the high absorption for both of these bands, yielding absorptions higher than 2 units for both wavenumbers in some pixels of the sample.

Fig. 9 shows the relative concentration maps for the three recovered pure spectra. These maps show clearly that 3 distinct spectra are present in these hyperspectroscopy images. A, D, E and G structures do not have any presence of the recovered pure spectra, since all pixels of these structures have zero value for relative concentration of any compound.

The first concentration map is related to first pure recovered spectra, and shows how paraffin is distributed in the samplings. The B structure cannot be seen in the first recovered concentration map, because this structure probably is an accumulation of API solvent, and is shown in the third recovered concentration map, according pure the recovered spectra (Fig. 8). The second concentration map
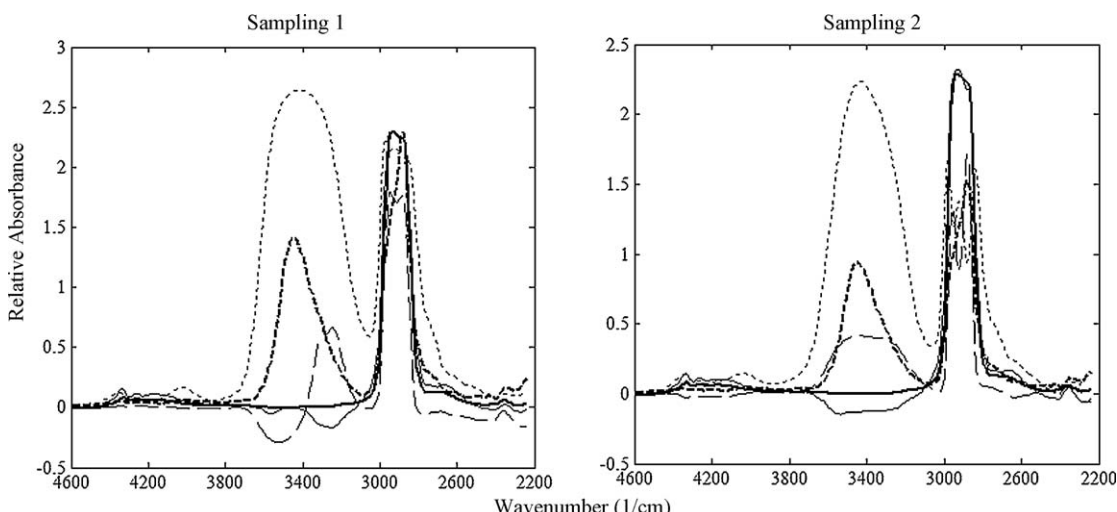

Fig. 8. Real spectra of vaseline and API solvent and integrated pure spectra recovered by MCR-ALS for first and second samplings.
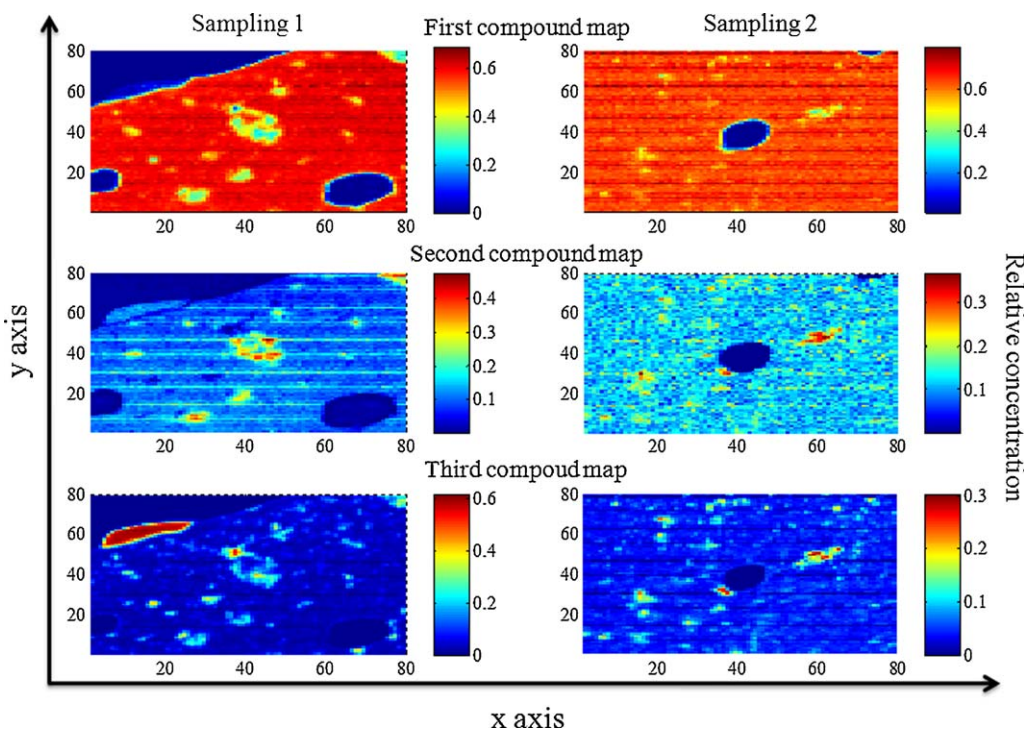
Fig. 9. Relative concentration maps recovered by MRC-ALS.

shows the distribution of the second recovered spectra, which corresponds to a mixture between paraffin and API solvent, showing a medium intensity spread on C and F structures.

5. Conclusions

In this work, three strategies (univariate analysis, principal component analysis and multivariate curve resolution) were applied to hyperspectroscopy data in order to verify if a tacrolimus ointment formulation presented only one phase under microscopic conditions. Multivariate methods presented advantages over univariate ones, since PCA and MCR-ALS allowed the analysis of the full data sets, facilitating the interpretation of the chemical composition of the pixels. However, MCR-ALS shown to be superior since it could recover pure spectra of data the matrix and generate relative concentration maps. From these concentration maps it was found that the microhomogeneity criterion was not satisfied for the composition of this ointment. This criterion could be satisfied by decreasing the solvent proportion using the presented technique for monitoring the microhomogeneity. Other possibility is using an API solvent which is more soluble in vaseline and will not affect the effectiveness of the ointment. Homogeneity is a fundamental quality parameter in semi-solid pharmaceutical dosages such as ointments, suspensions, gels and creams, and infrared imaging spectroscopy and chemometric methods have been demonstrated be powerful tools in the development process of dosage forms.

Acknowledgement

References

[1] European Pharmacopoeia 5.0, 5th ed., EDQM, Strasbourg, 2005.

[2] United States Pharmacopeia USP30-NF25, The National Formulary, Rockville, 2007.

[3] S. Venneti, H.E. Moss, M.H. Levin, M.R. Vagefi, S.C. Brozena, A. Pruitt, Z. Mourelatos, J.Q. Trojanowski, S.L. Galetta, L.J. Balcer, Asymmetric bilateral demyelinating optic neuropathy from tacrolimus toxicity, J. Neurol. Sci. 301 (2011) 112–115.

[4] A.S.B. Goebel, R.H.H. Neubert, J. Wohlrab, Dermal targeting of tacrolimus using colloidal carrier systems, Int. J. Pharm. 404 (2011) 159–168.

[5] A. Lisa, M.D. Beck, The efficacy and safety of tacrolimus ointment: a clinical review, J. Am. Acad. Dermatol. 53 (2005) S186–S194.

[6] D. Miyazaki, T. Takeshi Tominaga, A. Kakimaru-Hasegawa, Y. Nagata, J. Hasegawa, Y. Inoue, Therapeutic effects of tacrolimus ointment for refractory ocular surface inflammatory diseases, Ophthalmology 115 (2008) 988–992.

[7] J.M. Amigo, Practical issues of hyperspectral imaging analysis of solid dosage forms, Anal. Bioanal. Chem. 398 (2010) 93–109.

[8] A. de Juan, R. Tauler, R. Dyson, C. Marcolli, M. Rault, M. Mader, Spectroscopic imaging and chemometrics: a powerful combination for global and local sample analysis, Trends Anal. Chem. 23 (2004) 70–79.

[9] C. Gendrina, Y. Roggo, C. Collet, Vibrational chemical imaging and chemometrics for pharmaceutical applications: a review, J. Pharm. Biomed. Anal. 48 (2008) 533–553.

[10] Y. Roggo, A. Edmond, P. Chalus, M. Ulmschneider, Infrared hyperspectral imaging for qualitative analysis of pharmaceutical solid forms, Anal. Chim. Acta 535 (2005) 79–87.

[11] Y. Roggo, N. Jent, A. Edmond, P. Chalus, M. Ulmschneider, Characterizing process effects on pharmaceutical solid forms using near-infrared spectroscopy and infrared imaging, Eur. J. Pharm. Biopharm. 61 (2005) 100–110.

[12] C. Gendrin, Y. Roggo, C. Collet, Content uniformity of pharmaceutical solid dosage forms by near infrared hyperspectral imaging: a feasibility study, Talanta 73 (2007) 733–741.

[13] F. Clarke, Extracting process-related information from pharmaceutical dosage forms using near infrared microscopy, Vib. Spectrosc. 34 (2004) 25–35.

[14] W. Li, A. Woldu, R. Kelly, J. McCool, R. Bruce, H. Rasmussen, J. Cunningham, D. Winstead, Measurement of drug agglomerates in powder blending simulation samples by near infrared chemical imaging, Int. J. Pharm. 350 (2008) 369–373.

[15] C. Ravna, E. Skibstedb, R. Bro, Near-infrared chemical imaging (NIR-CI) on pharmaceutical solid dosage forms—comparing common calibration approaches, J. Pharm. Biomed. Anal. 48 (2008) 554–556.

[16] J.M. Amigo, J. Cruz, M. Bautista, S. Maspoch, J. Coello, M. Blanco, Study of pharmaceutical samples by NIR chemical-image and multivariate analysis, Trends Anal. Chem. 27 (2008) 696–713.

[17] J. Huang, H. Wium, K.B. Qvist, K.H. Esbensen, Multi-way methods in image analysis—relationships and applications, Chemom. Intell. Lab. Syst. 66 (2003) 141–158.

[18] K.L.A. Chan, S.V. Hammond, S.G. Kazarian, Anal. Chem 75 (2003) 2140–2146.

[19] O.Y. Rodionova, L.P. Houmøller, A.L. Pomerantsev, P. Geladi, J. Burger, V.L. Dorofeyev, A.P. Arzamastsev, Anal. Chim. Acta 549 (2005) 151–158.

Optimization of capillary electrophoresis method with contactless conductivity detection for the analysis of tobramycin and its related substances

Mohamed Nouri El-Attug [a,b], Jos Hoogmartens [a], Erwin Adams [a], Ann Van Schepdael [a,*]

[a] Laboratory for Pharmaceutical Analysis, Faculteit Farmaceutische Wetenschappen, Katholieke Universiteit Leuven, O & N 2, PB 923, Herestraat 49, B-3000 Leuven, Belgium
[b] Department of Pharmaceutical Chemistry, Faculty of Pharmacy, University of Tripoli, Tripoli, Libya

ARTICLE INFO

ABSTRACT

A method was validated and optimized to determine tobramycin (TOB) and its related substances. TOB is an aminoglycoside antibiotic which lacks a strong UV absorbing chromophore or fluorophore. Due to the physicochemical properties of TOB, capillary electrophoresis (CE) in combination with Capacitively Coupled Contactless Conductivity Detection (C^{4}D) was chosen.

The optimized separation method uses a background electrolyte (BGE) composed of 25 mM morpholinoethane–sulphonic acid (MES) adjusted to pH 6.4 by L-histidine (L-His). 0.3 mM cetyltrimethyl ammonium bromide (CTAB) was added as electroosmotic flow modifier in a concentration below the critical micellar concentration (CMC). Ammonium acetate 50 mg L^{-1} was used as internal standard (IS). 30 kV was applied in reverse polarity (cathode at the injection capillary end) on a fused silica capillary (65/43 cm; 75 μm id).

The optimized separation was obtained in less than 7 min with good linearity ($R^2 = 0.9995$) for tobramycin. It shows a good precision expressed as RSD on relative peak areas equal to 0.2% and 0.7% for intraday and interday respectively. The LOD and LOQ are 0.4 and 1.3 mg L^{-1} corresponding to 9 pg and 31 pg respectively.

1. Introduction

The United States Pharmacopeia (USP) [1] defines validation of analytical methods as the process by which it is established, by laboratory studies, that the performance characteristics of the method meet the requirements for the intended analytical applications. The USP has recommended a procedure for the validation of analytical methods.

Tobramycin (TOB) is an aminoglycoside antibiotic derived from nebramycin, an antibiotic complex produced by fermentation of the actinomycete *Streptomyces tenebrarius* [2]. It is a polycationic pseudo-oligosaccharide, which consists of two aminosugars joined by a glycosidic linkage in a central position to 2-deoxystreptamine. TOB is active against a broad spectrum of Gram-negative bacteria. It exerts a bactericidal activity against many bacterial strains involved in clinical infections. It is particularly indicated for the treatment of septicemia, complicated and recurrent urinary tract infections, lower respiratory infections, serious skin and soft tissue infections including burns and peritonitis, ophthalmic and central nervous system infections caused by organisms resistant to other antibiotics, including other aminoglycosides.

TOB is used in a variety of pharmaceutical applications, including ophthalmic suspensions, solutions and ointments, inhalation solutions and intravenous administrations. Like for other aminoglycosides, a narrow therapeutic index is implicated because of its potential oto- and nephrotoxicity encountered during its clinical use [3]. It has neither a chromophore nor fluorophore which limits optical detection (UV/vis and fluorescence). TOB can also be synthesized from kanamycin B [4]. The chemical structures of tobramycin and its major impurities are shown in Fig. 1.

TOB and kanamycin B are produced after base catalyzed hydrolysis of nebramine factor 5′ (6″-O carbamoyltobramycin) and 4 (6″-O carbamoylkanamycin B) respectively, produced by fermentation. Tobramycin and kanamycin B are hydrolyzed by acid to nebramine and neamine respectively. As TOB is produced by fermentation, beside the main component it also contains some related substances that result either from the incomplete purification or from degradation of the drug. Kanamycin B, nebramine and neamine (also known as neomycin A) are three known impurities of tobramycin reported in the Ph. Eur. [5].

The separation and detection of tobramycin and its impurities has been a great challenge, due to the polar basic nature and the lack of UV absorption properties. Several analytical methods have been used to determine it, such as paper chromatography [6], gas liquid chromatography after silylation [7] and spectrophotometry [8].

---

* Corresponding author. Tel.: +32 16 323440; fax: +32 16 323448.
E-mail address: ann.vanschepdael@pharm.kuleuven.be (A. Van Schepdael).
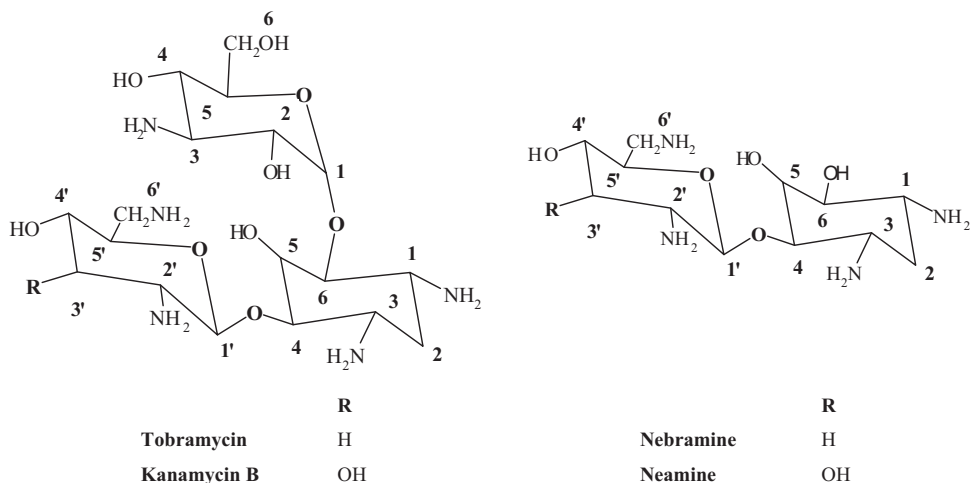
Fig. 1. Chemical structures of tobramycin and its major impurities.

LC and CE using pre and post-column derivatization of tobramycin [9–14] have been performed using o-phthalaldehyde (OPA) [9–11], 2,4,6-trinitrobenzenesulphonic acid [12] and 2,4-dinitrofluorobenzene [13]. However, these techniques can be tedious, time consuming, not safe and give problems with quantitation because of additional sample processing, variability of reaction completeness, possible instability of derivatized products and toxicity of some derivatization agents. Therefore it presents a limitation to its routine use. Direct detection using evaporative light scattering detection (ELSD) [15], mass spectrometry (MS) [16,17] and pulsed electrochemical detection (PED) [18,19] have also been described.

An ion-pair LC method using a poly(styrenedivinylbenzene) column as stationary phase combined with PED has been developed [18]. This method is currently prescribed in the Ph. Eur. [5] for the analysis of tobramycin. Beside with reversed phase chromatography, PED has also been used in combination with anion exchange chromatography for the detection of tobramycin and its impurities [19]. LC methods with electrochemical detection have shown good separation performance, but stability and operator experience are the major limitations. Because of that CE is increasingly being viewed as an alternative and a complement to LC for determination of drug related impurities [20]. Many investigators have used CE in the analysis of aminoglycosides combined with borate complexation [21], indirect detection methods [22] and amperometric detection [23]. Micellar electrokinetic capillary chromatography (MEKC) with UV detection for simultaneous determination of amikacin, tobramycin and kanamycin A, was performed in Tris buffer at pH 9.1 with a high concentration of sodium pentanesulphonate as an anionic surfactant [24]. However, these methods are less sensitive and selective for the related substances. CZE with amperometric detection has been reported for analysis of kanamycin and amikacin, but could only show selectivity for three components [23]. The determination of tobramycin in human serum has been reported using CE with Capacitively Coupled Contactless Conductivity Detection (CE-C^{4}D) [25].

The official method for the analysis of tobramycin in the European Pharmacopoeia (Ph. Eur.) [5] prescribes the use of thin layer chromatography (TLC) for identification and the test on kanamycin B and the assay are performed by LC-PED.

This work investigates the sensitivity and selectivity of CE with C^{4}D as a direct detection method for the analysis of tobramycin and its related substances. This mode of detection can be useful in capillary electrophoretic analyses of a broad scale of compounds, from low-molecular-mass highly mobile small inorganic and organic ions (e.g. halogenides, alkali metal ions, trifluoroacetic acid (TFA)) to alcohols, carbohydrates, proteins, aminoglycosides, etc. [26–28]. It can also be a good alternative to derivatization in case of non UV-absorbing substances.

2. Material and methods

2.1. Reagents, samples and solutions

All chemicals used were of analytical grade. 2-(N-morpholino)ethanesulphonic acid monohydrate (MES) and L-histidine (L-His) were purchased from Fluka (Sigma-Aldrich, Schnelldorf, Germany). N-cetyltrimethyl ammonium bromide (CTAB) and ammonium acetate were from Merck (Darmstadt, Germany). Sodium hydroxide was from Riedel-deHaën (Seelze, Germany), sodium chloride was from Fisher chemicals (Leicestershire, UK). Ammonium formate was from Fluka AG (Buchs Switzerland), formic acid from Acros Organics (Geel, Belgium) and sodium acetate from Applichem GmbH (Darmstadt, Germany). Tobramycin reference CRS was obtained from the European Pharmacopoeia EDQM (Strasbourg, France), tobramycin samples were obtained from different sources as Alcon Cusí (Barcelona, Spain), Biogal (Debrecen, Hungary) and Chongqing Daxin Pharmaceutical Co. Ltd. (Chongqing, China). Kanamycin B was acquired from WHO (Geneva, Switzerland). Neamine was prepared in the laboratory [29] and nebramine was obtained from Dr. Istvan Fabian (Lajos Kossuth University, Debrecen).

All solutions were prepared by using ultrapure MilliQ-water (Millipore, Milford, MA, USA) and were filtered with a 0.2 μm membrane filter syringe (Dassel, Germany).

The pH value of the buffers was measured and adjusted with the aid of a pH-meter Metrohm 691 (Herisau, Switzerland). MES buffers with pH values equal to or higher than 6.0 were prepared with MES (pK_a = 6) and the pH was adjusted with solutions of L-His. Stock solutions of 100 mM of MES, L-His and 10 mM of CTAB were prepared.

During method development, sample stock solutions of tobramycin and related impurities were individually prepared at a concentration of 1.0 g L^{-1} in water and stored at 7 °C, for at most one week.

2.2. Instrumentation and operating conditions

The experiments were performed on a P/ACE MDQ instrument (Beckman Coulter, Inc., Fullerton, CA, USA), coupled with an eDAQ

C^4D system (eDAQ, Denistone East, Australia). Data acquisition was done by 32 Karat^{TM} 4.0 software (Beckman Coulter, Inc., Fullerton, CA, USA).

Uncoated fused silica capillaries of 75 μm I.D. and 375 μm O.D. were purchased from Polymicro Technologies (Phoenix, AZ, USA). The total length was 65 cm and effective length 43 cm. New capillaries were conditioned at 45 °C by rinsing with 1 M NaOH (10 min), 0.1 M NaOH (30 min), wait for 30 min and water (5 min). Daily at the beginning of analysis, the capillary was rinsed with 1 M NaOH (5 min), 0.1 M NaOH (3 min), water (1 min) and BGE (2 min); all the steps were performed at 25 °C and 138 kPa pressure. The inlet/outlet vials were replaced every 3 runs.

During method development and later on, for method application to tobramycin analysis, the capillary was rinsed between runs for 1 min with 0.1 M NaOH, 1 min with water and 3 min with buffer at 138 kPa. Samples were hydrodynamically introduced at a pressure of 3.45 kPa for 5 s injection time and a separation voltage of −30 kV (cathode at the injection capillary end) at 25 °C was applied.

The eDAQ C^4D detector was employed at a peak-to-peak amplitude of 80 V and the frequency was 600 kHz. The data were processed using licensed PowerChrom v2 software (EDAQ, Denistone East, Australia). Further data acquisition was done by both PowerChrom v2 and 32 Karat^{TM} 4.0 softwares.

Table 1
Electrophoretic parameter settings applied in the method optimization, corresponding to low (−), central (0) and high (+) levels.

Parameter	Low value (−)	Central value (0)	High value (+)
pH	6.2	6.4	6.6
BGE (mM)	20	30	40
CTAB (mM)	0.2	0.4	0.6
Temp (°C)	22.5	25	27.5

2.3. Experimental design

Four experimental parameters (factors) were varied at levels under and above the central value: concentration of BGE (mM), pH, concentration of CTAB (mM) and capillary temperature (°C) (as shown in Table 1). The levels were chosen based on some pre-experiments and knowledge about the system. Factors were varied at the same time, making it possible to distinguish between the effects of a single variable and of interacting variables. Replicating center points are added to check for curvature (quadratic effects), and to obtain an independent estimate of the error to illustrate the repeatability of the method. A two level full factorial design was applied. For this design, the number of runs is equal to $2^k + n$, where k is the number of parameters and n is the number of
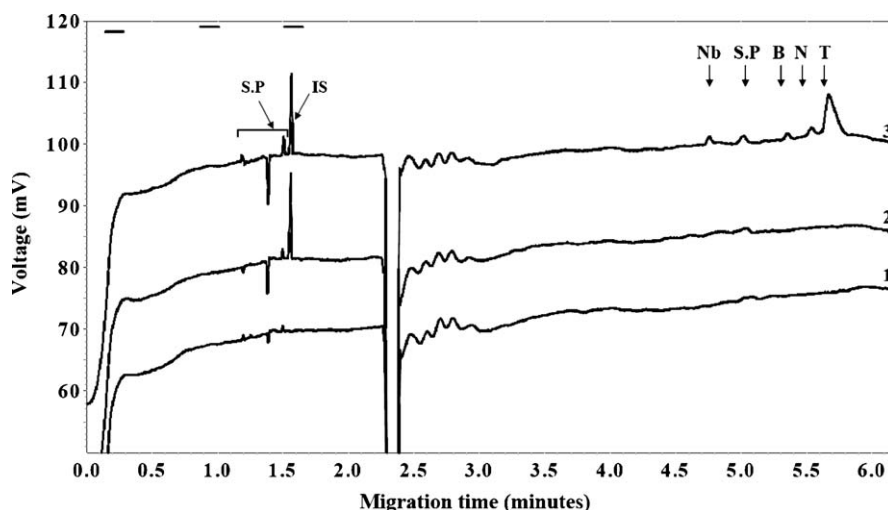

Fig. 2. Typical CE-C^4D electropherograms showing the separation of tobramycin from its impurities using CE; (1) blank (H$_2$O), (2) internal standard (ammonium acetate 50 mg L^{-1}) only and (3) samples dissolved in water: kanamycin B, nebramine and neamine 2.5 mg L^{-1} each and tobramycin 50 mg L^{-1}. S.P, system peak; IS, internal standard; B, kanamycin B; Nb, nebramine; N, neamine; T, tobramycin. Capillary, uncoated fused silica 75 μm I.D., 375 μm O.D. (65 cm total length, effective 43 cm to C^4D detector); voltage, 30 kV in reverse polarity; temperature, 25 °C; injection, inlet pressure 3.45 kPa for 5 s; BGE, 20 mM MES and 0.3 mM CTAB, adjusted by L-His to pH 6.4.
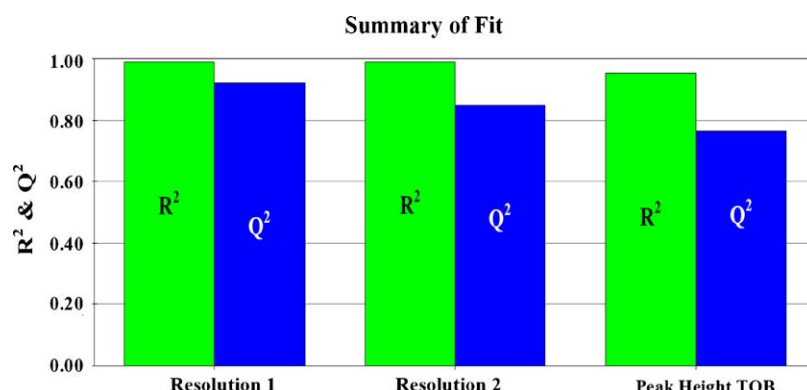

Fig. 3. Variations of the responses explained by the experimental design. The light shaded bars, R^2, denote the fraction of variation of the responses explained by the model and the dark shaded bars, Q^2, denote the fraction of variation of the responses that can be predicted by the model. Responses: resolution 1, resolution between kanamycin B and neamine; resolution 2, resolution between neamine and tobramycin; peak height TOB, peak height of tobramycin.
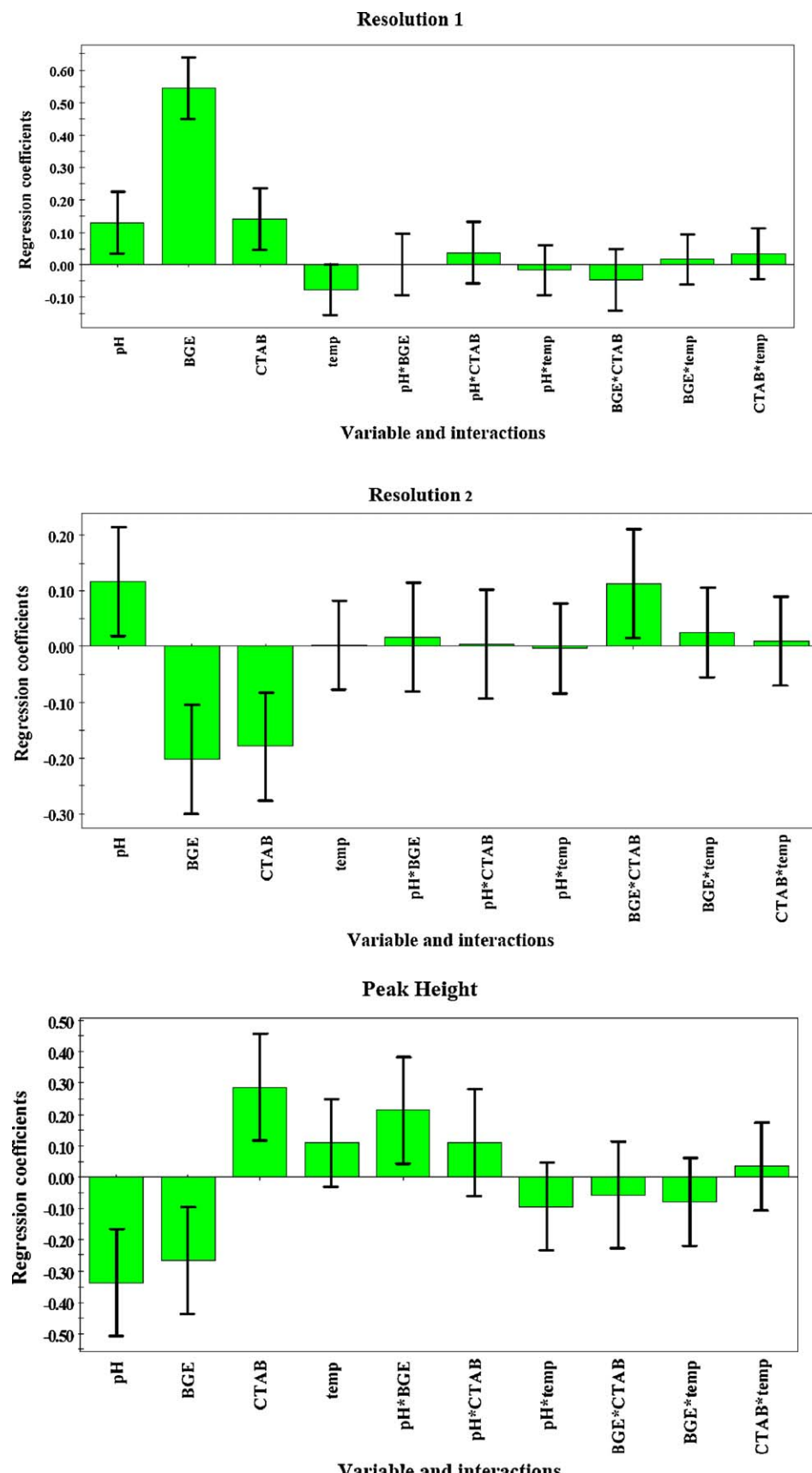
Fig. 4. Regression coefficient plots obtained from the optimization study. Rs1, resolution between kanamycin B and neamine and Rs2, resolution between neamine and tobramycin. pH, pH of the BGE; BGE, BGE concentration (mM); CTAB, CTAB concentration (mM) and temp, capillary temperature (°C).

center points, giving 19 experiments (i.e. 16 + the center point was replicated three times).

The responses investigated included the resolution between kanamycin B and neamine (Rs1), the resolution between neamine and tobramycin (Rs2) and the peak height of tobramycin (HT) in mV. With this it was concluded that all factors except capillary temperature had a significant effect on one or more responses at 95% confidence.

The statistical relationship between a response Y and the experimental variables X_i, X_j, ... is of the following form:

$$Y = \beta_0 + \beta_i X_i + \beta_j X_j + \beta_{ij} X_i X_j + \cdots + E \qquad (1)$$

where the β's are the regression coefficients and E is the overall experimental error.

The linear coefficients, β_i and β_j, describe the quantitative effect of the experimental variables in the model. The cross coefficient β_{ij} measures the interaction effect between the variables i and j.

All the experiments were carried out in a random order. Multiple linear regression (MLR) of the program Modde 5.0 software (Umetri, Umeå, Sweden) was used to calculate quantitative relations between the responses and the factors.

The statistical significance of the variables and interaction terms was tested at a significance level of $\alpha = 0.05$.

3. Results and discussion

3.1. Method development—separation BGE

The buffer pH as well as the ionic strength influence the electrophoretic mobility of the analytes through the capillary. Hence the choice of the BGE constituents is crucial. Accordingly in the present work, the buffer constituents MES-monohydrate and L-histidine were used and CTAB was added to the mixture as an electroosmotic flow modifier in a concentration less than 1.3 mM, the critical micellar concentration (CMC).

The mixture of MES and L-His is used for keeping the background conductivity as low as possible. MES and L-His both produce the necessary pH buffering.

According to the aim of the study different combinations were prepared from the stock solutions and tested in order to define the best combination for getting good selectivity and sensitivity for tobramycin and its related substances. The relevant responses evaluated were: the sensitivity by peak height and resolutions between kanamycin B and neamine (Rs1) and between neamine and tobramycin (Rs2).

A series of experiments was carried out in order to find the optimal pH and concentration of MES, L-His and CTAB for determining tobramycin. A BGE containing the following combination: 25 mM MES and 0.3 mM CTAB, at pH 6.4 adjusted by adding L-His, was chosen because it gave the highest peak height and good resolution between kanamycin B and neamine and good resolution between neamine and tobramycin.

The pH influence on the resolutions between tobramycin and its related substances was such that at higher pH best resolutions for Rs1 and Rs2 were obtained, but at the same time lowest peak height and so less sensitivity.

Under the optimized conditions of reverse polarity (cathode at the injection capillary end) and pH 6.4, the migration order was as follows: nebramine, kanamycin B, neamine and tobramycin. These compounds differ in the degree of substitution (number of amino
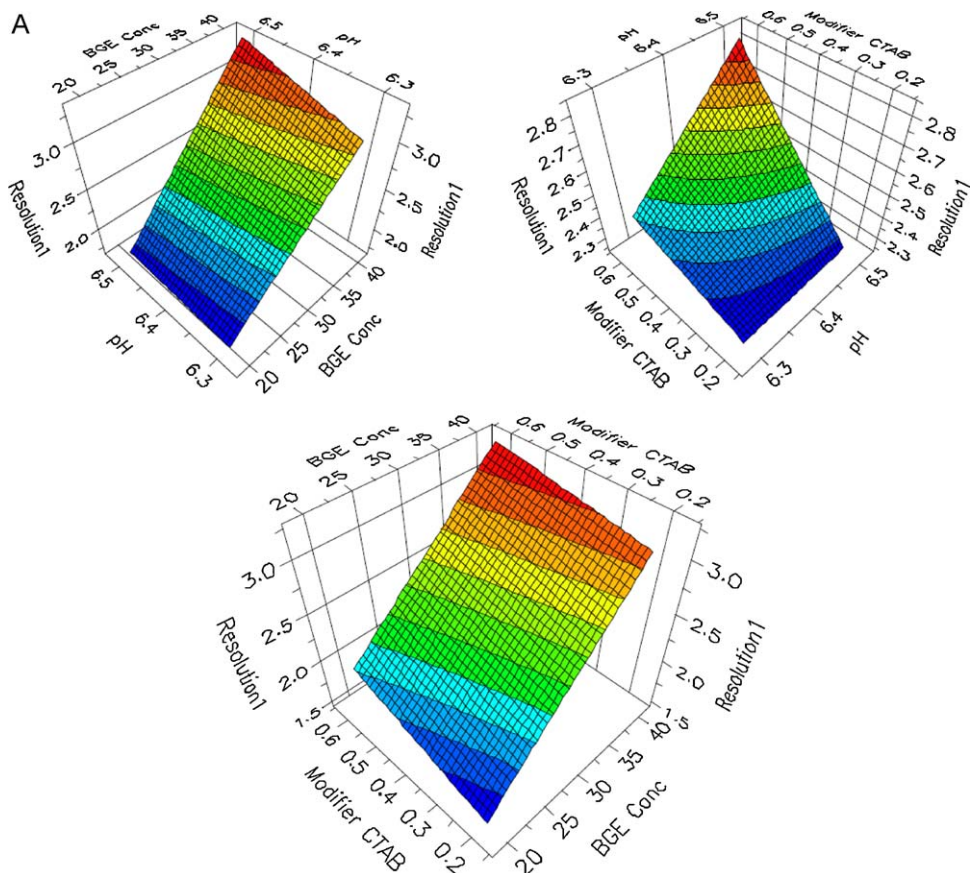

Fig. 5. (A) Response surface plot as a function of pH and BGE concentration (mM), pH and CTAB concentration (mM) and BGE concentration (mM) and CTAB concentration (mM) for Rs1. The other parameters are kept at their central values. (B) Response surface plot as a function of pH and BGE concentration (mM), pH and CTAB concentration (mM) and BGE concentration (mM) and CTAB concentration (mM) for Rs2. The other parameters are kept at their central value. (C) Response surface plot as a function of BGE concentration (mM) and CTAB concentration (mM), pH and CTAB concentration (mM) for peak height HT (mV). The other parameters are kept at their central values.
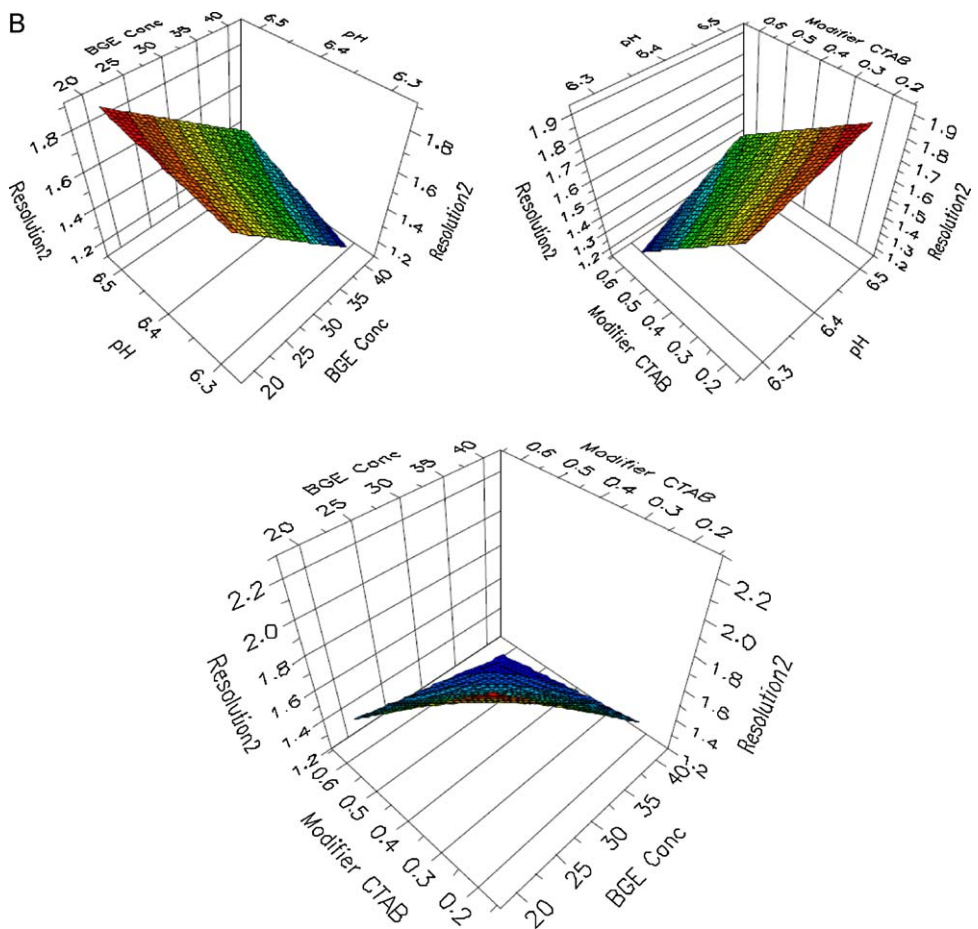
Fig. 5. (continued)

groups) which greatly affects the degree of compound ionization and thus the migration order. Tobramycin has five NH$_2$– groups in the molecular structure with pK_{a1} to pK_{a5} as 6.2, 7.4, 7.8, 8.3 and 8.9 [30]. Kanamycin B has five NH$_2$– groups with pK_{a1} to pK_{a5} as 5.79, 6.61, 7.66, 8.11 and 9.26. Neamine has four NH$_2$– groups in the molecular structure with pK_{a1} to pK_{a4} as 5.7, 7.6, 8.1 and 8.6.

Tobramycin migrates last because it has five protonated amino groups and one hydroxyl group less, nebramine migrates faster because it has four amino groups, one less than tobramycin and kanamycin B. The rank order of charge to mass ratio is TOB > neamine > kanamycin B > nebramine.

The separation voltage was optimized by plotting a curve of the generated current in function of the applied voltage. The linear range (where Ohm's law is valid) is the working range and the maximum voltage in this range (−30 kV) was adopted as the optimal separation voltage. To correct injection volume imprecision common in CE, an internal standard was used. Different compounds were tested during method development and finally ammonium acetate was chosen as internal standard at a concentration of 50 mg L^{-1}. Fig. 2 shows a separation obtained with the optimized parameters.

3.2. Method optimization

Performing the experiments according to a $2^k + n$ design as mentioned in Section 2.3, Table 1 produced the conclusion that most factors had a significant effect on the separation of one or more responses at 95% confidence.

A mathematical model was created, based on the total of 19 experiments. The variances of the responses were stabilized by a logarithmic transformation, which improved the model. Fig. 3 shows the fraction of variation of the responses explained by the model, R^2 and the fraction of variation of the responses that can be predicted by the model, Q^2. The possible values are in the range 0–1.0, with 1.0 revealing the existence of a model with an excellent predictive power. R^2 in our model was found to be between 0.99 and 0.96, and the values for Q^2 between 0.76 and 0.94.

The responses investigated included the resolution between kanamycin B and neamine (Rs1), resolution between neamine and tobramycin (Rs2) and the peak height of tobramycin (HT). The results expressed as regression coefficient plots are summarized in Fig. 4. These plots consist of bars, which are proportional to the regression coefficients. The bars denoted by one variable reflect the regression coefficient for the linear effect of that particular variable and the bars denoted by variable1 × variable2 the interaction between the two variables concerned. The 95% confidence interval is expressed in terms of an error line over the coefficient. When the interval includes zero, the variation of the response caused by changing the variable is smaller than the experimental error and the effect is considered to be not significant.

A positive regression coefficient stands for a positive effect on the responses studied, while a negative regression coefficient indicates a negative effect, as shown in Fig. 4. It can be observed that the pH of the BGE has a positive significant effect on Rs1, Rs2 and a negative significant effect on the HT of tobramycin. It means that increasing the pH of the BGE will increase Rs1, Rs2 and decrease the peak height of tobramycin causing less sensitivity. The concentration of the BGE was found to have a positive significant effect on Rs1 and negative significant effect on Rs2 and HT. This means that increasing the BGE concentration will improve Rs1 and
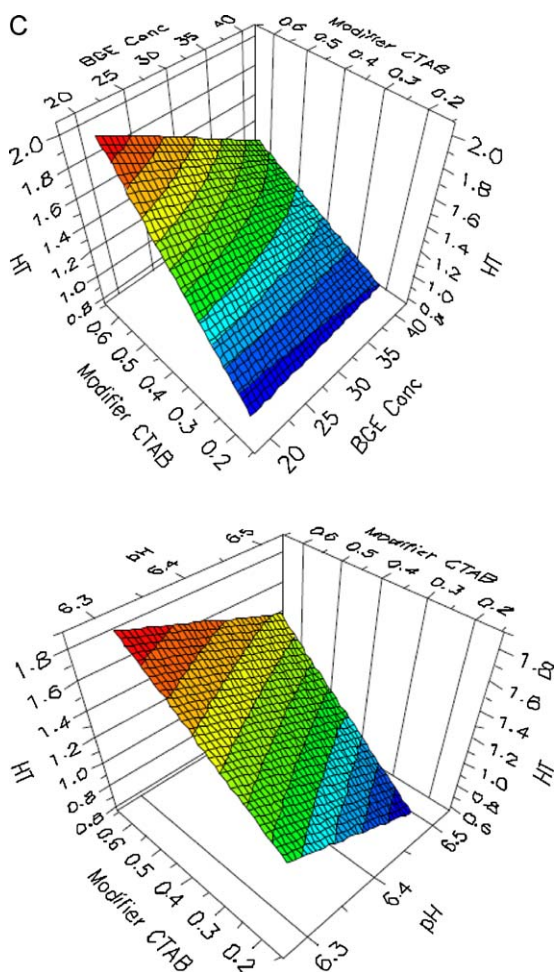
Fig. 5. (*continued*).

deteriorate Rs2 and HT. The concentration of CTAB was found to have a positive significant effect on Rs1, HT and a negative significant effect on Rs2. This means that increasing the CTAB concentration will improve Rs1 and peak height, but decrease Rs2. The capillary temperature was found to have no significant effect on Rs1, Rs2 and peak height. No significant interactions for Rs1, Rs2 and HT were found between the parameters studied, except a positive significant interaction for Rs2 between the concentration of BGE and CTAB and for peak height between pH and BGE concentration.

In order to better estimate the influence of the most important parameters on Rs1, Rs2 and HT, response surface plots were constructed. Fig. 5 shows the variation of Rs1, Rs2 and HT as a function of two significant parameters while the other parameters are kept constant at their central values. It is observed that in the range examined, the minimum resolution is 1.2 for Rs2. Therefore it can be concluded that selectivity is sufficient in the range examined. Hence the Rs1 will not be affected that much, and stay above 1.8. In order to get a good resolution for Rs2 that was considered as critical response, the factors were set to just below the center point value for the concentration of BGE and the concentration of CTAB. The pH was set to the center point level to compromise between resolutions 1, 2 and HT.

Based on those considerations, we define an optimal separation when the factors are 25 mM BGE at a pH of 6.4, an addition of 0.3 mM CTAB, 25 °C and −30 kV. This is adopted as optimized conditions for analyzing the commercial samples of tobramycin.

Table 2
Composition of commercial tobramycin and CRS expressed as is (% m/m).

Sample	Tobramycin	Kanamycin B	Neamine	Nebramine	Water content
CRS	91.6	ND	ND	ND	9.9
1	91.4	ND	ND	ND	9.5
2	91.6	ND	ND	ND	7.4
3	88.1	1.8	ND	ND	10.0

ND, not detected.

Electropherograms of the separations obtained by using these conditions are shown in Figs. 2 and 6.

3.2.1. Quantitative aspects

The precision, sensitivity and linearity of the method were evaluated as follows:

3.2.1.1. Sensitivity. For calculation, relative corrected peak areas were used. LOD and LOQ values correspond to 3 and 10 times the S/N. LOD and LOQ are expressed as percentage of a sample containing $1.0 \, g \, L^{-1}$ of tobramycin. Good sensitivity was observed, with LOD and LOQ estimated values of $0.4 \, mg \, L^{-1}$ (0.04% m/m) and $1.3 \, mg \, L^{-1}$ (0.1% m/m), these correspond to 9 pg and 31 pg, respectively.

3.2.1.2. Linearity for tobramycin. The optimized separation was obtained in less than 7 min with good linearity ($R^2 = 0.9995$) for tobramycin, with 9 concentration points injected in triplicate for the concentrations range from 1.5 to $1000 \, mg \, L^{-1}$. Ammonium acetate was used as internal standard at $50 \, mg \, L^{-1}$. For calculation, relative corrected peak areas were used.

The following regression equation was obtained: $y = 0.0131x - 0.0072$, $S_{yx} = 0.13$, where y: relative corrected peak area, x: concentration ($mg \, L^{-1}$), and S_{yx}: standard error of estimate. The intercept was found to be not statistically different from zero.

3.2.1.3. Repeatability for tobramycin. The system repeatability was performed by using the same sample, BGE and expressed as the relative standard deviation (% RSD) of the relative corrected peak areas, migration time and relative migration time. Intraday precisions were 0.2%, 0.6% and 0.5% ($n = 6$) respectively, and interday precisions were 0.7%, 0.8% and 0.8% ($n = 18$) respectively. The mean of migration time and relative migration time were 5.7 min, 3.5 ($n = 6$) and 5.7 min, 3.5 ($n = 18$) for intraday precision and interday precision respectively.

3.3. Application of the optimized CE-C4D method for analysis of tobramycin in real samples

The water content in the tobramycin CRS and commercial samples was determined by Karl Fischer titration as shown in Table 2.

The optimized method was applied for the analysis of tobramycin and its related impurities in commercial bulk samples.

A solution of $0.2 \, g \, L^{-1}$ was investigated for each commercial sample. The content of each sample was determined by using Tobramycin CRS (91.6% as is) and expressed as percent content of the main compound. Data obtained were in the range of 88.1–91.6%. There are no related substances above the detection limit in two samples, but sample number 3 which was obtained from Chongqing Daxin Pharmaceutical Co. Ltd. (Chongqing, China) has around 1.8% of kanamycin B as shown in Fig. 6 (electropherogram 3).

Improvement in analysis time was obtained compared to the method of Kaale et al. [14] using UV detection after derivatization, which needs 30 min (10 min for derivatization plus 20 min for separation) and to the LC-PED method, which needs more than 20 min
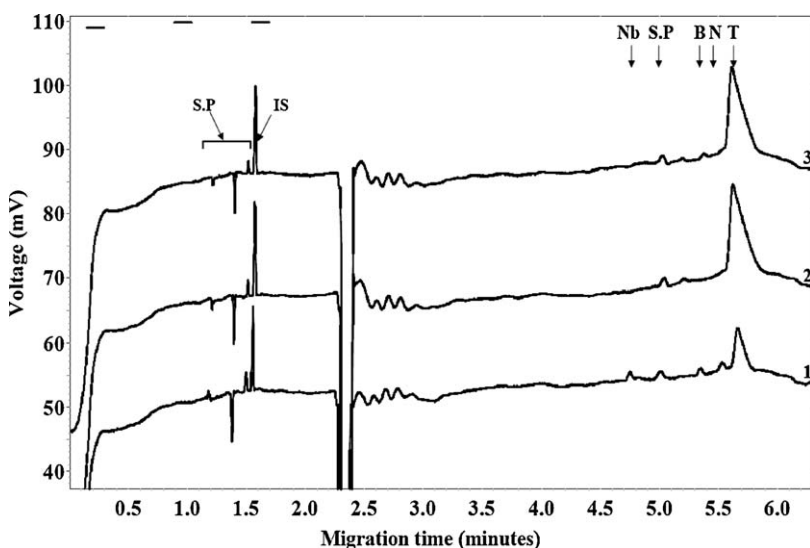
Fig. 6. Typical CE-C^{4}D electropherograms showing the separation of tobramycin from its impurities using CE; (1) samples dissolved in water: kanamycin B, nebramine and neamine 2.5 mg L^{-1} each and tobramycin 50 mg L^{-1}. (2) Tobramycin 0.2 g L^{-1} CRS and (3) commercial bulk sample, S.P, system peak; IS, internal standard (ammonium acetate 50 mg L^{-1}); B, kanamycin B; Nb, nebramine; N, neamine; T, tobramycin; CE conditions see Fig. 2.

for a two-step gradient for separation plus equilibration time of the PED instrument [7].

4. Conclusion

The goal of this work was the development, optimization and evaluation of a selective, simple and fast CZE method for the analysis of tobramycin and its related impurities in commercial samples.

A CZE method with C^{4}D detection was developed and validated for linearity, inter- and intra-day precision and sensitivity. Successful separation and good resolution between tobramycin and related substances were achieved. The described method yielded an effective improvement in simplicity and analysis time (7 min), which is important for routine application. The assay method was used to determine the content of commercial samples. The quantitative feature of this assay makes it a suitable assay for tobramycin.

This mode of detection can be useful for the analysis and assay of aminoglycosides such as tobramycin. It can also be a good alternative to derivatization in case of non UV-absorbing substances.

Acknowledgement

References

[1] Validation of Compendial Methods, United States Pharmacopeia XXIV, 2006, pp. 3050–3052.
[2] C.E. Higgins, R.E. Kaster, Nebramycin a new broad-spectrum antibiotic complex. II. Description of *Streptomyces tenebrarius*, Antimicrob. Agents Chemother. 7 (1967) 324–331.
[3] P. Federspil, W. Schatzle, E. Tiesler, Pharmacokinetics and ototoxicity of gentamicin, tobramycin and amikacin, J. Infect. Dis. 134 (1976) 200–205.
[4] Y. Takegi, T. Tsuchiya, S. Umezaya, H. Umezaya, Synthesis of 3′-deoxykanamycin B, J. Antibiot. 26 (1973) 403–406.
[5] European Pharmacopoeia, 7th ed., EDQM, Strasbourg, 2011, pp. 3103–3104.
[6] R.L. Hussey, Paper chromatography of tobramycin and some related compounds, J. Chromatogr. 92 (1974) 457–460.
[7] J.W. Mayhew, S.L. Gorbach, Gas–liquid chromatographic method for the assay of aminoglycoside antibiotics in serum, J. Chromatogr. 151 (1978) 133–146.
[8] S.S. Sampath, D.H. Robinson, Comparison of new and existing spectrophotometric methods for the analysis of tobramycin and other aminoglycosides, J. Pharm. Sci. 79 (1990) 428–431.
[9] H. Fabre, M. Sekkat, M.D. Blanchin, B. Mandrou, Determination of aminoglycosides in pharmaceutical formulations—II. High-performance liquid chromatography, J. Pharm. Biomed. Anal. 7 (1989) 1711–1718.
[10] F. Lai, T. Sheehan, Enhancement of detection sensitivity and cleanup selectivity for tobramycin through pre-column derivatization, J. Chromatogr. 609 (1992) 173–179.
[11] F. Wienen, U. Holzgrabe, A new micellar electrokinetic capillary chromatography method for separation of the components of the aminoglycoside antibiotics, Electrophoresis 24 (2003) 2948–2957.
[12] A.K. Dash, R. Suryanarayanan, A liquid-chromatographic method for the determination of tobramycin, J. Pharm. Biomed. Anal. 9 (1991) 237–245.
[13] H. Russ, D. McCleary, R. Katimy, J.L. Montana, R.B. Miller, R. Krishnamoorthy, C.W. Davis, Development and validation of a stability-indicating HPLC method for the determination of tobramycin and its related substances in an ophthalmic suspension, J. Liq. Chromatogr. Related Technol. 21 (1998) 2165–2181.
[14] E. Kaale, A. Van Schepdael, E. Roets, J. Hoogmartens, Development and validation of capillary electrophoresis method for tobramycin with precapillary derivatization and UV detection, Electrophoresis 23 (2002) 1695–1701.
[15] N.C. Megoulas, M.A. Koupparis, Development and validation of a novel HPLC/ELSD method for the direct determination of tobramycin in pharmaceuticals, plasma, and urine, Anal. Bioanal. Chem. 382 (2005) 290–296.
[16] M.X. Guo, L. Wrisley, E. Maygoo, Measurement of tobramycin by reversed-phase high-performance liquid chromatography with mass spectrometry detection, Anal. Chim. Acta 571 (2006) 12–16.
[17] B. Li, A. Van Schepdael, J. Hoogmartens, E. Adams, Characterization of impurities in tobramycin by liquid chromatography–mass spectrometry, J. Chromatogr. A 1216 (2009) 3941–3945.
[18] J. Szùnyog, E. Adams, E. Roets, J. Hoogmartens, Analysis of tobramycin by liquid chromatography with pulsed electrochemical detection, J. Pharm. Biomed. Anal. 23 (2000) 891–896.
[19] V.P. Hanko, J.S. Rohrer, Determination of tobramycin and impurities using high-performance anion exchange chromatography with integrated pulsed amperometric detection, J. Pharm. Biomed. Anal. 40 (2006) 1006–1012.
[20] A. Jouyban, E. Kenndler, Impurity analysis of pharmaceuticals using capillary electromigration methods, Electrophoresis 29 (2008) 3531–3551.
[21] C.L. Flurer, The analysis of aminoglycoside antibiotics by capillary electrophoresis, J. Pharm. Biomed. Anal. 13 (1995) 809–816.
[22] M.T. Ackermans, F.M. Everaerts, J.L. Beckers, Determination of aminoglycoside antibiotics in pharmaceuticals by capillary zone electrophoresis with indirect UV detection coupled with micellar electrokinetic capillary chromatography, J. Chromatogr. 606 (1992) 229–235.
[23] X.M. Fang, J.N. Ye, Y.Z. Fang, Determination of polyhydroxy antibiotics by capillary zone electrophoresis with amperometric detection at a nickel electrode, Anal. Chim. Acta 329 (1996) 49–55.
[24] H.H. Yeh, S.-J. Lin, J.-Y. Ko, C.-A. Chou, S.-H. Chen, Rapid and selective micellar electrokinetic chromatography for simultaneous determination of amikacin, kanamycin A, and tobramycin with UV detection and application in drug formulations, Electrophoresis 26 (2005) 947–953.
[25] W.S. Law, P. Kubáň, L.L. Yuan, J.H. Zhao, S.F.Y. Li, P.C. Hauser, Determination of tobramycin in human serum by capillary electrophoresis with contactless conductivity detection, Electrophoresis 27 (2006) 1932–1938.
[26] P. Kubáň, P.C. Hauser, Ten years of axial capacitively coupled contactless conductivity detection for CZE—a review, Electrophoresis 30 (2009) 176–188.

[27] M.N. El-Attug, B. Lutumba, J. Hoogmartens, E. Adams, A. Van Schepdael, Method development and validation for trifluoroacetic acid determination by capillary electrophoresis in combination with capacitively coupled contactless conductivity detection (CE-C4D), Talanta 83 (2010) 400–403.

[28] M.N. El-Attug, J. Hoogmartens, E. Adams, A. Van Schepdael, Capacitively coupled contactless conductivity detection (C4D) as an alternative detection mode in CE for the analysis of kanamycin sulphate and its related substances, J. Sep. Sci. 34 (2011) 2448–2454.

[29] P. Claes, F. Compernolle, H. Vanderhaeghe, Chromatographic analysis of neomycin. Isolation and identification of minor components, J. Antibiot. 27 (1974) 931–942.

[30] R. Pignatello, A. Mangiafico, L. Basile, B. Ruozi, P.M. Furneri, Amphiphilic ion pairs of tobramycin with lipoamino acids, Eur. J. Med. Chem. 46 (2011) 1665–1671.

Simultaneous determination of naringin, hesperidin, neohesperidin, naringenin and hesperetin of Fractus aurantii extract in rat plasma by liquid chromatography tandem mass spectrometry

Ling Tong [a,b], Dandan Zhou [b,c], Jun Gao [b], Yonghong Zhu [b], He Sun [b], Kaishun Bi [a,*]

[a] School of Pharmacy, Shenyang Pharmaceutical University, Wenhua Road 103, Shenyang 110016, China
[b] Tasly R&D Institute, Tianjin Tasly Group Co., Ltd., Tianjin 300402, China
[c] Institute of Chinese Materia Medica, Shanghai University of Traditional Chinese Medicine, Cailun Road 1200, Shanghai 201203, China

ARTICLE INFO

ABSTRACT

A liquid chromatography tandem mass spectrometry (LC–MS/MS) method was developed for the simultaneous determination of naringin, hesperidin, neohesperidin, naringenin and hesperetin in rat plasma, using liquiritin as the internal standard. Plasma samples extracted with a solid-phase extraction procedure were separated on a Zorbax SB-C18 analytical column (2.1 mm × 150 mm, 5 μm) and detected by electrospray ionization (ESI) in multiple reaction monitoring (MRM) mode. The calibration curves were linear over the range of 3.0–600 ng/ml for naringin, 0.5–100 ng/ml for hesperidin, 3.5–700 ng/ml for neohesperidin, 5.0–1000 ng/ml for naringenin and hesperetin, respectively. The lower limits of quantification were 0.5 ng/ml for naringin, hesperidin, naringenin and hesperetin, and 0.35 ng/ml for neohesperidin. Intra- and inter-day precision (RSD%) was less than 15% and accuracy (RE%) ranged from −3.3% to 4.8%. The validated method was successfully applied to investigate the pharmacokinetics of the major flavanones of Fructus aurantii extract after oral administration to rats.

© 2011 Published by Elsevier B.V.

1. Introduction

Fructus aurantii (Zhiqiao), the dried, mature fruit of Citrus aurantium L., is a well-known Traditional Chinese Medicine (TCM) with antioxidant [1], anti-tumor [2], antihypertension [3], anti-shock [4], etc. activity. Flavonoids are considered to be the major bioactive constituents of F. aurantii. Naringin, hesperidin, neohesperidin, naringenin and hesperetin (structures in Fig. 1), as the major citrus flavanone glycosides and aglycones had been investigated intensively, and were found to possess anti-oxidant, antiviral, anti-allergic, vasoprotective and anticarcinogenic properties [5–8].

Earlier publications have described several methods for determination of citrus flavanone glycosides and aglycones (naringin, hesperidin, naringenin or hesperetin) in biological samples utilizing HPLC–UV [9,10], microbore HPLC [11], GC–MS [12] and LC–MS/MS [13–17]. These researches usually aimed at pharmacokinetic or metabolic studies after the administration of reference substances or Tradititonal Chinese Medicine preparations (TCMp) containing F. aurantii. Li et al. [15] developed an LC–ESI/MS for analysis of naringin, hesperidin and neohesperidin in rat serum, but it showed unsatisfactory HPLC peak shape and no pharmacokinetic

data is provided. There are few papers published for simultaneous determination of citrus flavanone glycosides and aglycones (naringin, hesperidin, neohesperidin, naringenin and hesperetin) in biological fluids for pharmacokinetic study of F. aurantii extract. Yu et al. [16] published an LC–MS/MS method to determine ten major components of Da-Cheng-Qi decoction in dog plasma. In their paper, only three markers (naringin, naringenin and hesperidin) were selected in contrast to five in our study. The LLOQs were 3.13 ng/ml. F. aurantii extract contains abundant neohesperidin. However, few pharmacokinetic study on neohesperidin have been reported. It is necessary to develop a method for the quantitative analysis of this flavanone glycoside in plasma for the pharmacokinetic evaluation.

The aim of this study was to develop and validate a rapid and sensitive liquid chromatography–tandem mass spectrometry (LC–MS/MS) method for simultaneous quantification of naringin, hesperidin, neohesperidin, naringenin and hesperetin in rat plasma and to apply it to a pharmacokinetic study of F. aurantii extract.

2. Experimental

2.1. Chemicals and materials

Naringin, hesperidin, neohesperidin and liquiritin (I.S.) (purity > 98%) were received from the National Institute for
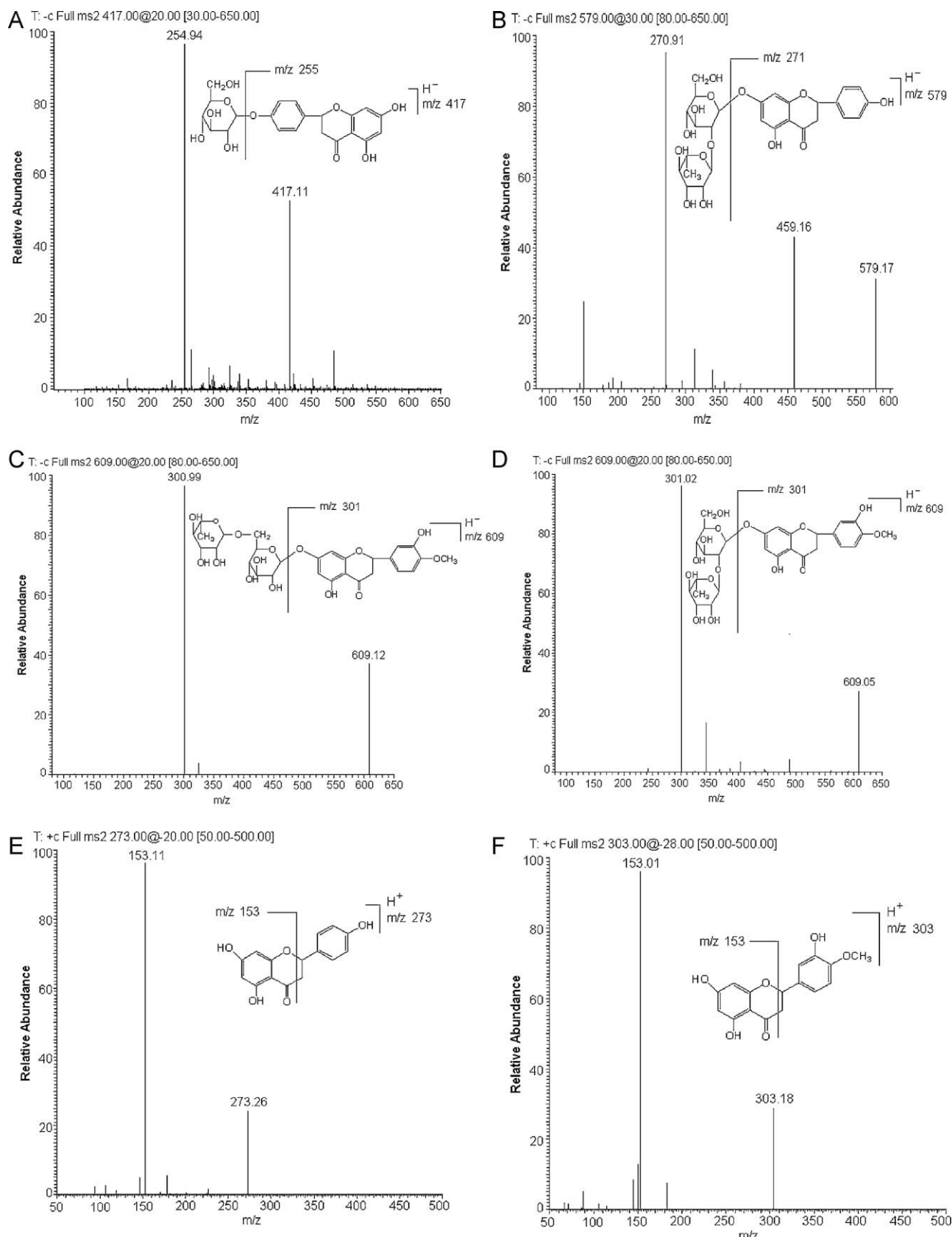
Fig. 1. Product ion mass spectra of [M−H]⁻ ions of (A) liquiritin (I.S.), (B) naringin, (C) hesperidin and (D) neohesperidin in negative mode, and [M+H]⁺ ions of (E) naringenin and (F) hesperetin in positive mode.
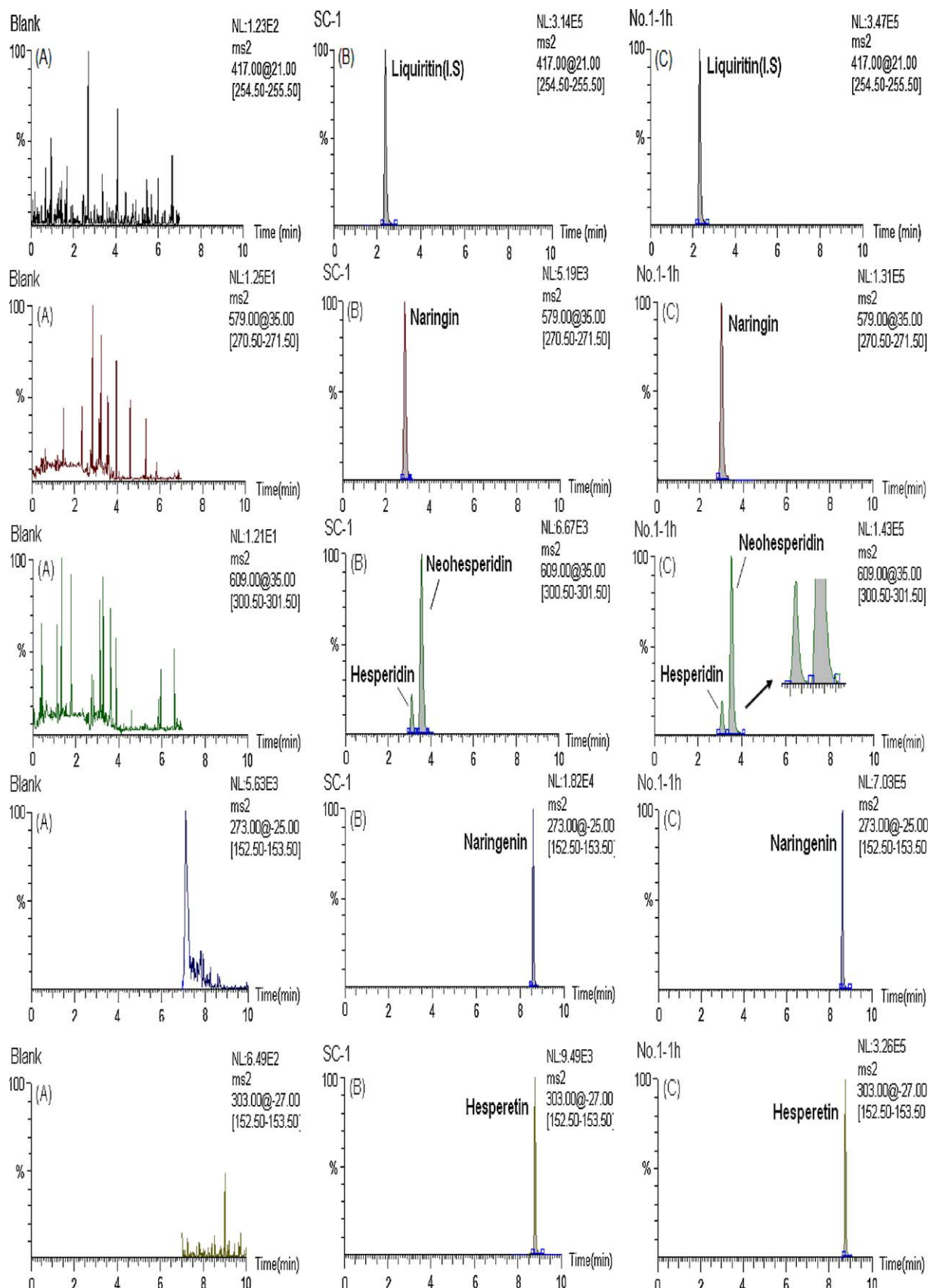
Fig. 2. Chromatograms of the flavonoids in (A) blank plasma, (B) blank plasma spiked with the five components and I.S. at the LLOQ (0.5 ng ml^{-1} naringin, 0.5 ng ml^{-1} hesperidin, 0.35 ng ml^{-1} neohesperidin, 0.5 ng ml^{-1} naringenin and 0.5 ng ml^{-1} hesperetin) and (C) plasma sample obtained 1 h after oral administration of *Fractus aurantii* extract.

Drug Control of China (Beijing, China). Naringenin and hesperetin (purity > 98%) were purchased from Delta Co. (Anhui, China). *F. aurantii* was purchased from the Medical Material Co. of Jiangxi province (Nanchang, China). HyperSep C$_{18}$ (SPE) cartridges (30 mg, 1 ml) were obtained from Thermo Co. (Waltham, MA, USA). Acetonitrile (Merck, Germany) and formic acid (Tedia, USA) were of HPLC grade, other chemicals were of analytical grade. Deionized water was prepared by Milli-Q system (Millipore, MA, USA).

2.2. Apparatus and LC–MS/MS conditions

The LC–MS/MS system consisted of a Surveyor^{TM} HPLC system and a TSQ Quantum triple quadrupole mass spectrometer equipped with an electrospray ionization (ESI) source (Thermo Finnigan, USA). Data acquisition was performed with Xcalibur 1.3 software.

Chromatographic separation was achieved at 30 °C on a Zorbax SB-C$_{18}$ column (150 mm × 2.1 mm i.d., 5 μm, Agilent, USA) and a C$_{18}$ guard column (5 μm, Phenomenex, USA). The mobile phase consisted of 0.1% formic acid water (A) and acetonitrile (B) using a gradient elution of 23–23% B at 0–3.0 min; 23–60% B at 3.0–3.5 min; 60–60% B at 3.5–9.0 min; 60–23% B at 9.0–12.0 min. The flow rate was 0.3 ml/min, and the injection volume was 20 μl.

Mass spectrometer was operated in negative mode for liquiritin (I.S.), naringin, hesperidin, neohesperidin and positive mode for naringenin and hesperetin. Quantification was obtained using multiple reaction monitoring (MRM) mode in two MS/MS scan segments. Segment I: 0.0–4.0 min in negative mode, liquiritin (I.S.), naringin, hesperidin and neohesperidin were monitored at m/z transitions of $417 \rightarrow 255$, $579 \rightarrow 271$, $609 \rightarrow 301$ and $609 \rightarrow 301$, with collision energies of 21 eV for liquiritin (I.S.) and 35 eV for naringin, hesperidin and neohesperidin, respectively. Segment II: 4.1–11.0 min in positive mode, naringenin and hesperetin were monitored at m/z transitions of $273 \rightarrow 153$ and $303 \rightarrow 153$, with collision energies of 25 eV, respectively. The MS parameters were as follows: spray voltage: 4.0 kV; heated capillary temperature: 350 °C; sheath gas (nitrogen): 35 psi; the auxiliary gas (nitrogen): 15 psi; the collision gas (argon) pressure: 1.5 mTorr. MS/MS operating conditions were optimized by infusion of the standard solution (1 μg/ml) of each analyte and I.S. into the ESI source via a syringe pump.

2.3. Preparation of F. aurantii extract

To calculate the administered dose of naringin, hesperidin, neohesperidin, naringenin and hesperetin, their contents in *F. aurantii* extract were quantitatively determined. The crude drug (10 g) was extracted twice by refluxing with boiling water (1:10, w/v) for 1.5 h and then filtered. The combined solution was concentrated under reduced pressure to give an extract of concentration equivalent to 0.4 g/ml *F. aurantii*, and stored at 4 °C until use. The HPLC analysis of the five flavanones was a modified version of a previously published method [18]. The contents of naringin, hesperidin, neohesperidin, naringenin and hesperetin in the extract were 0.812, 0.049, 1.090, 0.026 and 0.005 mg/g, respectively.

2.4. Preparation of standard and quality control samples

Stock solutions were prepared by dissolving the reference standards (100 μg/ml for naringin, hesperidin, neohesperidin, naringenin and hesperetin) and I.S. (100 μg/ml for liquiritin) in methanol. A series of standard mixture working solutions and the I.S. solution (150 ng/ml) were prepared freshly by further diluting the stock solutions with deionized water. All solutions were stored at 4 °C.

Calibration standards were prepared by spiking appropriate amount of the standard solutions in blank plasma (100 μl) to yield

final concentrations of 3, 9, 30, 75, 150, 300, 600 ng/ml for naringin; 0.5, 1.5, 5.0, 12.5, 25, 50, 100 ng/ml for hesperidin; 3.5, 10.5, 35, 87.5, 175, 350, 700 ng/ml for neohesperidin; 5, 15, 50, 125, 250, 500, 1000 ng/ml for naringenin and 5, 15, 50, 125, 250, 500, 1000 ng/ml for hesperetin, respectively. Three concentration levels of quality control (QC) samples were prepared containing naringin (9.0, 75, 480 ng/ml), hesperidin (1.5, 12.5, 80 ng/ml), neohesperidin (10.5, 87.5, 560 ng/ml), naringenin (15.0, 125, 800 ng/ml) and hesperetin (15.0, 125, 800 ng/ml) in the same manner.

2.5. Sample preparation

The SPE cartridges were conditioned and equilibrated with 1 ml of methanol, followed by 1 ml of water before use. Samples of plasma (100 μl), spiked with 100 μl of I.S. solution (150 ng/ml), 100 μl of deionized water (or standard solutions for calibration curve or QC samples) and 200 μl of 0.5% formic acid solution, were loaded onto SPE cartridges. After washed off with 1 ml of deionized water, the SPE cartridges were eluted with 1.0 ml methanol. The eluent was evaporated to dryness in vacuo at 40 °C. The residue was reconstituted with 100 μl of acetonitrile/water (20:80) and centrifuged at $10,000 \times g$ for 10 min under room temperature. The supernatant of 20 μl was injected into the LC–MS/MS.

2.6. Method validation

The specificity of the method was assessed by comparing lowest concentration in the calibration curves with blank rat plasma that had undergone the same pretreatment and analysis.

Calibration curves were confirmed by plotting the peak area ratio (y) of each analyte to I.S. versus plasma concentration (x) using weighed ($1/x^2$) least squares regression analysis. The limit of quantification (LOQ) was considered as the final concentration producing a signal-to-noise (S/N) ratio of 10.

The precision and accuracy were evaluated by assaying six replicates of QC samples at low, medium and high concentrations on the same day and three consecutive days. Precision was measured by intra- and inter-day relative standard deviation (RSD) and accuracy was described as relative error (RE).

The extraction recoveries were determined at three QC levels by comparing the peak area obtained from plasma sample spiked before extraction with those from plasma samples spiked after extraction. Similarly, the recovery of I.S. was evaluated at a single concentration of 150 ng/ml in the same way.

The matrix effect at three QC levels were assessed by comparing the absolute peak area of control plasma extracted and then spiked with a known amount of drug to that of neat standard samples at equivalent concentrations.

The stability of QC samples was evaluated by analyzing samples stored at room temperature for 4 h, three successive freeze (−20 °C)–thaw (room temperature) cycles, and processed samples under autosampler condition for 24 h. Samples were considered stable with the deviation from the nominal concentration within ±15.0%.

2.7. Application of the method and pharmacokinetic study

Six male Wistar rats, weighing 200 ± 20 g, were supplied by Vital River Lab Animal Technology Co., Ltd. (Beijing, China). The rats were housed under controlled environmental conditions (temperature 22 ± 2 °C; humidity $50 \pm 10\%$) with free access to food and drinking water until 12 h prior to experiments. After an oral administration of the *F. aurantii* extraction at a dose of 8 ml/kg, blood samples were collected into heparinized tubes from each rat by the puncture of the retro-orbital sinus prior to dosage and at 0.083, 0.167, 0.33, 0.67, 1.0, 2.0, 4.0, 6.0, 8.0, 10.0, 12.0, 24.0 and 30.0 h thereafter.

Following centrifugation (4000 × g for 10 min), plasma samples were stored at −20 °C until analysis. All pharmacokinetic parameters were processed by noncompartmental analysis using DAS 2.0 pharmacokinetic program (Chinese Pharmacological Society).

3. Results and discussion

3.1. Method development

According to the direct full-scan ESI mass spectra, the ion intensities of naringin, hesperidin, neohesperidin and I.S. was quite high in negative mode, while naringenin and hesperetin got greater sensitivity in positive mode. Product ion mass spectra of the five major flavanones in *F. Aurantii* extracts and I.S. are shown in Fig. 1. Naringin, hesperidin, neohesperidin and liquiritin (I.S.) are glycosides and their fragments were the result of the deprotonated ion [M−H]⁻ losing its glycons. Hesperidin and neohesperidin are isomers with identical product ion of 301. The MRM transitions on the negative ionization of naringin, hesperidin, neohesperidin and I.S. were selected at $579 \rightarrow 271$, $609 \rightarrow 301$, $609 \rightarrow 301$ and $417 \rightarrow 255$, respectively. For naringenin and hesperetin, the product ion mass spectra were recorded in positive ion mode from protonated molecular ions [M+H]⁺ and the most abundant fragment were the results of $[M+H - C_8H_8O]^+$ and $[M+H - C_9H_{10}O_2]^+$, respectively, at m/z both 153. Thus, the mass transition patterns, $273 \rightarrow 153$ and $303 \rightarrow 153$ were selected to monitor naringenin and hesperetin, respectively.

Different mobile phases were tested to optimize analytical performance. Acetonitrile, instead of methanol, was found to improve the resolution of hesperidin and neohesperidin. The addition of formic acid enhanced the sensitivity and improved the peak shape. The MRM chromatograms for each analyte are shown in Fig. 2. As mentioned, hesperidin and neohesperidin have identical precursor and product ions. Therefore, they were determined at the same channel with different retention times (Fig. 2). It was estimated that SPE could achieve satisfactory recoveries for both flavanone glycosides and aglycones after comparing several extraction procedures, though the recovery of analytes decreases as polarity decreases in SPE extraction.

3.2. Method validation

Representative chromatograms obtained from blank plasma, blank plasma spiked with the analytes (at LLOQs) and I.S., and plasma sample after an oral administration are shown in Fig. 2. No endogenous interference appeared around the retention time of the analytes and I.S. in drug-free specimens. The retention time of liquiritin (I.S.), naringin, hesperidin, neohesperidin, naringenin and hesperetin were 2.42, 2.91, 3.12, 3.59, 8.63 and 8.77 min, respectively.

The linear ranges, regression equations, LLOQs, and correlation coefficients obtained from typical calibration curves are shown in Table 1. All standard curves exhibited good linearity and the correlation coefficients (r) were higher than 0.9959. The LLOQs for naringin, hesperidin, neohesperidin, naringenin and hesperetin were 0.50, 0.50, 0.35, 0.50 and 0.5 ng/ml with coefficient of variation 10.3%, 13.1%, 9.31%, 9.75% and 12.7%, respectively. This sensitivity is better than described in [16].

As shown in Table 2, the method gave good precision and accuracy with the intra- and inter-day precision being ranged from 3.4% to 11% and 0.9% to 12%, respectively, while the accuracy ranged from −3.3% to 4.8%.

The extraction recoveries determined for all analytes are shown in Table 2. The mean extraction recovery of the I.S. was 94.9 ± 3.0%.

The observed matrix effects ranged from 98.1% to 107.6% for naringin, 86.1% to 101.2% for hesperidin, 94.7% to 103.5% for
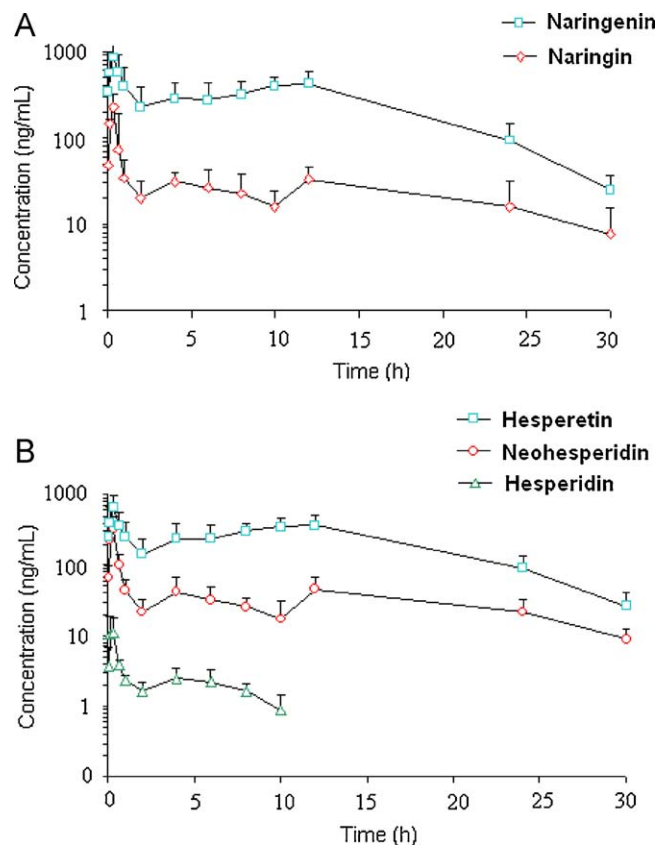

Fig. 3. Mean ± SD plasma concentration–time profiles for naringin, naringenin (A), neohesperidin, hesperetin and hesperidin (B) in rat plasma after oral administration of *Fractus aurantii* extract.

neohesperidin, 88.6% to 95.2% for naringenin and 81.8% to 98.5% for hesperetin, indicating a negligible matrix effect on the ionization of the analytes.

Results of the stability tests showed that all analytes were stable in plasma samples for 24 h in autosampler condition after preparation (RE: −4.9–7.2%, RSD < 10%), for 4 h at room temperature (RE: −9.5–11%, RSD < 8.9%), and within three freeze–thaw cycles (RE: −3.0–11%, RSD < 13%).

3.3. Results of pharmacokinetic study

The developed assay was sensitive enough to measure all the five compounds in rat plasma samples obtained following oral administration of *F. aurantii* extract. The plasma concentration–time profiles of these components in rat plasma are shown in Fig. 3 and the estimated pharmacokinetic parameters are shown in Table 3. According to DAS software, their concentration time courses conformed to a two-compartment pharmacokinetic model. Compared with an early paper [16], the main pharmacokinetic parameters of naringin, naringenin and hesperidin were different from the data obtained in our study. This might be the result of the difference between single herbal medicine and TCMp, as the latter has an influence of herb–herb interactions. The trend in concentration–time profiles of naringenin and hesperetin were basically consistent with Xu et al. report [17]: both had double peaks. In addition, the AUC$_{0\sim t}$ of naringenin and hesperetin were much higher than those of naringin, hesperidin and neohesperidin, although the administered doses of aglycones were rather less than those of the glycosides. The phenomenon might be attributed to the hydrolysis of flavanone glycosides (naringin, hesperidin and

Table 1
Regression data and LLOQs of the multi-components determined.

Components	Linear range (ng/ml)	Linear regression equation	Correlation coefficient (r)	LLOQ (ng/ml)
Naringin	3–600	$y = 0.00513x + 0.00109$	0.9967	0.50
Hesperidin	0.5–100	$y = 0.00701x - 0.00164$	0.9967	0.50
Neohesperidin	3.5–700	$y = 0.00595x - 0.00174$	0.9961	0.35
Naringenin	5–1000	$y = 0.00421x - 0.00037$	0.9964	0.50
Hesperetin	5–1000	$y = 0.00287x - 0.00075$	0.9959	0.50

Table 2
Precision, accuracy and extraction recoveries of naringin, hesperidin, neohesperidin, naringenin and hesperetin for LC–MS/MS method.

Components	Spiked (ng/ml)	Intra-day concentration measured (ng/ml)	Precision (%, RSD)	Accuracy (%, RE)	Inter-day concentration measured (ng/ml)	Precision (%, RSD)	Accuracy (%, RE)	Extraction recovery (%)
Naringin	9.0	8.946 ± 0.860	11	−0.60	9.121 ± 0.940	4.1	1.3	86.7 ± 4.6
	75.0	73.65 ± 5.867	8.0	−1.8	74.48 ± 6.319	7.1	−0.69	89.5 ± 3.6
	480.0	487.8 ± 33.99	7.0	1.6	487.6 ± 33.97	2.8	1.6	91.2 ± 3.7
Hesperidin	1.5	1.479 ± 0.113	7.7	−1.4	1.504 ± 0.128	4.1	0.29	84.1 ± 4.2
	12.5	12.84 ± 0.599	4.7	2.8	12.83 ± 0.851	0.9	2.6	88.7 ± 3.5
	80.0	77.44 ± 4.008	5.2	−3.2	79.04 ± 5.062	5.9	−1.2	87.9 ± 4.6
Neohesperidin	10.5	10.55 ± 0.932	8.8	0.45	10.26 ± 0.875	5.9	−2.3	88.6 ± 6.4
	87.5	86.92 ± 5.798	6.7	−0.7	87.32 ± 5.486	2.4	−0.21	91.3 ± 3.4
	560.0	586.9 ± 19.70	3.4	4.8	564.8 ± 41.48	8.3	0.86	90.1 ± 3.2
Naringenin	15.0	15.02 ± 1.408	9.4	0.13	15.28 ± 1.252	5.3	1.9	73.1 ± 3.3
	125.0	130.8 ± 8.154	6.2	4.6	124.7 ± 9.533	11	−0.24	78.1 ± 2.4
	800.0	824.9 ± 64.29	7.8	3.1	821.7 ± 64.10	8.3	2.7	76.2 ± 2.8
Hesperetin	15.0	14.88 ± 1.513	10	−0.82	15.14 ± 1.344	5.9	0.91	64.2 ± 2.9
	125.0	120.8 ± 7.684	6.4	−3.3	124.1 ± 9.147	12	−0.71	69.5 ± 1.9
	800.0	784.4 ± 55.33	7.1	−1.9	793.4 ± 60.54	4.0	−0.82	67.4 ± 3.3

Table 3
Estimated pharmacokinetic parameters for naringin, hesperidin, neohesperidin, naringenin and hesperetin in rat plasma (n = 6) after oral administration of *Fractus aurantii* extract.

Parameter	Naringin	Hesperidin	Neohesperidin	Naringenin	Hesperetin
C_{max} (ng/mL)	279.1 ± 53.83	17.04 ± 3.042	418.4 ± 72.08	1088 ± 198.7	791.0 ± 165.5
T_{max} (h)	0.28 ± 0.08	0.25 ± 0.09	0.28 ± 0.08	0.42 ± 0.21	0.42 ± 0.21
$t_{1/2}$ (h)	9.45 ± 2.88	3.17 ± 1.21	8.39 ± 1.45	4.43 ± 0.60	4.85 ± 0.51
K_e (1/h)	0.079 ± 0.022	0.245 ± 0.083	0.085 ± 0.014	0.159 ± 0.019	0.144 ± 0.016
$AUC_{0\sim t}$ (ng h/mL)	745.4 ± 304.5	23.41 ± 7.237	985.7 ± 410.8	7597 ± 2778	6548 ± 2416
$AUC_{0\sim\infty}$ (ng h/mL)	867.1 ± 337.4	27.33 ± 9.789	1111 ± 446.9	7786 ± 2842	6760 ± 2474
$MRT_{0\sim t}$ (h)	11.0 ± 1.20	3.91 ± 0.51	10.9 ± 0.58	10.4 ± 1.11	10.8 ± 0.90
CL/F (L/h-kg)	3.09 ± 1.02	6.31 ± 1.48	3.41 ± 0.84	0.012 ± 0.005	0.003 ± 0.001

neohesperidin) mediated by gastrointestinal bacteria after oral administration [19,9].

4. Conclusion

The method reported was the first LC–MS/MS quantitative assay of naringin, hesperidin, neohesperidin, naringenin and hesperetin in rat plasma samples following oral administration of *F. aurantii* extract. The method was specific, sensitive, accurate and reproducible, and was successfully applied to the pharmacokinetic studies of citrus flavanones in biological samples.

References

[1] F.A. van Acker, O. Schouten, G.R. Haenen, W.J. van der Vijgh, A. Bast, Flavonoids can replace alpha-tocopherol as an antioxidant, FEBS Lett. 473 (2000) 145–148.
[2] Y. Satoh, S. Tashiro, M. Satoh, Y. Fujimoto, J.Y. Xu, T. Ikekawa, Studies on the bioactive constituents of Aurantii Fructus Immaturus, Yakugaku Zasshi 116 (1996) 244–250.
[3] Y.T. Huang, G.F. Wang, C.F. Chen, C.C. Chen, C.Y. Hong, M.C. Yang, *Fructus aurantii* reduced portal pressure in portal hypertensive rats, Life Sci. 57 (1995) 2011–2020.
[4] X.W. Zhao, J.X. Li, Z.R. Zhu, D.Q. Sun, S.C. Liu, Anti-shock effects of synthetic effective compositions of fructus aurantii immaturus. Experimental study and clinical observation, Chin. Med. J. (Engl.) 102 (1989) 91–93.
[5] M. Zielińska-Przyjemska, E. Ignatowicz, Citrus fruit flavonoids influence on neutrophil apoptosis and oxidative metabolism, Phytother. Res. 22 (2008) 1557–1562.
[6] O. Benavente-García, J. Castillo, Update on uses and properties of citrus flavonoids: new findings in anticancer, cardiovascular, and anti-inflammatory activity, J. Agric. Food Chem. 56 (2008) 6185–6205.
[7] K. Itoh, M. Masuda, S. Naruto, K. Murata, H. Matsuda, Antiallergic activity of unripe Citrus hassaku fruits extract and its flavanone glycosides on chemical substance-induced dermatitis in mice, J. Nat. Med. 63 (2009) 443–450.
[8] R.K. Saha, T. Takahashi, T. Suzuki, Glucosyl hesperidin prevents influenza a virus replication in vitro by inhibition of viral sialidase, Biol. Pharm. Bull. 32 (2009) 1188–1192.
[9] S.L. Hsiu, T.Y. Huang, Y.C. Hou, D.H. Chin, P.D. Chao, Comparison of metabolic pharmacokinetics of naringin and naringenin in rabbits, Life Sci. 70 (2002) 1481–1489.
[10] F.I. Kanaze, E. Kokkalou, M. Georgarakis, I. Niopas, A validated solid-phase extraction HPLC method for the simultaneous determination of the citrus flavanone aglycones hesperetin and naringenin in urine, J. Pharm. Biomed. Anal. 36 (2004) 175–181.
[11] T.H. Tsai, Determination of naringin in rat blood, brain, liver, and bile using microdialysis and its interaction with cyclosporin a, a p-glycoprotein modulator, J. Agric. Food Chem. 50 (2002) 6669–6674.
[12] M. Spanakis, S. Kasmas, I. Niopas, Simultaneous determination of the flavonoid aglycones diosmetin and hesperetin in human plasma and urine by a validated GC/MS method: in vivo metabolic reduction of diosmetin to hesperetin, Biomed. Chromatogr. 23 (2009) 124–131.
[13] Y. Liu, F.G. Xu, Z.J. Zhang, R. Song, Y. Tian, Simultaneous determination of naringenin and hesperetin in rats after oral administration of Da-Cheng-Qi decoction by high-performance liquid chromatography–tandem mass spectrometry, Biomed. Chromatogr. 22 (2008) 736–745.

[14] T.Z. Fang, Y.G. Wang, Y. Ma, W.W. Su, Y. Bai, P.Y. Zhao, A rapid LC/MS/MS quantitation assay for naringin and its two metabolites in rats plasma, J. Pharm. Biomed. Anal. 40 (2006) 454–459.

[15] X.L. Li, H.B. Xiao, X.M. Liang, D.Z. Shi, J.G. Liu, LC–MS/MS determination of naringin, hesperidin and neohesperidin in rat serum after orally administrating the decoction of *Bulpleurum falcatum* L. and *Fractus aurantii*, J. Pharm. Biomed. Anal. 34 (2004) 159–166.

[16] Q. Yu, J. Xiang, W.F. Tang, M.Z. Liang, Y.P. Qin, F. Nan, Simultaneous determination of the 10 major components of Da-Cheng-Qi decoction in dog plasma by liquid chromatography tandem mass spectrometry, J. Chromatogr. B 877 (2009) 2025–2031.

[17] F.G. Xu, Y. Liu, H.J. Dong, R. Song, Z.J. Zhang, Pharmacokinetic comparison in rats of six bioactive compounds between Da-Cheng-Qi decoction and its parent herbal medicines, Nat. Prod. Commun. 5 (2010) 795–800.

[18] F. Pellati, S. Benvenuti, M. Melegari, High-performance liquid chromatography methods for the analysis of adrenergic amines and flavanones in *Citrus aurantium* L. var. amara, Phytochem. Anal. 15 (2004) 220–225.

[19] B. Ameer, R.A. Weintraub, J.V. Johnson, R.A. Yost, R.L. Rouseff, Flavanone absorption after naringin, hesperidin, and citrus administration, Clin. Pharmacol. Ther. 60 (1996) 34–40.

Model-based strategy for bioanalytical method comparison: Measurement of a soluble ligand as a biomarker

Theingi M. Thway [a,*], Jin Wang [a], Laura A. Brunner [a], Wen Gu [b], Ivan Magana [a], Guy Padbury [a], Mark Ma [a]

[a] Pharmacokinetics and Drug Metabolism, Amgen Inc., One Amgen Center Drive, Thousand Oaks, CA 91320, United States
[b] Biostatistics-Medical Sciences, Amgen Inc., One Amgen Center Drive, Thousand Oaks, CA 91320, United States

ARTICLE INFO

ABSTRACT

Ligand binding assays (LBAs) are often the method of choice for quantification of protein biomarkers and therapeutic biologics during drug development. Soluble ligand X is a glycoprotein. To understand the role of circulating ligand X in drug–target relationship, an analytical method (Method 1) was developed and validated to measure circulating ligand X and to support early clinical studies. Change in the detection reagent led to the development and validation of a second method (Method 2). Both methods measure total circulating ligand X levels. To ensure that the method specificities and data were consistent upon method change, the two methods were cross-validated using three distinct sample types: (1) recombinant ligand X (rLIGX) spiked in buffer, (2) authentic serum samples containing endogenous ligand X (eLIGX), and (3) serum samples collected from patients being dosed with the therapeutic antibody (incurred samples). Methods were considered comparable if the 90% confidence interval (90% CI) fell within 0.80–1.25 for all sample types. The results from the comparison reveal that two methods were comparable for rLIGX samples with the 90% CI of 0.90–1.07. However, with eLIGX samples, Method 1 produced higher mean (±SD) concentrations 675 (±316 pg/mL) than Method 2 195 (±97 pg/mL) and the two methods were considered not comparable as the 90% CI was 0.27–0.29. With the incurred samples, the comparison results also indicated the incomparability of these two methods as the 90% CI was 0.57–0.65. To describe the statistically relevant relationship between two methods in analyzing the serum samples, linear and quadratic regression models were applied to derive two conversion equations; one each for eLIGX and incurred samples. The applicability of the equations was verified with independent study data to indicate that the equations can be used to relate two different sets of study data. A model-based strategy presented here can serve as an explicatory paradigm for other analogous situations in the future.

1. Introduction

Membrane bound receptors and soluble ligands are often targets for therapeutic development. During clinical development, the dose–response relationship of the ligand or the target to the therapeutic antibody is often evaluated. The potential association of serum ligand or receptor levels to other distal biomarkers in different or diseased populations is also investigated; therefore, a reliable method of measuring the ligand or receptor biomarker concentrations in serum is necessary.

Ligand binding assays (LBAs) are often the method of choice for quantification of protein biomarkers and therapeutic biologics [1]. When feasible methods are developed, fit-for-purpose method validations are often performed for biomarkers intended to

support therapeutic development [2,3]. The validation parameters for biomarkers include accuracy, precision, selectivity, specificity, stability, and dilutional parallelism [2,3]. In contrast to LBAs that are intended to measure therapeutic biologics for PK assessments, LBAs for biomarkers need to use recombinant standards (normally of endogenous proteins) that may not be well characterized and/or not fully representative of the endogenous biomarkers [2]. Nonetheless, the biomarker methods are powerful tools in providing a relatively quantitative measurement of the protein of interest during the therapeutic development.

To measure circulating endogenous serum ligand X (eLIGX) in serum, recombinant ligand X (rLIGX) was used as a calibrator. Method 1 was first developed, validated, and implemented in few initial studies. A change in capture reagent led to the development and validation of a second method of measuring ligand X (Method 2). During drug development, when comparing the concentration values from different studies that used different analytical methods, the method cross-validation between the two methods need

* Corresponding author. Tel.: +1 805 447 1000; fax: +1 805 499 9027.
E-mail address: tthway@amgen.com (T.M. Thway).

to be performed. Thway et al. described the cross-validation of different LBAs intended to quantify analytes for pharmacokinetic assessment [4]. In addition, various statistical approaches were suggested for determining the comparability or equivalence of different methods [5–7]. We used a similar experimental design by including 30 incurred serum samples and a mean ratio with two-sided 90% confidence interval (CI) statistical approach to determine the comparability of two LBAs for ligand X measurement [4]. This report describes the use of an additional statistical strategy in method comparison for biomarker LBA. When two methods are not comparable, we determine the relationship factors between the two LBAs and verify the relationship factors with the study data. This distinctive strategy can be a powerful tool to compare the biomarker data from different methods or studies.

2. Methods and materials

2.1. Accuracy and precision of bioanalytical methods in buffer and serum

Method 1 and Method 2, both measuring ligand X in human serum, were developed and validated at Amgen Inc., Thousand Oaks, CA. Mouse anti-ligand X monoclonal antibody clone A, supplied by Amgen Inc., was used as a capture reagent in both methods and two different mouse anti-ligand X monoclonal antibodies were used as detection reagents in each method (Table 1). To establish the endogenous ligand X level, multiple lots of individual human serum were obtained from Bioreclamation Inc. (NY, USA) and measured in each method prior to method pre-study validations. Two levels of serum sample controls (low and high SSCs) were prepared by pooling human sera with similar level of endogenous ligand X and used to represent endogenous analytes in serum samples following the same approach presented by Wang et al. [3]. Due to the presence of endogenous ligand X in human serum matrix, the standard calibrators were prepared by spiking rLIGX (Amgen Inc., CA, USA) in 1X I-Block buffer (Applied Biosystems, CA, USA) with 10% Tween-20. During accuracy and precision runs, 5 quality control (QC) sample levels were prepared by spiking rLIGX (Amgen Inc., CA, USA) at the lower limit of quantification, low QC, high QC, and upper limit of quantification in assay buffer and 100% serum. The samples were analyzed in at least 3 replicates per level in 8 runs. The accuracy (%RE) and precision (%CV) of QCs spiked in buffer were evaluated from their nominal concentrations. The recoveries of rLIGX spiked QCs (%RE) in human serum were calculated from their nominal concentrations after subtraction of the endogenous concentration from the total observed concentration (endogenous

and spiked). Each method validation was conducted by performing at least 6 accuracy and precision runs and each run had 3 replicates each of 5 QC levels and two replicates of SSCs. The data from QCs spiked with rLIGX in buffer were used to calculate the total error of the method to establish the method acceptance criteria since the blank subtraction will not be done for the determination of the endogenous ligand level during the sample analysis. The assay ranges and the method acceptance criteria established during validation are summarized in Table 1.

2.2. Bioanalytical method comparison for ligand X Methods 1 and 2

Cross-validation of Methods 1 and 2 were conducted during the validation of Method 2.

Three sample types were included in the method cross-validation: recombinant ligand X spiked at 11 concentration levels in the buffer (rLIGX samples), 30 individual normal human serum samples (eLIGX samples) purchased commercially from Bioreclamation Inc. (NY, USA), and 30 incurred serum sample pools containing therapeutic antibody (TA) and eLIGX (incurred samples) from an Amgen-sponsored clinical study. All samples were analyzed with both methods. The rLIGX buffer samples were analyzed in two duplicates to evaluate possible differential results between the two methods. The %difference of results obtained by the two methods was calculated using the following formula:

$$\%\text{Difference} = \frac{[\text{Method 1}] - [\text{Method 2}]}{[\text{Method 2}]} \times 100.$$

2.3. Equivalence analysis for Methods 1 and 2

Data analysis was performed by using SAS V9.1 on a Windows XP Professional operating system. To evaluate the equivalence of Methods 1 and 2, data were log-transformed before statistical analysis. The mean difference and the corresponding two-sided 90% CI were calculated and were then transformed back to give the estimated ratio of the geometric means of the two methods and the 90% CI of the ratio. The p-value of the method difference was also provided. The two analytical methods were considered equivalent or comparable if the 90% CI of the ratio was completely contained within the equivalence range [0.80, 1.25]. Analyses were done separately for the three different sample types.

2.4. Study population and sample numbers from each study

Data from 4 clinical studies (study A, B, C, and D) are presented. Patient populations in studies A and B were healthy men or women with disease between 45 and 59 years of age. Study A has 18 placebo-treated subjects and study B had 16 placebo-treated subjects. Serum samples from each placebo-treated subject were collected on at least 3 time points per patient for the measurement of ligand X. For this research report, only the ligand X data from placebo subjects were used for the validation of the relationship factor.

Patient populations in study C were either healthy men or women with disease between 45 and 59 years of age. Patient populations in study D were all women with disease and aged 60+ years. Serum samples were collected at only 1 time point per subject. Forty samples from each study were compared.

2.5. Statistical modeling for the goodness of fit

All statistical analysis and model fitting were analyzed with SAS v9.1 in a Window XP Professional environment. Data were log-transformed before statistical analysis, and the results were

Table 1
Procedures, reagents and parameter of Methods 1 and 2.

| Parameters	Method 1	Method 2
Assay format	Chemiluminescence Sandwich Assay	Electrochemiluminescence Sandwich Assay
Measures ligand X	In the presence/absence of therapeutic Ab	In the presence/absence of therapeutic Ab
Coating Ab	Anti-ligand X MAb, clone A	Anti-ligand X MAb, clone A
Detection Ab	HRP labeled anti-ligand X MAb	Ruthenium labeled anti-ligand X MAb
Alkaline pretreatment	Yes	No
Assay range	300–75,000 pg/mL	50–50,000 pg/mL
Standards	Bias: −20% to 20% (−25% to 25% at LLOQ) Precision: ≤25%	Bias: −20% to 20% Precision: ≤15%
Quality controls	Bias: −30% to 30% Precision: ≤25%	Bias: −25% to 25% Precision: ≤25%
Samples	Precision: ≤25%	Precision: ≤15%
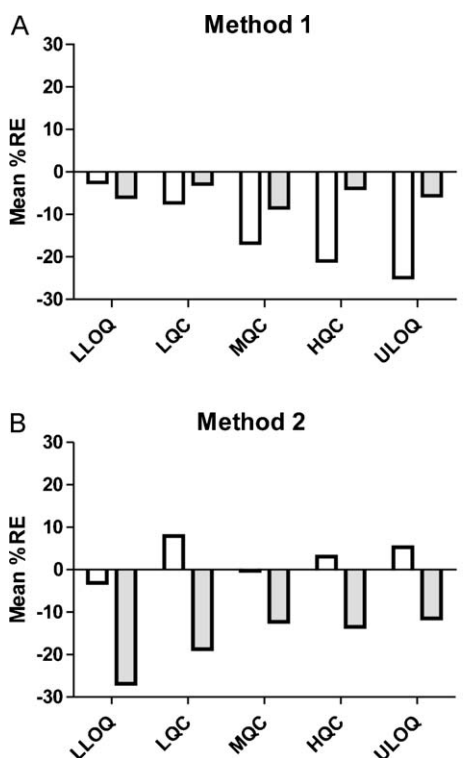
Fig. 1. Accuracy of Method 1 (A) and Method 2 (B) in measuring ligand X in serum and buffer. During accuracy and precision runs, 5 levels quality control (QC) samples were prepared by spiking rLIGX (Amgen Inc., CA, USA) at lower limit of quantification, low QC, high QC, and upper limit of quantification in assay buffer and 100% serum and %RE were calculated. Mean %RE indicated the cumulative results ($N = 24$) per level.

transformed back before reporting. Both linear and quadratic regression models were applied on the log-transformed data with Method 1 being the response and Method 2 being the covariate to model their relationship. The two nested models were compared by using the Chi-Square test. If the *p*-value of the nested comparison was less than 0.05, it indicated that the quadratic model performed significantly better than the linear model and it would be adopted as the final model. Otherwise, the simple linear regression model was used. In addition, goodness-of-fit of the final model was evaluated by using the residual plot and the residual normal plot. A 95% prediction interval of the relationship between Methods 1 and 2 was also evaluated. A prediction interval is an estimate in which future observations will fall, with a certain probability, given what has already been observed.

The back-calculated concentration results were fitted by using linear or quadratic regressions. The difference between Methods 1 and 2 was determined for both eLIGX and incurred samples.

3. Results

3.1. Accuracy of the methods

During the validation of each method, accuracy and precision parameters were tested by performing 6 analytical runs. Because of the presence of endogenous ligand X in human serum, the recoveries of QCs spiked in buffer were compared to that of serum. The %bias for QCs spiked in the buffer ranged from −21% to −2.5% and −3.1% to 7.9% in Methods 1 and 2, respectively (Fig. 1A and B). The %recoveries of QCs spiked in serum ranged from −8.5% to −2.9% and −26.9% to −11.5% in Methods 1 and 2, respectively. The highest inter-assay CVs were ≤27% for LLOQs and ≤20% for all other QCs in both methods. The high variability observed
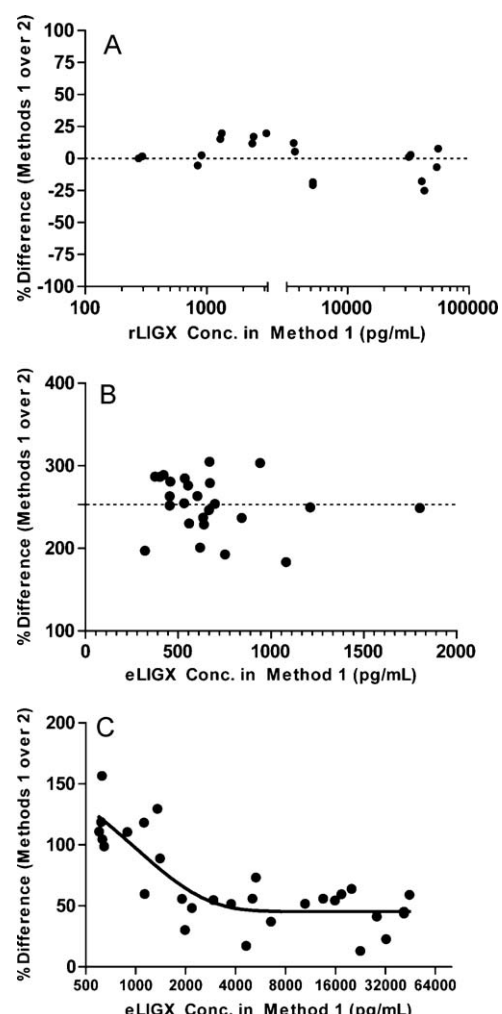

Fig. 2. Cross-validation of two ligand X methods using recombinant ligand X, rLIGX spiked samples (A), eLIGX samples (B) and incurred sample (C). (A) The results represent the %differences of Method 1 over Method 2 for rLIGX spiked samples at 10 different concentrations ranged from 0.275 to 55.7 ng/mL measured by Method 1. (B) The %differences of Method 1 over Method 2 for eLIGX samples (from 9 normal men, 3 normal women and 13 in diseased stage), measured in both methods. (C) The %differences of Method 1 over Method 2 for 30 incurred samples with the concentration ranging from 0.626 to 44.7 ng/mL.

at LLOQ was due to the accumulative errors of two measurements (endogenous and spiked total). The performance of QC was acceptable and the assay acceptance criteria were set as shown in Table 1.

3.2. Cross-validation of Methods 1 and 2 and equivalence testing

Method comparison was performed by using 3 different sample types: 11 rLIGX buffer samples (in duplicate), 30 eLIGX samples, and 30 incurred samples. A total of 21 results (1 data point was excluded due to high %CV) from rLIGX sample was used for data analysis. Using rLIGX samples, both methods measured similar concentrations in all spiked samples. The %difference of Method 1 over Method 2 is shown in Fig. 2A. Statistical analysis of rLIGX samples indicated that the ratio of geometric mean and 90% CI were 0.98 and 0.90–1.07, respectively (Table 2). The 90% CI was contained within the (0.80–1.25) equivalence interval (Table 2).

Using eLIGX samples, Method 1 consistently gave higher eLIGX concentrations than Method 2. Five sample pairs were excluded from comparison since 4 sample results measured by Method 2

Table 2
Equivalence between Methods 1 and 2.

Sample types	Geometric mean conc. measured by Method 1	Geometric mean conc. measured by Method 2	Ratio of Method 2 vs Method 1	90% CI of ratio	*p*-Value
rLIGX samples	4423.56	4503.00	0.98	[0.90, 1.07]	0.7075
eLIGX samples	177.27	623.28	0.28	[0.27, 0.29]	<0.0001
Incurred samples	2671.25	4387.43	0.61	[0.57, 0.65]	<0.0001

did not meet the analytical method acceptance criteria for %CV and 1 result was below the lower limit of quantification. The %difference in 25 samples ranged from 184 to 305% (Fig. 2B). The mean measured concentrations and standard deviation in eLIGX samples were $675 (\pm 316)$ pg/mL (3.5-fold higher) and $195 (\pm 97)$ pg/mL by Methods 1 and 2, respectively. Analysis of variance was performed, and the ratio of geometric means was determined to be 0.28. The 90% CI was 0.27–0.29 and was not contained within the (0.80–1.25) equivalence interval (Table 2).

Using incurred serum sample pools containing the therapeutic antibodies and eLIGX, a higher %difference (between 58% and 157%) was observed in samples containing an eLIGX concentration of <1900 pg/mL by Method 1 (Fig. 2C). A lesser %difference (between 13% and 73%) was observed in samples with an eLIGX concentration >1900 pg/mL. Analysis of variance was performed, and the ratio of geometric mean and the confidence intervals of the ratios were computed as 0.61 and 0.57–0.65, respectively (Table 2). The results indicated that Methods 1 and 2 were equivalent in measuring rLIGX but not comparable in measuring eLIGX concentrations.

3.3. Models to determine the relationship factors

Since the measured concentration values for eLIGX samples was not comparable between the two methods, a model-based strategy was planned to evaluate and compare historical study data measured by Method 1 with data from the studies in which Method 2 was used. To determine the relationship between the two methods for analyzing the eLIGX serum samples, both linear and quadratic regression models of method difference were compared on the log scale. The Chi-Square test for nested model comparison yielded a *p*-value of 0.4143. The quadratic model did not perform significantly better than the linear model in these samples; therefore, the linear model was chosen as the final model. Using the linear model, the following equation summarized their relationship for eLIGX samples:

$$\text{Method } 1 = \exp(1.51 + 0.95 \times \text{Log}(\text{Method } 2)) \tag{1.1}$$

or

$$\text{Method } 2 = \exp(-1.15 + 0.98 \times \text{Log}(\text{Method } 1)) \tag{1.2}$$

The *p*-value of the slope was 0.7280, indicating that the change in %difference vs concentration was not significant. When the concentration results measured by Method 2 were needed to compare the data obtained using Method 1, Eq. (1.1) could be used as a conversion factor. Similarly, when the concentration results measured by Method 1 were needed to compare the data obtained using Method 2, Eq. (1.2) could be used.

Similarly, for the incurred samples, both linear and quadratic models were fit to the log-transformed data to describe the relationship between Methods 1 and 2. The *p*-value of the nested model Chi-Square test was 0.0036, indicating that the quadratic model should be chosen as the final model. The quadratic regression and the model goodness-of-fit via the residual plot indicated that the quadratic model fit the data better. The following equations

summarized their estimated relationship for the incurred samples.

$$\text{Method } 1 = \exp(3.27 + 0.37 \times \text{Log}(\text{Method } 2) + 0.03$$
$$\times (\text{Log}(\text{Method } 2))^2) \tag{2.1}$$

or

$$\text{Method } 2 = \exp(-4.45 + 1.86 \times \text{Log}(\text{Method } 1) - 0.04$$
$$\times (\text{Log}(\text{Method } 1))^2) \tag{2.2}$$

The *p*-value of the slope was <0.0001 indicating that the decrease was significant.

From these models, two separate relationship factors were derived for two different sample types.

3.4. Confirmation and verification of the relationship factor/Eq. (1.1) or (1.2)

A 95% prediction interval of the relationship between Methods 1 and 2 was evaluated, and the results indicated that the model predicted data well (Fig. 3A). The same sets of data pairs were used to confirm whether Eq. (1.1) or (1.2) could be applied in adjusting the back-calculated ligand X concentrations. The eLIGX concentrations measured in 30 serum samples by Method 2 were adjusted with Eq. (1.1). The mean concentration adjusted by Eq. (1.1) was compared to the mean observed concentration quantified by Method 1 (Fig. 3B) or vice versa. The mean $(\pm SD)$ concentrations were $675 (\pm 316)$ pg/mL and $195 (\pm 97)$ pg/mL measured by Methods 1 and 2, respectively. After adjustment with Eq. (1.1), the concentration from Method 2 was $659 (\pm 318)$ pg/mL. The adjusted mean was comparable to the observed mean value $675 (\pm 316)$ pg/mL measured by Method 1 (Fig. 3B).

To verify this relationship factor with Eq. (1.1) or (1.2), additional independent data sets that were not used in deriving the relationship factor, were tested for further confirmation. In the first verification, Method 1 was used for study A and Method 2 was used for study B. The mean observed concentrations $(\pm SD)$ of placebo samples were $1190 (\pm 1104)$ pg/mL and $255 (\pm 94)$ pg/mL, respectively for studies A and B. The observed individual concentrations of placebo samples from study B were adjusted with Eq. (1.1). The mean adjusted concentration was compared to that of the mean concentrations of placebo samples from study A. Similarly, the observed individual concentrations of placebo samples from study A were adjusted with Eq. (1.2). The mean adjusted concentration was compared to that of mean concentrations of placebo samples from study B (Fig. 4A). In the second verification, Method 1 was used for study C and Method 2 was used for study D. The mean observed concentrations of samples were $821 (\pm 451)$ pg/mL and $258 (\pm 137)$ pg/mL, respectively, for studies C and D. The mean results of observed and adjusted concentration were comparable and shown in Fig. 4B using Eq. (1.1) or (1.2).

4. Discussion

LBA methods are the preferred tools for biomarker and PK assessment as a result of their high sensitivity, low cost, and high throughput. It is not uncommon that a change in any critical reagent (e.g., capture and/or detection antibodies) can lead to LBA method
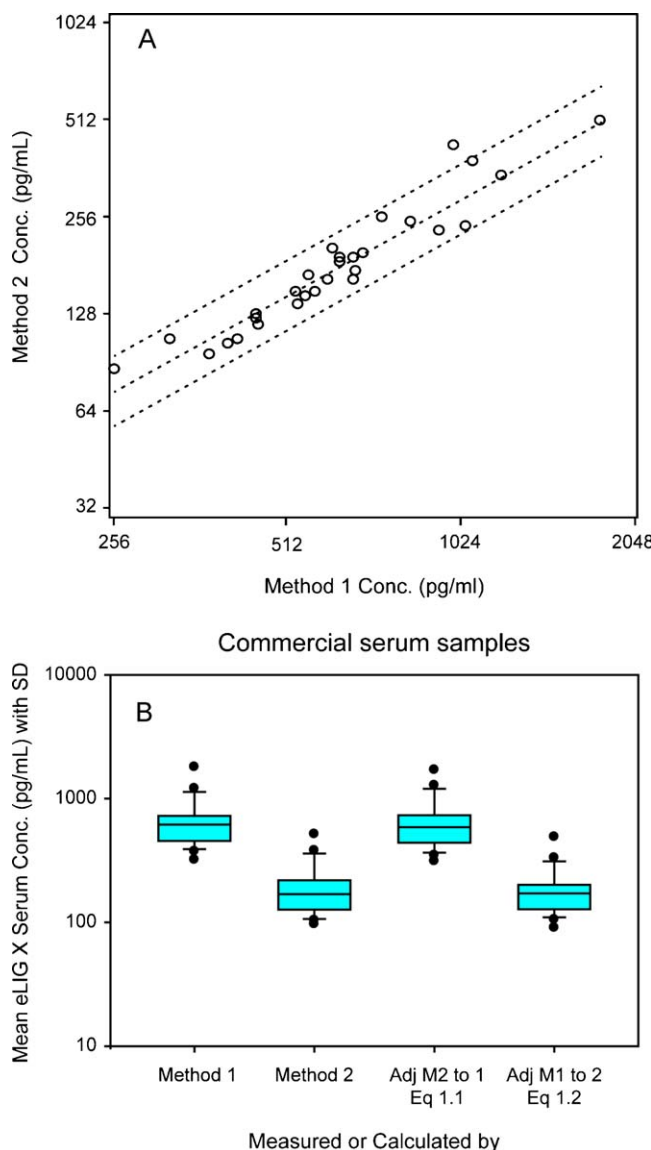
Fig. 3. (A) Model prediction with 95% confidence interval in data pair with eLIGX concentrations from 25 commercial samples. (B) The predicted LIGX concentrations were calculated with Eq. (1.1) or (1.2) on observed eLIGX concentrations of 25 sera measured by Method 1 or 2. The predicted LIGX concentrations were plotted against the observed LIGX concentrations.


Fig. 4. Verification of Eqs. (1.1) and (1.2) using two sets of data pair; study A vs B and study C vs D. eLIGX concentrations in studies A and C were measured using Method 1 while eLIGX concentrations in studies B and D were measured using Method 2. (A) eLIGX concentrations in placebo-dosed samples from study B had 3.5-fold lowered level than that of eLIGX concentrations in placebo-dosed samples from study A. The individual serum LIGX concentrations from Method 2 were adjusted with Eq. (1.1) and the mean concentration was computed. Then, the mean LIGX concentration from Method 2 was compared to those of Method 1. Similarly, individual serum LIGX concentrations from Method 1 were adjusted with Eq. (1.2) and the mean adjusted LIGX concentration from Method 1 was compared to those of Methods 1 and 2 prior to adjustment (Adj.M1to2) (B) eLIGX concentrations in serum samples from study D had 3.2-fold lowered level than that of eLIGX concentrations in serum samples from study C. Again, the individual serum LIGX concentrations from Method 2 or 1 were adjusted with Eq. (1.1) or (1.2), respectively and the mean adjusted LIGX concentrations were compared to those of Methods 1 and 2 prior to adjustment.

differences. In this paper, we have shown that the two methods are equivalent in measuring the recombinant LIGX and not equivalent in measuring the endogenous LIGX. We speculate that the lack of agreement between the two methods might be due to differences in binding affinity and/or recognition of epitopes between these antibodies and endogenous ligand. However, attempts to examine the actual biochemical basis leading to this disagreement between the two methods have been limited due to insufficient detection reagent from Method 1 and the near impracticality of purifying endogenous ligand. Since a different purification procedure for the detection reagent was used between the two methods, we investigated the potential role of this difference in the incomparability of the two methods; however, the data (not shown) suggested that the incomparability was not due to different purification processes. Based on these results and limitations, when possible, it is crucial to secure critical LBA reagent supplies in quantities sufficient to sustain long-term program support. Unfortunately, during the early stages of drug development, the quantity of well-characterized critical reagents can be limited. As drug development progresses, it is almost inevitable that different lots or different sources of critical reagents will be used in support of long-term studies. When multiple methods are used in the course of drug development, it is important to perform method comparison to ensure the consistency of the data obtained using different methods. If the original and newly developed methods, as in this presented case, are found not equivalent during method comparison, further method modification is required to re-establish the method comparability. Several attempts were made to optimize Method 2 including testing different conjugation ratio of the detection antibody, testing antibodies generated from other clones, and/or titering the detection reagent. Despite all these efforts, the method comparability still could not be restored. Therefore, an alternative approach was taken to examine the data comparability in supporting PK and pharmacodynamic (PD) analysis. Compared to other bioanalytical methods

(e.g., chromatographic methods) with wide linear standard calibration, LBAs, which demonstrate a narrow linear range, back calculation of standard concentration is achieved via non-linear regression models. Thus, a simple ratio or percentage difference is not suitable to determine the relationship between two LBAs. However, a statistical model can provide a conversion factor needed to verify the difference between the two methods and to compare the data generated from the different methods.

In this case, we have implemented a model-based statistical approach to determine the relationship between two methods for relevant sample types. Such a model-based approach was shown to be a valuable tool in determining comparability of data generated by different biomarker methods. In addition, data in this report demonstrated that different models are applicable for different sample types. During the statistical evaluation using multiple data sets and including additional verification, goodness-of-fit was evaluated on all relevant regression models. The 95% prediction intervals were valuable in evaluating various models. The final model may need to be further reconfirmed.

In summary, for any changes in bioanalytical methods, whether these are reagents, platforms, or procedures, method comparison is necessary. It is crucial to evaluate method equivalence to determine the impact of method changes. With thorough experimental method comparison design, which includes relevant sample types and sample numbers, this approach is useful in deriving statistically relevant relationships or conversion factors. In the presented case, the utility of a statistical model was implemented and proved to be valuable in the alignment of study results when the method equivalence could not be established. This approach can be applied to other similar situations where comparable data are required to perform PK/PD assessment.

5. Conclusion

Two bioanalytical methods of measuring serum ligand X concentration were developed and validated. The comparability of these two methods could not be established with incurred samples, and it led to the development of an alternative strategy that helped to compare data generated by using Method 1 with data generated by using Method 2. The two different relationship factors were derived from the most appropriate regression model for different sample types. Two relationship factors (Eqs. (1.1) and (1.2)) were confirmed and verified with additional study data. The results show that the equations describing the relationship between the two methods can be used when the data generated from one method are to be compared with that from the other. The model-based strategy presented can be applied when the cross-validation of different analytical methods fails and biomarker data from these methods are critical in understanding PK/PD relationship.

Acknowledgments

References

[1] J.W. Lee, M. Hall, Method validation of protein biomarkers in support of drug development or clinical diagnosis/prognosis, J. Chromatogr. B: Analyt. Technol. Biomed. Life Sci. 877 (2009) 1259–1271.
[2] J. Lee, V. Devanarayan, Y.C. Barrett, R. Weiner, J. Allinson, S. Fountain, S. Keller, I. Weinryb, M. Green, L. Duan, J.A. Rogers, R. Millham, P.J. O'Brien, J. Sailstad, M. Khan, C. Ray, J.A. Wagner, Fit-for-purpose method development and validation for successful biomarker measurement, Pharm. Res. 23 (2006) 12–328.
[3] J. Wang, J. Lee, D. Burns, D. Doherty, L. Brunner, M. Peterson, B. DeSilva, Fit-for-purpose method validation and application of a biomarker (C-terminal telopeptides of type 1 collagen) in Denosumab Clinical Studies, AAPS J. 11 (2009) 385–394.
[4] T.M. Thway, M. Ma, J. Lee, B. Sloey, Experimental and statistical approaches in method cross-validation to support pharmacokinetic decision, J. Pharm. Biomed. Anal. 49 (2009) 613–618.
[5] J.M. Bland, D.C. Altman, Statistical methods for assessing agreement between two methods of clinical measurement, Lancet 327 (1986) 1307–1310.
[6] J.M. Bland, D.C. Altman, Applying the right statistics: analysis of measurement studies, Ultrasound Obstet. Gynecol. 22 (2003) 85–93.
[7] J.O. Westgard, M.R. Hunt, Use and interpretation of common statistical tests in method-comparison studies, Clin. Chem. 19 (1973) 49–57.

Development and validation of a method using supported liquid extraction for the simultaneous determination of midazolam and 1′-hydroxy-midazolam in human plasma by liquid chromatography with tandem mass spectrometry detection

Camilla Svanström*, Gunnar P. Hansson, Leif D. Svensson, Carl Johan Sennbro

Department of Chemistry and Pharmaceutics, Active Biotech AB, Box 724, SE-22007 Lund, Sweden

ARTICLE INFO

ABSTRACT

The metabolic conversion of midazolam (MDZ) to its main metabolite 1′-hydroxy-midazolam (1-OH-MDZ) can be used as a probe drug for cytochrome P450 3A (CYP3A) activity. A sensitive method for the simultaneous determination of MDZ and its metabolite 1-OH-MDZ in human plasma using supported liquid extraction (SLE) in combination with liquid chromatography-tandem mass spectrometry (LC–MS/MS) detection was developed and validated. Plasma samples (100 μL) were diluted with 0.5 M NH_3 (aq) containing deuterated internal standards. The samples were extracted with ethyl acetate on a 96-well SLE-plate. Separation was performed on a Symmetry Shield RP18 column using an acidic gradient running from 2% to 95% methanol in 3 min. Detection was performed using a triple quadrupole mass spectrometer running in positive electrospray selected reaction monitoring (SRM) mode. The validated dynamic range was 0.2–100 nmol/L for both analytes. In the concentration range 0.6–75 nmol/L the extraction recoveries were in the ranges 91.2–98.6% and 94.5–98.3% for MDZ and 1-OH-MDZ, respectively. Matrix effects were more pronounced for MDZ than for 1-OH-MDZ but the response was still 75.4% or higher compared to a reference. The overall repeatability was within 2.2–7.6% for both analytes, the overall reproducibility was within 3.1–10.2% for both analytes and the overall accuracy bias was within −1.1 to 7.5% for both analytes. The method was successfully applied to determine the plasma concentrations of MDZ and 1-OH-MDZ in 14 healthy volunteers up to 24 h after administration of a single oral dose of 2 mg MDZ. The SLE technology was found to be convenient and suitable for sample preparation, and the developed method was found to be rapid, selective and reproducible for the simultaneous determination of MDZ and 1-OH-MDZ in human plasma.

© 2011 Elsevier B.V. All rights reserved.

1. Introduction

The metabolic conversion of midazolam (MDZ) to its main metabolite 1′-hydroxy-midazolam (1-OH-MDZ) is an established measure of human cytochrome P450 3A (CYP3A) activity [1–5]. MDZ is therefore often utilized in the pharmaceutical industry as a probe substrate in human drug–drug interaction (DDI) studies. Both induction and inhibition of metabolizing enzymes are complicating factors in drug development, potentially affecting the metabolism and clearance of many compounds [1,5–7]. The impact on the CYP3A enzyme subfamily is of special interest, as it is the main metabolizing enzyme for more than 50% of clinically used drugs [4,7]. MDZ is a sedative medical agent and in order to prevent unwanted side-effects in DDI studies conducted in healthy

volunteers, the administered doses of MDZ should be kept low [8]. Doses of 2 mg or lower are often used [4,8,9], resulting in maximum plasma concentrations of MDZ and its metabolites below 45 nmol/L. Therefore, the development of sensitive and robust methods for the determination of MDZ and its major metabolite 1-OH-MDZ in human plasma are important to support clinical development of new pharmaceuticals.

Several analytical methods for the determination of MDZ and 1-OH-MDZ have been described. However, these often hold insufficient LLOQ or demand complex sample preparations, often in combination with a need for large sample volumes [4,8–13]. The analytical method described herein was developed and validated in order to obtain a method that was both robust and sensitive, but also improved with respect to sample preparation for the simultaneous determination of MDZ and 1-OH-MDZ in human plasma. In order to achieve this, supported liquid extraction (SLE) in the 96-well plate format was evaluated in combination with liquid chromatography-tandem mass spectrometry (LC–MS/MS)

* Corresponding author. Tel.: +46 46 192099; fax: +46 46 192140.
*E-mail address:* camilla.svanstrom@activebiotech.com (C. Svanström).
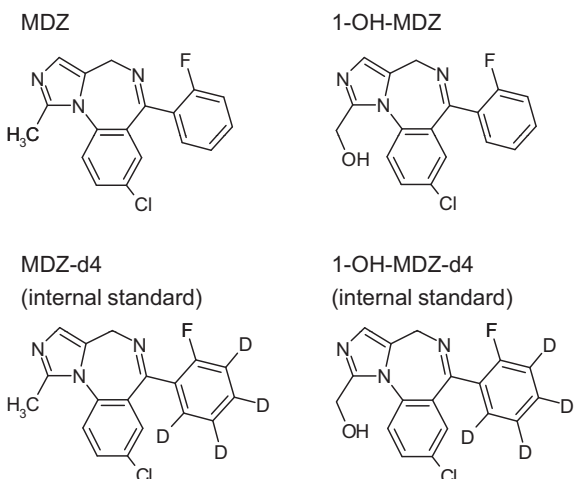
Fig. 1. Structural formula of MDZ, 1-OH-MDZ and their deuterated internal standards.

Fig. 2. Illustration of the front-flush configuration of the injection valve.

detection and stable isotope dilution. SLE is similar to liquid–liquid extraction (LLE) but differs from it in that the sample is totally absorbed onto a solid phase, containing a modified form of diatomaceous earth, on which the extraction occurs. The use of SLE in the 96-well format simplifies and also enables automation of the sample preparation. The aim of this study was to develop and validate an improved method for the simultaneous determination of MDZ and 1-OH-MDZ in human plasma using SLE in the 96-well format as sample preparation technique and to show that the method was applicable in a clinical DDI study.

2. Materials and methods

2.1. Chemicals

MDZ and 1-OH-MDZ were purchased from Toronto Research Chemicals (North York, Ontario, Canada) and the deuterated internal standards were purchased from Cerilliant Corporation (Round Rock, TX, USA). The chemical structure of the reference compounds are shown in Fig. 1. The purity of the reference compounds were 98% or higher. HPLC-quality acetonitrile and methanol were purchased from Fisher Scientific (Loughborough, Leicestershire UK). Ammonia (NH_3, 25% p.a.) and potassium hydroxide solution (KOH, 47% p.a.) were purchased from Merck (Darmstadt, Germany), trifluoroacetic acid (TFA, reagent grade $\geq$98%) was purchased from Sigma (St. Louis, MO, USA) and ethyl acetate (p.a.) was purchased from Fluka, Riedel-de Haën (Buchs, Switzerland). Deionized water was produced using a Milli-Q water purification system from Millipore (Bedford, MA, USA).

2.2. Equipment

Prior to extraction, the samples were centrifuged using an Eppendorf 5810R centrifuge with a swing-bucket rotor for micro plates (Eppendorf, Hamburg, Germany). For SLE extraction, ISO-LUTE SLE+, 200 mg Supported Liquid Extraction plates (Biotage, Uppsala, Sweden) were used. The samples were collected in 1 mL deep 96-well plates (Porvair Science, UK) which were sealed with a pierceable sealing foil (ABgene, Epsom, UK). During extraction, a vacuum manifold for 96-well plates (Waters Corporation, Milford, MA, USA) was used to monitor the pressure. For evaporation of the organic solvent a SPE Dry-96™ Sample Plate Concentrator (Argonaut, Foster City, CA, USA) was used.
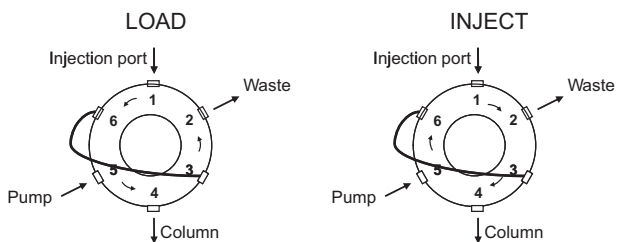
2.3. LC–MS/MS

The LC system used consisted of an HP 1100 binary pump from Agilent Technologies (Santa Clara, CA, USA) and a CTC HTS PAL autosampler from CTC analytics AG (Zwingen, Switzerland). In order to minimize the dwell volume of the system the standard gradient mixer was removed from the pump. The autosampler was equipped with a 6-port valve (Valco International, Schenkon, Switzerland) with a 20 μL external loop coupled in front-flush mode, the valve configuration is illustrated in Fig. 2. The effluent of the column was coupled to an API 3000™ triple quadrupole mass spectrometer from Applied Biosystems (Foster City, CA, USA) via an electrospray ion source operating in the positive mode. High-purity nitrogen gas was used as nebulizer, curtain and collision gas. Using collision induced fragmentation, quantitative analysis was performed with the mass spectrometer operating in the selected reaction monitoring (SRM) mode. The Analyst software version 1.4.2 from Applied Biosystems (Foster City, CA, USA) was used to control the LC–MS/MS system and to evaluate all acquired mass spectrometric data.

2.4. Standard solutions

2.4.1. Internal standard solutions

Internal standard stock solutions of MDZ-d4 and 1-OH-MDZ-d4 in methanol (about 20 μmol/L) were prepared by individual dilutions of the internal standard reference solutions.

An internal standard working solution containing 50 nmol/L each of the internal standards was prepared by adding aliquots of the internal standard stock solutions to 0.5 M NH_3 (aq). The internal standard working solution was stored in a refrigerator at 4–8 °C.

2.4.2. MDZ and 1-OH-MDZ stock and working solutions

Two stock solutions each of MDZ and 1-OH-MDZ (about 30 μmol/L and 60 μmol/L) in methanol were prepared. Working solutions containing both MDZ and 1-OH-MDZ (10 to 10 000 nmol/L) were prepared in methanol by further dilutions of the stock solutions. All stock solutions and working solutions were stored in a freezer at −20 °C.

2.4.3. MDZ and 1-OH-MDZ calibration standards and quality control samples

Calibration standards at eight different concentrations (0.10–98.3 nmol/L and 0.10–102 nmol/L for MDZ and 1-OH-MDZ, respectively) were prepared by spiking blank human plasma with known amounts of the working solutions containing a mix of MDZ and 1-OH-MDZ (1% (v/v) working solution in each calibration sample). Quality control (QC) samples at four different concentrations were prepared in the same way as the calibration standards. The nominal concentrations were 0.31, 0.60, 6.05, and 75.4 nmol/L for MDZ, and 0.29, 0.59, 5.97 and 73.5 nmol/L for 1-OH-MDZ. The calibration samples and QC samples were spiked in advance and stored frozen at −20 °C pending analysis.

2.5. Method development

2.5.1. LC–MS/MS method

Due to the fact that the analytical column, the autosampler wash solutions, the mobile phase composition and elution gradient were mainly generic for the instrument set-up it was not deemed necessary to further develop the LC method. However injection volume and back-flush vs. front-flush injection with partially filled loop was evaluated. The chromatographic conditions consisted of a mobile phase composition of 0.01% (v/v) TFA in methanol (A) and 0.01% (v/v) TFA in water (B). Two wash solutions were used to rinse the autosampler: a strongly alkaline methanol–water solution and an acidic organic solution consisting of acetonitrile with 0.2% (v/v) TFA. The analytes were separated from matrix components on a Symmetry Shield RP18, 30 mm × 2.1 mm column with 3.5 μm particles from Waters Corporation (Milford, MA, USA) using a gradient elution running from 2 to 95% (A) in 3 min followed by a wash out at 95% (A) for 0.5 min. The flow rate was 0.3 mL/min at ambient temperature and the chromatographic turnaround time was about 5 min.

The individual MS parameters for detection of MDZ and 1-OH-MDZ were automatically optimized using the Analyst Quantitative Optimization software.

2.5.2. Sample preparation

The parameters evaluated in method development were: extraction solvent, recovery of MDZ and 1-OH-MDZ after evaporation and reconstitution of the samples, and plasma volume to be extracted. Prior to extraction, the plasma samples were centrifuged at about $700 \times g$ for 5 min. At pH above 7.4 the azepine ring of MDZ is fully closed and the molecule becomes non-soluble in water [13]. Therefore, in order to enhance the extraction recovery, the plasma samples were diluted with 0.5 M NH$_3$ (aq) containing the deuterated internal standards prior to extraction. The diluted plasma samples were transferred to a SLE 96-well plate and absorbed onto the sorbent for about 5 min, with no breakthrough of liquid. After absorption, the samples were extracted by adding 1000 μL extraction solvent to each well. The extraction solvent was eluted by negative pressure and evaporated to dryness under a stream of heated nitrogen (35 °C) for approximately 20 min. Finally the residues were reconstituted in 100 μL methanol solution (aq) on a vortex mixer for approximately 15 min.

Ten different organic solvents or mixtures of solvents were investigated as extraction media for the SLE experiments. These were methyl acetate, ethyl acetate, tert-butyl acetate, toluene, toluene–isopropanol (99:1, v/v), ethyl acetate–hexane (9:1, v/v), ethyl acetate–heptane (3:1, v/v), hexane–dichloromethane (7:3, v/v) and isopropanol–dichloromethane (1:9, v/v). As a test solution for extraction experiments a plasma sample containing 30 nmol/L of both MDZ and 1-OH-MDZ was used.

The recoveries of MDZ and 1-OH-MDZ were investigated after evaporation and reconstitution in aqueous methanol solutions of various strengths (20, 30, 40 or 50%). The experiment was performed in a polypropylene 96-well plate. The test solutions were a mix of MDZ and 1-OH-MDZ in 50% methanol (aq) containing 0.61, 6.95, 75.6 nmol/L and 0.61, 7.04, 75.4 nmol/L for MDZ and 1-OH-MDZ, respectively. The test solutions were evaporated and then reconstituted in the aqueous methanol solutions. The unprocessed test solutions were used as reference.

The capacity of the 200 mg SLE-plate is 200 μL liquid and the manufacturer recommends the use of 100 μL plasma and 100 μL diluent. Here, a combination of 120 μL plasma and 80 μL diluent was also investigated.

2.6. Method validation

The evaluated parameters were SLE plate variation, selectivity, extraction recovery and matrix effects, dynamic range, LLOQ, accuracy and precision.

2.6.1. SLE+ plate variation

In total, seven SLE-plates (ISOLUTE SLE+, 200 mg, Biotage) packed with two different sorbent batches were used and evaluated during the experiments.

2.6.2. Selectivity

SLE extracts from human plasma were analyzed in order to confirm the absence of interfering peaks originating from endogenous compounds. Also the chromatographic selectivity between MDZ, 1-OH-MDZ and another hydroxylated metabolite, 4-hydroxymidazolam (4-OH-MDZ) was investigated.

2.6.3. SLE recovery and matrix effects

To investigate extraction recovery and matrix effects three different sets of samples were prepared and analyzed in replicates of six. The peak areas of the analytes were used in the evaluation. The samples prepared were spiked plasma samples prepared according to assay protocol (A), blank plasma samples prepared according to assay protocol with a reference solution added to the ethyl acetate prior to evaporation and reconstitution (B) and a reference solution in methanol, evaporated and reconstituted according to assay protocol (C). The following calculations were performed: extraction recovery (peak area (A)/peak area (B) × 100), matrix effect (peak area (B)/peak area (C) × 100) and total effect (peak area (A)/peak area (C) × 100). All sets of samples, containing a mix of MDZ and 1-OH-MDZ, were prepared and evaluated at three concentrations; 0.61, 6.95, 75.6 nmol/L and 0.61, 7.04, 75.4 nmol/L for MDZ and 1-OH-MDZ, respectively.

2.6.4. LLOQ, dynamic range and calibration graphs

The dynamic range and the LLOQ of the method were evaluated in the range 0.1–100 nmol/L for both MDZ and 1-OH-MDZ, based on expected pharmacokinetics of MDZ [9]. The dynamic range was evaluated by regression analysis and the LLOQ was defined as the lowest concentration of analyte where the back-calculated concentration could be determined with an accuracy bias of ±20% and a relative standard deviation (RSD) of ≤20%. After establishing the LLOQ and dynamic range of the method calibration standards in the ranges 0.21–98.3 nmol/L (n = 7) for MDZ, and 0.21–102 nmol/L (n = 7) for 1-OH-MDZ were evaluated at seven occasions.

2.6.5. Accuracy and precision of QC samples

QC samples at three concentrations: 0.60, 6.05, 75.4 nmol/L and 0.59, 5.97, 73.5 nmol/L, for MDZ and 1-OH-MDZ respectively, were analyzed and evaluated in replicates of six at three occasions and in replicates of four at four occasions.

2.6.6. Statistical evaluation

The Analyst software version 1.4.2 was used for integration of the chromatographic peak areas, for the calibration curve regression and for calculating the concentrations.

For the calculation of repeatability, the pooled relative standard deviation ($s_{r,p}$) was calculated. $s_{r,p}$ was calculated for each analyte at each concentration level using a formula obtained from the IUPAC Gold Book website [14].

For the calculation of reproducibility, the relative standard deviation (RSD) was calculated for all replicates at each concentration level for each analyte.

For the calculation of overall accuracy bias, the accuracy for all analyzed replicates was calculated at each concentration level for each analyte.

2.7. Method application

A clinical study including 14 healthy volunteers was initiated in order to evaluate the potential for drug interactions with a novel drug candidate via the CYP450 enzyme pathway. The subjects were orally administered a cocktail of five different CYP450 probe drugs including 2 mg MDZ. The metabolism of MDZ to its main metabolite 1-OH-MDZ reflected the activity of CYP3A enzyme. Blood and urine samples for analysis of the probe drugs and their metabolites were drawn on day 0 and day 12 of the study. The concentrations of MDZ and 1-OH-MDZ in plasma were analyzed at 11 time points (0, 0.5, 1, 1.5, 2, 4, 6, 8, 10, 12, and 24 h), for each subject on two occasions (day 0 and 12 of the study). The study protocol for the clinical trial was approved by the ethics committees of the participating study center before the start of the study, as were protocol amendments during study progression. All healthy volunteers provided written informed consent.

3. Results

3.1. Method development

3.1.1. LC–MS/MS method

Of the reconstituted sample extract 15 μL was injected onto the column using a partially filled 20 μL loop. To be able to inject 15 μL of the extract, the loop had to be mounted in front-flush mode or the chromatographic peak shapes of the analytes were distorted. The optimized MS conditions included an ion source temperature of 350 °C and an ion spray potential of 3500 V. Using collision induced fragmentation, quantitative analysis was performed with the mass spectrometer operating in positive electrospray (ESI) ionization and selected reaction monitoring (SRM) mode with unit resolution. The SRM transitions used for detection were m/z 326.1 > 291.3 and m/z 342.2 > 203.2 for MDZ and 1-OH-MDZ respectively. No cross-talk between the analytes was observed. Details of the optimized MS parameters are shown in Table 1.

3.1.2. Sample preparation

Of the ten organic solvents or mixtures of solvents investigated, ethyl acetate was considered to be the superior alternative showing excellent recoveries, satisfactory environmental aspects, ease of usage (pipettable) and sufficient volatility. Furthermore, the ethyl acetate extracts were visually clean and the noise and background levels observed in the SRM acquisitions were unusually low.

The recoveries of MDZ and 1-OH-MDZ after reconstitution in methanol solutions were in the ranges 70.3–93.4% and 83.0–105.3% for MDZ and 1-OH-MDZ, respectively. The results are shown in Table 2. Similar results were obtained for the internal standards. A solution consisting of 50% methanol (aq) was chosen for reconstitution of the samples.

We found that when extracting 120 μL plasma and 80 μL diluent, compared to extracting 100 μL plasma and 100 μL diluent, the peak areas of the analytes increased but the statistics such as precision and accuracy did not improve (data not shown). Therefore, 100 μL plasma was used for extraction further on.

3.2. Method validation

3.2.1. SLE+ plate variation

Comparison of the chromatograms regarding additional or interfering peaks showed that on one of the sorbent batches a small peak appeared in the SRM-transition for detection of 1-OH-MDZ, although that peak was separated from the peak of 1-OH-MDZ and did not interfere with the chromatography of 1-OH-MDZ.

3.2.2. Selectivity

The mass chromatograms of MDZ and 1-OH-MDZ showed extremely low background ionization and no interfering peaks were observed in either reference solutions or prepared plasma samples (Fig. 3A and B). The two hydroxylated metabolites 1-OH-MDZ and 4-OH-MDZ have the same molecular weight but showed unique product ions. Furthermore, they were chromatographically baseline separated, altogether indicating no interferences. Typical mass chromatograms of an extracted blank plasma sample and a sample with the concentration 0.2 nmol/L (LLOQ) of MDZ and 1-OH-MDZ are shown in Fig. 3.

3.2.3. SLE recovery and matrix effects

The extraction recoveries were in the ranges 91.2–98.6% and 94.5–98.3% for MDZ and 1-OH-MDZ, respectively. Matrix effects were more pronounced for MDZ than for 1-OH-MDZ but the response was still 75.4% or higher compared to a reference. The RSD in this experiment series was 13.3% or better. Similar results were obtained for the internal standards. The results are shown in Table 3.

3.2.4. LLOQ, dynamic range and calibration graphs

The LLOQ of the method was estimated to be 0.2 nmol/L for both MDZ and 1-OH-MDZ, i.e. the lowest calibration standard that was in compliance with the approval criteria. At LLOQ the reproducibility was 7.1% and 9.5% and the overall accuracy bias was −5.2% and −0.1% for MDZ (n = 7) and 1-OH-MDZ (n = 6), respectively. Calibration curves of MDZ and 1-OH-MDZ were obtained by plotting the peak area ratios of each analyte to its internal standard versus concentration. Using a quadratic regression (weight 1/concentration) the dynamic range of the method was estimated to be 0.2–100 nmol/L for both MDZ and 1-OH-MDZ. With few exceptions, the accuracies for the back-calculated values for the calibration standards were in compliance with the approval criteria ±15% (±20% at LLOQ) hence all calibration curves were approved and no analytical batches were rejected. The calibration curves were strongly reproducible and the correlation coefficient (r) was >0.999 for both MDZ and 1-OH-MDZ in all analytical batches.

3.2.5. Accuracy and precision of QC samples

With few exceptions, the accuracies of the QC samples were in compliance with the approval criteria of ±15% (±20% close to LLOQ). The overall results for the QC-samples are shown in Table 4.

3.3. Method application

The developed method was used for the analysis of human plasma samples from a clinical study with 14 healthy volunteers. In total 297 plasma samples were simultaneously analyzed for MDZ and 1-OH-MDZ in four analytical batches. No interfering peaks were detected in any of the plasma samples indicating a specific and selective method. Mass chromatograms from an incurred plasma sample are shown in Fig. 4. The sample was collected on day 0 of the study, 2 h after dosing and contained 15.7 nmol/L and 5.7 nmol/L of MDZ and 1-OH-MDZ, respectively. Of the analyzed plasma samples, 82% of the results were above LLOQ (0.2 nmol/L) and the C_{max} in the study was 87 nmol/L, which indicates sufficient calibration range for the given dose. On day 0 the compounds could be quantified up to 12 h after MDZ administration in most of the subjects, n = 13 and n = 11 for MDZ and 1-OH-MDZ, respectively. At 24 h MDZ and 1-OH-MDZ could be quantified in 3 and 2 subjects, respectively.

Table 1
SRM transitions and fragmentation parameters for the analytes and their internal standards.

Analyte	Precursor ion (m/z)	Product ion (m/z)	Dwell (ms)	DP (V)	FP (V)	CE (eV)	CXP (V)
MDZ	326.1	291.3	150	31	230	41	20
MDZ-d4	330.1	295.1	70	31	230	41	20
1-OH-MDZ	342.2	203.2	150	36	120	37	14
1-OH-MDZ-d4	346.2	203.2	70	36	120	37	14

DP, declustering potential; FP, focusing potential; CE, collision energy; CXP, cell exit potential.

Table 2
Recovery (%) of MDZ and 1-OH-MDZ at low, medium and high concentrations after reconstitution in methanol solutions with different strengths (20–50%).

Reconstitution solvent (% (v/v) methanol)	MDZ (nmol/L)			1-OH-MDZ (nmol/L)		
	0.61 ($n=3$)	6.95 ($n=3$)	75.6 ($n=3$)	0.61 ($n=3$)	7.04 ($n=3$)	75.4 ($n=3$)
Recovery with 20%	83.2	70.3	79.0	91.7	83.0	91.5
Recovery with 30%	93.4	81.0	81.1	84.6	94.2	95.0
Recovery with 40%	91.7	81.7	85.6	91.2	100.4	97.8
Recovery with 50%	93.2	91.9	90.4	88.6	105.3	98.4
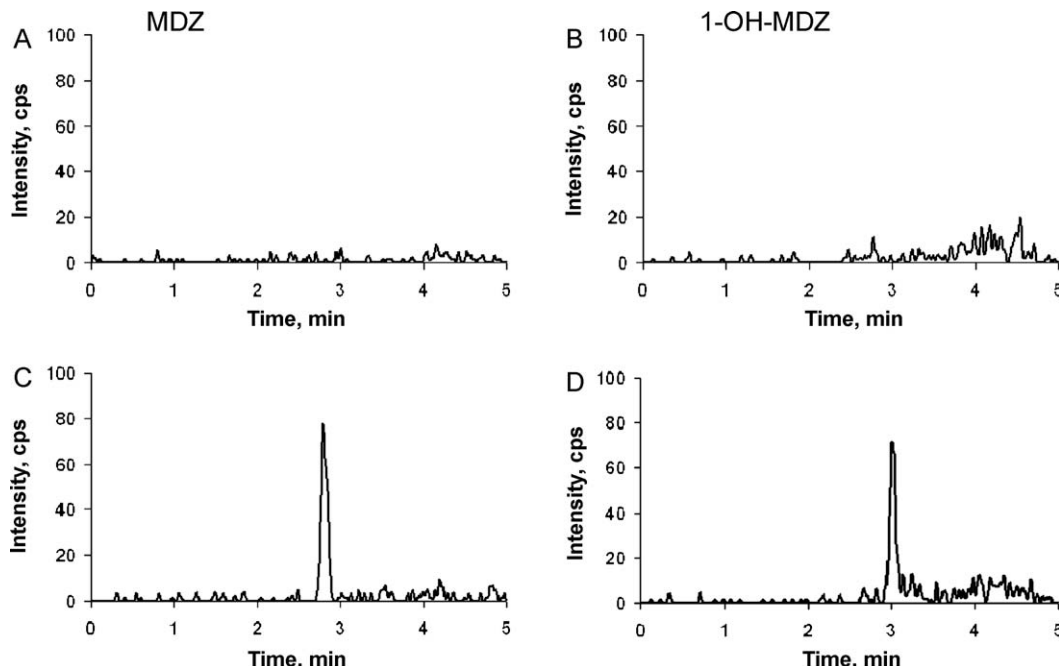
Fig. 3. Typical mass chromatograms of MDZ (A) and 1-OH-MDZ (B) from an extracted blank plasma sample and mass chromatograms of MDZ (C) and 1-OH-MDZ (D) from an extracted plasma sample containing 0.2 nmol/L (LLOQ) of MDZ and 1-OH-MDZ, respectively. The SRM transitions were 326.1 > 291.3 and 342.2 > 203.2 for MDZ and 1-OH-MDZ, respectively.

Average concentration–time profiles for MDZ and 1-OH-MDZ on day 0 are shown in Fig. 5.

4. Discussion

The method described herein utilizes SLE in the 96-well format in combination with LC–MS/MS and stable isotope dilution for the simultaneous determination of MDZ and its major metabolite 1-OH-MDZ in human plasma. This is the first time a method is reported that utilizes SLE as sample preparation

Table 4
The calculated overall accuracy bias, repeatability (intra-assay precision) and reproducibility (inter-assay precision) for the determination of MDZ and 1-OH-MDZ in QC-samples at three concentration levels. The QC-samples were analyzed and evaluated in replicates of six at three occasions and in replicates of four at four occasions.

	MDZ (nmol/L)			1-OH-MDZ (nmol/L)		
	0.60	6.05	75.4	0.59	5.97	73.5
Repeatability (%)	6.6	3.5	2.2	7.6	4.1	2.3
Reproducibility (%)	10.2	4.6	4.0	9.6	6.8	3.1
Accuracy bias (%)	4.0	7.0	5.7	7.5	−1.1	7.0

Table 3
Extraction recovery, matrix effect and total effect using absolute peak areas for the calculations.

|	MDZ (nmol/L)			1-OH-MDZ (nmol/L)		
	0.61 ($n=6$)	6.95 ($n=6$)	75.6 ($n=6$)	0.61 ($n=6$)	7.04 ($n=6$)	75.4 ($n=6$)
Extraction recovery (%)	96.7	91.2	98.6	94.5	95.5	98.3
Matrix effect (%)	75.4	87.0	83.2	91.0	105.5	94.6
Total effect (%)	72.9	79.4	82.1	86.0	100.7	93.0
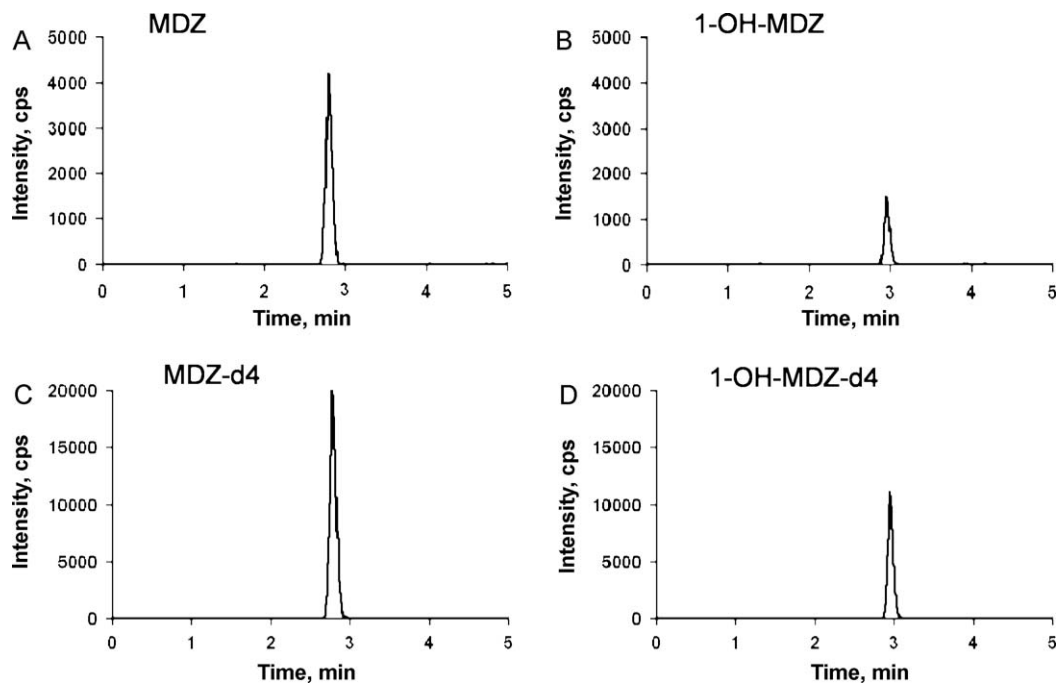
Fig. 4. Mass chromatograms from an incurred plasma sample collected 2 h after dosing on day 0 of the study, showing (A) MDZ at 15.7 nmol/L, (B) 1-OH-MDZ at 5.7 nmol/L, and their respective internal standard (C) and (D). The mass chromatograms show the raw data signals.

for the determination of these analytes. Our method shows superior sensitivity and selectivity compared to most methods previously reported in the literature [2,10–13]. Furthermore, the method is rapid, convenient to use and can be automated. The LLOQ of 0.2 nmol/L for both analytes was obtained using only 100 μL plasma for extraction. The evaluated quantification ranges (0.2–100 nmol/L for MDZ and 1-OH-MDZ) were sufficient to monitor the plasma concentrations from a clinical DDI study up to 24 h when a single oral dose of 2 mg MDZ had been administered. MDZ is a commonly used probe drug for the measuring of CYP3A activity and several bioanalytical methods for the determination of MDZ and 1-OH-MDZ have been described in the literature. Early methods utilizing UV-detection are generally not sensitive enough to support clinical DDI studies in which low doses of MDZ are to be administrated [10,13]. One method utilizing gas chromatography (GC) coupled to mass spectrometric detection obtained a LLOQ of 0.03 nmol/L although the sample preparation included time consuming extraction and

Fig. 5. Average plasma concentration–time profiles (±SD, lin–log) of MDZ and 1-OH-MDZ on day 0, after an oral dose of 2 mg MDZ. At 12 h $n = 13$ and $n = 11$ for MDZ and 1-OH-MDZ, respectively and at 24 h $n = 3$ and $n = 2$ for MDZ and 1-OH-MDZ, respectively.

derivatization steps [8]. Several sample preparation techniques for the analysis of MDZ and 1-OH-MDZ have been described in the literature and most of them, except LLE, are suitable for full automation. Still, the most frequently reported sample preparation technique is LLE, which is probably because it provides superior clean extracts and offers the possibility of concentrating the analytes during the extraction process. SLE in the 96-well plate format is a novel extraction technique in quantitative bioanalysis of small molecules. SLE is similar to LLE but differs from it in that the aqueous state is absorbed onto a solid phase that contains a modified form of diatomaceous earth on which the extraction occurs. Compared to traditional LLE, the SLE technology provides high analyte recoveries, eliminates emulsion formation, and shortens the sample preparation time [15,16]. The extraction conditions, i.e. pH and water immiscible solvent are often the same using LLE and SLE, which facilitates method transfer between the techniques. The use of SLE in the 96-well plate format combines the advantages of LLE and the 96-well format in a single technique which is rapid, easy to use and also enables automation of the sample preparation.

Due to its ability to provide superior sensitivity and specificity in complex matrices LC–MS/MS has emerged as the method of choice in supporting clinical and preclinical pharmacokinetic studies. With the LC–MS/MS technology, the use of a stable isotope as an internal standard is applicable. Stable isotope internal standards have the same chemical properties (molecular weight excluded) as the analyte. This results in robust methods in which the internal standard coelutes with the analyte and therefore compensates for effects such as ion suppression or ion enhancement, which may otherwise affect the results. Also, using the stable isotope dilution technique compensates for extraction recovery and injection malfunction. Altogether, LC–MS/MS in combination with isotope dilution is the state-of-the-art approach in the bioanalysis of small molecules.

Since the stabilities of MDZ and 1-OH-MDZ under various storage conditions have been well demonstrated in the literature, these parameters were not investigated in the validation. Plasma samples containing a mix of MDZ and 1-OH-MDZ have been shown
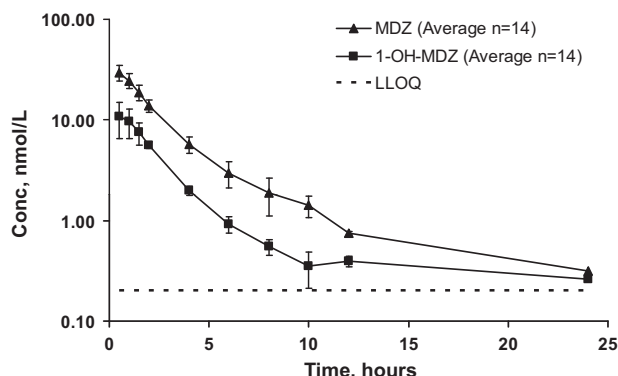
to be stable for at least 4 h at room temperature [11], at least 10 months stored in a freezer at −20 °C and they are not affected by three freeze-thaw cycles at −20 °C [9]. Stock solutions of MDZ and 1-OH-MDZ in methanol have been shown to be stable for at least 10 months stored in a freezer at −20 °C [9]. The short term stability of the internal standard working solution was investigated during the method development and no degradation of the internal standards was shown after one week stored in a refrigerator. Also, no issues regarding the stability of MDZ and 1-OH-MDZ were revealed during the sample preparation or in the reconstituted sample extracts stored at room temperature in the autosampler pending analysis.

After the development of this method, SLE-plates with higher capacity (400 mg compared to 200 mg) were launched; therefore a future improvement would be to evaluate these new plates. Also, the described method was developed on a LC–MS/MS system that was more than 10 years old, and using the same assay protocol on modern equipment would probably further improve the performance. Altogether, these improvements may lower the LLOQ of the method and as a result the doses of MDZ administrated to the healthy volunteers participating in clinical DDI studies could be even more decreased and hence further minimize unwanted side-effects for the study subjects.

5. Conclusions

SLE in combination with LC–MS/MS was found to be an excellent tool for the simultaneous determination of low levels of MDZ and 1-OH-MZ in human plasma. The method was found to be rapid, sensitive, selective and reproducible. The LLOQ 0.2 nmol/L for both analytes was achieved using only 100 μL plasma for the extraction. The validated dynamic range (0.2–100 nmol/L for MDZ and 1-OH-MDZ) was sufficient to monitor the plasma concentrations of both MDZ and 1-OH-MDZ for up to 24 h after a single oral dose of 2 mg MDZ in a clinical DDI study.

References

[1] G.E. Blakey, J.A. Lockton, J. Perrett, P. Norwood, M. Russel, Z. Aherne, J. Plume, Pharmacokinetic and pharmacodynamic assessment of a five-probe metabolic cocktail for CYPs 1A2, 3A4, 2C9, 2D6 and 2E1, Br. J. Clin. Pharmacol. 57 (2003) 162–169.

[2] V.A. Frerichs, C. Zaranek, C.E. Haas, Analysis of omeprazole midazolam and hydroxy-metabolites in plasma using liquid chromatography couples to tandem mass spectrometry, J. Chromatogr. B 824 (2005).

[3] S. Klieber, S. Hugla, R. Ngo, C. Arabeyre-Fabre, V. Meunier, F. Sadoun, O. Fedeli, M. Rival, M. Bourrie, F. Guillou, P. Maurel, G. Fabre, Contribution of the N-glucuronidation pathway to the overall in vitro metabolic clearance of midazolam in humans, Drug Metab. Dispos. 36 (2008) 851–862.

[4] B. Link, M. Haschke, M. Wenk, S. Krähenbühl, Determination of midazolam and its hydroxy metabolites in human plasma and oral fluid by liquid chromatography/electrospray ion trap mass spectrometry, Rapid Commun. Mass Spectrom. 21 (2007) 1532–1540.

[5] R. Mandrioli, L. Mercolini, M.A. Raggi, Benzodiazepine metabolism: an analytical perspective, Curr. Drug Metab. 9 (2008) 827–844.

[6] N.J. Plant, G.G. Gibson, Evaluation of the toxicological relevance of CYP3A4 induction, Curr. Opin. Drug Discov. Dev. 6 (2003) 50–56.

[7] S.-F. Zhou, Drugs behave as substrates, inhibitors and inducers of human cytochrome P450 3A4, Curr. Drug Metab. 9 (2008) 310–322.

[8] C.B. Eap, G. Bouchoux, K.P. Golay, P. Baumann, Determination of picogram levels of midazolam and 1- and 4-hydroxymidazolam in human plasma by gas chromatography-negative chemical ionization-mass spectrometry, J. Chromatogr. B 802 (2004) 339–345.

[9] M. Shimizu, T. Uno, H.-o. Tamura, H. Kanazawa, I. Murakami, K. Sugawara, T. Tateishi, A developed determination of midazolam and 1'-hydroxymidazolam in plasma by liquid chromatography-mass spectrometry: application of human pharmacokinetic study for measurement of CYP3A activity, J. Chromatogr. B 847 (2006) 275–281.

[10] S.L. Eeckhoudt, J.-P. Desager, Y. Horsmans, A.J.D. Winne, R.K. Verbeeck, Sensitive assay for midazolam and its metabolite 1'-hydroxymidazolam in human plasma by capillary high-performance liquid chromatography, J. Chromatogr. B 710 (1998) 165–171.

[11] V.A.P. Jabor, E.B. Coelho, N.A.G.d. Santos, P.S. Bonato, V.L. Lanchote, A highly sensitive LC–MS-MS assay for analysis of midazolam and its major metabolite in human plasma: application to drug metabolism, J. Chromatogr. B 822 (2005) 27–32.

[12] A. Kumar, H.J. Mann, R.P. Remmel, Simultaneous analysis of cytochrome P450 probes-dextromethorphan flurbiprofen and midazolam and their major metabolites by HPLC-mass-spectrometry/fluorescence after single-step extraction from plasma, J. Chromatogr. B 853 (2007).

[13] R. Lauber, M. Mosimann, M. Bührer, A.M. Zbinden, Automated determination of midazolam in human plasma by high-performance liquid chromatography using column switching, J. Chromatogr. B 654 (1994) 69–75.

[14] IUPAC, Compendium of Chemical Terminology, the Gold Book, 2nd ed., http://goldbook.iupac.org/ (accessed 8.4.11), doi:10.1351/goldbook.P04758.

[15] Biotage, Improve productivity and maximize analyte recovery, Technical note TN-0011.0105, 2006.

[16] L. Nguyen, W.-Z. Zhong, C.L. Painter, C. Zhang, S.V. Rahevendran, Quantitative analysis of PD 0332991 in xenograft mouse tumor tissue by a 96-well supported liquid extraction format and liquid chromatography/mass spectrometry, J. Pharm. Biomed. Anal. 53 (2010) 228–234.

Histone deacetylase 1 is required for Carbamazepine-induced CYP3A4 expression

Yin Wu [a,1], Xiaopeng Shi [a,1], Yonghong Liu [b], Xianzhi Zhang [c], Jinwen Wang [a], Xiaoxing Luo [d,**], Aidong Wen [a,*]

[a] Department of Pharmacy, Xijing Hospital, The Fourth Military Medical University, 127 Chang Le Xi Road, Xi'an, Shaanxi 710032, China
[b] Department of Neurology, Xijing Hospital, The Fourth Military Medical University, 127 Chang Le Xi Road, Xi'an, Shaanxi 710032, China
[c] Department of Health Service, School of Preventative Medicine, The Fourth Military Medical University, 169 Chang Le Xi Road, Xi'an, Shaanxi 710032, China
[d] Department of Pharmacology, School of Pharmacy, The Fourth Military Medical University, 169 Chang Le Xi Road, Xi'an, Shaanxi 710032, China

ARTICLE INFO

ABSTRACT

Carbamazepine (CBZ) is a commonly prescribed antiepileptic drug. Adverse effects and drug–drug interaction are the two major concerns for its clinic application. CBZ is mainly metabolized by cytochrome P450 (CYP) 3A4, a strong inducer of CYP3A4 as well, which in turn influences the pharmaceutical profiles of the co-administrated drugs. To date, little is known about the mechanisms underlying CBZ-induced CYP3A4 expression. In this study, we explored the possible roles of Pregnane X receptor (PXR) and the histone deacetylase 1 (HDAC1) on the CBZ-induced CYP3A4 expression. The results showed that: (1) Although the expression of PXR was increased in CBZ treated cells, PXR gene silencing surprisingly showed no significant effects on CBZ-induced CYP3A4 expression; (2) CBZ inhibited the binding of HDAC1 to the promoter of CYP3A4. In addition, both dominant negative form and siRNA of HDAC1 could repress the CBZ-induced CYP3A4 expression. These data, for the first time indicate that HDAC1, is required for the CBZ-induced CYP3A4 expression.

1. Introduction

Drugs metabolism in liver is mainly mediated by cytochrome P450. Among the P450 gene families, CYP3A4 is the predominant isoform of CYP3A enzymes and responsible for the metabolism of approximately half of commonly prescribed drugs [1]. Drug–drug interactions, one of the major concerns for rational drug administration, are thought to be mainly mediated by the activity of CYP3A4. Many drugs, especially xenobiotics can induce the expression of CYP3A4 and accelerate the elimination of concurrently used drugs, thereby altering the pharmacokinetic and pharmacodynamic profiles of those drugs, and sometimes leading to profound clinical consequences.

Carbamazepine (CBZ) is one of the most commonly prescribed drugs for treating partial seizures, generalized tonic–clonic seizures as well as trigeminal neuralgia [2]. It has also been administrated to patients with various psychiatric disorders, including acute mania, bipolar disorders and borderline personality disorders [3]. The bio-transformation of CBZ is mainly mediated by the activity of CYP3A4. In turn, it also shows a strong induction of CYP3A4, which influences the pharmaceutic profiles of CBZ and many co-administrated drugs, making the clinical usage of CBZ more cautious. For example, co-administration of CBZ and contraceptive drugs can increase the potential risks of un-intended pregnancy and deteriorate seizures [4]. Because of the CYP3A4 induction, it is suggested that patients should be followed up for 2–4 weeks after CBZ discontinuation to evaluate the antipsychotic adverse drug reactions [5]. Therefore, elucidating the mechanisms underlying the CBZ-induced CYP3A4 expression will be important for the rational administration of CBZ.

In the past decade, progress has been made in the molecular mechanisms responsible for the regulation of CYP3A4. On the promoter of CYP3A4, multiple transcription factor binding sites and histone acetylation sites were identified [6]. Among the transcription factors, Pregnane X receptor (PXR), was thought to be the major mediator of xenobiotics-induced CYP3A4 expression [7]. In addition, histone acetylation was also suggested to be associated with the ontogenic expression of CYP3A4. However, no direct evidence that PXR or histone acetylation contributes to the CBZ-induced CYP3A4 expression has been provided yet.

* Corresponding author at: Department of Pharmacy, Xijing Hospital, The Fourth Military Medical University, 127 Chang Le Xi Road, Xi'an, Shaanxi 710032, China. Tel.: +86 29 84773636; fax: +86 29 84773636.
** Co-corresponding author at: Department of Pharmacology, School of Pharmacy, The Fourth Military Medical University, 169 Chang Le Xi Road, Xi'an, Shaanxi 710032, China. Tel.: +86 29 84774591; fax: +86 29 84774591.
E-mail addresses: xxluo3@fmmu.edu.cn (X. Luo), adwen2011@gmail.com (A. Wen).
[1] These authors contribute equally to this paper.

In the present study, we explored the possible roles PXR and HDAC1 in CBZ-induced CYP3A4 expression, and for the first time, showed that HDAC1 was required for CBZ-induced CYP3A4 expression.

2. Materials and methods

2.1. Cell culture and treatment

Human liver tissues, from liver biopsy of patients with primary or secondary liver tumors, were collected according to the Declaration of Helsinki and the institutional guidelines of the Xijing Hospital, The Fourth Military Medical University, Xi'an, China, and with the informed written consent of each patient. Hepatocytes were isolated by trypsin digestion and cultured at 1.5×10^6 cells/well of a six-well plate with DMEM containing 10% fetal calf serum (FCS). After two days, cultures were maintained for 24 h in Williams'E medium supplemented with 100 nM dexamethasone, 2 mM L-glutamine, 1% ITS-G, 100 U/ml penicillin, and 100 U/ml streptomycin (Invitrogen). HepG2 cells were obtained from ATCC and maintained by DMEM containing 10% FCS.

For CBZ (Sigma) treatment, cells were incubated with 1 μM, 10 μM, 100 μM CBZ for 48 h. An equivalent amount of DMSO and 10 μM rifampicin (RIF) was used as negative and positive controls respectively. For Procyanidin-B3 (Pro-B3, National Institute for the Control of Pharmaceutical and Biological Products, Beijing, China) treatment, cells were challenged by 500 μM Pro-B or 10 μM CBZ plus 500 μM Pro-B respectively for 48 h.

For siRNA interference, dsRNA was synthesized according the following sequence which had been demonstrated to be effective in silencing the expression of PXR: UUUCAUCU-GAGCGUCCAUCAGCUCC [8]; HDAC1: GCAGAUGCAGAGAUUCAAU; and HDAC2 GCAGCGUCUCUUUGAGAAC [8]. High-purity scramble sequence (Low GC) siRNA oligonucleotides were used as negative control. Transfection of siRNA was conducted with Lipofectamine 2000 transfection reagent (Invitrogen) according to the manufacturer's instructions. A final concentration of 100 nM siRNA was incubated with the transfection complexes for 48 h.

For stable transfection, HepG2 cells expressing dominant negative HDAC1 or dominant negative HDAC2 plasmids [8] were selected with G418 (800 μg/ml) for 2 weeks.

2.2. Real time PCR

Total RNA was extracted using Trizol reagents (Invitrogen). cDNA was synthesized from 1 μg of total RNA using AMV Reverse Transcriptase (Takara) at 37 °C for 1 h in the presence of random hexamers. One tenth was used for real time RT-PCR amplification using the Light Cycler apparatus (Stretegene Mx3500P). The primers for CYP3A4 and PXR are as the followings: CYP3A4 forward primers: GCAGGAAAGCTCCATGCA-CATAG; reverse primers: GAGAAGCCAGGTTTCCATGG. PXR forward primers: ACTTACCACCAAGCAGTCCAAGAG; reverse primers: CTCATCTGCGTTGACACTGG. The measurements were performed in triplicates. Expression of CYP3A4 and PXR mRNA was normalized to housekeeping gene glyceraldehyde-3-phosphate dehydrogenase (GAPDH). Relative differences in real time RT-PCR among samples were determined using the $\Delta\Delta CT$ method as described in the Stretegene instructions. The ΔCT value for each sample was determined using the CT value obtained from the means of triplicates. The $\Delta\Delta CT$ was calculated by subtracting control ΔCT values from the corresponding experimental ΔCT. The resulting values were converted to fold-changes over control by raising 2 to the power of $-\Delta\Delta CT$.

2.3. Luciferase reporter assay

A chimera p3A4-luc reporter construct containing the basal promoter (−362/+53) with proximal PXR response element and the distal xenobiotic responsive enhancer module (−7836/−7208) of the CYP3A4 gene 5′-flanking region was inserted to pGL3-Basic reporter vector [9]. A 1.5 kbp segment upstream the starting code of PXR was cloned into pGL3-Basic to make pPXR-luc plasmid. HepG2 cells were transiently transfected by lipofection 2000 with 300 ng/well of p3A4-luc or pPXR-luc reporter in 24-well plates. CBZ and Pro-B treatments were as described. Rellina (5 ng/well) was used as internal control. 24 h after transfection, cells were lyzed and luciferase activity was measured and normalized by the readings of rellina luciferase in each well.

2.4. Chromatin immunoprecipitation (ChIP)

ChIP was performed with minor modifications of the procedure described by ChIP kit (Upstate), using approximately $1.5–2 \times 10^7$ HepG2 cells cross-linked with 1% formaldehyde for 10 min at room temperature. Cell pellets were re-suspended in cell lysis buffer and incubated on ice for 10 min. The nuclei were pelleted and resuspended in nuclei lysis buffer (50 mM Tris–HCl [pH 8.1], 10 mM EDTA, 1% SDS plus protease inhibitor cocktail) and incubated on ice for 10 min. Chromatin was sheared to a size range of 0.3–0.5 kbp by sonication in a crushed-ice/water bath with four 20-s bursts of 200 W with a 30-s interval between bursts using a Bioruptor (Diagenode). Chromatin was pre-cleared for 1.5 h at 4 °C with 50% gel slurry of protein A–agarose beads saturated with salmon sperm DNA and BSA. Pre-cleared chromatin was diluted 3-fold in IP dilution buffer provided by the kit, and 10% of the supernatants were kept as inputs. The diluted chromatin was incubated overnight on a rotating platform at 4 °C with mouse anti-HDAC1 antibody (1:200, Millipore). The immune complexes were recovered by 1 h incubation at 4 °C with 50% gel slurry of either protein A–agarose. Cross-linking was reversed by adding NaCl to a final concentration of 0.3 M and incubated overnight at 65 °C in the presence of RNase A. Samples were then digested with proteinase K at 45 °C for 1.5 h. DNA was purified by chromatography on QIAquick® columns (PCR purification kit, Qiagen), eluted by water, and an aliquot was used for analysis by PCR. Touch down PCR reactions were performed using primers specific for the human Cyp3A4 promoter region. The primers sequences were: forward primer: TTCTTTGCCAACTTC-CAAGG; reverse primer: TCTGTGTTGCTCTTTGCTGG.

2.5. Statistical analyses

All experiments were repeated three times. ANOVA was performed for statistical analysis. When significant differences were found, post hoc comparisons were made using the Tukey honestly significant difference test. p value less than 0.05 was considered significant in all instances. Representative figures were shown and data presented as means ± standard error (S.E.).

3. Results and discussion

3.1. CBZ induces the expression of CYP3A4

Many clinically used anti-epileptic drugs display inductive effects on p450, which in turn affects the clearance of co-administered drugs, complicating the clinical use of these drugs. A typical example is CBZ. It is mainly metabolized by CYP3A4 [9], a cytochrome with wide inter-individual variation in population.
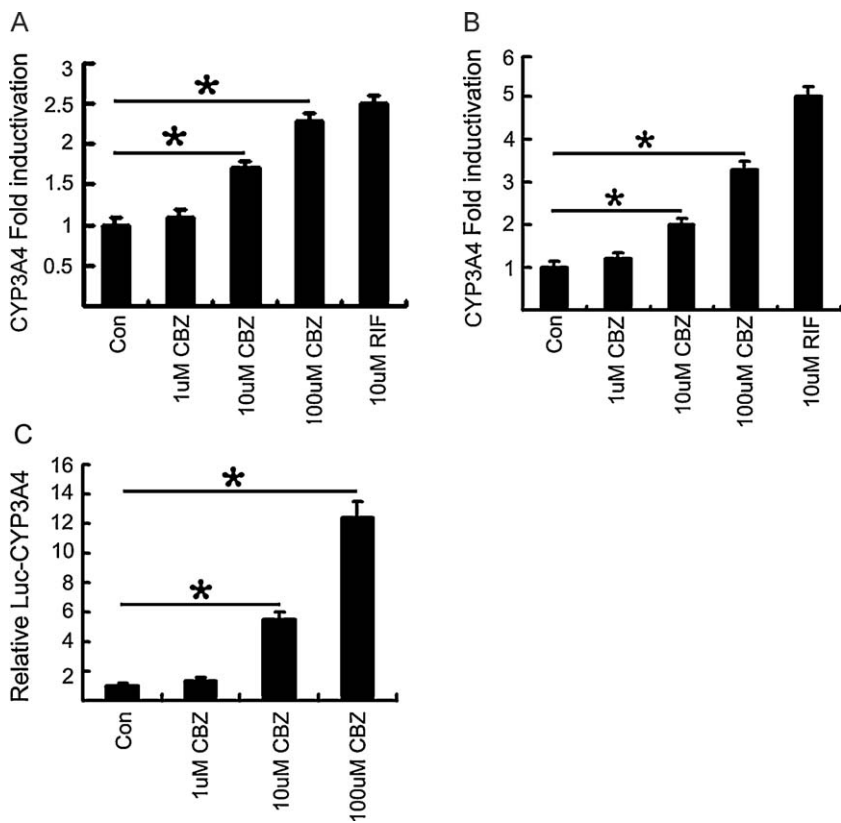
Fig. 1. CBZ induced CYP3A4 expression. Real time RT-PCR results of CBZ-induced CYP3A4 in HepG2 cells (A) and primary cultured human hepatocytes (B). Luciferase reporter assay of the expression of CYP3A4 promoter in CBZ treated cells (C). * indicates significant changes ($p < 0.05$) compared with control ($n = 3$).

We first examined the effects of CBZ on the expression of CYP3A4. HepG2 and primary cultured hepatic cells were treated by CBZ (from 1 μM to 100 μM) for 48 h. DMSO and 10 μM RIF were used as blank and positive controls respectively. CBZ dose dependently promoted the expression of CYP3A4 in HepG2 cells (Fig. 1A). The primary cultured hepatocytic cells were more sensitive to CBZ stimulation as same dose of CBZ induced more dramatic increase of CYP3A4 (Fig. 1B). To further confirm the inductive effect of CBZ on CYP3A4, we examined the transcription of CYP3A4 promoter under the treatment of CBZ. The luciferase reporter assay showed that the transcription of CYP3A4 promoter was significantly enhanced by CBZ dose dependently (Fig. 1C). These results indicate that CBZ induces the expression of CYP3A4 effectively *in vitro*.

3.2. CBZ-induced CYP3A4 expression is independent of PXR expression

Both genetic and epigenetic mechanisms have been suggested to be responsible for regulating the expression of CYP3A4. Gene polymorphism was originally proposed to contribute to the polymorphism of many p450 genes, including CYP3A4 [10]. However, rare evidence was identified by human study on the polymorphism of CYP3A4, indicating the existence of other regulatory mechanisms for the expression of CYP3A4 [11]. Through bioinformatic analysis, researchers have identified multiple transcription factor binding sites on the promoter of CYP3A4. Among those transcription factors, PXR has been suggested to be the most important [12]. Many drugs induce CYP3A4 expression through the activity of PXR [13]. Therefore, we examined the effects of PXR silencing on the expression of CBZ-induced CPY3A4 expression. We first stimulated HepG2 cells by 100 μM CBZ for 48 h and then measured the expression of PXR by real time RT-PCR. The results showed that 100 μM

CBZ induced a 3.5 fold increase of PXR mRNA expression compared with blank control (Fig. 2A), which was consistent with previous reports [14,15]. PXR siRNA suppressed the expression of PXR to about 20% of blank control (Fig. 2A). CBZ treatment in combination with PXR siRNA decreased the expression of PXR to a similar level as blank control ($p < 0.05$) (Fig. 2A). Furthermore, we checked the expression of CYP3A4 by co-stimulation with CBZ and PXR siRNA. Surprisingly, both real time RT-PCR and luciferase assay showed that PXR siRNA did not affect the expression of CYP3A4 significantly ($p > 0.05$) (Fig. 2B and C). These results indicated that although PXR was induced by CBZ, it might not contribute much to the CBZ-induced CYP3A4 expression.

3.3. CBZ inhibits the binding of HDAC1 to the promoter of CYP3A4

Since PXR expression is dispensable for CBZ-induced CYP3A4 expression, we hypothesized that chromatin modification might be responsible for the CBZ-induced CYP3A4 expression. DNA methylation has been demonstrated to be critical for regulating the expression of P450 genes, for example, CYP1B1 [14]. Our bioinformatic analysis showed that there was no CpG island in the promoter region of CYP3A4, precluding the possible regulation of CYP3A4 by DNA methylation. Because many anti-epileptic drugs, including CBZ are histone acetylation regulators [15,16], we then asked if histone acetylation were involved in regulating the expression of CYP3A4. HepG2 cells were treated with histone acetyltransferase inhibitor Procyanidin B3 (Pro-B3) to see if Pro-B3 could reduce the CBZ-induced CYP3A4 expression. The results showed that, 500 μM Pro-B3 reduced 100 μM CBZ induced CYP3A4 expression by about 48% ($p < 0.05$) (Fig. 3A), suggesting the involvement of histone acetylation in CBZ-induced CYP3A4 expression. ChIP assay was further performed to examine the binding of HDAC1
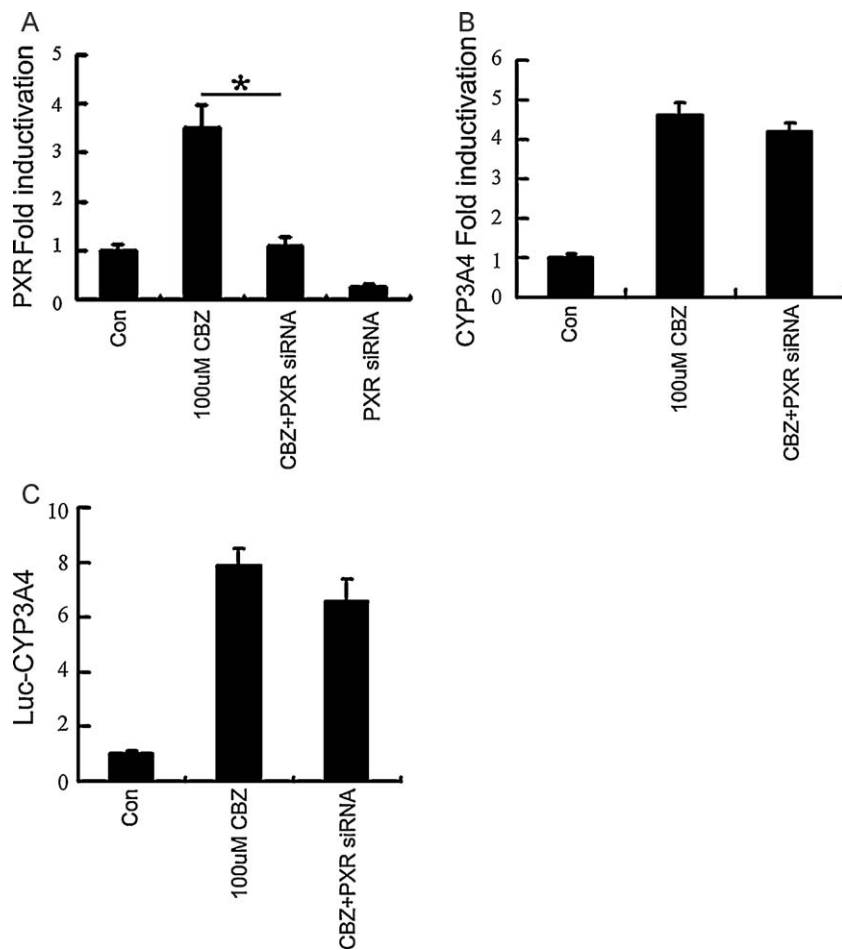
Fig. 2. Effects of PXR silencing on CBZ-induced CYP3A4 expression. Real time RT-PCR results of CBZ-induced PXR expression and siRNA interference of CBZ-induced PXR expression (A). Real time RT-PCR results of the effects of PXR siRNA on CBZ-induced CYP3A4 expression (B). Luciferase reporter assay of the expression of CYP3A4 promoter in CBZ treated cells treated with PXR siRNA (C). * indicates significant changes ($p < 0.05$) compared with control ($n = 3$).
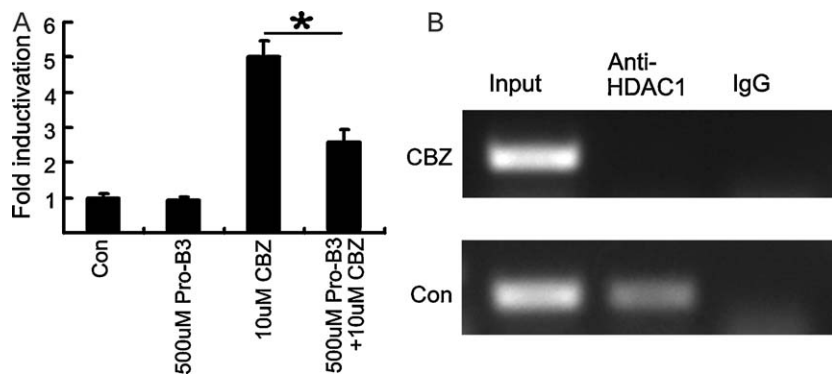

Fig. 3. Involvement of histone acetylation of CYP3A4 promoter in the CBZ-induced CYP3A4 expression. 500 μM Pro-B3 partially reduced CBZ-induced CYP3A4 expression (A). CBZ inhibited the binding of HDAC1 to the promoter of CYP3A4 (B). * indicates significant changes ($p < 0.05$) compared with control ($n = 3$).

to the promoter of CYP3A4. The results showed that in normal condition, HDAC1 bound to the promoter of CYP3A4. CBZ treatment inhibited the binding of HDAC1 to the promoter of CYP3A4 (Fig. 3B).

3.4. HDAC1 is required for the CBZ-induced CYP3A4 expression

To test whether HDAC1 were involved in CBZ-induced CYP3A4 expression, we first knocked down the expression of HDAC1 and HDAC2 respectively by siRNA, and then checked the CBZ-induced CYP3A4 expression. The results showed that HDAC1 silencing reduced the CBZ-induced CYP3A4 expression by 48.9% ($p < 0.05$), while HDAC2 silencing had no significant effect on the CBZ-induced CYP3A4 expression (Fig. 4A). To further confirm the results, we transfected and obtained the HepG2 cell lines that stably expressed dominant negative mutants of HDAC1 or HDAC2. DN-HDAC1 dramatically reduced the CBZ-induced CYP3A4 expression by 54.9% ($p < 0.05$), while DN-HDAC2 did not affect the expression of CYP3A4 (Fig. 4B). Taken together, our data, for the first time, revealed a role of HDAC1 in mediating the CBZ-induced CYP3A4 expression,
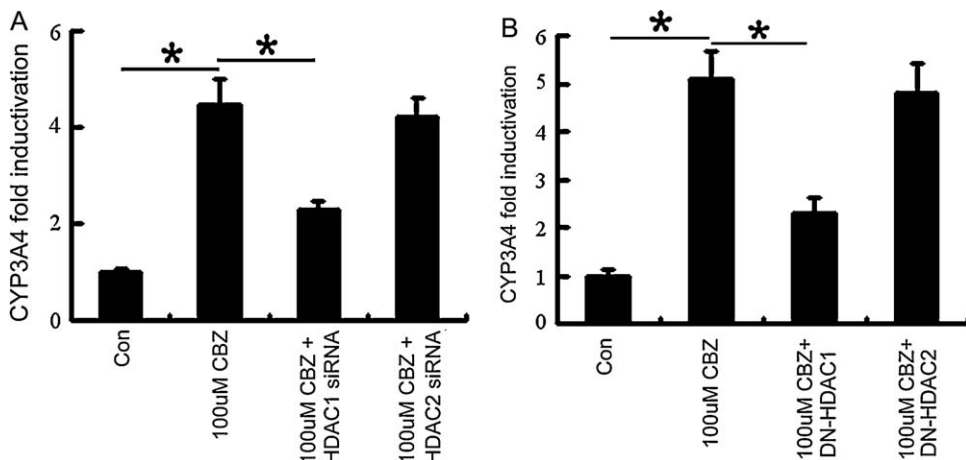
Fig. 4. Involvement of HDAC1 in the CBZ-induced CYP3A4 expression. HDAC1 siRNA inhibited the CBZ-induced CYP3A4 expression (A). DN-HDAC1 suppressed the CBZ-induced CYP3A4 expression (B). * indicates significant changes ($p < 0.05$) compared with control ($n = 3$).

providing a potential target for antagonizing the unwanted increase of CYP3A4 upon CBZ administration.

4. Conclusion

CBZ can efficiently induce the expression of CYP3A4 *in vitro*. PXR expression can be induced by CBZ but does not contribute to CBZ-induced CYP3A4 expression. HDAC1 is involved in CBZ-induced CYP3A4 expression.

Acknowledgements

References

[1] K.E. Thummel, G.R. Wilkinson, In vitro and in vivo drug interactions involving human CYP3A, Annu. Rev. Pharmacol. Toxicol. 38 (1998) 389–430.
[2] E. Beghi, E. Perucca, The management of epilepsy in the 1990. Acquisitions, uncertainties and priorities for future research, Drugs 49 (1995) 680–694.
[3] C.L. Ernst, J.F. Goldberg, Antidepressant properties of anticonvulsant drugs for bipolar disorder, J. Clin. Psychopharmacol. 23 (2003) 182–192.
[4] A. Sabers, Pharmacokinetic interactions between contraceptives and antiepileptic drugs, Seizure 17 (2008) 141–144.
[5] D.K. Strack, S.G. Leckband, J.M. Meyer, Antipsychotic prescribing practices following withdrawal of concomitant carbamazepine, J. Psychiatr. Pract. 15 (2009) 442–448.
[6] H. Qiu, M. Mathas, S. Nestler, C. Bengel, D. Nem, U. Godtel-Armbrust, T. Lang, S. Taudien, O. Burk, L. Wojnowski, The unique complexity of the CYP3A4 upstream region suggests a nongenetic explanation of its expression variability, Pharmacogenet. Genomics 20 (2010) 167–178.
[7] E.G. Schuetz, Lessons from the CYP3A4 promoter, Mol. Pharmacol. 65 (2004) 279–281.
[8] W. Lei, K. Zhang, X. Pan, Y. Hu, D. Wang, X. Yuan, G. Shu, J. Song, Histone deacetylase 1 is required for transforming growth factor-beta1-induced epithelial-mesenchymal transition, Int. J. Biochem. Cell Biol. 42 (2010) 1489–1497.
[9] B. Goodwin, E. Hodgson, C. Liddle, The orphan human pregnane X receptor mediates the transcriptional activation of CYP3A4 by rifampicin through a distal enhancer module, Mol. Pharmacol. 56 (1999) 1329–1339.
[10] A. Westlind, L. Lofberg, N. Tindberg, T.B. Andersson, M. Ingelman-Sundberg, Interindividual differences in hepatic expression of CYP3A4: relationship to genetic polymorphism in the 5'-upstream regulatory region, Biochem. Biophys. Res. Commun. 259 (1999) 201–205.
[11] D. Anglicheau, C. Legendre, P. Beaune, E. Thervet, Cytochrome P450 3A polymorphisms and immunosuppressive drugs: an update, Pharmacogenomics 8 (2007) 835–849.
[12] E. Sandanaraj, S. Lal, V. Selvarajan, L.L. Ooi, Z.W. Wong, N.S. Wong, P.C. Ang, E.J. Lee, B. Chowbay, PXR pharmacogenetics: association of haplotypes with hepatic CYP3A4 and ABCB1 messenger RNA expression and doxorubicin clearance in Asian breast cancer patients, Clin. Cancer Res. 14 (2008) 7116–7126.
[13] J.M. Lehmann, D.D. McKee, M.A. Watson, T.M. Willson, J.T. Moore, S.A. Kliewer, The human orphan nuclear receptor PXR is activated by compounds that regulate CYP3A4 gene expression and cause drug interactions, J. Clin. Invest. 102 (1998) 1016–1023.
[14] W. Habano, T. Gamo, T. Sugai, K. Otsuka, G. Wakabayashi, S. Ozawa, CYP1B1, but not CYP1A1, is downregulated by promoter methylation in colorectal cancers, Int. J. Oncol. 34 (2009) 1085–1091.
[15] S. Eyal, B. Yagen, E. Sobol, Y. Altschuler, M. Shmuel, M. Bialer, The activity of antiepileptic drugs as histone deacetylase inhibitors, Epilepsia 45 (2004) 737–744.
[16] A.S. Beutler, S. Li, R. Nicol, M.J. Walsh, Carbamazepine is an inhibitor of histone deacetylases, Life Sci. 76 (2005) 3107–3115.

Investigation of the disposition of loxapine, amoxapine and their hydroxylated metabolites in different brain regions, CSF and plasma of rat by LC–MS/MS

Yin Cheong Wong, Siu Kwan Wo, Zhong Zuo*

School of Pharmacy, Faculty of Medicine, The Chinese University of Hong Kong, Shatin, New Territories, Hong Kong Special Administrative Region

ABSTRACT

Loxapine represents an interesting example of old "new" drug and is recently drawing attention for its novel inhalation formulation for the treatment of both psychiatric and non-psychiatric disorders. It is extensively metabolized to several active metabolites with diverging pharmacological properties. To further pursue the contribution of metabolites to the overall outcome after loxapine administration, quantification of both loxapine and its active metabolites is essential. The current study developed a rapid liquid chromatography–tandem mass spectrometry (LC–MS/MS) method for the simultaneous quantification of loxapine and its five metabolites (amoxapine, 7-hydroxy-loxapine, 8-hydroxy-loxapine, 7-hydroxy-amoxapine and 8-hydroxy-amoxapine) in rat brain tissues, plasma and cerebrospinal fluid (CSF). By evaluating the effects of perchloric acid and methanol on analyte recovery, the extraction methods were optimized and only small amounts of sample (100 μl for plasma and less than 100 mg for brain tissue) were required. The lower limits of quantification (LLOQs) in brain tissue were 3 ng/g for loxapine and amoxapine and 5 ng/g for the four hydroxylated metabolites of loxapine. The LLOQs were 1 ng/ml for loxapine and amoxapine and 2 ng/ml for the four hydroxylated metabolites in plasma, and 10 ng/ml for all analytes in CSF. The developed method was applied to a pharmacokinetic study on rats treated with a low-dose loxapine by oral administration. Four hours after loxapine dosing, high levels of 7-hydroxy-loxapine were found throughout the ten brain regions examined (68–124 ng/g), while only trace amount of loxapine was measured in brain (<5 ng/g) and plasma (<3 ng/ml). The method provides a useful tool for both preclinical and clinical investigations on the dispositions of loxapine and its metabolites, which would help to elucidate their roles in neurotherapeutics.

© 2011 Elsevier B.V. All rights reserved.

1. Introduction

Loxapine, a tricyclic, dibenzoxazepine antipsychotic, is a treatment option in situations where rapid tranquillization is needed [1]. Although it is usually classified as a typical antipsychotic, it is structurally similar to other atypical antipsychotics such as clozapine and olanzapine. It is suggested that loxapine might have atypical antipsychotic properties according to the observations from both clinical [2,3], *in vivo* [4] and *in vitro* [5] studies and such "atypicality" is more prominent at lower loxapine doses (less than 50 mg per day). Furthermore, administration of low-dose loxapine (5 or 10 mg) through a novel inhalation device was found to be effective in the management of acute agitation [6] and acute migraine attack [7].

In humans, loxapine is extensively metabolized by cytochrome P450 (CYP) isozymes to amoxapine (i.e. *N*-desmethyl-loxapine), 7-hydroxy-loxapine (7-OH-loxapine) and 8-hydroxy-loxapine

(8-OH-loxapine), which are further metabolized to 7-hydroxy-amoxapine (7-OH-amoxapine) and 8-hydroxy-amoxapine (8-OH-amoxapine) [8,9] (Fig. 1). The pharmacological properties of these five metabolites differ markedly. Amoxapine is marketed as an antidepressant but it is also found to be effective in the treatment of schizophrenia [10,11]. The 7-hydroxylated metabolites have higher affinities to the dopamine D_2 and serotonin $5HT_{2A}$ receptors than loxapine [5]. The 8-hydroxylated metabolites are considered inactive as they have relatively low affinities to dopamine and serotonin receptors. However, they did show certain pharmacological activities in *in vitro* systems [5,12]. Both loxapine, amoxapine and the four hydroxylated metabolites can be detected in the plasma of patients taking oral loxapine [13] and the plasma levels of metabolites are comparable to or even higher than that of loxapine [13,14]. Therefore, it is highly likely that these metabolites contribute to the therapeutic and/or adverse effects of loxapine and it is worth investigating the dispositions of loxapine and its metabolites in brain and blood.

There are two published assays [13,14] on the concurrent determination of loxapine and these five metabolites in human plasma based on HPLC–UV methods. However, these assays suffered from

---

* Corresponding author. Tel.: +852 3943 6832; fax: +852 2603 5295.
 *E-mail address:* joanzuo@cuhk.edu.hk (Z. Zuo).
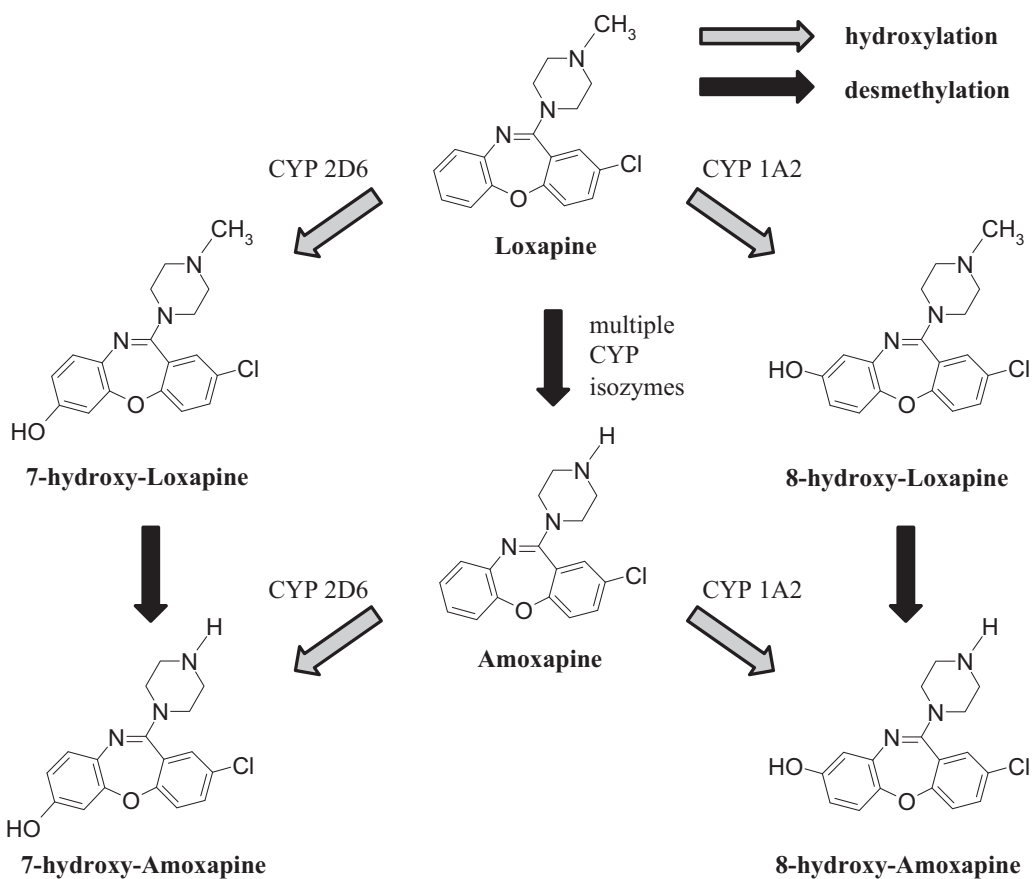
Fig. 1. Summary of metabolic pathways of loxapine.

long run time (35 min) [14], low extraction recoveries (41–59%) and poor sensitivities (limit of detection 3.5–6.3 ng/ml) [13]. Recently, a liquid chromatography–tandem mass spectrometry (LC–MS/MS) method was developed for the simultaneous analyses of human plasma loxapine, amoxapine, 7-OH-loxapine and 8-OH-loxapine but not 7-OH-amoxapine and 8-OH-amoxapine [15]. In addition, all the assays mentioned above were developed for plasma sample analyses, which might not be suitable for tissue analyses.

Although loxapine has been clinically applied for the treatment of schizophrenia since 1970s and a considerable amount of metabolites has been observed in the plasma of patients taking loxapine, it is surprising to find that the disposition of loxapine metabolites in brain remains unknown. The lacking of selective and sensitive method for concurrent quantification of loxapine and its five metabolites, which have different physiochemical properties, could be one of the major reasons. An early method by Cooper and Kelly [16] on the determination of loxapine and these five metabolites in human serum, tissue and urine involved the use gas–liquid chromatography (GLC) and derivatization was needed. Unfortunately, the hydroxylated metabolites were not well resolved on the GLC chromatogram, which in turn hampered the quantification of these metabolites in the brain tissue of a patient overdosed with loxapine [17], which is the only report on loxapine metabolite disposition in animal brain. The disposition of loxapine metabolites in different brain regions remains unknown and information on the dispositions of loxapine and its metabolites in cerebrospinal fluid (CSF) is not available either.

For *in vivo* pharmacokinetic studies in laboratory animals such as rats, the amount of sample (plasma, brain tissue and CSF)

available for quantitative drug analyses is much lower than that from human studies. There is a need to develop an assay that is sensitive enough to concurrently quantify loxapine and its metabolites in the small amount of samples obtained from laboratory animals, especially when the dose of drug given is low. The main aim of the study is to develop a rapid, sensitive and selective method for simultaneous determination of loxapine, amoxapine and their 7- and 8-hydroxylated metabolites in different biological matrices (rat brain tissues, CSF and plasma) using LC–MS/MS. The developed method was applied to investigate the dispositions of loxapine and its metabolites in rat brain, plasma and CSF after oral administration of low-dose loxapine.

2. Materials and methods

2.1. Materials and chemicals

Loxapine succinate, amoxapine and doxepin hydrochloride (internal standard, IS) were obtained from Sigma (St. Louis, MO, USA). 7-OH-loxapine, 8-OH-loxapine, 7-OH-amoxapine and 8-OH-amoxapine were purchased from Tianchen Scientific Inc. (Alberta, Canada). Acetonitrile (ACN, HPLC grade) was obtained from RCI Labscan (Bangkok, Thailand). Methanol (HPLC grade) and perchloric acid (70%, w/w) were obtained from Merck (Darmstadt, Germany). All other reagents were of at least analytical grade and were used without further purification. Distilled and deionized water was used for the preparation of all solutions. Oasis mixed-mode cation-exchange (MCX) cartridges (1 ml, 30 mg) used for solid phase extraction (SPE) were supplied by Waters (Milford, USA).

2.2. Preparation of stock solutions, calibration standards and quality control (QC) samples

Master stock solutions of loxapine and the five metabolites were prepared separately in methanol at concentration of 0.1 mg/ml as free base, except for 7-OH-amoxapine which was prepared at 0.04 mg/ml. The stock standard mixture solution was prepared by mixing and diluting the six master stock solutions with methanol to reach a concentration of 10 μg/ml for each analyte. These stock solutions were stored at −20 °C, which were reported to be stable for at least 3 months [13]. The working standard mixture solutions were freshly prepared by serial dilution of the stock standard mix solution with 50% ACN in water to produce final concentrations of 4, 8, 12, 20, 40, 120, 180, 240, 480, 640, 800 and 1000 ng/ml before analysis. The master stock solution and working standard of the IS (doxepin hydrochloride) were prepared in methanol at 0.1 mg/ml and in 50% ACN in water at 50 ng/ml, respectively.

Calibration standards and QC samples were prepared by spiking the appropriate amount of working standards to relevant drug-free biological matrices. To 100 μl plasma, 25 μl IS working standard and 25 μl working standard mixture were spiked to yield the concentrations of 1, 2, 5, 10, 30, 60, 120, 200 and 250 ng/ml for the six target analytes with 12.5 ng/ml IS. To 100 mg (wet weight) brain tissue (obtained from minced rat whole brain), 0.5 volume (i.e. 50 μl) of IS working standard and the appropriate amount of working standard mixture (e.g. 25 μl) were spiked to yield the concentrations of 3, 5, 10, 30, 60, 100 and 150 ng/g with 25 ng/g IS. Artificial CSF (aCSF) containing 125 mM NaCl, 2.5 mM KCl, 1.2 mM $CaCl_2$, 0.9 mM $MgCl_2$, 25 mM $NaHCO_3$, 0.5 mM Na_2HPO_4, 0.5 mM KH_2PO_4, 3.7 mM glucose, and 6.5 mM urea was prepared as described previously [18]. Appropriate amount of working standard mixture (e.g. 25 μl) was spiked into 300 μl blank aCSF to yield the concentrations of 10, 15, 30, 60, 120, 200 and 300 ng/ml for each analyte. To 25 μl of the above aCSF samples, 25 μl IS working standard and 150 μl ACN–0.1% formic acid in water (1:1, v/v) were added to generate 6.25 ng/ml IS in the final mixture. QC samples were prepared at three concentrations (low, medium, high) at 3, 45 and 160 ng/ml for plasma; 7, 45 and 125 ng/g for brain tissue; and 20, 100 and 250 ng/ml for aCSF. All calibration standards and QC samples were subjected to the sample extraction as described in Section 2.3.

2.3. Sample extraction procedure

2.3.1. Plasma

To 100 μl plasma sample obtained from pharmacokinetic study, 25 μl IS working standard (prepared in Section 2.2) was added. After protein precipitation with 1 ml perchloric acid (10%, w/w), the sample was centrifuged at 16,000 × g for 10 min. The whole supernatant was then loaded to the MCX cartridge which was preconditioned with 1 ml methanol followed by 1 ml 1% formic acid in water. The cartridge was subsequently rinsed with 1 ml 1% formic acid in water and then 1 ml methanol followed by drying under vacuum for 25 min. The analytes were eluted with 1 ml 1% ammonia in methanol. The eluent was then evaporated to dryness under nitrogen stream at 40 °C water bath and the residue was reconstituted with 100 μl reconstitute solvent (ACN–0.1% formic acid in water (1:1, v/v)). After centrifugation at 16,000 × g for 5 min, supernatant was taken for LC–MS/MS analysis.

To optimize plasma sample extraction process, effects of concentration and volume of perchloric acid on the recoveries of analytes were evaluated by using different concentrations (5, 10 or 16.7%, w/w) and volumes (100, 500, or 1000 μl) of perchloric acid in the protein precipitation step. Blank plasma (100 μl) spiked with working standard mixture (120 ng/ml for each analyte) and IS (12.5 ng/ml) was subjected to the same protein precipitation and SPE procedures as mentioned above. Recovery was calculated by comparing the peak area of extracted standard to that obtained by direct injection of the equivalent amount of standard prepared in neat reconstitute solvent into the LC–MS/MS.

2.3.2. Brain tissue

For the brain samples obtained from pharmacokinetic study, the whole brain of each rat was dissected into different anatomical regions, minced (cut into small pieces by scissors) and weighted. To prepare the homogenate, 0.5 volume (0.5 μl/mg tissue) of IS working standard followed by 1 volume (1 μl/mg tissue) of methanol and 7 volumes (7 μl/mg tissue) of perchloric acid (10%, w/w) were added as homogenization medium. The sample was homogenized by ultrasonic probe (Microson XL-2000, Misonix, USA) for 20–30 s. The homogenate was then centrifuged at 1500 × g for 30 min and 400 μl of the supernatant was loaded to the MCX cartridge and the analytes were extracted as described in Section 2.3.1.

To optimize brain tissue sample extraction process, effects of methanol and perchloric acid on the recoveries of the analytes were evaluated. Various combinations of methanol and perchloric acid (with perchloric acid at different concentrations and different volume ratios of methanol:perchloric acid) were added to blank brain tissue (200 mg) spiked with working standard mixture (100 ng/g for each analyte) and IS (25 ng/g). The tissue was subjected to the same homogenization and SPE procedures as mentioned above.

2.3.3. CSF

To 25 μl CSF sample obtained from pharmacokinetic study, 25 μl IS working standard and 150 μl reconstitute solvent (ACN–0.1% formic acid in water (1:1, v/v)) were added and the mixture was directly injected to the LC–MS/MS for analysis.

2.4. LC–MS/MS conditions

The LC–MS/MS system consisted of Agilent 1200 series LC pumps and auto-sampler (Agilent, CA, USA), coupled with an ABI 2000 Q-Trap triple quadrupole mass spectrometer with an electrospray ionization (ESI) source (AB Sciex Instruments, CA, USA). Chromatographic separation was achieved by an Alltima C_{18} column (150 mm × 4.6 mm i.d., 5 μm particle size, Alltech) equipped with a guard filter (Unifilter 0.5 μm, Thermo). The two mobile phases were (A) ACN and (B) 0.1% formic acid in water. The HPLC gradient started at 85% B and was linearly decreased to 50% B over 4.5 min. Then the gradient was quickly declined to 10% B in 0.5 min and was maintained at 10% B for 3 more minutes. The gradient returned to the original condition of 85% B in 0.5 min and was held at 85% B for the next 5.5 min to equilibrate the column before next injection. The flow rate was set at 1 ml/min and the total running time was 14 min. The temperatures of the auto-sampler and the column were set at 4 °C and ambient, respectively. Prior to the ionization source, 60% of the HPLC column effluent stream was split off by a split tee and thus only 40% of the effluent was introduced. In addition, the first 3.5 min of the column effluent was diverted to waste to reduce interference (e.g. inorganic salts). The injection volume was 25 μl.

The MS/MS system was operated under positive mode and multiple reaction monitoring (MRM) mode. The MS conditions were: ion spray voltage at +5.5 kV; nitrogen as nebulizer gas, auxiliary gas and curtain gas at 30, 70 and 30 psi, respectively; collision gas set at medium and auxiliary gas temperature at 400 °C. Other MS parameters of each analyte, including the MRM transitions, were optimized by direct infusion of the individual authentic standard into the mass spectrometer (Table 1). The data acquisition was performed with Analyst software 1.4.1 (AB Sciex Instruments, CA, USA).

Table 1
Optimized LC–MS/MS parameters for loxapine, its metabolites and IS.

Analyte	Q1 *m/z*	Q3 *m/z*	DP (V)	EP (V)	CEP (V)	CE (V)	CXP (V)	Dwell time (ms)
Loxapine	328	271	66	10.0	22	27	6	200
Hydroxyloxapine[a]	344	287	66	10.5	20	27	14	200
Amoxapine	314	271	66	10.0	18	27	8	200
Hydroxyamoxapine[b]	330	287	70	9.5	22	27	14	200
Doxepin	280	107	56	8.5	16	29	4	200

Q1 *m/z*, mass-to-charge ratio of precursor ion; Q3 *m/z*, mass-to-charge ratio of fragment ion; DP, declustering potential; EP, entrance potential; CEP, collision cell entrance potential; CE, collision energy; CXP, collision cell exit potential.

[a] Hydroxyloxapine represents 7- and 8-hydroxyloxapine.
[b] Hydroxyamoxapine represents 7- and 8-hydroxyamoxapine.

2.5. Method validation

The developed method was validated according to the guidelines for Bioanalytical Method Validation published by the U.S. Food and Drug Administration (FDA) in 2001 [19].

2.5.1. Linearity and range

Calibration samples were prepared by spiking IS and different amounts of analytes to the matrices (Section 2.2) followed by extraction process stated in Section 2.3. Calibration curves were generated by plotting the peak area ratio of analyte to IS against the analyte concentration. Linearity was considered satisfactory if the coefficient of determination (R^2) of the plot was higher than 0.99. The lower limit of quantification (LLOQ) was defined as the lowest concentration of the calibration curve at which the accuracy (relative error) was within ±20% of the nominal concentration and the precision (relative standard deviation, RSD) was less than 20%, and with a signal-to-noise peak height ratio greater than 5:1.

2.5.2. Accuracy and precision

Intra-day accuracy and precision were determined within one day by analyzing five replicates of the QC samples at three concentrations (low, medium and high) (Section 2.2). The inter-day accuracy and precision were determined on three separate days. Concentrations of the analytes were determined from calibration curve prepared according to what has been described in Section 2.5.1. Accuracy within ±15% of the nominal concentration and precision with RSD less than ±15% were considered to be acceptable.

2.5.3. Recovery and stability

The recoveries were calculated by comparing the peak area of the analyte spiked to matrix followed by sample extraction to that prepared in neat reconstitute solvent. Stability tests were evaluated in triplicates of the three levels of QC samples. For freeze–thaw stability, the QC samples were subjected to three freeze (−80 °C)–thaw (room temperature) cycles before sample extraction. Auto-sampler stability was assessed by comparing the extracted and reconstituted QC samples that were placed in the auto-sampler (4 °C) for 24 h.

2.5.4. Assay selectivity and matrix effects

The specificity of the assay was evaluated by analyzing the blank sample matrix for interference. Matrix effects were calculated by comparing the peak area of the analyte spiked after sample extraction of blank brain tissue or plasma with that prepared in neat reconstitute solvent [20]. Since no sample extraction process was involved in the assay of CSF (Section 2.3.3), the matrix effect for CSF was not evaluated.

2.6. Application to pharmacokinetic study in rats

The study was approved by the Department of Health of Hong Kong and the Animal Ethics Committee, The Chinese University of Hong Kong. One day before the pharmacokinetic experiment, the male Wistar rats (180–220 g, $n = 4$) were anesthetized with an intraperitoneal dose of ketamine (90 mg/kg) and xylazine (10 mg/kg) followed by cannulation surgery of a polythene tube in the right jugular vein. The rats were allowed to recover and were fasted overnight. Loxapine solution was first prepared by dissolving 6.8 mg loxapine succinate in 1 ml of 2.5% Solutol in normal saline. The solution was diluted 10-folds with normal saline before administration. Four hundred microliters of this diluted solution was administered to rat by oral gavage, equivalent to a loxapine dose at 1 mg/kg rat body weight (free base). About 200 µl of blood was sampled at 3, 5, 10, 15, 20, 30, 45, 60, 120, and 240 min and collected in a centrifuge tube containing heparin. Plasma was obtained by centrifugation of the blood at $16,000 \times g$ for 5 min. At 240 min, the rats were exsanguinated by cardiac puncture under anesthesia and their CSFs (about 50–100 µl) were obtained by cisternal puncture. The whole brain was then removed from skull, quickly rinsed with cold normal saline (4 °C) and was wiped by tissue paper to remove excess water. The brain was then dissected into ten anatomical regions including: (1) olfactory bulb; (2) anterior cortex; (3) middle cortex; (4) posterior cortex; (5) hippocampus; (6) striatum; (7) midbrain/thalamus/hypothalamus; (8) cerebellum; (9) medulla/pons; and (10) trigeminal nerve. Meninges and blood vessels were removed and each region was weighted. All samples were frozen at −80 °C until analysis.

Plasma pharmacokinetic parameters were calculated by WinNonlin (version 2.1) using non-compartmental analysis. Area under the curve (AUC) was calculated using linear/log trapezoidal method. Analyte with a concentration lower than the LLOQ was considered as 0 ng/ml (plasma or CSF) or 0 ng/g (brain tissue) in the calculation. Samples with analyte concentrations higher than the upper limit of quantification (ULOQ) were diluted with reconstitute solvent and measured again.

3. Results and discussion

3.1. Optimization of LC and MS conditions

Composition of the mobile phase had significant effects on the retention time and peak shape of the analytes. Isobaric ions (i.e. 7-OH-loxapine and 8-OH-loxapine; 7-OH-amoxapine and 8-OH-amoxapine) were monitored at the same mass transition. In order to chromatographically separate the 7- and 8-hydroxylated isomers, the gradient was started with a low content of ACN (15%), followed by a gradual increase in ACN for the initial 4.5 min. It was found that starting the gradient with a high proportion of ACN or rapid increment of ACN in the initial period would lead to co-elution of these isobaric ions. However, once the separation of the hydroxylated metabolites was achieved, the content of ACN should be raised to prevent peak broadening or tailing of the subsequent non-hydroxylated analytes (i.e. amoxapine, IS and loxapine). Furthermore, increasing the concentration of the formic acid in the mobile phase (B) from 0.1% to 0.5% or 1% would suppress the
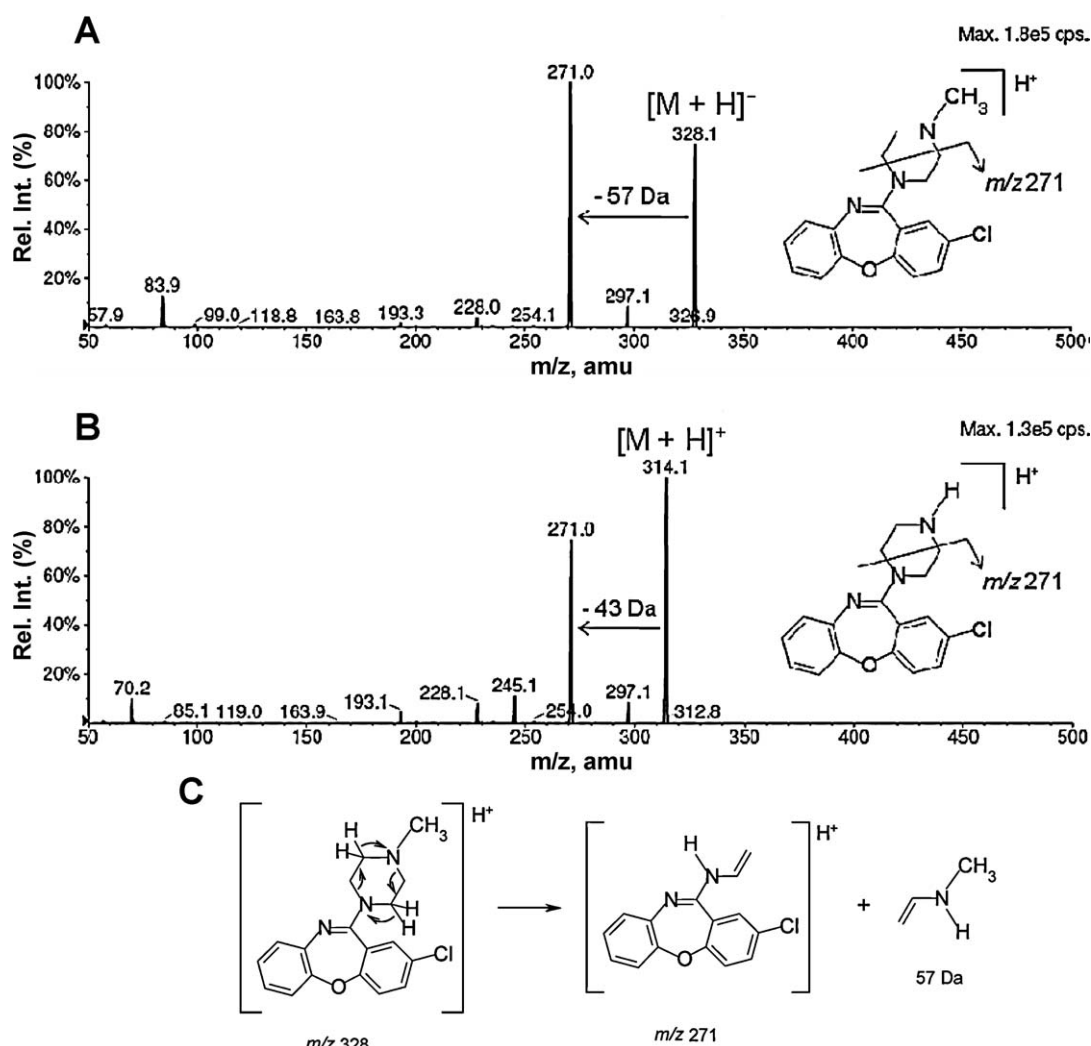
Fig. 2. Product ion spectra of [M+H]⁺ ion of loxapine (A), amoxapine (B) and proposed fragmentation pathway of [M+H]⁺ ion of loxapine (C).

signal intensity of the analytes. Other analytical columns (cyano, phenyl and C_8) and mobile phases (ammonium hydroxide at pH 10; methanol) had been evaluated but only the current method achieved optimal peak shapes and resolution. For the choice of IS, imipramine, a tricyclic antidepressant with a strong MS signal, was initially used. Later, it was found that doxepin, which also contains a tricyclic backbone and tertiary amine functional group, had a closer retention time to the target analytes and less peak tailing than imipramine. Therefore, doxepin was adopted as IS.

By using positive ESI, abundant protonated molecular ions ([M+H]⁺) of loxapine, amoxapine and their hydroxylated metabolites were generated and upon collision-induced dissociation, produced specific fragment ion(s) that can be used for identification and quantification. Fig. 2 shows the product ion spectra of the [M+H]⁺ ion of loxapine and amoxapine. The most intense fragment ion of m/z 271, formed by the loss of C_3H_7N (57 Da) and C_2H_5N (43 Da) respectively, were proposed to be arisen from the cleavage of C–N bonds from the piperazine moiety (Fig. 2). Other fragment ions were found in low abundance. For 7- and 8-hydroxylated metabolites, similar fragmentation pattern were observed (i.e. the predominant fragment ions were arisen from the loss of corresponding C_3H_7N or C_2H_5N). Consequently, these ions were selected for MRM monitoring.

The optimized MS parameters of each analyte are listed in Table 1. Representative chromatograms of a brain sample (100 mg) spiked with 7 ng/g of analytes and 25 ng/g of IS, and a brain sample of striatum (109 mg, with 25 ng/g of IS added) from a rat 4 h after oral administration of loxapine at 1 mg/kg are shown in Fig. 3A and B, respectively. To check the effect of carryover, injection of 100 μl neat ACN following calibration standards at ULOQs was conducted for all the three biological matrices. Carryover was found to be acceptable since the related peak areas observed were less than 10% of the corresponding analyte peak areas at LLOQs. Our method is the first report on determination of both loxapine and its five metabolites simultaneously in brain, plasma and CSF by LC–MS/MS.

3.2. Extraction of loxapine and metabolites from biological matrices

3.2.1. Plasma

The extraction recoveries of analytes in plasma using various concentrations and volumes of perchloric acid are shown in Table 2. Recoveries from extraction with perchloric acid at 10% (w/w) were consistently higher than that from perchloric acid at 5%; however, a further increase of perchloric acid to 16.7% led to a slight reduction in the extraction recovery. Furthermore, extraction with 100 μl perchloric acid had lower recovery than that from larger volumes (500 or 1000 μl). Probably the loss of sample during sample loading
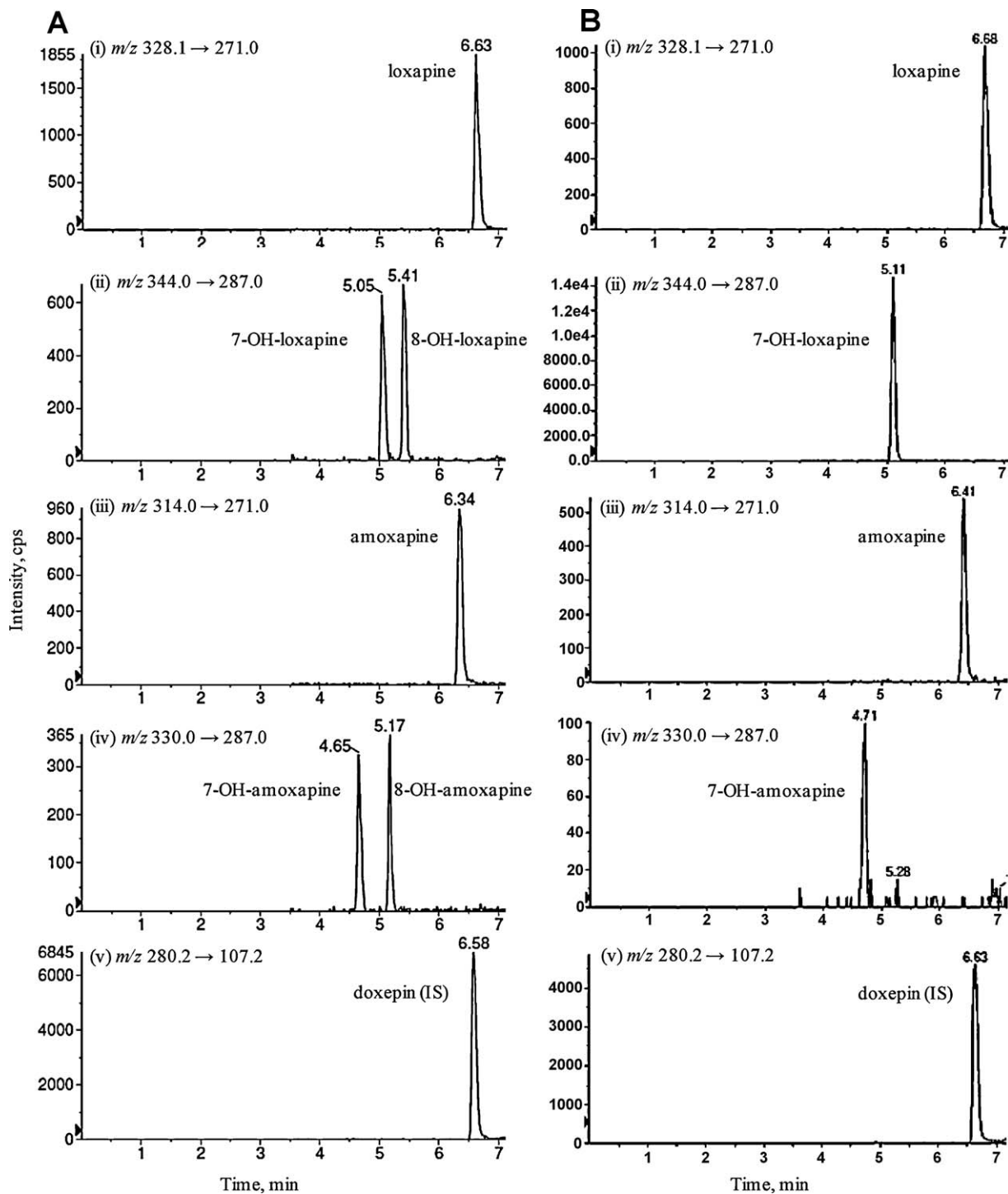
Fig. 3. Representative extracted ion chromatograms of: (A) a blank rat brain sample (100 mg) spiked with 7 ng/g of analytes and 25 ng/g of IS and (B) a rat brain striatum sample (109 mg with 25 ng/g of IS) obtained 4 h after oral administration of loxapine at 1 mg/kg.

to MCX was proportionately larger for small supernatant volumes. Finally, 1 ml 10% (w/w) perchloric acid was selected and employed in the subsequent plasma assays as it achieved the highest recoveries of loxapine and its five metabolites. By optimizing the extraction procedure, the present method offers an advantage of a small sample size (100 μl plasma), which is much smaller than those reported from literature (300 μl [15] to 3 ml [13,14,16]) and is crucial for rat studies with limited sample size. Also it could reduce the depletion of animal blood volume due to serial blood samplings in the pharmacokinetic study.

3.2.2. Brain tissue

In preparing brain tissue homogenate, perchloric acid and methanol were added to enhance the extraction of the target analytes which were lipophilic and highly tissue-bound. The recoveries of analytes using various combinations of these two reagents were summarized in Table 3. By increasing the volume ratio of methanol:perchloric acid from 200:1400 to 1400:200, extraction recoveries of the 7-hydroxylated metabolites were dramatically reduced with subtle decrease in recoveries for other analytes. Among the same methanol:perchloric acid volume ratio, switching

Table 2
Effect of perchloric acid on the extraction recoveries of analytes in 100 μl plasma ($n = 3$).

Concentration of perchloric acid (%, w/w)	Volume (μl)[a]	Recovery (%)[b]						
		Loxapine	7-OH-loxapine	8-OH-loxapine	Amoxapine	7-OH-amoxapine	8-OH-amoxapine	IS
5	100	30 ± 3	41 ± 6	44 ± 4	39 ± 5	46 ± 10	46 ± 7	18 ± 2
	500	50 ± 1	59 ± 1	62 ± 1	61 ± 1	68 ± 1	62 ± 1	33 ± 1
	1000	45 ± 11	49 ± 7	52 ± 11	52 ± 12	58 ± 3	47 ± 13	29 ± 8
10	100	48 ± 8	63 ± 6	75 ± 11	72 ± 11	67 ± 3	69 ± 10	27 ± 2
	500	66 ± 16	66 ± 10	81 ± 14	85 ± 20	73 ± 9	71 ± 10	39 ± 11
	1000	<u>73[c] ± 18</u>	<u>73 ± 12</u>	<u>89 ± 16</u>	<u>95 ± 17</u>	<u>79 ± 11</u>	<u>79 ± 8</u>	44 ± 15
16.7	100	49 ± 5	62 ± 8	78 ± 15	76 ± 13	65 ± 9	57 ± 27	30 ± 5
	500	50 ± 36	54 ± 20	70 ± 23	65 ± 31	59 ± 22	66 ± 13	34 ± 24
	1000	65 ± 22	63 ± 9	81 ± 12	80 ± 15	67 ± 10	72 ± 11	<u>47 ± 16</u>

[a] Volume of perchloric acid added to 100 μl plasma.
[b] Data presented as mean ± S.D.
[c] The highest recovery value of each analyte was underlined.

the concentration of perchloric acid did not yield a consistent effect, although recoveries of the hydroxylated metabolites using 16.7% (w/w) perchloric acid seemed to be lower than that using 5% or 10%. Finally, one volume (1 μl/mg tissue) of methanol with 7 volumes (7 μl/mg tissue) of 10% (w/w) perchloric acid was chosen for extraction of analytes in brain tissue. The choices of low methanol to perchloric acid ratio and low concentration of perchloric acid are in line with Sugita et al. [21] for the extraction of imipramine and its desmethylated and hydroxylated metabolites in rat brain. Again, through extraction optimization, the present method offers an advantage that it only requires a small volume of tissue (100 mg or less), whereas a much larger amount of tissue (1 g) is required in the GLC assay reported by Cooper and Kelly [16].

3.2.3. Sample cleanup by SPE

Apart from the current sample extraction with MCX, we had investigated other extraction methods such as liquid–liquid extractions (with various combinations of diethyl ether, ethyl acetate, and n-hexane), other SPE cartridges (WCX and HLB) and different protein precipitation agents (formic acid, acetic acid, phosphoric acid and ACN); however, the recoveries of analytes in brain tissue and plasma were lower than that of the present method. Moreover, other cleanup procedures such as increasing the ammonia concentration of the MCX eluent (from 1% to 2% or 5% in methanol) or changing the evaporation method from using nitrogen stream to

vacuum concentrator had also been tried but showed no apparent variation on the recoveries of all analytes.

3.3. Method validation

3.3.1. Linearity and range

The LLOQs, the lowest point of the calibration curve, were 1 ng/ml for loxapine and amoxapine and 2 ng/ml for the four hydroxylated metabolites in plasma; 3 ng/g for loxapine and amoxapine and 5 ng/g for the four hydroxylated metabolites in brain tissue; and 10 ng/ml for all the six analytes in aCSF. The ULOQs, the highest point of the calibration curve, were 250 ng/ml, 150 ng/g and 300 ng/ml for all analytes in plasma, brain tissue and aCSF, respectively. Within these ranges the calibration curves of the three biological matrices achieved good linearity ($R^2 > 0.99$). Comparing with previous assays on concurrent determination of these six analytes in plasma [13,14,16], the present LC–MS/MS method offers comparable or slightly higher sensitivities while a much smaller sample size (100 μl) is required (versus up to 3 ml from these reports as mentioned above). The relatively high LLOQ of CSF might have originated from the dilution effect since the CSF samples were diluted with reconstitute solvent before direct LC–MS/MS analysis. Nevertheless, dilution of the untreated CSF samples with reconstitute solvent which had a composition similar to the mobile phase was necessary to minimize the unfavorable changes in LC–MS/MS

Table 3
Effect of methanol and perchloric acid on the extraction recoveries of analytes in 200 mg brain tissue ($n = 3$).

Volume (μl)[a]		Concentration of perchloric acid (%, w/w)	Recovery (%)[b]						
Methanol	Perchloric acid		Loxapine	7-OH-loxapine	8-OH-loxapine	Amoxapine	7-OH-amoxapine	8-OH-amoxapine	IS
200	1400	5	44 ± 12	43 ± 1	69 ± 1	73 ± 10	54 ± 4	65 ± 1	18 ± 5
		10	57 ± 10	<u>46 ± 11</u>	<u>81 ± 20</u>	<u>90 ± 23</u>	<u>57 ± 10</u>	51 ± 19	25 ± 7
		16.7	<u>58[c] ± 13</u>	36 ± 3	76 ± 16	87 ± 18	45 ± 3	60 ± 4	<u>29 ± 8</u>
600	1000	5	39 ± 12	30 ± 7	69 ± 5	73 ± 7	37 ± 9	<u>66 ± 5</u>	23 ± 8
		10	40 ± 12	27 ± 5	70 ± 4	77 ± 3	37 ± 5	64 ± 4	25 ± 7
		16.7	41 ± 16	5 ± 4	55 ± 13	65 ± 22	7 ± 6	41 ± 18	25 ± 6
1000	600	5	29 ± 11	1 ± 0	36 ± 9	53 ± 15	1 ± 1	45 ± 8	16 ± 7
		10	26 ± 7	0 ± 0	31 ± 3	52 ± 8	0 ± 0	40 ± 3	13 ± 4
		16.7	32 ± 15	0 ± 0	31 ± 7	65 ± 26	0 ± 0	36 ± 1	20 ± 11
1400	200	5	41 ± 9	20 ± 5	57 ± 12	58 ± 11	25 ± 8	44 ± 10	<u>29 ± 9</u>
		10	44 ± 13	2 ± 2	55 ± 11	65 ± 18	2 ± 2	43 ± 8	28 ± 9
		16.7	31 ± 8	0 ± 0	41 ± 9	56 ± 14	0 ± 0	36 ± 2	18 ± 5

[a] Volume of methanol and perchloric acid added to 200 mg brain tissue.
[b] Data presented as mean ± S.D.
[c] The highest recovery value of each analyte was underlined.

chromatograms (e.g. shift in analyte retention time, distortion of peak shape) in addition to the dilution of endogenous interferences.

The present assay also applies to brain tissues and CSFs, the full validation of which have not been reported to date. Except for that reported by Cooper and Kelly [16], there has been no previous report on the determination of loxapine or its metabolites in brain tissue or CSF. However, Cooper and Kelly had not presented the assay validations on brain tissue nor did they report the detection limit or LLOQ of analytes in brain tissue.

3.3.2. Accuracy and precision

The results for intra-day and inter-day accuracy and precision of the assay are shown in Table 4. For all the three biological matrices tested, both the accuracy (within ±15% bias) and precision (RSD less than ±15%) met the criteria set by the guidance on Bioanalytical Method Validation from FDA (2001).

3.3.3. Recovery and stability

Recoveries of analytes in the three biological matrices are shown in Table 5. It was noticed that recoveries of analytes in plasma samples ranged from 60% to 84% and were consistent across the concentration range studied. Such plasma recoveries were comparable to that reported by Zimmer at al. (76–95%) [15] who also used cation exchange SPE as the extraction method, and were higher than that using liquid–liquid extractions (41–59% by Hue et al. [13] and 45–85% by Cheung et al. [14]). This suggests that SPE might be a better method for the concurrent extractions of the tricyclic drug loxapine and its metabolites than liquid–liquid extractions. Among all analytes investigated, loxapine and amoxapine had higher recoveries (72–85%) in brain tissue than their hydroxylated metabolites (50–66% for 7-hydroxylated metabolites; 59–79% for 8-hydroxylated metabolites). For aCSF samples, recoveries of all the analytes were at least 75%.

For stability tests, three replicates of three levels of QC samples were included. After three freeze–thaw cycles, the percentages of all analytes remaining were 91–114%, 93–110% and 86–102% in plasma, brain tissue and aCSF, respectively. In addition, after 24 h in the auto-sampler (4 °C), there were 95–107%, 94–109% and 89–105% of all analytes remaining in plasma, brain tissue and aCSF, respectively.

3.3.4. Assay selectivity and matrix effects

The extracted ion chromatograms of blank plasma, brain tissues and CSF (not shown) did not show any interfering peaks or signal at the retention times of the target analytes, suggesting a good selectivity of the assay. For the evaluation of matrix effects in plasma and brain tissue, three replicates of three levels of QC samples were included. It was found that the matrix effects were more prominent on the four hydroxylated metabolites. For plasma, signal suppression ranged from 0% to 16% for all analytes at all QC levels, except for 7-OH-loxapine with suppression of 22% at 3 ng/ml. For brain tissue, signal suppressions of the four hydroxylated metabolites ranged from 8% to 26%, while the signal suppression or enhancement on loxapine and amoxapine was less than 9% at all QC levels. RSDs of the three replicates were always less than 15%. The results justified the use of relevant biological matrices in the preparation of calibration standards and QC samples.

3.4. Application to pharmacokinetic study in rats

3.4.1. Plasma pharmacokinetic profiles

The pharmacokinetic profiles of loxapine and its metabolites in rat plasma after oral administration of low-dose loxapine (1 mg/kg) are shown in Fig. 4 and the pharmacokinetic parameters are summarized in Table 6. Loxapine was rapidly metabolized to amoxapine, 7-OH-loxapine and 7-OH-amoxapine, leaving a low

Table 4
Intra- and inter-day accuracy and precision of the developed assay.

	Matrices	Spiked	Loxapine		7-OH-loxapine		8-OH-loxapine		Amoxapine		7-OH-amoxapine		8-OH-amoxapine	
			Accuracy (%)	RSD (%)	Accuracy (%)	RSD (%)	Accuracy (%)	RSD (%)	Accuracy (%)	RSD (%)	Accuracy (%)	RSD (%)	Accuracy	RSD
Intra-day (n = 5)	Brain	7 ng/g	97.3	4.3	101.2	4.5	97.7	8.0	105.2	7.6	102.8	4.2	105.8	7.0
		45 ng/g	102.5	3.7	101.7	11.2	96.8	11.8	99.7	11.3	97.5	7.3	98.5	7.3
		125 ng/g	101.6	9.8	111.8	10.2	97.2	11.8	101.6	9.1	93.4	3.0	102.8	7.1
	aCSF[a]	20 ng/ml	104.8	6.7	100.9	7.2	97.0	4.1	103.7	5.8	104.9	8.1	103.4	8.2
		100 ng/ml	89.5	6.6	92.0	3.7	96.0	1.3	94.6	2.1	96.6	4.1	95.5	4.0
		250 ng/ml	88.2	2.2	98.0	9.4	98.2	6.3	93.5	6.3	96.6	8.8	98.9	8.3
		3 ng/ml	101.0	2.4	89.0	3.4	88.5	6.2	100.4	5.6	104.7	4.5	105.0	9.5
	Plasma	45 ng/ml	98.9	11.6	97.0	8.4	98.9	4.8	104.0	7.2	106.8	8.7	104.2	7.0
		160 ng/ml	92.7	3.4	99.4	4.1	99.0	3.1	97.6	4.6	101.8	3.3	99.2	3.6
Inter-day (n = 3)	Brain	7 ng/g	92.4	2.9	102.0	8.6	96.9	6.4	102.3	6.8	106.6	5.9	103.2	10.6
		45 ng/g	103.1	9.4	89.7	8.3	86.8	3.8	93.3	13.1	94.8	7.4	100.1	7.8
		125 ng/g	97.7	8.6	97.7	11.8	101.1	12.5	108.3	5.0	93.7	4.8	98.7	11.5
	aCSF	20 ng/ml	102.9	11.1	96.7	9.2	93.7	7.9	97.8	4.7	102.5	10.0	100.7	11.5
		100 ng/ml	98.7	5.6	94.7	1.6	97.0	2.3	97.2	2.0	96.8	3.2	94.3	3.3
		250 ng/ml	97.6	5.9	98.5	3.8	98.8	3.1	97.0	4.2	94.8	2.3	96.8	2.6
		3 ng/ml	94.5	7.4	96.0	5.8	93.5	6.3	103.6	6.8	97.6	9.9	97.9	9.6
	Plasma	45 ng/ml	108.4	2.4	103.0	7.9	95.5	9.4	99.9	2.8	97.1	10.9	107.2	6.6
		160 ng/ml	96.8	3.4	104.3	0.5	101.4	9.1	99.5	0.3	103.0	2.1	102.9	3.8

[a] aCSF, artificial cerebrospinal fluid.

Table 5
Extraction recoveries of the tested analytes in brain, aCSF and plasma ($n = 7$).

Matrices	Spiked amount/concentration	Extraction recovery (%)[a]					
		Loxapine	7-OH-loxapine	8-OH-loxapine	Amoxapine	7-OH-amoxapine	8-OH-amoxapine
Brain	7 ng/g	75.5 ± 4.1	53.4 ± 4.6	60.6 ± 8.2	76.9 ± 7.8	49.9 ± 5.9	58.8 ± 7.1
	45 ng/g	72.1 ± 8.9	53.7 ± 7.4	65.5 ± 7.4	74.1 ± 7.2	53.8 ± 6.8	70.4 ± 5.8
	125 ng/g	77.4 ± 8.1	65.6 ± 6.5	78.5 ± 5.1	85.0 ± 7.2	62.1 ± 6.7	76.4 ± 9.2
aCSF[b]	20 ng/ml	75.0 ± 8.8	89.3 ± 3.2	84.0 ± 6.0	83.3 ± 7.0	86.9 ± 3.9	89.6 ± 5.6
	100 ng/ml	76.2 ± 4.3	89.2 ± 4.7	88.5 ± 6.3	86.3 ± 4.1	87.4 ± 9.4	89.5 ± 9.6
	250 ng/ml	77.4 ± 2.7	90.9 ± 5.0	90.6 ± 5.2	85.7 ± 3.7	90.2 ± 7.3	93.6 ± 6.7
Plasma	3 ng/ml	78.6 ± 8.6	66.7 ± 8.1	78.3 ± 4.3	84.1 ± 9.6	63.8 ± 8.3	71.1 ± 9.0
	45 ng/ml	62.6 ± 7.3	60.5 ± 5.4	63.8 ± 6.8	65.8 ± 8.2	60.2 ± 5.6	60.8 ± 4.1
	160 ng/ml	76.7 ± 5.8	68.5 ± 3.7	78.6 ± 6.5	77.5 ± 6.3	69.6 ± 6.1	68.9 ± 4.4

[a] Data presented as mean ± S.D.
[b] aCSF, artificial cerebrospinal fluid.

Table 6
Plasma pharmacokinetic parameters of loxapine and its metabolites after oral treatment of 1 mg/kg loxapine.[a]

Parameters[b]	Loxapine	7-OH-loxapine	Amoxapine	7-OH-amoxapine
C_{max} (ng/ml)	2.5 ± 1.7	37.0 ± 15.2	59.8 ± 28.5	44.5 ± 9.2
t_{max} (min)	12.5 ± 2.9	83.8 ± 106.1	23.8 ± 7.5	87.5 ± 103.1
$AUC_{0-240\,min}$ (ng min/ml)	141.7 ± 156.4	4492.8 ± 814.8	5006.5 ± 1943.5	5910.7 ± 1294.8

$AUC_{0-240\,min}$, area under the plasma concentration–time curve from 0 to 240 min.

[a] Data presented as mean ± S.D.
[b] C_{max}, maximum plasma concentration; t_{max}, time to the maximum plasma concentration.

concentration of loxapine in plasma (less than 3 ng/ml) throughout the 4-h study period. Amoxapine attained peak plasma concentration earlier than that of the 7-hydroxylated metabolites. The plasma concentration versus time profiles of the two 7-hydroxylated metabolites were rather similar with double peaks observed at 30 min and 60 min. This might suggest that 7-OH-amoxapine was mainly generated from the hydroxylation of amoxapine rather than from the desmethylation of 7-OH-loxapine since there was no time lag between the formation of 7-OH-amoxapine and the formation of 7-OH-loxapine. In contrast to the 7-OH metabolites, 8-OH-loxapine and 8-OH-amoxapine could not be detected (<LLOQ), which was in good agreement with the previous finding that 8-OH-amoxapine was not detectable in either serum or brain of rats treated with intraperitoneal injection of amoxapine [22].

3.4.2. Brain distribution study

Fig. 5 shows the rat brain distribution of analytes at 4 h after oral administration of loxapine at 1 mg/kg. High levels of

Fig. 4. Loxapine and metabolites concentration–time profiles in rat plasma after oral administration of loxapine at 1 mg/kg. Data represent mean ± S.E. ($n = 4$). 8-OH-loxapine and 8-OH-amoxapine were found to be lower than LLOQ.

7-OH-loxapine (68–124 ng/g) was found throughout the ten examined brain regions (Fig. 5, top) despite its low plasma level at 4 h (13.6 ng/ml), resulting in a brain-to-plasma ratio of around 5–10. Among these brain regions examined, striatum exhibited the highest level of 7-OH-loxapine. This can be rationalized by the fact that loxapine and its 7-hydroxylated metabolites work as dopamine antagonists and have high affinities to the dopamine receptors that are densely localized in striatum. Compared with 7-OH-loxapine, the brain levels of loxapine, amoxapine and 7-OH-amoxapine were relatively low (less than 5 ng/g, Fig. 5, bottom). This further supports the notion that the metabolites, particularly the 7-hydroxylated metabolites, do play an important role after loxapine administration. The reason why the brain level of 7-OH-loxapine was much higher than that of amoxapine and 7-OH-amoxapine despite their similar plasma concentrations at 4 h is not clear. It could be due to either higher penetration or affinity of 7-OH-loxapine towards brain tissue or its lower brain elimination rate than the other metabolites. In conformity with observations from plasma, the two 8-hydroxylated metabolites were not present in detectable quantity (<LLOQ) in brain tissue. An early neuropharmacological evaluation conducted by Latimer [23] represents the only report on the regional distribution of loxapine in the brain of laboratory animals treated with loxapine. In rats intravenously injected with 5 mg/kg loxapine, mesencephalon (midbrain) consistently exhibited higher loxapine levels than cortex, diencephalon and cerebellum throughout the first 60 min. However, the analysis of brain tissue was based upon the hydrolysis of loxapine to an aromatic amine responding to a Bratton–Marshall reaction. Whether such assay could reliably differentiate loxapine from its structurally similar metabolites, particularly the 7-OH-loxapine that are present in substantial amount in brain as observed in the present study, is uncertain.

3.4.3. CSF disposition

Neither the parent drug nor the metabolites were detected in the CSF of rats at 4 h after oral loxapine administration. However, using the present LC–MS/MS method, at 4 h after intravenous injection of loxapine at the same dose (1 mg/kg), trace amounts of loxapine (approx. 4 ng/ml) and 7-OH-loxapine (approx. 6 ng/ml) were
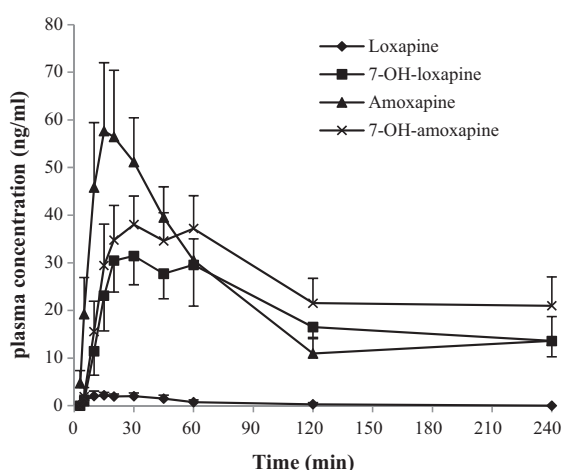
Tissue concentration (ng/g)

## Tissue concentration (ng/g)
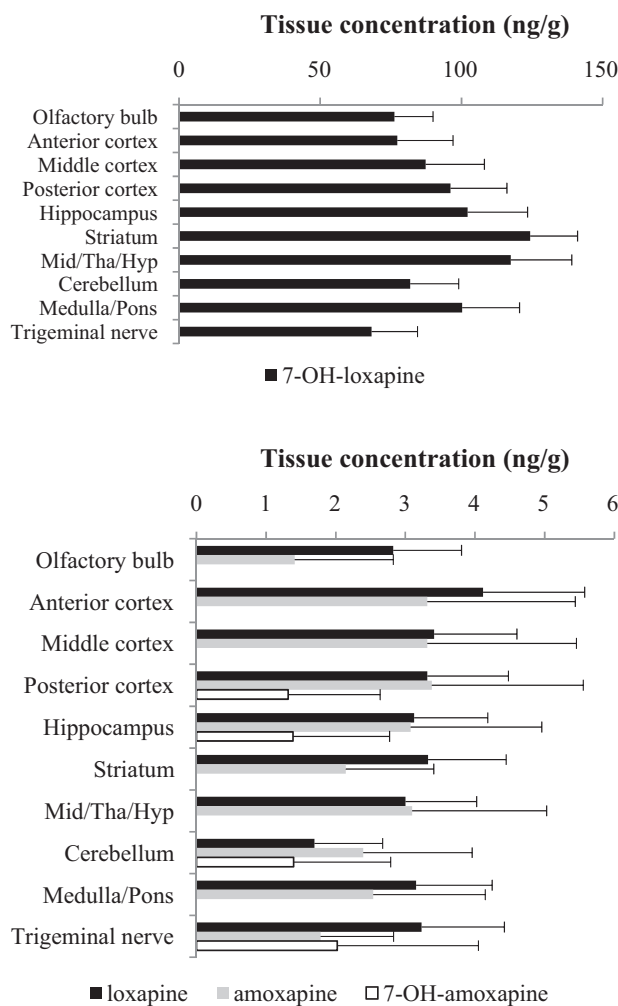
Fig. 5. Brain regional distributions of 7-OH-loxapine (top), and loxapine, amoxapine and 7-OH-amoxapine (bottom) 4 h after oral administration of loxapine at 1 mg/kg. Data represent mean ± S.E. (*n* = 4). 8-OH-loxapine and 8-OH-amoxapine were found to be lower than LLOQ. Mid/Tha/Hyp: the region containing midbrain, thalamus and hypothalamus.

detected in the CSF of rats while the average concentrations of loxapine and 7-OH-loxapine across different brain regions were around 150 ng/g and 300 ng/g, respectively (unpublished data). A previous *in vivo* rat study on tricyclic antipsychotics (clozapine, quetiapine and chlorpromazine) revealed that these drugs exhibited high tissue bindings (with unbound fractions in brain less than 3%) and at 1 h after oral dosing the concentrations of parent drug in brain tissue were 13–535 folds higher than that in CSF and were 7–25 folds higher than that in blood [24]. Taken together with the present observations, these findings suggest that tricyclic compounds, including loxapine and its metabolites, have preferential disposition in brain tissue, leaving low concentrations of unbound drug in CSF and plasma.

3.5. Implications on the treatment of various CNS disorders by loxapine

The present findings represent the first report on the regional distribution of loxapine metabolites in animal brain and CSF and also the first report on the plasma pharmacokinetic profiles of loxapine metabolites in laboratory animal after loxapine administration. Low-dose loxapine (1 mg/kg in rat, equivalent to 9.7 mg in a 60 kg human adult [25]) was investigated in the present study while for the previous rat pharmacokinetic studies the doses of

loxapine were much higher (from 5 mg/kg [23] to 7–10 mg/kg [26] or even 50 mg/kg [27]). Testing loxapine at a relatively low dose could avoid the saturation of metabolic enzymes and other unfavorable physiological changes, and thus the result should be more reflective of the actual dispositions of loxapine and metabolites. The level of metabolites far exceeded that of the parent drug in both plasma and brain, suggesting that these active metabolites might play a predominant role in the therapeutic outcomes and/or toxicities during the loxapine treatment course, in particular when the drug is given at low doses in which saturation of metabolite formation is less likely to happen. As discussed above, loxapine and its five metabolites exhibit differential pharmacokinetic and pharmacotherapeutic behaviors. Due to such complexity, it is necessary to monitor all these analytes and only through well-designed studies and accurate analytical measurements that the role of loxapine metabolites can be elucidated.

Interestingly, it is suggested that loxapine might actually behave as atypical antipsychotic (elicit fewer extrapyramidal side-effects), especially at lower doses (<50 mg/day) [2,3,5]. Low-dose loxapine (5 or 10 mg) delivered via a novel dry powder inhaler was also effective in the acute management of agitation [6] and migraine [7], with the indication on agitation now pending FDA approval. Therefore there is a need to re-evaluate the pharmacological properties of low-dose loxapine after acute or chronic administration. The developed LC–MS/MS assay, which offers high sensitivity (low ng/ml or ng/g level), small sample size requirement (100 μl for plasma or less than 100 mg for brain tissue) and versatility in different biological matrices, is a useful tool for both preclinical and clinical investigations of loxapine and its active metabolites in the treatment of various CNS disorders.

4. Conclusions

This is the first report to describe a LC–MS/MS assay for the simultaneous quantification of loxapine, amoxapine and their four hydroxylated metabolites (7-OH-loxapine, 8-OH-loxapine, 7-OH-amoxapine and 8-OH-amoxapine) in different biological matrices (brain, CSF and plasma) in rat. Through optimization of the extraction process, only small amount of sample is required for the assay. The method was fully validated and has been successfully applied to the pharmacokinetic study of loxapine and its metabolites in systemic circulation and regional distribution study in brain and CSF after oral administration of low-dose loxapine (1 mg/kg) in rat. Given its sensitivity and reliability, the present method represents a practical tool for further investigations on the disposition of loxapine and its active metabolites after low-dose loxapine treatment, which could help clarify the roles of these species in the CNS. In addition, the current methodologies could probably be applied to the analyses of other tricyclic drugs (for example, many of the antipsychotics and antidepressants) which are also extensively metabolized by CYP enzymes to active desmethylated and hydroxylated metabolites.

References

[1] A. Chakrabarti, A. Bagnall, P. Chue, M. Fenton, V. Palaniswamy, W. Wong, J. Xia, Loxapine for schizophrenia, Cochrane Database Syst. Rev. (2007) CD001943.
[2] H.Y. Meltzer, K. Jayathilake, Low-dose loxapine in the treatment of schizophrenia: is it more effective and more atypical than standard-dose loxapine, J. Clin. Psychiatry 60 (1999) 47–51.

[3] W.M. Glazer, Does loxapine have atypical properties? Clinical evidence, J. Clin. Psychiatry 60 (1999) 42–46.

[4] Z. Li, J. Ichikawa, H.Y. Meltzer, A comparison of the effects of loxapine with ziprasidone and thioridazine on the release of dopamine and acetylcholine in the prefrontal cortex and nucleus accumbens, Psychopharmacology (Berlin, Germany) 167 (2003) 315–323.

[5] L. Ereshefsky, Pharmacologic and pharmacokinetic considerations in choosing an antipsychotic, J. Clin. Psychiatry 60 (Suppl. 10) (1999) 20–30.

[6] L. Citrome, Aerosolised antipsychotic assuages agitation: inhaled loxapine for agitation associated with schizophrenia or bipolar disorder, Int. J. Clin. Pract. 65 (2011) 330–340.

[7] R.L. Hale, P. Munzar, J.D. Rabinowitz, Method for treating pain with loxapine and amoxapine, U.S. Pat. Appl. Publ. 2003-719540; 2002-429405 (2004) 14.

[8] K. Huie, A. Reed, L. Takahashi, J. Cassella, Characterization of loxapine human metabolism, Drug Metab. Rev. 40 (2008) 210–211.

[9] C.P. Granvil, J. Chen, M.V. Padval, P.J. Elliot, In vitro metabolism of CRx-119, a novel syncretic drug candidate, in human liver microsomes and recombinant P450 enzymes, Drug Metab. Rev. 38 (2006) 94.

[10] R. Apiquian, A. Fresan, R. Ulloa, C. de la Fuente-Sandoval, M. Herrera-Estrella, A. Vazquez, H. Nicolini, S. Kapur, Amoxapine as an atypical antipsychotic: a comparative study vs risperidone, Neuropsychopharmacology 30 (2005) 2236–2244.

[11] I.B. Chaudhry, N. Husain, S. Khan, S. Badshah, B. Deakin, S. Kapur, Amoxapine as an antipsychotic: comparative study versus haloperidol, J. Clin. Psychopharmacol. 27 (2007) 575–581.

[12] A. Fulton, T. Norman, G.D. Burrows, Ligand binding and platelet uptake studies of loxapine, amoxapine and their 8-hydroxylated derivatives, J. Affect. Disord. 4 (1982) 113–119.

[13] B. Hue, B. Palomba, M. Giacardy-Paty, T. Bottai, R. Alric, P. Petit, Concurrent high-performance liquid chromatographic measurement of loxapine and amoxapine and of their hydroxylated metabolites in plasma, Ther. Drug Monit. 20 (1998) 335–339.

[14] S.W. Cheung, S.W. Tang, G. Remington, Simultaneous quantitation of loxapine, amoxapine and their 7- and 8-hydroxy metabolites in plasma by high-performance liquid chromatography, J. Chromatogr. 564 (1991) 213–221.

[15] J.S.D. Zimmer, S.R. Needham, C.D. Christianson, C.M. Piekarski, C.N. Sheaff, K. Huie, A.R. Reed, L. Takahashi, Validation of HPLC–MS/MS methods for analysis of loxapine, amoxapine, 7-OH-loxapine, 8-OH-loxapine and loxapine N-oxide in human plasma, Bioanalysis 2 (2010) 1989–2000.

[16] T.B. Cooper, R.G. Kelly, GLC analysis of loxapine and amoxapine in serum, tissues, and urine, Methodol. Anal. Toxicol. 3 (1985) 99–106.

[17] T.B. Cooper, R. Bost, I. Sunshine, Postmortem blood and tissue levels of loxapine and its metabolites, J. Anal. Toxicol. 5 (1981) 99–100.

[18] A. Chodobski, J. Szmydynger-Chodobska, M.D. Vannorsdall, M.H. Epstein, C.E. Johanson, AT1 receptor subtype mediates the inhibitory effect of central angiotensin II on cerebrospinal fluid formation in the rat, Regul. Pept. 53 (1994) 123–129.

[19] US Food and Drug Administration, Center for Drug Evaluation and Research, Guidance for Industry: Bioanalytical Method Validation, 2001.

[20] B.K. Matuszewski, M.L. Constanzer, C.M. Chavez-Eng, Strategies for the assessment of matrix effect in quantitative bioanalytical methods based on HPLC-MS/MS, Anal. Chem. 75 (2003) 3019–3030.

[21] S. Sugita, A. Kobayashi, S. Suzuki, T. Yoshida, K. Nakazawa, High-performance liquid chromatographic determination of imipramine and its metabolites in rat brain, J. Chromatogr. 421 (1987) 412–417.

[22] A. Kobayashi, K. Fujita, K. Nakazawa, In rat brain amoxapine enhances dopamine metabolism: pharmacokinetic variations of the effect, Eur. J. Pharmacol. 215 (1992) 43–49.

[23] C.N. Latimer, Neuropharmacologic evaluation of oxilapine, a potent psychoactive agent, J. Pharmacol. Exp. Ther. 166 (1969) 151–162.

[24] J. Watson, S. Wright, A. Lucas, K.L. Clarke, J. Viggers, S. Cheetham, P. Jeffrey, R. Porter, K.D. Read, Receptor occupancy and brain free fraction, Drug Metab. Dispos. 37 (2009) 753–760.

[25] US Food and Drug Administration, Center for Drug Evaluation and Research, Guidance for Industry: Estimating the Maximum Safe Starting Dose in Initial Clinical Trials for Therapeutics in Adult Healthy Volunteers, 2005.

[26] J.P. Krise, W.N. Charman, S.A. Charman, V.J. Stella, A novel prodrug approach for tertiary amines. 3. In vivo evaluation of two N-phosphonooxymethyl prodrugs in rats and dogs, J. Pharm. Sci. 88 (1999) 928–932.

[27] G. Nakova, E. Tomov, R. Georgieva, Study on the resorption of cloxazepine succinate in experimental animals and the use of high performance liquid chromatography (HPLC), Eksp. Med. Morfol. 21 (1982) 39–43.

An ultra-pressure liquid chromatography–tandem mass spectrometry method for the simultaneous determination of three physalins in rat plasma and its application to pharmacokinetic study of *Physalis alkekengi* var. *franchetii* (Chinese lantern) in rats

Yunliang Zheng[a], Yong Chen[a], Yiping Ren[b], Lianjun Luan[a], Yongjiang Wu[a],*

[a] College of Pharmaceutical Sciences, Zhejiang University, 338 Yuhangtang Road, Hangzhou 310058, China
[b] Zhejiang Provincial Center for Disease Prevention and Control, 630 Xincheng Road, Hangzhou 310051, China

ARTICLE INFO

ABSTRACT

An ultra-high pressure liquid chromatography–tandem mass spectrometry (UPLC–MS/MS) method was developed for the quantification of three major ingredients in Chinese lantern preparations (CLP) in rat plasma. Following extraction by ethyl acetate, the analytes were separated on an Acquity UPLC BEH Shield RP C_{18} column using a gradient mobile phase system of acetonitrile–water. Electrospray ionization (ESI) tandem interface was employed prior to mass spectrometric detection. The calibration curves were linear over the range of 5.0–500.0 ng/ml for physalin D, 2.3–230.0 ng/ml for physalin G and 0.71–71.0 ng/ml for 4,7-didehydroneophysalin B. The average extraction recoveries, examined at four concentration levels, carried from 57.1% to 76.9%, and the accuracies ranged from 94.0% to 113.3% with precision (RSD) <15%. The validated method was successfully applied to the determination of the three physalins in rat plasma after intragastric administration of CLP suspension.

© 2011 Elsevier B.V. All rights reserved.

1. Introduction

The use of natural products in the treatment of a variety of diseases has been increasing due to the considerable number of medicinal plants with proven biological activities applicable to the treatment of some diseases [1]. The calyces of *Physalis alkekengi* var. *franchetii* (Solanaceae) (Chinese lantern) are used as a traditional herbal medicine in China for the treatment of sore throat, cough, eczema, hepatitis, urinary problems, and tumors [2,3]. Physalins are the major steroidal constituents of Chinese lantern, and their rare 13,14-seco-16,24-cycloergostane skeletons ($C_{28}H_{30-34}O_{9-12}$) have been established by X-ray crystallographic analysis [4–6]. The physalins have been studied extensively during the past 20 years and are reported to have many activities: physalins B and F are able to reduce the percentage of leishmania-infected macrophages and the intracellular parasite number in vitro at concentrations non-cytotoxic to macrophages [7]; physalin B and D display considerable cytotoxicity against several cancer cell lines, showing IC_{50} values in the range of 0.58–15.18 µg/ml for physalin B, and 0.28–2.43 µg/ml for physalin D, the in vivo (administered

intraperitoneally) antitumor activity is related to the inhibition of tumor proliferation, as observed by the reduction of Ki67 staining in tumors of treated animals [8]; physalin F and G can cause the reduction in nitric oxide production by macrophages stimulated with lipopolysaccharide and interferon-γ [9]. In addition, physalins also have anti-inflammatory [10–12] and cytotoxic [13–15] activities.

Previous studies mainly focused on the isolation, characterization and biological activities of physalins from Chinese lantern, whereas, few pharmacokinetic study of physalins has been reported. In our previous study, we found that several physalins (e.g. physalin B and physalin H) could not be absorbed through intragastric administration, which is a key factor for new drug discovery and rational use of Chinese lantern. Therefore, pharmacokinetic studies of physalins are of great importance for the further development and the rational use of Chinese lantern. The purpose of this study is to develop and validate an analytical method for the simultaneous determination of physalins in biological matrix, and then study their pharmacokinetic behaviors.

Several analytical methods have been reported for the quantification of physalins [16–18]. However, all these methods are concentrating only on one or two physalins in Chinese lantern using HPLC with UV detection at 220 nm or 230 nm. Single wavelength spectrophotometric detection, particularly in the end absorption

* Corresponding author. Tel.: +86 571 88208455; fax: +86 571 88208455.
E-mail address: yjwu@zju.edu.cn (Y. Wu).

region, lacks the specificity desirable for quantitation in biological matrices, thus the effort to develop more sensitive methods for the simultaneously quantify multiple active components of the raw materials of Chinese lantern in biological matrices are necessary for pharmacokinetic studies. Compared to HPLC–UV method, UPLC–MS/MS analytical method is a more powerful approach, especially in the analysis of multi-components in complicated matrices, to rapidly quantify multi-ingredients due to its rapid separation power, low detection limit, high specificity and resolution. In order to study the pharmacokinetics property of physalin D, we have reported an UPLC–MS/MS method for quantification of it in rat plasma [19]. However, as we know, composition of Chinese lantern is complex, so as to explain its pharmacokinetic properties, we should study pharmacokinetics properties of more compounds in Chinese lantern.

In the present study, we developed and validated a sensitive and rapid UPLC–MS/MS method in MRM mode for the simultaneous determination of three bioactive physalins in Chinese lantern: physalin D, physalin G and 4,7-didehydroneophysalin B in rat plasma using physalin H as the internal standard (IS) (Fig. 1). The method was successfully applied to pharmacokinetic study of them after intragastric administration of CLP suspension.

2. Experimental

2.1. Chemical reagents and animals

Chinese lantern was bought from Bozhou, Anhui province and was authenticated by Associate Professor Juan-Hua Xu from College of Pharmaceutical Sciences, Zhejiang University.

The standards of physalin D, physalin G, 4,7-didehydroneophysalin B and physalin H (IS; not present in the CLP) were isolated in our laboratory. Their structures (Fig. 1) were identified by comparing UV, IR, ^{1}H and ^{13}C NMR, 2D NMR data with corresponding references [20–23]. The purity of each compound was determined to be above 97% by LC–MS and NMR.

HPLC grade acetonitrile and methanol were purchased from Merck (Darmstadt, Germany). Deionized water was purified using a Milli-Q system (Millipore, Milford, MA, USA). Male Sprague-Dawley (SD) rats, weighing 160 ± 20 g ("20" is a standard deviation: SD), were obtained from the Zhejiang University Laboratory Animal Center.

2.2. Instrument and analytical conditions

LC analysis was performed using a Waters Acquity Ultra Performance LC (UPLC) system (Waters, Milford, MA, USA). Chromatographic separation was performed on an Acquity UPLC BEH Shield RP C_{18} column (100 mm × 2.1 mm, 1.7 μm particle size; Waters, Milford, MA, USA). A linear gradient elution programme was used with solvent A (water) and solvent B (acetonitrile) as follows: 32% B (initial), 32–40% B (0–3.5 min), 40–55% B (3.5–5.0 min), 55–100% B (5.0–5.2 min), 100–100% B (5.2–6.2 min), 100–32% B (6.2–6.5 min). The flow rate was 0.3 ml/min and the injection volume was 2 μl. The column and sample temperatures were maintained at 35 °C and 4 °C, respectively.

Determination was performed using a Micromass Quattro Ultima triple-quadrupole mass spectrometer equipped with an ESI source (Waters, Manchester, UK). The parameters of the mass spectrometer under the ESI$^+$ mode were as follows: capillary voltage,
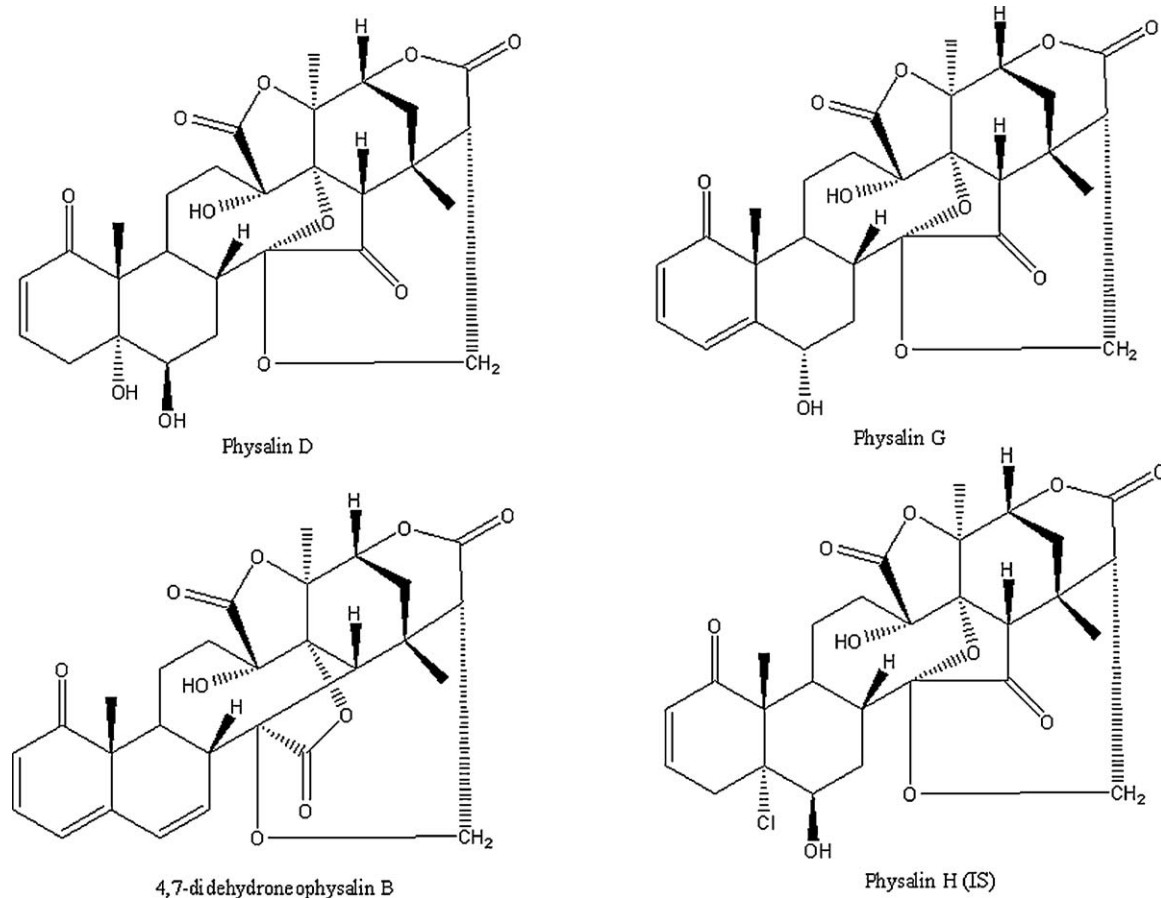

Fig. 1. Chemical structures of physalin D, physalin G, 4,7-didehydroneophysalin B and physalin H (IS).

Table 1
ESI$^+$-MS/MS parameters on the parent and daughter ions (m/z) and collision energy of the three analytes and IS.

Analytes	Parent ions (m/z)	Daughter ions (m/z)	Collision energy (eV)
Physalin D	545.3	509.3	8
Physalin G	527.3	135.4	35
4,7-Didehydroneophysalin B	509.2	171.3	25
Physalin H (IS)	563.3	545.2	18

3.50 kV; cone voltage, 35 V; source temperature, 120 °C; aperture, 0.5; cone gas, 52 l/h; desolvation temperature, 350 °C; desolvation gas, 580 l/h; argon collision gas pressure, 2.7×10^{-3} mbar; ion energy1, 1 eV; collision gradient, 1.0 and ion energy2, 1 eV. The parameters on the m/z and collision energy of parent ions and quantitative daughter ions for the three analytes and IS are summarized in Table 1.

2.3. Calibration standards and quality control (QC) sample preparation

Accurately weighed solid portions of standards (10.00 mg, 11.50 mg, 14.20 mg, 15.00 mg for physalin D, physalin G, 4,7-didehydroneophysalin B and IS, respectively) were dissolved in methanol to prepare stock solutions separately: 1.000 mg/ml for physalin D, 1.150 mg/ml for physalin G, 1.420 mg/ml for 4,7-didehydroneophysalin B and 1.500 mg/ml for IS. Working solutions used for spiking plasma were all freshly prepared by diluting the stock solution with 50% acetonitrile aqueous solution to appropriate concentrations.

Calibration standard samples were prepared by freshly spiking the appropriate working solution into blank pooled plasma to prepare concentrations of 5.0–500.0 ng/ml for physalin D, 2.3–230.0 ng/ml for physalin G, 0.71–71.0 ng/ml for 4,7-didehydroneophysalin B, and processed as described in the preparation of sample solution (Section 2.5). The QC samples (at four concentration levels, refer to Tables 3–5) used for the recovery study, intra-day and inter-day accuracy, precision and stability study were prepared in the same way as the preparation of calibration standard samples, and then stored at −20 °C until analysis.

2.4. Preparation of Chinese lantern preparations (CLP)

Powdered Chinese lantern (200 g) was extracted for two times (1.5 h each time) with 3000 ml of water by refluxing, and then filtered. The combined filtrates were concentrated to 500 ml by using a rotary evaporator in vacuum. Stirring with a glass rod, 1500 ml of ethanol was added into the 500 ml concentrated solution. After filtering and recovering ethanol, the residual liquid was extracted by CH_2Cl_2 (2×500 ml). Then the CH_2Cl_2 extract was evaporated to dryness using rotary evaporator at a maximum temperature of 45 °C, yield about 2.0 g of CLP.

2.5. Preparation of sample solution

Plasma samples were removed from −20 °C storage and thawed under ambient conditions. An aliquot of 50 μl of plasma was extracted employing a liquid–liquid extraction technique after the addition of 20 μl of (600 ng/ml) IS solution and 300 μl of ethyl acetate. After vortex for 90 s and centrifugation at 15,000 rpm for 5 min, 200 μl of the organic phase was transferred into a centrifuge tube and evaporated to dryness under a nitrogen stream at room temperature. The residue was reconstituted in 200 μl of 50% acetonitrile aqueous solution. After centrifugation at 15,000 rpm for 10 min, 2 μl of the supernatant was injected into the UPLC–MS/MS system.

2.6. Method validation

The method was validated in terms of specificity, calibration curve, sensitivity, matrix effect, accuracy, precision and stability mainly according to the European Medicines Agency (2009) guidelines for validation of bioanalytical method [24].

2.6.1. Specificity, linearity and sensitivity

Specificity was evaluated by using six pre-dose plasma samples from different rats and compared them with six spiked lower limit of quantification (LLOQ) in blank plasma. Blank plasma samples and spiked LLOQ matrix were extracted, and then analyzed by UPLC–MS/MS for potential interfering peaks within the range of the retention time of each analyte.

Calibration curves were constructed from the peak-area ratios of each analyte to IS versus plasma concentrations using a $1/x^2$ weighted linear least-squares regression model. The LLOQ was determined as the lowest concentration point of the standard curve. The lower limit of detection (LLOD) was defined as the amount that could be detected with a signal-to-noise ratio of 3.

2.6.2. Extraction recovery and matrix effect

Extraction recovery was measured for four concentration levels of QC samples ($n = 5$). The blank matrix was prepared as described in Section 2.5, without adding any standard. The extraction recovery was determined by comparing the analyte and IS peak area obtained from QC samples with those originally dissolved with blank matrix.

Matrix effect was determined by comparing the analytes and IS peak area dissolved with blank matrix against those dissolved with 50% acetonitrile aqueous solution.

2.6.3. Precision, accuracy and stability

The intra-day and inter-day precision and accuracy were carried out through quantifying four levels of QC samples ($n = 5$) on the same day and on four consecutive validation days, respectively. The results of the intra-day and inter-day precisions were presented with the relative standard deviation (RSD, %), whilst percentage difference between amount spiked and determined was taken as the measures of accuracy.

The post-preparation stability was tested by determining the extracted QC samples stored in the auto-sampler (4 °C) for 24 h; the freeze and thaw stability was carried out by assaying QC plasma samples undergoing three freeze (−20 °C)–thaw (room temperature) cycles, and the storage stability was evaluated by determining QC plasma samples at five replicates stored at −20 °C for 25 days.

2.7. Pharmacokinetic analysis

Six male SD rats (160 ± 20 g) were used in pharmacokinetic studies. The rats were fasted for 12 h and had free access to water before dosing. Each rat received an intragastric administration of 0.5 g/kg CLP (equivalent to 35.6 mg/kg of physalin D, 13.9 mg/kg of physalin G and 32.6 mg/kg of 4,7-didehydroneophysalin B). The CLP was suspended in 0.5% carboxymethyl cellulose sodium (CMC-Na) (w/v). Blood samples (about 300 μl) were collected in heparinized tubes via the postorbital venous plexus veins from each

Table 2
Linear regression data, LLOD and LLOQ of the investigated components.

Analytes	Regressive equation	R^2	Test range (ng/ml)	LLOD (ng/ml)	LLOQ (ng/ml)
Physalin D	$Y = 0.80x - 2.91$	0.9987	5.0–500.0	1.0	5.0
Physalin G	$Y = 0.66x + 0.15$	0.9985	2.3–230.0	0.2	2.3
4,7-Didehydroneophysalin B	$Y = 2.64x - 1.06$	0.9977	0.71–71.0	0.08	0.71

Table 3
Extraction recovery and matrix effect of the developed method and the repeatability of the extraction procedure ($n = 5$).

Analytes	QC conc. (ng/ml)	Recovery (%)	Matrix effect (%)
Physalin D	5.0	62.7 ± 8.1	103.0 ± 7.3
	10.0	57.1 ± 5.9	98.2 ± 10.0
	100.0	67.2 ± 5.8	108.1 ± 4.0
	300.0	61.1 ± 6.6	98.9 ± 8.1
Physalin G	2.3	59.9 ± 6.6	105.9 ± 8.9
	4.6	60.5 ± 4.1	103.9 ± 9.9
	46.0	74.3 ± 5.9	107.7 ± 3.6
	138.0	70.2 ± 6.2	104.1 ± 11.5
4,7-Didehydroneophysalin B	0.71	71.9 ± 4.7	98.7 ± 6.7
	1.42	76.9 ± 8.1	96.0 ± 4.1
	14.2	75.7 ± 4.4	106.3 ± 6.8
	42.6	71.2 ± 2.4	99.3 ± 7.3

Table 4
Precision and accuracy from QC samples of rat plasma extracts (n = four days and five replicates per day).

Analytes	QC conc. (ng/ml)	Intra-day (RSD, %)	Inter-day (RSD, %)	Accuracy (%)
Physalin D	5.0	10.4	14.9	94.0
	10.0	10.9	14.6	103.0
	100.0	8.9	8.0	101.9
	300.0	8.1	11.4	101.7
Physalin G	2.3	8.0	13.0	100.0
	4.6.0	4.5	6.7	97.8
	46.0	6.5	11.0	108.5
	138.0	4.9	4.1	98.3
4,7-Didehydroneophysalin B	0.71	10.4	11.9	94.4
	1.42	4.5	5.3	105.6
	14.2	4.6	7.9	98.6
	42.6	6.0	7.2	101.6

Table 5
Stability of the three analytes in rats plasma under different storage conditions ($n = 5$).

Analytes	QC conc. (ng/ml)	Autosampler 4 °C for 24 h	Three freeze–thaw cycles	Storage at −20 °C to 25 days
Physalin D	5.0	101.6 ± 3.1	95.2 ± 11.0	91.6 ± 2.5
	10.0	94.0 ± 4.5	108.7 ± 13.5	106.3 ± 9.4
	100.0	103.2 ± 3.2	94.9 ± 7.2	97.7 ± 9.2
	300.0	101.9 ± 9.1	101.6 ± 10.5	102.8 ± 7.3
Physalin G	2.3	96.1 ± 6.7	98.2 ± 13.9	98.9 ± 6.5
	4.6	98.5 ± 8.7	97.2 ± 5.7	103.0 ± 6.8
	46.0	100.0 ± 3.4	99.9 ± 5.1	90.4 ± 3.0
	138.0	98.9 ± 3.8	97.7 ± 4.5	97.5 ± 5.8
4,7-Didehydroneophysalin B	0.71	102.2 ± 4.0	101.4 ± 14.2	105.6 ± 10.6
	1.42	106.9 ± 5.8	105.2 ± 4.4	105.0 ± 11.9
	14.2	101.1 ± 6.0	99.2 ± 3.8	94.3 ± 7.3
	42.6	100.2 ± 8.7	98.8 ± 6.6	100.8 ± 9.8

All values are represented as the percent of measured concentration from nominal concentration (accuracy %).

rat at 0, 5, 10, 20, 40, 70, 100, 130, 170, 230, 410, 530, 720 and 1340 min after administration, and were immediately centrifuged at 600 rpm for 5 min, and then stored at −20 °C until analysis. The pharmacokinetic parameters $t_{1/2}$ (the biological half-life), CL (total body clearance) and AUC_{0-t} (area under curve) were calculated by drug and statistics (DAS) software, version 2.0 (Shanghai, China). The parameter t_{max} (the time to reach peak concentration) was obtained from the time point corresponding to peak concentration of each analyte in rat plasma. C_{max} (the peak concentration) was determined from peak concentration of each analyte in rat plasma after intragastric administration.

3. Results and discussion

3.1. Selection of IS

It is necessary to use an IS to get high accuracy when a mass spectrometer is equipped with LC as the detector. An ideal IS should be

a structurally similar analog or stable isotope-labelled compound. Considering the isotope-labelled compounds are difficult to obtain, physalin H is chosen for quantification as the IS due to its similarity with the analytes in structure, mass spectrographic behavior, chromatographic behavior and solubility, which is better than luteolin that was used in our previous study [19].

3.2. Optimization of mobile phase and MS parameters

Different mobile phases (methanol–water, acetonitrile–water with or without formic acid or ammonium acetate) and various gradient elution processes were investigated to optimize analytical performance. We found that the response of physalin G decreased with the increased ammonium acetate concentration in the mobile phase, and the responses of the analytes and IS were not improved when adding formic acid to mobile phase. When the mobile phase consisted of acetonitrile and water, the responses were higher and peaks were of better shape than that of methanol–water system. Therefore, the acetonitrile–water system was selected as the mobile phase.

MS examination of the analytes and IS standard solutions in positive and negative ESI modes by direct full scan method revealed that signals obtained from the positive electrospray ionization source mode had a good resolution and high intensity to permit quantitative measurement. The optimization of daughter ions and their collision energy was performed by the daughter scan mode. The daughter ions were confirmed based on their signal intensity. The final MS/MS parameters are summarized in Table 1, and the product spectra and fragmentation reactions of the four compounds are shown in Fig. 2.
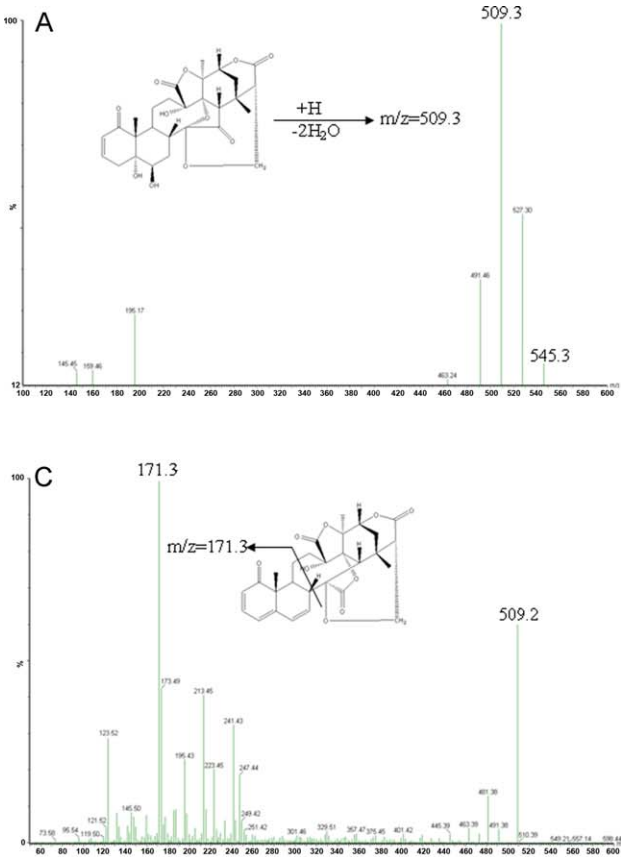
3.3. Optimization of sample pretreatment

Protein precipitation was initially developed with methanol and acetonitrile, but the recoveries of physalin G and 4,7-didehydroneophysalin B were found below 50%. Liquid–liquid extraction (LLE) of the three analytes and IS from plasma samples was then explored. Different types of solvents were tested to extract the analytes and IS. Although the analytes and IS could be extracted with dichloromethane and ethyl acetate, the results showed that ethyl acetate offered better recoveries for all of the analytes. Compared with the more recent and popular technique of solid-phase extraction (SPE), purification with LLE resulted in less potential interfering compounds, and it is simple and much more economical. In addition, the IS, which has a structure similar to the analytes, also has a better recovery under current conditions.

3.4. Method validation

3.4.1. Specificity

The typical chromatograms of physalin D, physalin G and 4,7-didehydroneophysalin B and IS are presented in Fig. 3. Under the described chromatographic conditions, a good separation was achieved and no significant peak was observed in any of the blank plasma samples for the three analytes and IS. The retention times of physalin D, physalin G and 4,7-didehydroneophysalin B and IS were 2.31, 2.75, 4.95 and 4.84 min, respectively.

3.4.2. Linearity and sensitivity

The quantitative capability of the system employing UPLC–MS/MS method was tested in the assay. Plasma sam-
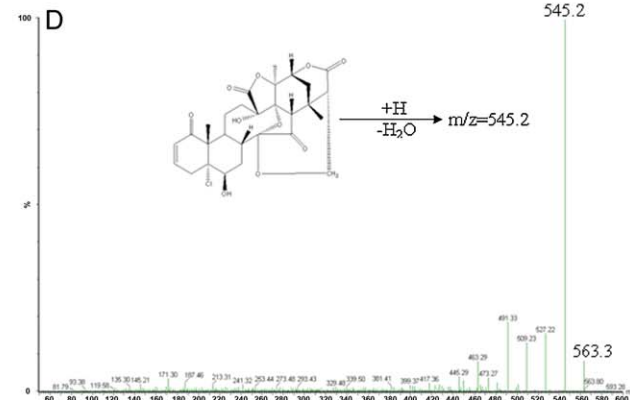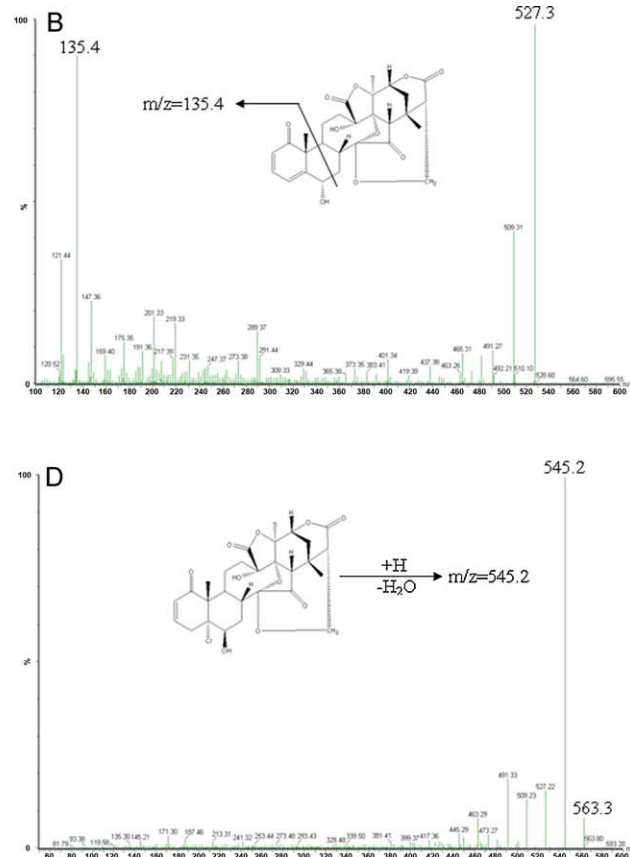
Fig. 2. The product spectra and fragmentation reactions of the four compounds in positive electrospray ionization mode (A) physalin D; (B) physalin G; (C) 4,7-didehydroneophysalin B; and (D) IS.
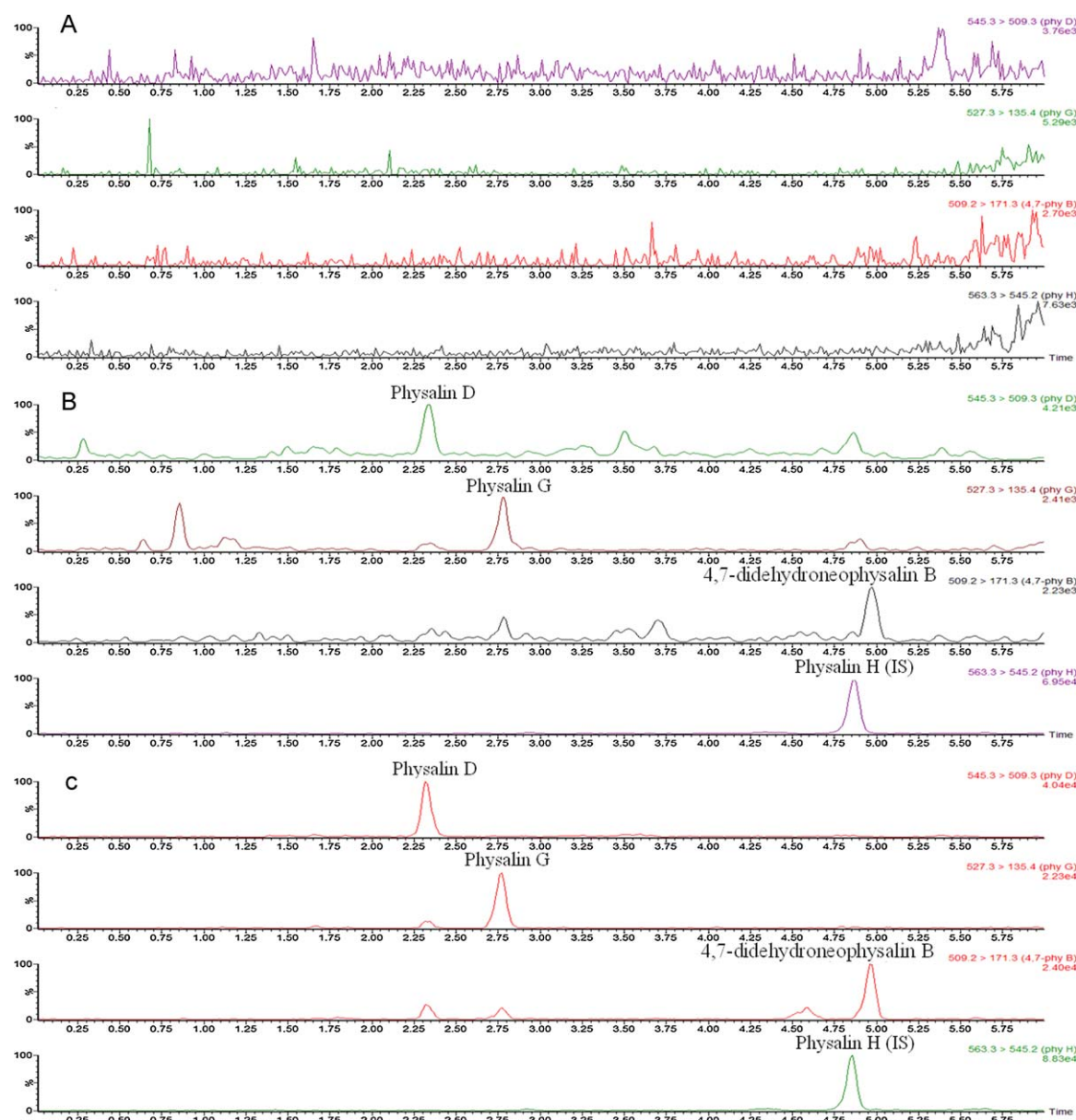
Fig. 3. Representative MRM chromatograms of physalin D, physalin G, 4,7-didehydroneophysalin B and IS in rat plasma. (A) Blank plasma; (B) blank plasma spiked with 5.0, 2.3, 0.71 and 60.0 ng/ml for physalin D, physalin G, 4,7-didehydroneophysalin B and IS, respectively; (C) rat plasma samples collected at 40 min after intragastric administration of CLP at a dose of 0.5 g/kg (23.5, 10.1, 13.8 and 60.0 ng/ml for physalin D, physalin G, 4,7-didehydroneophysalin B and IS, respectively).

ples were quantified by using the ratio of the peak area of analyte to that of IS as the assay parameter. Table 2 shows the results of the standard calibration curves, linearity (R^2), LLOD and LLOQ. The calibration curves are linear with $R^2 > 0.998$, and these limits are sufficient for this pharmacokinetic study.

3.4.3. Extraction recovery and matrix effect

A single-step LLE method (Section 2.5) with ethyl acetate proved to be simple, rapid and successful, with extraction recovery rates between 57.1 and 76.9% at the four concentrations of QC samples for the three analytes, and the recovery of IS was (74.1 ± 6.3%), indicating that the LLE method was acceptable. The extraction recovery and matrix effect data of the three analytes are shown in Table 3, and the matrix effect of the IS was about 106.8% (RSD: 8.7%). These data indicated that the sample preparation method is satisfied and resulted in no appreciable matrix effect for the analytes.

3.4.4. Accuracy and precision

The intra- and inter-day precisions were analyzed by injecting replicates of QC samples. Table 4 summarizes the intra- and inter-day precisions and accuracy of the method. The intra- and inter-day precision (RSD) ranged 4.5–10.9% and 4.1–14.9%, respectively. The accuracy derived from QC samples was between 94.0 and 113.3% for all the QC levels of the three analytes. The results demonstrate that the precision and accuracy of this assay are within the acceptable range.

3.4.5. Stability

Stability of the analytes during the sample processing procedures and storing was evaluated by analysis of four levels of QC samples. The results are shown in Table 5. The results indicated that these analytes in rat plasma were all stable for three cycles of freeze–thaw, 24 h in the auto-sampler (4 °C), 25 days at −20 °C with accuracy in the range of 90.4–113.3%.

Table 6

Pharmacokinetic parameters of physalin D, physalin G and 4,7-didehydroneophysalin B after intragastric administration of Chinese lantern preparation to six male SD rats (values are mean ± standard deviation).

Parameters	Unit	Phyalin D	Physalin G	4,7-Didehydroneophysalin B
C_{max}	ng/ml	47.6 ± 4.1	20.9 ± 4.4	23.6 ± 4.9
$t_{1/2z}$	min	220.6 ± 62.6	482.4 ± 205.0	368.7 ± 72.1
T_{max}	min	70.0 ± 0.0	70.0 ± 0.0	70.0 ± 0.0
CL	l/min/kg	4.4 ± 0.6	3.2 ± 0.7	8.7 ± 1.9
$AUC_{(0-t)}$	ng min/ml	7515.6 ± 859.0	3674.4 ± 691.5	3649.3 ± 771.2
$AUC_{(0-\infty)}$	ng min/ml	8216.6 ± 1031.0	4473.8 ± 1047.6	3889.2 ± 887.8
$MRT_{(0-t)}$	min	205.1 ± 19.6	281.5 ± 84.5	293.3 ± 26.0
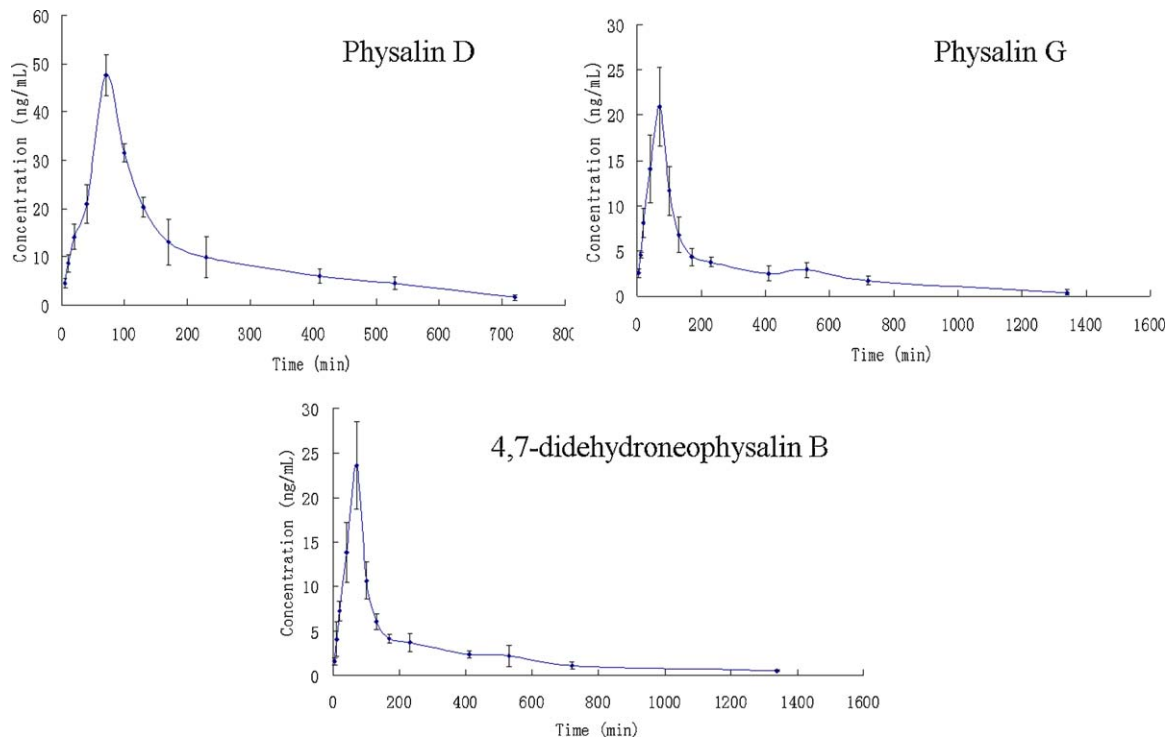
Fig. 4. Mean (±SD, $n = 6$) plasma concentration of physalin D, physalin G, 4,7-didehydroneophysalin B as a function of time following intragastric administrations (dose at 0.5 mg/kg) of CLP suspension to rats.

3.5. Pharmacokinetic study

This method was applied to the pharmacokinetic study of physalin D, physalin G and 4,7-didehydroneophysalin B in rats after intragastric administration of CLP. The assay was proved to be sensitive enough for the determination of the three compounds in rat plasma. The pharmacokinetic parameters are presented in Table 6. The mean plasma concentration–time profiles are illustrated in Fig. 4.

The results shown in Fig. 4 and Table 6 suggested that the plasma concentrations of all the three compounds reached C_{max} at 70 min, which indicated they were all absorbed very quickly by rats, the elimination of physalin D was the quickest of the three compounds, which, to some extent, consisted with our previous study [19].

Our preliminary experiment found that CLP was mainly consisted of physalins, and the three active analytes used in this study occupied about 15% of the CLP. Considering the structures of physalins are similar, the pharmacokinetic properties of the three analytes used in this study will be useful to preliminary presume other physalins' pharmacokinetic properties, and to promote the efficacy and safety of Chinese lantern and to avoid its adverse effects.

4. Conclusion

To our knowledge, this is the first fully validated UPLC–MS/MS method for the simultaneous quantification of physalin D, physalin G and 4,7-didehydroneophysalin B in biological matrix. The method proved to be specific, sensitive, accurate and precise. Liquid–liquid extraction was employed for the extraction of these components from the plasma samples. The developed method provided a simple sample preparation and a stable analytical result for the determination of these physalins in plasma samples. This method was successfully applied in the determination of the three major components of CLP in rat plasma after intragastric administration. The results showed that the three physalins have similar absorption and elimination behavior.

References

[1] B. Stephen, K. Richard, Commonly used herbal medicines in the United States: a review, Am. J. Med. 116 (2004) 478–485.
[2] Chinese Pharmacopoeia Committee, Pharmacopoeia of The People's Republic of China, vol. 1, Chemical Industry Press, Beijing, 2005, pp. 250–251.

[3] S. Helvaci, G. Kokdil, M. Kawai, N. Duran, G. Duran, A. Guvenc, Antimicrobial activity of the extracts and physalin D from *Physalis alkekengi* and evaluation of antioxidant potential of physalin D, Pharm. Biol. 48 (2010) 142–150.

[4] M. Kawai, T. Matsuura, T. Taga, K.J. Osaki, Crystal and molecular structure of 5a-acetoxy-6-bromohexahydrophysalin A, Chem. Soc. B (1970) 812–815.

[5] M. Kawai, B. Makino, T. Taga, Y. Miwa, T. Yamamoto, T. Furuta, H. Yamamura, Y. Butsugan, K. Ogawa, M. Hayashi, Crystal structures of 5α,6α-epoxy and 2,3-dihydro derivatives of physalin B, a 13,14-seco-16,24-cyclosteroid, and their ¹H NMR spectral analysis, Bull. Chem. Soc. Jpn. 67 (1994) 222–226.

[6] T. Taga, Y. Miwa, K. Machida, M. Kawai, Y. Buisugan, Structure of 4,7-didehydroneophysalin B, acid-induced rearrangement product of physalin A, Acta Crystallogr. C 47 (1991) 2188–2191.

[7] E.T. Guimarães, M.S. Lima, L.A. Santos, I.M. Ribeiro, T.B.C. Tomassini, R.R. Santos, W.L.C. Santos, M.B.P. Soares, Activity of physalins purified from Physalis angulata in in vitro and in vivo models of cutaneous leishmaniasis, J. Antimicrob. Chemoth. 64 (2009) 84–87.

[8] H.I.F. Magalhaes, M.L. Veras, M.R. Torres, A.P.N.N. Alves, O.D.L. Pessoa, E.R. Silveira, L.V. Costa-Lotufo, M.O. Moraes, C. Pessoa, In-vitro and in-vivo antitumour activity of physalins B and D from Physalis angulata, J. Pharm. Pharmacol. 58 (2006) 235–241.

[9] M.B.P. Soares, M.C. Bellintani, I.M. Ribeiro, T.C.B. Tomassini, R.R. Santos, Inhibition of macrophage activation and lipopolysaccharide-induced death by seco-steroids purified from Physalis angulata L, Eur. J. Pharmacol. 459 (2003) 107–112.

[10] A.T. Vieira, V. Pinho, L.B. Lepsch, C. Scavone, I.M. Ribeiro, T. Tomassini, R.R. Santos, M.B.P. Soares, M.M. Teixeira, D.G. Souza, Mechanisms of the anti-inflammatory effects of the natural secosteroids physalins in a model of intestinal ischaemia and reperfusion injury, Br. J. Pharmacol. 146 (2005) 244–251.

[11] N.B. Pinto, T.C. Morais, K.M.B. Carvalho, C.R. Silva, G.M. Andrade, G.A.C. Brito, M.L. Veras, O.D.L. Pessoa, V.S. Rao, F.A. Santos, Topical anti-inflammatory potential of physalin E from Physalis angulata on experimental dermatitis in mice, Phytomedicine 17 (2010) 740–743.

[12] D. Brustolim, J.F. Vasconcelos, L.A.R. Freitas, M.M. Teixeira, M.T. Farias, Y.M. Ribeiro, T.C.B. Tomassini, G.G.S. Oliveira, L.C.P. Carvalho, R.R. Santos, M.B.P. Soares, Activity of physalin F in a collagen-induced arthritis model, J. Nat. Prod. 73 (2010) 1323–1326.

[13] P.C. Kuo, T.H. Kuo, A.G. Damu, C.R. Su, E.J. Lee, T.S. Wu, R. Shu, C.M. Chen, K.F. Bastow, T.H. Chen, K.H. Lee, A. Physanolide, A novel skeleton steroid, and other cytotoxic principles from Physalis angulata, Org. Lett. 8 (2006) 2953–2956.

[14] A.G. Damu, P.C. Kuo, C.R. Su, T.H. Kuo, T.H. Chen, K.F. Bastow, K.H. Lee, T.S. Wu, Isolation, structures, and structure-cytotoxic activity relationships of withanolides and physalins from Physalis angulata, J. Nat. Prod. 70 (2007) 1146–1152.

[15] H.I.F. Magalhaes, M.L. Veras, O.D.L. Pessoa, E.R. Silveira, M.O. Moraes, C. Pessoa, L.V. Costa-Lotufo, Preliminary investigation of structure–activity relationship of cytotoxic physalins, Lett. Drug Des. Discov. 3 (2006) 9–13.

[16] R. Shi, L.Y. Jia, Q.S. Sun, D.D. Yu, RP-HPLC determination of three active components in *Physalis alkekengi* L. var. *franchetii* (Msst.) Makino, Chin. J. Pharm. Anal. 28 (2008) 260–262.

[17] H.D. Zhao, C.X. Lin, C.X. Yin, T. Yu, X. Feng, Q. Cai, Determination of 4,7-didehydro-neophysalinB in *Physalis alkekengi* L. var. *franchetii* (mast.) Mskino Calyces by HPLC, J. Liaoning Univ. TCM 10 (2008) 129–130.

[18] X. Dong, Y.Q. Liu, Q. Cai, Determination of physalin P in *Physalis alkekengi* L. var. *franchetii* (mast.) Mskino Calyces by HPLC, Chin. Tradit. Patent Med. 31 (2009) 1304–1306.

[19] Y.J. Wu, Y.L. Zheng, N. Chen, L.J. Luan, X.S. Liu, Plasma pharmacokinetics and tissue distribution study of physalin D in rats by ultra-pressure liquid chromatography with tandem mass spectrometry, J. Chromatogr. B 879 (2011) 443–448.

[20] T. Matsuura, M. Kawai, Bitter principles of *Physalis alkekengi* var *francheti*: structure of physalin B, Tetrahedron Lett. 10 (1969) 1765–1766.

[21] R.L. Row, S.K. Reddy, S.N. Sarma, T. Matsuura, R. Nakashima, New pyhsalins from Physalis alngulata and Physalis land folia. Structure and reactions of physalins D, I, G and K, Phytochemistry 19 (1980) 1175–1181.

[22] R.L. Row, S.N. Sarma, T. Matsuura, R. Nakashima, Physalins E and H, new physalins from *Physalis angulata* and *P. lancifolia*, Phytochemistry 17 (1978) 1641–1645.

[23] R. Sunayama, M. Kuroyanagi, K. Umehara, A. Ueno, Physalin and neophysalins from *Physalis alkekengi* var. *francheti* and their differentiation inducing activity, Phytochemistry 34 (1993) 529–533.

[24] European Medicines Agency, Guideline on Validation of Bioanalytical Methods, Committee for Medicinal Products for Human Use, London, 2009.

Fast simultaneous quantitative analysis of FTY720 and its metabolite FTY720-P in human blood by on-line solid phase extraction coupled with liquid chromatography–tandem mass spectrometry

Corinne Emotte, Fany Deglave, Olivier Heudi *, Franck Picard, Olivier Kretz

Novartis Pharma AG, DMPK/Bioanalytics, CH-4002 Basel, Switzerland

ARTICLE INFO

ABSTRACT

Fingolimod (Gilenya®; FTY720), has been recently approved for the treatment of multiple sclerosis in Europe and in the USA. In the present study, we have developed and validated a rapid and sensitive liquid chromatography–tandem mass spectrometry (LC–MS/MS) method to simultaneously quantify FTY720 and FTY720-P in human blood. The sample preparation involves the sample dilution with a solution made of dimethylhexylamine (DMHA), ortho-phosphoric acid and methanol prior to the on-line solid phase extraction (SPE) on a C_{18} cartridge. The samples were then eluted on a C_{18} column with a gradient elution of DMHA solution and acetonitrile and analyzed by LC–MS/MS using electrospay ionization in positive mode. The analysis time between 2 samples was 7.5 min. Standard curves were linear over the ranges of 0.0800 ng/mL (LLOQ) to 16.0 ng/mL for FTY720 and 0.100 ng/mL (LLOQ) to 20.0 ng/mL for FTY720-P with correlation coefficient (r^2) greater than 0.997. The method selectivities for FTY720 and FTY720-P were demonstrated in six different batches of human blood. Intra-run and inter-run precision and accuracy within $\pm20\%$ (at the LLOQ) and $\pm15\%$ (other levels) were achieved during a 3-run validation for quality control samples (QCs). In addition, stability data obtained during freeze–thaw (3 cycles), at room temperature (24 h), and in an auto-sampler were determined and reported. The method robustness was demonstrated by the consistent data obtained by reanalyzing human blood samples for several clinical studies. In addition comparative data for FTY720 and FTY720-P were obtained between our current method and those of two available separate LC–MS/MS assays. The results of the present work demonstrated that our bioanalytical LC–MS/MS method is rapid, sensitive, specific and reliable for the simultaneous quantitative analysis of FTY720 and FTY720-P in human blood.

© 2011 Elsevier B.V. All rights reserved.

1. Introduction

Fingolimod (Gilenya; FTY720), a synthetic compound based on the fungal secondary metabolite myriocin, has been recently approved for the treatment of multiple sclerosis in Europe and in the USA. FTY720 mechanism of action is unique as it reduces the number of circulating lymphocytes by preventing their egress from lymph nodes [1–4]. FTY720 is mainly phosphorylated by sphingosine kinase type II to its active metabolite FTY720-phosphate (FTY720-P), an analogue of sphingosine-1-phosphate (S1P) [1]. The relevance of S1P in cellular processes has been emphasized by identifying its function as a ligand on a family of G-protein coupled receptors from which five subtypes (S1P1–S1P5) exist [5]. It has

been shown that the imbalance between FTY720/FTY720-P could have a great impact on the mode of action of FTY720 [6,7] both *in vitro* and *in vivo*. Thus, it is essential to develop fast and reliable method for the quantitative analysis of FTY720 and FTY720-P in biological matrices. Analytical methods for quantitative analysis of FTY720 and related analogs involved high-performance liquid chromatography (HPLC) coupled with fluorescent detection [8–10]. Since these compounds are not naturally fluorescent, a derivatization step is needed to enhance their detection by fluorescence. As a consequence, these methods required either laborious chemical derivatization procedure or longer running time which makes the approach not suitable for high-throughput quantitative analysis. Liquid chromatography coupled to tandem mass spectrometry (LC–MS/MS) has been applied to the quantification of FTY720 in blood samples [11,12]. With these methods low sensitivity was achieved as well as short analysis time. However none of them were applied to the simultaneous analysis of FTY720 and its phosphorylated metabolite FTY720-P in whole blood samples. In an attempt to quantify FTY720 and FTY720-P in blood samples, two separate

* Corresponding author at: Novartis Institute for Biomedical Research, DMPK/Bioanalytics Fabrikstrasse 14 WSJ-153.3.02, CH-4056 Basel, Switzerland. Tel.: +41 79 535 96 11; fax: +41 61 696 85 84.

*E-mail addresses:* olivier.heudi@novartis.com, heudio@hotmail.fr (O. Heudi).
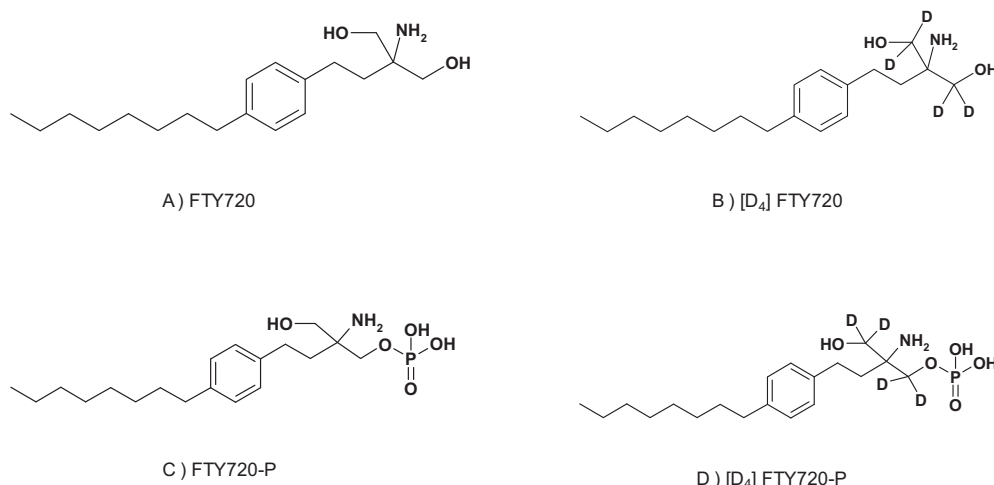
Fig. 1. Chemical structures of FTY720 (A), FTY720-P (B), and that of their internal standards [D$_4$] FTY720 (C) and [D$_4$] FTY720-P (D).

time consuming LC–MS/MS methods were developed (see material and method section for the full details of these two methods). The FTY720 method involves a liquid/liquid extraction (LLE) procedure while the one developed for FTY720-P uses protein precipitation (PPT). Both of these methods required at least 0.1 mL of blood sample each, and are performed on two separate LC–MS/MS instruments. It became evident that an improved LC–MS/MS bioanalytical method aiming at the simultaneous determination of FTY720 and FTY720-P would represent an obvious advantage.

In the present study, we have developed and validated a rapid and sensitive liquid chromatography–tandem mass spectrometry (LC–MS/MS) method to simultaneously quantify FTY720 and FTY720-P in human blood.

2. Experimental

2.1. Chemicals and reagents

Acetic acid (100% anhydrous), ortho-phosporic acid, methanol, isopropanol, ethanol, acetonitrile and tetrahydrofuran were obtained from Merck KGaA (Darmstadt, Germany). Formic acid, TFA and ammonium formiate were purchased from Fluka (Buchs, Switzerland). 1.5-Dimethylhexylamine, 99% was obtained from Sigma–Aldrich (St Louis, MO, USA). MilliQ grade water was produced by a Millipore system (Bedford, MA, USA). The different human blood batches used for the preparation of Cs and QCs were obtained from the internal blood bank. FTY720, FTY720-P, [D$_4$]FTY720 and [D$_4$]FTY720-P were synthesized in-house. The structures of these compounds are shown in Fig. 1.

2.2. Solution preparation

The ammonium buffer and the HPLC mobile phase (A) used in the present study were prepared as the following.

Buffer Ammonium formiate buffer: 1.26 g of ammonium formiate was dissolved in 500 mL water and then 450 µL of a 5% formic acid aqueous solution was added.

HPLC mobile phase A: in a 2000 mL flask, 1.635 mL of DMHA was mixed with 75 mL of buffer ammonium formiate and then water was added filled in to the mark.

2.3. Instrumentation

The on-line SPE system consisted of a Prospekt-2 apparatus (Spark Holland, Emmen, Netherlands) composed of an

Table 1
SRM transitions and ion optics parameters for FTY720, FTY720-P and that of their respective internal standard [D$_4$]FTY720 and [D$_4$]FTY720-P.

Compounds	Declustering potential (V)	Collision energy (eV)	Collision cell exit potential (V)
FTY720	46	21	16
[D$_4$]FTY720	76	21	22
FTY720-P	106	25	18
[D$_4$]FTY720-P	86	23	18

auto-sampler (Endurance), a solvent delivery unit (SDU) and an automatic cartridge exchange (ACE) module. The cartridges used were HySphere C$_{18}$, HD 7 mm from Spark (Holland, Emmen, Netherlands). The HPLC system consisted of a Shimadzu LC-10ADVP mobile phase delivery pump (Kyoto, Japan). The HPLC analytical column used was a Gemini C$_{18}$-NX (30 mm × 2.0 mm, 5 µm) from Phenomenex (Torrance, CA, USA).

Mass spectrometric detection was performed on an API 5000 triple quadrupole mass spectrometer from AB/MDS Sciex (Ontario, Canada) equipped with a Turbo V Ionspray source operating in the positive mode. Data acquisition was performed with Analyst 1.4.2 software distributed by AB/MDS Sciex. The curtain gas, ion source gas 1, ion source gas 2 and collision gas (all nitrogen) were set at 40, 30, 40 and 4 instrument units, respectively. The spray voltage was 5500 V, the heater temperature was 650 °C, the interface heater was turned on, and the entrance potential was set to 10 V. Data acquisition was performed with a dwell time of 50 ms for each transition. Specific settings for each compound are shown in Table 1. Under these MS conditions, the predominant analyte precursor ion was the protonated species [H+H]$^+$. The different monitored transitions used were as follows: FTY720 (m/z) 308.3 → 255.4; [D$_4$]FTY720 (m/z) 312.4 → 259.2; FTY720-P (m/z) 388.1 → 255.2 and [D$_4$]FTY720-P (m/z) 392.2 → 259.3 (Fig. 2A–D).

2.4. Preparation of stock and working solutions

Stock solutions containing both FTY720 and FTY720-P were prepared in pure methanol to give a final concentration of 1.6 µg/mL (FTY720) and 1.50 µg/mL (FTY720-P) for the calibration standards (Cs) preparation; 1.28 µg/mL (FTY720) and 1.20 µg/mL (FTY720-P) for quality control samples (QCs) preparation. Individual working calibration standard (Cs) solutions with concentrations of 0.400, 0.8, 2.00, 4.00, 8.00 and 16.0 ng/mL (FTY720) and 0.500, 1.00, 2.50, 5.00, 10.0 and 20.0 ng/mL (FTY720-P) were prepared after serial dilutions of the stock solution with methanol. The working Quality
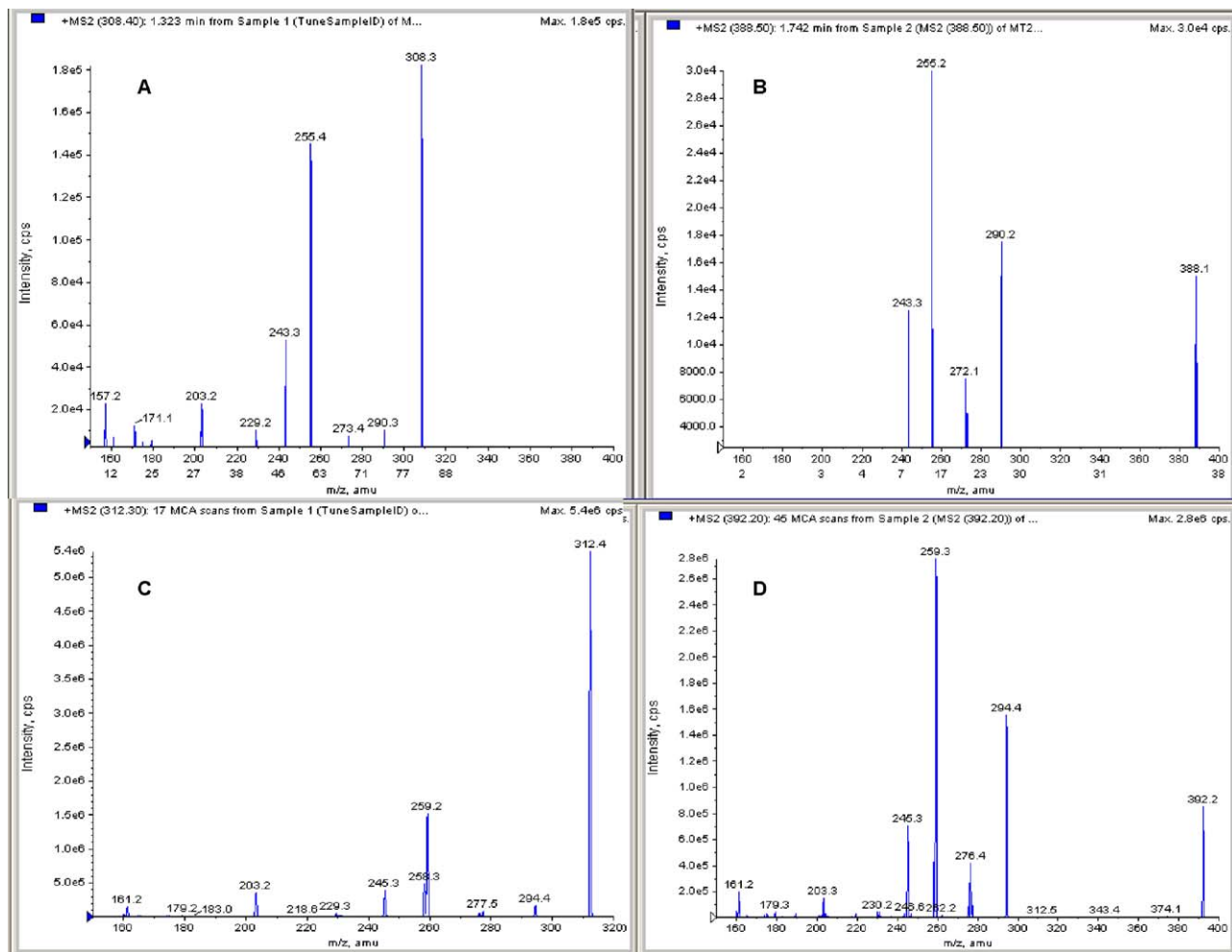
Fig. 2. The collision assisted dissociation mass spectra of: FTY720 (A), (B) FTY720-P (B), (C) [D$_4$]FTY720 and [D$_4$]FTY720-P (D).

Control sample (QCs) solutions with concentrations of 2.40, 12.0 and 1200 ng/mL (FTY720) and 3.00, 15.0, and 1500 ng/mL (FTY720-P) were prepared in the same manner.

2.5. Preparation of Cs and QCs

Two different batches of human blood were used for the preparation of Cs and QCs. The Cs samples were prepared by spiking each FTY720 and FTY720-P individual working Cs solution with blank human blood. This yielded Cs concentrations of 0.08 (LLOQ), 0.40, 0.80, 2.00, 4.00, 8.00 and 16.0 ng/mL (FTY720) and 0.100 (LLOQ), 0.500, 1.00, 2.50, 5.00, 10.0 and 20.0 ng/mL (FTY720-P). The QCs were prepared in the same manner to give final concentrations of 0.08, 0.240, 2.40 and 12.0 ng/mL (FTY720) and 0.1, 0.300, 3.00 and 15.0 ng/mL (FTY720-P).

2.6. Sample preparation

A volume of 100 μL of blood Cs, QCs or study samples was transferred into a 96-well, then 50 μL of the DMHA solution containing each internal standard and 20 μL of a 3% ortho-phosphoric acid solution were added. The samples were vortexed and 250 μL of pure methanol was added. The plate was shaken for 10 min and centrifuged (10 min, 5888 × g, 5 °C). After the centrifugation an aliquot

of the supernatant (150 μL) was directly injected onto the SPE-LC/MS/MS system.

2.7. SPE, LC, and MS conditions

The cartridges were conditioned with 2000 μL solution of acetonitrile/methanol/0.5% acetic acid/0.025% TFA (50/50/1/1, v/v/v/v) and subsequently with 1000 μL of DMHA solution (mobile phase A). Next, the cartridges were successively washed with 1500 μL acetonitrile/DMHA (50/50, v/v), 2600 μL tetrahydrofuran, 2600 μL isopropanol/ethanol (50/50, v/v) and 3000 μL acetonitrile/DMHA (50/50, v/v) solutions. Then 150 μL of diluted blood (calibration standards, QCs, and study samples) were loaded onto the cartridge using 2000 μL DMHA solution and the cartridge washed with 5000 μL of aqueous solution of phosphoric acid at 0.1% followed by 2000 μL methanol/water (50/50, v/v) and 2000 μL aqueous solution of phosphoric acid at 0.1%. After completion of the sample preparation cycle, the cartridge was switched in-line with the mobile phases to desorb the analytes and transfer them into the LC column (Scheme 1, elute position). After 60 s of elution, the cartridge was switched back off-line (Scheme 1, load position), replaced by a new one and the sample preparation cycle started again with the next sample. The total time of the SPE cycle was less than the chromatographic run-time. Thus, once synchronized, the time of sample cleanup is virtually nonexistent after processing the first cartridge.
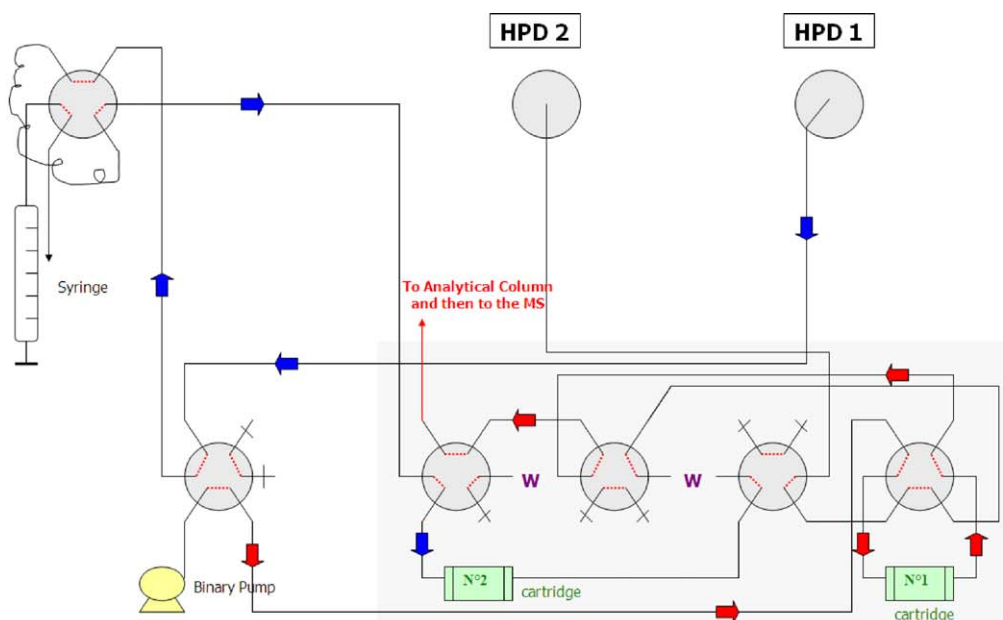
Action	Solvent and volume	Velocity	Position	Time
Place cartridge				
Activation	a) ACN/MeoH/TFA/Acetic acid (50/50/0.025/0.5 v/v/v/v) (2 mL)	5 mL/min	Load	0.4 min
	b) DMHA solution (1 mL)	5 mL/min	Load	0.2 min
Auto-sampler washing conditions	Port 1: Acetonitrile/DMHA (50/50, v/v)			
	Port 2: Tetrahydrofuran			
	Port 3: Isopropanol/ethanol (50/50, v/v)			
Sample loading	a) 150 µL diluted blood sample			
	b) DMHA solution (2 mL)	2 mL/min	Load	1 min
Washing solution for the SPE part	a) 0.1% aqueous solution of phosphoric acid (5 mL)	2.5 mL/min	Load	0.5 min
	b) Methanol/Water (50/50, v/v) (1 mL)	2.5 mL/min		0.4 min
	c) 0.1% aqueous solution of phosphoric acid (2 mL)	2.5 mL/min		0.8 min
Output signal				
Elute	Mobile phase	0.4 mL	Elute	
Wait			Load	
Start new cycle				

Scheme 1. On-line SPE-LC–MS/MS programming.

The mobile phases DMHA solution (A) and acetonitrile/isopropanol (80/20, v/v) (B) were delivered at either 400 µL/min or 800 µL/min as described in Table 2.

2.8. LC–MS/MS method for FTY720 quantitative analysis in blood samples

The method consists of a liquid–liquid extraction of blood samples using a 75/25 (v/v) mixture of tert-butyl methylether and dichloromethane as organic solvent. Briefly, 500 µL of blood sample were transferred to 10 mL extraction tubes. A volume of 50 µL of internal standard ([D$_4$]FTY720) at a concentration of 20 ng/mL in methanol and 500 µL of 100 mM aqueous solution of NaOH were added to the tubes before vortex-mixing. After 10 min centrifugation at 2000 × g at 15 °C, the aqueous phase was frozen on dry ice and the supernatant was transferred into a new tube. The organic

Table 2
Gradient program used for the LC-analysis of FTY720 and FTY720-P.

Time (min)	% of mobile phase B	Pump flow rate (µL/min)
0.01	30	400
1.00	30	400
2.50	100	400
3.50	100	400
3.58	100	800
4.00	100	800
4.08	30	400
5.50	30	400

Mobile phase A: DMHA solution.
Mobile phase B: Pure acetonitrile.
The time that separates two sample injections corresponds to 7.5 min.

solution was evaporated to dryness under a stream of nitrogen at approx. 37 °C. The dry residue was reconstituted in 150 μL of a 80/20 (v/v) mixture of methanol and 0.1% trifluoroacetic acid in water. The tubes were shaken for 3 s on a vortex mixer, ultrasonicated and centrifuged at $3220 \times g$ for 10 min at 15 °C. The solution was transferred into injection vial and 75 μL were injected onto the LC–MS/MS system. The samples were analyzed on a Eclipse XDB-C18 particle size 3.5 μm, 50 mm length 4.6 mm internal diameter (Agilent technologies, Wilmington, DE, USA) at 40 °C using a gradient with water acidified with 0.15 formic acid and methanol solution as eluents at a constant flow rate of 1.0 mL/min with at total run-time of 8 min. Mass spectrometer (API 4000 triple quadrupole) was operated in the positive mode ion mode (APCI+) with a source temperature set at 600 °C. According to the full scan precursors, the product ions and collision energies (CE) were as follows: m/z $308 \rightarrow 255$ for FTY720 (CE 21V) and m/z $312 \rightarrow 259$ for [D_4]FTY720 (CE 21V).

2.9. LC–MS/MS method for FTY720-P quantitative analysis in blood samples

FTY720-P was extracted from the blood samples by protein precipitation with methanol. Briefly, a volume of 100 μL of blood sample was transferred to a 5-mL polypropylene tube. After addition of 100 μL of internal standard ([D_4]FTY720-P at a concentration of 20 ng/mL in methanol) and 1 mL of methanol, the tubes were shaken for 2–3 min on a vortex mixer. After 10 min centrifugation at $2500 \times g$, the supernatant was transferred into a 5-mL polypropylene tube and the organic phase was evaporated to dryness under a nitrogen stream at approximately 37 °C. The dry residue was dissolved in 200 μL water–methanol solution (80:20, v/v). The tubes were shaken for 2–3 min on a vortex mixer and an aliquot was transferred into a vial containing a polypropylene insert. The capped vials were placed in the auto-sampler and 20 μL was injected onto the analytical column. The samples were analyzed on a C_{18} Gemini 5 μm (30 mm × 2.0 mm) column equipped with a guard Gemini C18 5 μm (4 mm × 2.0 mm) (Phenomenex, Torrance, CA, USA) at 25 °C using a gradient with dimethylhexylamine solution and acetonitrile as eluents at a constant flow rate of 0.4 mL/min with at total run-time of 7 min. Mass spectrometer (API 4000 triple quadrupole) was operated in the positive mode ion mode (ESI+) with an elctrospray voltage of 5000 V at 650 °C. According to the full scan precursors, to the product ions and collision energies (CE) were as follows: m/z $388 \rightarrow 255$ for FTY720-P (CE 21V) and m/z $392 \rightarrow 259$ for [D_4]FTY720-P (CE 21V).

3. Results and discussion

3.1. Method development and sample preparation

In the present study we have used stable isotope labeled compounds that contain deuterium atoms as IS (Fig. 1). The fact that all four deuterium atoms are located to the carbon atoms adjacent to the hydroxy groups (which are lost during the MS fragmentation of FTY720 and FTY720-P) may lead to the deuterium hydrogen exchange during the collision-induced dissociation (CID). To address this point, precursor ion product scans were performed for the two IS used. As shown in Fig. 3, there is no deuterium–hydrogen exchange during the CID as only parents compounds ([D_4]FTY720 (Fig. 3A) and [D_4]FTY720-P (Fig. 3B)) were found in the MS spectra. In addition, in the neutral loss mass scan of H_3PO_4 (MW = 98) spectra of [D_4]FTY720-P the only mass found corresponded to that of [D_4]FTY720-P (Fig. 3C). These data demonstrated that there is no deuterium–hydrogen exchange during the MS fragmentation of both IS used for this study.
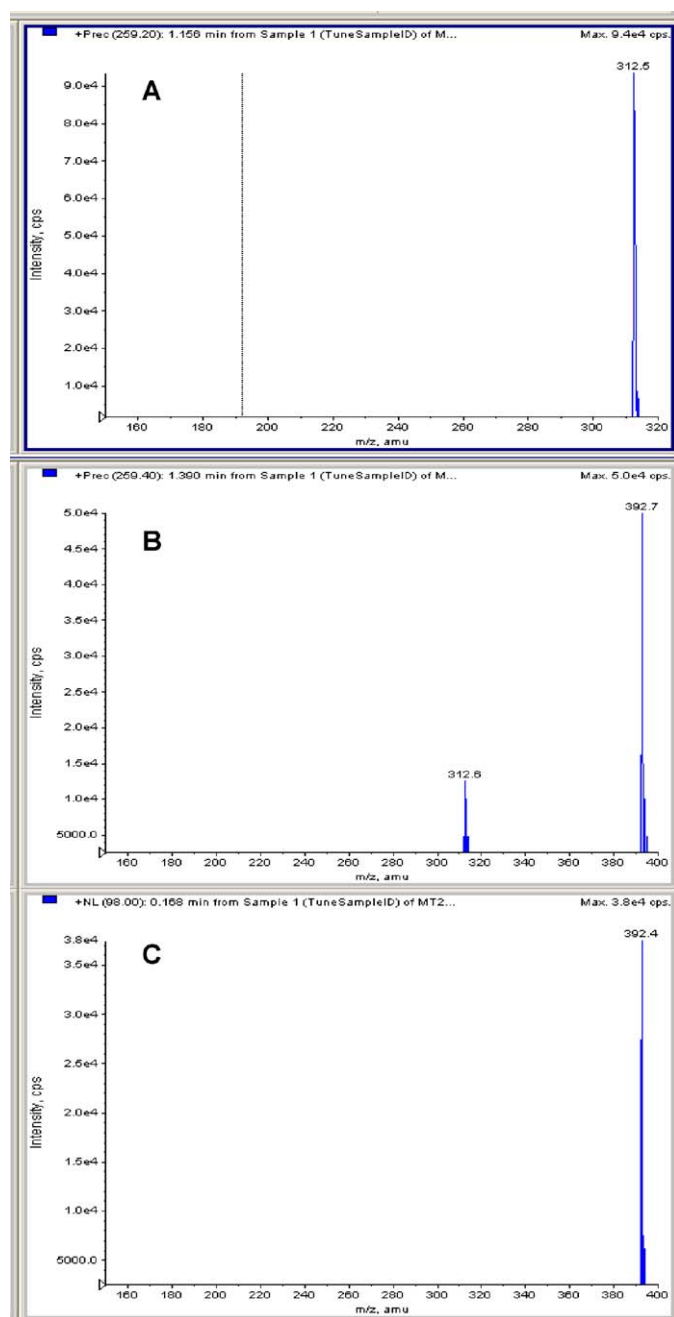

Fig. 3. Precursor ion scan for [D_4]FTY720 (A) and [D_4]FTY720-P (B) and (C) neutral loss scan (C) for [D_4]FTY720-P.

The major challenge in developing a simultaneous method for the quantitative analysis of FTY720 and FTY720-P is that one of the analytes is highly water-soluble (e.g. FTY720-P) whereas the other one is highly hydrophobic (FTY720). Thus, there is often a loss of one or the other analyte using the standard two-phase LLE methods and this could compromise the recovery and the method sensitivity for either FTY720 or FTY720-P. PPT has been used for the extraction of FTY720 related compounds prior the LC–MS/MS analysis [13] because of its simplicity. However during our method development, we found that, samples originating from blood PPT were not always compatible with LC–MS/MS analyses as we observed some sensitivity loss and MS clogging during the sample analysis (data not shown). Consequently, neither LLE nor PPT was selected as the sample preparation approach for the present work. SPE has been
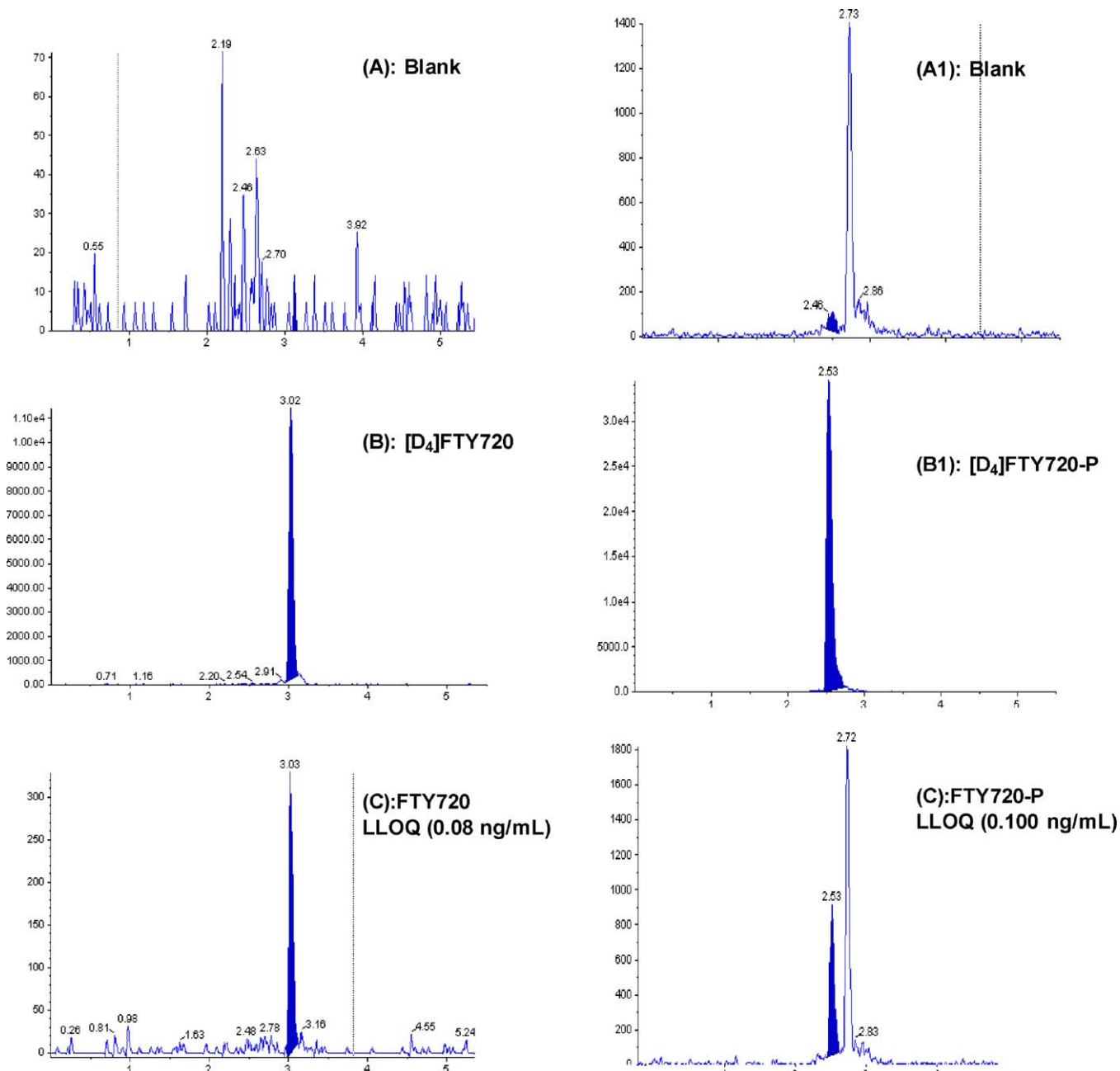
Fig. 4. Representative SRM chromatograms of extracted blank blood sample without (A) FTY720 (m/z 308.3 → 255.4); (A1) FTY720-P (m/z 388.1 → 255.2); or extracted blank blood sample spiked with the IS (zero control sample) of (B) [D_4]FTY720 (m/z 312.4 → 259.2) and (B1) [D_4]FTY720-P (m/z 392.2 → 259.3) and representative SRM chromatograms of extracted blood sample spiked at the low limit of quantification (LLOQ) of (C) FTY720 (m/z 308.3 → 255.4) and (C1) FTY720-P (m/z 388.1 → 255.2). FTY720 (retention time (Rt), 3.02 min); [D_4]FTY720 (Rt, 3.03 min); FTY720-P (Rt, 2.53 min); [D_4]FTY720-P (Rt: 2.53 min).

used for FTY720-P related compounds extraction from biological matrices. Due to the zwitterionic nature of FTY720-P, it was not possible to use a cationic or ionic sorbent for the sample extraction. In fact we have observed low recovery of FTY720-P when using mixed mode cation or anion exchange sorbent. Thus the C_{18} sorbents were used for the simultaneous on-line extraction of FTY720 and FTY720-P. The latter approach was used for the following reasons: (i) the direct injection of diluted blood sample (ii) SPE can be automated and operated on-line with LC–MS/MS detection and thus offering speed, high sensitivity by the sample pre-concentration and (iii) the large choice of C_{18} cartridges that can selectively retain both FTY720 and FTY720-P. In the present study we have developed an extraction procedure using on-line SPE to efficiently recover FTY720 and FTY720-P from diluted blood samples. During the method development, several loading solutions with various ratios of acetonitrile, methanol and water were tested but none of them gave a satisfactory retention of FTY720-P onto the SPE C_{18} HySphere cartridge. As a consequence, we failed to detect FTY720-P peak by LC–MS/MS under these conditions (data not shown). Ion-pairing salts with more volatility such as DMHA were successfully employed to retain polar compound on C_{18} column [14,15]. In the present work, a formate buffer containing DMHA (DMHA solution)

Table 3
Concentration of QCs results in human blood and accuracy and precision of the method in spiked human blood for FTY720.

Run date	FTY720 nominal concentration (ng/mL)							
	0.0800	%Bias	0.240	%Bias	2.40	%Bias	12.0	%Bias
	FTY720 measured concentration in (ng/mL)							
Day 1	0.0657	−17.9	0.246	2.5	2.48	3.3	12.2	1.7
	0.0768	−4.0	0.248	3.3	2.32	−3.3	11.8	−1.7
	0.0705	−11.9	0.243	1.3	2.40	0.0	11.2	−6.7
	0.0574	−28.3[a]	0.273	13.8	2.56	6.7	11.9	−0.8
	0.0693	−13.4	0.243	1.3	2.26	−5.8	11.5	−4.2
	0.0700	−12.5	0.238	−0.8	2.42	0.8	12.1	0.8
Intra-run mean (ng/mL)	0.0683		0.249		2.41		11.8	
Intra-run %CV	9.4		5.0		4.5		3.2	
Intra-run %Bias	−14.6		3.8		0.4		−1.7	
n	6		6		6		6	
Day 2	0.0891	11.4	0.240	0.0	2.36	−1.7	11.8	−1.7
	0.0870	8.8	0.227	−5.4	2.35	−2.1	11.6	−3.3
	0.0894	11.8	0.236	−1.7	2.35	−2.1	11.9	−0.8
	0.0841	5.1	0.248	3.3	2.36	−1.7	11.6	−3.3
	0.0862	7.8	0.265	10.4	2.30	−4.2	11.8	−1.7
	0.0927	15.9	0.263	9.6	2.31	−3.8	11.5	−4.2
Intra-run mean (ng/mL)	0.0881		0.247		2.34		11.7	
Intra-run %CV	3.4		6.2		1.1		1.3	
Intra-run %Bias	10.1		2.9		−2.5		−2.5	
n	6		6		6		6	
Day 3	0.0741	−7.4	0.245	2.1	2.30	−4.2	12.4	3.3
	0.0806	0.8	0.251	4.6	2.29	−4.6	11.9	−0.8
	0.0844	5.5	0.253	5.4	2.39	−0.4	11.9	−0.8
	0.0785	−1.9	0.254	5.8	2.35	−2.1	11.7	−2.5
	0.0794	−0.8	0.232	−3.3	2.34	−2.5	11.5	−4.2
	0.0797	−0.4	0.231	−3.8	2.44	1.7	12.4	3.3
Intra-run mean (ng/mL)	0.0795		0.244		2.35		12.0	
Intra-run %CV	4.2		4.3		2.4		3.1	
Intra-run %Bias	−0.6		1.7		−2.1		0.0	
n	6		6		6		6	
Mean (ng/mL)	0.0786		0.246		2.37		11.8	
Inter-run %CV	11.9		5.0		3.1		2.7	
Inter-run %Bias	−1.8		2.5		−1.3		−1.7	
n	18		18		18		18	

[a] >20%Bias.
Mean and S.D. expressed in ng/mL.

improved the retention of FTY720-P on SPE cartridge without compromising that of FTY720. As a consequence, this solution was used to dilute and load the blood samples onto the cartridge.

The mobile phase regulates chromatography behavior and appropriate ionization. To obtain the optimal mobile phase, various ratios of methanol, acetonitrile and water were tested. The acetonitrile could lower the running time of each sample within 2.0 min, but broaden peak was obtained for FTY720 and almost no retention for FTY720-P (data not shown). An increase in the methanol content improved the sensitivity and peak shape of FTY720, but the retention of FTY720-P was not enough. In addition, the acidic modifier, formic acid or acetic acid did not improve the sensitivity and the peak shapes. Finally, mobile phases consisting of DMHA solution (A) and acetonitrile/isopropanol (80/20, v/v) were optimal for the retention of FTY720-P and that of FTY720.

3.2. Selectivity

The selectivity was investigated by analyzing six individual blank extracted blood samples. There was no significant interference at the expected retention times of FTY720 (Fig. 4A) and FTY720-P (Fig. 4A1). Moreover, there were no interferences between FTY720 or FTY720-P peak and their respective IS. The Representative chromatograms of blank blood sample spiked with the IS (zero sample) at the concentrations used in this study for

[D$_4$]FTY720 and [D$_4$]FTY720-P are depicted in Fig. 4B and B1, respectively. This demonstrated that our LC–MS/MS assay is highly specific for the simultaneous determination of FTY720 and FTY720-P in human blood.

3.3. Sensitivity

The LLOQ was defined as the lowest concentration on the calibration curve of FTY720 and FTY720-P measured with acceptable precision and accuracy (i.e. coefficient of variation (CV) and relative error <20%) and with at least five times response compared to blank response. Shown in Fig. 4C and C1 are the representative chromatograms of FTY720 and that of FTY720-P at the respective LLOQ of 0.08 ng/mL and 0.1 ng/mL. As can be noticed, with 150 µL injection, FTY720 and FTY720-P peaks at the LLOQ were above the requirement for a reliable quantification.

3.4. Calibration

Blood calibration curves for FTY720 and FTY720-P were constructed using peak area ratios of each analyte to that of its IS and applying a weighted ($1/x^2$) least-squares linear regression analysis. Daily variations of calibration regression coefficient (R^2) and the linear regression fit equations were as follows: 0.9947 and $y = 00.3751x + 0.02769$ for FTY720 and 0.9977 and

Table 4
Concentration of QCs results in human blood and accuracy and precision of the method in spiked human blood for FTY720-P.

Run date	FTY720P nominal concentration (ng/mL)							
	0.100	%Bias	0.300	%Bias	3.00	%Bias	15.0	%Bias
	FTY720P measured concentration (ng/mL)							
Day 1	0.116	16.0	0.256	−14.7	3.17	5.7	15.8	5.3
	0.107	7.0	0.291	−3.0	3.43	14.3	15.8	5.3
	0.121	21.0[a]	0.291	−3.0	2.89	−3.7	14.8	−1.3
	0.138	38.0[a]	0.327	9.0	2.74	−8.7	15.3	2.0
	0.104	4.0	0.274	−8.7	2.84	−5.3	12.9	−14.0
	0.0909	−9.1	0.363	21.0[b]	2.73	−9.0	16.8	12.0
Intra-run mean	0.113		0.300		2.97		15.2	
Intra-run %CV	14.2		12.9		9.4		8.7	
Intra-run %Bias	13.0		0.0		−1.0		1.3	
n	6		6		6		6	
Day 2	0.118	18.0	0.285	−5.0	3.00	0.0	14.0	−6.7
	0.0934	−6.6	0.278	−7.3	2.82	−6.0	14.5	−3.3
	0.104	4.0	0.333	11.0	2.95	−1.7	14.9	−0.7
	0.106	6.0	0.290	−3.3	3.12	4.0	15.5	3.3
	0.0997	−0.3	0.330	10.0	2.84	−5.3	14.8	−1.3
	0.122	22.0[a]	0.285	−5.0	2.79	−7.0	13.9	−7.3
Intra-run mean	0.107		0.300		2.92		14.6	
Intra-run %CV	10.2		8.2		4.3		4.1	
Intra-run %Bias	7.0		0.0		−2.7		−2.7	
n	6		6		6		6	
Day 3	0.125	25.0[a]	0.286	−4.7	3.12	4.0	15.5	3.3
	0.0879	−12.1	0.321	7.0	2.91	−3.0	15.0	0.0
	0.0971	−2.9	0.329	9.7	2.89	−3.7	15.9	6.0
	0.0990	−1.0	0.287	−4.3	3.15	5.0	15.8	5.3
	0.0760	−24.0[a]	0.270	−10.0	2.89	−3.7	14.7	−2.0
	0.0833	−16.7	0.315	5.0	3.16	5.3	16.9	12.7
Intra-run mean	0.0947		0.301		3.02		15.6	
Intra-run %CV	18.1		7.8		4.5		5.0	
Intra-run %Bias	−5.3		0.3		0.7		4.0	
n	6		6		6		6	
Mean conc. (ng/mL)	0.105		0.301		2.97		15.2	
Inter-run %CV	15.3		9.3		6.3		6.5	
Inter-run %Bias	5.0		0.3		−1.0		1.3	
n	18		18		18		18	

Mean and S.D. expressed in ng/mL.

[a] >20%Bias.

[b] >15%Bias.

$y = 0.2214x + 0.01029$ for FTY720-P. The calibration curve parameters obtained on each of the three days were suitable for the quantification of FTY720 and FTY720-P in the samples during the intra- and inter-day validations, dilution and stability tests.

3.5. Precision and accuracy

For FTY720 and FTY720-P, precision (expressed as percent relative standard deviation, %CV) and accuracy (expressed as percent error, %bias) were calculated for the four QCs concentrations. At least five replicates of each QC point were analyzed every day to determine the intra-day accuracy and precision. This process was repeated over 3 days in order to determine the inter-day accuracy and precision. The intra-run QCs accuracies were within the range ±20% at the LOQ and ±15% at the other concentration levels with at least 3/4 of the individual back-calculated values fulfilling these acceptance criteria (Tables 3 and 4). The inter-run precision and accuracy values for FTY720 ranged from 2.7 to 11.9% (n = 18) and between −1.8 to 2.5% (n = 18), respectively (Table 4). The inter-run precision and accuracy values for FTY720-P ranged from 6.3 to 15.3% (n = 18) and between −1.0 to 5.0% (n = 18), respectively (Table 5). These results clearly demonstrated that our on-line

SPE-LC–MS/MS analytical method is reliable for the quantitative analysis of FTY720 and FTY720-P in human blood samples.

3.6. Stability of blood sample during storage

The assessment of FTY720 stabilities were performed on spiked QCs at 0.240 and 12.0 ng/mL whereas spiked QCs at concentration of 0.300 and 15.0 ng/mL were used to study those of FTY720-P one. The bench-top stability over 6 h, the three freeze–thaw cycles and the auto-sampler stability evaluated at 5 °C over 90 h were successfully validated for FTY720 and FTY720-P with good accuracy and precision data (Table 5).

3.7. Dilution effect

The dilution test was determined using a 1000-fold QCs dilution with blank blood for FTY720 and FTY720-P prior their extraction and assayed in 5 replicates along with Cs and QCs in a validation run. As can be seen in Table 6, the measured concentrations of FTY720 and FTY720-P in these QCs were comparable to the nominal values, with accuracy of 10.8% (FTY720) and 11.6% (FTY720-P), demonstrating that samples with higher concentration can be diluted with blank blood to obtain acceptable data.

Table 5
Room temperature, freeze–thaw and auto-sampler stability of FTY720 and FTY720-P ($n = 3$).

	Room temperature[a]	Freeze–thaw cycles[b]	Auto-sampler[c]
FTY720			
Nominal concentration (ng/mL)	0.240	0.240	0.240
Measured concentration (ng/mL)			
Sample 1	0.242	0.247	0.278
Sample 2	0.236	0.230	0.226
Sample 3	0.245	0.251	0.267
Mean (ng/mL)	0.241	0.243	0.257
%CV	1.9	4.6	10.7
%Bias	0.4	1.1	7.1
Nominal concentration (ng/mL)	12.0	12.0	12.0
Measured concentration (ng/mL)			
Sample 1	12.7	11.9	12.1
Sample 2	13.5	12.3	12.9
Sample 3	12.5	12.9	12.3
Mean (ng/mL)	12.9	12.4	12.4
%CV	4.10	4.07	3.35
%Bias	7.5	3.1	3.6
FTY720-P			
Nominal concentration (ng/mL)	0.300	0.300	0.300
Measured concentration (ng/mL)			
Sample 1	0.256	0.255	0.373
Sample 2	0.327	0.238	0.32
Sample 3	0.315	0.289	0.305
Mean (ng/mL)	0.299	0.261	0.333
%CV	12.7	10.0	10.7
%Bias	−0.2	−13.1	10.9
Nominal concentration (ng/mL)	15.0	15.0	15.0
Measured concentration (ng/mL)			
Sample 1	15.1	15.8	15.6
Sample 2	17.2	15.6	15.3
Sample 3	15.8	15.9	14.7
Mean (ng/mL)	16.0	15.8	15.2
%CV	6.67	0.97	3.01
%Bias	6.9	5.1	1.3

[a] The room temperature stability was determined after 6 h period of storage.
[b] Stability after 3 freeze–thaw cycles at or below −70 °C.
[c] Auto-sampler stability at 5 °C for 90 h.

Table 6
Precision and accuracy of dilution QC samples ($n = 5$) for FTY720 and FTY720-P.

Initial Concentration (ng/mL)	10,000	
Dilution factor	1000	
	Measured concentration (ng/mL)	Final measured concentration (ng/mL)
FTY720		
Sample 1	11.0	11,000
Sample 2	10.6	10,600
Sample 3	10.6	10,600
Sample 4	12.2	12,200
Sample 5	11.0	11,000
Mean (ng/mL)		11,080
%CV		5.93
%Bias		10.8
FTY720-P		
Sample 1	10.8	10,800
Sample 2	10.8	10,800
Sample 3	11.0	11,000
Sample 4	11.2	11,200
Sample 5	12.0	12,000
Mean (ng/mL)		11,160
%CV		4.46
%Bias		11.6

Table 7
Carryover in extracted blood blank samples following injection of the ULOQ for FTY720, FYP720-P, [D_4] FTY720, and [D_4] FTY720-P.

	Blank 1	Blank 2	Blank 3	Blank 4
FTY720				
Measured peak area	671	400	0	0
Peak area at the LLOQ in QCs ($n = 3$)	2940			
Carryover (%)	22.8	13.6	0	0
[D_4] FTY720				
Measured peak area	26.1	12.3	20.4	30.3
Peak area of ISTD in QCs ($n = 3$)	40,833			
Carryover (%)	0	0	0	0
FTY720-P				
Measured peak area	0	0	0	0
Peak area at the LLOQ in QCs ($n = 3$)	311			
Carryover (%)	0	0	0	0
[D_4] FTY720-P				
Measured peak area	213	457	358	153
Peak area of ISTD in QCs ($n = 3$)	10,097			
Carryover (%)	2.1	4.5	3.5	1.5

3.8. Carryover

In the current assay, the combination of the different solvents (see the Scheme 1) used to wash the syringe and the injection port multiple times before and after each injection was proven to be satisfactory to reduce the carry-over of FTY720. As can be seen in Table 7, the level of FTY720 in a second blank extracted sample injected right after the ULOQ was below 15% of the LLOQ signal. With further injections of extracted blank samples, the amount of FTY720 found was zero. The carry-over issue has been encountered during previous analysis of FTY720-P related compound and this has been attributed to their zwitterionic nature [16]. In the current assay, we were able to efficiently reduce the carry over of FTY720-P when using a solution of acetonitrile/DMHA solution to wash the injection port. As can be seen in Table 7, FTY720-P was not detected in a first blank extracted sample injected right after the ULOQ. We believe that DMHA modifies the zwitterionic nature FTY720-P, which eliminates the carry-over.

3.9. Incurred samples reproducibility (ISR)

Matrix effects due to metabolites present in study samples from dosed subjects can be difficult to predict and compensate for in advance. A reproducibility test of incurred samples gives valuable information on the robustness of the method and should be performed as early as possible. During the method validation blood samples from human receiving different doses of FTY720 were also considered for analysis. The blood sample volume, approximately 1 mL was collected on tubes coated with sodium citrate as anti-coagulant. A total of 30 samples were re-analyzed for both FTY720 and FTY720-P within an interval of time less than 1 month. The %bias between the re-analyzed concentrations and the original concentrations were all below 20% (Table 8) and this met the acceptance criteria set for incurred sample re-analysis [17]. In addition, ISR was successfully performed for each analysed clinical study (data not shown).

3.10. Methods comparison

Two separate LC–MS/MS bioanalytical methods were originally developed for the analysis of FTY720 and FTY720-P in human blood sample. The FTY720 method was validated within the curve range of 0.08–80.0 ng/mL using 0.50 mL blood sample with a run time of 6.5 min. The method consists in (i) a liquid–liquid extraction of blood samples using a 75/25 (v/v) mixture of tert-butyl methyl-ether and dichloromethane as organic solvent (ii) evaporation to dryness and reconstitution in the mobile phase and (iii)

Table 8
Incurred samples reanalysis data for FTY720 and FTY720-P.

Patient nr.	FTY720 concentration (ng/mL)			FTY720-P concentration (ng/mL)		
	First determination	Second determination	Bias (%)	First determination	Second determination	Bias (%)
0001_05105	1.92	1.88	−2.0	1.09	1.01	−7.1
0001_05105	1.05	0.950	−9.9	0.561	0.508	−9.4
0001_05106	2.36	2.31	−1.9	1.36	1.30	−4.5
0001_05106	1.20	1.08	−10.2	0.706	0.624	−11.5
0001_05107	2.27	1.87	−17.7	1.19	1.07	−9.6
0001_05107	1.09	1.02	−6.6	0.563	0.517	−8.2
0001_05108	3.03	2.64	−12.8	1.52	1.37	−9.6
0001_05108	1.36	1.20	−11.5	0.760	0.686	−9.7
0001_05109	2.11	1.72	−18.3	1.03	0.905	−12.1
0001_05110	2.47	2.15	−12.8	1.06	1.03	−2.8
0001_05104	2.38	2.18	−8.7	1.55	1.38	−10.6
0001_05104	2.23	2.26	1.4	1.48	1.38	−6.9
0001_05104	2.76	2.48	−10.2	1.64	1.58	−3.6
0001_05104	2.88	2.59	−10.3	1.80	1.77	−1.4
0001_05104	3.13	2.84	−9.2	2.06	1.93	−5.9
0001_05104	2.84	2.72	−4.4	1.93	1.89	−2.5
0001_05104	2.79	2.57	−7.9	1.57	1.45	−8.0
0001_05104	2.27	2.32	2.2	1.42	1.49	5.0
0001_05105	2.94	2.63	−10.5	1.87	1.54	−17.8
0001_05105	2.60	2.32	−10.8	1.29	1.22	−5.5
0001_05106	3.59	3.38	−5.7	2.10	1.99	−4.9
0001_05106	2.98	2.74	−7.8	1.48	1.47	−0.6
0001_05107	3.14	2.92	−6.9	1.74	1.67	−4.3
0001_05107	2.56	2.42	−5.7	1.20	1.13	−6.1
0001_05108	4.12	3.61	−12.3	2.23	2.02	−9.2
0001_05108	3.61	3.54	−1.9	1.96	1.89	−3.7
0001_05109	3.12	2.86	−8.3	1.57	1.45	−7.5
0001_05109	2.46	2.23	−9.6	1.17	1.09	−6.5
0001_05110	3.74	3.49	−6.9	1.51	1.41	−6.7
0001_05110	3.56	3.39	−4.8	1.35	1.31	−3.3
Total number of samples:					31	
Number of samples meeting the acceptance criteria:					31	
Number of results meeting the acceptance criteria (%):					100	

LC–MS/MS of FTY720 in positive mode using APCI as the ionization technique. The FTY720-P method was validated within the curve range 1.5–500 ng/mL using 0.1 mL blood sample with a run time of 9.5 min. The method consists on (i) blood protein precipitation with a methanol solution containing the internal standard (ii) evaporation to the dryness and reconstitution in the mobile phase and (iii) LC–MS/MS analysis of samples in positive mode using ESI as the ionization technique.

These two methods were used separately to analyze 62 human clinical samples (31 for each compound) and the results found were compared with those obtained with our current method. Shown in Fig. 5 are the comparative concentration data for FTY720 and FTY720-P between the two single methods and our simultaneous quantitative method. It can be noticed that excellent correlation between the results obtained with the single and the combo LC–MS/MS methods as indicated by a coefficient of correlation higher than 0.98. Moreover, with a slope value of 1.14, it confirms that comparable data were obtained between our method and the two single methods for both FTY720 and FTY720-P on incurred samples.

4. Conclusions

We have developed and validated a sensitive, rapid and reliable method for the simultaneous determination of FTY720 and FTY720-P in human blood sample. The method has been successfully applied to the analysis of human clinical samples. In addition, the robustness has was demonstrated by the reanalysis of human incurred samples. The data of our new bioanalytical LC–MS/MS method were comparable to those obtained with the single methods. Thus having a single method will obviously (i) reduce the amount of blood volume taken from patients, which is highly desirable to support clinical studies with FTY720; (ii) increase the sample throughout analysis with less consumption of solvent.

$$y = 1.1434x - 0.0247$$
$$R^2 = 0.9867$$
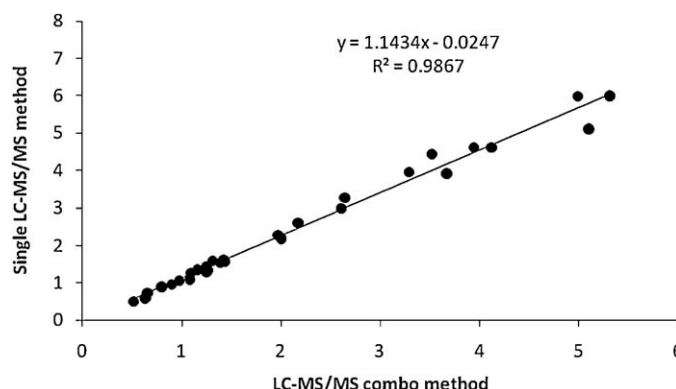
Fig. 5. Comparison of FTY720 and FTY720-P concentration (ng/mL) by the respective single and the simultaneous bioanalytical (combo) methods.

References

[1] V. Brinkmann, M.D. Davis, C.E. Heise, R. Albert, S. Cottens, R. Hof, C. Bruns, E. Prieschl, T. Baumruker, P. Hiestand, C.A. Foster, M. Zollinger, K.R. Lynch, The immune modulator FTY720 targets sphingosine 1-phosphate receptors, J. Biol. Chem. 277 (2002) 21453–21457.
[2] S. Mandala, R. Hajdu, J. Bergstrom, E. Quackenbush, J. Xie, J. Milligan, R. Thornton, G.J. Shei, D. Card, C. Keohane, M. Rosenbach, J. Hale, C.L. Lynch, K. Rupprecht, W. Parsons, H. Rosen, Alteration of lymphocyte trafficking by sphingosine-1-phosphate receptor agonists, Science 296 (2002) 346–349.

[3] H. Rosen, G. Sanna, C. Alfonso, Egress: a receptor-regulated step in lymphocyte trafficking, Immunol. Rev. 195 (2003) 160–177.
[4] M.G. Sanna, S.K. Wang, P.J. Gonzalez-Cabrera, A. Don, D. Marsolais, M.P. Matheu, S.H. Wei, I. Parker, E. Jo, W.C. Cheng, M.D. Cahalan, C.H. Wong, H. Rosen, Enhancement of capillary leakage and restoration of lymphocyte egress by a chiral S1P1 antagonist in vivo, Nat. Chem. Biol. 2 (2006) 434–441.
[5] T. Hla, Sphingosine 1-phosphate receptors, Prostaglandins 64 (2001) 135–142.
[6] V. Brinkmann, A. Billich, T. Baumruker, P. Heining, R. Schmouder, G. Francis, S. Aradhye, P. Burtin, Fingolimod (FTY720): discovery and development of an oral drug to treat multiple sclerosis, Nat. Rev. Drug Discov. 9 (2010) 883–897.
[7] H. Potteck, B. Nieuwenhuis, A. Luth, M. van der Giet, B. Kleuser, Phosphorylation of the immunomodulator FTY720 inhibits programmed cell death of fibroblasts via the S1P3 receptor subtype and Bcl-2 activation, Cell Physiol. Biochem. 26 (2010) 67–78.
[8] A. Kihara, M. Ikeda, Y. Kariya, E.Y. Lee, Y.M. Lee, Y. Igarashi, Sphingosine-1-phosphate lyase is involved in the differentiation of F9 embryonal carcinoma cells to primitive endoderm, J. Biol. Chem. 278 (2003) 14578–14585.
[9] Y.M. Lee, K. Venkataraman, S.I. Hwang, D.K. Han, T. Hla, A novel method to quantify sphingosine 1-phosphate by immobilized metal affinity chromatography (IMAC), Prostaglandins Other Lipid. Mediat. 84 (2007) 154–162.
[10] J.K. Min, H.S. Yoo, E.Y. Lee, W.J. Lee, Y.M. Lee, Simultaneous quantitative analysis of sphingoid base 1-phosphates in biological samples by o-phthalaldehyde precolumn derivatization after dephosphorylation with alkaline phosphatase, Anal. Biochem. 303 (2002) 167–175.
[11] E.V. Berdyshev, I. Gorshkova, A. Skobeleva, R. Bittman, X. Lu, S.M. Dudek, T. Mirzapoiazova, J.G. Garcia, V. Natarajan, FTY720 inhibits ceramide synthases and up-regulates dihydrosphingosine 1-phosphate formation in human lung endothelial cells, J. Biol. Chem. 284 (2009) 5467–5477.
[12] P. Salm, C.R. Warnholtz, S.V. Lynch, P.J. Taylor, Measurement and stability of FTY720 in human whole blood by high-performance liquid chromatography-atmospheric pressure chemical ionization-tandem mass spectrometry, J. Chromatogr. B: Anal. Technol. Biomed. Life Sci. 843 (2006) 157–163.
[13] T. Lan, H. Bi, W. Liu, X. Xie, S. Xu, H. Huang, Simultaneous determination of sphingosine and sphingosine 1-phosphate in biological samples by liquid chromatography–tandem mass spectrometry, J. Chromatogr. B 879 (2011) 520–526.
[14] E.N. Fung, Z. Cai, T.C. Burnette, A.K. Sinhababu, Simultaneous determination of Ziagen and its phosphorylated metabolites by ion-pairing high-performance liquid chromatography–tandem mass spectrometry, J. Chromatogr. B: Biomed. Sci. Appl. 754 (2001) 285–295.
[15] R. Tuytten, F. Lemiere, W.V. Dongen, E.L. Esmans, H. Slegers, Short capillary ion-pair high-performance liquid chromatography coupled to electrospray (tandem) mass spectrometry for the simultaneous analysis of nucleoside mono-, di- and triphosphates, Rapid Commun. Mass Spectrom. 16 (2002) 1205–1215.
[16] E.V. Berdyshev, I.A. Gorshkova, J.G. Garcia, V. Natarajan, W.C. Hubbard, Quantitative analysis of sphingoid base-1-phosphates as bisacetylated derivatives by liquid chromatography–tandem mass spectrometry, Anal. Biochem. 339 (2005) 129–136.
[17] D.M. Fast, M. Kelley, C.T. Viswanathan, J. O'Shaughnessy, S.P. King, A. Chaudhary, R. Weiner, A.J. DeStefano, D. Tang, Workshop report and follow-up – AAPS Workshop on current topics in GLP bioanalysis: assay reproducibility for incurred samples – implications of Crystal City recommendations, AAPS J. 11 (2009) 238–241.

Metabolomic study of insomnia and intervention effects of Suanzaoren decoction using ultra-performance liquid-chromatography/electrospray-ionization synapt high-definition mass spectrometry

Bo Yang[a], Aihua Zhang[a], Hui Sun[b], Wei Dong[a], Guangli Yan[a], Tingli Li[c], Xijun Wang[a,*]

[a] National TCM Key Lab of Serum Pharmacochemistry, Heilongjiang University of Chinese Medicine, and Key Laboratory of Chinese Materia Medica, Ministry of Education, Heping Road 24, Harbin 150040, China
[b] Department of Pharmaceutical Analysis, Heilongjiang University of Chinese Medicine, Heping Road 24, Harbin 150040, China
[c] Department of TCM Pharmacology, Heilongjiang University of Chinese Medicine, Heping Road 24, Harbin 150040, China

A B S T R A C T

Metabolomics is the comprehensive assessment of endogenous metabolites of a biological system in a holistic context, and its property consists with the global view of traditional Chinese medicine (TCM). *Suanzaoren* decoction (SZRD), an ancient TCM formulae, has been used for treating insomnia for centuries, and its mechanism remains unclear completely. This paper was designed to explore globally metabolomic characters of the insomnia and the therapeutic effects of SZRD. Ultra-performance liquid-chromatography/electrospray-ionization synapt high-definition mass spectrometry (UPLC/ESI-SYNAPT-HDMS) combined with pattern recognition approaches including principal component analysis (PCA), partial least squares-discriminant analysis (PLS-DA) and orthogonal projection to latent structures discriminate analysis (OPLS-DA) were integrated to approximate the comprehensive metabolic signature and discover differentiating metabolites. The changes in metabolic profiling were restored to their baseline values after SZRD treatment according to the PCA score plots. Altogether, the current metabonomic approach based on UPLC/ESI-SYNAPT-HDMS indicate 20 ions (9 in the negative mode, 11 in the positive mode) as "differentiating metabolites". The alterations in these metabolites were associated with perturbations in amino acid and fatty acid metabolism, in response to insomnia through immune and nervous system. Of note, we found that SZRD increases sleep activity and exhibits binding affinity for serotonin receptors. These results implicate the therapeutic effects of SZRD may mediate through serotonergic activation. Our findings also show the robust UPLC/ESI-SYNAPT-HDMS techniques is promising for metabolites profiling analysis of TCM and open new perspectives to using metabolomics platform to resolve special TCM issues.

© 2011 Elsevier B.V. All rights reserved.

1. Introduction

Metabolomics was originally proposed as a method of functional genomics, an emerging subject of the post-genome era, which, together with genomics, transcriptomics and proteomics, jointly constitutes the 'Systems Biology' [1,2]. It has recently demonstrated significant potential in many fields such as responses to environmental stress, toxicology, nutrition, studying global effects of genetic manipulation, cancer, comparing different growth stages, diabetes, disease diagnosis and natural product discovery [3]. Depending on a series analysis of different sample spectra and combination with chemical pattern recognition methods, metabolomics can be used to identify organisms in pathophysiological state, drug toxicity and efficacy [4]. Metabolomics holds the promise of a comprehensive, non-invasive analysis of metabolic biomarkers that could detect early-stage disease, identify disease post-surgery, and help to monitor treatment response. Surprisingly, the global metabolite profile involves measuring low molecular-weight metabolites (<1 kDa) in complex biofluids/tissues to study perturbations in response to physiological challenges, toxic insults or disease processes [5]. As the newest of the "omics" sciences, metabolomics has brought much excitement to the field of life sciences as a potential translational tool, especially its method and design resemble those of traditional Chinese medicine (TCM). Increasing evidence demonstrates that TCM is playing an important role in the treatment of many complex diseases and are being accepted by more and more people [6,7]. As a systemic approach, metabonomics adopts a 'top-down' strategy to reflect the terminal symptoms of metabolic

* Corresponding author. Tel.: +86 451 82110818; fax: +86 451 82110818.
 E-mail addresses: phar_research@hotmail.com, xijunwangls@126.com
(X. Wang).

network of biological systems in holistic context [8,9]. This trait is in concert with the holistic efficacy of TCM, indicating that metabolomics has the potential to impact our understanding of the TCM theory [3]. Marker metabolites can be therapeutic targets as well [10]. The systemic thinking and strategy of the metabolomics and its aim at grasping integral function have provided unprecedented enlightenment for the modem TCM research.

The sedative–hypnotic medications, including benzodiazepines and non-benzodiazepines, are the most common treatments for insomnia. However, concerns regarding patterns of inappropriate use, dependence and adverse effects have led to caution in prescribing those sedative–hypnotic medications. TCM has been commonly used for treating insomnia in Asian countries for centuries. A traditional Chinese herb remedy, SZRD, has been efficiently and widely used as a tranquilizing agent to treat insomnia for thousands of years in Asia [11]. SZRD which was reported originally in 'Synopsis of the golden chamber' written by Zhang Zhongjing (Han Dynasty) [12], is the most commonly prescribed Chinese herbal formulae with the effects of hypnosis, sedation and anti-convulsion and has been used to treat insomnia and anxiety in the clinical practice [13,14]. It consists of five herbal medicines: *Semen Ziziphi Spinosae* (18 g), *Poria* (10 g), *Rhizoma Chuanxiong* (5 g), *Rhizoma Anemarrhenae* (10 g) and *Radix Glycyrrhizae* (3 g) [15]. Although SZRD has been used to improve sleep disruption in insomniac patients, its mechanism is still unclear.

Sleep is essential for basic survival, and insufficient sleep leads to a variety of dysfunctions. Problems with sleep are one of the commonest reasons for seeking medical attention. Knowledge gained from basic research into sleep in animals has led to marked advances in the understanding of human sleep, with important diagnostic and therapeutic implications. Insomnia is an extremely common symptom in the context of psychiatric disorders. It is estimated that more than 27% people in the world suffer from insomnia and this figure is expected to grow by the middle of the 21st century [16]. Sleep disturbance is a common health problem among adults, and enhancing sleep quality is an issue of significant importance to healthcare providers [17,18]. Insomnia can also impair attention and memory, and its growing prevalence, especially among "knowledge workers", motivates a detailed exploration of its impact on human behavior. Several behavioral and imaging studies have examined the effects of sleep deprivation on attention, memory, and emotion processing. As sleep quality worsens into insomnia, individuals may seek assistance from medication. However, sedative and hypnotic drugs possess seriously adverse effects. Many Chinese medicinal products have been traditionally used for the treatment of insomnia, however, few literatures reported about the detailed therapeutic mechanisms how these Chinese medicines trigger the promotion of sleep. In trying to approach the rationale of formula design in TCM, here we use the treatment of insomnia with SZRD as a working model.

Recent advances of instrumentation and computation has enabled the simultaneous analysis of a large number of metabolites. UPLC coupled with MS has proven to be an effective combination for metabolites identifications and quantifications due to its excellent resolution and sensitivity. The aim of the current study was to obtain a systematic view of dissection of mechanisms of SZRD as an effective treatment for sleeping disorder. We wished to identify multiple metabolites that could facilitate the understanding of the actions of SZRD and aid their incorporation into future improvement of TCM therapy. Thus, a robust Waters UPLC/ESI-SYNAPT-HDMS system and Waters UPLC BEH C_{18} column with a 1.7 μm particle size was utilized and designed to elucidate the treatment for sleeping disorder of SZRD on *Drosophila* with sleep deprivation by light stimulus.

2. Materials and methods

2.1. Ethics statement

All studies were performed in accordance with the recommendations of the Guide for the Care and Use of Laboratory Animals of Heilongjiang University of Chinese Medicine. The protocol was approved by the Animal Experimental Ethical Committee of Heilongjiang University of Chinese Medicine. All efforts were made to ameliorate suffering of animals.

2.2. Animals

The wild-type *Drosophila melanogaster* (Canton S) was provided by Beijing University. *D. melanogaster* adult of the wild-type strain Canton-S were collected within 24 h after eclosion and kept at 25 °C, humidity ($55 \pm 5\%$), under 12:12-h light–dark cycle conditions either in population vials that housed 50 flies and contained 5 ml of 5% sucrose 1% agar or in individual monitor tubes that housed a single fly and contained 150 μl of 5% sucrose 1% agar for the duration of the experiment. Individual flies were acclimated for 5 days. The locomotor activity was measured using the Drosophila Activity Monitoring System (DAMS, Trikinetics Inc., USA).

2.3. Animals sampling and handling

Seven-day drosophila were randomly divided into 3 groups with 10 drosophila in each (male, 5; female, 5): the Control; Model and SZRD groups. The drosophila in the model and SZRD groups were performed by light sleep deprivation method. In the experiments with sleep deprivation, at the seventh night, the drosophila were sleep deprived by handling starting at 19:00 light onset, restored the 10 min light period for each whole time point from 20:00 to 7:00 am day 8. The whole procedure of light sleep deprivation was holding for 3 consecutive days. The drosophila in the control and model groups were administrated with normal nutrient medium in the whole procedure for 10 consecutive days and anaesthetized by CO_2 on day 10. Flies were anaesthetized by CO_2 and killed on day 8 (8:00 a.m.). Drosophila was shattered and extracted from methanol and by centrifugation at 3000 rpm for 10 min at 4 °C and stored at −20 °C for metabolomic analysis.

2.4. Chemicals and reagents

Acetonitrile (HPLC grade) was purchased from Merck (Darmstadt, Germany); methanol (HPLC grade) was purchased from Fisher Corporation (Michigan, USA); distilled water was purchased from Watson's Food & Beverage Co., Ltd. (Guangzhou, China); formic acid was of HPLC grade, and was produced from Honeywell Company (Morristown, NJ, USA); leucine enkephalin was purchased from Sigma–Aldrich (MO, USA). All other reagents were of analytical grade. *Semen Ziziphi Spinosae*, *Poria*, *Rhizoma Chuanxiong*, *Rhizoma Anemarrhenae* and *Radix Glycytthizae* were purchased from Harbin Tongrentang Drug Store (Harbin, China). All crude drugs were authenticated by Prof. Xijun Wang, Department of Pharmacognosy of Heilongjiang University of Chinese Medicine. SZRD was prepared in our laboratory according to the method recorded in "Synopsis of the golden chamber", and the decoction was transformed into the freeze-dried powder. Nutrient medium preparation: Maizena (14 g), saccharobiose (10 g), agar (1 g) and distilled water (153 ml) are stirred and boiled for 2–3 min, then add in yeast powder (1 g) and propionic acid (0.8 ml) miscing. SZRD was added in nutrient medium.

According to the original composition and preparation method of SZRD recorded in 'Synopsis of the golden chamber written', SZRD was prepared in the following procedure. *Semen Ziziphi Spinosae*

(18 g) was crushed to power (40 mesh size) and immersed in 1000 ml deionized water for 1 h and then decocted to boil keeping for 30 min until the volume of water reduced to about 400 ml, then 6 g *Poria*, 6 g *Rhizoma Chuanxiong*, 6 g *Rhizoma Anemarrhenae* and 3 g *Radix Glycytthizae* were added, and kept it boiling for 10 more minutes. The extracted solution was filtered through 6 layer gauzes and made to a concentration of 1 g crude drug per milliliter, and finally the solution was freeze-dried. Twenty milligrams of the freeze-dried powder were extracted with 20 ml methanol for 30 min under ultrasonics. The methanol extraction was centrifuged at 10,000 rpm for 5 min at 4 °C, and the supernatant was filtered through a 0.22 μm-filter, the filtrate was used for UPLC analysis.

2.5. UPLC–Q-TOF-HDMS analysis

The UPLC–MS analysis was performed on a Waters ACQUITY UPLC system (Waters Corporation, Milford, USA) coupled with a Waters Micromass Q-tof microTM Synapt High Definition Mass Spectrometer (Manchester, UK) equipped with electrospray ionization. For the reversed-phase UPLC analysis, the ACQUITY UPLC^{TM} BEH C$_{18}$ column (100 mm × 2.1 mm i.d., 1.7 μm, Waters Corp, Milford, USA) was used. The column temperature was maintained at 45 °C; the flow rate of the mobile phase was 0.40 ml/min; the injection volume was fixed at 5.0 μl. Mobile phase A consisted of 0.1% formic acid in acetonitrile, while mobile phase B consisted of 0.1% formic acid in water. The column was eluted with a linear gradient of 1–50% B over initial to 2.0 min, 50–70% B over 2.0–7.0 min, 70–99% B over 7.0–11.0 min and held at 99% B for 2.0 min, returned to 1% B for 0.5 min and then held for 1.5 min at an eluent flow rate of 0.40 ml/min.

For the UPLC–HDMS analysis, the optimal conditions were as follows: capillary voltage of 2500 V, desolvation temperature of 250 °C, sample cone voltage of 35 V, extraction cone voltage of 4.0 V, microchannel plate voltage of 1600 V, collision energy of 4 eV, source temperature of 120 °C, cone gas flow of 50 l/h and desolvation gas flow of 700 l/h for positive ion mode; capillary voltage of 2300 V, desolvation temperature of 300 °C, sample cone voltage of 45 V, extraction cone voltage of 4.0 V, microchannel plate voltage of 1600 V, collision energy of 4 eV, source temperature of 100 °C, cone gas flow of 50 l/h and desolvation gas flow of 700 l/h for negative ion mode. A "purge-wash-purge" cycle was employed on the auto-sampler, with 90% aqueous formic acid used for the wash solvent and 0.1% aqueous formic acid used as the purge solvent, this ensured that the carry-over between injections was minimized. The mass spectrometric full-scan data were acquired in the positive ion mode from 100 to 1000 Da with a 0.1 s scan time. Data were centroided and mass was corrected during acquisition using an external reference (Lock-Spray^{TM}) consisting of a 0.2 ng/ml solution of leucine enkephalin infused at a flow rate of 100 μl min^{-1} via a lockspray interface, generating a reference ion for positive ion mode ([M+H]$^+$ = 556.2771) and negative ion mode ([M−H]$^-$ = 554.2615) to ensure accuracy during the MS analysis.

2.6. Data processing and multivariate data analysis

The mass data acquired were imported to Markerlynx (version 4.1, Waters Corporation, MA, USA) within Masslynx software (version 4.1) for peak detection and alignment. All data were normalized to the summed total ion intensity per chromatogram, and the resultant data matrices were introduced to EZinfo 2.0 software for PCA, PLS-DA and OPLS analyses. Metabolite peaks were assigned by MS/MS analysis or interpreted with available biochemical databases, such as HMDB, http://www.hmdb.ca/; KEGG, http://www.genome.jp/kegg/; METLIN, http://metlin.scripps.edu/; MassBank, http://www.massbank.jp/. Potential markers were extracted from S-plots constructed following analysis with OPLS,

and markers were chosen based on their contribution to the variation and correlation within the data set. Other statistical analyses used include one-way analysis of variance (ANOVA), least significant difference (LSD) test and independent sample *t*-test. They were performed with SPSS 17.0. Statistical differences are considered significant when the test *p* value is less than 0.05.

3. Results and discussion

Using the optimal reversed-phase UPLC–HDMS conditions described above, the representative Based Peak Intensity (BPI) chromatograms of drosophila samples collected are presented in Fig. 1. Low molecular mass metabolites could be separated well in the short time of 14 min due to the minor particles (sub-1.7 μm) of UPLC. The OPLS-DA approach separated samples into two blocks was applied to obtain better discrimination as a result of sleep deprivation between the control and model groups, indicating that the insomnia model was successfully reproduced (Fig. 2A and B). The corresponding PLS-DA loadings plot indicated that differentiating metabolites were attributable to the clustering observed in the scores plot (Fig. 3). To exhibit the responsibility of each ion for these variations more intuitively, S-plots and VIP-value plots were combined (Fig. 4). The green point graph is the S-plot, and most of the ions were clustered around the origin point; only a few of them scattered in the margin region, and just these few ions contributed to the clustering observed in the score plot and were also the differentiating metabolites. The red point graph is the VIP-value plot, which represents the value of each ion. The farther away from the origin, the higher the VIP value of the ions was. The green points and red points were in one-to-one correspondence in the combination. Combining the results of the OPLS analysis with S-plots and VIP-value plots, the UPLC–HDMS analysis platform provided the retention time, precise molecular mass and MS/MS data for the structural identification of biomarkers. Finally, potential biomarkers of significant contribution was characterizated 11 in positive mode and 9 in negative mode, respectively (Tables 1 and 2). According to the protocol detailed above, the robust UPLC–HDMS segregation analysis platform provided the retention time, precise molecular mass and MS/MS data for the structural identification of biomarkers. The precise molecular mass was determined within measurement errors (<5 ppm) by Q-TOF, and meanwhile, the potential elemental composition, degree of unsaturation and fractional isotope abundance of compounds were obtained. The presumed molecular formula was searched in Chemspider, Human Metabolome Database, METLIN and other databases to identify the possible chemical constitutions and to determine the potential structures of the ions. Taking one ion as example, the identification procedure was as follows. According to the protocol detailed above, the ion at Rt = 3.04 and [M+H]$^+$ = 274 has a high VIP value. This ion might contain an odd number of nitrogen atoms because its precise molecular weight was 274.2744, and its molecular formula was speculated as C$_{16}$H$_{35}$NO$_2$ from the analysis of its elemental composition and fractional isotope abundance. Degree of unsaturation was calculated as 0, indicating that it was a ring compound. The main fragment ions analyzed by MS/MS screening were m/z 228.1992, 175.1490, 147.1256 and 81.0655, which could correspond to lost −C$_3$H$_{10}$, −C$_7$H$_{15}$, −C$_9$H$_{19}$ and −C$_{12}$H$_{28}$, respectively. Finally, it was speculated as N-lauryl-diethanolamine after searching in the database. All of the potential biomarkers identified are shown in Tables 1 and 2 and Fig. 5.

We utilized metabolomic approach further to delineate metabolic changes of insomnia after dosing SZRD regiment treatment. Metabolomic trajectory analysis has been found that SZRD dosing regiment can be regulated back towards their baseline levels to that of control group. With regard to information analyst

Table 1
Potential biomarkers identified of insomnia drosophila in positive model.

No.	VIP	Formula	Observed [M+H]$^+$	Rt	Actual-M	Proposed compound	MS/MS	Losses
1	27.72	$C_{16}H_{35}NO_2$	274.2744	3.04	273.2668	N-Lauryl diethanolamine	228.1992	$-C_3H_{10}$
							175.1490	$-C_7H_{15}$
							147.1256	$-C_9H_{19}$
							102.0608	$-C_{12}H_{28}$
							81.0655	$-C_{10}H_{27}NO_2$
2	22.45	$C_{18}H_{39}NO_3$	318.2978	3.07	317.2930	2-Aminooctadecane-1,3,4-triol	256.2679	$-C_2H_6O_2$
							177.1187	$-C_6H_{23}NO_2$
							105.0707	$-C_{14}H_{29}O$
							87.0462	$-C_{14}H_{33}NO$
3	20.64	$C_{18}H_{39}NO_2$	302.3048	3.91	301.2981	(2S,3R)-2-aminooctadecane-1,3-diol	211.2065	$-C_4H_{13}NO$
							89.0595	$-C_4H_9O_2$
							73.0328	$-C_3H_5O_2$
4	17.48	$C_{20}H_{43}NO_2$	330.3375	5.18	329.3294	2,2′-(Hexadecylimino)	211.1942	$-C_7H_{19}O$
							184.1793	$-C_9H_{22}O$
							117.0869	$-C_{15}H_{33}$
							69.0682	$-C_{15}H_{35}NO_2$
5	17.24	$C_{22}H_{47}NO_2$	358.3651	6.61	357.3607	2,2′-(Octadecylimino)diethanol	285.2761	$-C_5H_{13}$
							241.2369	$-C_7H_{17}O$
							180.1748	$-C_{10}H_{26}O_2$
							109.0957	$-C_{14}H_{35}NO_2$
							71.0829	$-C_{18}H_{39}O_2$
6	14.56	$C_{21}H_{38}O_4$	355.2805	8.64	354.2770	Ricinoleic acid, methyl ester, acetate	313.2772	$-C_2H_2O$
							131.1097	$-C_{14}H_{24}O_2$
							71.0871	$-C_{16}H_{28}O_4$
7	14.19	$C_{36}H_{69}NO_5S$	628.4999	8.83	627.4896	Ditetradcyl N-(4-sulfany lbutanoyl)-L-aspartate	584.4768	$-C_2H_4O$
							553.4100	$-C_4H_{11}O$
							443.3358	$-C_{11}H_{21}O_2$
							355.2825	$-C_{15}H_{31}NOS$
							257.2662	$-C_{20}H_{35}O_4S$
							171.1433	$-C_{26}H_{51}NO_3S$
							93.0246	$-C_{30}H_{65}NO_4S$
8	13.75	$C_{10}H_{12}N_2O$	176.0850	9.21	175.0949	Serotonin	146.0649	$-CH_5N$
							94.0408	$-C_4H_7N_2$
							65.0258	$-C_6H_{10}NO$
9	12.24	$C_{28}H_{44}N_2O_3$	457.3482	9.44	456.3352	15-Hydroxy-N-methyl-9-oxo-N-(2-pyridin-2-ylethyl)prost-13-en-1-amide	391.2977	$-C_5H_6$
							339.2353	$-C_6H_{14}O_2$
							301.2815	-301.2769
							282.2799	$-C_{10}H_9NO_2$
							57.0706	$-C_{24}H_{36}N_2O_3$
10	11.91	$C_{29}H_{46}N_2O_3$	471.3629	9.84	470.3508	N-octadecanoyl tryptophan	427.3368	$-CH_2NO$
							315.2898	$-C_7H_{10}NO_3$
							177.1160	$-C_{18}H_{32}NO_2$
							133.0864	$-C_{20}H_{36}NO_3$
11	11.78	$C_{13}H_{16}N_2O_2$	232.1212	10.19	232.121185	Melatonin	202.0896	$-CH_3N$
							106.0405	$-C_6H_9N_2O$
							92.0152	$-C_8H_{13}NO$
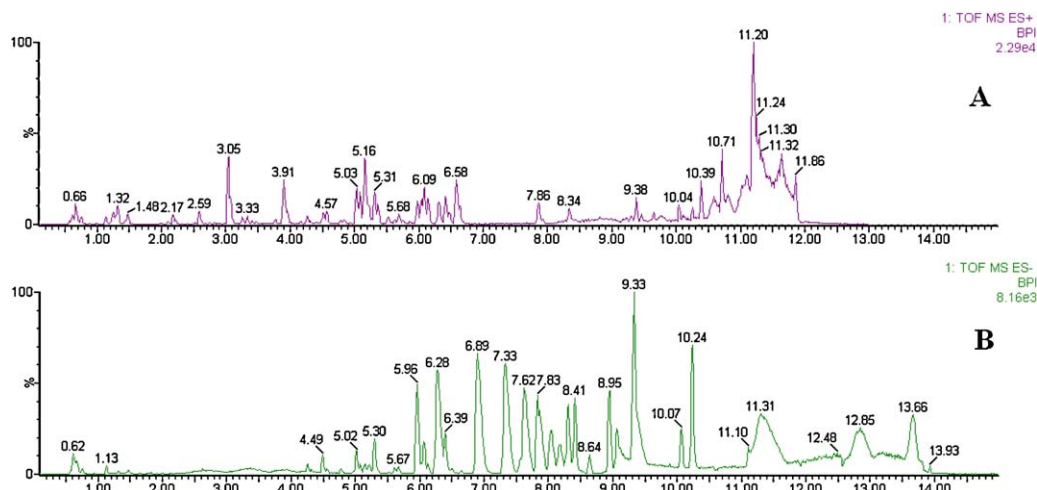
Fig. 1. BPI chromatograms derived from UPLC–HDMS in (A) positive mode and (B) negative mode.

Table 2
Potential biomarkers identified of insomnia drosophila in negative model.

No.	VIP	Formula	Observed [M−H]⁻	Rt	Actual-M	Proposed compound	MS/MS	Losses
12	21.17	$C_{18}H_{32}O_2$	279.2911	9.33	280.2402	Linoleic acid	208.2101	$-C_3H_3O_2$
							196.1442	$-C_6H_{11}$
							181.1190	$-C_7H_{14}$
							171.1448	$-C_8H_{12}$
							155.1172	$-C_9H_{16}$
							87.0439	$-C_{14}H_{24}$
13	13.01	$C_{15}H_{26}N_4OS$	309.2186	6.21	310.1827	1′-(Cyclopropylcarb-amothioyl)-1,4′-bi piperidine-4′-carboxamide	285.1849	$-C_2$
							278.1532	$-CH_3O$
							266.1505	$-C_2H_3O$
							221.1457	$-C_3H_6NS$
							127.1063	$-C_8H_{12}N_3S$
14	12.41	$C_{17}H_{30}N_4O_2S$	353.2073	6.65	354.2089	2-{[4-(3-Methoxypropyl)-5-propyl-4H-1,2,4-triazol-3-yl]sulfanyl}-1-(3-methylpiperidin-1-yl)ethanone	284.1307	$-C_5H_9$
							283.1778	$-C_2H_2N_2O$
							155.0118	$-C_{11}H_{24}N_3$
							137.9843	$-C_{13}H_{29}NO$
							136.0243	$-C_{11}H_{14}N_3O_2$
							96.9628	$-C_{14}H_{30}N_3O$
15	12.05	$C_{23}H_{46}N_2OS$	397.3085	7.04	398.3331	N-(hexadecyl-carbamothioyl) hexanamide	133.0857	$-C_{18}H_{32}O$
							71.0861	$-C_{18}H_{34}N_2OS$
16	11.65	$C_{28}H_{46}N_2S$	441.3432	7.46	442.3382	5-Heptadecyl-N-phenyl-2,3-dihydro-1H-pyrrole-1-carbothioamide	253.1738	$-C_{14}H_{20}$
							191.1654	$-C_{15}H_{24}NS$
							149.0254	$-C_{20}H_{38}N$
							136.0214	$-C_{21}H_{39}N$
							97.1015	$-C_{21}H_{32}N_2S$
							85.1002	$-C_{22}H_{32}N_2S$
17	9.22	$C_{31}H_{53}N_3$	466.3271	8.37	467.3239	4′-(Hexadecahydropyren-1-yl)-2,2′:6′,2″-terpiperidine	302.2828	$-C_{10}H_{16}N_2$
							175.1361	$-C_{19}H_{35}N_2$
							133.0867	$-C_{22}H_{41}N_2$
							71.0863	$-C_{26}H_{41}N_3$
							57.0712	$-C_{27}H_{43}N_3$
18	8.46	$C_{11}H_{12}N_2O_3$	219.0848	8.45	220.0848	5-Hydroxy-L-tryptophan	177.1125	$-CO_2$
							101.0597	$-C_6H_4N_2O$
							73.0305	$-C_8H_8N_2O$
19	7.99	$C_{19}H_{31}ClN_2O$	337.2019	9.04	338.2125	1-(3-Chlorophenyl)-3-dodecylurea	177.1084	$-C_9H_{17}Cl$
							151.0959	$-C_{11}H_{19}Cl$
							133.0860	$-C_{11}H_{21}OCl$
							57.0709	$-C_{15}H_{21}N_2OCl$
20	7.19	$C_{20}H_{32}O_5$	351.2250	4.65	352.2249	Prostaglandin D2	279.2242	$-C_2O_3$
							243.1425	$-C_4H_{12}O_3$
							171.1452	$-C_{10}H_{12}O_3$
							87.0412	$-C_{16}H_{24}O_3$
							73.0302	$-C_{17}H_{26}O_3$

of PCA, which was shown in Fig. 6, the control and insomnia drosophila groups were significantly divided into two classes after sleep deprivation treatment, indicating that the model of insomnia was successfully reproduced. SZRD regiment developed the distant tendency to the diverse extent of model group, demonstrating that SZRD could have some therapeutic effect on the insomnia. Interestingly, SZRD exhibited good prevention role of insomnia and kept animals in the normal situation, because there were no distinct clustering differences between control group and SZRD treatment. Of note, distinct clustering differences were observed after SZRD treatment in comparison with the model group; it has been found that dosing regiment can be regulated back towards their baseline levels to that of control group. In order to more clearly characterize treatment sleep effects of SZRD, the intensity level of 20 markers in the different groups was analyzed (Fig. 7) and, we have found that content of the key markers closered to normal group. Thus, SZRD may regulate metabolism of these markers to efficiently use for sleeping disorder. Additionally, a correlation coefficient analysis was applied to investigate the connections between biomarkers and corresponding groups (Fig. 8). The plot shows how the each biomarker in relation to group and represents the feature of group. Variables situated upper are positively correlated to group and those situated opposite are negatively correlated to the group. The markers 4, 10, 14, 16, such as 2,2′-(hexadecylimino), 2-{[4-(3-methoxypropyl)-5-propyl-4H-1,2,4-triazol-3-yl]sulfanyl}-1-(3-methylpiperidin-1-yl)ethanone, 5-heptadecyl-N-ph-enyl-2,3-dihydro-1H-pyrrole-1-carbothioamide, 5-heptadecyl-N-phenyl-2,3-dihydro-1H-pyrrole-1-carbothioamide have the negative correlation with control group; others have the positive correlation with control group, indicating normal sleep characteristic. Correlations between markers 8, 11, 18, 20 with the control group while being relatively high when compared to the other variables, therefore the change in serotonin, melatonin, 5-hydroxy-L-tryptophan, prostaglandin D2 has the strongest association with normal characteristics and are enough to suggest that these markers can principally represent the insomnia model in this study. The markers 4, 10, 14, 16 have the positive correlation with model group; others have the negative correlation with model group, shows the overall metabolic profile of Drosophila caused a significant disturbance via sleep deprivation. The markers 4, 10, 14, 16 have the negative correlation with SZRD group; others have the positive correlation with SZRD group, consistent with the control group. The above conclusion is consistent with PCA results in Fig. 6. Interestingly,
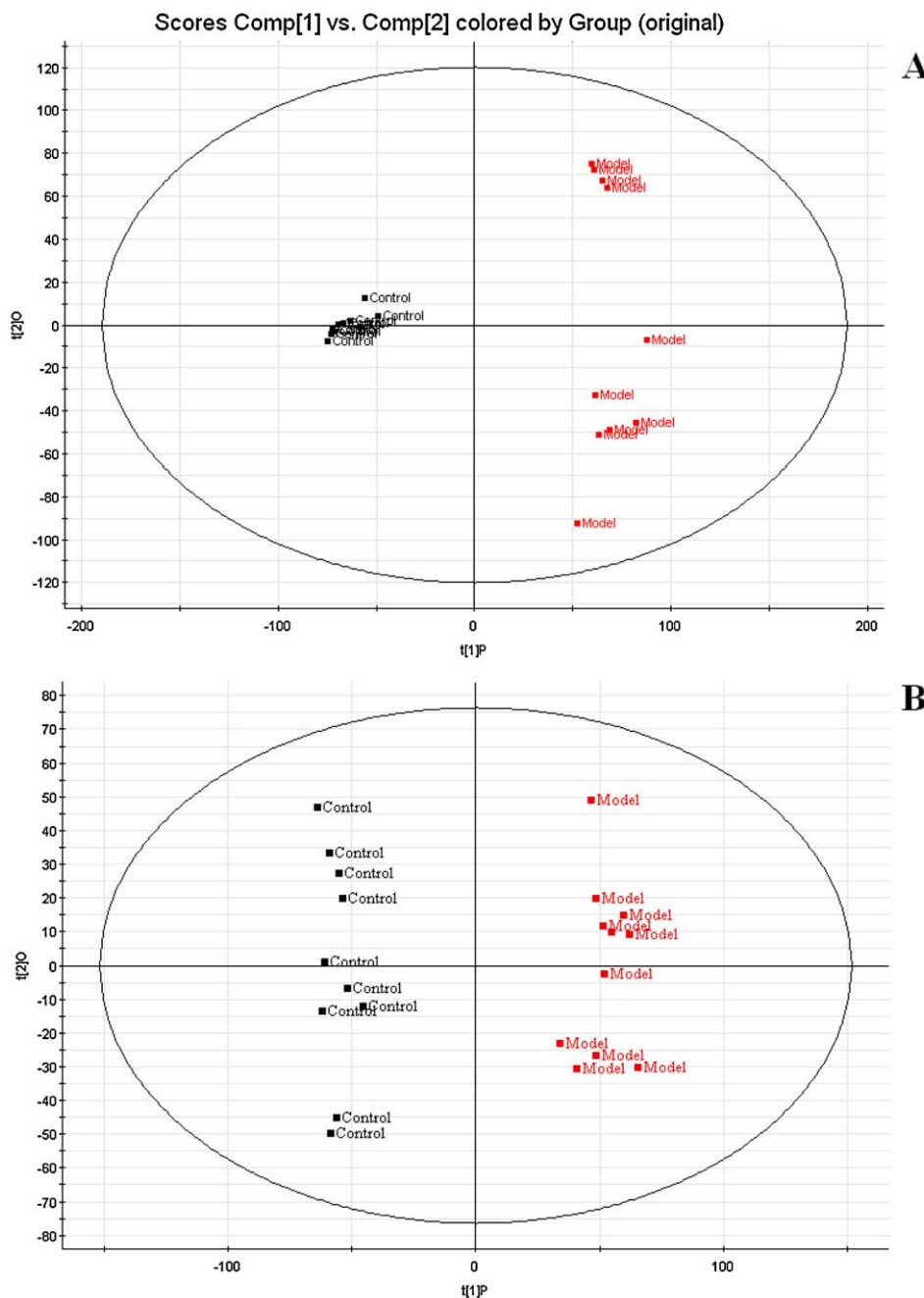
Fig. 2. OPLS-DA model results for control and model group. Significant metabolomic difference was shown between control and model group. One data point stands for one subject (A, positive mode; B, negative mode. ■, control group; ■, model group).

these results provide evidence for the dissection of the mode of action of clinically well established SZRD for insomnia.

Insomnia is a common problem that for many sufferers persists chronically and may result from a wide range of causes [19]. Specific treatments address particular underlying medical disorders. General therapeutic approaches, including pharmacologic and behavioral strategies, may have broad applicability to insomnia patients. Many different medications and substances have been used in an attempt to improve sleep. Insomnia is a common problem requiring appropriate recognition and management. Despite recent advances in the development of newer hypnotics in western medicine, a significant proportion of patients with insomnia, both locally and internationally, consume TCM [20]. Sedative–hypnotic medications, including benzodiazepines and non-benzodiazepines, are usually prescribed for the insomniac patients; however, the

addiction, dependence and adverse effects of those medications have drawn much attention. In contrast, SZRD, a classic traditional Chinese medicine formulae, has been efficiently used for insomnia relief in China, although its mechanism remains unclear [21]. This study was designed to further elucidate the underlying mechanism of SZRD on sleep regulation. Metabolomics is a powerful new technology that allows for the assessment of global metabolic profiles in easily accessible biofluids and biomarker discovery in order to distinguish between diseased and non-diseased status [5,22–24]. The use of metabonomics for the screening of biomarker patterns and elucidation of biochemical processes during the postgenomic era has increased contemporaneously with progress in global systems biology. At present study, a insomnia model was constructed, and dynamic metabolic profiles of treated drosophila with SZRD were investigated with UPLC–HDMS combined with multivariate
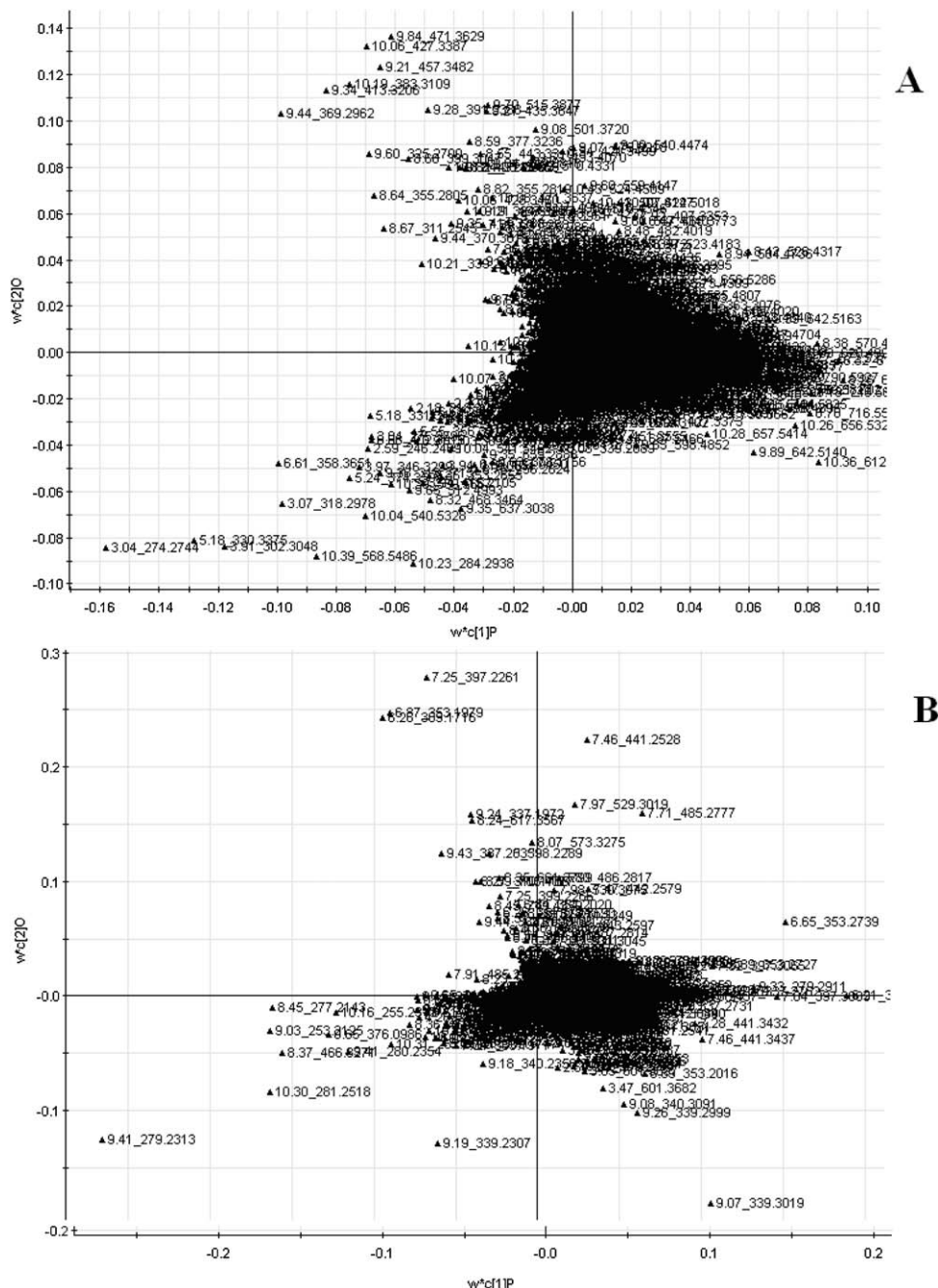
Fig. 3. Loading plot of PLS-DA of insomnia drosophila. The loading plot represents the impact of the metabolites on the clustering results. PLS-DA loading plots displayed variables positively correlated with score plots. Statistically and significantly different metabolites responsible for the discrimination of the two groups were identified between the control and model group (A, positive mode; B, negative mode).

statistical analysis. We utilized this approach to delineate hypnotic property of SZRD. Interestingly, metabolomic trajectory analysis has been found that dosing SZRD regiment can be regulated back towards their baseline levels to that of control group, showed potent therapeutic efficacy. Importantly, we found that SZRD activated an array of factors involved in amino acid metabolism and lipid metabolism, etc.

Metabolic analysis of insomnia were inferred from changes in the intermediates during substance metabolism in the present study. Further analysis revealed that metabolites identified together are important for the host response to insomnia through immune system and nervous system, etc. Melatonin is a biogenic amine that is found in animals, plants and microbes. In mammals,

melatonin is produced by the pineal gland which is located in the center of the brain but outside the blood–brain barrier. The secretion of melatonin increases in darkness and decreases during exposure to light, thereby regulating the circadian rhythms of several biological functions, including the sleep–wake cycle [25]. In particular, melatonin regulates the sleep–wake cycle by chemically causing drowsiness and lowering the body temperature. Melatonin is also implicated in the regulation of mood, learning and memory, immune activity, dreaming, fertility and reproduction. Melatonin is also an effective antioxidant. Most of the actions of melatonin are mediated through the binding and activation of melatonin receptors. Individuals with insomnia disorders may have lower than normal levels of melatonin and that the deficits were associated
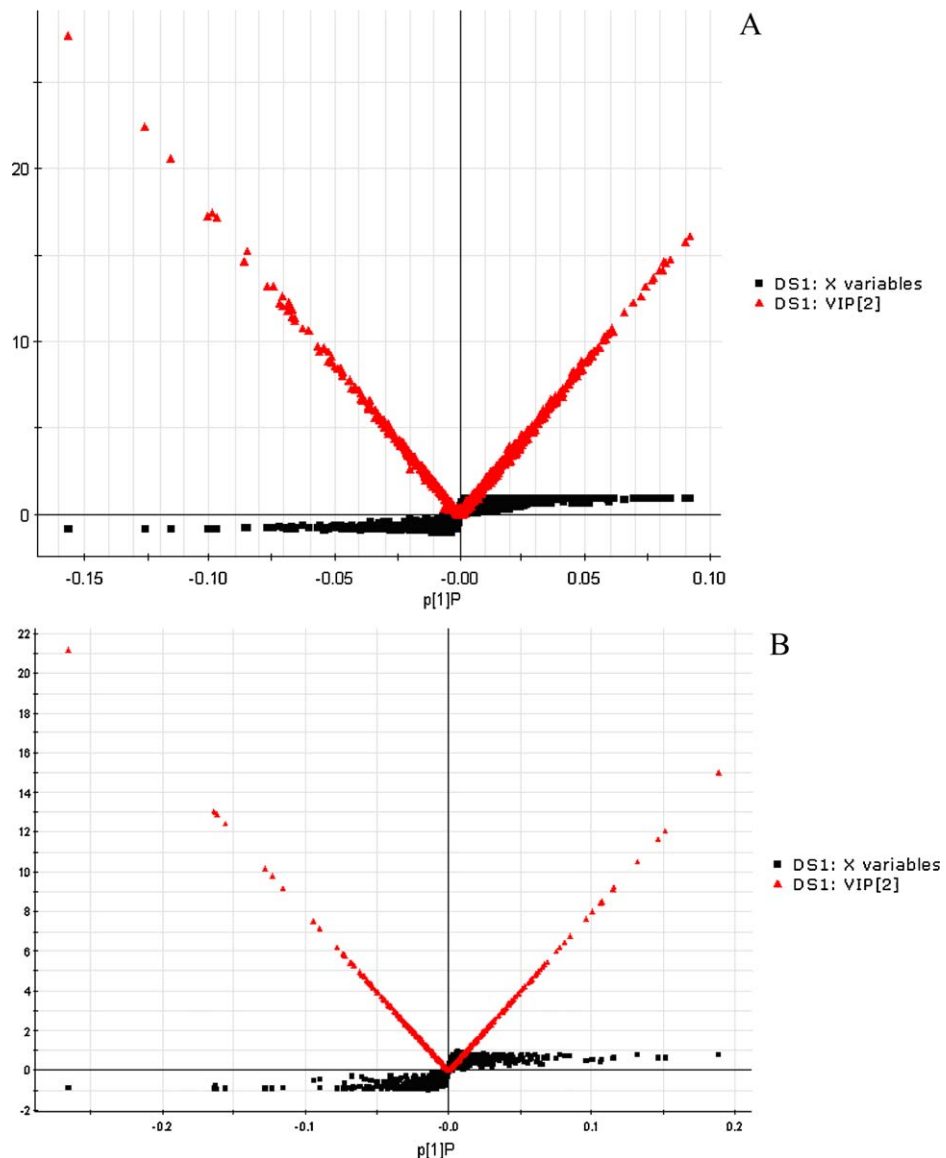
Fig. 4. Combination plot of S-plot and VIP values. The red point graph is the VIP-value plot, which represents the value of each metabolites. The farther away from the origin, the higher the VIP value of the metabolites was. The black points and red points were in one-to-one correspondence in the combination (A, positive mode; B, negative mode). (For interpretation of the references to color in this figure legend, the reader is referred to the web version of the article.)

with low activity of the melatonin. Reduced melatonin production has also been proposed as a likely factor in the significantly higher insomnia rates in night workers. Serotonin (5-hydroxytryptamine, 5-HT) is a biochemical messenger and regulator, synthesized from the essential amino acid L-tryptophan. Serotonin in the nervous system acts as a local transmitter at synapses, and as a paracrine or hormonal modulator of circuits upon diffusion, allowing a wide variety of 'state-dependent' behavioral responses to different stimuli [26,27]. Serotonin is widely distributed in the nervous system of vertebrates and invertebrates and some of its behavioral effects have been preserved along evolution [28]. Such is the case of aggressive behavior and rhythmic motor patterns, including those responsible for feeding. In vertebrates, which display a wider and much more sophisticated behavioral repertoire, serotonin also modulates sleep, the arousal state, sexual behavior, and others, and deficiencies of the serotonergic system causes disorders such as depression, obsessive–compulsive disorder, phobias, posttraumatic stress disorder, epilepsy, and generalized anxiety disorder. Serotonin has three different modes of action in the nervous system: as transmitter, acting locally at synaptic

boutons; upon diffusion at a distance from its release sites, producing paracrine (also called volume) effects, and by circulating in the blood stream, producing hormonal effects. The three modes can affect a single neuronal circuit [29]. Serotonin has been claimed to help alleviate insomnia, depression, and headaches [30]. So, serotonin might be useful biomarker for insomnia. Prostaglandin D2 (or PGD2) is a prostaglandin that is actively produced in various organs such as the brain, spleen, thymus, bone marrow, uterus, ovary, oviduct, testis, prostate and epididymis, and is involved in many physiological events. It is potent endogenous somnogens and plays a critical role in the regulation of physiological sleep [31]. PGD2 binds to the prostaglandin D2 receptor which is a G-protein-coupled receptor. Its activity is mainly that promotes sleep; regulates body temperature, olfactory function, hormone release, and nociception in the central nervous system; prevents platelet aggregation; and induces vasodilation and bronchoconstriction. PGD2 is also released from mast cells as an allergic and inflammatory mediator, through receptor-mediated G-protein linked signaling pathways. In mammalian systems, it is efficiently converted into more stable arachidonate metabolites, such as PGD2,
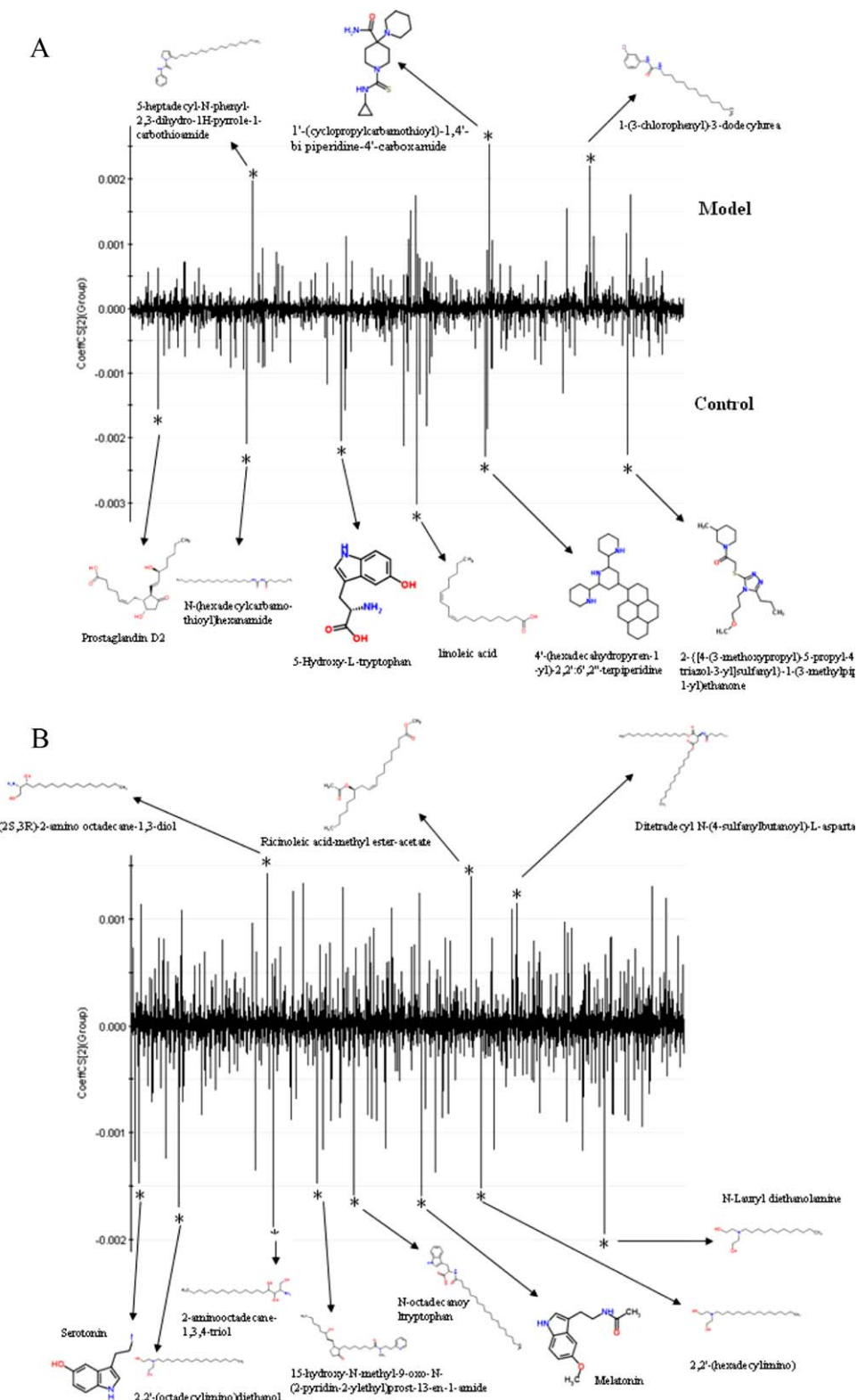
Fig. 5. Loading plots of OPLS-DA model of potential biomarkers identified in negative model (A) and positive (B) model.

PGE2, PGF2a by the action of three groups of enzymes, PGD synthases, PGE synthases and PGF synthases, respectively [32]. PGD2 has been proposed to be essential for the initiation, maintenance and plays pivotal roles in the regulation of the physiological sleep and shown to reduce promptly and effectively the amounts of sleep during the period of infusion [33]. The presence of PGD2 suggests that sleep was disturbed. So, PGD2 might appear to contribute to the insomnia and has a close relationship with insomnia. 5-Hydroxy-L-tryptophan is synthesized by the pineal gland. Daily rhythms in pineal methoxyindole metabolism have been described in rodents and humans (5-hydroxy-L-tryptophan level are coincident with serotonin levels in rodents pineal) and 5-hydroxy-L-tryptophan at its highest during the daylight hours and fall markedly soon after the onset of darkness, coincident with increases in the
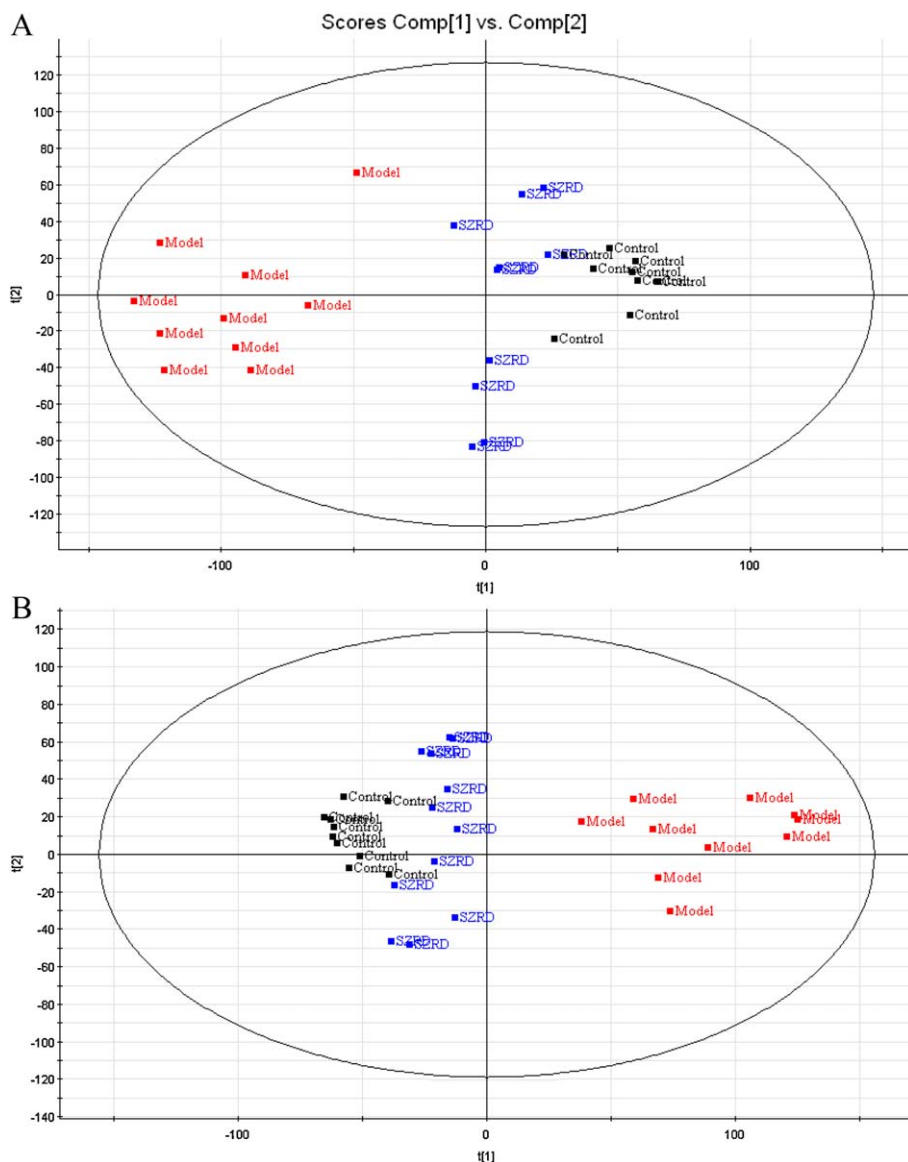
Fig. 6. Trajectory analysis of PCA Score plots for the insomnia drosophila after regimens SZRD treatment in positive model (A) and negative model (B).
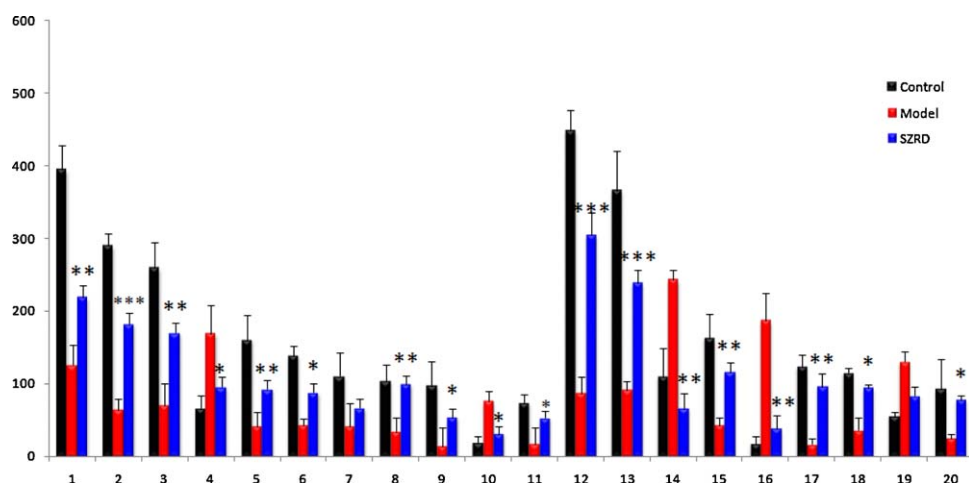
Fig. 7. Differential expression levels (mean) of biomarkers in different groups. The "asterisk" indicated the statistical significance of the biomarkers changes by Student's t-test: $^*p < 0.05$; $^{**}p < 0.01$; $^{***}p < 0.001$.
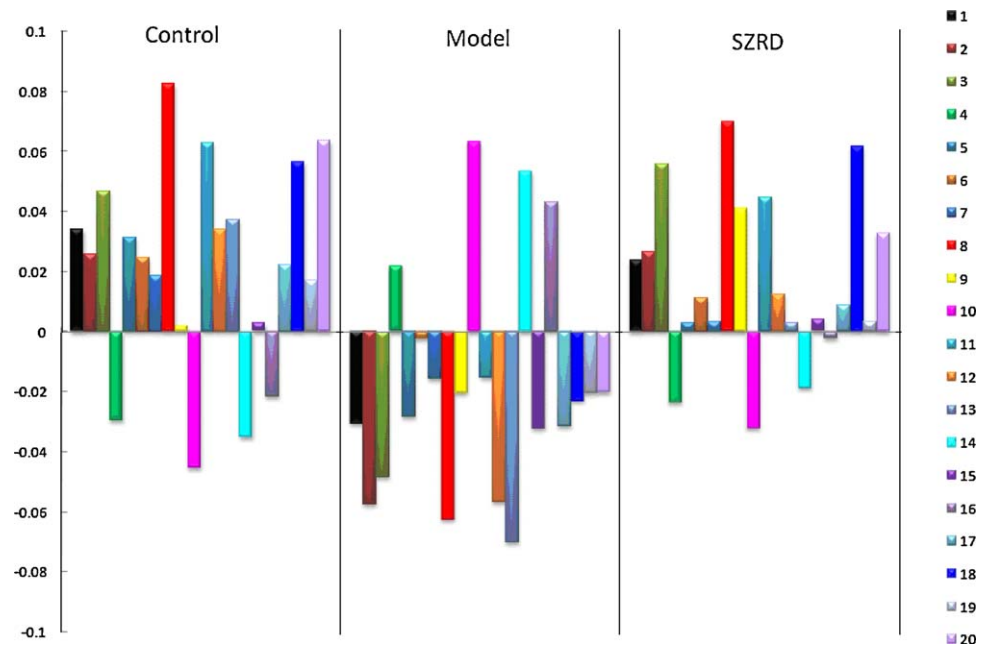
Fig. 8. Correlation coefficient analysis between groups with corresponding markers in different groups. Variables are presented in 3 groups, Control, Model and SZRD. Values of correlations are shown in the vertical axis (upper for positive correlations and low for negative correlations) and corresponding markers represented to the right of the bars. Numbers consist with Tables 1 and 2.

levels of pineal melatonin and the activities of pineal serotonin-N-acetyltransferase and hydroxyindole-O-methyltransferase. The fact that the levels of 5-hydroxy-ʟ-tryptophan and melatonin vary in parallel suggests that the major factor generating the methoxyindole rhythms is not serotonin-N-acetyltransferase activity, but perhaps a change in the availability (for metabolism) of "stored" serotonin. 5-Hydroxy-ʟ-tryptophan is frequently seen in sleep disruption, nightly restlessness, sundowning, and other circadian disturbances disease [30]. After sleep deprivation, the presence of 5-hydroxy-ʟ-tryptophan, suggests a potential monitoring role for insomnia progression. Thus, 5-hydroxy-ʟ-tryptophan might be sensitive indicator biomarker of insomnia. However, other markers was warranted the further mechanistic exploration of this formulae.

4. Conclusion

The present results demonstrate the dissection of the action of clinically well established TCM formulae such as SZRD should be possible by application of advanced analytical research approaches at the global metabolomics levels. This study may be considered a useful pilot trial in exploring the value of traditional formulae on a larger scale and in helping to bridge Western and the Eastern medicines in the era of systems biology. In conclusion, this is the first demonstration of metabolomic approach to delineate metabolic changes in insomnia after dosing SZRD regiment treatment. In this study, a model of insomnia drosophila was constructed, and dynamic metabolic profiles were investigated with UPLC–HDMS combined with multivariate statistical analysis, potential biomarkers of significant contribution was characterizated 9 in negative mode and 11 in positive mode. Of note, SZRD regiment developed the distant tendency to the diverse extent of model group and could be regulated back towards their baseline levels to that of control group, demonstrating that SZRD could have good prevention role of insomnia and keep animals in the normal situation. Analysis of correlations revealed that serotonin, melatonin, 5-hydroxy-ʟ-tryptophan, prostaglandin D2 have the strongest association with normal characteristics. We found that

SZRD increases sleep activity and exhibits binding affinity for serotonin receptors. These results implicate the hypnotic effect of SZRD and its effects may be mediated through serotonergic activation. It provided strong evidence that the hypnotic effect of SZRD occurred at the level of global metabolomics. By using a metabolomic approach, this study also exemplifies that metabolomics could provide a very promising way to elucidate therapeutic mechanisms of TCM.

References

[1] E. Holmes, R.L. Loo, J. Stamler, M. Bictash, I.K. Yap, Q. Chan, T. Ebbels, M. De Iorio, I.J. Brown, K.A. Veselkov, M.L. Daviglus, H. Kesteloot, H. Ueshima, L. Zhao, J.K. Nicholson, P. Elliott, Human metabolic phenotype diversity and its association with diet and blood pressure, Nature 453 (2008) 396–401.
[2] J.K. Nicholson, I.D. Wilson, Understanding 'global' systems biology: metabonomics and the continuum of metabolism, Nat. Rev. 2 (2003) 668–676.
[3] X. Wang, H. Sun, A. Zhang, W. Sun, P. Wang, Z. Wang, Potential role of metabolomics apporoaches in the area of traditional Chinese medicine: as pillars of the bridge between Chinese and Western medicine, J. Pharm. Biomed. Anal. 55 (2011) 859–868.
[4] J.K. Nicholoson, J. Connelly, J.C. Lindon, E. Holmes, Metabonomics: a platform for studying drug toxicity and gene function, Nat. Rev. 1 (2002) 153–161.
[5] A. Sreekumar, L.M. Poisson, T.M. Rajendiran, A.P. Khan, Q. Cao, J. Yu, B. Laxman, R. Mehra, R.J. Lonigro, Y. Li, M.K. Nyati, A. Ahsan, S. Kalyana-Sundaram, B. Han, X. Cao, J. Byun, G.S. Omenn, D. Ghosh, S. Pennathur, D.C. Alexander, A. Berger, J.R. Shuster, J.T. Wei, S. Varambally, C. Beecher, A.M. Chinnaiyan, Metabolomic

profiles delineate potential role for sarcosine in prostate cancer progression, Nature 457 (2009) 910–914.

[6] L. Wang, G.B. Zhou, P. Liu, J.H. Song, Y. Liang, X.J. Yan, F. Xu, B.S. Wang, J.H. Mao, Z.X. Shen, S.J. Chen, Z. Chen, Dissection of mechanisms of Chinese medicinal formula Realgar-Indigo naturalis as an effective treatment for promyelocytic leukemia, Proc. Natl. Acad. Sci. U.S.A. 105 (2008) 4826–4831.

[7] Q.Y. Zhang, J.H. Mao, P. Liu, Q.H. Huang, J. Lu, Y.Y. Xie, L. Weng, Y. Zhang, Q. Chen, S.J. Chen, Z. Chen, A systems biology understanding of the synergistic effects of arsenic sulfide and Imatinib in BCR/ABL-associated leukemia, Proc. Natl. Acad. Sci. U.S.A. 106 (2009) 3378–3383.

[8] M. Kusano, H. Redestig, T. Hirai, A. Oikawa, F. Matsuda, A. Fukushima, M. Arita, S. Watanabe, M. Yano, K. Hiwasa-Tanase, K. Ezura, K. Saito, Covering chemical diversity of genetically-modified tomatoes using metabolomics for objective substantial equivalence assessment, PLoS One 6 (2011) e16989–e17000.

[9] J.K. Nicholson, J.C. Lindon, Systems biology: metabonomics, Nature 455 (2008) 1054–1056.

[10] A.K. Arakaki, J. Skolnick, J.F. McDonald, Marker metabolites can be therapeutic targets as well, Nature 456 (2008) 443–444.

[11] P.L. Yi, C.H. Tsai, Y.C. Chen, F.C. Chang, Gamma-aminobutyric acid (GABA) receptor mediates suanzaorentang, a traditional Chinese herb remedy, -induced sleep alteration, J. Biomed. Sci. 14 (2007) 285–297.

[12] Z.J. Zhang, Prescription of Jinkuiyaolue, People's Medical Publishing House, Beijing, 2002.

[13] C.Y. Chen, Y.F. Chen, H.Y. Tsai, What is the effective component in Suanzaoren decoction for curing insomnia? Discovery by virtual screening and molecular dynamic simulation, J. Biomol. Struct. Dyn. 26 (2007) 57–64.

[14] S.J. Zhang, Z.X. Chen, Y.W. Lin, Y.H. Cheng, S.L. Liu, C.J. Wang, Clinical observation of modified Suan Zao Ren decoction on insomnia of chronic hepatitis B patients, Zhong Yao Cai 30 (2007) 1482–1484.

[15] Y.J. Li, K.S. Bi, Study on the therapeutic material basis of traditional Chinese medicinal preparation Suanzaoren decoction, Chem. Pharm. Bull. (Tokyo) 54 (2006) 847–851.

[16] M. Murphy, B.A. Riedner, R. Huber, M. Massimini, F. Ferrarelli, G. Tononi, Source modeling sleep slow waves, Proc. Natl. Acad. Sci. U.S.A. 106 (2009) 1608–1613.

[17] M.W. Mahowald, C.H. Schenck, Insights from studying human sleep disorders, Nature 437 (2005) 1279–1285.

[18] R. Faubel, E. Lopez-Garcia, P. Guallar-Castillón, T. Balboa-Castillo, J.L. Gutiérrez-Fisac, J.R. Banegas, F. Rodríguez-Artalejo, Sleep duration and health-related quality of life among older adults: a population-based cohort in Spain, Sleep 32 (2009) 1059–1068.

[19] D.N. Neubauer, Pharmacologic approaches for the treatment of chronic insomnia, Clin. Cornerstone 5 (2003) 16–27.

[20] L.C. Chen, I.C. Chen, B.R. Wang, C.H. Shao, Drug-use pattern of Chinese herbal medicines in insomnia: a 4-year survey in Taiwan, J. Clin. Pharm. Ther. 34 (2009) 555–560.

[21] P.L. Yi, C.P. Lin, C.H. Tsai, J.G. Lin, F.C. Chang, The involvement of serotonin receptors in suanzaorentang-induced sleep alteration, J. Biomed. Sci. 14 (2007) 829–840.

[22] C. Barbas, E.P. Moraes, A. Villaseñor, Capillary electrophoresis as a metabolomics tool for non-targeted fingerprinting of biological samples, J. Pharm. Biomed. Anal. 55 (2011) 823–831.

[23] M.Y. Choi, C. Chai, J.H. Park, J. Lim, J. Lee, S.W. Kwon, Effects of storage period and heat treatment on phenolic compound composition in dried Citrus peels (Chenpi) and discrimination of Chenpi with different storage periods through targeted metabolomic study using HPLC-DAD analysis, J. Pharm. Biomed. Anal. 54 (2011) 638–645.

[24] C. Ma, K. Bi, M. Zhang, D. Su, X. Fan, W. Ji, C. Wang, X. Chen, Metabonomic study of biochemical changes in the urine of Morning Glory Seed treated rat, J. Pharm. Biomed. Anal. 53 (2010) 559–566.

[25] M.S. Rahman, B.H. Kim, A. Takemura, C.B. Park, Y.D. Lee, Effects of moonlight exposure on plasma melatonin rhythms in the seagrass rabbitfish, Siganus canaliculatus, J. Biol. Rhythms 19 (2004) 325–334.

[26] M. Deuschle, M. Schredl, C. Schilling, S. Wüst, J. Frank, S.H. Witt, M. Rietschel, M. Buckert, A. Meyer-Lindenberg, T.G. Schulze, Association between a serotonin transporter length polymorphism and primary insomnia, Sleep 33 (2010) 343–347.

[27] S. Leu-Semenescu, I. Arnulf, C. Decaix, F. Moussa, C. Clot, C. Boniol, Y. Touitou, R. Levy, M. Vidailhet, E. Roze, Sleep and rhythm consequences of a genetically induced loss of serotonin, Sleep 33 (2010) 307–314.

[28] R. Rosenberg, D.J. Seiden, S.G. Hull, M. Erman, H. Schwartz, C. Anderson, W. Prosser, W. Shanahan, M. Sanchez, E. Chuang, T. Roth, APD125, a selective serotonin 5-HT(2A) receptor inverse agonist, significantly improves sleep maintenance in primary insomnia, Sleep 31 (2008) 1663–1671.

[29] F.F De-Miguel, C. Trueta, Synaptic and extrasynaptic secretion of serotonin, Cell. Mol. Neurobiol. 25 (2005) 297–312.

[30] K. Klarskov, K.L. Johnson, L.M. Benson, G.J. Gleich, S. Naylor, Eosinophilia-myalgia syndrome case-associated contaminants in commercially available 5-hydroxytryptophan, Adv. Exp. Med. Biol. 467 (1999) 461–468.

[31] Y. Urade, Molecular mechanisms of insomnia, Nippon Rinsho 67 (2009) 1489–1493.

[32] S. Saito, H. Tsuda, T. Michimata, Prostaglandin D2 and reproduction, Am. J. Reprod. Immunol. 47 (2002) 295–302.

[33] W.M. Qu, Z.L. Huang, X.H. Xu, K. Aritake, N. Eguchi, F. Nambu, S. Narumiya, Y. Urade, O. Hayaishi, Lipocalin-type prostaglandin D synthase produces prostaglandin D2 involved in regulation of physiological sleep, Proc. Natl. Acad. Sci. U.S.A. 103 (2006) 17949–17954.

Short communication

Structure of the major degradant of *ezetimibe*

Zsuzsanna Sánta*, János Kóti, Katalin Szőke, Krisztina Vukics, Csaba Szántay Jr.

Gedeon Richter Plc, 1103 Budapest Gyömrői út 19-21, Hungary

ABSTRACT

In a recent contribution to this Journal Gajjar and Shah described the isolation and structure elucidation of the major alkaline degradant of *ezetimibe*, a lipid lowering agent [A.K. Gajjar, V.D. Shah, J. Pharm. Biomed. Anal. 55 (2011) 225–229]. Based on ^{1}H NMR, ^{13}C NMR and mass spectrometric studies the authors concluded that the structure of the degradant is 5-(4-fluorophenyl)-2-[(4-fluorophenylamino)-(4-hydroxyphenyl) methyl]-pent-4-enoic acid. In a subsequent "Letter to the Editor" submitted to the Journal, Barhate and Mohanra pointed out that the aforementioned structure is inconsistent with the spectroscopic data reported by Gajjar and Shah, consequently it must be wrong [Ch.R. Barhate, K. Mohanra, J. Pharm. Biomed. Anal. 55 (2011) 1237–1238]. However, Barhate and Mohanra did not offer a correct structure in their critical letter. Based on the cited NMR data we realised that previously we had had the same degradant in hand and had unambiguously determined its structure from detailed ^{1}H, ^{13}C, COSY, H-C HSQC, H-C HMBC and 1D-NOESY NMR investigations. Herein we report the correct structure to be (2R,3R,6S)-N,6-bis(4-fluorophenyl)-2-(4-hydroxyphenyl)-3,4,5,6-tetrahydro-2H-pyran-3-carboxamide. However, the structure is not new and was described earlier [G.Y.S.K. Swamy et al., Acta Cryst. E 61 (2005) o3608–o3610; K. Filip et al., J. Mol. Struct. 991 (2011) 162–170]. The aim of our present communication is to bring together the various threads of analytical effort involving this degradant into a compact and hopefully instructive conclusion on the pages of this Journal. For the sake of completeness and clarity we also list the correct NMR spectral assignments for *ezetimibe* which was also given partly erroneously in the earlier literature, and we propose a mechanism for the formation of the degradant.

© 2011 Elsevier B.V. All rights reserved.

1. Introduction

A vast range of increasingly powerful structure-elucidation spectroscopic techniques are becoming more and more accessible and almost routinely applicable worldwide. Consequently one may easily think that there is hardly any reason to be sceptical about the correctness of the structures reported in the modern literature, especially when the compound in question is available in pure form and relatively large quantities (several hundreds of milligrams), and contains only a few heteroatoms. However, practice shows that the fact that we (can) have an abundance of structurally relevant spectral data in our hands does not necessarily make structure elucidation a mechanical process, and misinterpreting those data is always a possibility that one should take into account. For example, from a meticulous survey of the papers published between 2007 and 2008 in the *Journal of Natural Products*, Carvalho and co-workers concluded that out of 198 publications featuring new natural products whose structure had been determined by NMR, 47 had at least one new compound for which alternative structures would also be consistent with the reported NMR

data, but these alternatives had apparently not been considered and ruled out by the authors of the pertinent papers [1]. Likewise, an incorrect structure for the major degradant (herein referred to as "compound **X**") of *ezetimibe*, a lipid lowering agent with the structure (3R,4S)-1-(4-fluorophenyl)-3-[(3S)-3-(4-fluorophenyl)-3-hydroxypropyl]-4-(4-hydroxyphenyl)azetidin-2-one (**1**), was published recently in this Journal [2]. Based on ^{1}H NMR, ^{13}C NMR and mass spectrometric studies, in their paper Gajjar and Shah concluded that the structure of **X** is 5-(4-fluorophenyl)-2-[(4-fluorophenylamino)-(4-hydroxyphenyl) methyl]-pent-4-enoic acid (2) (see Fig. 1). The mistake was quickly spotted by Barhate and Mohanra, who published a "Letter to the Editor" [3] in which they drew attention to the fact that structure **2** is incompatible with the NMR data provided for **X** in [2]. Following up on the observations of Barhate and Mohanra, here we note only one conspicuous detail which shows clearly why structure **2** must be incorrect: the ^{13}C spectrum of **X** lacks non-aromatic unsaturated carbon peaks. In their critical letter however Barhate and Mohanra did not propose an alternative structure for **X**. Since we also had compound **X** in our hands, in the present article we give the correct structure for **X** as based on our own detailed NMR studies. Although the structure elucidation procedure did not require sophisticated methods, we discuss the problem in some detail to avoid a similar line of thought as was made in [2].

---

* Corresponding author. Tel.: +36 1 5057055.
  E-mail address: zs.santa@richter.hu (Z. Sánta).
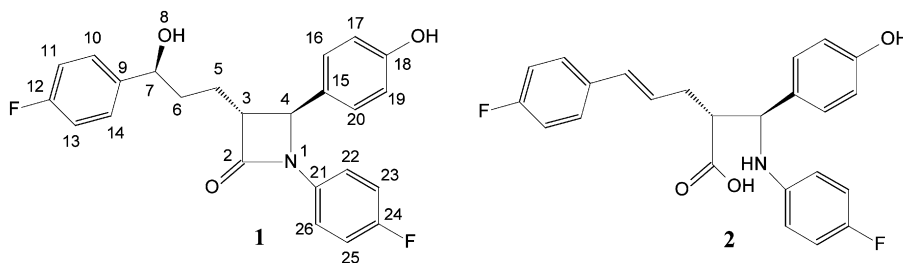
Fig. 1. Structure of *ezetimibe* (**1**) and **2**.

Our literature search disclosed that compound **X** was already separated and identified, first from its crystal structure by Swamy et al. [4] who also listed its NMR data (however, the structural identification was not based on NMR). Subsequently a detailed NMR and IR characterization was given for **X** by Filip et al. [5]. However, a careful inspection of the literature data reveals some errors and ambiguities. For example, according to our own NMR measurements performed in various solvents some of the NMR data and assignments given for **X** in [4] are incorrect. Moreover the degradant's NMR chemical shifts listed in [5] turn out to have been measured in DMSO (without the authors mentioning it and using a misleading footnote in that respect), but the discussion in the text is based on NMR data measured in CDCl$_3$. Other related literature reports NMR data for *ezetimibe* [6–8] without assignments, or again with partially wrong data and assignments [9]. Therefore we find it useful to fill the analytical gaps and to clarify the ambiguities the different authors left in their spectral data and assignments corresponding to compound **X** and the parent compound *ezetimibe* [2,4–9]. We also added ^{19}F NMR data.

2. Experimental

2.1. Thin-layer chromatography

TLC was performed using precoated Silica gel 60 F$_{254}$ TLC plates and visualized with ultraviolet light at 254 nm followed by perchloric acid dyeing reagent.

2.2. Preparation of **X**

2.2.1. By NaOH
0.82 g (2.0 mmol) *ezetimibe* (**1**) was dissolved in 50 ml methanolic sodium hydroxide solution (0.2 g NaOH in 50 ml methanol) The reaction was heated at 80 °C for 30 min. The reaction was monitored by thin-layer chromatography (EtOAc:*n*-hexane = 2:1, starting material R_f = 0.52, product R_f = 0.66). After completion, the mixture was cooled to room temperature then neutralized with 5 ml 1 M hydrochloric acid. The methanol was evaporated, the residue was diluted with 15 ml water. The crystalline product was filtered and washed with 10 ml water. Yield: 0.80 g.

2.2.2. By Bu$_4$NF
100 mg (0.24 mmol) *(3R,4S)-1-(4-Fluorophenyl)-3-[(S)-3-(4-fluorophenyl)-3-hydroxypropyl]-4-(4-hydroxyphenyl)-azetidin-2-one (ezetimibe)* was dissolved in 2 ml acetonitrile and 50 mg (0.16 mmol) tetrabutylammonium fluoride hydrate was added. The reaction was stirred at room temperature for 20 h. The reaction was monitored by TLC (EtOAc:*n*-hexane = 2:1, starting material R_f = 0.52, product R_f = 0.66). The acetonitrile was evaporated, the residue was dissolved in a mixture of 10 ml EtOAc and 10 ml 10% aqueous citric acid solution. The mixture was stirred for 15 min, and then separated. The organic layer was dried over sodium sulfate, filtered, the solvent evaporated in vacuum. The residue was crystallized from *n*-hexane. Yield: 90 mg.

2.3. NMR spectroscopy

NMR measurements were performed at 298 K on a Varian 500 MHz NMR spectrometer equipped with a HCN PFG Triple Resonance ^{13}C Enhanced Cold Probe operating at 500 MHz for ^{1}H and 125 MHz for ^{13}C, using DMSO-d_6 and CDCl$_3$ as solvent. ^{19}F measurements were performed on a Varian 400 MHz NMR spectrometer equipped with an ATB 1H/^{19}F/{^{15}N-^{31}P} PFG Probe operating at 376 MHz for ^{19}F. The chemical shifts were referenced either to TMS (^{1}H) or solvent (^{13}C, DMSO: 39.50, CDCl$_3$: 77.0 ppm). Direct ^{1}H–^{13}C, long-range ^{1}H–^{13}C, scalar and dipolar spin–spin connectivities were established from 1D ^{1}H, ^{13}C, ^{1}H–^{1}H gCOSY, ^{1}H–^{13}C gHSQC (J = 140 Hz), ^{1}H–^{13}C gHMBC (J = 8 Hz) and 1D NOESY (mix. time: 500 ms, relax. delay: 1 s) experiments, respectively. All pulse sequences were applied by using the standard spectrometer software package.

2.4. Mass spectrometry

Both low and high-resolution MS measurements were performed on a Finnigan MAT 95XP mass spectrometer using EI (electron impact) ionization (70 eV, 220 °C source temperature, perfluorokerosene reference compound).

3. Results and discussion

3.1. Alkaline degradation of ezetimibe

Although we had in hand compound **X**, we had derived it previously from an alternative synthetic process (see Section 2.2.2). Therefore we reproduced the process described in [2] exactly so as to ensure that our identification of **X** can be based on a full synthetic compatibility with Ref. [2]. As expected, the synthesis yielded **X** which could be separated by crystallisation from water (see Section 2.2.1). The purity of the sample was enough to prove the identity of the materials derived from the two processes.

3.2. Structure elucidation of compound **X**

MS and HRMS measurements showed a molecular ion peak for **X** at *m/z* 409 M$^+$, which is the same for ezetimibe and accords with the statements of [2].

For easier comparison of the data and the deductions presented in [2], we discuss the NMR spectra of **X** measured in DMSO, although the separation of the signals is much better in CDCl$_3$. In the NMR spectra recorded by us for **X** the ^{1}H NMR chemical shifts as well as the ^{13}C NMR chemical shifts accord eminently with those reported in [2], providing further proof that our compound **X** is identical with the major degradant discussed in [2]. The ^{1}H NMR spectrum of **X** showed 21 protons: 7 in the aliphatic region, 12 in the aromatic region and 2 exchangeable OH or NH protons. The number
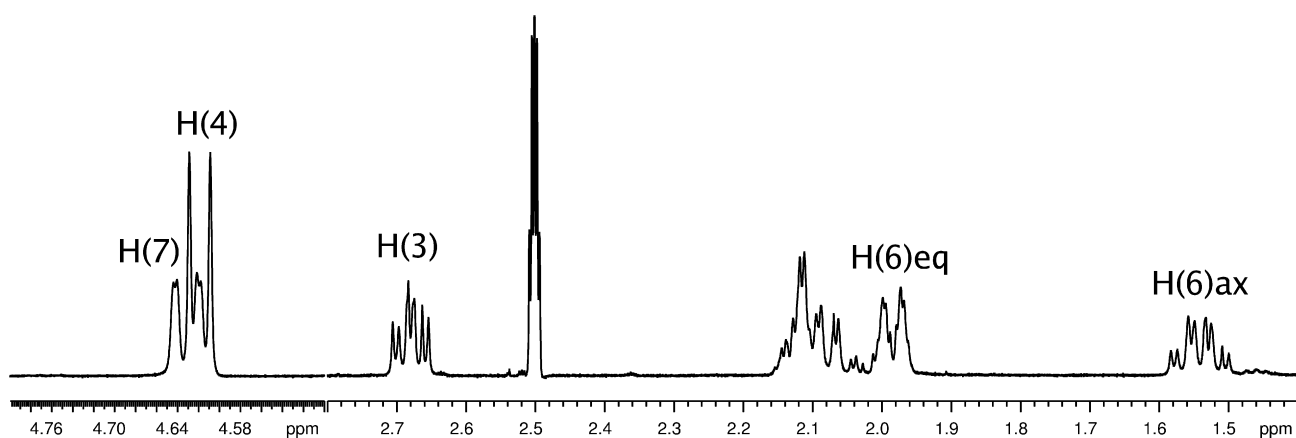
Fig. 2. ¹H NMR spectrum of **X**, aliphatic part.

of protons born by each carbon atom in **X** could be determined from an edited HSQC measurement, showing 2 CH₂-s, 3 aliphatic CH-s and 12 aromatic CH-s—in that respect nothing has changed in comparison with the starting material **1**. From this experiment we could also determine that 2 of the aliphatic CH-s are connected to a heteroatom, most probably an O, as based on their ¹³C chemical shifts being around 80 ppm; this is a new feature and suggests a cyclic rather than an open-chained structure (signal assignments are listed in Table 1). This statement is also supported by the fact that the ¹H resonances of one of the CH₂-s are far from each other (1.54 and 1.99 ppm) and show multiplicity features that are characteristic of axial and equatorial protons, respectively, located on the central carbon of a $-CH_{ax}-CH_{ax}H_{eq}-CH_{ax}CH_{eq}-$ moiety within a 6-membered cyclic system with a chair-like geometry (quartet-like and doublet-like signals). Although the ¹H signals at 4.62 and 4.63 ppm overlap, their fine coupling pattern could be conveniently analyzed in a well-resolved 500 MHz ¹H spectrum: the signal at 4.62 ppm is a doublet with a vicinal coupling of $J = 10$ Hz, and the one at 4.63 ppm is a doublet–multiplet also with a vicinal coupling of $J = 10$ Hz (Fig. 2). The whole set of aliphatic spin–spin connections can be determined from a 2D gCOSY spectrum (4.62–2.69–2.10–1.98–1.55–4.63).

The HMBC experiment showed us that the 2 CH carbons having a ¹³C chemical shift around 80 ppm must be directly connected to 2 different aromatic rings (Fig. 3, peaks 3, 4, 8 and 9) and in 2/3-bond proximity of each other (peaks 1 and 2). Likewise, according to the HMBC spectrum both of the exchangeable protons are 2 bonds away from 2 different aromatic rings (peaks 5 and 6) and one of them is also in a 2/3-bond proximity of a carboxyl derivative group (peak 7). Assuming that the structure of **X** must be closely related to *ezetimibe*, from these pieces of information we can unambiguously infer the structure of **X** to be **3** (see Fig. 4). (For an easier comparison of the assignments with those given in [2] the same skeletal numbering was used as in [2]).

The configurations of the stereocenters (i.e., C(3), C(4) and C(7)) in **3** could be readily and unambiguously deduced from the measured ¹H–¹H vicinal couplings in the tetrahydropyran ring, since the observed couplings uniquely fit the relative configurations only as indicated in **3**, with the C(3)–H$_{β,ax}$, C(4)–H$_{α,ax}$ and C(7)–H$_{α,ax}$ protons all being axial in a predominant chair conformation of the tetrahydropyran ring in which each bulky substituent is equatorial. 1D NOESY experiments also confirmed this geometry. In particular, strong NOE-s were observed between H(6)$_{β,ax}$ and Ar$_β$-H(10,14) and H(3)$_{β,ax}$ and Ar$_β$-H(16,20), but no NOE was detected between H(7)$_{α,ax}$ and H(6)$_{β,ax}$ or between H(4)$_{α,ax}$ and H(3)$_{β,ax}$. Furthermore, upon mechanistic considerations **3** is most likely derived from **1** via an S$_N$2 reaction on C(4) by the OH group (Scheme 1),
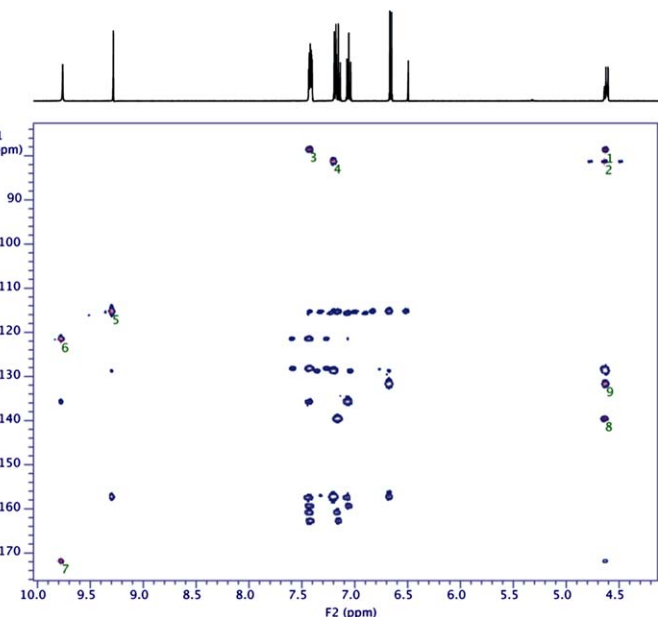
Fig. 3. Relevant part of the HMBC spectrum of **X** (The numbered peaks refer to the following correlations: (1) H4–C7; (2) H7–C4; (3) H10–C7; (4) H16–C4; (5) OH–C17; (6) NH–C22; (7) NH–CO; (8) H7–C9; (9) H4–C15.).

Fig. 4. Structure of compound **X** (**3**).

in which case C(3) and C(7) retain their configurations but C(4) is inverted. On the one hand this mechanism rationalizes the formation of **3** from **1**; on the other hand the relative configuration that follows from such a mechanism accords with what has been inferred for **3** from NMR. Moreover, since *ezetimibe* is an optically
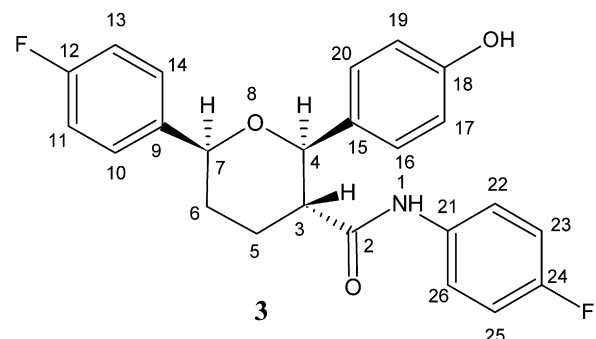
Table 1
NMR signals and assignments for the degradant (**X**) and *ezetimibe* (**1**).

Assignment	DMSO		CDCl₃[a]	
	^{1}H	^{13}C (J_{CF})	^{1}H	^{13}C (J_{CF})
Degradant (X)				
NH-1	9.76 (1H) s	–	8.14 (1H) s	–
2	–	171.3	–	171.4
3	2.69 (1H) m (~ddd J 11.1 10.0 4.4)	49.9	2.54 (1H) m (~ddd J 11.8 9.8 2.6)	51.9
4	4.62 (1H) d J 10.0	80.7	4.72 (1H) d J 10.0	81.4
5	2.02–2.15 (2H) m	28.2	ax: 2.29 (1H) qd J 13.0[b] 4.0 eq: 2.18 (1H) dm J 13.3	27.7
6	ax: 1.55 (1H) qd J 12.4[b] 4.4 eq: 1.98 (1H) dm J 12.9	32.4	ax: 1.58 (1H) qd J 13.3 4.1 eq: 1.98 (1H) dm J 13.3	32.6
7	4.63 (1H) dd J 11.2 1.8	78.0	4.62 (1H) dd J 11.5 2.2	78.9
9	–	139.0 d (3.0)	–	138.4 d (2.9)
10, 14	7.42 (2H) m	127.7 d (8.2)	7.39 (2H) m	127.2 d (7.8)
11, 13	7.16 (2H) m~t	114.8 d (21.2)	7.01 (2H) m~t	114.8 d (21.3)
12	–	161.3 d (242.6)	–	161.8 d (245)
15	–	131.2	–	131.7
16, 20	7.19 (2H) m~d	128.2	7.28 (2H) m~d	127.7
17, 19	6.66 (2H) m~d	114.7	6.78 (2H) m~d	115.2
18	–	156.7	–	156.7
21	–	135.2 d (2.5)	–	133.8 d (2.7)
22, 26	7.42 (2H) m	120.9 d (7.9)	7.26 (2H) m	122.0 d (7.8)
23, 25	7.06 (2H) m~t	115.1 d (22.2)	6.90 (2H) m~t	114.9 d (21.5)
24	–	157.9 d (240)	–	158.9 d (242.5)
Ar-OH	9.28 (1H) s	–	8.57 (1H) s	–
F	−115.6; −119.4		−115.6; −118.6	
Ezetimibe (**1**)				
2	–	167.4	–	167.7
3	3.05–3.11 (1H) m	59.4	3.05–3.11 (1H) m	60.1
4	4.80 (1H) d J 2.1	59.6	4.57 (1H) d J 2.4	61.1
5	1.69–1.78 + 1.78–1.84 (2 × 1H) m[a]	24.5	1.90–2.01 (2H) m[c]	24.9
6	1.66–1.74 (2H) m	36.4	1.84–1.94 (2H) m[c]	36.5
7	4.46–4.52 (1H) m	71.1	4.64–4.69 (1H) m	72.4
OH-8	5.29 (1H) d J 4.1	–	3.83 (1H) d J 3.9	–
9	–	142.2 d (2.9)	–	140.6 d (2.9)
10, 14	7.30 (2H) m	127.5 d (7.8)	7.30 (2H) m	127.3 d (8.1)
11, 13	7.11 (2H) m	114.7 d (21.0)	7.01 (2H) m	114.9 d (21.3)
12	–	161.0 d (242)	–	161.8 d (245)
15	–	127.9	–	127.8
16, 20	7.21 (2H) m[c]	127.6	7.15 (2H) m~d	127.0
17, 19	6.75 (2H) m~d	115.7	6.85 (2H) m~d	116.0
18	–	157.4	–	157.4
21	–	134.0 d (2.4)	–	133.9 d (2.7)
22, 26	7.20 (2H) m[c]	118.3 d (7.8)	7.25 (2H) m	118.2 d (7.8)
23, 25	7.13 (2H) m	115.8 d (23.0)	6.92 (2H) m	115.5 d (22.8)
24	–	158.0 d (240.5)	–	158.6 d (243)
Ar-OH	9.53	–	8.82	–
F	−116.4; −118.8		−115.7; −118.5	

[a] A few drops of DMSO was added for better solubility.
[b] Average coupling constant.
[c] Determined from HSQC spectrum.
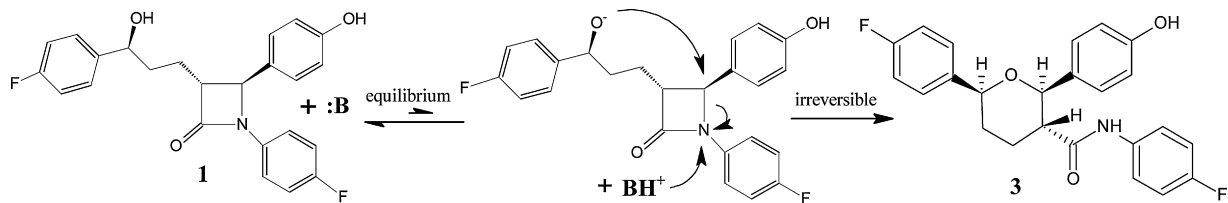
Scheme 1. Mechanism for the formation of **3** from *ezetimibe*.

pure substance with the absolute configuration shown in **1**, this mechanism tells us that C(3), C(4) and C(7) must have the absolute configuration as represented by **3**.

Based on our observations, namely, that the degradation of *ezetimibe* requires definitely a medium with proton accepting capability (water, alcohols), but being not necessarily basic (although basic conditions accelerate the degradation), on the other hand slightly acidic media avert the transformation, we came to the conclusion that the presence of the alcoholate form is essential for the reaction. Since the formation of the tetrahydropyranyl ring is rapid and irreversible, the anion formed in equilibrium only in a low population is sufficient to complete the reaction.

4. Conclusion

In the present article we gave the structure of the main degradant (**X**) of *ezetimibe* (**1**), which was incorrectly identified in a recent paper. The correct structure of **X** is

(2*R*,3*R*,6*S*)-*N*,6-bis(4-fluorophenyl)-2-(4-hydroxyphenyl)-3,4,5,6-tetrahydro-2*H*-pyran-3-carboxamide.

References

[1] E.M. Carvalho, F.A. Periera, J. Junker, How well does NMR behave in natural products structure determination? A survey of natural products published in 2007 and 2008, Poster presented at the 50th Experimental NMR Conference, March 29–April 3, 2009, Asilomar, California.

[2] A.K. Gajjar, V.D. Shah, Isolation and structure elucidation of major alkaline degradant of ezetimibe, J. Pharm. Biomed. Anal. 55 (2011) 225–229.

[3] Ch.R. Barhate, K. Mohanra, What is the degradation product of ezetimibe? J. Pharm. Biomed. Anal. 55 (2011) 1237–1238.

[4] G.Y.S.K. Swamy, K. Ravikumar, L.K. Wadhwa, R. Saxena, S. Singh, (2*R**,3*R**,6*S**)-*N*,6-Bis(4-fluorophenyl)-2-(4-hydroxyphenyl)-3,4,5,6-tetrahydro-2*H*-pyran-3-carboxamide, Acta Cryst. E 61 (2005) o3608–o3610.

[5] K. Filip, K. Bankowski, K. Sidoryk, J. Zagrodzka, M. Laszcz, K. Trzcinska, A. Szyprowska, P. Cmoch, W. Maruszak, Physicochemical characterization of ezetimibe and its impurities, J. Mol. Struct. 991 (2011) 162–170.

[6] G. Wu, Y. Wong, X. Chen, Z. Ding, A novel one-step diastereo- and enantioselective formation of *trans*-azetidinones and its application to the total synthesis of cholesterol absorption inhibitors, J. Org. Chem. 64 (1999) 3714–3718.

[7] S.B. Rosenblum, T. Huynh, A. Afonso, H.R. Davis Jr., N. Yumibe, J.W. Clader, D.A. Burnett, Discovery of 1-(4-fluorophenyl)-(3*R*)-[3-(4-fluorophenyl)-(3*S*)-hydroxypropyl]-(4*S*)-(4-hydroxyphenyl)-2-azetidinone (SCH 58235): a designed, potent, orally active inhibitor of cholesterol absorption, J. Med. Chem. 41 (1998) 973–980.

[8] L. Kvaerno, M. Werder, H. Hauser, E.M. Carreira, Synthesis and in vitro evaluation of inhibitors of intestinal cholesterol absorption, J. Med. Chem. 48 (2005) 6035–6053.

[9] B. Ramana, B.A. Sharmaa, R. Butalab, P.D. Ghugareb, A. Kumarb, Structural elucidation of a process-related impurity in ezetimibe by LC/MS/MS and NMR, J. Pharm. Biomed. Anal. 52 (2010) 73–78.

Short communication

A validated LC–MS/MS assay for the simultaneous determination of the anti-leukemic agent dasatinib and two pharmacologically active metabolites in human plasma: Application to a clinical pharmacokinetic study

Michael T. Furlong[a],[*], Shruti Agrawal[b], Dara Hawthorne[a], Michael Lago[c], Steve Unger[d], Linda Krueger[d], Bruce Stouffer[a]

[a] Bristol-Myers Squibb, Research and Development, Analytical and Bioanalytical Development, Route 206 & Province Line Road, Princeton, NJ 08543, USA
[b] Bristol-Myers Squibb, Research and Development, Discovery Medicine and Clinical Pharmacology, Route 206 & Province Line Road, Princeton, NJ 08543, USA
[c] Bristol-Myers Squibb, Research and Development, Discovery Chemical Synthesis-Radiochemistry, Route 206 & Province Line Road, Princeton, NJ 08543, USA
[d] Worldwide Clinical Trials, Drug Development Solutions, Bioanalytical Sciences, 8609 Cross Park Dr, Austin, TX 78754, USA

A B S T R A C T

Dasatinib (Sprycel®) is a potent antitumor agent prescribed for patients with chronic myeloid leukemia (CML). To enable reliable quantification of dasatinib and its pharmacologically active metabolites in human plasma during clinical testing, a sensitive and reliable liquid chromatography–tandem mass spectrometry (LC–MS/MS) method was developed and validated. Samples were prepared using solid phase extraction on Oasis HLB 96-well plates. Chromatographic separation was achieved isocratically on a Luna phenyl–hexyl analytical column. Analytes and the stable labeled internal standards were detected by positive ion electrospray tandem mass spectrometry. The assay was validated over a concentration range of 1.00–1000 ng/mL for dasatinib and its two active metabolites. Intra- and inter-assay precision values for replicate QC control samples were within 5.3% for all analytes during the assay validation. Mean QC control accuracy values were within ±9.0% of nominal values for all analytes. Assay recoveries were high (>79%) and internal standard normalized matrix effects were minimal. The three analytes were stable in human plasma for at least 22 h at room temperature, for at least 123 days at −20 °C, and following at least six freeze–thaw cycles. The validated method was successfully applied to the quantification of dasatinib and two active metabolites in a human pharmacokinetic study.

© 2011 Elsevier B.V. All rights reserved.

1. Introduction

Approximately 5000 people in the USA alone are diagnosed each year with chronic myeloid leukemia (CML) [1]. Genetic insights into this malignancy facilitated the identification of the Bcr–Abl kinase as a tractable drug target to combat CML [2]. The introduction of imatinib (Gleevec™) as the first marketed inhibitor of Bcr–Abl has resulted in substantially improved prognoses for patients afflicted with CML [3,4]. Unfortunately, many patients are either intolerant to or develop resistance against imatinib [5,6]. Many such patients have benefited from the introduction of 2nd-generation Bcr–Abl inhibitors such as dasatinib (Spyrycel®) and nilotinib (Tasigna®) [7]. Both of these agents are pharmacologically active in most instances of imatinib-resistant CML [7]. Although originally approved to treat imatinib-resistant or intolerant CML patients, dasatinib has recently been approved as a first line therapy as a consequence of superior performance in a comparative efficacy trial with imatinib [8].

Dasatinib is extensively metabolized in humans via oxidative (Phase I) and conjugative (Phase II) pathways [9]. Several metabolites of dasatinib possess significant anti-leukemic activity. The N-dealkylated metabolite, M4, is approximately equipotent compared to dasatinib, while the N-oxide metabolite, M5, is approximately 10-fold less potent [9]. Given the pharmacological activity of M4 and M5, it was imperative that metabolites M4 and M5 be quantified along with dasatinib itself during clinical development in order to fully understand their contribution to the efficacy profile of this compound. Two validated LC–MS/MS methods have recently been described to support simultaneous quantification of dasatinib and other Brc–Abl inhibitors in human plasma [10,11]. However, neither of these assays was developed to quantify dasatinib metabolites. Herein, we report the development, validation and successful application of the first LC–MS/MS assay capable of quantifying dasatinib and two pharmacologically active metabolites.

* Corresponding author. Tel.: +1 609 252 5069; fax: +1 609 252 3315.
E-mail address: michael.furlong@bms.com (M.T. Furlong).
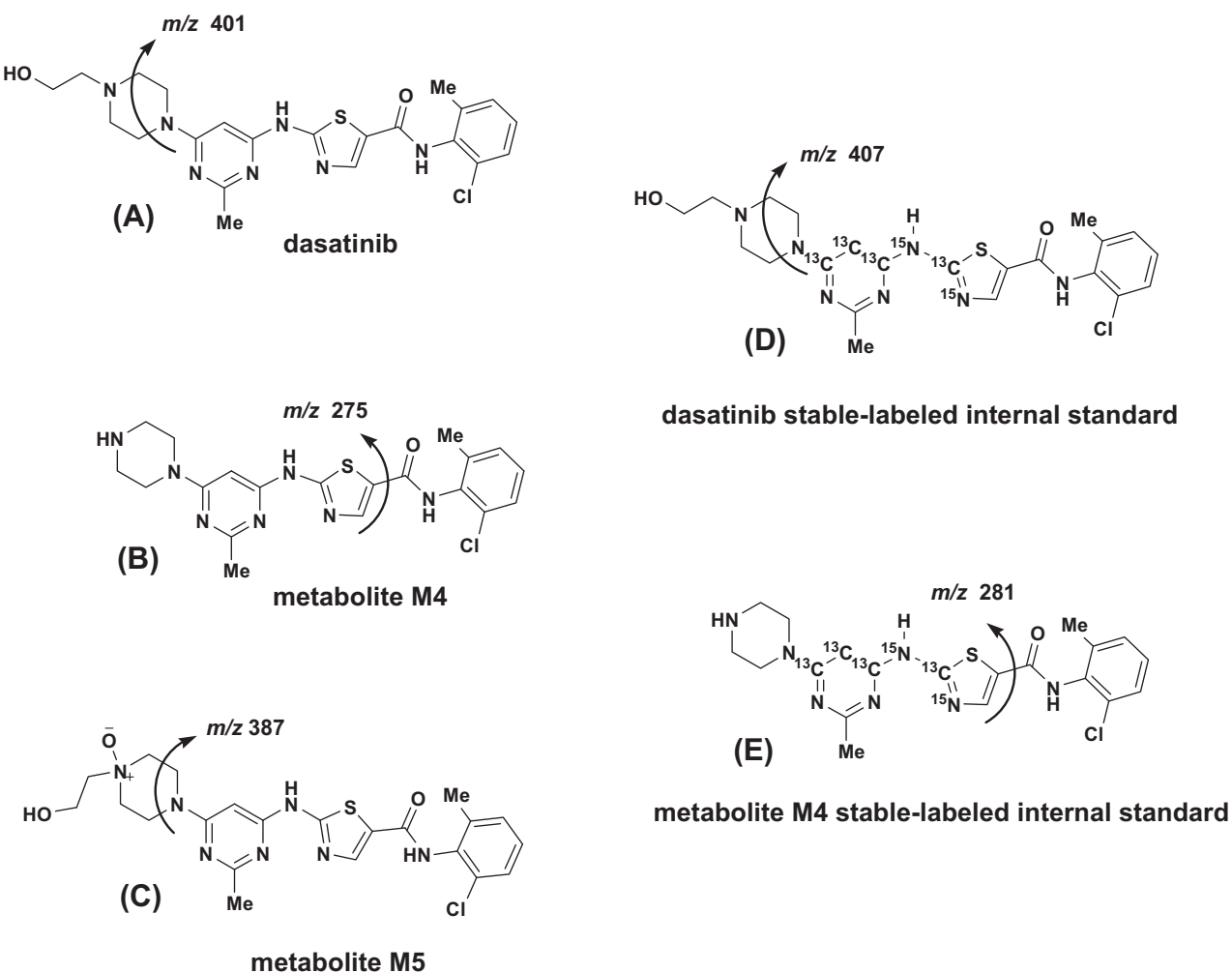
Fig. 1. Chemical structures of analytes and internal standards. The stable-labeled internal standard for dasatinib was used to quantify dasatinib and M5. Arrows indicate the proposed fragmentation pathways leading to the product ions monitored in the assay.

2. Experimental

2.1. Materials and reagents

Dasatinib, metabolites M4 and M5, and stable isotope-labeled internal standards were synthesized at Bristol-Myers Squibb Research & Development (Fig. 1). Control human K_3EDTA plasma was purchased from Bioreclamation Inc. (Hicksville, NY, USA). Reagent grade ammonium acetate and phosphoric acid were purchased from Sigma-Aldrich (St. Louis, MO, USA). HPLC grade methanol was purchased from Mallinckrodt (St. Louis, MO). Formic acid (90%) was purchased from Fisher (Pittsburgh, PA, USA). Deionized water was obtained using a Continental Research Grade UF/Polishing System Model #LBPUO 1002 (Continental Water Systems Corporation, US Filter, Houston, TX, USA).

2.2. Liquid chromatography–tandem mass spectrometry

Experiments were conducted using a Shimadzu LC-10 AT pump (Columbia, MD, USA), and a Perkin Elmer Series 200 autosampler (Norwalk, CT, USA) coupled to an MDS-Sciex API 4000 triple quadrupole mass spectrometer equipped with a TurboIonspray™ source (Concord, Ontario, Canada). All evaluations were performed at unit resolution in the positive ion electrospray (ESI) mode. Chromatographic separation was achieved on a phenyl–hexyl Luna column (50 mm × 2.0 mm 3 micron particle size (Phenomenex, Torrance, CA, USA). The mobile phase composition was ammonium acetate (pH 3.0; 0.1 M)–water–methanol (10:37:53, v:v:v). Following sample injection (5 μl) onto the LC–MS/MS system, analytes were separated under isocratic conditions at a flow rate of 0.3 mL/min. The cycle time of the method was 3.0 min per injection.

Optimal mass spectrometer parameters employed for detection of all analytes and internal standards detection were as follows: ionspray voltage (IS) +5000 V, temperature 400 °C, nebulizer gas (GS1) 50, TurboIonSpray gas (GS2) 75, collision-activated dissociation (CAD) gas 10, collision gas 6, declustering potential (DP) +80 V, and entrance potential (EP) +10 V. Collision energy (CE) settings for dasatinib, M4, M5, $[^{13}C_4, ^{15}N_2]$ stable isotope-labeled dasatinib, and $[^{13}C_4, ^{15}N_2]$ stable-labeled M4 were 39, 44, 43, 43, and 44 eV, respectively. Collision cell exit potential (CXP) settings for dasatinib, M4, M5, $[^{13}C_4, ^{15}N_2]$ stable isotope-labeled dasatinib, and $[^{13}C_4, ^{15}N_2]$ stable isotope-labeled M4 were 6, 17, 26, 10, and 17 eV, respectively. The MRM (Multiple Reaction Monitoring) transitions were m/z 488 → 401 for dasatinib, m/z 444 → 275 for M4, m/z 504 → 387 for M5, m/z 494 → 407 for $[^{13}C_4, ^{15}N_2]$ stable isotope-labeled dasatinib, and m/z 450 → 481 for $[^{13}C_4, ^{15}N_2]$ stable isotope-labeled M4. Dwell times were 200 milliseconds for dasatinib, M4 and M5; 150 millisecond dwell times were used for the stable isotope-labeled internal standards.

2.3. LC–MS/MS data acquisition and processing

MRM data acquisition, chromatographic peak integration, and chromatographic review were performed using Sciex Analyst, version 1.4 software. Data regression using peak area ratios of the analyte to the internal standard was carried out using Watson Laboratory Information Management Software (Thermo Fisher Scientific, Waltham, MA, USA). Calibration standards were fitted to a $1/x^2$ weighted linear regression model and the equation of this curve was then used to calculate the predicted concentrations in all samples within the analytical runs. Intra- and inter-assay assay CVs for validation analytical run QC samples were calculated within Watson using a one-way analysis of variance (ANOVA).

2.4. Preparation of calibration standards and quality control (QC) samples

Combined analyte spiking solutions were prepared in methanol. Calibration standards and QC samples were prepared by adding appropriate volumes of combined analyte spiking solutions to blank human plasma. The final calibration standard concentrations were 1, 2, 5, 10, 50, 100, 250, 500, 750, and 1000 ng/mL. Final QC samples concentrations were 1, 3, 35, 400, 800, and 5000 ng/mL.

2.5. Sample preparation

The combined internal standard working solution used during sample extraction was prepared fresh daily in 0.5% aqueous phosphoric acid at a concentration of 100 ng/mL for each internal standard ([$^{13}C_4$,$^{15}N_2$] stable-labeled dasatinib and [$^{13}C_4$,$^{15}N_2$] stable-labeled M4). Plasma samples were extracted by solid phase extraction (SPE) using Oasis HLB 96-well micro-elution plates (Waters Corporation, Milford, MA, USA) as follows: Prior to SPE, a 200 μL aliquot of combined internal standard working solution was added to all plasma samples except matrix blank samples, to which a 200 μL aliquot of 0.5% aqueous phosphoric acid solution was added. SPE plates were conditioned sequentially with 200 μL of methanol and 200 μL of 0.5% aqueous phosphoric acid. Plasma samples were applied to the conditioned plates and allowed to elute slowly via gravity. The plates were sequentially washed with 0.5% phosphoric acid and methanol:water (10:90, v:v). Plates were eluted by gravity with 50 μL of methanol. The eluted samples were diluted with 75 μL of water and submitted for LC–MS/MS analysis.

2.6. LC–MS/MS assay validation

Validation of the LC–MS/MS method was carried out in accordance with the FDA Guidance for Industry – Bioanalytical Method Validation [12] and Bristol-Myers Squibb Standard Operating Procedures. Accuracy, precision and sensitivity were established in three core analytical runs for dasatinib and M5; a fourth analytical run was included for M4 due to insufficient M4 dilution QC samples (3/6) passing for accuracy in one of the three core analytical runs. The LLOQ was evaluated by spiking the three analytes into 6 unique human plasma lots at 1.00 ng/mL followed by extraction and quantification. Specificity was assessed for potential matrix interferences in six lots of blank human plasma by extraction and inspection of the resulting chromatograms for interfering peaks at the retention times of the 3 analytes and internal standards. Specificity was similarly assessed for potential internal standard-derived interferences using six lots of internal standard-spiked blank plasma. The recovery of dasatinib, M4, M5, and the internal standards from human plasma during extraction was determined at 50 and 800 ng/mL by comparing the response ratios in human plasma samples spiked with the analytes prior to extraction with those spiked post-extraction. The matrix effect was determined

at concentrations of 50 and 800 ng/mL for dasatinib, M4, M5, and the internal standards by dividing the analyte peak area responses in human plasma spiked post-extraction by the analyte responses spiked in reconstitution solution. Capability of dilution was evaluated using QC samples that were prepared at a concentration of 5000 ng/mL and subsequently diluted ten-fold with blank human plasma prior to analysis.

2.7. Stability evaluation

To assess the stability of the three analytes in plasma, QC samples were subjected to the following stability stress conditions: short-term room temperature, freeze/thaw cycling (−20 to 25 °C) and long-term frozen stability (−20 °C). Reinjection reproducibility was also assessed for extracted samples by reinjection of an entire analytical run after storage at room temperature. To assess the potential for analyte degradation during study sample blood collection and plasma harvesting, the stability of all three analytes in blood was assessed at +4 °C and room temperature. The stability of the analytes in stock solutions during short and long-term storage at +4 °C and at room temperature was also assessed.

2.8. Pharmacokinetic study

To demonstrate the utility of the validated LC–MS/MS assay, results from a clinical study conducted in healthy subjects are presented here. Subjects ($n = 20$) received a 100 mg dasatinib dose on Day 1 after an overnight fast. Blood samples were collected at 0, 0.5, 1, 1.5, 2, 3, 4, 5, 6, 8, 12 and 24 h from a peripheral vein using Becton Dickinson Vacutainers, which contained K_3EDTA as the anticoagulant. Plasma was harvested via centrifugation and stored at −20 °C until analysis. Plasma samples were analyzed for dasatinib, M4 and M5. Single dose pharmacokinetic parameters were derived from plasma concentration–time data by noncompartmental methods using Kinetica™ 4.2 in eToolbox version 2.4.

3. Results and discussion

3.1. Assay validation and stability evaluation

Validation analytical run calibration curves were linear over the concentration range 1.00–1000 ng/mL for dasatinib as well as metabolites M4 and M5. The mean linear regression equations of the calibration curves for dasatinib, M4 and M5 were: $y = 0.003253(\pm 0.000468)\ x + 0.000296(\pm 0.000110)$, $y = 0.00444(\pm 0.000508)\ x + (0.000117 \pm 0.000273)$ and $y = (0.002069 \pm 0.000125)\ x + (0.000014 \pm 0.000103)$ respectively, where y was the concentration of the analyte and x was the peak area ratio of the analyte to the internal standard. Correlation coefficients (R^2) were >0.9951 for all analytes in all validation analytical runs, indicating a good fit of the calibration data to the regression lines. Precision and accuracy data obtained for quality control samples from the core validation analytical runs are summarized in Table 1. Stability data are summarized in Table 2. Plasma QC samples were considered to be stable under the stress conditions tested if the observed concentrations of at least 2/3 of the stressed QC replicates were within ±15.0% of their respective theoretical values. Stock solutions were considered to be stable under the stress conditions tested if the internal standard-normalized peak area response of the stressed solution differed by ≤5% from the response of a freshly prepared stock solution.

Representative LLOQ samples for dasatinib, as well as metabolites M4/M5, are shown in Fig. 2. Analysis of six unique lots of human plasma showed no significant interfering peaks at the retention times of any of the analytes or internal standard samples. Minor matrix-derived peaks, even when present, were considered to be

Table 1
Quality control ANOVA summary for dasatinib and metabolites M4/M5.

Nominal concentration (ng/mL)	LLOQ 1.00			QCL 3.00			QCM 400			QCH 800			QCDil 5000		
	Dasatinib	M4	M5	Dasatinib	M4	M5	Dasatinib	M4	M5	Dasatinib	M4	M5	Dasatinib	M4	M5
Mean observed conc.	0.94	0.97	0.99	2.73	2.83	2.74	400	422	405	791	841	823	5340	5520	5620
%DIFF	−6.0	−3.0	−1.0	−9.0	−5.7	−8.7	0.1	5.5	1.3	−1.2	5.1	2.9	6.8	10.4	12.5
Between run precision (%CV)	5.1	3.1	3.0	0.9	3.2	4.2	2.9	0.0[a]	5.3	3.9	1.8	3.7	5.9	0.6	1.1
Within run precision (%CV)	4.5	7.9	5.9	3.4	3.9	5.3	0.9	2.0	1.4	3.0	3.2	3.1	8.9	8.0	5.3
Total variation (%CV)	6.8	8.5	6.6	3.5	5.1	6.8	3.0	2.0	5.5	4.9	3.7	4.8	10.7	8.0	5.4
n	18	24	18	18	24	18	18	24	18	18	24	18	18	24	18
Number of runs	3	4	3	3	4	3	3	4	3	3	4	3	3	4	3

%CV indicates %coefficient of variation; %DIFF indicates %difference (inter-run accuracy); QCL indicates low quality control concentration; QCM indicates medium quality control concentration; QCH indicates high quality control concentration; QCDil indicates dilution quality control concentration.

[a] No significant additional variation was observed as a result of performing the assay in different runs.

insignificant because their peak areas were less than or equal to 20% of the analyte peak area of the corresponding LLOQ sample. No interferences were observed in blank plasma lots spiked with internal standards. Mean recoveries were 86.5%, 100.6%, 83.3%, 79.2% and 85.8% for dasatinib, M4, M5, $[^{13}C_4,^{15}N_2]$ dasatinib and $[^{13}C_4,^{15}N_2]$ M4, respectively. Internal standard-normalized matrix effects were minimal for all analytes and internal standards. Matrix effect values were 0.960, 0.948, 0.985, 0.959 and 0.992 for dasatinib, M4, M5, $[^{13}C_4,^{15}N_2]$ dasatinib and $[^{13}C_4,^{15}N_2]$ M4, respectively.

3.2. Evaluation of potential matrix variability

Evaluation of precision and accuracy in unique matrix lots at the LLOQ during validation provides insight into the ability of an internal standard to normalize lot to lot or subject to subject variations in analyte response. When quantifying small molecule analytes in complex biological matrices such as plasma, stable isotope-labeled internal standards are typically preferred over structural analog internal standards. This is because the very similar
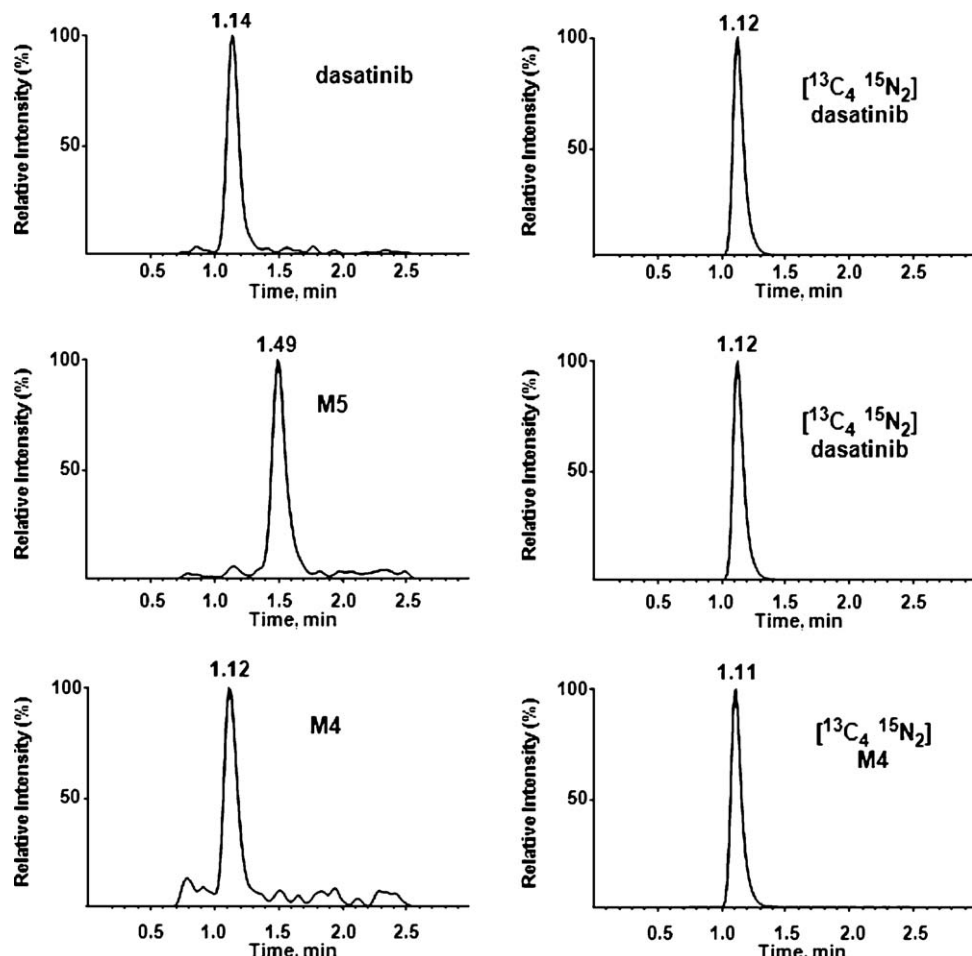
Fig. 2. Representative chromatograms at the lower limit of quantification (1.00 ng/mL). Left panels – analytes; right panels – internal standards.

Table 2
Summary of stability data for dasatinib, metabolite M4 and metabolite M5.

Conditions	Minimum stability
Short term room temperature stability in human plasma	22 h
Frozen stability in human plasma (−20 °C)	123 days
Freeze–thaw stability in human plasma (−20 to 25 °C)	6 cycles
Reinjection reproducibility of extracted samples (room temperature)	135 h
Stability in human blood (+4 °C and room temperature)	30 min
Stock solution in methanol – storage stability (+4 °C)	166 days
Stock solution in methanol – storage stability (room temperature)	6 h
Combined working IS solution in 0.5% phosphoric acid (room temperature)	24 h

chemical properties and chromatographic retention times of the analyte and stable isotope-labeled internal standard are believed to more reliably facilitate a proportional change in detector response for both compounds caused by lot- or subject-dependent changes in extraction efficiency and/or matrix suppression/enhancement components [13,14]. For the method validation and pharmacokinetic study described herein, stable-labeled internal standards were available for dasatinib and metabolite M4; however no stable-labeled internal standard was available for metabolite M5. Therefore, the $[^{13}C_4,^{15}N_2]$ stable-labeled internal standard for dasatinib was used to quantify both M5 and dasatinib. Based on their distinct chemical structures (Fig. 1) and distinct chromatographic retention times (Fig. 2), the reliability of $[^{13}C_4,^{15}N_2]$ dasatinib as an internal standard for M5 had to be carefully evaluated.

Table 3 summarizes the results of the matrix variability evaluations carried out at the LLOQ (1.00 ng/mL) of all three analytes. As expected, good accuracy and precision was observed for dasatinib and metabolite M4, both of which were evaluated using their stable-labeled analog internal standards. Metabolite M5 also showed favorable precision and accuracy results despite not having the benefit of a stable-isotope labeled internal standard. These data indicated that quantification of all three analytes would not be adversely affected by subject to subject variability in extraction efficiency and/or matrix effects during pharmacokinetic study samples analysis.

3.3. Application of the validated LC–MS/MS method to a human pharmacokinetic study

Fig. 3 shows mean (±SD) plasma-concentration time profiles for dasatinib, metabolite M4 and metabolite M5, along with their corresponding single dose pharmacokinetic parameters in healthy subjects. The mean exposures (±SD) of M4 and M5, relative to dasatinib, as calculated by ratio of individual AUC0-∞ values, were 3.3

Table 3
Matrix variability evaluation in multiple plasma lots at the lower limit of quantification (1.00 ng/mL).

Plasma lot number	LLOQ (1.00 ng/mL)		
	Dasatinib	M4	M5
1	0.92	0.95	1.11
2	0.91	0.85	1.13
3	0.94	1.06	1.16
4	0.92	0.91	1.08
5	0.89	0.92	1.04
6	0.95	0.96	1.04
Mean observed conc.	0.92	0.94	1.09
%DIFF	−7.8	−5.8	9.3
S.D.	0.021	0.070	0.049
%CV	2.3	7.4	4.5

%DIFF: %difference; S.D.: standard deviation: %CV: %coefficient of variation.

Parameter	Dasatinib	M4	M5
Cmax (ng/mL)	85.6 (36)	4.0 (52)	2.7 (42)
AUC$_{0-\infty}$ (ng.h/mL)	294.0 (33)	19.9 (43)	16.7 (43)
Tmax (h)	1.0 (0.5-3.0)	1.5 (1.0-4.0)	1.8 (1.5-6.0)

Fig. 3. Mean (+SD) plasma concentration–time profiles and pharmacokinetic data of dasatinib, M4 and M5 following administration of dasatinib to healthy subjects. Data were obtained from N = 20 subjects. C_{max} and AUC0-∞ data are represented as geometric means (%CV) and T_{max} is represented as median (minimum–maximum).

(±0.9)% and 5.6 (±1.5)%, respectively. These results demonstrated that M4 and M5 are minor metabolites of dasatinib and therefore do not contribute significantly to clinical efficacy. These trends were seen in this pharmacokinetic study and in other studies during clinical development of this drug.

4. Conclusion

In summary, development, validation and application of the LC–MS/MS assay described in this report was critical in demonstrating that despite the potent intrinsic anti-leukemic activity of metabolites M4 and M5, their relatively low observed exposures in dasatinib-treated cancer patients ensured that these metabolites would likely not contribute meaningfully to the efficacy of this compound.

References

[1] American Cancer Society, Cancer Facts & Figures, 2010, p. 14.
[2] Y. Chen, C. Peng, D. Li, S. Li, Molecular and cellular bases of chronic myeloid leukemia, Protein Cell 1 (2010) 124–132.
[3] H. Brenner, A. Gondos, D. Pulte, Recent trends in long-term survival of patients with chronic myelocytic leukemia: disclosing the impact of advances in therapy on the population level, Haematologica 93 (2008) 1544–1549.
[4] A. Hochhaus, S.G. O'Brien, F. Guilhot, B.J. Druker, S. Branford, L. Foroni, J.M. Goldman, M.C. Mueller, J.P. Radich, M. Rudoltz, M. Mone, I. Gathmann, T.P. Hughes, R.A. Larson, Six-year follow-up of patients receiving imatinib for the first-line treatment of chronic myeloid leukemia, Leukemia 23 (2009) 1054–1061.
[5] H.M. Kantarjian, M. Talpaz, S. O'Brien, F. Giles, G. Garcia-Manero, S. Faderl, D. Thomas, J. Shan, M.B. Rios, J. Cortes, Dose escalation of imatinib mesylate can overcome resistance to standard-dose therapy in patients with chronic myelogenous leukemia, Blood 101 (2003) 473–475.
[6] B.J. Druker, F. Guilhot, S.G. O'Brien, I. Gathmann, H. Kantarjian, N. Gattermann, M.W.N. Deininger, R.T. Silver, J.M. Goldman, R.M. Stone, F. Cervantes, A. Hochhaus, B.L. Powell, J.L. Gabrilove, P. Rousselot, J. Reiffers, J.J. Cornelissen, T. Hughes, H. Agis, T. Fischer, G. Verhoef, J. Shepherd, G. Saglio, A. Gratwohl, J.L.

Nielsen, J.P. Radich, B. Simonsson, K. Taylor, M. Baccarani, C. So, L. Letvak, R.A. Larson, Five-year follow-up of patients receiving imatinib for chronic myeloid leukemia, N. Engl. J. Med. 355 (2006) 2408–2417.

[7] B. Stein, B.D. Smith, Treatment options for patients with chronic myeloid leukemia who are resistant to or unable to tolerate imatinib, Clin. Ther. 32 (2010) 804–820.

[8] H. Kantarjian, N.P. Shah, A. Hochhaus, J. Cortes, S. Shah, M. Ayala, B. Moiraghi, Z. Shen, J. Mayer, R. Pasquini, H. Nakamae, F. Huguet, C. Boque, C. Chuah, E. Bleickardt, M.B. Bradley-Garelik, C. Zhu, T. Szatrowski, D. Shapiro, M. Baccarani, Dasatinib versus imatinib in newly diagnosed chronic-phase chronic myeloid leukemia, N. Engl. J. Med. 362 (2010) 2260–2270.

[9] L.J. Christopher, D. Cui, C. Wu, R. Luo, J.A. Manning, S.J. Bonacorsi, M. Lago, A. Allentoff, F.Y.F. Lee, B. McCann, S. Galbraith, D.P. Reitberg, K. He, A. Barros Jr., A. Blackwood-Chirchir, W.G. Humphreys, R.A. Iyer, Metabolism and disposition of dasatinib after oral administration to humans, Drug Metab. Dispos. 36 (2008) 1357–1364.

[10] A. Haouala, B. Zanolari, B. Rochat, M. Montemurro, K. Zaman, M.A. Duchosal, H.B. Ris, S. Leyvraz, N. Widmer, L.A. Decosterd, Therapeutic Drug Monitoring of the new targeted anticancer agents imatinib, nilotinib, dasatinib, sunitinib, sorafenib and lapatinib by LC tandem mass spectrometry, J. Chromatogr. B: Analyt. Technol. Biomed. Life Sci. 877 (2009) 1982–1996.

[11] S. De Francia, A. D'Avolio, F. De Martino, E. Pirro, L. Baietto, M. Siccardi, M. Simiele, S. Racca, G. Saglio, F. Di Carlo, G. Di Perri, New HPLC-MS method for the simultaneous quantification of the antileukemia drugs imatinib, dasatinib, and nilotinib in human plasma, J. Chromatogr. B: Analyt. Technol. Biomed. Life Sci. 877 (2009) 1721–1726.

[12] FDA Guidance for Industry, Bioanalytical Method Validation, 2001.

[13] I. Fu, E.J. Woolf, B.K. Matuszewski, Effect of the sample matrix on the determination of indinavir in human urine by HPLC with turbo ion spray tandem mass spectrometric detection, J. Pharm. Biomed. Anal. 18 (1998) 347–357.

[14] E. Stokvis, H. Rosing, J.H. Beijnen, Stable isotopically labeled internal standards in quantitative bioanalysis using liquid chromatography/mass spectrometry: necessity or not? Rapid Commun. Mass Spectrom. 19 (2005) 401–407.

Short communication

A stability indicating simultaneous dual wavelength UV–HPLC method for the determination of potential impurities in fampridine active pharmaceutical ingredient

Saji Thomas*, Sanjeev Shandilya, Amber Bharti, Ashutosh Agarwal

Jubilant Life Sciences Ltd., Analytical Research Department, R&D Centre, C-26, Sector-59, Noida, Uttar Pradesh 201 301, India

ABSTRACT

A novel, sensitive, stability indicating simultaneous dual wavelength reverse phase UV–HPLC method has been developed for the quantitative determination of potential impurities of fampridine active pharmaceutical ingredient. Efficient chromatographic separation was achieved on a C18 stationary phase in gradient mode and quantitation by ultraviolet dual wavelength detection. The method was validated according to ICH guidelines with respect to specificity, precision, linearity and accuracy. Regression analysis showed correlation coefficient value greater than 0.999 for fampridine and its seven impurities. Detection limit as low as 0.003% was achieved for fampridine *N*-oxide and 0.01% for other impurities. Accuracy of the method was established based on the recovery obtained between 93.3% and 110.0% for all impurities. The method was found to be specific, selective to the degradation products and robust. Peak purity analysis by PDA detector confirmed the specificity of the method. Major degradation of the drug substance was found to occur under oxidative stress conditions to form fampridine *N*-oxide.

© 2011 Elsevier B.V. All rights reserved.

1. Introduction

Dalfampridine is the first drug approved in the United States by USFDA to improve walking in patients with multiple sclerosis and is chemically known as 4-aminopyridine or fampridine. Ampyra® is an extended release tablet formulation of dalfampridine which was previously called Fampridine-SR. Fampridine is a potassium channel-blocker that enhances conduction in focally demyelinated axons, improves synaptic transmission and potentiates muscle contraction. It has shown efficacy in patients with all five major types of multiple sclerosis namely relapsing, remitting, secondary progressive, progressive relapsing and primary progressive [1–4].

A HPLC method has been reported in literature for the quantitative determination of fampridine in pharmaceutical formulations [5]. However extensive survey revealed that no stability indicating HPLC method has been reported including major pharmacopoeias such as USP, EP, JP and BP for the quantitative determination of potential impurities of fampridine active pharmaceutical ingredient. Therefore it was felt necessary to develop an accurate, rapid, specific and stability indicating method for the determination of potential impurities of fampridine. The present ICH drug stability test guideline [6] suggests that stress studies should be carried out on a drug substance to establish its inherent stability characteristics, leading to separation of degradation impurities and hence supporting the suitability of the proposed analytical procedure, which must be fully validated [7,8].

The presence of impurities in active pharmaceutical ingredient (API) can have a significant impact on the quality, safety and efficacy of drug products. Therefore, it is important to have a stability indicating validated method for the quantitative determination of potential impurities in the drug substance.

The present work deals with method development, method validation and forced degradation study of fampridine. One of the impurities was found to have absorbance at higher wavelength hence simultaneous dual wavelength detection was proposed. To the best of our knowledge, no LC methods have been reported so far for the impurity profile study of fampridine active pharmaceutical ingredient.

2. Experimental

2.1. Materials and chemicals

Sample of fampridine API (Batch No. FAM/11001), standards of Imp-6, Imp-7 were obtained from Chemical Research Department

Table 1

Fampridine

List of potential impurities in fampridine.

S. no.	Name	Structure	Mol. wt	Assigned code	Source
1	Isoniacin		123.03	Imp-1	Process impurity
2	Niacin		123.03	Imp-2	Process impurity
3	Isonicotinamide		122.05	Imp-3	Process impurity
4	3-Aminopyridine		94.05	Imp-4	Isomeric impurity
5	2-Aminopyridine		94.05	Imp-5	Isomeric impurity
6	Fampridine-N-oxide		110.05	Imp-6	Oxidative degradant
7	3-Hydroxy-4-aminopyridine		110.05	Imp-7	Metabolite

of Jubilant Life Sciences Limited (Noida, India). Imp-1, Imp-2, Imp-3, Imp-4 and Imp-5 were purchased from Sigma Aldrich Corporation (St. Louis, MO, USA). Deionized water was prepared using a Milli-Q plus water purification system from Millipore (Bedford, MA, USA). HPLC grade methanol, acetonitrile, 1-octane sulphonic acid sodium salt monohydrate, ammonium acetate, orthophosphoric acid, and triethylamine were purchased from Qualigens India Limited (Mumbai, India).

2.2. High performance liquid chromatography

Samples were analysed on a Waters alliance 2690 separation module equipped with 2487 UV detector (Waters Corporation, Milford, MA, USA) using a Xterra RP18 (250 mm × 4.6 mm, particle size 5 μm, Waters Corporation, Milford, MA, USA). The mobile phase consisted of a mixture of A, 10 mM 1-octane sulphonic acid sodium salt monohydrate, 10 mM ammonium acetate and 0.1% triethylamine adjusted to pH 4.00 ± 0.05 with ortho phosphoric acid–methanol (95:5, v/v) and B, methanol–mobile phase A (80:20, v/v) with a timed gradient programme (T_{min}A:B): $T_0$97:3, T_{15}90:10, T_{30}70:30, T_{35}97:3, and T_{60}97:3. The injection volume was 20 μL for a sample concentration of 0.75 mg/mL prepared in mobile phase-A. Detector wavelength was fixed at 240 nm and

282 nm and the column was maintained at 40 °C throughout the analysis.

2.3. Photo stability

Photo stability studies were carried out using a photo stability chamber model TP 0000090G (Thermo Lab equipments Pvt. Ltd., Mumbai, India). Study was performed on dark control and photolytic exposed sample in a way to get the minimum exposure of 1.2 million lux hours for light and 200 W h/m² for ultraviolet region.

2.4. Preparation of stock solution for method validation

A test preparation of 750 μg/mL of fampridine API sample was prepared by dissolving the appropriate amount in mobile phase-A. A stock solution of impurities was prepared by dissolving 7.5 mg each of Imp-1, Imp-2, Imp-3, Imp-4, Imp-5, Imp-6, Imp-7 and 7.5 mg of fampridine in 20 mL of mobile phase-A and further diluted 5–100 mL with mobile phase-A. From this stock solution a standard solution containing 1.125 μg/mL of each impurity and 1.125 μg/mL of fampridine was prepared. This standard solution was also used for checking solution stability and robustness parameters.

Table 2
Method validation summary report.

Parameter	Impurity-1	Impurity-2	Impurity-3	Impurity-4	Impurity-5	Impurity-6	Impurity-7	Fampridine
System suitability								
RT	2.77	2.99	4.97	10.65	14.69	5.99	18.49	11.97
RRT	0.23	0.25	0.42	0.89	1.23	0.50	1.54	1.00
R_s	–	1.31	9.85	14.71	5.30	3.89	8.27	2.92
N	4469	5278	8509	17,642	17,950	6159	25,179	6927
T	1.03	1.18	1.09	1.05	1.09	1.09	1.02	1.76
RF	1.92	2.79	2.29	0.67	1.13	0.23	1.25	1.00
Linearity								
r	0.9999	0.9999	0.9999	0.9998	0.9999	1.0000	0.9998	0.9999
Slope	181,191	124,531	151,834	521,853	308,426	956,989	278,843	347,526
Intercept	−45	−224	63	−443	−277	−142	−1126	−159
Detection limit (%)	0.01	0.01	0.01	0.01	0.01	0.003	0.01	0.01
Quantitation limit (%)	0.03	0.03	0.03	0.03	0.03	0.01	0.03	0.03
Precision % RSD (n = 6)	1.17	1.89	2.73	0.77	3.42	0.81	2.39	1.41
Accuracy at QL level (n = 3)								
Amount added (%)	0.030	0.033	0.030	0.030	0.030	0.010	0.030	0.030
Amount recovered (%)	0.029	0.033	0.029	0.028	0.028	0.011	0.028	0.030
% recovery	96.67	100.00	96.67	93.33	93.33	110.00	93.33	100.00
Accuracy at 100% level (n = 3)								
Amount added (%)	0.152	0.151	0.150	0.150	0.149	0.151	0.149	0.150
Amount recovered (%)	0.144	0.148	0.144	0.144	0.142	0.145	0.141	0.150
% recovery	94.74	98.01	96.00	96.00	95.30	96.03	94.63	100.00
Accuracy at 150% level (n = 3)								
Amount added (%)	0.228	0.226	0.224	0.225	0.224	0.226	0.224	0.225
Amount recovered (%)	0.216	0.221	0.216	0.216	0.214	0.219	0.212	0.230
% recovery	94.74	97.79	96.43	96.00	95.54	96.90	94.64	102.22

n, number of determinations; RT, retention time; RRT, relative retention time; R_s, USP resolution; RF, response factor; N, number of theoretical plates; T, USP tailing factor; r, correlation coefficient.

3. Results and discussion

3.1. Method development

The main aim of the chromatographic method development was to achieve the separation of closely eluting impurities namely Imp-1, Imp-2, Imp-4, Imp-5 and to retain fampridine peak. Impurities were named based on their elution pattern. The details of

potential impurities of fampridine were listed in Table 1. Fampridine, Imp-4 and Imp-5 were co-eluted when different stationery phases like C8, C18, and phenyl were used in different mobile phases containing phosphate, ammonium and combination of these two buffers along with acetonitrile, methanol, with pH ranging from 3 to 6. Tailing was observed to be more at higher pH. Use of Xterra-RP18 column and introduction of 1-octane sulphonic acid sodium salt ion pair reagent was the major factor
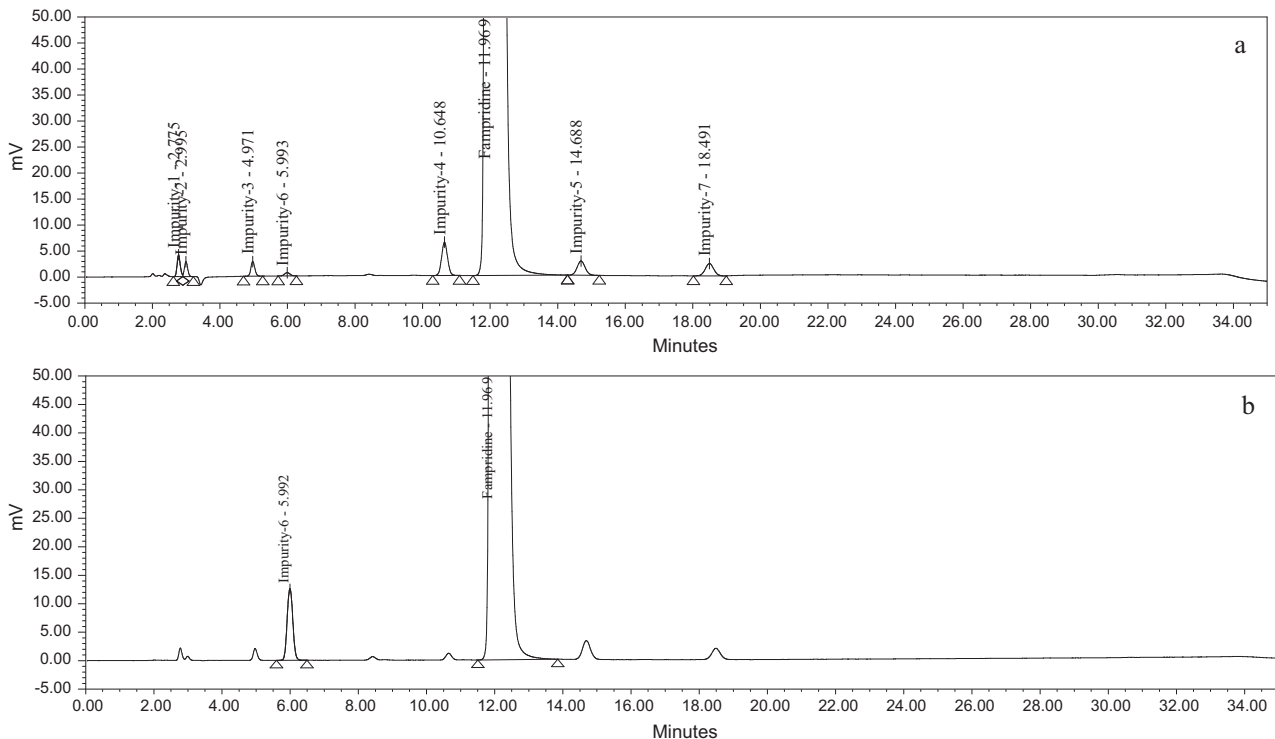
Fig. 1. (a) Chromatogram of fampridine spiked with impurities at 240 nm. (b) Chromatogram of fampridine spiked with impurities at 282 nm.
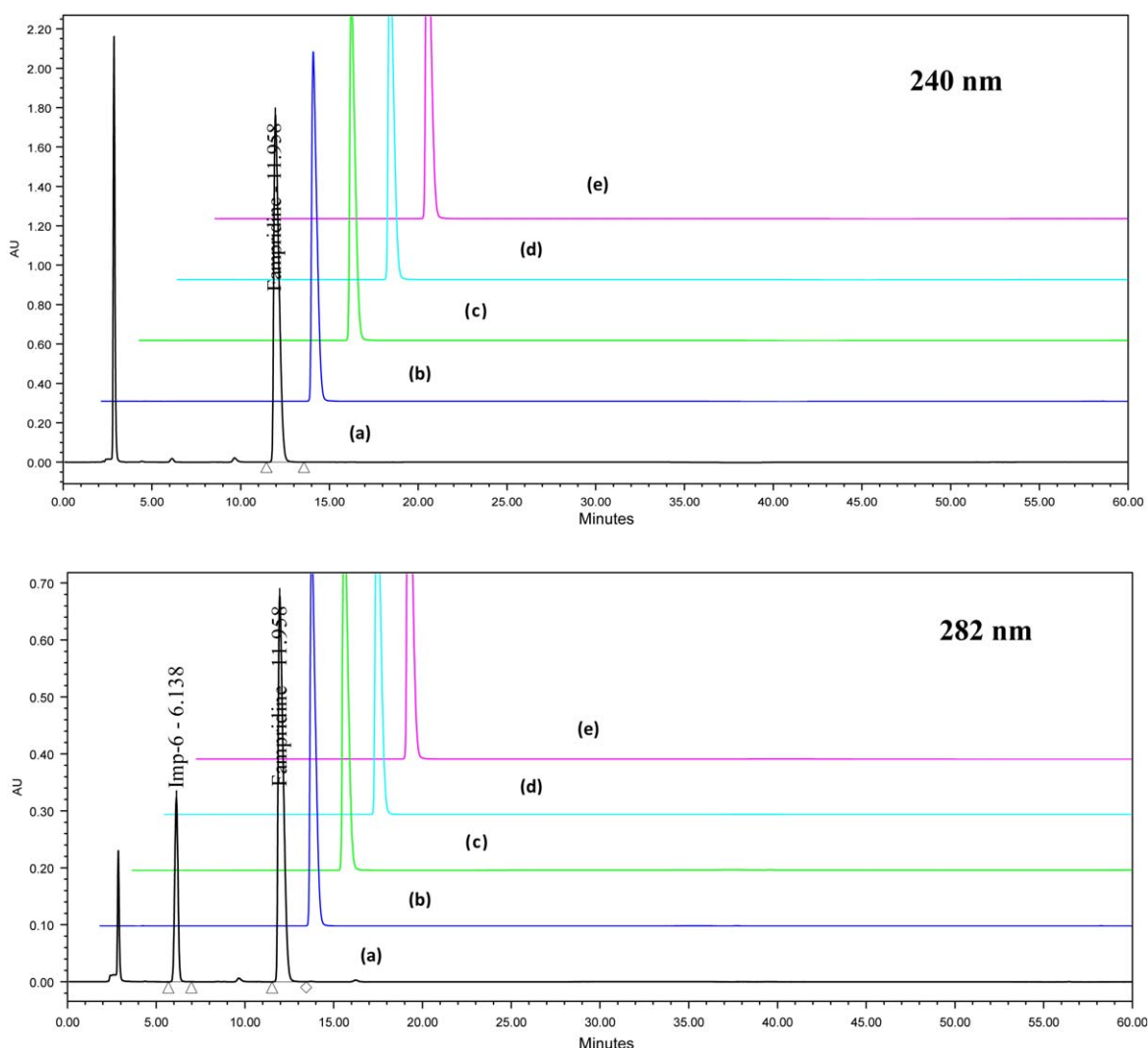
Fig. 2. (a) Typical chromatogram of fampridine under stress conditions at 240 nm: (a) oxidative degradation, (b) acid hydrolysis, (c) base hydrolysis, (d) thermal degradation, and (e) photolytic degradation. (b) Typical chromatogram of fampridine under stress conditions at 282 nm: (a) oxidative degradation, (b) acid hydrolysis, (c) base hydrolysis, (d) thermal degradation, and (e) photolytic degradation.

in achieving the desired resolution of closely eluting impurities and retention of fampridine peak. Use of triethylamine and 40 °C column temperature reduced the tailing of fampridine peak. In the new method, resolution between fampridine and Imp-4 was found to be more than 2.0 (Table 2) and the peak tailing was less than 2.0. After several experiments for gradient profile, chromatographic conditions were optimized as described under Section 2.2.

4. Method validation

The newly developed method was validated to establish specificity, precision, linearity, accuracy, sensitivity, robustness and system suitability according to ICH guidelines. Validation study was carried out for the analysis of Imp-1, Imp-2, Imp-3, Imp-4, Imp-5, Imp-6 and Imp-7. The system suitability and selectivity were checked by injecting 750 μg/mL of fampridine solution containing 0.15% of all impurities (Fig. 1). Method validation results are summarized in Table 2.

4.1. Specificity

Specificity is the ability of the method to unequivocally assess the analyte response in the presence of its potential impurities. Specificity was established by injecting fampridine co-spiked with potential impurities. Forced degradation study was performed to demonstrate the stability indicating power and specificity of the proposed method. The stress conditions employed for degradation study included acid (1 N HCl, 80 °C, for 3 h), base (1 N NaOH, 80 °C, for 3 h), thermal (105 °C, for 24 h), oxidation (30% H_2O_2, 30 °C, for 15 min), photolytic (1.2 million lux h/and 200 W h/m^2) and water hydrolysis (80 °C, for 3 h).

4.2. Results of forced degradation and identification of major degradant impurity

Fampridine molecule was found to be very stable during stress conditions in acid, base, thermal, photolytic and water hydrolysis. In oxidative degradation condition, significant degradation was observed and the impurity formed at RRT of 0.51 and was identified

as fampridine *N*-oxide. Chromatograms of forced degradation study have been depicted in Fig. 2. Peak purity of stressed samples of fampridine was checked using a SPD M20A photo diode array detector (Shimadzu Corporation, Japan). Degradation studies and peak purity test results derived from PDA detector confirmed that the fampridine peak was homogenous and pure in all the stress samples. The developed LC method was found to be specific in the presence of Imp-1, Imp-2, Imp-3, Imp-4, Imp-5, Imp-6, Imp-7 and their degradation products confirmed the stability indicating power of the newly developed method.

4.3. Precision

The precision of the related substances method was checked by injecting six individual preparations of (750 µg/mL) fampridine spiked with 0.15% of each impurity. Percentage RSD for peak areas of each impurity was calculated. Precision was also determined by performing the same procedures on a different day (inter-day precision). The intermediate precision (ruggedness) of the method was also evaluated by a different analyst and different instrument in the same laboratory. Percentage RSD of areas of each impurity was within 4.0, confirming the good precision at low level of the developed analytical method.

4.4. Sensitivity

The sensitivity was determined by establishing the detection limit (DL) and quantitation limit (QL) for all impurities by injecting a series of dilute solutions with known concentration. The detection limit and quantitation limit for Imp-1, Imp-2, Imp-3, Imp-4, Imp-5 and Imp-7 were about 0.01% and 0.03% respectively. DL and QL for Imp-6 were 0.003% and 0.01% respectively, indicating high sensitivity of the method. The precision at QL concentration for all impurities was below 4%.

4.5. Linearity and range

A linearity test solution for related substance method was prepared by diluting the impurity stock solution to the required concentrations. The solutions were prepared at six concentration levels. From QL to 150% of the permitted maximum level of impurity (i.e. QL, 0.075%, 0.1125%, 0.15%, 0.1875% and 0.225%) was subjected to linear regression analysis with the least squares method. Calibration equation obtained from regression analysis was used to calculate the corresponding predicted responses. The residuals and sum of the residual squares were calculated from the corresponding predicted responses. The correlation coefficient obtained was greater than 0.999 for all impurities. The result showed an excellent correlation between the peak area and concentration of all impurities. Standard deviation of peak area was significantly low and RSD was below 4.0%. Linearity was established between ranges of QL to 0.225% of the analyte concentration (750 µg/mL).

4.6. Accuracy

The accuracy of the method was evaluated in triplicate at three concentration levels, i.e. QL, 100% level (0.15% of the drug substance) and 150% level (0.225% of the drug substance). The percentage of recovery for each impurity was calculated at each level.

The percentage recovery of all impurities ranged from 93.3% to 110.0% indicating the accuracy of the method.

4.7. Robustness

To determine the robustness of the developed method, experimental conditions were deliberately changed and the resolution between fampridine and Imp-4 was evaluated. Close observation of analysis results of deliberately changed chromatographic conditions (flow rate, pH, mobile phase composition and column temperature) revealed that the resolution between Imp-4 and fampridine was greater than 2.0, illustrating the robustness of the method.

4.8. Solution stability

The solution stability of fampridine and its related impurities was demonstrated by leaving both spiked and unspiked sample solution in tightly capped HPLC vials at 25 °C in auto sampler. Content of each impurity was determined every 4 h against freshly prepared standard solution. The solution stability experiments data confirmed that sample solutions were stable up to 24 h.

5. Conclusion

The newly developed RP-LC method for quantitative determination of fampridine related substances was found to be sensitive, precise, accurate specific and stability indicating. The major oxidative degradant was identified as fampridine *N*-oxide. This newly developed method has been validated as per regulatory requirements and can be used for routine and stability studies for the quantitative determination of potential impurities in fampridine drug substance.

Acknowledgements

References

[1] J.E.F. Reynolds, Martindale the Complete Drug Reference, 35th ed., Royal Pharmaceutical Society of Great Britain, 2008, p. 574.
[2] K.C. Hayes, P.J. Potter, J.T. Hsieh, M.A. Katz, A.R. Blight, R. Cohen, Pharmacokinetics and safety of multiple oral doses of sustained-release 4-aminopyridine (Fampridine-SR) in subjects with chronic, incomplete spinal cord injury, Arch. Phy. Med. Rehabil. 85 (2004) 29–34.
[3] T. Vollmer, H.R. Henney, Pharmacokinetics and tolerability of single escalating doses of fampridine sustained-release tablets in patients with multiple sclerosis: a phase I–II, open-label trial, Clin. Ther. 31 (2009) 2206–2210.
[4] T. Vollmer, A.R. Blight, H.R. Henney III, Steady-state pharmacokinetics a tolerability of orally administered fampridine sustained-release 10-mg tablets in patients with multiple sclerosis: a 2-week, open-label, follow-up study, Clin. Ther. 31 (2009) 2215–2223.
[5] R.F. Donnelly, Chemical stability of 4-aminopyridine capsules, Can. J. Hospital Pharm. 57 (2004) 284–287.
[6] ICH Guidelines, Stability testing of new drug substances and drug products: text and methodology Q1 A (R2), February 2003.
[7] ICH Guidelines, Validation of analytical procedures stability testing of new drug substances and drug products: text and methodology Q2 (R1), November 2005.
[8] ICH Guidelines, Impurities in new drug substances Q3A (R2), October 2006.

Short communication

Chemiluminescence determination of terbutaline sulfate in bovine urine and pharmaceutical preparations based on enhancement of the 2-phenyl-4, 5-di (2-furyl) imidazole–potassium ferricyanide system

Lu Han, Yumin Zhang, Jing Kang, Jieli Tang, Yihua Zhang*

College of Chemistry, Jilin University, Changchun 130012, PR China

ABSTRACT

In this paper, a novel chemiluminescence (CL) system, 2-phenyl-4, 5-di (2-furyl) imidazole (PDFI)–potassium ferricyanide, for the determination of terbutaline sulfate was described. The method was based on enhancement of CL emission of PDFI–potassium ferricyanide system in the presence of terbutaline sulfate. Under the optimum conditions, the enhanced chemiluminescence intensity is linearly related to the concentration of terbutaline sulfate. The proposed method has been successfully applied to the determination of terbutaline sulfate in bovine urine and pharmaceutical preparations with satisfactory results. Furthermore, the possible mechanism of chemiluminescence reaction was also discussed briefly.

© 2011 Elsevier B.V. All rights reserved.

1. Introduction

Chemiluminescence (CL) analysis has received increasing attention over the years. It has been applied in many different fields, particularly in pharmaceutical and biomedical analysis. Most of the CL methods involve inhibition or catalysis of the redox reaction of CL reagents such as luminol, lucigenin and gallic acid. Therefore, the interests in the research of CL reagents and CL labeling reagents for pharmaceutical analysis have increased in recent years. Imidazole derivatives are a new type of luminescent material with unique optical properties, and have been successfully used in CL analysis. Lophine (2, 4, 5-triphenylimidazole) has been known as a potential chemiluminogenic compound since 1877 [1] and has been used for the determination of some trace metal ions [2]. Recently, new lophine derivatives were synthesized and their properties were determined [3]. It was also reported that lophine analogues having 2-furyl group at both 4- and 5-positions gave stronger CL intensity than lophine [4]. But these compounds synthesized were rarely used in CL analysis for the determination of drugs.

Terbutaline sulfate, 2-tert-butylamino-1-(3, 5-dihydroxy-phenyl) ethanol hemisulfate, is a synthetic β_2-adrenoceptor that is widely used as a bronchodilator for treatment of bronchial asthma, chronic bronchitis, and emphysema [5]. It could stimulate

protein accretion and inhibit the adipose accumulation of animal. So terbutaline sulfate as feed additives was used to increase lean meat percentage of beef and pork. The use of growth promoters for fattering purposes in cattle has been banned for reasons of fair trade and consumer protection in the European Union since 1988 [6]. Therefore, the determination of such drug is important for quality assurance of pharmaceutical preparations, and the evaluation of terbutaline sulfate misuse in animals.

Many analytical methods have been developed for determination of terbutaline sulfate, including HPLC [7,8], LC–MS [9], CE [10], CE–MS [11], and voltammetry [12]. Usually, HPLC and CE are applied to the determination of terbutaline sulfate in real samples. The determination of drugs in biological fluids by HPLC usually requires several sample preparation processes or off-line solid phase extraction, which is time-consuming and may lead to variability in the results. Compared with CL method, these methods require expensive instruments and complex sample pre-treatment. So CL method has been developed for the determination of terbutaline sulfate. The potassium ferricyanide–rhodamine 6G and luminol–permanganate CL system were applied to the determination of terbutaline sulfate in human urine and pharmaceutical preparations [13,14]. Molecularly imprinted polymer–CL method was also proposed to determine terbutaline sulfate in human serum [15].

In this paper, 2-phenyl-4, 5-di (2-furyl) imidazole (PDFI) was synthesized according to the method reported in literature [16]. A novel chemiluminescence (CL) system, PDFI–potassium ferri-cyanide system, for the determination of terbutaline sulfate was

---

* Corresponding author. Tel.: +86 0431 85168352 6.
  E-mail address: yihuazh47@yahoo.com.cn (Y. Zhang).
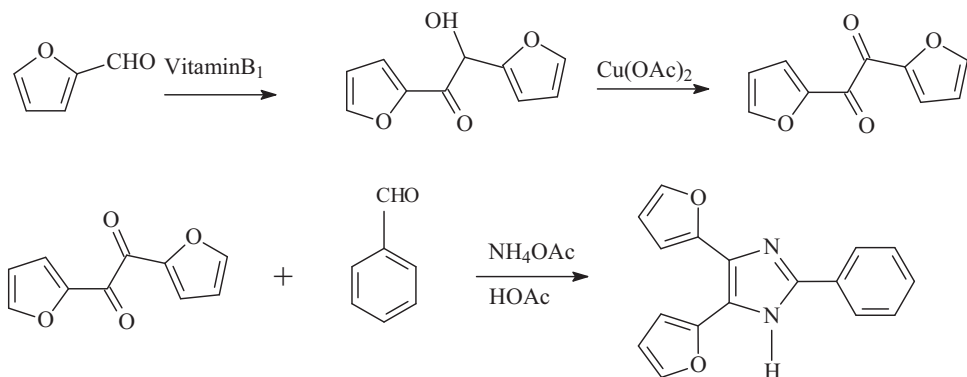
Fig. 1. Scheme for the synthesis of 2-phenyl-4, 5-di (2-furyl) imidazole.

described. The method was based on enhancement of CL emission of PDFI–potassium ferricyanide system in the presence of terbutaline sulfate. The possible enhancement mechanism was also further investigated. The method was applied to the determination of terbutaline sulfate in bovine urine and pharmaceutical preparations, and the obtained results were satisfactory. The proposed method has the advantages of simplicity, rapidity, and sensitivity.

2. Experimental

2.1. Reagents and chemicals

All the reagents were of analytical reagent grade and all solutions were prepared with double-distilled water. NaOH, KCl, NaCl, $CaCl_2$, $Ni(NO_3)_2 \cdot 6H_2O$, $BaCl_2 \cdot 2H_2O$, $CdCl_2$, $MnSO_4 \cdot H_2O$, $Cr(NO_3)_3 \cdot 9H_2O$, $Pb(NO_3)_2$, $CuSO_4 \cdot 5H_2O$, potassium ferricyanide were purchased from Beijing Chemical Plant in China. $CoCl_2 \cdot 6H_2O$ was purchased from Shanghai Chemical Plant in China. NH_4Cl was purchased from Tianjin Chemical Plant 1.

Terbutaline sulfate (Institute of Pharmaceutical and Biomaterial Authentication of China) was used as standard. Terbutaline sulfate tablets were obtained from local drug stores.

The 1.0×10^{-3} mol/L stock solution of PDFI was prepared by dissolving 7.1 mg of PDFI with ethanol and then diluting to 25 mL and the working solution (1×10^{-4} mol/L) was prepared by diluting the stock solution with water.

2.2. Synthesis of PDFI

Firstly, furil was synthesized via the benzoin condensation of furfural, and then PDFI was prepared by the condensation reaction of furil with benzaldehyde, ammonium acetate and acetic acid in water bath at 60–70 °C. This method was known as Debus [16]. The synthetic route is briefly shown in Fig. 1.

2.3. Apparatus

The CL analysis was conducted on a laboratory-built steady injection CL system. The schematic diagram of the system is shown in Fig. 2. The steady injection system consists of two peristaltic pumps and a sixteen-hole eight-way valve. The CL emission is detected by an ultra-weak luminescence analyzer. Data acquisition and treatment are performed with BPCL software running under Windows XP.

The fluorescence spectrum was recorded with a RF-5301 spectrofluorimeter (Shimadzu, Japan). The absorbance were obtained on an Australian GBC Cintra 10e UV–vis Spectrometer with the wavelength range of 200–800 nm.

2.4. Procedure

Experimental results were obtained by using the following operation parameters: sample loop volume, 200 μL; sampling time, 10 s; sample injection time, 20 s; the PMT negative voltage, −1000 V; the integral time of the CL signal, 60 s. 200 μL of PDFI solution and 200 μL analyte standard solution (or sample solution) were first added into the sample cell, and then the potassium ferricyanide and NaOH solution were simultaneously injected into the sample cell with the steady injection system.

The operation mode is as follows: (1) Fig. 2a, pumps P_1 and P_2 were activated, and valve V was in the loading position. The pump P_1 was used to deliver potassium ferricyanide solution into the sample $loop_1$ (SL_1) and the pump P_2 was used to deliver NaOH solution into the sample $loop_2$ (SL_2). (2) Fig. 2b, pumps P_1 and P_2 were activated, and valve V was in the injection position. The pumps P_1 and P_2 were used to deliver the air current. The potassium ferricyanide solution and NaOH solution were simultaneously pumped into chemifold R and mixed. The mixed solution was carried into sample cell S and reacted with the mixture of PDFI solution and analyte standard solution (or sample solution) in the sample cell S. The CL signal was measured and recorded. The concentration of analyte was quantified by measuring the enhanced CL intensity, $\Delta I = I_s - I_0$, where I_0 and I_s are CL intensity in the absence and presence of terbutaline sulfate, respectively.

2.5. Preparation of sample

2.5.1. Pharmaceutical preparations

At least 20 terbutaline sulfate tablets (labeled content 2.5 mg per tablet) were weighed. The average tablet weight was calculated from the weight of 20 tablets. They were ground to a homogeneous fine powder. A portion of the powder corresponding to 2.5 mg was weighed and dissolved with 100 mL double-distilled water. The obtained solution was centrifugalized for 30 min at 4000 r/min. The supernatant was further diluted with water so that the concentration of terbutaline sulfate was in the concentration range of the calibration curve.

2.5.2. Bovine urine

The bovine urine samples were real-life samples. Bovine urine samples obtained from suburb cattle farm were analyzed. Urine samples from 2 bovines were taken, respectively by collecting the urine from spontaneous urinating animals directly into precleaned glass flasks. Glass flasks were immediately taken to the laboratory and stored at 4 °C before analysis. All samplings were performed in the early morning. The sample was filtered with microporous filtering film of 0.65 μm and centrifugalized at 4000 r/min for 30 min to remove the proteins. 500 μL of the deproteinized bovine urine
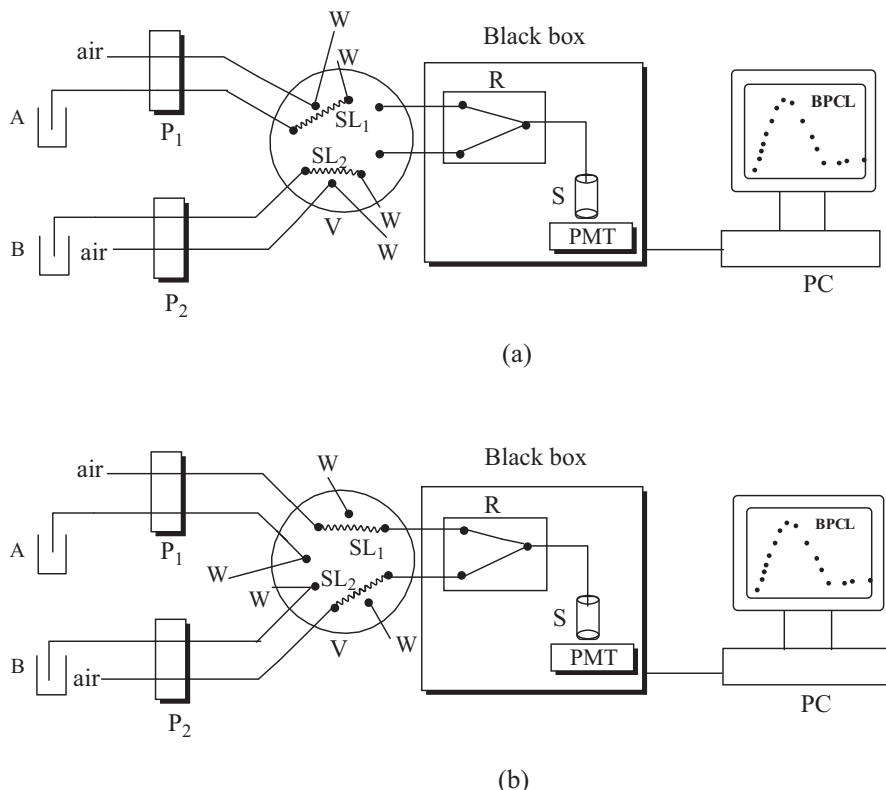
Fig. 2. Schematic diagram of the steady-injection CL system: (a) loading position and (b) injection position. A: potassium ferricyanide; B: NaOH solution; P_1, P_2: peristaltic pump; SL: sample loop; V: eight-way valve; R: chemifold; S: sample cell; PMT: photomultiplier tube; PC: computer; W: waste.

was then transferred to a 50 mL volumetric flask and diluted to the mark with water. To obtain low CL background, the sample solution was diluted 10 times when it was analyzed.

3. Results and discussion

3.1. Condition optimization of the CL system

The effect potassium ferricyanide concentration on the CL intensity was examined. It was found that the CL intensity increased along with the increases of potassium ferricyanide concentration. When the concentration was higher than 1.0×10^{-3} mol/L, the CL intensity decreased. The produced CL was partly absorbed by potassium ferricyanide, which was called self-absorption. So the CL intensity decreases with the increase of the concentration of potassium ferricyanide in system. So 1.0×10^{-3} mol/L was chosen as the optimum concentration for potassium ferricyanide.

The effect of NaOH concentration was investigated in the range of 5.0×10^{-4}–0.25 mol/L. The maximum CL intensity was obtained when the concentration of NaOH was 0.05 mol/L.

The influence of PDFI concentration on the CL intensity was investigated. The maximum CL intensity could be obtained when the concentration of PDFI was 1.0×10^{-4} mol/L. Therefore, 1.0×10^{-4} mol/L was selected for the present work.

3.2. Performance of the proposed method

Under the optimized experimental conditions, the enhanced CL intensity was linearly related to the concentration of terbutaline sulfate in the range of 0.05–10 μg/mL. The detection limit was 0.01 μg/mL and the relative standard deviation for 1.0 μg/mL terbutaline sulfate ($n = 11$) was 2.7%. The regression equation was $\Delta I = (2077.7 \pm 2374.4) + (0.18 \times 10^6 \pm 545.7)C$; C is the concentration of terbutaline sulfate (μg/mL), $S_{y/x}$ is 4884.8 and the correlation coefficient is 0.9999 ($n = 7$).

3.3. Interference studies

In order to assess the selectivity of the proposed method, we chose some foreign species that may exist in the samples used in the study. The influence of the foreign species was investigated by analyzing a standard solution of 1.0 μg/mL terbutaline sulfate. The tolerance of foreign species was taken as the highest concentration yielding an error less than ±5% in the CL signal of terbutaline sulfate. The results showed that no interference could be observed for 1000-fold Na^+, K^+, Ba^{2+}, Ca^{2+}, Mn^{2+}, Cd^{2+}, NH_4^+, 500-fold Pb^{2+}, urea, DL-β-phenylalanine, L-asparagine, 250-fold Cr^{3+}, Co^{2+}, L-tryptophan, 100-fold glucose, 5-fold L-tyrosine, and 0.5-fold Cu^{2+}, ascorbic acid.

3.4. Possible mechanism of CL reaction

The emission spectra of PDFI–potassium ferricyanide and PDFI–potassium ferricyanide–terbutaline sulfate CL reaction systems in the absence and presence of terbutaline sulfate were examined The results showed that the maximum emission appeared at 525 nm for the two reaction system, and the relative CL intensity was higher in the presence of terbutaline sulfate (Fig. 3a and b). The fluorescence (FL) emission spectrum of PDFI was further examined (Fig. 3c). It can be seen that the characteristic emission peak of PDFI is 436 nm. These results revealed that the luminophor of PDFI–potassium ferricyanide and PDFI–potassium ferricyanide–terbutaline sulfate systems is not PDFI but the intermediate product, which is the oxidation product of PDFI. The mechanism was similar with the mechanism of lophine CL [17].
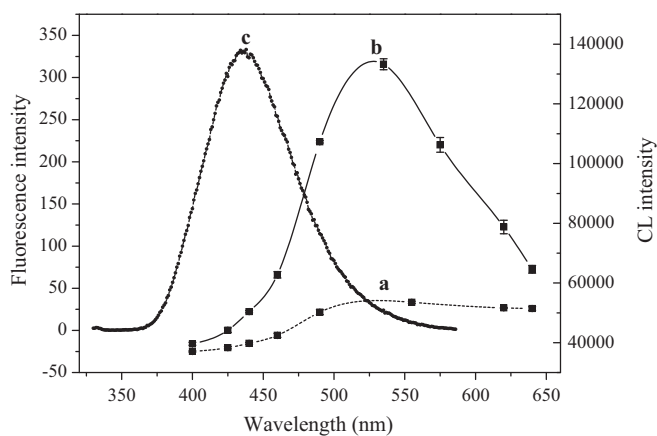
Fig. 3. The fluorescence emission spectra of PDFI (c); condition: PDFI, 1 μmol/L. The CL spectra of PDFI–potassium ferricyanide system (a) and PDFI–potassium ferricyanide–terbutaline sulfate system (b); conditions: PDFI, 1.0×10^{-4} mol/L; potassium ferricyanide, 1.0×10^{-3} mol/L; NaOH, 0.05 mol/L; terbutaline sulfate, 10 μg/mL.

Table 1
Determination of terbutaline sulfate in bovine urine ($n = 5$).

Sample	Added (μg/mL)	Found (μg/mL)	Recovery (%)	RSD (%)
	0.5	0.46	92	3.2
Sample 1	1.0	0.99	99	4.5
	2.0	2.16	108	2.7
	0.5	0.48	96	3.3
Sample 2	1.0	0.99	99	3.7
	2.0	2.10	105	2.6

3.5. Application

3.5.1. Determination of terbutaline sulfate in bovine urine

Two parallel bovine urine samples were analyzed. Because the difference between CL signals obtained with samples and blank was less than ±5%. The terbutaline sulfate in the two bovine urine samples was undetectable. So the spiked samples were analyzed. The spiked samples were prepared by adding standard solution of terbutaline sulfate into bovine urine. The results obtained for analyzing the spiked bovine urine samples are shown in Table 1. Recoveries from 92% to 108% were obtained. The recovery means the percentage of the true amount of terbutaline sulfate recovered during the proposed procedure.

3.5.2. Determination of terbutaline sulfate in pharmaceutical preparations

In order to investigate the precision of the proposed method, this method was applied the determination of terbutaline sulfate

In alkaline medium, polyhydroxyphenols can be oxidized to semiquinone radical, which is unstable and can further produce $O_2^{\bullet-}$ or $^1O_2^\bullet$ [18]. The $O_2^{\bullet-}$ reacts with PDFI to form an intermediate product. And then the intermediate product emits light from excitation state, and thus the CL emission was enhanced. The CL mechanism is shown in Fig. 4.
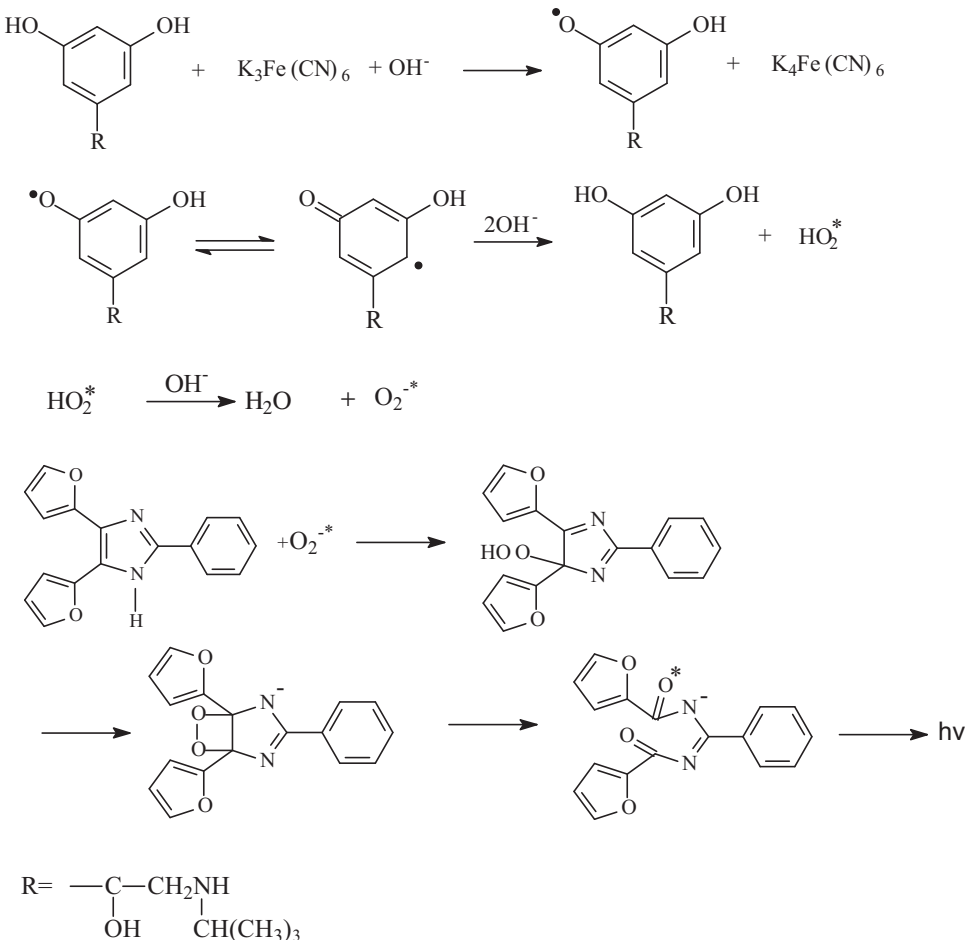
Fig. 4. Scheme for the mechanism of the CL.

Table 2
Analytical results of pharmaceutical preparations.

Sample	Label (mg/tablet)	Proposed method		UV–vis spectrophotometry		Relative error (%)
		Content (mg/tablet)	RSD (%)	Content (mg/tablet)	RSD (%)	
Terbutaline sulfate tablet	2.50	2.39	4.9	2.44	1.6	−2.0

in pharmaceutical preparations. The comparison between the proposed CL method and UV–vis spectrophotometry was also carried out. The detection limit was 0.17 μg/mL when UV–vis spectrophotometry was applied to the determination of terbutaline sulfate. As can be seen from Table 2, there is a good agreement between results obtained by the two methods.

4. Conclusion

In the work, a novel CL system for determining terbutaline sulfate was proposed. A kind of imidazole derivative, PDFI, was synthesized and used as CL reagent in this system. This method has been successfully applied to the determination of terbutaline sulfate in bovine urine and pharmaceutical preparations. Moreover, the application of imidazole derivatives should be widened in CL analysis.

References

[1] B.R. Radziszewski, Untersuchungen über hydrobenzamid, amarin und lophin, Chem. Ber. 10 (1877) 70–75.
[2] A. MacDonald, K.W. Chan, T.A. Nieman, Lophine chemiluminescence for metal ion determinations, Anal. Chem. 51 (1979) 2077–2082.
[3] N. Fridman, M. Kaftory, S. Speiser, Structures and photophysics of lophine and double lophine derivatives, Sens. Actuators B 126 (2007) 107–115.
[4] K. Nakashima, Y. Fukuzaki, R. Nomura, R. Shimoda, Y. Nakamurafl, N. Kurodafl, S. Akiyama, K. Irgum, Fluorescence and chemiluminescence properties of newly developed lophine analogues, Dyes Pigments 38 (1998) 127–136.
[5] R. Ventura, L. Damasceno, M. Farré, J. Cardoso, J. Segura, Analytical methodology for the detection of β2-agonists in urine by gas chromatography–mass spectrometry for application in doping control, Anal. Chim. Acta 418 (2000) 79–92.
[6] L. Martineau, M.A. Horan, N.J. Rothwell, R.A. Little, Salbutamol, a beta 2-adrenoceptor agonist increases skeletal muscle strength in young men, Clin. Sci. 8 (1992) 615–621.
[7] K.H. Kim, H.J. Kim, J.H. Kim, S.D. Shin, Determination of terbutaline enantiomers in human urine by coupled achiral–chiral high-performance liquid chromatography with fluorescence detection, J. Chromatogr. B 751 (2001) 69–77.
[8] V.L. Herring, J.A. Johnson, Simple method for determination of terbutaline concentration by high-performance liquid chromatography, J. Chromatogr. B 741 (2000) 307–312.
[9] D.R. Doerge, S. Bajic, L.R. Blankenship, S.W. Preece, M.I. Churchwell, Determination of β-agonist residues in human plasma using liquid chromatography/atmospheric pressure chemical ionization mass spectrometry and tandem mass spectrometry, J. Mass Spectrom. 30 (1995) 911–916.
[10] S. Li, J.S. Wang, S.L. Zhao, Determination of terbutaline sulfate by capillary electrophoresis with chemiluminescence detection, J. Chromatogr. B 877 (2009) 155–158.
[11] W.Z. Lu, R.B. Cole, Determination of chiral pharmaceutical compounds, terbutaline, ketamine and propranolol, by on-line capillary electrophoresis–electrospray ionization mass spectrometry, J. Chromatogr. B 714 (1998) 69–75.
[12] N. Yilmaz, S.A. Özkan, B. Uslu, Z. Şentürk, İ. Biryol, Determination of terbutaline based on oxidation voltammetry, J. Pharm. Biomed. Anal. 17 (1998) 349–355.
[13] Z.P. Wang, Z.J. Zhang, Z.F. Fu, X. Zhang, Sensitive flow-injection chemiluminescence determination of terbutaline sulfate based on enhancement of the luminol–permanganate reaction, Anal. Bioanal. Chem. 378 (2004) 834–840.
[14] Y. Lv, Z.J. Zhang, Y.F. Hu, D.Y. He, S.H. He, A novel chemiluminescence method for determination of terbutaline sulfate based on potassium ferricyanide oxidation sensitized by rhodamine 6G, J. Pharm. Biomed. Anal. 32 (2003) 555–561.
[15] D.Y. He, Z.J. Zhang, H.J. Zhou, Y. Huang, Micro flow sensor on a chip for the determination of terbutaline in human serum based on chemiluminescence and a molecularly imprinted polymer, Talanta 69 (2006) 1215–1220.
[16] H. Debus, Ueber die einwirkung des ammoniaks auf glyoxal, Liebigs Ann. Chem. 107 (1858) 199–208.
[17] M. Tsunenaga, H. Iga, M. Kimura, Location effect of an OH group on the chemiluminescence efficiency of 4-hydroperoxy-2-(o-, m-, or p-hydroxyphenyl)-4,5-diphenyl-4H-isoimidazoles, Tetrahedron Lett. 46 (2005) 1877–1880.
[18] N.P. Evmiridis, Prospects of using chemiluminescence emission generated during oxidation of pyrogallol with periodate for the determination of pyrogallol with flow injection, Analyst 113 (1988) 1051–1056.

Short communication

Subcritical water extraction of alkaloids in *Sophora flavescens* Ait. and determination by capillary electrophoresis with field-amplified sample stacking

Haiyan Wang [a], Yuchao Lu [a], Jie Chen [a], Junchao Li [b], Shuhui Liu [a,c,*]

[a] *College of Science, Northwest A&F University, No. 3 Taicheng Road, Yangling, Shaanxi 712100, China*
[b] *College of Life Sciences, Northwest A&F University, No. 3 Taicheng Road, Yangling, Shaanxi 712100, China*
[c] *Shaanxi Key Laboratory of Molecular Biology for Agriculture, No. 3 Taicheng Road, Yangling, Shaanxi 712100, China*

ARTICLE INFO

ABSTRACT

The extraction and determination of cytisine, sophocarpine, matrine, sophoridine and oxymatrine in *Sophora flavescens* Ait. were performed using subcritical water extraction and capillary electrophoresis with field-amplified sample stacking. The effects of extraction temperature, pressure, time and cycle number on the extraction yields were investigated systematically for accelerated solvent extraction with ethanol (ASE) and accelerated solvent extraction with water (subcritical water extraction, SWE). The extraction yields obtained using SWE, ASE, water ultrasonic extraction and chloroform soaking extraction methods were compared. The electrophoresis separation buffer was monosodium phosphate (pH 3.0; 110 mM)-isopropanol (85:15, v/v). The effect of phosphoric acid added to the sample matrix on the reproducibility of the peak heights of the analytes was also examined. Cytisine, sophoridine and oxymatrine showed good linearity ($R^2 > 0.999$) within 0.125–4.0 μg/mL, and sophocarpine and matrine exhibited good linearity ($R^2 > 0.998$) within 0.0625–2.0 μg/mL, with the detection limits in the range of 0.004–0.0013 μg/mL. The five alkaloid contents in medicinal plants from different sources and *Sophora* instant granule were determined and compared.

© 2011 Elsevier B.V. All rights reserved.

1. Introduction

Sophora flavescens Ait. (*Sophora*), in the family *Fabaceae*, is a traditional Chinese medicine. Researchers at home and abroad have studied its chemical components, which are mainly quinolizidine alkaloids and flavonoids. Thus far, over twenties alkaloids have been isolated from the root, leaves or flowers of *Sophora* which are reported to exhibit sedative, analgesic and other central nervous system inhibition effects [1] as well as antipyretic, anti-tumor, anti-myocardial activities [2].

The extraction methods of the alkaloids in *Sophora* are mainly chloroform soaking extraction [3–8] and solvent reflux extraction [9,10] in which shortcomings include long extraction time, high cost of non-environmental friendly organic solvents, and organic solvent residuals in the products extracted. Only a couple of research groups used ultrasonic extraction [11,12] and supercritical fluid extraction [13].

Accelerated solvent extraction (ASE) is a new highly efficient sample preparation technique for extraction of solid or semi-solid

samples. ASE becomes more preferred because of its apparent advantages such as less solvent consumption, automatic procedure for simultaneous extraction of multiple samples, short sample preparation time, and higher extraction recoveries. However, ASE using organic solvents is not a promising extraction procedure in term of environment issue. Subcritical water extraction (SWE) uses pure water as the solvent and is an innovative green sample preparation technique. Subcritical water is also called superheated water, pressurized hot water, whose polarity, surface tension and viscosity can be changed by controlling temperature and pressure. When the temperature is increased, the polarity decreases, and the solubility of organic compounds in the subcritical water increases dramatically. The device used for ASE is also suitable for SWE [14]. Several reviews on SWE have been published recently [15,16].

So far, capillary electrophoresis (CE) has been widely used in pharmaceutical analysis due to its high separation efficiency, low consumption of organic solvent and in-line sample enrichment. Several papers described the determination of alkaloids in *Sophora* using CE [5–8]. Due to its self-limiting nature, the reproducibility of CE is poor, especially when using in-line field-amplified sample stacking (FASS), in which an internal standard has to be added during the quantitative analysis [6–8]. However, the selection of the internal standard substances is rather difficult. They often interfere with other peaks from real samples, and some are quite toxic and harmful.

* Corresponding author at: College of Science, Northwest A&F University, No. 3 Taicheng Road, Yangling, Shaanxi 712100, China. Tel.: +86 029 87092226; fax: +86 029 87092226.

E-mail address: shliu815@126.com (S. Liu).
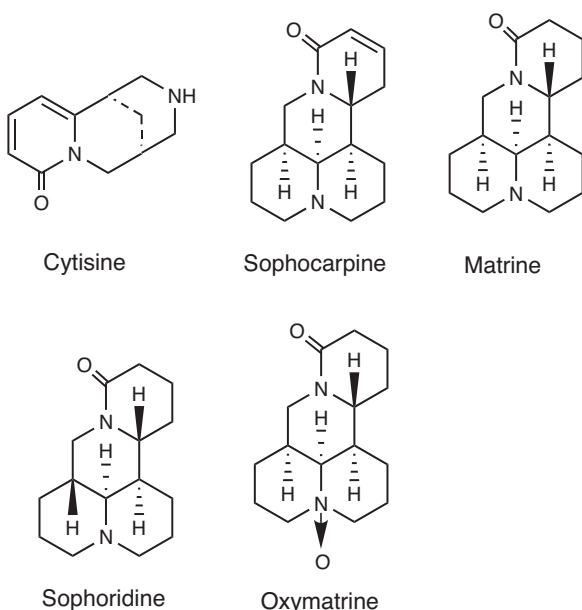
Scheme 1. The structures of the five alkaloids.

In this paper, the extraction of five active compounds (Scheme 1) from *Sophora* using SWE was investigated and compared with ASE, water ultrasonic extraction and chloroform soaking extraction. The contents of the analytes were analyzed using CE with FASS, for which the effort was made to improve the reproducibility. By integrating SWE and CE, we attempted to provide a new, efficient and environmentally friendly analysis approach for the medicinal plant quality control.

2. Materials and methods

2.1. Instruments and apparatus

All electrophoresis experiments were performed on a Beckman P/ACE^{TM} MDQ Capillary Electrophoresis System equipped with a photodiode array detector (PDA) and controlled by System Gold software (Beckman Coulter Inc., Fullerton, CA, USA). Uncoated fused-silica capillaries with a total length of 50 cm (40 cm to the detector) and 50 μm I.D., from Ruipu Chromatogram Equipment Company (Yongnian County, Hebei Province, China) were maintained at 25 °C in a cartridge with a 100 μm × 800 μm detection window. The PDA was set at an acquisition range from 190 to 300 nm (bandwidth of 6 nm), at a spectral acquisition rate of 4 Hz. Electropherograms were recorded at 214 nm. Peak identity was confirmed by post-run diode-array detection analysis of the absorption maximum of individual peaks in a mixture. Separation was performed at a constant voltage of 25 kV (anode at injection end). The pH of all solutions was measured by pH 213 equipment (Hanna instruments, Italy). Water was purified using Millipore Direct-Q 3 system (Millipore Corporation, Bedford, MA, USA).

A new capillary was rinsed with 0.1 M sodium hydroxide for 30 min, deionized water for 30 min, and finally with the background electrolyte (BGE) solution for 30 min before use. Between each run, the capillary was rinsed with water for 1 min, 0.1 M sodium hydroxide for 3 min, water for 1 min, and then the BGE for 5 min, successively. The electrolytes were filtered through 0.22 μm mixed cellulose ester filters (Shanghai Minimo Separation Technology Co. Ltd.) prior to use.

2.2. Chemicals and samples

Cytisine and matrine were purchased from Aladdin reagent company (Shanghai, China). Sophoridine was supplied by the National Institute for the Control of Pharmaceutical and Biological Products of China (NICPBP, Beijing, China). Sophocarpine and oxymatrine were purchased from Sigma–Aldrich (St. Louis, MO, USA). Sodium hydroxide and sodium dihydrogen phosphate (all of analytical grade) were from Tianjin BODI Chemical Reagent Co. Ltd. (Tianjing, China). Ethanol, methanol and 2-propanol (of HPLC grade) were purchased from Luomiou Chemical Reagent Co. Ltd. (Tianjing, China).

The crude drug *Sophora* root was obtained from different sources, including a local hospital, a local drug store and the campus of Northwest A&F University (Yangling, Shannxi Province, China), which were all authenticated by Prof. Junchao Li (College of Life Sciences, Northwest A&F University). After being dried naturally and ground into a fine powder (60 mesh), the samples were stored at dry place under room temperature. *Sophora* instant granule, which was a new commercial product made from the crude drug *Sophora* root, was purchased from a local hospital.

Stock solution of 200 mM sodium dihydrogen phosphate was prepared by dissolving the corresponding substance in water. The pH of the run buffer was adjusted with 0.2 M hydrochloric acid or 0.2 M sodium hydroxide. Stock standard solutions with cytisine (200 μg/mL), sophocarpine (100 μg/mL), matrine (100 μg/mL), sophoridine (200 μg/mL) and oxymatrine (200 μg/mL) were prepared in water and stored at 4 °C in a refrigerator, when in use, diluted to the final concentration with water.

2.3. Sample extraction

2.3.1. Accelerated solvent extraction method

A Dionex ASE 200 Accelerated Solvent Extractor was performed. First, 0.5 g *Sophora* sample was accurately weighed, mixed thoroughly with 3.0 g diatomite and then transferred to an 11-mL stainless steel extraction cell. A filter paper was placed on the bottom of the extraction cell. Ethanol was used as the extraction solvent. Extraction pressure, temperature, static time and cycles are specified in Section 3.2 (preheating period, 5 min). After extraction, the thimble was rinsed with fresh extraction solvent (60% of the extraction cell volume) and purged with a flow of nitrogen (150 psi during 90 s). Solvent was collected in a 40 ml vial and then transferred to a 25 ml flask, which was rotary evaporated at 50 °C. The residue was redissolved in 25 mL of water. Then, 1 mL of the sample solution was diluted to an appropriate concentration with water, filtered through a 0.22-μm filter and then analyzed.

2.3.2. Subcritical water extraction

The same ASE 200 (Dionex, USA) instrument was used. First, 0.5 g *Sophora* sample was accurately weighed, mixed thoroughly with 3.0 g diatomite and then transferred to an 11-mL stainless steel extraction cell. Water was deoxygenated by degassing for 20 min prior to its use as extraction solvent. The same conditions were used as in Section 2.3.1. After finishing extraction, water was added to the extraction solution to reach a final volume of 25 mL. Then, 1 mL of the sample solution was diluted to an appropriate concentration with water, filtered through a 0.22-μm filter and then analyzed.

2.3.3. Ultrasonic extraction

First, 0.5 g *Sophora* sample was weighed and placed in an Erlenmeyer flask with a plug. Then, 25 mL of water was added as the extraction solvent. The mixture was weighed and shaken until it was mixed well. The sample was allowed to sit at room temperature for 3 h, followed by ultrasonic extraction for 30 min. The flask was weighed again, and the lost water was made up. The mixture was
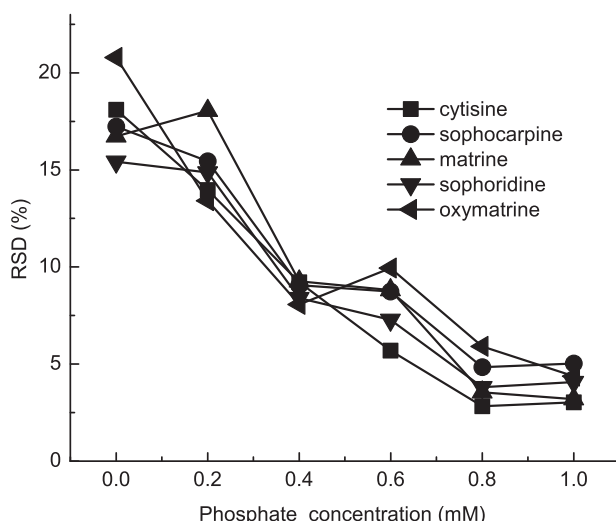
Fig. 1. The influence of phosphoric acid added to a sample solution on the reproducibility of the analyte peak heights. Each analyte, 1 μg/mL; buffer: monosodium phosphate (pH 3.0; 110 mM)-isopropanol (85:15, v/v); water plug: 0.5 psi × 3 s; injection: 8 kV × 8 s.

shaken, centrifuged and filtered. Then, 1 mL of the sample solution was diluted to an appropriate concentration with water, filtered through a 0.22-μm filter and analyzed.

2.4. Soaking extraction

According to the *Sophora* extraction method described in the 1995 edition of Chinese Pharmacopoeia [17], 0.5 g *Sophora* sample was weighed and placed in an Erlenmeyer flask with a plug. After 25 mL of chloroform was added as the extraction solvent, 0.3 mL of concentrated ammonia was added to the mixture, which was then shaken until it was mixed well. The flask was incubated at room temperature overnight (16 h), then centrifuged and filtered. The extraction solution was rotary evaporated at 40 °C, and the residue was redissolved in 50 mL of water. Then, 1 mL of the sample solution was diluted to an appropriate concentration with water, filtered through a 0.22-μm filter and analyzed.

3. Results and discussion

3.1. Development of CE analysis method

Based on the pilot experiments and our previous paper [8], monosodium phosphate (pH 3.0; 110 mM)-isopropanol (85:15, v/v) was used as the electrophoresis buffer. The FASS was conducted by preparing the samples in water and electro-injecting. Although a water plug was injected at 0.5 psi for 3 s to improve the reproducibility [8], it could not meet the requirements without the addition of an internal standard. Phosphoric acid was chosen to add into a sample solution to overcome this drawback [18]. As can be seen in Fig. 1, the addition of phosphoric acid improved the reproducibility significantly. Nevertheless, the amount of phosphoric acid added had certain effects on the stacking efficiency. With the addition of a small amount of phosphoric acid, the protonation of the analytes was increased, which helped the electrostacking and increased the analyte peak heights. The addition of more phosphoric acid to the sample caused an increase in solution conductivity, which decreased the field strength for sample electro-injection, thus the heights of analytes peaks declined. Based on these considerations, 0.8 mM phosphoric acid was appropriate concentration. The electropherogram of a five-standard mixture solution is shown in Fig. 2(a).
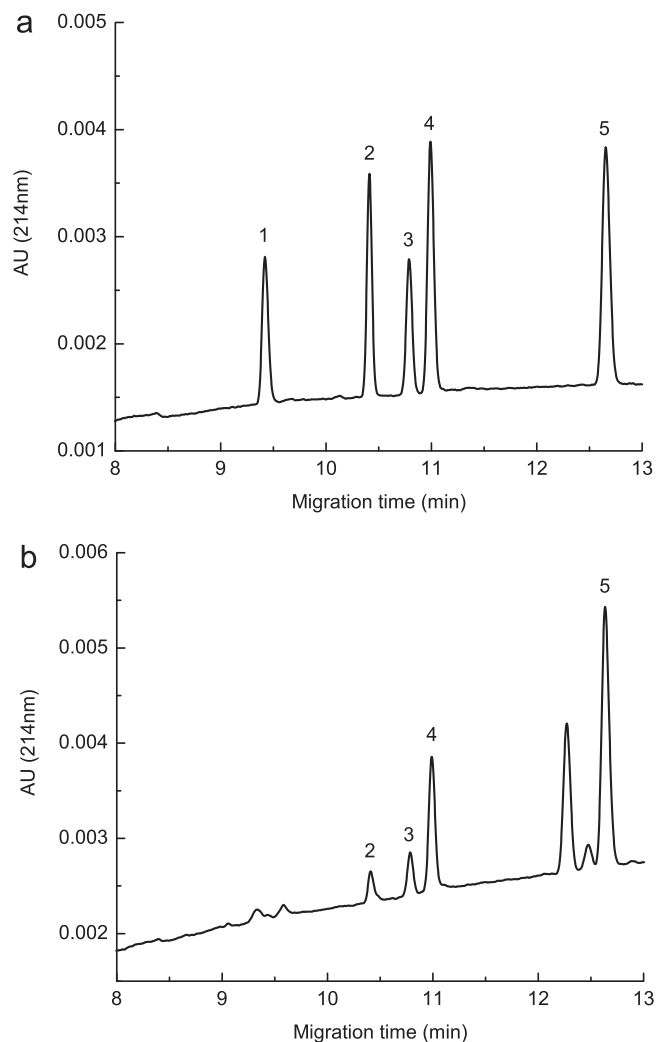
Fig. 2. Electropherogram of a standard mixture solution (a) and the extract of *Sophora* using SWE (b). Both the standard and the actual sample solution were supplemented with 0.8 mM phosphoric acid. Other conditions as described in Fig. 1. 1 = cytisine, 2 = sophocarpine, 3 = matrine, 4 = sophoridine, 5 = oxymatrine.

Under the optimal electrophoresis conditions, the correlation between the concentrations of the analytes and the peak heights was analyzed. Cytisine, sophoridine and oxymatrine showed good linearity ($R^2 > 0.999$) within 0.125–4.0 μg/mL, and sophocarpine and matrine exhibited good linearity ($R^2 > 0.998$) within 0.0625–2.0 μg/mL, respectively. The RSD values of the migration times and peak heights that were determined by five replicate injections of a standard mixture solution under the optimum conditions were below 1.5% and 4.8%, respectively. The detection limits calculated using a signal-to-noise criterion of 3 were in the range of 0.004–0.0013 μg/mL.

3.2. Optimization of SWE and ASE

In this study, after *Sophora* samples (from the campus of Northwest A&F University) were extracted, the contents of the five active compounds was determined by CE under optimized conditions developed to indicate the influence of different extraction methods and extraction conditions on extraction efficiency.

3.2.1. Effect of temperature and pressure

Pressure and temperature are the two most important physical parameters in SWE and ASE, and they have both theoretical and

Table 1
Extraction efficiency of the alkaloids from *Sophora flavescens* Ait. via SWE and ASE expressed as the alkaloids contents of three replicates ±%RSD.

	Content of the alkaloids (mg/g, ±%RSD, $n = 3$)				
	Sophocarpine	Matrine	Sophoridine	Oxymatrine	Total alkaloids
SWE					
Temperature (°C)					
70	0.20 ± 4.2	0.76 ± 4.1	6.25 ± 4.5	11.85 ± 3.3	19.06
100	0.65 ± 3.2	1.77 ± 4.4	7.01 ± 3.9	13.50 ± 2.1	22.93
130	1.53 ± 2.8	3.75 ± 3.8	7.40 ± 4.0	8.03 ± 5.0	20.71
160	3.08 ± 3.1	6.03 ± 4.9	7.64 ± 4.3	5.88 ± 3.6	22.63
190	3.29 ± 2.1	6.85 ± 2.8	7.85 ± 4.8	4.81 ± 4.1	22.80
Pressure (psi)					
600	0.58 ± 2.6	1.50 ± 3.0	6.48 ± 4.3	12.68 ± 4.1	21.24
1000	0.60 ± 3.3	1.72 ± 2.2	6.95 ± 2.7	13.25 ± 3.8	22.52
1500	0.73 ± 1.6	1.75 ± 0.4	7.09 ± 2.5	13.38 ± 2.9	22.95
2000	0.60 ± 3.9	1.49 ± 3.5	6.45 ± 2.8	12.41 ± 4.8	20.95
Extraction time (min)					
5	0.64 ± 4.1	1.73 ± 3.0	6.91 ± 3.2	12.92 ± 2.6	22.20
8	0.63 ± 1.3	2.10 ± 2.6	7.05 ± 0.6	14.39 ± 0.4	24.16
11	0.82 ± 3.0	1.76 ± 3.3	7.87 ± 2.5	13.50 ± 1.8	23.95
14	0.69 ± 5.2	1.75 ± 4.4	7.17 ± 3.4	12.74 ± 3.0	22.35
Cycles					
1	0.57 ± 4.0	0.95 ± 4.3	6.76 ± 2.7	14.77 ± 1.9	23.05
2	0.63 ± 1.3	2.10 ± 2.6	7.05 ± 0.6	14.39 ± 0.4	24.16
3	0.67 ± 5.1	1.72 ± 3.7	6.66 ± 4.5	13.47 ± 2.5	22.52
ASE					
Temperature (°C)					
70	0.10 ± 5.1	0.46 ± 4.5	3.87 ± 1.6	11.42 ± 5.1	15.85
100	0.15 ± 3.6	1.25 ± 3.4	6.63 ± 4.8	10.83 ± 5.7	18.86
130	0.58 ± 3.3	2.28 ± 4.8	5.67 ± 2.9	7.38 ± 5.2	15.91
160	0.93 ± 2.9	3.05 ± 2.1	5.15 ± 4.0	5.25 ± 4.9	14.38
Pressure (psi)					
600	0.14 ± 4.2	1.20 ± 5.5	5.83 ± 3.1	9.77 ± 3.7	16.94
1000	0.18 ± 4.8	1.24 ± 5.4	6.55 ± 5.6	10.43 ± 2.6	18.40
1500	0.14 ± 4.7	0.96 ± 4.2	5.35 ± 2.8	9.73 ± 4.3	16.18
2000	0.19 ± 5.2	1.35 ± 3.9	6.42 ± 1.6	10.97 ± 4.5	18.93
Extraction time (min)					
5	0.13 ± 2.3	1.26 ± 0.7	6.22 ± 1.9	11.11 ± 1.1	18.72
8	0.24 ± 3.2	1.45 ± 3.6	6.27 ± 1.7	9.70 ± 1.9	17.66
11	0.25 ± 1.9	1.46 ± 3.3	6.48 ± 3.2	9.98 ± 1.6	18.17
14	0.16 ± 3.2	1.28 ± 0.9	6.13 ± 3.8	10.12 ± 5.3	17.69
Cycles					
1	0.09 ± 5.1	0.60 ± 4.9	5.68 ± 4.6	11.71 ± 4.2	18.08
2	0.11 ± 2.7	1.27 ± 2.5	6.32 ± 3.7	10.89 ± 3.7	18.60
3	0.17 ± 5.1	1.33 ± 5.5	6.00 ± 5.2	9.50 ± 1.9	17.00

practical implications for the extraction process. In this experiment, the effect of temperature on the yields of extracted compounds was investigated with an extraction pressure of 1000 psi, a static extraction time of 5 min and a cycle number of 2 (Table 1). When SWE was used, the yields of sophocarpine, matrine and sophoridine had upward tendencies with increasing temperature from 70 to 190 °C. The yield of oxymatrine increased firstly with temperature ranging from 70 to 100 °C, then dropping significantly from 100 to 190 °C (cytisine could not be detected in all the samples). When ASE was used, increasing the temperature from 70 to 160 °C increased the yields of sophocarpine and matrine. The yield of sophoridine first increased and then decreased, with the highest yield at 100 °C. The yield of oxymatrine decreased with increasing temperature. With an extraction solvent of either water or ethanol, the total alkaloid yield reached its maximum at 100 °C.

At an extraction temperature of 100 °C, a static extraction time of 5 min and a cycle number of 2, four levels of pressure (600, 1000, 1500, 2000 psi) were applied to the extraction, and the corresponding extracted yields are reported in Table 1. For SWE with increasing extraction pressure, the yields of sophocarpine, matrine, sophoridine and oxymatrine first increased slightly and then decreased, and the yield of each active compound reached its maximal level at 1500 psi, which was then selected as the optimal value for SWE. For ASE with increasing extraction pressure, the

yields of sophocarpine, matrine, sophoridine and oxymatrine first increased, then decreased and increased again. The maximum levels reached at both 1000 psi and 2000 psi. Since the latter was excluded because of a safety issue with the equipment, 1000 psi was selected in the subsequent experiments. It is also noticed that the extraction pressure did not influence the yields as obviously as the extraction temperature.

3.2.2. Effect of extraction time and cycle number

When SWE was used, the effect of extraction time on the yield of the active compound was examined with an extraction temperature of 100 °C, an extraction pressure of 1500 psi and a cycle number of 2 (Table 1). With increasing extraction time, the yield of each analyte generally showed an initial increasing and then decreasing trend, and the total alkaloid yield reached its maximum at 8 min. The effect of the extraction time on the yield by ASE was tested with an extraction temperature of 100 °C, an extraction pressure of 1000 psi and a cycle number of 2 (Table 1). As the extraction time increased, the yields of sophocarpine and matrine and sophoridine showed the same variance trend as in SWE, while the yield of oxymatrine decreased firstly and then kept stable. An extraction time of 5 min was chosen due to the highest total yield obtained.

The effect of the cycle number on the yield was examined for SWE with an extraction temperature of 100 °C, an extraction

Table 2
Comparison of the alkaloid contents in medicinal plant from different sources and *Sophora* instant granule (mg/g, n = 3).

Samples	Sophocarpine		Matrine		Sophoridine		Oxymatrine		Total alkaloids content
	Content	RSD%	Content	RSD%	Content	RSD%	Content	RSD%	
Crude No. 1	2.21	4.0	5.50	2.0	2.33	3.3	28.34	1.2	38.37
Crude No. 2	1.21	3.8	3.72	4.4	6.09	6.2	21.04	5.5	32.06
Crude No. 3	0.63	1.3	2.10	2.6	7.05	0.6	14.39	0.4	24.17
Granule	14.56	2.7	51.81	2.1	0.00	–	13.73	7.5	84.11

pressure of 1500 psi and an extraction time of 8 min (Table 1). The yield of sophocarpine showed a slight upward trend with increasing cycle number. The yields of matrine and sophoridine first increased and then decreased, showing the maximal levels at 2 cycles. However, the yield of oxymatrine decreased with an increase in cycle number. The effect of the cycle number on the yields was investigated for ASE with an extraction temperature of 100 °C, an extraction pressure of 1000 psi and an extraction time of 5 min (Table 1). The yields of sophocarpine and matrine showed upward trends with increasing cycle number. Sophoridine manifested an initial upward and then downward yields. The yield of oxymatrine dropped obviously with increasing cycle number. The total alkaloid yields reached their maximal levels at a cycle number of 2 whichever extraction method was used.

In summary, the optimal SWE conditions were as follows: an extraction temperature of 100 °C, an extraction pressure of 1500 psi, a static extraction time of 8 min and a cycle number of 2. The optimal ASE conditions were as follows: an extraction temperature of 100 °C, an extraction pressure of 1000 psi, a static extraction time of 5 min and a cycle number of 2.

3.2.3. Recovery yields

Six replicates of 0.5 g *Sophora* sample were accurately weighed, in which appropriate amounts of cytisine, sophocarpine, matrine, sophoridine and oxymatrine were spiked then. After extracting and analyzing under the optimal SWE/CE and ASE/CE conditions, the recoveries of the analytes were determined. For SWE, the average recoveries of six replicates of spiked samples ranged from 95% to 119%, and for ASE, the average recoveries ranged from 62% to 106%. The relatively standard deviations of the recoveries (n = 6) were < 8.7% indicating the reported method achieved satisfactory repeatability.

3.3. Comparison of different extraction methods

After establishing the optimal conditions for SWE and ASE, the extraction efficiencies of the different extraction methods were compared based on the extraction yields (Fig. 3). Compared with other methods, SWE showed a relatively high yield for each analyte. When ASE was performed, the yield of oxymatrine was the lowest among the four methods, but this method seemed to be slightly better than chloroform soaking extraction and water ultrasonic extraction for matrine and sophoridine. Chloroform soaking extraction and water ultrasonic extraction were particularly effective in terms of extraction of oxymatrine, but they worked less efficiently for other three alkaloilds. For the total alkaloild yields, SWE manifest to be the best, closely followed by water ultrasonic extraction, which gave a higher value than chloroform soaking extraction and ASE.

Additionally, as SWE and water ultrasonic extraction used water as solvent, which is suitable for CE analysis without solvent evaporation, which is a serious advantage in terms of sample preparation time as well as the accuracy of the method. As can be seen from the
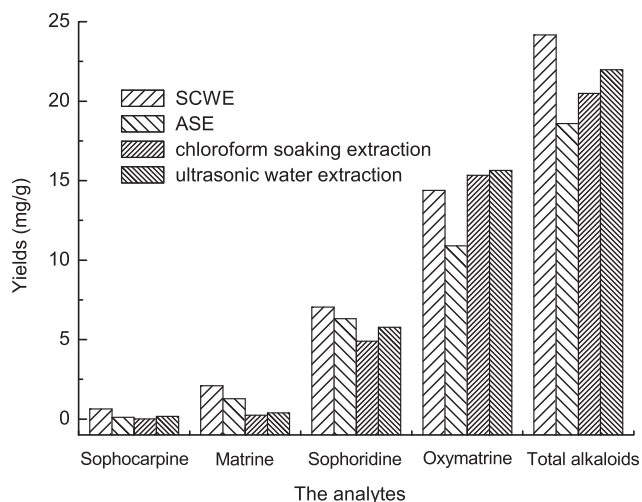
Fig. 3. Comparison of the yield of each analyte using different extraction methods.

results, SWE is preferred to the other three extraction methods for the extraction of alkaloids in *Sophora*.

3.4. Comparison of analytes contents in different medicines

The SWE-CE method developed was used to extract and analyze the alkaloids in *Sophora* samples from different sources and *Sophora* instant granule, and the electropherogram of a real sample is illustrated in Fig. 2(b), the contents in Table 2. The amounts of matrine and oxymatrine in the three crude samples were close to those extracted by supercritical fluid extraction [13]. It is also noted that the amounts of matrine and sophocarpine in the instant granule manifested ca. 10–20 times higher than those in the crude samples, while the amount of oxymatrine in the former fell within the same range in the latter, and sophoridine could not be detected in the former. A conclusion can be drawn that the production process of *Sophora* instant granule from crude *Sophora* plants influenced the content ratio of the active compounds to a great degree, which should be noticed.

4. Conclusions

This study describes an efficient and environmentally friendly extraction and analysis approach for the determination of alkaloids in *Sophora*. SWE exhibited the highest extraction efficiency for the total alkaloid yield. And its particular advantages over traditional extraction methods lies on a short extraction time, no need for organic solvent consumption and high extraction efficiency. Adding a certain amount of acid to the sample matrix was a simple way to improve the electro-injection reproducibility in CE with field amplified stacking. Due to the advantages of both SWE and CE, this method may have a promising potential in application to the quality control of natural medicine.

Acknowledgements

References

[1] Y.F. Miao, B. Wu, W.Q. Zhang, Y.M. Qiu, B. Li, X.J. Lu, Neuroprotective effect of sophocarpine against transient focal cerebral ischemia via down-regulation of the acid-sensing ion channel 1 in rats, Brain Res. 1382 (2011) 245–251.

[2] A.D. Kinghorn, M.F. Balandrin, Quinolizidine alkaloids of the leguminosae: structural types, analysis, chemotaxonomy and biological activities, in: S.W. Pelletier (Ed.), Alkaloids: Chemical and Biological Perspectives, vol. 2, Wiley, New York, 1984, pp. 105–148.

[3] B.Q. Wang, Z.G. She, X.H. Wang, X.L. Hu, Determination of matrine by thin layer chromatography-fluorescence quenching, Chin. J. Anal. Chem. 25 (1997) 693–695.

[4] F.Q. Yang, J.Q.T.Y. Zhang, Y. Ito, Preparative separation of alkaloids from the root of Sophora flavescens Ait. by pH-zone-refining counter-current chromatography, J. Chromatogr. A 822 (1998) 316–320.

[5] J.Y. Yin, Y.H. Xu, J. Li, E.K. Wang, Analysis of quinolizidine alkaloids in Sophora flavescens Ait. by capillary electrophoresis with tris(2,2′-bipyridyl) ruthenium (II)-based electrochemiluminescence detection, Talanta 75 (2008) 38–42.

[6] Y.Q. Yu, P.L. Ding, D.F. Chen, Determination of quinolizidine alkaloids in Sophora medicinal plants by capillary electrophoresis, Anal. Chim. Acta 523 (2004) 15–20.

[7] Y.J. Wu, Q. Shao, Z.Q. Zhen, Y.Y. Cheng, Determination of quinolizidine alkaloids in Sophora flavescens and its preparation using capillary electrophoresis, Biomed. Chromatogr. 20 (2006) 446–450.

[8] S.H. Liu, Q.F. Li, X.G. Chen, Z.D. Hu, Field-amplified sample stacking in capillary electrophoresis for on-column concentration of alkaloids in Sophora flavescens Ait., Electrophoresis 23 (2002) 3392–3397.

[9] J.P. Lai, X.W. He, Y. Jiang, F. Chen, Preparative separation and determination of matrine from the Chinese medicinal plant Sophora flavescens Ait. by molecularly imprinted solid-phase extraction, Anal. Bioanal. Chem. 375 (2003) 264–269.

[10] X.Y. Su, L. Kong, X. Lia, X.G. Chen, M. Guo, H.F. Zou, Screening and analysis of bioactive compounds with biofingerprinting chromatogram analysis of traditional Chinese medicines targeting DNA by microdialysis/HPLC, J. Chromatogr. A 1076 (2005) 118–126.

[11] L. Zhang, L. Xu, S.S. Xiao, Q.F. Liao, Q. Li, J. Liang, X.H. Chen, K.Sh. Bi, Characterization of flavonoids in the extract of Sophora flavescens Ait. by high-performance liquid chromatography coupled with diode-array detector and electrospray ionization mass spectrometry, J. Pharm. Biomed. Anal. 44 (2007) 1019–1028.

[12] J.Z. Song, H.X. Xu, S.J. Tian, P.P. But, Determination of quinolizidine alkaloids in traditional Chinese herbal drugs by nonaqueous capillary electrophoresis, J. Chromatogr. A 857 (1999) 303–311.

[13] J.Y. Ling, G.Y. Zhang, Z.J. Cui, C.K. Zhang, Supercritical fluid extraction of quinolizidine alkaloids from Sophora flavescens Ait. and purification by high-speed counter-current chromatography, J. Chromatogr. A 1145 (2007) 123–127.

[14] Y. Cheng, S.M. Li, Analytical method development of long-chain ketones in PM2.5 aerosols using accelerated solvent extraction and Gc/FID/MSD, Int. J. Environ. Anal. Chem. 84 (2004) 367–378.

[15] J. Kronholm, K. Hartonen, M.L. Riekkola, Analytical extractions with water at elevated temperatures and pressures, Trends Anal. Chem. 26 (2007) 396–412.

[16] C.C. Teo, S.N. Tan, J.W.H. Yong, C.S. Hew, E.S. Ong, Pressurized hot water extraction (PHWE), J. Chromatogr. A 1217 (2010) 2484–2494.

[17] Pharmacopoeia Commission of the Ministry of Public Health, The People's Republic of China, Pharmacopoeia of the People's Republic of China: Part 1, Guangdong Academic Press, 1995, pp. 176–177.

[18] C.X. Zhang, W. Thormann, Head-column field-amplified sample stacking in binary system capillary electrophoresis. 2. Optimization with a preinjection plug and application to micellar electrokinetic chromatography, Anal. Chem. 70 (1998) 540–548.

Short communication

UPLC MS/MS assay for routine quantification of dabigatran – A direct thrombin inhibitor – In human plasma

Xavier Delavenne [a,b,*], Julie Moracchini [a], Silvy Laporte [b], Patrick Mismetti [b], Thierry Basset [a,b]

[a] Laboratory of Pharmacology and Toxicology, University Hospital, F-42055 Saint-Etienne, France
[b] Thrombosis Research Group (EA 3065), University Jean Monnet, F-42023 Saint-Etienne, France

A B S T R A C T

This article described the development and full validation of rapid and accurate liquid chromatography method, coupled with tandem mass spectrometry detection, for quantification of dabigatran in human plasma with $[^{13}C_6]$-dabigatran as internal standard. Plasma pretreatment involved a single step protein precipitation with methanol. Separation was performed by ultra performance reversed-phase chromatography on an Acquity UPLC BEH C8 100 mm × 1 mm × 1.7 μm column using a gradient elution mode. The mobile phase was a mix of distilled water containing 0.1% formic acid and methanol containing 0.1% formic acid. Specific multiple reaction monitoring transitions were recorded in positive electrospray ionization. The method was linear over the concentration range of 2–500 μg/L. The intra- and inter-day precision values were below 11.3% and accuracy was within 93.8% and 108.8% for all QC levels (5, 75 and 400 μg/L). The lower limit of quantification was 2 μg/L. Total analysis time was to 10 min including sample preparation.

1. Introduction

Dabigatran etexilate is a novel oral direct thrombin inhibitor. In recent studies, dabigatran demonstrated its efficacy for prophylaxis and treatment of thromboembolic event during orthopedic surgery and curative treatment of hypercoagulability in atrial fibrillation [1,2].

Contrary to vitamin K antagonist (VKA), no laboratory monitoring was advised for this drug because its pharmacokinetic profile is supposed to be more predictable [3,4]. However EMEA underlined the low bioavailability and very large interindividual variability of dabigatran exposition in case of renal impairment, elderly patients or extreme weights [5]. From that point, some arguments are in favor of a monitoring assay [6]. First, dabigatran is eliminated at 80% by kidney leading to accumulation in renal impaired patients. Second, it is also a substrate of P-glycoprotein (P-gp) and may be subject to drug–drug interactions [7,8]. P-gp inductors or inhibitors can respectively decrease or increase its bioavailability. In these situations, dabigatran accumulation could increase bleeding risk and may require therapeutic drug monitoring.

Several methods were previously published for quantification of dabigatran in phase II/III studies [1,3,7–11]. None of them

presented the complete analytical process used and validation criteria according the FDA guidelines [12]. The purpose of this work was to develop a fully validated and routinely available ultra performance liquid chromatography coupled with tandem mass spectrometry (UPLC MS/MS) method by for quantification of dabigatran in human plasma.

2. Materials and methods

2.1. Chemicals and reagents

Dabigatran and $[^{13}C_6]$-dabigatran were purchased from Alsachim (Strasbourg, France). LC MS grade methanol and acetonitrile were obtained from Fisher Scientific GmbH (Schwerte, Germany) and distilled water from Aguettant (Lyon, France). Hydrochloric acid 0.1 N was obtained from Sigma–Aldrich (St. Quentin Fallavier, France). A 0.2 μm polyvinylidene fluoride filter was used for mobile phases and was provided by Interchim (Montluçon, France).

2.2. Stock solutions, calibration standards and quality control samples

Stock solutions of dabigatran and internal standard $[^{13}C_6]$-dabigatran were prepared in methanol/HCl 0.1 N (90/10, v/v) at a concentration of 50 μg/L, and stored at −20 °C. Working solutions were prepared freshly on each day of analysis as serial dilutions

* Corresponding author at: Laboratory of Pharmacology and Toxicology, University Hospital, F-42055 Saint-Etienne, France. Tel.: +33 4 7712 7464; fax: +33 4 7712 7311.
E-mail address: xavier.delavenne@chu-st-etienne.fr (X. Delavenne).

in methanol. Calibration curve standards and quality control (QC) samples were prepared in blank human plasma (Etablissement Français du Sang). Calibrator concentrations were 0, 2, 10, 50, 100, 250 and 500 μg/L and QC levels were 5, 75 and 400 μg/L. Calibration curves and QC samples were prepared from separate working solutions. Internal standard (IS) solution was prepared at a concentration of 200 μg/L by diluting $[^{13}C_6]$-dabigatran in methanol.

2.3. Sample preparation

A 100 μL aliquot of plasma sample, calibrator or QC was added into a 1.5 mL polypropylene tube with 900 μL of methanol/HCl 0.1 N (90/10, v/v) containing the internal standard $[^{13}C_6]$-dabigatran at the concentration of 50 μg/L. The mixture was vortexed and centrifuged at 14,000 rpm for 5 min at room temperature. The supernatant was transferred to an autosampler vial and 10 μL was injected into the in the ultra performance liquid chromatography (UPLC) system using a temperature-controlled autosampler device (10 °C).

2.4. Liquid chromatography

Chromatographic analysis was performed using an Acquity ultra performance liquid chromatograph system coupled to a Quattro Micro triple quadrupole mass spectrometer from Waters (Saint-Quentin en Yvelines, France). The instrument was equipped with an electrospray ionization source. Separation was achieved at 40 °C using an Acquity UPLC BEH C8 100 mm × 1 mm × 1.7 μm (Waters). The mobile phase was a mix of A: distilled water containing 0.1% formic acid and B: methanol containing 0.1% formic acid. A 0.2 μm polyvinylidene fluoride filter provided by Interchim (Montluçon, France) was used to filter mobile phases. The gradient was: 0–0.3 min, 10% B; 0.3–0.6 min: linear from 10 to 90% B; 0.6–2.3 min: 90% B; 2.5 min return to initial conditions until 4.5 min. The flow rate was 0.18 mL/min.

2.5. Tandem mass spectrometry

The instrument was equipped with an electrospray ionization source. The analytes were detected in multiple reaction monitoring mode (MRM) using the positive ionization mode. Mass spectrometer parameters were: capillary voltage 3 kV; extractor 4 V; lens voltage 0.3 V; source temperature 140 °C; desolvatation temperature 400 °C; cone gas flow 50 L/h; desolvatation gas flow 500 L/h. Dry nitrogen (>99.5%) produced by N2 generator F-DBS (Courtaboeuf, France) was used as desolvatation and nebulization gas and argon (>99.999%, Mecer, France) was used as collision gas. The system control and data acquisition were performed using MassLynx V4.1 software (Waters).

2.6. Method validation

The method was validated according to internationally accepted recommendations [12].

2.6.1. Linearity, accuracy and precision
Linearity accuracy and precision were evaluated using calibrators and QC levels. Linear regression analysis was carried out on the standard curve generated by plotting peak areas ratio of dabigatran and IS versus concentration of dabigatran. Standard curves were constructed by least-squares linear regression analysis using a weighting factor of 1/concentration. Intra and inter-day precisions were assessed by analysis of spiked QC samples six times during the same day and on six different days. The mean accuracy was determined by comparing the measured concentrations

against the theoretical concentration $((1 - (\text{theoretical concentration} - \text{mean concentrations})/\text{theoretical concentration}) \times 100)$ for the 3 level QC samples.

2.6.2. Limit of detection and quantification
Lower limit of detection (LLOD) and lower limit of quantification (LLOQ) were determined by direct injection of decreasing amounts of dabigatran in plasma samples and were calculated as the concentration giving peaks with a signal-to-noise ratio of 3 and 10 respectively. For LLOQ precision should be better than 20% and accuracy in the range of 80–120%.

2.6.3. Stability
Samples stability was determined at three level of concentration ($n = 6$). Short-term temperature stability was assessed by thawing at room temperature (25 °C) three level samples and keeping at this temperature for 6 and 12 h. Long-term stability was assessed by storing aliquots at −20 °C for 5, 7, 30 and 45 days. The freeze/thaw stability was evaluated after three complete freeze/thaw cycles (−20 to 25 °C) on consecutive days. Post-preparative stability was evaluated by storing samples in autosampler 12 h at 4 °C. Dabigatran was considered stable if the relative error (RE (%) = (measured concentration − reference concentration)/reference concentration × 100) was below 15% for different conditions.

2.6.4. Selectivity
To investigate selectivity, plasma samples from 10 different dabigatran free subjects were analyzed without addition of IS.

2.6.5. Matrix effect
The matrix effects were investigated by direct infusion of dabigatran and $[^{13}C_6]$-dabigatran into the mass spectrometer detector during the chromatographic analysis of 6 different blank plasma extracts. The standard solution of dabigatran and IS at 2 mg/L were infused at a flow rate of 30 μL/min during the chromatographic analysis. The chromatographic signals in each MRM transition were analyzed to check for any signal disturbance at the analytes retention times.

3. Results and discussion

3.1. Liquid chromatography

Representative chromatograms of drug free, LLOQ and supposed over exposed human plasma samples are shown in Fig. 1. Dabigatran and IS retention times and peak shape did not varied over the whole validation period (data not shown). Retention time was near 1.6 min for dabigatran and IS, total run time of 4.5 min allowed return to initials conditions.

3.2. Mass spectrometry

In positive electrospray ionization, quantification was performed by addition of 472.19→324.17 m/z and 472.19→306.13 m/z MRM transitions for [dabigatran +H]$^+$. Internal standard was monitored by 478.32→330.18 m/z MRM. Qualification transitions were 472.19→289.09 m/z and 478.32→295.10 m/z for dabigatran and internal standard, respectively. Fig. 2 presents MS and MS/MS mass spectrums for both analytes. Optimized mass spectrometer parameters for each compound were cone voltage 35 V, collision energy 20 V and dwell time 0.17 s.
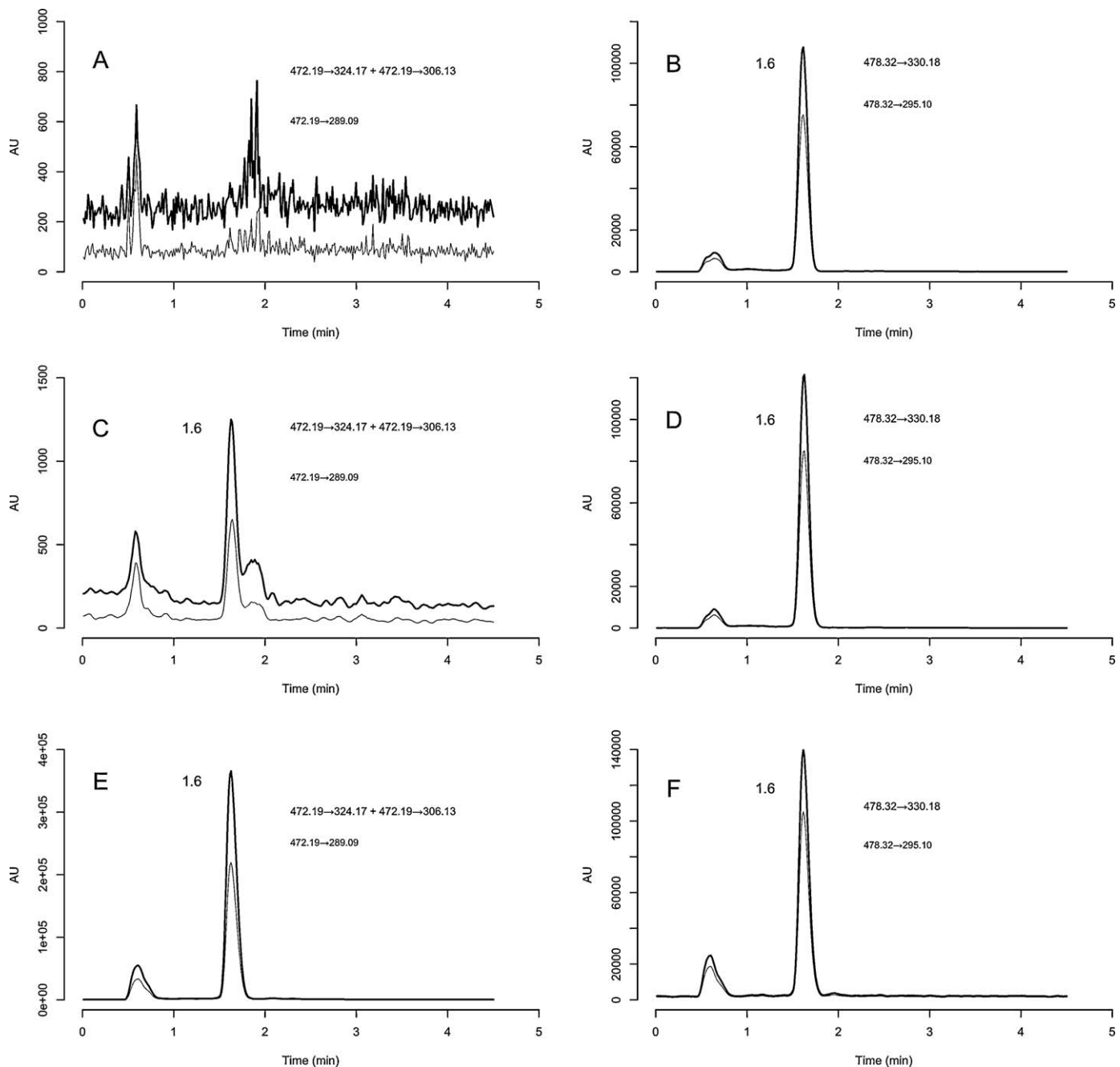
Fig. 1. Representative chromatograms of a negative sample (A, B), dabigatran LLOQ = 2 μg/L (C, D) and case (E, F). A, C and E represent dabigatran chromatograms; B, D and F represent [$^{13}C_6$]-dabigatran chromatograms.

3.3. Method validation

3.3.1. Linearity, accuracy and precision

Dabigatran calibration curve was linear between 1 and 500 μg/L. Typical calibration curve equation was $y = 0.00425x - 0.00132$. Where y represents the ratio of dabigatran peak area to that of IS and x the plasma concentration. The relative standard deviations of slopes and intercepts for 10 calibration curves were below 6% and mean r^2 was above 0.9998. The inter- and intra-day precision and accuracy measured at the three QC levels were summarized in Table 1. Relative standard deviations were less than 11.3% for both inter- and intra-day precision. Accuracy was within 93.9% and 108.8%. The above values were within the acceptable range, the method is considered accurate and precise.

3.3.2. Limit of detection and quantification

LLOD and LLOQ were 1 μg/L and 2 μg/L, respectively, with an injection volume of 10 μL. For LLOQ the precision and accuracy were 7.1% and 97%.

Table 1
Method validation, precision and accuracy.

	Dabigatran		
Theoretical concentration μg/L	5	75	400
Intra-day ($n = 6$)			
Precision (%)	6.3	3.0	2.2
Accuracy (%)	98.4	102.3	99.8
Inter-day ($n = 6$)			
Precision (%)	11.9	4.8	5.8
Accuracy (%)	108.8	93.9	101.5
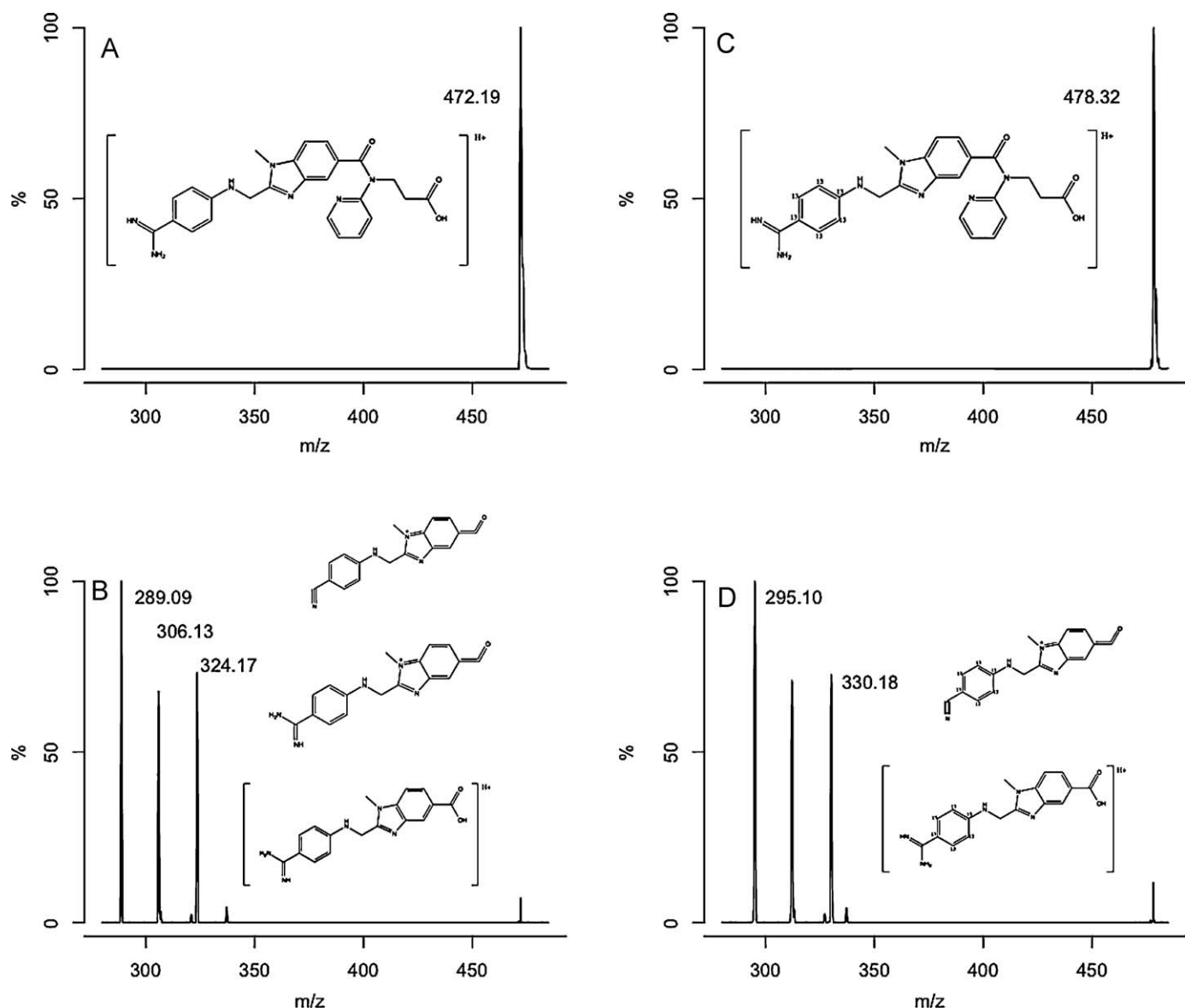
Fig. 2. Dabigatran and [$^{13}C_6$]-dabigatran mass spectrums, MS (A, C) and MS/MS (B, D).

3.3.3. Stability

Short-term, long-term, post-preparative storage and three freeze–thaw cycles indicated that dabigatran was stable in human plasma and post-preparative matrix (Table 2). The overall dispersion did not exceeded 7% (CV%) and relative error 15%.

3.3.4. Selectivity

No relevant interferences were observed on dabigatran and IS detection channels in ten different dabigatran free human samples.

3.3.5. Matrix effect

No significant matrix effect was observed on each monitored channels at the retention time of dabigatran and IS (1.6 min) in 6 blank plasma. Moreover the impact of matrix effect would be balanced by isotopically labeled IS (Fig. 3).

3.4. Case report

As an illustration, we report the case of 75 years old patient treated with dabigatran in prevention of venous thromboembolism after a major orthopedic surgery. This patient presented a major bleeding episode for which physicians suspected an accumulation of dabigatran. After quantification, the concentration of dabigatran was over 7000 µg/L (Fig. 1), which is far above therapeutic range observed in phase II/III (100–500 µg/L) [9]. Regarding the context

Table 2
Stability (*n* = 6).

Dabigatran concentration (µg/L)		
Short term mean (relative error%)		
0 h	4.5 (ref)	76.3 (ref)	359.0 (ref)
6 h	4.8 (6.7)	75.3 (−1.3)	359.3 (0.1)
12 h	4.3 (−4.4)	77.2 (1.2)	349.0 (−2.8)
Long term mean (relative error%)		
5 day	4.6 (2.2)	75.4 (−1.2)	369.5 (2.9)
7 day	4.2 (−6.7)	72.9 (−4.5)	346.3 (−3.5)
15 day	4.7 (4,4)	69.4 (−9.0)	345.8 (−3.7)
30 day	4.2 (−6.7)	72.9 (−4.5)	346.3 (−3.5)
45 day	5.1 (13.3)	70.9 (−7.1)	344.7 (−4.0)
Freeze-thaw stability mean (relative error%)		
	3,9 (−13.3)	70,0 (−8.3)	349.0 (−2.8)
Post-preparative stability mean (relative error%)		
	4.6 (2.2)	78.3 (2.6)	362.7 (1.0)
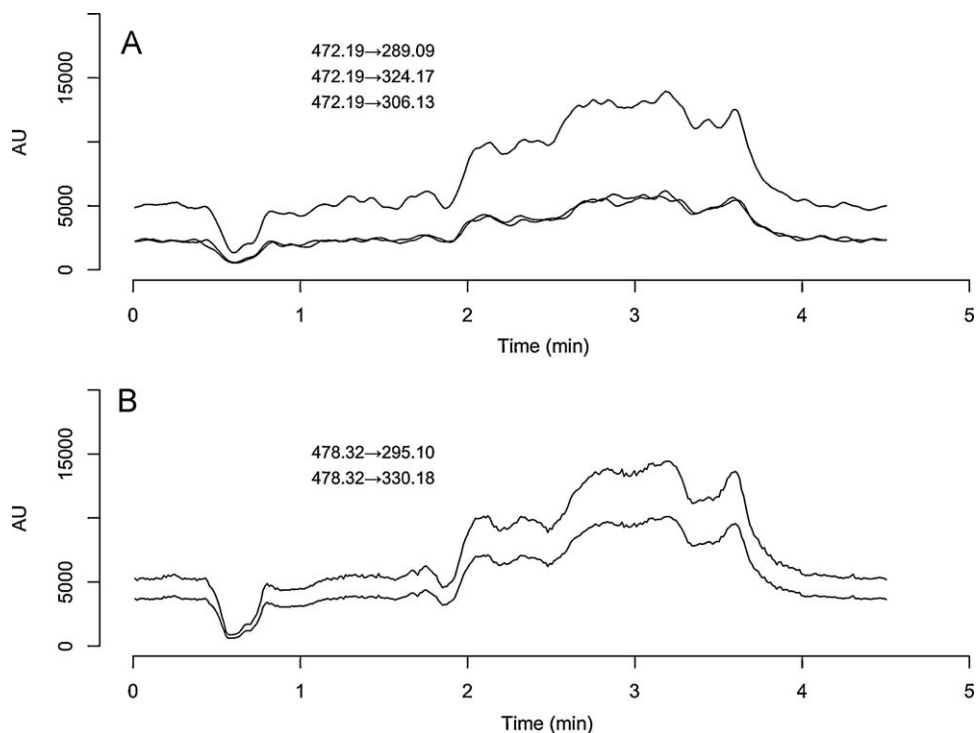
Fig. 3. Representative chromatograms of matrix effect experience on dabigatran (A) and [^{13}C$_6$]-dabigatran (B) monitored transitions.

of major bleeding, a full validation of dilution process was not considered. However, a 10 000 μg/L plasma QC was spiked and further diluted it in the same condition as the case, i.e. 50 μL of sample plus 950 μL of drug free plasma. The QC measured concentration was 9782 μg/L.

4. Conclusion

In conclusion, this paper described the development and full validation of a single step preparation, rapid (about 10 min), sensible and accurate ultra performance liquid chromatography method using tandem mass spectrometry detection for dabigatran quantification in human plasma. This method is totally compatible with other UPLC MS/MS routine activities and could be applied to 24/7 clinical toxicology to monitor dabigatran accumulation and therapeutic drug monitoring [13].

References

[1] B.I. Eriksson, O.E. Dahl, H.R. Büller, R. Hettiarachchi, N. Rosencher, M.-L. Bravo, L. Ahnfelt, F. Piovella, J. Stangier, P. Kälebo, P. Reilly, B.I.S. Group, A new oral direct thrombin inhibitor, dabigatran etexilate, compared with enoxaparin for prevention of thromboembolic events following total hip or knee replacement: the BISTRO II randomized trial, Journal of Thrombosis and Haemostasis 3 (2005) 103–111.

[2] S.J. Connolly, M.D. Ezekowitz, S. Yusuf, P.A. Reilly, L.I. Wallentin, Randomized evaluation of long-term anticoagulation therapy, newly identified events in the RE-LY trial, The New England Journal of Medicine 363 (2010) 1875–1876.

[3] J. Stangier, K. Rathgen, H. Stähle, D. Gansser, W. Roth, The pharmacokinetics, pharmacodynamics and tolerability of dabigatran etexilate, a new oral direct thrombin inhibitor, in healthy male subjects, British Journal of Clinical Pharmacology 64 (2007) 292–303.

[4] H. Bounameaux, G. Reber, New oral antithrombotics: a need for laboratory monitoring. Against, Journal of Thrombosis and Haemostasis 8 (2010) 627–630.

[5] EMEA, CHMP assessment report for Pradaxa, 2008.

[6] P. Mismetti, S. Laporte, New oral antithrombotics: a need for laboratory monitoring, Journal of Thrombosis and Haemostasis 8 (2010) 621–626.

[7] S. Blech, T. Ebner, E. Ludwig-Schwellinger, J. Stangier, W. Roth, The metabolism and disposition of the oral direct thrombin inhibitor, dabigatran, in humans, Drug Metabolism and Disposition 36 (2008) 386–399.

[8] J. Stangier, H. Stahle, K. Rathgen, W. Roth, K. Shakeri-Nejad, Pharmacokinetics and Pharmacodynamics of dabigatran etexilate, an oral direct thrombin inhibitor, are not affected by moderate hepatic impairment, The Journal of Clinical Pharmacology 48 (2008) 1411–1419.

[9] K.-H. Liesenfeld, H.G. Schäfer, I.F. Trocóniz, C. Tillmann, B.I. Eriksson, J. Stangier, Effects of the direct thrombin inhibitor dabigatran on ex vivo coagulation time in orthopaedic surgery patients: a population model analysis, British Journal of Clinical Pharmacology 62 (2006) 527–537.

[10] J. Stangier, H. Stähle, K. Rathgen, R. Fuhr, Pharmacokinetics and pharmacodynamics of the direct oral thrombin inhibitor dabigatran in healthy elderly subjects, Clinical Pharmacokinetics 47 (2008) 47–59.

[11] I.F. Troconiz, C. Tillmann, K.-H. Liesenfeld, H.-G. Schafer, J. Stangier, Population pharmacokinetic analysis of the new oral thrombin inhibitor dabigatran etexilate (BIBR 1048) in patients undergoing primary elective total hip replacement surgery, The Journal of Clinical Pharmacology 47 (2007) 371–382.

[12] FDA, Guidance for Industry, Bioanalytical Method Validation, 2001.

[13] X. Delavenne, J.P. Gay-Montchamp, T. Basset, HPLC MS/MS method for quantification of meprobamate in human plasma: application to 24/7 clinical toxicology, Journal of Chromatography B: Analytical Technologies in the Biomedical and Life Sciences 879 (2011) 215–218.

Short communication

FT-NIR spectroscopy for rapid and simple determination of nimesulide in rabbit plasma for pharmacokinetic analysis

P.V. Ajayakumar [a,*], Debabrata Chanda [b], Anirban Pal [b], Mahendra P. Singh [b], A. Samad [c]

[a] Analytical Chemistry Department, CSIR – Central Institute of Medicinal and Aromatic Plants, P.O. CIMAP, Lucknow 226015, India
[b] In-vivo Testing Facility, Molecular Bioprospection Department, CSIR – Central Institute of Medicinal and Aromatic Plants, P.O. CIMAP, Lucknow 226015, India
[c] Microbiology and Plant pathology Department, CSIR – Central Institute of Medicinal and Aromatic Plants, P.O. CIMAP, Lucknow 226015, India

ARTICLE INFO

ABSTRACT

High-throughput analysis of a large number of samples for pharmacokinetic study is necessary in drug development and pharmacovigilance. Usually, drug quantification for pharmacokinetics and bio-availability is achieved through matrix extraction and HPLC analysis, which is time, labour and cost intensive method. A prompt and solvent free method is the quest for such analysis in the present times. Pharmacokinetic analysis of nimesulide from plasma samples of rabbits through Fourier transform near infrared (FT-NIR) spectroscopy analysis combined with partial least squares (PLS) regression model was undertaken with validation through HPLC analysis. Pharmacokinetic parameters obtained through FT-NIR and HPLC were found to be statistically similar with errors below the acceptable limits. The study demonstrates the use of FT-NIR for pharmacokinetics and bio-availability studies. This high throughput method analyses more than 50 samples in an hour without solvents usage and provide ample scope for automation and commercial utilization.

© 2011 Elsevier B.V. All rights reserved.

1. Introduction

Near infrared (NIR) spectroscopy is a noninvasive, relatively low cost optical technique, portable, useful for real-time measurement of changes in tissues in relation to oxygenation and perfusion [1], body fat [2], qualitative and quantitative measurements of various chemicals in foods, pharmaceuticals, materials, medical, agricultural produce etc. [3]. In addition, Fourier transform near infrared (FT-NIR) is extensively used in different fields of the pharmaceutical industry like prediction of tablet properties of raw-mixed powders before compression [4]; quantitative measurement of components in intact tablets [5,6]; raw materials, intermediate and finished product forms including gels [7] and development of solid dosage forms [8] besides others. Recently, FT-NIR has extensively being explored for studies in urology [1,9]; sports medicine [10], real-time study of brain vascular and metabolic activities [11]. Much of the appeal of NIR technique is because of the fact that wealth of chemical and physical information can be obtained with in seconds often without the need for any sample preparation.

Although Fourier transform infrared spectroscopy (FT-IR) has been used for determining molecular concentrations of different bio-active analytes in various biological matrices like blood, serum, plasma and urine [12], the use of FT-NIR in the bio-analysis of

pharmacophore in biological samples like blood, urine, plasma or serum samples has not yet been reported. There is a tremendous need and scope for novel and high throughput analytical method for bioanalysis in the course of drug discovery and development [13]. Hence in the present experiment, we have done pharmacokinetics study of nimesulide in rabbit through FT-NIR analysis of plasma samples and validated the same through HPLC analysis.

Nimesulide (4-nitro-2-phenoxymethanesulfonanide) was chosen because of its continuing use in India and other developing countries as a prominent, selective cyclooxygenase (COX-2) inhibitor in inflammatory conditions as well as the easiest availability of high-performance liquid chromatography (HPLC) methods and IR data for the purpose of cross validation. The pharmacokinetics aspects of nimesulide have been documented in human [14] and some animal species using traditional methods [15,16], but none has explored the novel method of calculating kinetic parameters from FT-NIR generated data. Rabbits were preferred to other rodents because its heart and cardiac circulation are closely similar to those of human [17].

2. Materials and methods

2.1. Animals

Adult male and female New Zealand white rabbits (2.5 kg body weight), six in numbers, being maintained at the in vivo testing

---

facility, CIMAP, Lucknow, India were used for the study. The animals were acclimatized to the experimental environment for 7 days before the actual experimentation. The animals were re-used after a wash period of 21 days. The protocols used were duly approved by Institutional Animal Ethics Committee (IAEC) through CPCSEA, Government of India.

2.2. Chemicals

Nimesulide and Cremophore EL were obtained from Sigma Chemicals, India. HPLC grade solvents were obtained from Merck India Ltd., India

2.3. Treatment of animals with nimesulide and collection of samples

A clear aqueous solution of nimesulide was prepared in 10% cremophore EL in 0.9% sodium chloride (NaCl) in water. Nimesulide was injected at 5 mg kg^{-1} body weight intraperitonially (i.p.) to the rabbits. Blood samples were collected in heparinised tubes, in duplicate, at 0, 5, 15, 30, 60, 120, 240, 360 and 480 min after the administration of the drug. Clear plasma samples were collected from the blood samples after centrifugation at 5000 × g for 5 min at 4 °C.

2.4. FT-NIR analysis

The plasma samples thus obtained were used directly for the Fourier transform near infrared (FT-NIR) analysis. The FT-NIR absorbance spectra from 10,000 cm^{-1} to 4000 cm^{-1} at a resolution of 4.0 cm^{-1} (using Antaris II Analyzer, Thermo Fisher Scientific, USA) in transmission mode, using indium gallium arsenide (InGaAs) detector were recorded for each sample. To reduce sampling error, the three vials (0.5 mm cell with 170 μl rabbit plasma) of samples from each plasma sample prepared in the previous step were analysed individually. The plasma obtained from the blood collected at zero (0) minute (just before the administration of the drug) was considered as the blank and the background measurements were taken using the blank before every spectral measurement.

Data acquisition, spectral mathematical treatments and partial least squares (PLS) regression were done using TQ Analyst Software (Thermo Fisher Scientific, USA). The second derivative of absorbance spectra smoothed with Norris derivative (segment length 19, gap between points 2) was used for all regression work. For path length corrections, standard normal variate (SNV) path length was chosen.

2.5. Sample preparation for nimesulide assay

Plasma samples (275 μl) were vigorously vortexed with the addition of acetonitrile (1000 μl) in a microcentrifuge tube for the extraction of nimesulide; the tubes were then centrifuged at 1000 × g for 5 min and the solvent phases were separated in fresh microcentrifuge tubes. After the evaporation of the solvent phase, the samples were reconstituted in 100 μl of acetonitrile which were then subjected to high-performance liquid chromatography (HPLC) analysis. A standard solution of nimesulide, in acetonitrile, was used for calibration of the HPLC peaks.

2.6. HPLC analysis

For the calibration, as well as cross validation of PLS model developed using FT-NIR data, HPLC analysis were done as described by Toutain, et al. [15] and Rao, et al. [16], using an HPLC system with UV detector (LC 10A with SPD 10AT) from Shimadzu, Japan connected with a SymmetryShield (Waters) RP-18, column. The UV detector was set at 210 nm and the analyses were carried out using the same series of the extracted plasma samples used in the FT-NIR analysis.

2.7. Kinetic analysis

Pharmacokinetic parameters were calculated following the procedure as reported earlier [18] using the software PK87.

The whole experiments were conducted three times in order to verify the reproducibility of the method. The spectra obtained from first and second rounds of experiments were used for calibration and validation of the PLS model. The spectra from the third round of the experiment were used only for prediction, and the predicted values were compared with the results from the HPLC analysis.

2.8. Calibration in raw plasma samples

A stock solution of nimesulide (5 mg ml^{-1}) was prepared in double distilled water containing 0.9% NaCl and 12.5% cremophore EL. Two fold serial dilution of this nimesulide stock solution ranging from 2.5 mg ml^{-1} to 0.02 mg ml^{-1} was prepared in freshly collected rabbit plasma. Four replicates of the eight dilutions were subjected to FT-NIR analysis using plasma as blank.

3. Results and discussion

The raw absorbance spectra recorded for nimesulide in rabbit plasma, taken at different time intervals after the i.p. injection, are shown in Fig. 1. The FT-NIR data from first and second rounds of the experiment were randomly split into calibration set (64 samples, 4 rabbits) and validation set (32 samples, 2 rabbits). All the data from the third round of the experiment were used as prediction set (48 samples, 6 rabbits). The two validation animals were selected randomly in each time interval.

The visual analysis of the second derivative spectra gave peaks and dips with an indication that at wave number ranges 6430–6360 cm^{-1} (Fig. 2), 5364–5290 cm^{-1} and 4849–4833 cm^{-1} the y-axis values change in the same way as the concentration of the drug, quantified through HPLC analysis, in the collected blood samples. At wave numbers ranging between 5364 and 5290 cm^{-1}, the spectra showed a dip. The FT-IR spectrum of the pure drug showed prominent peaks at wave numbers 3284, 1590, 1488, 1342, 1282 and 1247 cm^{-1} [19]. So the significant contribution of the FT-NIR band obtained at 6430–6360 cm^{-1} could be from the combination of overtones arised from N–H stretching and N–H deformation. Similarly, the major contribution for the band at 4849–4833 cm^{-1} might be influenced strongly by the combination of overtone from asymmetric C–O stretching and asymmetric N–O stretching.

PLS regression models were built using these three wavelength ranges viz., 6430–6360 cm^{-1}, 5364–5290 cm^{-1} and 4849–4833 cm^{-1}. Two latent variables were used to make the PLS models. This number was used because of two reasons. One reason is that the TQ Analyst Software selected the two variables in its calculations, and the other reason is that it gave lower root mean squares error of cross validation (RMSECV). In order to find the closeness between reference value (value obtained through HPLC analysis) and the value found by the calibration model, RMSEP (root mean square error of prediction) was also calculated using the formula:

$$\text{RMSEP} = \frac{\sum_i (Yi_{\text{pre}} - Yi_{\text{HPLC}})^2}{n}$$

where n is the number of samples used for prediction. Similarly, root mean square error of calibration (RMSEC) and root mean square error of validation (RMSEV) were also calculated.
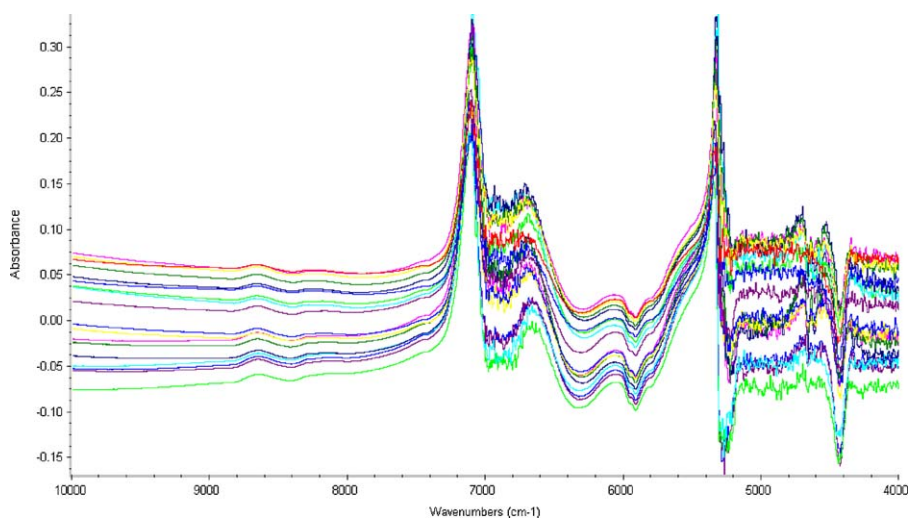
Fig. 1. Raw FT-NIR spectra of plasma samples at different time interval, after the i.p. injection of nimesulide.

The PLS calibration model gave RMSEC of 2.11 ng, RMSEV of 2.89 ng and RMSEP of 2.54 ng. As the animal to animal variations is an influencing factor in the drug interaction, these values and variations are within the acceptable limits. Fig. 4 shows the calibration curve plotted using the concentration of nimesulide predicted using the FT-NIR method and the concentration of nimesulide measured using the HPLC method. The straight line curve showed a slope of 1.02 and an intercept of 0.79.

The curve obtained from the PLS calibration model of the plasma samples fortified with nimesulide also gave comparable results with a straight line having regression equation $1.03x + 5.96$ and r^2 value of 0.99.

The relative error was calculated using the equation:

$$\text{Error}\,(\%) = \frac{Y_{\text{HPLC}} - Y_{\text{pre}}}{Y_{\text{HPLC}}} \times 100$$

where Y is the value of nimesulide content in the plasma. The plasma obtained after 5 min of the i.p. injection showed 100% error because the FT-NIR model developed failed to recognise the nimesulide related components in the spectra. There after the average relative error reduced to a range between −12.71% at 360 min and −1.83% at 60 min after the i.p. injection. The minus sign indicates that the average predicted values of nimesulide (Y_{pre}) are numerically greater than that of the values obtained from HPLC analysis (Y_{HPLC}). The percentage relative errors concerning the measurements are shown in Fig. 5. From this figure, it is possible to note that, in general, the relative errors decreased as the concentration of nimesulide increased in the rabbit plasma. The figure depicts a random distribution of the errors. The random distribution of relative errors is an indication of linear behaviour of the data [6]. Thus, it is clearly established that there is linearity in the measurements. If we consider all the 126 samples obtained in between 15 min and 480 min, then the average relative error is only −5.92%. Relative errors lower than ±6% are acceptable for quality control [20]. From the graph, it may be noted that most of the validation samples have errors of similar level.

Paired t-test was also performed to check for any significant difference in the concentration of nimesulide in plasma samples predicted and determined using HPLC method. The t-value obtained was 0.47, and at the 95% confidence level, the critical value of t is 4.64 ($p = 0.32$). It can be concluded that the HPLC method and the PLS model developed using FT-NIR data do not significantly have different values for the determination of nimesulide in the plasma.
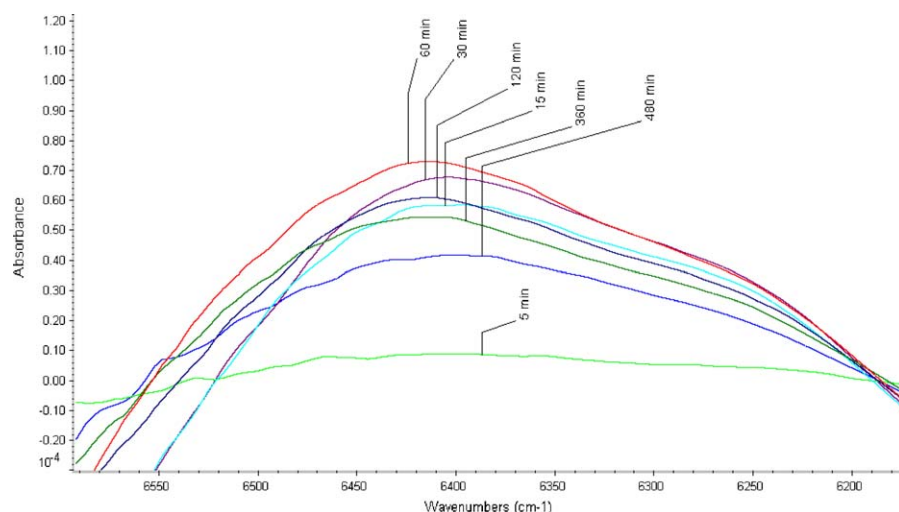
Fig. 2. FT-NIR secondary derivative spectra of plasma samples collected from nimesulide injected rabbits at different time after the i.p. injection. The wave number range 6430–6360 cm^{-1}.

Table 1
PK Parameters obtained from the calculations using the raw data and PK87 software.

Parameters	Using data from the HPLC analysis		Using data from the model (predicted)		Relative error percentage of means
	Mean value (a)	STDEV	Mean value (b)	STDEV	[($a-b$)/a] 100
K(a) (min^{-1})	0.0136	0.0005	−0.0133	0.00046	2.21
Lambda (Z) (min^{-1})	0.0089	0.00032	−0.0089	0.00076	0
Absorbtion half time (min)	50.77	1.29	52.03	1.36	−2.47
Elimination half time (min)	77.98	2.76	78.20	7.33	−0.28
AUC (0 to tn) (ng min ml^{-1})	18929.76	560.53	19902.18	655.66	−5.14
AUC (0 to ∞) (ng min ml^{-1})	19518.65	551.55	20547.26	694.52	−5.27
AUMC (0 to tn) (ng min ml^{-1})	3305768.82	108639.31	3544892.25	138872.9	−7.23
AUMC (0 to ∞) (ng min ml^{-1})	3654867.30	109909.11	3714492.75	859841.6	−1.63
MRT (min)	187.27	3.18	191.17	5.69	−2.08
Clearance (ml min^{-1})	10.25	0.29	9.74	0.33	4.97
VD (area) L	69.24	3.63	65.88	5.83	−4.86
C_max (ng ml^{-1})	75.29	6.65	76.62	7.22	−1.84
C_max_calculated (ng ml^{-1})	70.01	3.04	71.24	2.65	−1.76
T_max (min)	60	0	60	0	0
T_max_calculated (min)	83.56	2.28	84.11	2.81	0.01

The developed NIR model could not give correct measure of the nimesulide content in the plasma at 5 min readings. At 5 min, HPLC analysis indicated the presence of nimesulide in blood (0.64 ng ml^{-1}). Thus, it can be assumed that the model is less sensitive than HPLC method, to the active component. This low sensitivity may be due to the preprocessing applied to the spectra. However, the model was clearly able to distinguish the samples with different concentrations of nimesulide in the blood samples collected after 5 min of i.p. injection. Hence, the further pharmacokinetics parameters of the nimesulide in rabbit were calculated, and the results are shown in Table 1.

In both FT-NIR and HPLC analysis, it was clearly apparent that the plasma drug concentration continued to increase and reached a maximum at 60 min after the i.p. injection. There after, the drug concentration decreased gradually and reached a very low concentration at 480 min after the injection of the drug. Except at 5 min after the i.p. injection, the predicted values obtained from FT-NIR analysis were numerically closer to the values obtained from HPLC

serum analysis (Table 2). The nimesulide concentration in plasma vs. time curves showed quite similar trends in both FT-NIR based prediction and HPLC based analysis (Fig. 3) i.e., a rapid distribution phase and a slower elimination phase. Fig. 4 shows the calibration curve plotted using the concentration of nimesulide predicted using the NIR method and the concentration of nimesulide measured using the HPLC method.

The drug concentration in plasma was highest (76.51 ± 7.38 ng ml^{-1} by FT-NIR method; 75.13 ± 6.81 ng ml^{-1} by HPLC method) at 60 min after i.p. injection and there after declined gradually and reached 5.62 ± 1.14 ng ml^{-1} by the FT-NIR based method (5.23 ± 0.29 ng ml^{-1} by HPLC measurement) at 480 min after i.p. (Table 2). The pharmacokinetic parameters like maximum concentration (C_max), maximum concentration calculated (C_max_calc), maximum absorption time (T_max), maximum absorption time calculated (T_max_calc), absorption half time, elimination half time, mean residence time, clearance rate, etc. obtained from both FT-NIR based PLS model analysis and HPLC

Table 2
Concentration of nimesulide in plasma at different times of observations in rabbits.

| Time (h)	Predicted from our model		HPLC analysis	
	Mean value (ng ml^{-1})	STDEV (ng ml^{-1})	Mean value (ng ml^{-1})	STDEV (ng ml^{-1})
0.08	0	0	0.64	0.05
0.25	23.39	1.70	21.82	1.71
0.5	56.62	2.29	55.04	2.42
1	76.51	7.38	75.13	6.81
2	65.13	1.96	63.56	2.03
4	47.16	1.71	44.21	1.85
6	24.80	2.49	22.01	1.62
8	5.62	1.14	5.22	0.29
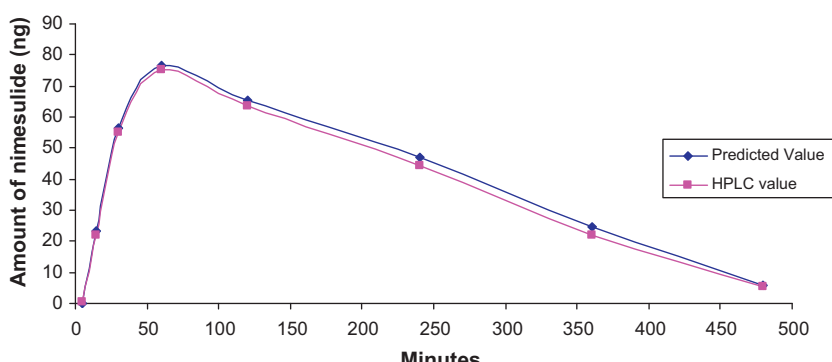
**Fig. 3.** Time–concentration of nimesulide curve obtained for treated rabbits.
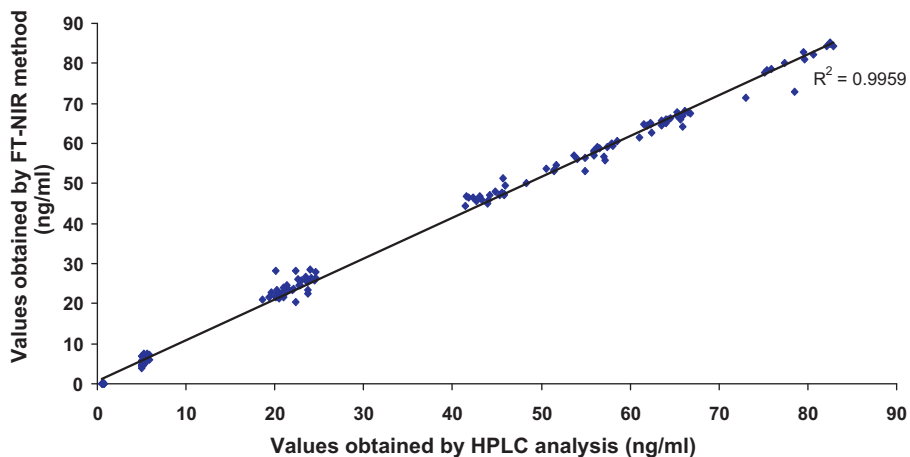
Fig. 4. Calibration curve for nimesulide content in the plasma samples obtained after i.p. injection.
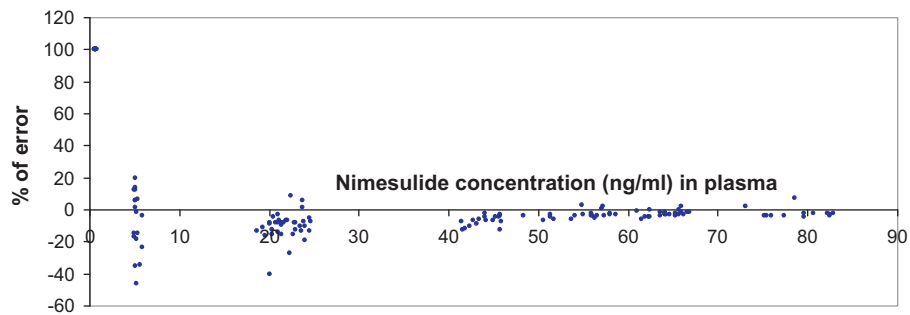

Fig. 5. Relative error for nimesulide content obtained by the FT-NIR analysis.

based analysis were numerically close to each other (Table 1). There were no significant difference between the values obtained by the two methods ($p > 0.05$). Thus, it is clearly established that the PLS model developed using the FT-NIR data gave comparable results, in both the quantity of nimesulide present in blood plasma and the data obtained from pharmacokinetics study with those data, with HPLC method. The percentage of error difference between the two methods was less than 6%. Hence, the newly developed FT-NIR data based PLS model can be used in the pharmacokinetics and bio-availability study of nimesulide.

Although methods like enzyme analysis, gas chromatography (GC) combined with or without mass spectrometry (MS), HPLC etc, are available to generate drug quantification data for the pharmacokinetics parameters and bio-availability studies, still many are depending on HPLC data. For all the routinely using methods, the extraction of the drug molecule from the blood plasma is required. In addition to the cost of solvents required for HPLC running, cost of solvents required for extraction and the process required are adding the total cost of analysis per samples as well as the time required for the analysis of one sample. In the method that we developed, there is no requirement of sample extraction, and thus no extra chemical is added to or subtracted from the plasma samples. Further, FT-NIR analysis does not require more than a minute to obtain the quantity of drug present in the sample. Thus, this method is much faster than the available HPLC methods and is environmental friendly. Most of the HPLC based protocols for nimesulide analysis available in the literature require 4.5–7.0 min to obtain the peak for nimesulide or its main metabolite 4-hydroxy nimesulide after injecting the sample into the instrument system. Our strategy is faster than the method reported by Ptácek et al. [21] in 2001. Their method can examine only 20 samples in an hour where as our method can give the result of more than 50 samples in an hour and is much more cost effective

than the other methods because no extraction, solvents and standards (after developing the model) are required. The latest in the queue, by Schebb et al., in 2011, reports [22] that an ultra fast online solid phase extraction liquid chromatography electrospray tandem mass spectrometry (SPE–LC–ESI–MS/MS) based method can determine diclofenac concentration in approximately 2 min rounding up to 30 samples in an hour. The FT-NIR based method is not only a high throughput analysis method but also provides further scope of automation and compliant with the requirements of green analytical chemistry.

There are only two reports available in pharmacokinetics study of nimesulide in rabbits. In the first study, availability of nimesulide was examined, using HPLC, in aqueous humor after the administration of an ophthalmic preparation [23] and in the next one lithium content is noted after the co-administration of nimesulide and lithium [24]. There is no reports perce as far as pharmacokinetics study of nimesulide in the rabbit is concerned.

To the best knowledge of the authors, there is no report of pharmacokinetics and bio-availability after i.p. administration of nimesulide to human or rabbits. The rabbit's heart and cardiac circulation are very closely resemble those of human [17]. The T_max_calc obtained in the present study (84.11 ± 2.81 min) is in good agreement with T_max of humans (73–165 min; 100 mg dosage), through the oral route [25], where as the elimination half life (78.2 ± 7.33 min) obtained for rabbit is less than that of human (108–284 min).

4. Conclusion

This is the first report of demonstrating the capability of FT-NIR measurements in the pharmacokinetics and bio-availability studies. Here, we have performed in vivo measurements of nimesulide

content in the plasma samples of rabbits after an i.p. injection in order to study kinetic behaviour of nimesulide. We have identified nimesulide-specific features in these in vivo spectra. The results suggest that FT-NIR transmission technique can be used for rapid and convenient analysis of drug content in plasma without any extraction procedure. The error of this method is within that expected range for pharmaceutical assays. The ease of use and rapid generation of results gives FT-NIR a distinct advantage over other analytical techniques. Since India is emerging as a centre of clinical research and pharmacovigilance, where a large number of drug exposed population is to be scanned, the FT-NIR method that have high speed and yet economical, may provide a viable alternate to the existing methods.

Acknowledgement

References

[1] L. Stothers, B. Shadgan, A. Macnab, Urological application of near infrared spectroscopy, Can. J. Urol. 15 (2008) 4399–4409.

[2] H. Azizian, J.K.G. Kramer, S.B. Heymsfield, Fourier transform near infrared spectroscopy: a newly developed: non-invasive method to measure body fat, Lipids 43 (2008) 97–103.

[3] S. Takeno, T. Bamba, Y. Nakazawa, E.O.A. Fukusaki, A. Kobayashi, A high-throughput and solvent-free method for measurement of natural polyisoprene content in leaves by Fourier transform near infrared spectroscopy, J. Biosci. Bioeng. 106 (2008) 537–540.

[4] M. Otsuka, I. Yamane, Prediction of tablet properties based on near infrared spectra of raw mixed powders by chemometrics: scale-up factor of blending and tableting processes, J. Pharm. Sci. 98 (2009) 4296–4305.

[5] C. Abrahamsson, J. Johansson, S. Andersson-Engels, S.F.S. Svanberg, Time resolved NIR spectroscopy for quantitative analysis of intact pharmaceutical tablets, Anal. Chem. 77 (2005) 1055–1059.

[6] W.F.C. Rocha, A.L. Rosa, J.A. Martins, R.J. Poppi, Determination and validation of nimesulide in pharmaceutical formulation by near infrared spectroscopy, J. Braz. Chem. Soc. 21 (2010) 1929–1936.

[7] M.S. Kemper, E.J. Magnuson, S.R. Lowry, W.J. McCarthy, N. Aksornkoae, D.C. Watts, et al., Use of FT-NIR transmission spectroscopy for the quantitative analysis of an active ingredient in a translucent pharmaceutical topical gel formulation, AAPS PharmSci. 3 (2001), doi:10.1208/ps030323, article 23 (2001).

[8] E. Rasanen, N. Sandler, Near infrared spectroscopy in the development of solid dosage forms, J. Pharm. Pharmacol. 59 (2007) 147–149.

[9] A.J. Macnab, L. Stothers, Development of a near infrared spectroscopy instrument for application in urology, Can. J. Urol. 15 (2008) 42233–44240.

[10] V. Quaresima, R. Lepanto, M. Ferrari, The use of near infrared spectroscopy in sports medicine, J. Sports Med. Phys. Fitness 43 (2003) 1–13.

[11] F. Crespi, Near-infrared spectroscopy (NIRS): a non-invasive in vivo methodology for analysis of brain vascular and metabolic activities in real time in rodents, Curr. Vasc. Pharmacol. 5 (2007) 305–321.

[12] C. Petibois, K. Gionnet, M. Goncalves, A. Perromat, M. Moenner, G. Deleris, Analytical performances of FT-IR spectrometry and imaging for concentration measurements within biological fluids, cells and tissues, Analyst 131 (2006) 640–647.

[13] N.R. Srinivas, Changing need for bioanalysis during drug development, Biomed. Chromatogr. 22 (2008) 235–243.

[14] C.M. Rolim, V. Porta, S. Storpirtis, Quantitation of nimesulide in human plasma by high-performance liquid chromatography with ultraviolet absorbance detection and its application to a bioequivalence study, Arzneimittelforschung 57 (2007) 537–541.

[15] P.L. Toutain, C.C. Cester, T. Haak, S. Metge, Pharmacokinetics profile and in vitro selective cyclooxygenase-2 inhibition by nimesulide in the dog, J. Vet. Pharmacol. Ther. 24 (2001) 35–42.

[16] G.S. Rao, J.K. Malik, V.B. Siddaraju, N.C. Shankaramurthy, Pharmacokinetics and bioavailability of nimesulide in goats, J. Vet. Pharmacol. Ther. 30 (2007) 157–162.

[17] S.A. Saeed, S. Ahmed, Anti-ischemic effects of nimesulide, a cyclooxygenase-2 inhibitor on the ischemic model of rabbit induced by isoproterenol, Arch. Pharm. Res. 29 (2006) 977–983.

[18] D. Chanda, S.C. Debnath, S.K. Das, T.K. Mandal, A. Bhattacharyya, A. Choudhury, A.K. Chakraborty, Metabolism of metamitron in goat following a single oral administration of a nontoxic dose level: a continued study, J. Agric. Food Chem. 52 (2004) 7377–7381.

[19] A. Prasad, M.L. Sharma, S. Kanwar, R. Rathee, S.D. Sharma, A practical large scale synthesis of nimesulide – a step ahead, JSIR 64 (2005) 756–760.

[20] The United States Pharmacopoeia, 25th revision, U.S. Pharmacopocia Convention, Rockville, 2002.

[21] P. Ptácek, J. Macek, J. Klíma, Rapid and simple high-performance liquid chromatographic determination of nimesulide in human plasma, J. Chromatogr B: Analyt. Technol. Biomed. Life Sci. 758 (2001) 183–188.

[22] N.H. Schebb, B. Inceoglu, T. Rose, K. Wagner, B.D. Hammock, Development of an ultra fast online-solid phase extraction (SPE) liquid chromatography electrospray tandem mass spectrometry (LC–ESI–MS/MS) based approach for the determination of drugs in pharmacokinetic studies, Anal. Methods 3 (2011) 420–428.

[23] A. Maltese, F. Maugeri, C. Bucolo, Rapid determination of nimesulide in rabbit aqueous humor by liquid chromatography, J. Chromatogr. B: Analyt. Technol. Biomed. Life Sci. 804 (2004) 441–443.

[24] S. Sidhu, A. Kondal, S. Malhotra, S.K. Garg, P. Pandhim, Effect of nimesulide co-administration on pharmacokinetics of lithium, Indian J. Exp. Biol. 42 (2004) 1248–1250.

[25] A. Bernareggi, Clinical pharmacokinetics of nimesulide, Clin. Pharmacokinet. 35 (1998) 247–274.

Short communication

Effects and mechanism characterization of ionic liquids as mobile phase additives for the separation of matrine-type alkaloids by liquid chromatography

Min Bian [a,b,c], Zunjian Zhang [a,b,*], Hao Yin [c]

[a] Key Laboratory of Drug Quality Control and Pharmacovigilance (China Pharmaceutical University), Ministry of Education, PR China
[b] Center for Instrumental Analysis, China Pharmaceutical University, Nanjing 210009, PR China
[c] College of Science, Nanjing University of Technology, Nanjing 210009, PR China

ABSTRACT

The mechanism for the separation of matrine-type alkaloids (sophoridine, sophoramine, sophocarpine, matrine, and oxymatrine) on a C_{18} column with a mobile phase containing room temperature ionic liquids (RTILs) as additive was studied in the current work by investigating several factors that influenced chromatographic behavior, including mobile phase pH, buffer solution concentration, ionic liquid concentration, and length of alkyl groups in RTILs. Peak efficiency was selected as the criterion for chromatographic efficiency whereas peak efficiency was also selected for triethylamine (TEA). The addition of RTILs in a mobile phase demonstrated superior effects on the separation of these basic compounds because of the increase in peak efficiency. The difference between RTILs and TEA and the changes in retention factors caused by the additives concentration, depending on the acidity of the mobile phase, showed the dual nature of the ionic liquids. This allowed both the constituting anion and cation to participate in the retention mechanism. Furthermore, the chromatographic behaviors of analytes with a mobile phase containing RTILs having different lengths of alkyl groups at different concentrations, complied with the stoichiometric displacement model for retention (SDM-R). This clarified the significant role of competitive adsorption between solutes and additives on the stationary phase.

© 2011 Published by Elsevier B.V.

1. Introduction

Room temperature ionic liquids (RTILs) have numerous desirable properties, such as excellent solvation qualities, wide temperature range, nonvolatility, and high electrical conductivity. RTILs consist of relatively large organic cations, and weak coordinators of organic or inorganic anions. Interestingly, when the length and branching of alkyl chains of cations and species of anion are varied, RTILs show different properties and thus, can be applied for specific purposes.

Recently, RTILs have been used in separation and chemical analysis. For example, they are used as solvent for liquid–liquid extraction [1], running electrolytes for capillary electrophoresis [2], components for gas chromatography stationary phases [3], and additives for high-pressure liquid chromatography (HPLC) mobile phases [4–6].

RTILs have been found to be more helpful particularly as low concentration additives. Adding RTILs to HPLC mobile phases can shield the acidic silica surface, improve the peak shape, and reduce

the peak broadening. Jiang et al. investigated the effects of 1-alkyl-3-methylimidazole ionic liquids as mobile phase additives for the separation of ephedrines on a C_{18} column [4]. Because the coating of ionic liquid cations on the surface of C_{18} formed a bilayer to compete with the sample molecules in HPLC, the retention time of ephedrines shortened. Subsequently, the effects of RTILs as additives for the separation of catecholamines [5] and nucleotides [6] have been reported in literature.

The matrine-type alkaloids, including oxymatrine (OMT), sophoridine (SRI), sophoramine (SA), matrine (MT), sophocarpine (SC), etc. belong to the group of quinolizidine bio-alkaloids. These have visible antidiarrheal effects, which facilitate killing of amoebae and Giardia lamblia stiles [7]. Because of these significant biological activities, interest in the separation and determination of matrine-type alkaloids has grown. Several methods, such as HPLC, CE, and TLC have been applied [8–10].

Unquestionably, HPLC is the most widely used technique for the separation of matrine-type alkaloids because of its simplicity and general applicability [11]. But based on previous research, the addition of classical ammonia depressors to the mobile phase did not fully remove the negative effects of residual silanol on the retention of matrine-type alkaloids, even with the employment of purified and less acidic silica supports [12,13]. Furthermore, the presence of ammonia depressors causes the slow equilibration of

the chromatographic system when the mobile phase is changed [14]. For this reason, ionic liquids have become good candidates for the efficient suppression of residual silanols.

At present, the effects of RTILs as mobile phase additives for the separation of matrine-type alkaloids in HPLC have not been reported. Therefore, in the present paper, 1-butyl-3-methlomidazolium tetrafluoroborate (BMIM BF$_4$), a typical and easily available RTIL, was selected as an additive for the separation of matrine-type alkaloids. The mobile phase pH, salt concentration, and the length of RTIL alkyl groups were also investigated to clarify the mechanism of this separation. Peak efficiency was selected as the criterion for chromatographic efficiency while the peak efficiency was also selected for TEA.

2. Experimental

2.1. Apparatus

The HPLC system used is composed of a Shimadzu pump (model LC-20AD, Japan), Shimadzu UV detector (model SPD-20A), and a 7125 injector with a 20 μl sample loop (model 7725i, Rheodyne, USA). An ODS column (silica particle size: 5 μm, 4.6 mm × 150 mm I.D.) (Ledon Technology Co., Suzhou, China) was employed. The flow rate was 0.7 ml min^{-1}. The signal was monitored at 220 nm and recorded by LC Solution of Class-VP (Shimadzu, Japan).

2.2. Reagents

MT, OMT, and SRI used in separation tests were purchased from the National Institute for the Control of Pharmaceutical and Biological Products (Beijing, China). SA and SC were purchased from Shanghai Tauto Biotech Co. Ltd. (Shanghai, China). The RTILs 1-butyl-3-methylimidazole tetrafluroborate (C$_4$minBF$_4$, 97.4%), 1-hexyl-3-methylimidazole tetrafluroborate (C$_6$minBF$_4$, 96.6%), 1-octyl-3-methylimidazole tetrafluroborate (C$_8$minBF$_4$, 97.7%), 1-decyl-3-methylimidazole tetrafluroborate (C$_{10}$minBF$_4$, 95.8%), and 1-dodecyl-3-methylimidazole tetrafluroborate (C$_{12}$minBF$_4$, 97.0%) were synthesized based on the procedures described in literature [15].

The reagents, including methylimidazole, chlorobutane, chlorohexane, chlorooctane, chlorododecane, acetone, sodium fluoborate, dichloromethane, and ethyl acetate used in the synthesis were of analytical grade. Mobile phases were prepared using acetonitrile and the selected amount of additives which were degassed ultrasonically prior to use. Double distilled water was used throughout the procedure.

3. Results and discussion

3.1. Effects of additives on the retention behavior of matrine-type alkaloids

Fig. 1 shows the result of separating matrine-type alkaloids obtained with 20 mM of phosphate buffer–acetonitrile (90%/10%, v/v) mobile phases containing 5.2 mM BMIM BF$_4$ as an additive at pH 5.8. The detection wavelength was achieved at 220 nm, and the rate-flow was 0.7 ml min^{-1}. The chromatograms showed that the compounds could be completely separated.

3.2. Effect of mobile phase pH and phosphate buffer concentration

The dissociation constants (pK_a) of the five matrine-type alkaloids in water are in the range of 7–9 [16] (Table 1), which means that they are in their cationic state in the working pH range (3 < pH < 7). Moreover, alkaloids should be separated in the buffer mobile phase because the volatile ionization of analytes can lead
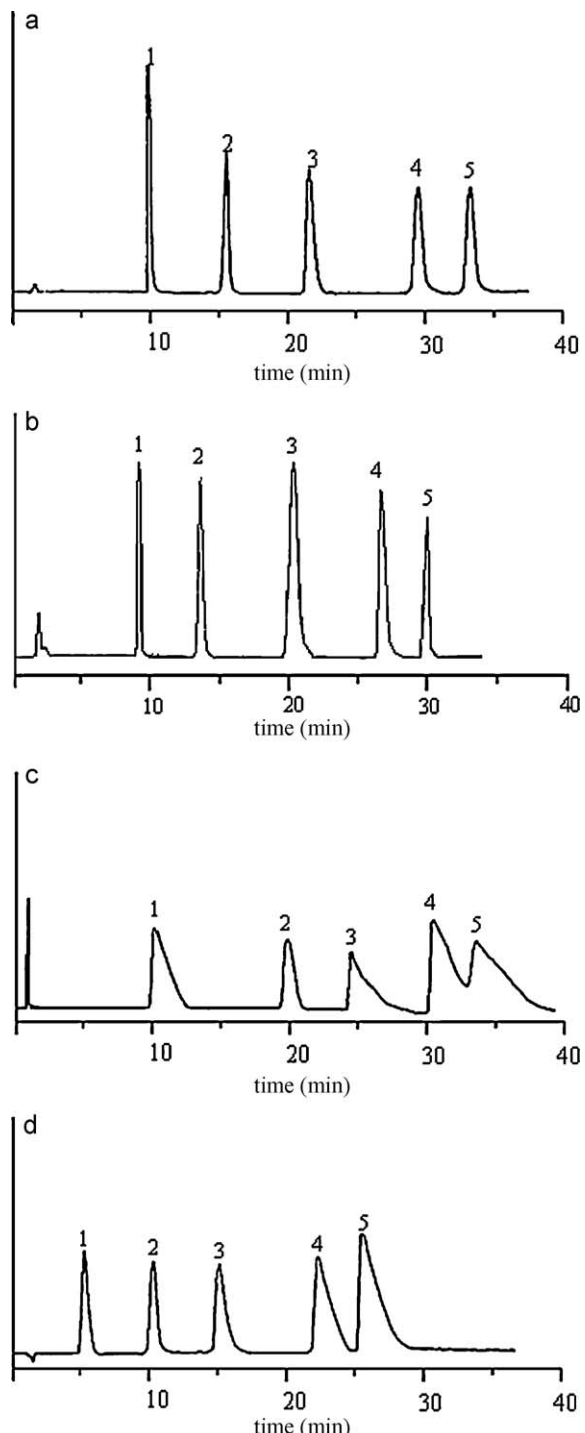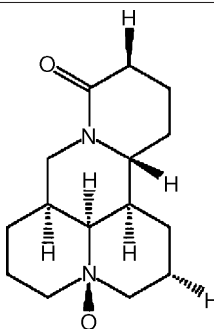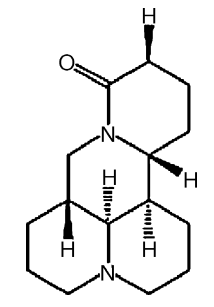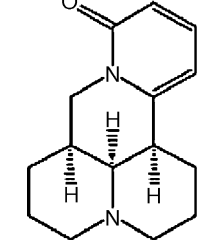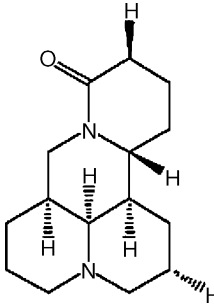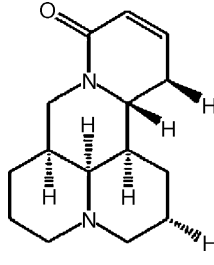

Fig. 1. Chromatograms of matrine-type alkaloids with a 20 mM phosphate buffer–acetonitrile 90%/10% (v/v) mobile phase containing 5.2 mM BMIM BF$_4$ at pH 5.8 (a); with 80 mM phosphate buffer–acetonitrile 90%/10% (v/v) mobile phase containing 5.2 mM BMIM BF$_4$ at pH 3.4 (b); with the 20 mM phosphate buffer–acetonitrile 90%/10% (v/v) mobile phase without additives (c) and containing 3.6 mM [0.05% (v/v)] of TEA (b) at pH 5.8. Chromatographic conditions: column, C$_{18}$ (5 μm, 4.6 mm × 150 mm I.D.); rate flow, 0.7 ml min^{-1}; detection, 220 nm. Peaks: (1) OMT, (2) SRI, (3) SA, (4) MT, and (5) SC.

to peak distortion at different points [17] and the effects of chromatographic behavior on analyte retention are related to changes in buffer solution concentration [18]. To determine the effects of salt concentration, the changes in k' at different salt concentrations were respectively examined at pH 3.4 and pH 6.4. At pH 6.4, k' generally decreased along with the increases of buffer solution

Table 1
Structures and dissociation constants of the five matrine-type alkaloids.

Compound	Structure	pKa [17]
Oxymatrine (OMT)		7.14
Sophoridine (SRI)		8.97
Sophoramine (SA)		7.02
Matrine (MT)		8.24
Sophocarpine (SC)		7.68

concentrations in the range of 0–100 mM. When the buffer solution concentration increased to 100 mM, the minimum k' generated and the tailings of peaks were reduced. However, the general observed effect of the increase in buffer solution concentration at pH 3.4 was an increase of k'.

The distinction between pH 3.4 and 6.4 can be explained by the theory of He et al. and Flieger [4,18] guiding the chaotropic effect. When chaotropic salts are used as mobile additives for the separation of matrine-type alkaloids, two types of models are present in the retention process: one is competition between the analyte polar group and imidazolium cations with the silanol group, which causes k to decrease, and the other is the adsorption of ion-pairs consisting of chaotropic anions and cationic solutes into the stationary phase, which causes k to increase. At a lower pH (3.4), the increase in k is caused by the predominant ion-pair complex formation effect between additives and alkaloids, whereas the decrease in k is probably caused by the predominant competition effect between additives and protonation alkaloids for adsorption on the stationary phase surface at a higher pH (6.4).

Peak efficiencies, expressed as theoretical plates (N), undoubtedly improved with the increase in buffer solution concentration (Fig. 1b and Fig. 2). Flieger [18] showed that the variation of retention factor with a change in buffer solution concentration is due to the change of column saturation capacity. However, the column damage caused by salt precipitates stemming from high salt concentrations is undoubtedly prevented.

3.3. The effect of concentration of RTILs and the length of RTILs alkyl groups

The addition of different BMIM BF$_4$ concentrations in the range of 2.6–83.4 mM to the mobile phase was initially used to study the effect of RTIL concentration on the separation of matrine-type alkaloids. Results showed that retention factors not only decreased with increases in BMIM BF$_4$ concentration, but log k' was also linearly related to log c (c is the concentration of BMIM BF$_4$ in the mobile phase). The relationship was validated to comply with the stoichiometric displacement model for retention (SDM-R) of other studies. The mathematical expression of SDM-R is as follows [19–21]:

$$\log k' = \log I - Z \log a_D \tag{1}$$

where k' is the retention factor and a_D stands for the solvent activity in the bulk solution. When other conditions remain unchanged, the ionic liquid additive is viewed as the displacer in the alkaloid separation system and a_D is the ionic liquid concentration in the mobile phase. Log I is the affinity of 1 mol of solute to the stationary phase. Z represents the total moles of the solvent released or adsorbed for every 1 mol of solute, together with its corresponding contact area on the adsorbent surface during the adsorption or desorption process. Both log I and Z are constants for the given condition, which make Eq. (1) a linear equation.

Even when the length of RTIL alkyl groups increases, the linear relationship and SDM-R still exists. Therefore, the five kinds of ionic liquid 1-alkyl-3-methylimidazole tetrafluoroborate (C$_n$mimBF$_4$, n = 4, 6, 8, 10, 12) having various alkyl chains were prepared with N-methylimidazole and alkyl bromides. The effect of RTIL concentration in mobile phase and the lengths of RTIL alkyl groups were both investigated.

All retention data for analytes were determined according to the reports in the literature [19]. Fortunately, plots of log k' versus log a_D showed straight lines in relation to the value of the linear correlation coefficient. Values were mostly higher than 0.9 and within the additive concentration in the range of 10.4 mM < a_D < 83.2 mM. This is consistent with Eq. (1).

Table 2 shows the stoichiometric parameters and linearity obtained from the plotting of log k' versus log a_D with the mobile phase containing C$_n$mimBF$_4$ (n = 4–10) as displacers. Based on these data, the following conclusions were drawn. First, the good linear relationship between the retention time of each solute and the concentration changes in ionic liquid demonstrated that the retention behavior of all solutes under the given condition was consistent with SDM-R. The retention mechanism in the retention process was validated. Equilibrium was established when the imidazolium cations in the displacer were absorbed on the surface

Table 2
Stoichiometric parameter of different analytes with five homologous displacers.

n	OMT			SRI			SA			MT			SC		
	Z	$\log I$	r	Z	$\log I$	r	Z	$\log I$	r	Z	$\log I$	r	Z	$\log I$	r
4	0.2272	0.9570	0.9833	0.2580	1.2063	0.9995	0.1611	1.2614	0.9797	0.1906	1.4147	0.9956	0.1774	1.4685	0.9822
6	0.1991	0.9797	0.9636	0.2232	1.2088	0.9824	0.1367	1.2880	0.9607	0.1836	1.4401	0.9954	0.1347	1.4689	0.9933
8	0.1738	0.9790	0.9984	0.2017	1.2219	0.9950	0.1199	1.3023	0.9662	0.1568	1.4389	0.9900	0.0726	1.4415	0.9126
10	0.1600	0.9797	0.9797	0.1971	1.2407	0.9994	0.1086	1.3308	0.9176	0.1128	1,4233	0.9883	0.0818	1.4896	0.9826
12	0.1443	1.0057	0.9453	0.1776	1.2528	0.9869	0.0784	1.3245	0.9423	0.1227	1.4543	0.9976	0.0697	1.5051	0.0697

n is the number of carbon atom of RTILs alkyl groups.

of the stationary phase. Equilibrium, which existed between the displacer and stationary phase with a certain displacer concentration ($a_D > 10.4$ mM), was broken when the separated solutes entered into the chromatographic column and were absorbed by the stationary phase (separating the solutes is a precondition if the adsorption affinity of the separated solutes is more than that of the displacer). Because of stronger adsorption, the solutes were absorbed while a certain amount of ionic liquid displacer was released from the adsorbent and returned to the mobile phase. This indicates the competitive adsorption that is predominant between the separated elements and the displacer.

Second, the value of Z, which is a parameter of measurement in the SDM-R model, is an expression parameter showing the characteristics of a displacing agent in mobile phase under a given condition. Table 2 shows that the Z value of the same solute generally decreased with an increase in the length of the alkyl groups. Z represents the total amounts by moles of the displacer released or adsorbed for every 1 mol of solute together with its corresponding contact area on the adsorbent surface during the adsorption or desorption process. When the contact area between the solute and the solid adsorbent is invariable, the longer the alkyl group is, the larger the size of the displacer molecule will be. The fewer the total amount of displacer, the lower the value of Z will be. An abnormal increase of Z value was probably caused by ion-pair complex formation effect between additives and alkaloids.

Third, $\log I$, which is related to retention factor, is the affinity of 1 mol of solute to the stationary phase. This could be used to express the functional capability between the solute and the stationary phase and is relevant to the retention factor. Specifically, an increase in $\log I$ lead to an increase in k'. Table 2 shows that the retention factor increased generally with the increase in the lengths of the alkyl groups and $\log I$, which resulted in severe ruggedness. When the resolution fulfilled the requirements, the shorter length of the alkyl group facilitated better result.

3.4. Comparative study of ionic liquid and triethylamine (TEA) as mobile phase additives

Triethylamine (TEA) is the most popular silanol suppressing agent. A comparative study on the retention, peak shape, and peak efficiency of five matrine-type alkaloids chromatographed with aqueous-organic mobile phases containing ionic liquid or TEA was conducted.

Fig. 1 shows the chromatograms obtained with 20 mM of phosphate buffer–acetonitrile 90%/10% (v/v) mobile phase without additive (Fig. 1c) and containing 3.6 mM [0.05% (v/v)] TEA (Fig. 1d) at pH 5.8. The chromatograms show that the resolution was significantly higher when the analyte was working with the mobile phase containing TEA compared with that without an additive. However, RTILs were significantly more effective than TEA.

The tailing observed with the 3.6 mM TEA mobile phase could be reduced by increasing the TEA concentration, but the resolution factor would decrease. Furthermore, TEA decreased the retention

of analytes more than BMIM BF$_4$ did. The observed differences of the two additives have been explained in previous studies [22,23].

As proposed in Ref. [22], the RTIL cation could be adsorbed on the stationary phase surface, and imidazolium cations can interact with silanol groups. The suppression of the silanol–cationic solute interaction decreases the retention factors of the positively charged solutes. Similarly, TEA is mainly in the positive TEA$^+$ form at pH 5.8 and associates with silanol groups. This silanol screening effect is helpful for improving peak efficiency and shape. However, the decrease in retention factors is a side effect.

Nevertheless, the BF$_4^-$ anions have a chaotropic character that allows them to associate with cationic solutes in the presence of the ionic liquid additives. Phosphate anions are more kosmotropic and unable to undergo ion pairing with cations. To understand why BF$_4$ ion-pairing increases the solute retention factors, the ion-pairs have been determined to possess more affinity for the C$_{18}$ alkyl chains of the stationary phase compared with the cationic solutes. Moreover, the two effects, including competitive adsorption with solutes on the stationary phase and ion-pairing with solutes, can compensate each other in the presence of RTIL additives. However, competitive adsorption between solutes and additives on the stationary phase plays a major role in this process according to the SDM-R.

The chosen phosphate buffer contains H$_2$PO$_4^-$ kosmotropic anions that possess water-structure properties. Due to their ability to form hydrogen bonds, their stronger hydration and greater polarity enhance the aqueous solution structure. When the pH rises, the loss of protons of phosphate anions and breakage of hydrogen bonds increase the chaotropic effect. Hence, the increase of buffer concentration results in the increase of retention time. However, the result indicates that k' generally decreases along with the increase in buffer solution concentrations at pH 6.4. This may be due to the fact that the lower pH ensures more protonation of the alkaloids than the higher pH does. Simultaneously, the fraction of the analytes present as ion pairs with anionic additives is very small at higher pH. Moreover, according to the assumptions of chaotropic theory, if the effect of chaotropic mobile phase additives on base retention is examined, these bases should be transferred into cationic forms. Therefore, lower pH of phosphate buffer is preferred.
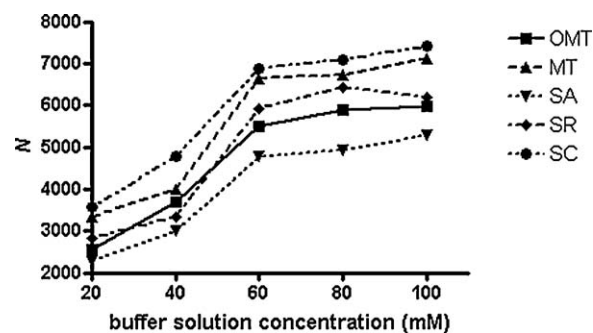

**Fig. 2.** Effect of buffer solution concentration on peak efficiency of five matrine-type alkaloids.
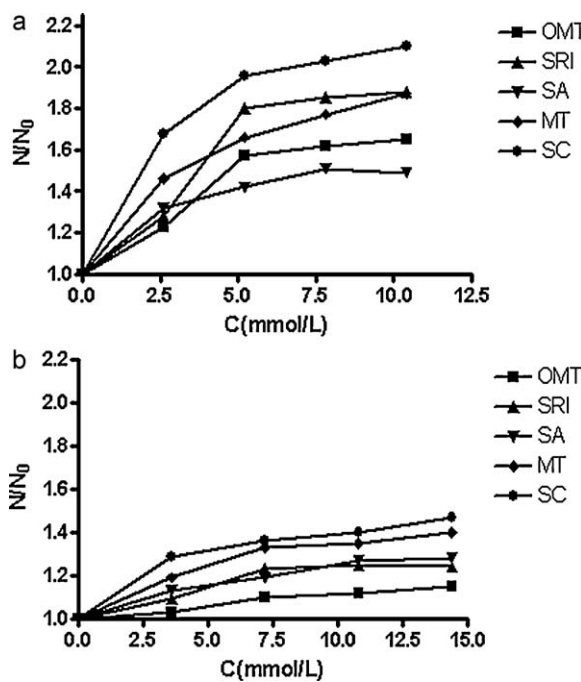
Fig. 3. Relative efficiency changes (N/N_0, where N_0 is the number of plates without additive) observed on the matrine-type alkaloid peaks with a mobile phase containing (a) BMIM BF$_4$ or (b) TEA at different concentrations. Other chromatographic conditions are the same as those in Fig. 1.

The effects of the addition of TEA or RTILs are better peak shape and enhanced efficiency. Therefore, in the present study, the dependence of peak efficiency on the concentration of additives in the mobile phase was investigated. Peak efficiencies were expressed as theoretical plates (N). The improvement in peak efficiencies observed on the matrine-type alkaloid peaks was expressed as N/N_0, and the ratio was derived from the plate count measured with an additive over the plate count obtained with the same compound and the same mobile phase without an additive. The results showed peak efficiencies were significantly improved by TEA and BMIM BF$_4$ (Fig. 3). However, the addition of TEA cannot completely eliminate tailing, even with the increased concentration. As mentioned, the resolution would decrease when the TEA concentration is increased, and this should be avoided.

4. Conclusions

To clarify systematically the effectiveness and mechanism of separation of matrine-type alkaloids with mobile phase containing RTILs in HPLC, the mobile phase pH, phosphate buffer concentration, and the length of RTIL alkyl groups were studied. The results demonstrated that the separation of alkaloids should be undertaken at weak acidity conditions. The retention factor increased under elevated phosphate buffer concentration at pH 3.4 and decreased at pH 6.4, which may be attributed to the ion-pair complex formation effect between additives and alkaloids at low pH and to the competition effect between additives and protonation alkaloids for adsorption on the stationary phase surface at relatively high pH.

In the process of investigating the effects of RTIL concentration and length of RTIL alkyl groups, chromatographic behaviors were accidently discovered and consequently validated to comply with SDM-R. The validation further clarified that the competitive adsorption between ionic liquids as displacer and analytes was the main process.

In addition, RTILs and TEA as mobile additives were compared. As a result, although the peak efficiencies had a significant improvement, the ionic liquid BMIM BF$_4$ was found superior to TEA. Moreover, BMIM BF$_4$ had little influence on the solute retention factors, whereas TEA significantly affected the factors as shown by the decrease. This difference was caused by the dual nature of ionic liquids which facilitated the participation of both the constituting anion and cation in the retention mechanism. The cations mostly interacted with the stationary phase silanol groups, and the anions were responsible for the possible ion-pairing with the cationic solutes. The two effects were beneficial on the chromatographic figure of merit. However, the cation effect was shown to be predominant based on SDM-R, although this needs to be verified by further experiments.

References

[1] A. Kumar, Salt effects on Diels–Alder reaction kinetics, Chem. Rev. 101 (2001) 1–19.
[2] T.F. Jiang, Y.L. Gu, B. Liang, J.B. Li, Y.P. Shi, Q.Y. Ou, Dynamically coating the capillary with 1-alkyl-3-methylimidazole-based ionic liquids for separation of basic proteins by capillary electrophoresis, Anal. Chim. Acta 479 (2003) 249–254.
[3] D.W. Armstrong, L.F. He, Y.S. Liu, Examination of ionic liquids and their interaction with molecules, when used as stationary phases in gas chromatography, Anal. Chem. 71 (1999) 3873–3876.
[4] L.J. He, W.Z. Zhang, L. Zhao, X. Liu, S.X. Jiang, Effect of 1-alkyl-3-methylimidazolium-based ionic liquids as the eluent on the separation of ephedrines by liquid chromatography, J. Chromatogr. A 1007 (2003) 39–45.
[5] W. Zhang, L. He, Y. Gu, X. Liu, S.X. Jiang, Effect of ionic liquids as mobile phase additives on retention of catecholamines in reversed-phase high-performance liquid chromatography, Anal. Lett. 36 (2003) 827–839.
[6] W.Z. Zhang, L.J. He, X. Liu, S.X. Jiang, Ionic liquids as mobile phase additives for separation of nucleotides in high performance liquid chromatography, Chin. J. Chem. 22 (2004) 549–552.
[7] X. Chen, C.Q. Yi, X.Q. Yang, X.R. Wang, Liquid chromatography of active principles in *Sophora flavescens* root, J. Chromatogr. B 812 (2004) 149–163.
[8] L.X. Jin, Y.Y. Cui, G.D. Zhang, HPLC analysis of alkaloids in *Sophora flavescens* Ait, Acta Pharm. 28 (1993) 136–139.
[9] L. Zhang, W.T. Liu, R.W. Zhang, Z.W. Wang, Z.D. Shen, Pharmacokinetic study of matrine, oxymatrine and oxysophocarpine in rat plasma after oral administration of *Sophora flavescens* Ait. extract by liquid chromatography tandem mass spectrometry, J. Pharm. Biomed. Anal. 47 (2008) 892–898.
[10] Y.Q. Cheng, H.L. Chen, Y.Q. Li, X.G. Chen, Z.D. Hu, Separation and determination of aloperine, sophoridine, matrine and oxymatrine by combination of flow injection with microfluidic capillary electrophoresis, Talanta 3 (2004) 491–496.
[11] J. Sun, J.J. Mao, X.H. Liu, Y.J. Wang, Y.H. Sun, Z.G. He, Separation and mechanism elucidation for six structure-like matrine-type alkaloids by micellar liquid chromatography, J. Sep. Sci. 32 (2009) 2043–2050.
[12] S.D. Rogers, J.G. Dorsey, Chromatographic silanol activity test procedures: the quest for a universal test, J. Chromatogr. A 892 (2000) 57–65.
[13] J.J. Gilroy, J.W. Dolan, L.R. Snyder, Selectivity evaluation for several new chromatographic columns, including sub-2 micron columns, for continued method development efficiency, J. Chromatogr. A 1000 (2003) 757–778.
[14] L.R. Snyder, J.J. Kirkland, J.L. Glajch, Practical HPLC Method Development, 2nd ed., Wiley, New York, 1997, 178 p.
[15] P.J. Dyson, M.C. Srinivasan, T. Vine, T. Welton, D.J. Williams, A.J.P. White, T. Zigras, Organometallic synthesis in ambient temperature chloroaluminate(III) ionic liquids. Ligand exchange reactions of ferrocene, J. Chem. Soc. Dalton Trans. 19 (1997) 3465–3469.
[16] J.A. Dean, Lange's Handbook of Chemistry., 2nd ed., Science Publishing House, Beijing, 2003.
[17] L.R. Snyder, J.J. Kirkland, Introduction to Modern Liquid Chromatography, 2nd ed., Wiley-Interscience, New York, 1979.
[18] J. Flieger, Effect of mobile phase composition on the retention of selected alkaloids in reversed-phase liquid chromatography with chaotropic salts, J. Chromatogr. A 1175 (2007) 207–216.
[19] X.D. Geng, F.E. Regnier, Retention model for proteins in reversed-phase liquid chromatography, J. Chromatogr. 296 (1984) 15–30.
[20] M.T.W. Hearn, M.I. Aguilar, High-performance liquid chromatography of amino acids, peptides and proteins. LXXIII. Investigations on the relationships between molecular structure, retention and band-broadening properties of polypeptides separated by reversed-phase high-performance liquid chromatography, J. Chromatogr. 397 (1987) 47–70.
[21] B.G. Belenkii, A.M. Podkladenko, O.I. Kurenbin, V.G. Mal'tsev, D.G. Nasledov, S.A. Trushin, Peculiarities of zone migration and band broadening in gradient reversed-phase high-performance liquid chromatography of proteins with respect to membrane chromatography, J. Chromatogr. 64 (1993) 1–15.
[22] M.J. Ruiz-Angel, S. Carda-Broch, A. Berthod, Ionic liquids versus triethylamine as mobile phase additives in the analysis of β-blockers, J. Chromatogr. A 1119 (2006) 202–208.
[23] A. Berthod, M.J. Ruiz-Angel, S. Huguet, Nonmolecular solvents in separation methods: dual nature of room temperature ionic liquids, Anal. Chem. 77 (2005) 4071–4080.

Short communication

Capillary zone electrophoresis as a potential technique for the simultaneous determination of sulfadoxine and pyrimethamine in tablet formulations

N'Cho Christophe Amin [a,b], Marie-Dominique Blanchin [a], Michèle Aké [b], Huguette Fabre [a,*]

[a] Laboratoire de Chimie Analytique, Contrôle physico-chimique des médicaments, Institut des Biomolécules Max Mousseron, UMR 5247, Faculté de Pharmacie, BP 14491, 34093 Montpelier, France
[b] Université de Cocody, UFR Sciences Pharmaceutiques, Laboratoire de Chimie analytique, chimie minérale et chimie générale, BPV 34 Abidjan, Côte d'Ivoire

ARTICLE INFO

ABSTRACT

A novel, simple and rapid capillary zone electrophoresis method with UV detection has been developed for the simultaneous determination of pyrimethamine and sulfadoxine in tablet formulations. The compounds are separated in 6 min in a fused silica capillary, 30 cm long (20 cm to detector) $\times$ 50 μm using a 100 mM phosphate buffer pH 7.2 as background electrolyte, a 330 V cm^{-1} electric field and a detection wavelength of 214 nm. Analysis of different tablet formulations has shown a good agreement with the liquid chromatography method described in the United States Pharmacopoeia. Main advantages of the CZE method are the rapid set-up of instrumentation and capillary equilibration, short analysis time and low running cost.

© 2011 Elsevier B.V. All rights reserved.

1. Introduction

Because each year, in the malaria-endemic areas of Africa, around 25 millions of pregnant women are at risk of *Plasmodium falciparum* during their pregnancy [1], a preventive antimalaria treatment for pregnant women has been recommended by World Health Organisation. The national policy which has been adopted in Côte d'Ivoire is to use pyrimethamine (PYR) and sulfadoxine (SDX) in combination for this purpose [2]. In this antimalaria chemotherapy, PYR which is a dihydrofolate inhibitor is combined in a synergetic effect with SDX, a sulfonamide which inhibits dihydropteroate synthetase. The two active substances sequentially block the two enzymes involved in the biosynthesis of folic acid within *P. falciparum*. Among separation methods, liquid chromatography (LC) methods have been described for the simultaneous determination of SDX and PYR in tablets [3–6], cleaning validation swabs [7] or human plasma [8–10]. Capillary electrophoresis (CE) methods have been reported for the determination of sulfonamides in food, pharmaceuticals and water [11–13] or for the determination of PYR as drug substance or in drug formulations [14–16] but there are no CE methods reported for a simultaneous determination of SDX and PYR in pharmaceuticals. Since alternative or complementary methods may be of interest to guarantee the quality of the drug or to detect drug adulteration, or counterfeit medicines [17], the possibility of using CE for the simultaneous determination of PYR and SDX in tablets has been investigated.

2. Experimental

2.1. Chemicals

PYR, SDX, procaine hydrochloride (PRO) and phenobarbital (PHE) were from Sigma Aldrich (Saint Quentin Fallavier, France). All other chemicals were of analytical grade from different suppliers. Fansidar® (Roche), Maloxine® (Exphar) and Ubigen SP® (Ubithera) commercial tablet formulations, were purchased from a pharmacy in Côte d'Ivoire. Amalar® (Micro Labs Ltd.), Fansidar® (Roche), Malabase® (Ronak), Maloxine® (Tycol Pharm, London, UK, Britlodge Ltd.; SW Pharma, China) tablets were purchased from a street market in Abidjan. All formulations had a declared content of 500 mg of SDX and 25 mg of PYR per tablet.

2.2. Solutions

2.2.1. Background electrolyte solution

100 mM sodium dihydrogenophosphate aqueous solution adjusted to pH 7.2 with a 0.1 M sodium hydroxide solution and filtered through a 0.45 μm Millipore membrane filter, type HVLP.

* Corresponding author. Tel.: +33 4 11 75 95 88.
E-mail address: huguette.fabre@univ-montp1.fr (H. Fabre).
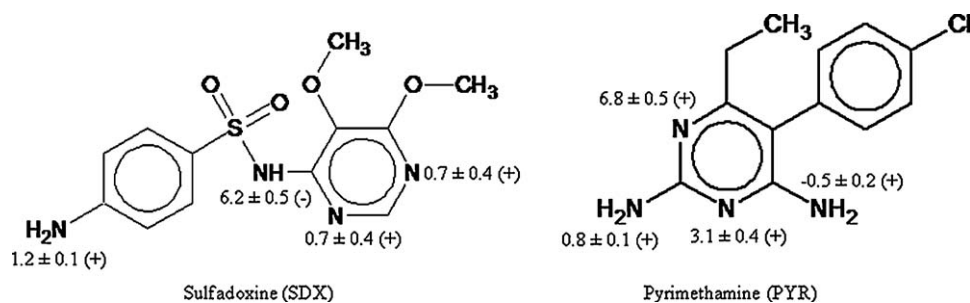
Fig. 1. Chemical structure and pK_as of sulfadoxine (SDX) and pyrimethamine (PYR).

2.2.2. Standard solution

A solution (24.0 mg l^{-1} PYR and 480.0 mg l^{-1} SDX) is prepared in a volumetric flask by sonication of an accurately weighed amount of PYR and SDX in acetonitrile (17% of the flask volume). After addition of 0.1% aqueous phosphoric acid solution to volume, the resulting solution (solution S) is sonicated for 5 min. A volume of 1 ml of internal standard (IS) solution (PRO, 300 mg l^{-1} and PHE, 2520 mg l^{-1} in acetonitrile – 0.1% phosphoric acid solution, 1:1, v/v) is added to 5 ml of solution S. This working standard solution contains PYR, 20 mg l^{-1}; SDX, 400 mg l^{-1}; PRO, 50 mg l^{-1} and PHE, 420 mg l^{-1}.

2.2.3. Test solution

Test solutions corresponding to theoretical PYR, 20 mg l^{-1}; SDX, 400 mg l^{-1} concentrations are prepared from an accurate amount of powdered tablet following the same procedure. After centrifugation of the extract at 5000 rpm for 5 min, 1 ml of the IS solution is added to 5 ml of supernatant. Standard and test solutions are stable for at least 24 h at ambient temperature.

2.3. Apparatus and operating conditions

A Beckman P/ACE MDQ (Fullerton, CA) instrument with a photodiode array detector was used with a fused-silica capillary, 30 cm long (20 cm to the detector), 50 μm internal diameter (TSP, Composite Metal Services, Hallow, Worcs, UK), housed in a cartridge with a 200 μm × 800 μm detector window. Prior to its first use, the capillary was pre-conditioned by washing at 20 psi for 20 min with a 0.1 M sodium hydroxide solution, and then flushed with water for 5 min. Every working day a preconditioning was carried out with 0.1 M sodium hydroxide followed by water and electrolyte buffer at 20 psi for 5 min. Optimised operating conditions for analysis were as follows: capillary rinse, 0.1 M HCl (1 min; 20 psi), 0.1 M NaOH (1 min; 20 psi), electrolyte (2 min; 20 psi); sample introduction (anodic side, 3 s, 0.3 psi); wait, water (0 s); separation, 330 V cm^{-1} with a 0.17 min ramp voltage, cartridge temperature, 25 °C ($i = 80$ μA); detection at 214 nm.

3. Results and discussion

3.1. Method optimisation

3.1.1. Selection of background electrolyte and separation conditions

The respective pK_a values of 6.8 (+) and 6.2 (−) [18] of PYR and SDX (Fig. 1) allow their separation under cationic (PYR) and anionic (SDX) forms in a pH range of 5–8. Different phosphate buffer solutions were tested in this range. An optimal separation was obtained with a phosphate buffer pH 7.2 at high concentration (100 mM) to improve peak efficiency by a stacking effect. Using a short length capillary (30 cm) to achieve the separation in the shortest time possible and applying a moderate voltage (10 kV) at a 25 °C separation temperature resulted in an acceptable current developed

(80 μA). Under these conditions, a minimum of 50 separations can be achieved with the same set of separation vials without noticeable drift of migration times (MTs) due to buffer depletion.

3.1.2. Selection of a sample solvent

Different sample solvents were investigated. Methanol, mixtures of methanol–water or methanol–phosphoric acid used in different ratios, resulted in a tailing peak for PYR. Using the sample solvent described in the USP (0.1% phosphoric acid–acetonitrile, 83:17, v/v) resulted in better peak shapes which can be explained by the stacking effect of acetonitrile in the presence of salt [19].

3.1.3. Selection of internal standards

The use of an IS is needed for quantitative analysis in CE to take into account small variations of the injected volumes due to the injection system. Because there is a disproportion in PYR and SDX, it was decided to use two different ISs for quantification. Among potential candidates, PRO (pK_a 9) and tetracaine (pK_a 8.5) were tested for PYR, and PHE (pK_a 7.4), benzoic acid (pK_a 4.3) and sorbic acid (pK_a 4.76) for SDX. PRO and PHE were selected as they give peaks well resolved (Fig. 2), close to the analytes and do not increase the analysis time.

3.1.4. Selection of detection wavelength

Due to the low concentration of PYR in the tablet extract, detection at a low wavelength is needed for sensitivity. A 214 nm wavelength (which allows the use of an instrument equipped with
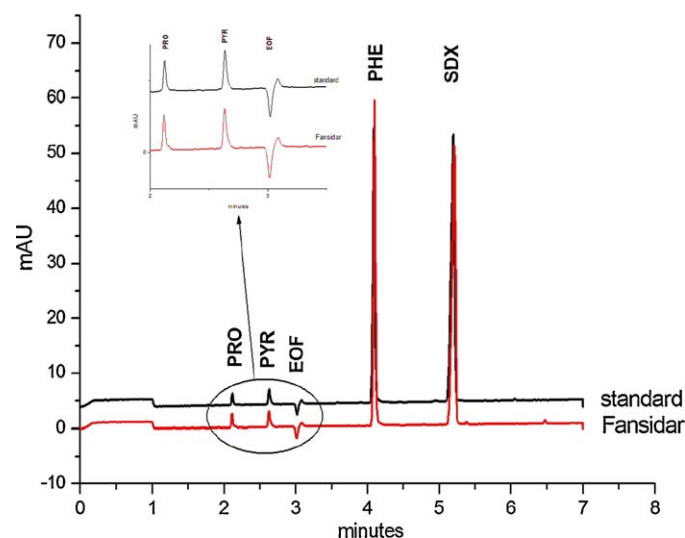

Fig. 2. Electropherograms of a standard solution of PYR and SDX (upper trace) and a test solution of Fansidar (lower trace). Conditions: 100 mM phosphate buffer pH 7.2; capillary, 50 μm I.D. × 30 cm; inj 3 s, 0.3 psi, PYR 20 mg l^{-1}, SDX 400 mg l^{-1}; 10 kV; 25 °C; detection, λ = 214 nm.
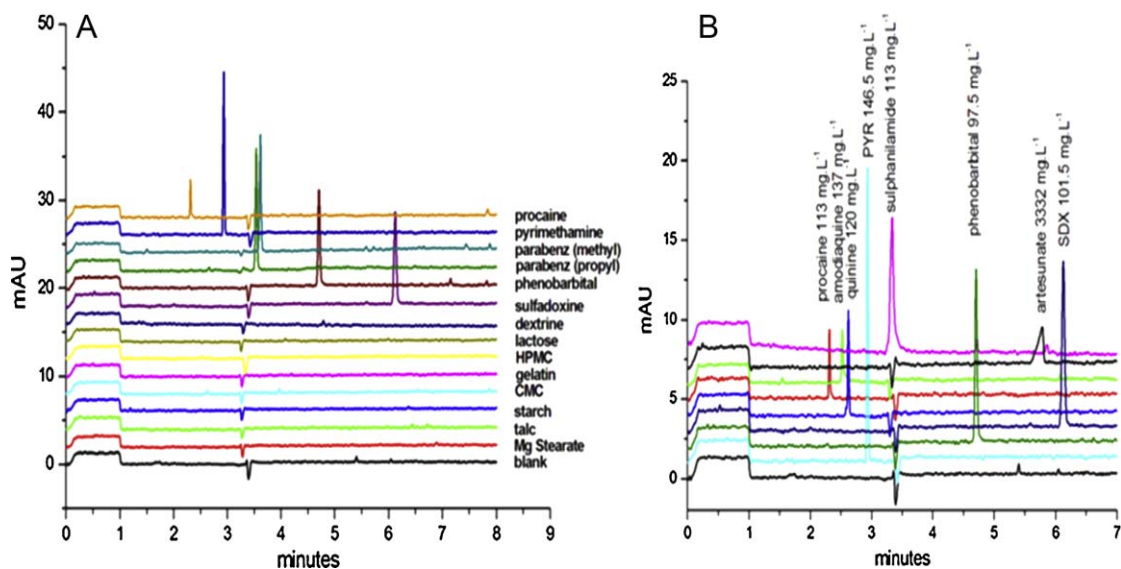
Fig. 3. Selectivity towards formulation excipients (A) and common antimalarials (B). Experimental conditions were as in Fig. 2.

a filter for detection) gave the best signal-to-noise ratio for PYR and allowed a simultaneous determination of the analytes.

3.2. Evaluation of method performances

3.2.1. Selectivity

No interference was noted with the ingredients present in the different tablet formulations analysed (Table 1) at the MTs of the active substances and ISs (Fig. 3A). The selectivity was also assessed towards sulfanilic acid and sulfanilamide, degradation products of SDX [20]. Sulfanilamide (pK_a 10.4), which is unionised migrates with the EOF (Fig. 3B) and sulfanilic acid (pK_a 3.2) is eluted at 18 min. As it was also considered that the method could be potentially applicable to detect counterfeit antimalarial formulations [17], the selectivity was also tested towards common antimalarials sold in Côte d'Ivoire: (artemether, lumefantrine, artesunate, amodiaquine and quinine). Artemether was not soluble in the dissolving solvent. Lumefantrine pK_as 8.7 (+), 13.5 (−) was not detected within 20 min. It is assumed that this very hydrophobic compound precipitates in the background electrolyte. Amodiaquine (pK_as 5.8 (+), 9.6 (+) and 10.2 (−)) and quinine pK_as 4.1 (+), 8.4 (+), 12.8 (−) migrate as cations and artesunate pK_a 4.3 (−), as an anion at pH 7.2 which is in agreement with their pK_a values [18], and are separated from PYR, SDX and IS (Fig. 3B).

3.2.2. Linearity of the response function

The linearity of the response function (corrected peak areas, CPA analyte/IS) vs analyte concentration was assessed over the range

5.0–25.0 mg l^{-1} for PYR and 100–500 mg l^{-1} for SDX at 5 concentration levels corresponding to 25, 50, 75, 100 and 125% of the target concentration (PYR, 20 mg l^{-1}; SDX, 400 mg l^{-1}). Three series of mixed calibration solutions were prepared independently over 3 days, each time from a different stock solution. Regression equations were:

$$\text{CPA (PYR/PRO)} = (0.0676 \pm 0.0013)\,\text{PYR mg l}^{-1}$$
$$- (0.012 \pm 0.021); \quad r^2 = 0.995$$

$$\text{CPA (SDX/PHE)} = (0.00298 \pm 0.00003)\,\text{SDX mg l}^{-1}$$
$$+ (0.026 \pm 0.010); \quad r^2 = 0.999$$

with the confidence intervals calculated at $\alpha = 0.05$. Analysis of variance showed that the relationship is linear and that the regression line passes through or close to the origin.

3.2.3. Relative migration times and corrected peak area precision

The precision of the system was assessed by injecting 7 times successively standard and test solutions at the target concentration. The RSD values were typically better than 0.1% for relative migration times, RMTs (MTs relative to IS) and in the range 0.5–2% for relative corrected peak areas, RCPAs (CPAs relative to IS). Similar RMTs (1.35 for PYR and 1.23 for SDX) were obtained on a same day, on different days, on different capillaries and different instruments. RMTs can be used together with UV spectra to confirm the identity of the drugs.

Table 1
Excipients of the different pharmaceutical formulations analysed.

Excipients	Ubithera®	Fansidar®	Maloxine®	Malabase®
Sodium carboxymethylcellulose (CMC)			×	
Dextrine	×			
Gelatin		×		
Hydroxypropyl methylcellulose (HPMC)	×			
Lactose		×		
Magnesium/calcium stearate	×	×	×	×
Sodium methyl hydroxybenzoate			×	×
Sodium propyl hydroxybenzoate			×	×
Starch	×	×	×	×
Talc		×	×	×

Amalar® unknown excipients.

Table 2
HPLC and CE determinations of SDX and PYR in commercial tablet formulations expressed as % of the label claim. Average of duplicate assays (except Fansidar, pharmacy, $n = 7$).

	EC PYR %	SDX %	HPLC PYR %	SDX %
Pharmaceuticals sold in a pharmacy				
Fansidar®	101.7	101.1	100.9	99.9
Maloxine®	97.9	100.0	98.5	98.8
Ubigen SP®	96.5	97.9	99.0	96.9
Pharmaceuticals sold on the street market				
Amalar®	98.2	100.8	98.0	99.6
Fansidar®	98.0	100.7	95.7	100.1
Malabase®	96.3	99.9	99.0	99.5
Maloxine® Tycol	91.0	92.1	92.0	91.2
Maloxine® Britlodge	97.2	88.1	94.5	87.4
Maloxine® SW Pharma	97.6	93.6	98.7	92.8

3.2.4. Limit of detection (LOD) and quantification (LOQ)

The LOD (signal-to-noise ratio of 3) and the LOQ (signal-to-noise ratio of 10) evaluated from a test solution at the target concentration, were $0.8\,\mathrm{mg\,l^{-1}}$ and $2.5\,\mathrm{mg\,l^{-1}}$, respectively, for both compounds. These limits correspond to 0.8 mg (LOD) and 2.5 mg (LOQ) of active substance per tablet.

3.2.5. Analysis of formulations. Cross-validation

Different formulations were analysed by the proposed CE method and the LC method described in the USP monograph "sulfadoxine and pyrimethamin tablet" [5]. Table 2 presents the comparative results of duplicate assays in different formulations, except for Fansidar (commercial formulation) for which 7 replicate determinations were performed to test the repeatability of the entire analytical procedure. Similar results are obtained using LC and CE. The repeatability of the analytical procedure ($n = 7$) for Fansidar expressed as the RSD was 1.94% for PYR and 0.7% for SDX in CZE, which is comparable with the results found in LC (1.06% for PYR and 0.7% for SDX).

4. Conclusion

CZE is a valuable technique for the simultaneous determination of PYR and SDX in tablet formulations. The method proposed shows good performances with respect to selectivity, linearity and precision. Cross validation with the USP LC method demonstrates the validity of the CE assays in different tablet formulations. Main advantages of the CZE method developed by comparison with the USP LC method are the rapid set-up of instrumentation and capillary equilibration, short run time (6 min) and low running cost (long lifetime of the capillary and consumption of a few millilitres of separation buffer per day). In contrast, the USP method that uses a phenyl column requires about 2 h for equilibration and a run time of 16 min and this stationary phase presents a rather poor stability. The specificity of the CE method towards common antimalarial suggests to use it to detect counterfeit tablets of SDX and PYR.

Acknowledgment

References

[1] WHO, World Health Organization Regional Office for Africa, A Strategic Framework for Malaria Prevention and Control During Pregnacy in the African Region, Brazzaville, 2004, pp. 1–27.

[2] Programme National de lutte contre le Paludisme, Ministère chargé de la santé, Abidjan, 2004, pp. 1–33.

[3] A. Abdo-Rabbo, A. Bassili, H. Atta, The quality of antimalarials available in Yemen, Malar. J. 4 (2005) 28–35.

[4] O. Onwujekwe, H. Kaur, N. Dike, E. Shu, B. Uzochukwu, K. Hanson, V. Okoye, P. Okonkwo, Quality of anti-malarial drugs provided by public healthcare providers in south-east Nigeria, Malar. J. 8 (2009) 22–31.

[5] USP33-NF28 reissue, United States Pharmacopoeia-National Formulary (Ed.), Baltimore, Maryland, United States, 2010.

[6] M. Arayne, N. Sultana, F. Siddiqui, S. Naseem, F. Qureshi, Simultaneous determination of pyrimethamine, sulfadoxine, mefloquine, and ibuprofen in pharmaceutical formulations by RP-HPLC, Med. Chem. Res. 19 (2010) 1043–1054.

[7] M.B. Boca, Z. Apostolides, E. Pretorius, A validated HPLC method for determining residues of a dual active ingredient anti-malarial drug on manufacturing equipment surfaces, J. Pharm. Biomed. Anal. 37 (2005) 461–468.

[8] H. Astier, C. Renard, V. Cheminel, O. Soares, C. Mounier, F. Peyron, J.F. Chaulet, Simultaneous determination of pyrimethamine and sulphadoxine in human plasma by high-performance liquid chromatography after automated liquid-solid extraction, J. Chromatogr. B 698 (1997) 217–223.

[9] Y. Bergqvist, S. Eckerbom, H. Larsson, M. Malek-Zade, Reverse-phase liquid chromatographic method for the simultaneous determination of the antimalarial drugs sulfadoxine, pyrimethamine, mefloquine and its major metabolites in plasma, J. Chromatogr. Biomed. Appl. 109 (1991) 169–177.

[10] B.A. Sinnaeve, T.N. Decaestecker, P.G. Risha, J.P. Remon, C. Vervaer, J.F. Van Bocxlaer, Liquid-chromatographic–mass spectrometric assay for simultaneous pyrimethamine and sulfadoxine determination in human plasma samples, J. Chromatogr. A 1076 (2005) 97–102.

[11] T. Li, Z.-G. Shi, M.-M. Zheng, Y.-Q. Feng, Multiresidue determination of sulfonamides in chicken meat by polymer monolith microextraction and capillary zone electrophoresis with field-amplified sample stacking, J. Chromatogr. A 1205 (2008) 163–170.

[12] R. Hoff, T.B.L. Kist, Analysis of sulfonamides by capillary electrophoresis, J. Sep. Sci. 32 (2009) 854–866.

[13] F.J. Lara, A.M. García-Campaña, C. Neusüss, F. Alés-Barrero, Determination of sulfonamide residues in water samples by in-line solid-phase extraction-capillary electrophoresis, J. Chromatogr. A 1216 (2009) 3372–3379.

[14] R.B. Taylor, R.G. Reid, Analysis of antimalarial drugs by CZE and MEKC. Part 1. Critical factors affecting separation, J. Pharm. Biomed. Anal. 11 (1993) 1289–1294.

[15] J. Cao, R.F. Cross, The separation of dihydrofolate reductase inhibitors and the determination of pK_a values by capillary electrophoresis, J. Chromatogr. A 695 (1995) 297–308.

[16] J. Berzas Nevado, P. Castaneda, J. Liq, Micellar electrokinetic capillary chromatography as an alternative method for the determination of sulfonamides and their associated compounds, J. Liq. Chromatogr. Relat. Technol. 22 (1999) 1975–1986.

[17] R.D. Marini, E. Rozet, M.L.A. Montes, C. Rohrbasser, S. Roht, D. Rhème, P. Bonnabry, J. Schappler, J.L. Veuthey, P. Hubert, S. Rudaz, Reliable low-cost capillary electrophoresis device for drug quality control and counterfeit medicines, J. Pharm. Biomed. Anal. 53 (2010) 1278–1287.

[18] Y. Bergqvist, N. Lindegårdh, in: P. Schlagenhauf-Lawlor (Ed.), Travelers' Malaria, McGraw-Hill, New York, 2008, p. 248.

[19] Z.K. Shihabi, Peptide stacking by acetonitrile–salt mixtures for capillary electrophoresis, J. Chromatogr. A 744 (1996) 231–240.

[20] K. Louati, F. Mistiri, M. Kallel, F. Safta, Stress degradation study on sulfadimethoxine and development of a validated stability-indicating HPLC assay, Ann. Pharm. Fr. 69 (2011) 91–99.

Short communication

Quantitative analysis of atractylenolide I in rat plasma by LC–MS/MS method and its application to pharmacokinetic study

Yujuan Li [a,*], Yushi Zhang [a], Zhimin Wang [b], Jingjing Zhu [b], Yuan Tian [a], Bo Chen [a]

[a] School of Life Science, Beijing Institute of Technology, No.5 Zhongguancun South Street, Beijing 100081, China
[b] Institute of Chinese Materia Medica, China Academy of Chinese Medical Sciences, Beijing 100007, China

ARTICLE INFO

ABSTRACT

A new high-performance liquid chromatography/tandem mass spectrometry (LC–MS/MS) was developed for quantitative analysis of atractylenolide I in rat plasma using buspirone as internal standard (I.S.). Rat plasma samples were deproteined with methanol and acetonitrile (1:1, v/v). Atractylenolide I and I.S. were separated on a Phenomenex Gemini C_{18} column (50 mm × 2.0 mm, 5 μm) with gradient mobile phase at the flow rate of 0.4 ml/min. The detection was performed by positive ion electrospray ionization (ESI) in multiple reaction monitoring (MRM) mode. The linear calibration curve of atractylenolide I in rat plasma ranged 2.0–5000 ng/ml ($R > 0.9979$). The limit of detection (LOD) and the limit of quantification (LOQ) were 0.6 ng/ml and 2.0 ng/ml, respectively. Both accuracy and precision of the assay were satisfactory. The recoveries of atractylenolide I and I.S. were 91.4% and 87.8%, respectively. This fully validated method was applied to a pharmacokinetic study of atractylenolide I in rats administered with 20 g/kg Atractylodis extract. The main pharmacokinetic parameters T_{max} (the time to peak), C_{max} (the concentration to peak), $T_{0.5}$ (the biological half time), and K_e (the elimination rate constant) were 0.81 ± 0.11 h, 7.99 ± 1.2 ng/ml, 1.94 ± 0.27 h, 0.365 ± 0.06/h, respectively.

© 2011 Elsevier B.V. All rights reserved.

1. Introduction

Traditional Chinese Medicine (TCM) is the natural therapeutic agent used for prevention and treatment of diseases for thousands' of years in China. Atractylodis (the dried root and stem of *Atractylodes macrocephala Koidz*) is one of the TCM listed in Chinese Phaemacopoeia [1]. It shows anti-tumor, anti-inflammatory and anti-bacterial effects [2–4]. It also could inhibit gastrointestinal smooth muscle [5]. Atractylodis is rich of volatile oil and lactones [6,7]. Recently, atractylenolide I, one single compound isolated from Atractylodis, has attracted more and more attention because of its multiple therapeutic effects. It has been reported that atractylenolide I showed aromatase inhibiting activity, anti-bacterial activity and gastroprotective activity [8,9]. Atractylenolide I could also inhibit uterine contraction [10]. Anticancer effect of atractylenolide I has been proved in different cancer cells [11–15].

Reversed-phase high performance liquid chromatography (RP-HPLC) with evaporation light scattering detection and UV detection has been reported for determination of atractylenolide I in Atractylodis herb [16,17]. Until now, two pieces of paper reported that a capillary gas chromatography-selected ion monitoring mass spectrometry method and an RP-HPLC method with UV detection for quantification of atractylenolide I in rat plasma. In those paper, atractylenolide I was administered to rats as a single component [18,19]. However, owing to the complexity of chemical constituents in this herbal medicine, reports are unavailable regarding analytical methods for quantification and pharmacokinetic study of atractylenolide I in Atractylodis. Furthermore, HPLC–MS method for determination of atractylenolide I in animals or human has not been reported elsewhere.

In order to support preclinical pharmacokinetic studies of Atractylodis and make better use of TCM preparations containing this herb, it is critical to develop a new method for determination of atractylenolide I in Atractylodis from biological matrices. In the current paper, a simple, rapid and sensitive HPLC–MS/MS method for quantification of atractylenolide I in the plasma of rat after oral administration of the Atractylodis extract was developed for the first time. The preliminary pharmacokinetic behavior of atractylenolide I in rat plasma after oral administration of Atractylodis extract was firstly elucidated.

2. Experimental

2.1. Chemicals and reagents

Atractylodis extract and atractylenolide I (98.8%, purity) were supplied from Shanghai TCM University, Shanghai, China.

Atractylodis was extracted with 95% ethanol and then evaporated to dryness to get the extract. Buspirone used as internal standard (I.S., 98.6%, purity) was purchased from National Institute for the Control of Pharmaceutical and Biological Products, Beijing, China. Methanol and acetonitrile were of chromatographic grade from Fisher Company (Iowa, USA). Formic acid was of analytical grade purchased from Mairida Technologies (Beijing, China). The blank rat plasma was obtained from healthy Wistar rat (the Experimental Animal Institute of the Medical Science Academy of China).

2.2. Stock solutions and standard samples

The standard stock solution was prepared by dissolving 10.0 mg of atractylenolide I in 100 ml of methanol to obtain a nominal concentration of 0.1 mg/ml. The internal standard stock solution was prepared by dissolving appropriate amount of buspirone in the mixture solvent of methanol and acetonitrile (1:1, v/v) to obtain a nominal concentration of 0.1 μg/ml. All the stock solutions were kept at 4 °C before use.

Calibration curves were prepared by spiking 50 μl of the appropriate standard solution to 50 μl of blank rat plasma at concentrations of 2.0, 5.0, 20.0, 50.0, 200, 500, 1000, 2000 and 5000 ng/ml. Quality control (QC) samples (0.2, 200 and 5000 ng/ml) were independently prepared.

2.3. Chromatography and mass spectrometry

LC–MS/MS analysis was performed on Waters Acquity UPLC system coupled to a Waters Quattro Premier XE Mass Spectrometer (Waters Company, Milford, USA). MassLynx and Quanlynx (Waters Company, Milford, USA) software version 4.1 was used for instrument control and quantification, respectively. The LC system was equipped with a Phenomenex Gemini column (2.0 mm × 50 mm, 5 μm, Phenomenex Company, CA, USA). The mobile phase consisted of a mixture of 0.1% formic acid in water (A) and 0.1% formic acid in methanol (B). The gradient elution was programmed as follows: 0 min 10% B, 1 min 10% B, 3 min 90% B, 4 min 90% B, 4.01 min 10% B, 5 min stop. The flow rate was set at 0.4 ml/min and the column temperature was maintained at 25 °C. The injection volume was 10 μl.

The mass spectrometer was operated in the positive electrospray ionization (ESI) mode with multiple reaction monitoring (MRM). MRM parameters were optimized using direct infusion experiments of standard compounds. Nitrogen was used as desolvation gas (600 l/h) and cone gas (50 l/h). The capillary voltage was set at 3.2 kV with the source temperature at 110 °C for atractylenolide I and I.S. Collision energies for atractylenolide I and I.S. were 20 V and 30 V, respectively. Cone voltage were set at 37 V for atractylenolide I and 42 V for I.S., respectively. The desolvation temperature was kept at 300 °C. The precursor-to-product ion transitions were monitored at m/z 231.1 → 185.1 for atractylenolide I and at m/z 386.4 → 122.1 for buspirone.

2.4. Extraction procedure

To 50 μl plasma sample, 150 μl of I.S. solution (the mixture solvent of methanol–acetonitrile (1:1, v/v) were added for protein precipitation. The mixture was vortexed for 60 s and centrifuged at 5000 rpm for 10 min. The supernatant was filtered through 0.45 μm membrane. 10 μl of aliquot was injected onto the LC–MS/MS system for analysis.

2.5. Assay validation

Calibration curve was obtained by plotting the peak area ratio of atractylenolide I to I.S. against the corresponding atractylenolide

I concentrations. Linearity was assessed by weighted linear regression with the weighting factor $1/x^2$ (x was the concentration of atractylenolide I in rat plasma). The selectivity was determined by comparison the blank rat plasma with real samples. The limit of quantification (LOQ) was defined as the lowest drug concentration on the calibration curve of atractylenolide I determined with an accuracy (relative error, RE) and precision (relative standard deviation, R.S.D.) of less than 20%. The limit of detection (LOD) was defined as signal/noise ratio of 3.

The accuracy was defined as the percentage of deviation (RE) of the observed concentrations from the nominal concentrations. Six replicate QC samples at each concentration were analyzed in a single sequence for within-day assessment. For between-day assessment six replicate QC samples at each concentration were analyzed on three occasions. The precision of the assay was determined by calculating the R.S.D. Recovery was calculated by comparing the observed concentrations with the spiked concentrations with low (2 ng/ml), medium (200 ng/ml) and high concentration (5000 ng/ml) QC samples.

The stability of atractylenolide I in rat plasma at room temperature for 6 h, at −20 °C for 30 days and after three freeze–thaw cycles was assessed. The concentration of atractylenolide I from three storage conditions was compared to the initial concentration of freshly prepared samples.

2.6. Pharmacokinetic study

The method was applied to a pharmacokinetic study of atractylenolide I in rats. Wistar rats (200 ± 20 g, three males and three females were supplied by Experimental Animal Institute of the Medical Science Academy, Beijing, China. The rats were fasted for 12 h and had free access to water before dosing. Rats was administered a single dose of 20 g/kg Atractylodis extract, and then blood samples were collected at scheduled time points (0, 0.5, 1,2, 3, 4, 6, 8, 12, 18, 24 and 36 h). The blood samples were then centrifuged at 3000 rpm for 10 min immediately and then the plasma samples were prepared and obtained. The plasma samples were kept at −20 °C until analysis.

The plasma concentrations of atractylenolide I at different time points were expressed as mean ± S.D. The concentration versus time curve was plotted. All the pharmacokinetic parameters were calculated by DAS 2.0 statistical software (Mathematical Pharmacology Professional Committee of China).

3. Results and discussion

3.1. Method development

In order to obtain a sensitive mass response of the compounds, the transitions of the targets and the main parameters, such as cone, capillary and collision voltages, desolvation and source temperatures were investigated carefully. All MS parameters were optimized to find the most abundant and characteristic molecular and product ions. Full scan product ion spectra of atractylenolide I and I.S. were investigated with MRM mode. For atractylenolide I, typical fragment ion of m/z 185.1 was observed. The characteristic fragment ion of m/z 122.1 for I.S. was selected. Their fragmentation pathways are shown in Fig. 1.

Different compositions of the mobile phase (methanol and water) were investigated in present study. Initially, isocratic mobile phase was adopted to separate atractylenolide I and I.S. However, atractylenolide I was difficult to be well separated from other lactone components, such as atractylenolide II and atractylenolide III in Atractylodis extract because of their extremely similar structures. Finally, gradient mobile phase was utilized to separate
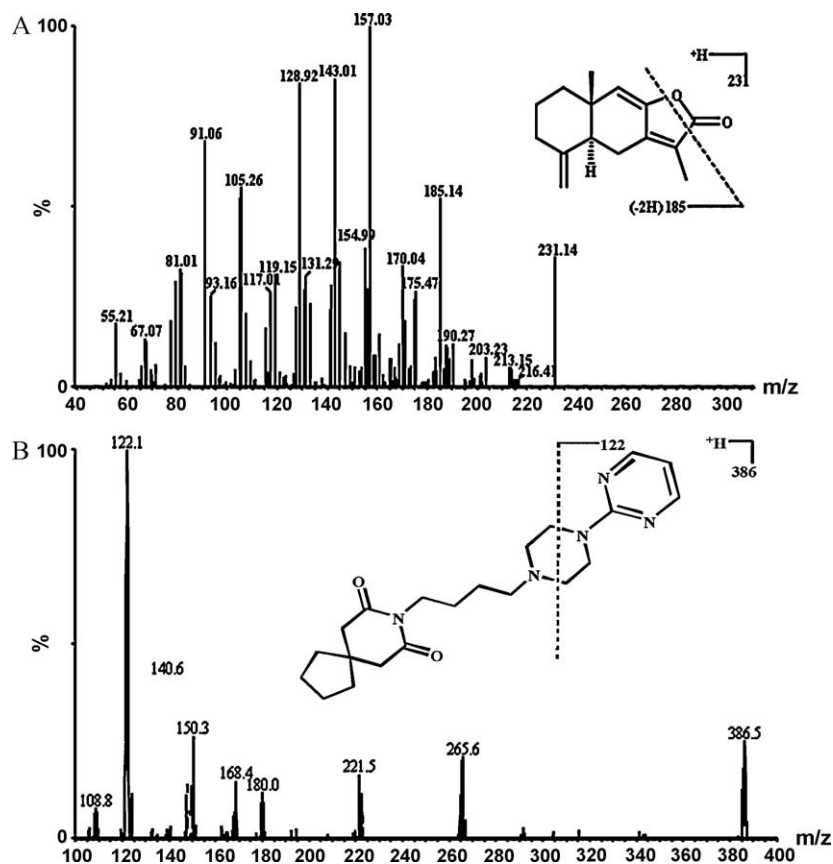
Fig. 1. Full-scan product ion spectra of [M+H]$^+$ ions and fragmentation pathways for (A) atractylenolide I and (B) buspirone.

Table 1
Precision and accuracy for the determination of atractylenolide I in rat plasma by LC/MS/MS method (n = 6).

Nominal concentration (ng/ml)	Calculated concentration (ng/ml)	Intra-day R.S.D. (%)	Inter-day R.S.D. (%)	Accuracy RE (%)
2.00	1.844	6.2	8.9	−7.8
200	209.2	3.4	3.1	4.6
5000	5170	1.6	4.8	3.4

atractylenolide I and I.S. with sharp peaks and appropriate analysis time. Under the optimal HPLC–MS/MS conditions, the representative MRM chromatograms of atractylenolide I and I.S. are shown in Fig. 2. The retention times of atractylenolide I and I.S. were 2.27 min and 3.65 min, respectively. Each chromatographic run was completed within 4 min.

Different protein precipitation solvents, such as methanol, acetonitrile, were tested. Finally, a mixture of methanol–acetonitrile (1:1, v/v) was used as the optimal solvent because no significant ion suppression effect was observed. This very simple protein precipitation method could also increase the recoveries of atractylenolide I and I.S. with good repeatability.

Compared with previous GC–MS method for determination of atractylenolide I in rat plasma [18], the present HPLC–MS/MS method supplied shorter run time (3.65 min) than 10 min reported earlier. Furthermore, the protein precipitation procedure seemed simpler than liquid–liquid extraction method.

3.2. Assay validation

The calibration curve was linear over the concentration range of 2.0–5000 ng/ml. The intercept, slope and correlation coefficient of calibration equation were 12.1, 202.4 and 0.9979, respectively.

The LOD and LOQ were 0.6 ng/ml and 2.0 ng/ml, respectively. Intra- and inter-day precisions (R.S.D.) and accuracy for quantification of atractylenolide I in rat plasma were summarized in Table 1. Intra- and inter-day precisions ranged from 1.6% to 8.9%. Accuracy (RE) was between −7.8% and 3.4% for atractylenolide I at three concentrations in rat plasma. Both precision and accuracy of this assay were satisfactory.

Recovery result was shown in Table 2. The recoveries of atractylenolide I at low, medium and high spiked levels were 90.1%, 90.8% and 93.4%, respectively. The average recovery of atractylenolide I was 86.7%. The recovery of I.S. was 87.8%. Moreover, good repeatability of atractylenolide I recovery experiment was obtained with RSD values less than 7.6%.

Table 2
The extraction recoveries of atractylenolide I and I.S. in rat plasma by LC/MS/MS method (n = 6).

| Compound	Added concentration (ng/ml)	Extract recovery (%)	R.S.D. (%)
I.S.	100	87.8	3.2
AO-I	2.00	90.1	7.6
	200	90.8	2.8
	5000	93.4	3.3
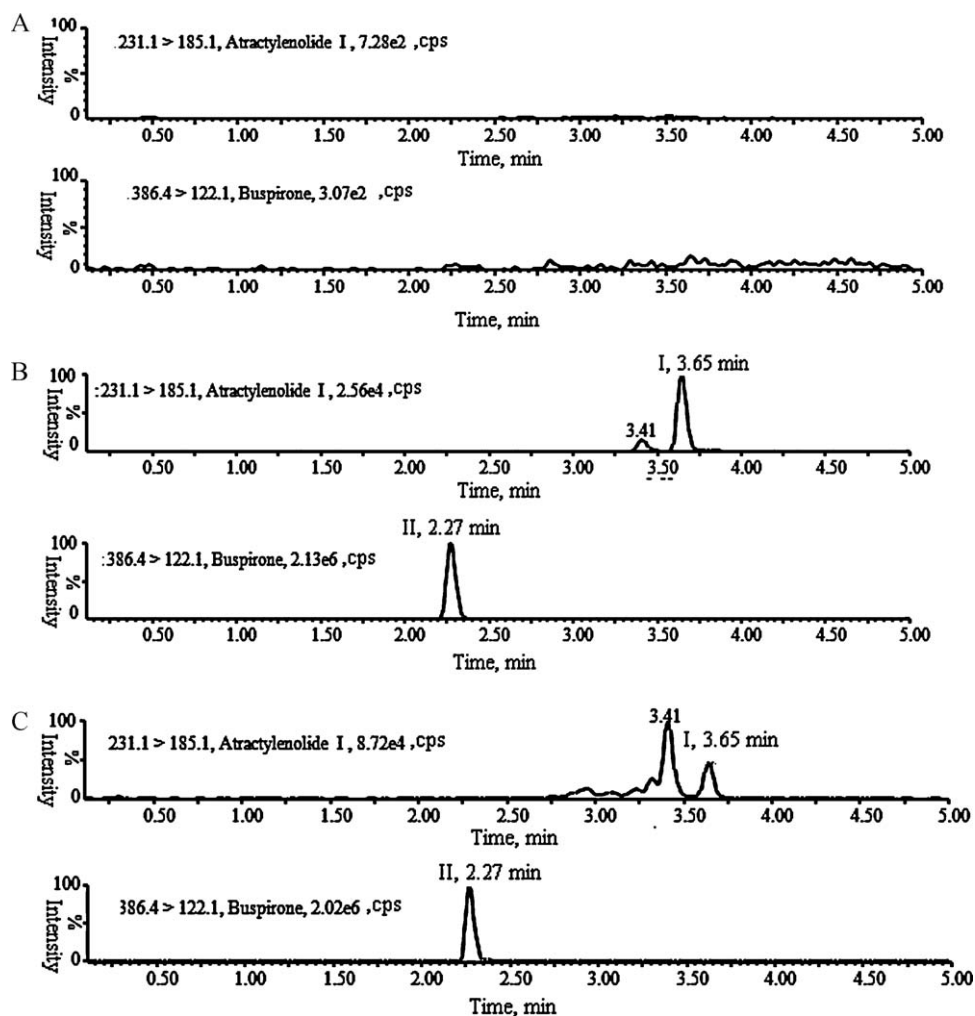
Fig. 2. Typical chromatograms of (A) blank plasma, (B) blank plasma spiked with atractylenolide I (100 ng/ml) and I.S. (100 ng/ml) and (C) a real plasma sample collected at 1 h after an oral dose of 20 g/kg Atractylodis. Peak I, atractylenolide I; Peak II, I.S.

The stability results of atractylenolide I under three storage conditions were listed in Table 3. Atractylenolide I in rat plasma at room temperature was stable for 6 h with RE less than 8.3%. The stability of atractylenolide I in rat plasma at −20 °C for 30 days ranged from −1.8% to 3.1% (RE). The stability of atractylenolide I after three freeze–thaw cycles was below 6.4% (RE). Stability results showed that atractylenolide I was stable under different conditions.

Table 3
Stability of atractylenolide I in rat plasma at different conditions determined by LC/MS/MS method ($n = 6$).

Conditions	Spiked concentration (ng/ml)		
	2.00	200	5000
Freeze–thaw stability (RE, %)			
0 cycle	2.1	−4.3	4.8
3 cycles	3.2	6.4	−3.7
Storage stability at −20 °C (RE, %)			
0 day	3.1	−4.0	1.4
30 days	2.8	−1.8	2.0
Processed plasma samples at 20 °C RE, %)			
0 h	8.3	−2.9	6.3
6 h	7.6	−2.7	1.9

3.3. Pharmacokinetic study

Mean plasma concentration–time profile of atractylenolide I after oral administration of Atractylodis extract was shown in Fig. 3. The main pharmacokinetic parameters were listed in Table 4. Atractylenolide I was found to be absorbed quickly within 1 h.
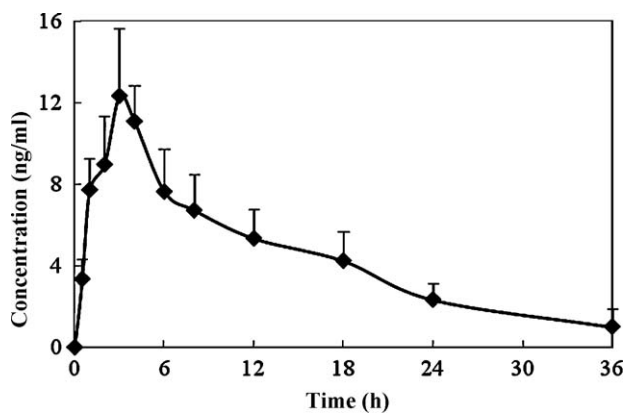
Fig. 3. Mean plasma concentration-time profile of atractylenolide I determined by LC/MS/MS method after oral administration of 20 g/kg Atractylodis extract to rats. Each point represents the mean ± S.D. ($n = 6$).

Table 4
Pharmacokinetic parameters of atractylenolide I after oral administration of Atractylodis extract (20 g/kg) to rats ($n = 6$, Mean ± S.D.).

Parameters	Values	Parameters	Values
K_e (/h)	0.365 ± 0.06	AUC_{0-T} (µg h/l)	22.2 ± 1.9
$T_{0.5}$ (h)	1.94 ± 0.27	$AUC_{0-\infty}$ (µg h/l)	22.6 ± 1.8
T_{max} (h)	0.81 ± 0.11	CL (l/h/kg)	978.2 ± 117.3
C_{max} (µg/l)	7.99 ± 1.2	Vc (l/kg)	2768.6 ± 751.5

The time to reach peak concentration (T_{max}) was 0.81 ± 0.11 h. Peak concentration (C_{max}) ranged from 6.79 to 9.19 µg/l, respectively. The biological half-life ($T_{0.5}$) was 1.94 h with values between 1.67 and 2.21 h. The elimination rate constant (K_e) and area under curve (AUC_{0-T}) were 0.365 ± 0.06 h, and 22.21 ± 1.9 µg h/l, respectively.

The dose of 20 g/kg Atractylodis extract was decided by our previous in vitro everted intestinal Sac model experiments (data not published). The contents of atractylenolide I, II and III in Atractylodis extract are 0.053%, 0.025% and 0.072%, respectively. During method development, simultaneous determination for atractylenolide I, II and III in blank rat plasma was performed. While, atractylenolide II in real samples of rats ingested Atractylodis extract was not detected at any time point under present chromatographic condition. Though atractylenolide III could be determined in rat plasma samples at different time points, the pharmacokinetic curve of atractylenolide III showed an irregular pattern. All these interesting phenomena still need further study.

4. Conclusions

A rapid, simple and sensitive LC–MS/MS method was developed for quantification of atractylenolide I in rat plasma for the first time. This method was completely validated and applied to a pharmacokinetic study of atractylenolide I after oral administration of 20 g/kg Atractylodis extract to Wistar rats. The preliminary pharmacokinetic behavior of atractylenolide I in Atractylodis was firstly elucidated.

Acknowledgement

References

[1] Pharmacopoeia of the People's Republic of China, vol. 2, Chemical Industry Press, Beijing, 2010, p. 95.

[2] C.Q. Li, L.C. He, H.Y. Dong, J.Q. Jin, Screening for the anti-inflammatory activity of fractions and compounds from Atractylodes macrophala koidz, J. Ethnopharmacol. 114 (2007) 212–217.

[3] H. Dong, L. He, M. Huang, Y. Dong, Anti-inflammatory components isolated from Atractylodes macrocephala Koidz, Nat. Prod. Res. 22 (2008) 418–427.

[4] S.I. Jeong, S.Y. Kim, S.J. Kim, B.S. Hwang, T.H. Kwon, K.Y. Yu, S.H. Hang, K. Suzuki, K.J. Kim, Antibacterial activity of phytochemicals isolated from *Atractylodes japonica* against methicillin-resistant *staphylococcus aureus*, Molecules 15 (2010) 7395–7402.

[5] K.T. Wang, L.G. Chen, C.H. Wu, C.C. Chang, C.C. Wang, Gastroprotective activity of atractylenolide III from *Atractylodes ovata* on ethanol-induced gastric ulcer in vitro and in vivo, J. Pharm. Pharmacol. 62 (2010) 381–388.

[6] W.W. Ye, Y. Shao, R.H. Hu, Study on chemical constituents in Atractylodes macrocephala Koidz, China Sci. Technol. Achiev. 23 (2008) 41–44.

[7] W. Chen, G.F. He, M.H. Jiang, Research on Atractylodes macrocephala Koidz in recent ten years, J. Lishizhen Herbal Med. 18 (2007) 338–340.

[8] H. Jiang, J. Shi, Y. Li, Screening for compounds with aromatase inhibiting activities from Atractylodes macrocephala Koidz, Molecules 16 (2011) 3146–3151.

[9] C. Wang, H. Duan, L. He, Inhibitory effect of atractylenolide I on angiogenesis in chronic inflammation in vivo and in vitro, Eur. J. Pharmacol. 612 (2009) 143–152.

[10] Y.Q. Zhang, S.B. Xu, Y.C. Lin, Q. Li, X. Zhang, Y.R. Lai, Antagonistic effects of 3 sesquiterpene lactones from Atractylodes macrocephala Koidz on rat uterine contraction in vitro, Acta Pharmacol. Sin. 21 (2000) 91–96.

[11] Y. Liu, Z. Jia, L. Dong, R. Wang, G. Qiu, A randomized pilot study of atractylenolide I on gastric cancer cachexia patients, Evid. Based Complement Alternat. Med. 5 (2008) 337–344.

[12] C.Q. Li, L.C. He, J.Q. Jin, Atractylenolide I and atractylenolide III inhibit lipopolysaccharide-induced TNF-alpha and NO production in macrophages, Phytother. Res. 21 (2007) 347–353.

[13] C.C. Wang, S.Y. Lin, H.C. Cheng, W.C. Hou, Pro-oxidant and cytotoxic activities of atractylenolide I in human promyeloleukemic HL-60 cells, Food Chem. Toxicol. 44 (2006) 1308–1315.

[14] Y. Ye, G.X. Chou, H. Wang, J.H. Chu, W.F. Fong, Z.L. Yu, Effects of sesquiterpenes isolated from largehead Atractylodes Rhizome on growth, migration, and differentiation of B16 melanoma cells, Therapies 10 (2011) 92–100.

[15] C.C. Wang, L.G. Chen, L.L. Yang, Cytotoxic activity of sesquiterpenoids from Atractylodes ovata on leukemia cell lines, Planta Med. 68 (2002) 204–208.

[16] C. Li, X. Zhang, Simultaneous determination of five effective components in Sijunzi bolus using high performance liquid chromatography-evaporation light scattering detection, Se Pu 28 (2010) 64–67.

[17] D. Shou, S. Dai, J. Zhang, H. Li, Z. Yu, Simultaneous determination of atractylenolide III, atractylenolide I and atractylon in Artactylodis macrocephala using microbore liquid chromatography, Se Pu 26 (2008) 637–639.

[18] C. Wang, S. Wang, Q. Chen, L. He, A capillary gas chromatography-selected ion monitoring mass spectrometry method for the analysis of atractylenolide I in rat plasma and tissues, and application in a pharmacokinetic study, J. Chromatogr. B: Analyt. Technol. Biomed. Life Sci. 863 (2008) 215–222.

[19] C. Li, L. He, Y. Hu, Pharmacokinetics of atractylenolide I from Atractylodes macrocephala Koidz in rats by RP-HPLC, Asian J. Pharmacodyn. Pharmacokinet. 7 (2007) 283–288.

Short communication

An LC–MS/MS method for the determination of ofloxacin in 20 μl human plasma

Sandra A. Meredith *, Peter J. Smith, Jennifer Norman, Lubbe Wiesner

Division of Clinical Pharmacology, University of Cape Town, Medical School, Observatory, 7925 Cape Town, South Africa

ARTICLE INFO

ABSTRACT

A sensitive and selective liquid chromatography–tandem mass spectrometry method was developed and validated for the determination of ofloxacin in 20 μl human plasma over the concentration range of 0.078–20 μg/ml. Sample preparation was achieved by protein precipitation with acetonitrile and methanol containing the internal standard (Gatifloxacin). Chromatographic separation was achieved on a Luna 5 μm PFP (110 A, 50 × 2 mm) column with acetonitrile and water containing 0.1% formic acid (50:50, v/v) as the mobile phase, at a flow rate of 400 μl/ml. The within-day and between-day precision determinations for ofloxacin, expressed as the percentage coefficient of variation, were lower than 7% at all test concentrations. Recovery of ofloxacin was greater than 70% and reproducible at the low, medium and high end of the dynamic range. No significant matrix effects were observed for the analyte or internal standard. The assay was successfully used to examine the pharmacokinetics of ofloxacin as part of a study to characterize the pharmacokinetics of a number of anti-tuberculosis drugs utilized in the treatment of multi-drug resistant tuberculosis (MDR-TB).

© 2011 Elsevier B.V. All rights reserved.

1. Introduction

The occurrence of multidrug-resistance (MDR) strains of tuberculosis (TB) contributes significantly to the increased incidence of TB. Ofloxacin is used as a second-line drug for the treatment of MDR-TB [1,2]. It is a broad-spectrum, chemotherapeutic antimicrobial agent belonging to the Fluoroquinolone (quinolones) drug class. Quinolones target bacterial DNA gyrase, an enzyme that controls the supercoiling of DNA and separating of linked DNA molecules. Inhibition of DNA gyrase by the quinolones effects DNA replication, transcription, repair and recombination [3,4].

A number of papers on the determination and quantification of ofloxacin by High Performance Liquid Chromatography (HPLC) with UV or fluorescence detection have been published, with the limit of detection being around 20–25 ng/ml. The drawback of these methods however, is that large plasma volumes (between 0.2 and 1.0 ml) are required [3,5–7]. For pediatric patients this is not ideal, particularly when numerous samples are needed [8]. To minimise the volume of blood sampling, drug assays requiring smaller sample volumes are essential.

Advances in HPLC coupled with triple quadrupole mass spectrometry (LC–MS/MS) technology have revolutionized drug analysis in biological samples. Today LC–MS/MS is heralded the gold standard for drug analysis, with vast improvements in sensitivity, selectivity and throughput [9]. The aim of this work was to develop a sensitive LC–MS/MS method using low plasma volumes to facilitate pharmacokinetic studies and therapeutic drug monitoring in paediatric patients. We describe here a robust LC–MS/MS method coupled with a simple protein precipitation extraction method for the determination of ofloxacin in 20 μl human plasma.

2. Experimental

2.1. Materials and chemicals

Methanol (LiChrosolv®), acetonitrile (LiChrosolv®), formic acid (pro analysis) and water (LiChrosolv®) were purchased from Merck kGaA, Darmstadt, Germany. The ofloxacin reference standard (EP) was supplied by Industrial Analytical (Kyalami, RSA) and gatifloxacin (internal standard) supplied by Toronto Research Chemicals (TRC, Ontario, Canada). Drug free plasma was obtained from Western Province Blood Transfusion Services at the Groote Schuur Hospital, South Africa. A Phenomenex Luna, PFP(2) 100 A, 50 mm × 2.0 mm column (Phenomenex, USA) was used for retaining ofloxacin and the internal standard.

2.2. Chemical structure

Chemical structure of ofloxacin is presented in Fig. 1.

* Corresponding author at: Division of Clinical Pharmacology, University of Cape Town, Medical School, H50, Old Main Building, Groote Schuur Hospital, Observatory, 7925 Cape Town, South Africa. Tel.: +27 21 406 6479; fax: +27 21 406 6152.
*E-mail address:* sandra.meredith@uct.ac.za (S.A. Meredith).
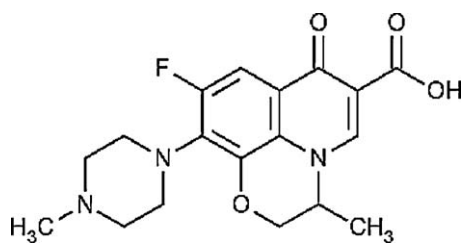
Fig. 1. Chemical structure of ofloxacin.

2.3. Instrumentation

The mobile phase was delivered with an Agilent 1200 series binary pump and the samples injected with an Agilent 1200 High Performance Autosampler (Agilent, CA, USA). Detection was performed by an AB Sciex API 3200 Q Trap mass spectrometer (AB Sciex, Ontario, Canada) fitted with a Turbo V^{TM} ion source.

2.4. Preparation of calibration

Calibration standards and quality controls (QC) were prepared in blank human plasma, and the preparation procedure performed on ice. Ofloxacin stock solution (SS1) was prepared in a mixture of acetonitrile and water (50:50, v/v) at 1000 μg/ml. Blank plasma (10 ml) was spiked with SS1 for the highest calibration standard (20 μg/ml) and serial dilutions were performed with blank plasma to attain the additional calibration standards (10, 5, 2.5, 1.25, 0.623, 0.313, 0.156 and 0.078 μg/ml). The same methodology was used for the preparation of the high, medium and low QCs (16, 8 and 0.25 μg/ml, respectively). The calibration standards and QC standards were briefly vortexed, aliquoted into polypropylene tubes and stored at approximately −70 °C.

2.5. Extraction procedure

The extraction procedure was performed on ice and in polypropylene test tubes. The plasma samples were thawed on ice, briefly vortexed, and 20 μl placed into polypropylene tubes. A mixture of acetonitrile and methanol (80:20, v/v) containing internal standard (gatifloxacin) at 200 ng/ml was added to precipitate the proteins. The samples were vortexed for 1 min, ultrasonicated for 5 min, vortexed for a further 30 s, and centrifuged for 5 min at 16,000 rcf. The supernatant (160 μl) was transferred to clean polypropylene tubes and evaporated under nitrogen at 30 °C for 20 min.. Mobile phase (100 μl), which consisted of acetonitrile and water with 0.1% formic acid (50:50, v/v), was added to the dry samples. The samples were vortexed for 30 s, transferred to a 96 well polypropylene plate, and 5 μl were injected onto the HPLC column.

2.6. Mass spectrometry

Electrospray ionization (ESI) was performed in the positive ion mode with nitrogen as the nebulizing, turbo spray and curtain gas with the optimum values set at 50, 60 and 20 psi, respectively. The heated nebulizer temperature was set at 500 °C. The ionspray voltage was set at 4000 V. The instrument response was optimised for ofloxacin and the internal standard by infusing a solution of the compounds dissolved in mobile phase at a constant flow. The pause time was set at 5 ms, the dwell time at 150 ms, and the collision gas (N2) was set to medium (arbitrary values).

The AB Sciex API 3200 Q Trap mass spectrometer was operated at unit resolution in the multiple reaction monitoring (MRM) mode, monitoring the transition of the protonated molecular ion m/z 362.1 to the product ions at m/z 318.3 for ofloxacin, and the protonated molecular ion m/z 376.1 to the product ions m/z 332.4 for gatifloxacin. The instrument was interfaced with a computer running Applied Biosystems Analyst version 1.4.2 software.

2.7. Liquid chromatography

Chromatography was performed on a Phenomenex Luna, PFP (50 mm × 2.0 mm, 5 μm) analytical column. The mobile phase consisted of acetonitrile and water with 0.1% formic acid and was delivered with a gradient (10–70% acetonitrile over 5 min, brought back to 10% in 0.1 min, and kept at 10% acetonitrile for another 2.9 min) at a flow rate of 400 μl/min for 8 min. The analytical column was kept in a column compartment at a constant temperature of 20 °C. An Agilent 1200 series autosampler injected 5 μl onto the HPLC column. The injection needle was rinsed with mobile phase (acetonitrile and water with 0.1% formic acid (50:50, v/v)) for 10 s using the flush port wash station. The samples were cooled to 4 °C while awaiting injection. A representative raw chromatogram at the lower limit of quantification (LLOQ) for ofloxacin is presented in Fig. 2.

2.8. Method validation

2.8.1. Calibration standards and quality controls
The calibration curve for ofloxacin was validated by analysing plasma QC samples in six fold at high, medium, and low concentrations (16, 8 and 0.25 μg/ml, respectively) over a period of 3 days to determine the intra- and inter-day accuracy and precision. The QC values were interpolated from the calibration curve. The calibration curve contained 10 different concentrations spanning a concentration range of 0.078–20 μg/ml. Calibration curves were constructed using a weighted quadratic regression (1/concentration) of the peak area ratio of ofloxacin to the internal standard versus nominal concentration.

2.8.2. Recovery
Recovery was evaluated at high, medium and low concentrations (16, 8 and 0.25 μg/ml, respectively). Blank plasma was extracted and the dried samples reconstituted with mobile phase and spiked with ofloxacin to generate the reference samples (containing matrix components). The high, medium and low QC standards were used as the test samples. Recoveries were calculated by comparing the peak areas of the extracted samples with those of the reference samples.

2.8.3. Stock solution stability
Stock solutions of ofloxacin and the internal standard were prepared in a mixture of acetonitrile and water (50:50, v/v). The test stocks were left at room temperature and the reference stocks at −70 °C for 6 h. Both the ofloxacin reference and test stocks were diluted with mobile phase (spiked with either the reference or test stock of internal standard) at a mid-level concentration (5 μg/ml) and were analysed with a valid calibration curve. In addition, reference stocks stored at −70 °C for at least a year were diluted and compared with freshly prepared stocks to determine long-term stability at −70 °C.

2.8.4. Freeze and thaw stability
To ascertain freeze–thaw stability, high (16 μg/ml) and low (0.25 μg/ml) QC standards were frozen, put through three freeze (at −70 °C) and thaw (at room temperature) cycles and analysed against a valid calibration curve.

2.8.5. Benchtop stability
To establish benchtop stability, high (16 μg/ml) and low (0.25 μg/ml) QC standards were frozen at −70 °C, left on the bench

■ XIC of +MRM (4 pairs): 362.127/318.300 Da from Sample 1 (B6) of 1044.wiff (Turbo Spray)   Max. 60.0 cps.
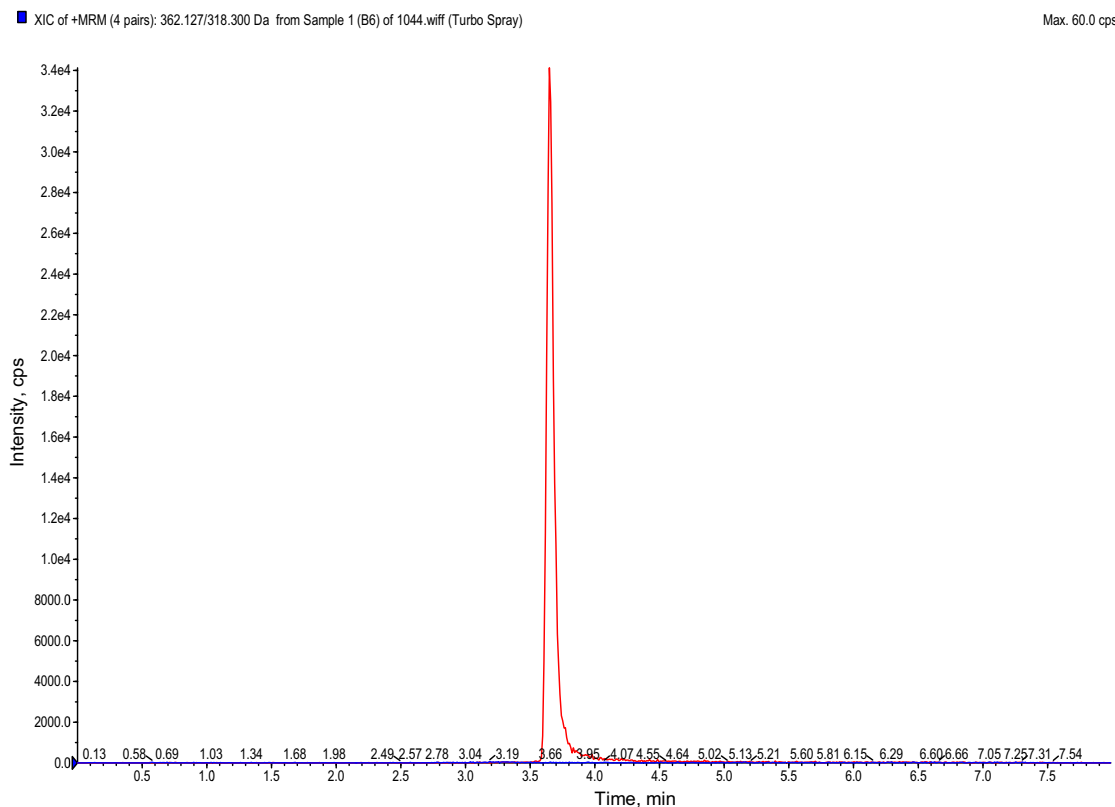
Fig. 2. Chromatogram of a blank plasma sample with internal standard.

at room temperature for 4 h, and were analysed against a valid calibration curve.

2.8.6. On-instrument stability

A 72 h on-instrument stability evaluation of ofloxacin and the internal standard was performed. Six high QCs were extracted and pooled, and analysed over four days. The samples were extracted and analysed on day 1, left on the autosampler and analysed again after 24, 48 and 72 h.

2.8.7. Matrix effects evaluation

Matrix effects were evaluated both visually and quantitatively. The publication by Matuszewski et al. was followed to evaluate the influence of co-eluting matrix components on ofloxacin and internal standard ionization [10]. Blank plasma from six different plasma sources was extracted. The dried samples were reconstituted with mobile phase and spiked with ofloxacin at a high concentration (20 μg/ml), and diluted with mobile phase for a relatively low concentration (2 μg/ml). The quantitative assessment of matrix effects was obtained by comparing the peak area ratios. Visualization of the matrix effects was achieved by post-column infusion [11]. A continuous infusion of ofloxacin and gatifloxacin was introduced by a Harvard infusion pump through a T-piece connector to the mass spectrometer while plasma samples were injected. A change in response would indicate ion suppression or enhancement.

2.8.8. Haemolysis evaluation

The effect of haemolysis on analyte quantitation was evaluated at 1% and 2% haemolysed blood present in plasma at a relatively high (16 μg/ml) and a relatively low (0.2 μg/ml) concentration. The measured concentration of the test samples were determined and compared with the measured concentration of the reference samples to calculate the overall accuracy.

2.8.9. Specificity

The high specificity of MS/MS detection prevents the detection of compounds that do not produce the specific parent ion in the Q1 scan and the specific product ion in the Q3 scan. Specificity was assessed by analysing extracts from six different plasma sources.

2.8.10. Effect of concomitant medication on the assay

Nine commonly administered anti-tuberculosis drugs, likely to be co-administered with ofloxacin, were evaluated. The drugs; linezolid, terizidone, ethionamide, cycloserine, pyrazinamide, ethambutol, rifampicin, kanamycin and capreomycin, were spiked into plasma at 250 ng/ml (test plasma). The reference plasma contained the same volume of solvent used to prepare the stock solutions of the drugs. The effect on analyte quantitation was evaluated at high, medium and low concentrations (16, 8 and 0.25 μg/ml, respectively). The peak area of ofloxacin and the internal standard of the test samples were compared with that of the reference samples to calculate the overall accuracy.

3. Results and discussion

The protein precipitation extraction method for ofloxacin performed well during validation. The calibration range was validated between 0.078 μg/ml and 20 μg/ml. A quadratic regression, with peak area ratio (drug/internal standard) against concentration with 1/concentration (1/x) weighting, was fitted to the calibration curve. The combined accuracy and precision statistics of the quality controls (N = 18; high, medium and low) were between 97.1% and 102.4%, and 2.8% and 5.2%, respectively. The percentage recovery for ofloxacin was greater than 70% (N = 3) and reproducible over three levels. According to FDA guidelines, recovery of the analyte need not be 100%, but should be consistent, precise and reproducible [12]. At a relatively low, medium and high concentration the %
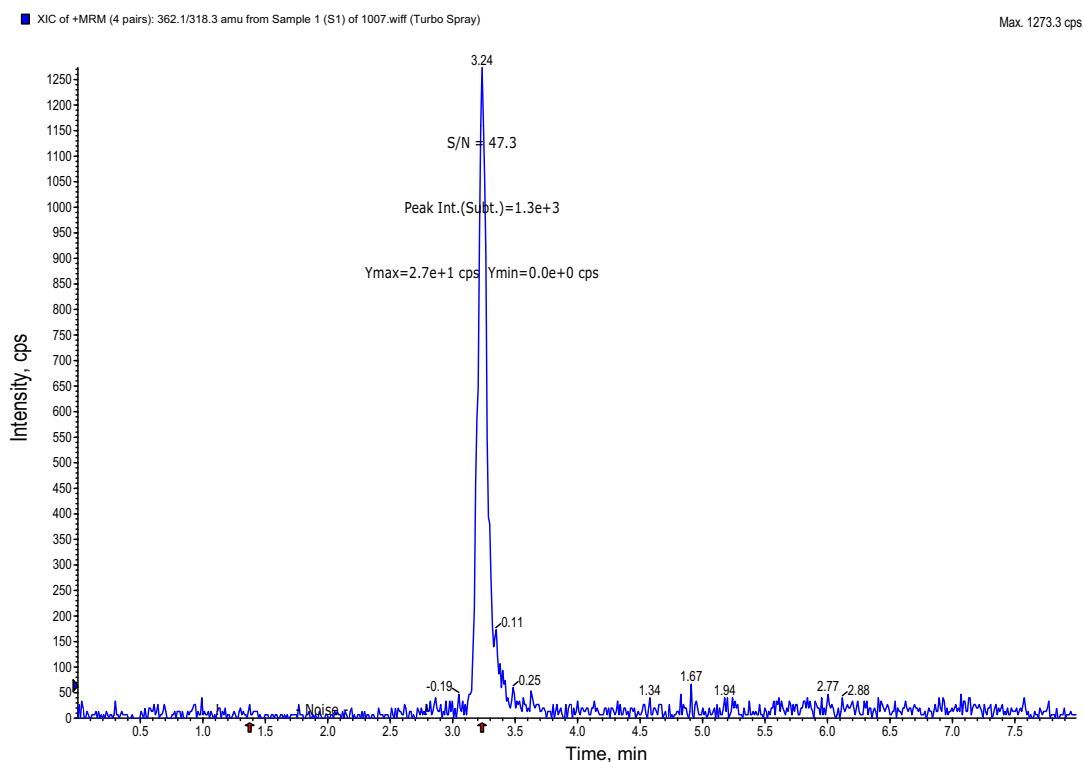
Fig. 3. Chromatogram of an ofloxacin calibration standard at LLOQ (0.078 μg/ml).

recovery was 76.5 (CV% = 3.5), 77.3 (CV% = 0.4) and 74.5 (CV% = 8.8), respectively. The CVs comply with these guidelines.

Long-term storage of the ofloxacin stock solution in a mixture of acetonitrile and water (50:50, v/v) at −70 °C for a period longer than one year was examined. The accuracy of the stored stock solution samples compared to freshly prepared samples is 106.9 (CV% = 5.0, N = 2). Ofloxacin stock solution showed acceptable stability after 6 h at room temperature. The accuracy of the stock solution test samples compared to the reference samples is 90.1% (CV% = 5.9, N = 3). However, stocks solutions were stored at −70 °C until required for standard and quality control preparation, and was spiked immediately into plasma after being thawed. Freeze–thaw stability was evaluated over three freeze–thaw cycles on consecutive days at the high and low concentrations. The observed concentrations were within 4% of the nominal concentrations, demonstrating that ofloxacin is stable through three freeze–thaw cycles. The accuracy of ofloxacin benchtop stability over 4 h is 90.8% (CV% = 10, N = 5) at 16 μg/ml and 96.6% (CV% = 2.7, N = 5) at 0.25 μg/ml, indicating that ofloxacin is stable at room temperature for up to 4 h. Lastly, sample extracts of ofloxacin and the internal standard are also stable on-instrument at 5 °C for up to 72 h. The calculated accuracies of the ratios (N = 5) were all well within 15% of the reference (ratios on day 1). After 24 h (day 2) the accuracy was 99.5%, after 48 h (day 3) it was 100.4%, and after 72 h (day 4), 101.5%.

The effect of matrix components was evaluated both quantitatively and visually at a relatively high and relatively low concentration. Quantitative assessment was performed using 6 different plasma sources. The coefficient of variation of the 6 peak areas of ofloxacin and the internal standard was 7.3% at the high level and 5.1% at the low level (Table 1). In addition, no change in response for ofloxacin or the internal standard was observed in the post-column infusion experiment. No significant matrix effects were observed for ofloxacin or the internal standard, gatifloxacin. The effect of haemolysis on analyte quantitation was evaluated at 1% and 2% haemolysed blood present in plasma. The accuracy of the haemolysed sample (N = 6) at a relatively high

Table 1
Assessment of matrix effects of 6 different matrices at a high and low concentration.

	H level (20 μg/ml)	L Level (2 μg/ml)
Mean ratio of peak areas	121	169
SD	8.81	8.69
CV%	7.3	5.1

(16 μg/ml) experiment was 96.6% (CV% = 6.2) and 96.7% (CV% = 4.6) for 1% and 2% haemolysed blood, respectively. The accuracy at the relatively low (0.2 μg/ml) experiment was 100.9% (CV% = 6.2) and 101.2 (CV% = 1.5) for 1% and 2% haemolysed blood, respectively. The presence of haemolysed blood was found to have no impact on ofloxacin quantitation. Similarly, no significant effect on analyte quantitation was observed in the presence of other drugs likely to be co-administered with ofloxacin. The accuracy of the test sample containing the nine drugs (N = 3) at a relatively high concentration (16 μg/ml) was 91.8% (CV% = 5.2), at a mid-level concentration (8 μg/ml) was 91.1% (CV% = 6.7), and at a relatively low concentration was 93.2% (CV% = 7.6).

Due to the high specificity of MS/MS detection, no interfering or late eluting peaks were found when analysing blank plasma (Fig. 2). This is confirmed with the analysis of extracts from six different plasma sources. The lower limit of quantification (LLOQ) for the method, when injecting 5 μl onto the column, is 0.078 μg/ml (Fig. 3). The signal to noise at LLOQ was well above the minimum international accepted criteria (S/N > 5). The accuracy for the LLOQ (N = 6) was 95.7% (CV% = 6.6), well within acceptable limits (accuracy within 80–120%, precision below 20%). If necessary, sensitivity of the method could be improved by raising the injection volume.

4. Application to clinical pharmacokinetics studies

The validated method performed well during sample analysis of clinical samples generated during a clinical study conducted at DP Marais Hospital, Cape Town, South Africa. The objective of the study
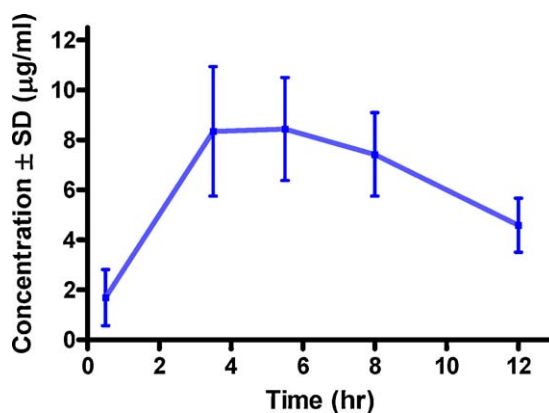
Fig. 4. Concentration vs. time profile of ofloxacin ($N = 16$).

was to characterize the population pharmacokinetics of a number of second line anti-tuberculosis drugs utilized in the treatment of MDR-TB. The assay was applied to determine the levels of ofloxacin in human plasma following oral administration of 800 mg. A representative mean concentration versus time profile (up to 12 h) of ofloxacin for this pharmacokinetic study of anti-tuberculosis therapy in patients with MDR-TB is presented in Fig. 4 (16 patients).

The precision (total-assay coefficients of variation; CV %) for ofloxacin during sample analysis were less than 8% at high (16 μg/ml), medium (8 μg/ml) and low (0.25 μg/ml) QC levels. The LLOQ was 0.078 μg/ml.

5. Conclusion

A simple protein-precipitation extraction method coupled with LC–MS/MS detection has been developed and fully validated for the determination of ofloxacin, with a quantification limit of 0.078 μg/ml. This method is specific, sensitive and reproducible and has been successfully used to quantify ofloxacin in a clinical pharmacokinetic study. A number of methods using HPLC coupled with UV or fluorescence detection [3,5–7] allow for the quantification of ofloxacin, but require plasma volumes equal to or greater than 200 μl. The LC–MS/MS method described here uses a much lower plasma volume (20 μl) and injection volume (5 μl), with good sensitivity at the LLOQ. The lower plasma volume is important for pharmacokinetic studies and therapeutic drug monitoring in children, and the low injection volume offers the possibility of enhancing sensitivity. This method can be used for pharmacokinetic studies and therapeutic drug monitoring in patients, including children, with MDR-TB.

References

[1] H. Tomioka, Prospects for the development of new antimycrobacterial drugs, J. Infect. Chemother. 6 (2000) 8–20.
[2] S.M. Hwang, D.D. Kim, S.J. Chung, C.K. Shim, Delivery of ofloxacin to the lung and alveolar macrophages via hyaluronan microspheres for the treatment of tuberculosis, J. Control. Release 129 (2008) 100–106.
[3] J. Macek, E. Ptáček, Determination of Ofloxacin in human plasma using high-performance liquid chromatography and fluorescence detection, J. Chromatogr. B: Biomed. Sci. Appl. 673 (1995) 316–319.
[4] D.C. Hooper, J.S. Wolfson, Fluoroquinolone antimicrobial agents, Clin. Microbiol. Rev. 2 (1989) 378–424.
[5] C. Wongsinsup, W. Taesotikul, S. Kaewvichit, S. Sangsrijan, S. Sangsrijan, Simple extraction and determination of ofloxacin in human plasma by high-performance liquid chromatography with fluorescence detector, CMU Nat. Sci. 8 (2009) 165–174.
[6] M. Amini, Kh. Abdi, M. Darabi, A. Shafiee, Determination of ofloxacin in plasma by HPLC with UV detection, J. Appl. Sci. 5 (2005) 1655–1657.
[7] D.K. Xu, A.Z. Ding, Y.S. Yuan, Y. Diao, Determination of ofloxacin in human plasma and studies of its pharmacokinetics using HPLC method, Yao Xue Xue Bao 27 (1992) 462–466.
[8] R. Kauffman, G. Kearns, Pharmacokinetic studies in pediatric patients, clinical and ethical considerations, Clin. Pharmacokinet. 23 (1992) 10–29.
[9] J.L. Veuthey, S. Souverain, S. Rudaz, Column-switching procedures for the fast analysis of drugs in biologic samples, Ther. Drug Monit. 26 (2004) 161–166.
[10] B.K. Matuszewski, M.L. Constanzer, C.M. Chavez-Eng, Strategies for the assessment of matrix effect in quantitative bioanalytical methods based on HPLC–MS/MS, Anal. Chem. 75 (2003) 3019–3030.
[11] R. Bonfiglio, R.C. King, T.V. Olah, K. Merkle, The effects of sample preparation methods on the variability of the electrospray ionization response for model drug compounds, Rapid Commun. Mass Spectrom. 13 (1999) 1175–1185.
[12] Guidance for Industry Bioanalytical Method Validation, Department of Health and Human Services, Food and Drug Administration, Rockville, USA, 2001.

Chemical profiling of the cytotoxic triterpenoid-concentrating fraction and characterization of ergostane stereo-isomer ingredients from *Antrodia camphorata*

Ying-Chi Du[a,1], Tung-Ying Wu[a,1], Fang-Rong Chang[a,b,c,d], Wan-Yu Lin[a], Yu-Ming Hsu[a], Fu-Ting Cheng[a], Chi-Yu Lu[e], Ming-Hong Yen[a], Ya-Ting Tsui[a], Hsuan-Lun Chen[a], Ming-Feng Hou[c], Mei-Chin Lu[a,f,g,*], Yang-Chang Wu[a,h,i,**]

[a] *Graduate Institute of Natural Products, College of Pharmacy, Kaohsiung Medical University, Kaohsiung 807, Taiwan*
[b] *Research and Development Center of Chinese Herbal Medicines and New Drugs, College of Pharmacy, Kaohsiung Medical University, Kaohsiung 807, Taiwan*
[c] *Cancer Center, Kaohsiung Medical University Hospital, Kaohsiung 807, Taiwan*
[d] *Department of Marine Biotechnology and Resources, National Sun Yat-sen University, Kaohsiung 804, Taiwan*
[e] *Department of Biochemistry, College of Medicine, Kaohsiung Medical University, Kaohsiung 807, Taiwan*
[f] *Graduate Institute of Marine Biotechnology, National Dong Hwa University, Pingtung 944, Taiwan*
[g] *National Museum of Marine Biology & Aquarium, Pingtung 944, Taiwan*
[h] *Graduate Institute of Integrated Medicine, College of Chinese Medicine, China Medical University, Taichung 404, Taiwan*
[i] *Natural Medicinal Products Research Center, and Center for Molecular Medicine, China Medical University Hospital, Taichung 404, Taiwan*

ARTICLE INFO

ABSTRACT

Antrodia camphorata (AC), also known as *Antrodia cinnamomea*, an endemic species in Taiwan, is one of the treasured medicinal mushrooms. AC is traditionally used for its chemopreventive biofunctions. In this investigation, we report a convenient method for concentrating the antiproliferative active triterpenoid-rich fraction (FEA), from ethanolic extract of AC (EEAC). A series of stereo-isomers of zhankuic acids (**1**–**8**) from the FEA was purified by HPLC using an efficient acidic solvent system. The structures of compounds **1**–**8** were elucidated based on spectroscopic data analysis, and the absolute configuration of α-chiral carboxylic acid at C-25 in the structures was assigned based on reaction with (*R*)- and (*S*)-1-(9-anthryl)-2,2,2-trifluoroethanol. Major ingredients of FEA (eight ergostanes **1**–**8** and two lanostanes **9**–**10**) were further characterised by high-performance liquid chromatography-photodiode array detection/mass spectrometry (HPLC-PDA/MS). Compounds **1**–**8** and their pair mixture forms (antcin K, antcin C, zhankuic acid C, and zhankuic acid A) were subjected to anti-proliferative assay against three human leukemia cell lines. Among them, the derivatives with carbonyl group at C-3 showed cytotoxicity with IC$_{50}$ values ranging from 16.44 to 77.04 μg/ml.

1. Introduction

Antrodia camphorata (AC, also known as *Antrodia cinnamomea*), by name Chang-Chih, is an endemic fungus in Taiwan. Hundreds years before, the Taiwanese aborigines found that the wild AC had a special effect to relief hangover syndrome. It was also used in folk medicine for the treatment of food and drug detoxication, diarrhea, abdominal pain, hypertension, skin itching, and cancer [1,2]. Because of the potential pharmaceutical value of its biologically active ingredients, the fruiting bodies of AC are regarded as one of the health treasure troves of Taiwan [3]. Due to scarcity in nature and the difficulty in its artificial cultivation, the average price of AC is higher than the Truffle (*Tuber magnatum*), which is considered as one of the most expensive mushrooms worldwide. Several research groups have studied the phytochemical constituents of AC fruiting bodies and their pharmacological activities [4]. However, few studies have focused on analyzing the active components of AC fruiting bodies and their pharmacological mechanism of action [5–8].

In our previous study, we reported that the ethanolic extract from wild fruiting bodies of *A. camphorata* (EEAC) could induce HL 60 cell apoptosis via histone hypoacetylation, up-regulation of histone deacetyltransferase 1, and down-regulation of histone

* Corresponding author at: Graduate Institute of Marine Biotechnology, National Dong Hwa University, Pingtung 944, Taiwan. Tel.: +886 8 8825038; fax: +886 8 8825087.
** Corresponding author at: Graduate Institute of Integrated Medicine, College of Chinese Medicine, China Medical University, Taichung 404, Taiwan. Tel.: +886 4 22057153; fax: +886 4 22060248.
E-mail addresses: jinx6609@yahoo.com.tw (M.-C. Lu), yachwu@mail.cmu.edu.tw (Y.-C. Wu).
[1] These authors contributed equally to this study.

acetyltransferase activities [9]. Moreover, after fractionation of EEAC and cytotoxicity evaluation of different fractions, we found that the ethyl acetate fraction (FEA), which showed characteristic ^{1}H NMR signals of triterpenoids, was the cytotoxic active fraction of EEAC. In this bio-guided fractionation procedure, the cytotoxic components of EEAC can be attributed to FEA. The aforementioned results encouraged us to carry out further chemical and cytotoxic analyses targeting the active fraction, FEA. In the current study, the chemical profile of FEA active components (the triterpenoid-rich fraction from *A. camphorata*) was illustrated by isolation, purification, and structural elucidation of the major ergostane and lanostane derivatives by NMR and HPLC-PDA/MS.

Chiral centers present in the skeleton of bioactive botanical secondary metabolites, which are generated by specific enzyme systems in biosynthesis, are always an important issues in drug discovery. The dramatic effect of chirality on the activity and/or toxicity of any therapeutic entity was always explored and monitored. Zhankuic acids, the most abundant triterpenoid of AC, were reported to be present in a mixture of a stereo-isomeric pairs with a chiral center at C-25 [10]. So far, only zhankuic acid A was successfully separated into two isolated peaks using capillary electrophoresis [11], however other zhankuic acids, such as antcin K, antcin C, zhankuic acid C, zhankuic acid A, etc., have never been obtained in a pure form utilizing the isolation procedures embedded by previous studies [4]. Separating chiral components of isomeric mixture is crucial for understanding the mechanism of action of each isomer and the adverse effect of the undesired isomer on human body [12,13]. The lack of studies on separating pure isomers of ergostane triterpenes from AC was the driving force to investigate the possibility of developing an efficient method for their separation. In this current study, purification and structural elucidation for a series of pure stereo-isomers of ergostane triterpenes (**1**–**8**) are described herein, and their chemical profiling and cytotoxic activities were also investigated.

2. Materials and methods

2.1. General experimental procedures

Melting points were determined using a Fisher-Johns melting point apparatus (Thermo Fisher Scientific Inc., Rockford, USA), and the values presented are uncorrected. Optical rotations were measured with a JASCO DIP-370 digital polarimeter (JASCO Inc., Tokyo, Japan). UV spectra were obtained on a JASCO V-530 UV-Vis spectrophotometer (JASCO Inc., Tokyo, Japan). The IR spectra were measured on a Mattson Genesis II spectrometer (Thermo Fisher Scientific Inc., Rockford, USA). ^{1}H and ^{13}C NMR spectra were recorded on VNMRS-600 (Varian Inc., Palo Alto, USA), Varian Unity plus-400 (Varian Inc., Palo Alto, USA) and Gemini 2000-200 (Varian Inc., Palo Alto, USA) NMR spectrometers. Chemical shifts were reported in parts per million (δ), and coupling constants (J) were expressed in Hertz. LRESIMS were measured on a VG Biotech Quattro 5022 mass spectrometer (VG Biotech, Altrincham, England). Silica gel 60 (230–400 mesh) (Merck KGaA, Darmstadt, Germany) and Sephadex LH-20 (Sigma–Aldrich Corp., St. Louis, USA) were used for column chromatography. TLC analysis was carried out on silica gel GF$_{254}$ pre-coated plates (Merck KGaA, Darmstadt, Germany) and compounds were visualized using 50% H_2SO_4, followed by heating on a hot plate. HPLC isolation was performed with a Hitachi L-7100 series HPLC (Hitachi Inc., Tokyo, Japan), equipped with a Bischoff RI detector and a Shimadzu LC-10AT series HPLC (Shimadzu Inc., Tokyo, Japan) with a SPD-10A UV-Vis detector or photodiode array detector. The Hypersil ODS (250 mm × 10 mm I.D., 5 μm) (Thermo Fisher Scientific Inc., Rockford, USA) and Cosmosil 5C-18-MS-II (250 mm × 10 mm I.D., 5 μm) (Nacalai Tesque, Kyoto, Japan) columns were utilized for HPLC separation.

2.2. Preparation of the ethanol extracts from wild fruiting bodies (EEAC)

The ethanolic extract of AC wild fruiting bodies (EEAC) was prepared as reported previously [9]. In brief, the mushroom was refluxed with ethanol at 75 °C in a 1:10 (w/v) ratio for 2 h. The extract was cooled and allowed to precipitate at 4 °C overnight. The extract supernatant was further filtered to remove any precipitate, and then the filtrate was lyophilised and stored at −70 °C before use.

2.3. Fractionation of the ethanolic extract from wild fruiting bodies (EEAC)

We utilized four different methods for the efficient fractionation of AC wild fruiting bodies ethanolic extract (Fig. S1). In Type 1, EEAC (11.0 g) was extracted with *n*-hexane to obtain the *n*-hexane fraction (FNH, 1.4 g) and the first residue. The first residue was further extracted with EtOAc to obtain the ethyl acetate fraction (FEA, 6.8 g) and the second residue. The second residue was further extracted with EtOH to obtain the ethanol fraction (FET, 1.1 g) and the third residue (0.6 g). In Type 2, EEAC (101.9 mg) was fractionised by liquid–liquid partition between EtOAc and H_2O to obtain the ethyl acetate fraction (FEA-EEAC, 79.6 mg) and the water fraction (FW1-EEAC, 20.0 mg). In Type 3, EEAC (100.3 mg) was fractionised by liquid–liquid partition between $CHCl_3$ and H_2O to yield chloroform (FCl3-EEAC, 77.6 mg) and water (FW2-EEAC, 23.6 mg) fractions. In Type 4, EEAC (100.9 mg) was fractionised by liquid–liquid partition between CH_2Cl_2 and H_2O to obtain the dichloromethane fraction (FCl2-EEAC, 76.9 mg) and the water fraction (FW3-EEAC, 23.5 mg).

2.4. Isolation of major components from the ethyl acetate fraction (FEA) utilizing Type 1 process

FEA (6.8 g) was separated by silica gel column (5 cm × 20 cm) chromatography using gradient mixtures of *n*-hexane–EtOAc–MeOH (10:1:0, 5:1:0, 1:1:0, 0:1:0, 0:40:1, 0:30:1, 0:20:1 and 0:10:1, respectively) as eluents. According to TLC results, seventeen fractions were obtained. The fourth fraction (fraction 4, 588.4 mg) was chromatographed on Sephadex LH-20 (3.5 cm × 50 cm) using EtOAc–CH_2Cl_2–MeOH (1:1:6) as the eluent, yielding three fractions. Fraction 4-1 (568.6 mg) was further chromatographed on silica gel column (3 cm × 20 cm) using $CHCl_3$–MeOH (35:1) as eluent to yield three fractions. Fifty milligrams from fraction 4-1-2 (240.3 mg) were purified with reverse-phase HPLC (RI detector; Hypersil ODS, 250 mm × 10 mm; MeOH–H_2O, 90:10) to offer dehydroeburicoic acid (**10**) (10.3 mg; flow rate: 2 ml/min; R_t 26.9 min). The sixth fraction (fraction 6, 970.9 mg) was chromatographed with EtOAc–CH_2Cl_2–MeOH (1:1:6) on Sephadex LH-20 (3.5 cm × 50 cm) to render three fractions. Fraction 6-2 (901.0 mg) was separated by silica gel column (3.5 cm × 15 cm) with $CHCl_3$–MeOH (40:1) as eluent and further purified with reverse-phase HPLC (RI detector; Hypersil ODS, 250 mm × 10 mm; ACN–H_2O, 75:25) to obtain a mixture of zhankuic acid A epimers (77.5 mg; flow rate: 2 ml/min; R_t 12.4 min). The tenth fraction (fraction 10, 132.6 mg) was chromatographed using preparative TLC with CH_2Cl_2–MeOH (15:1) to afford five fractions. Fraction 10-2 (85.0 mg) was further purified with reverse-phase HPLC (RI detector; Hypersil ODS, 250 mm × 10 mm; ACN–H_2O, 70:30) to provide a mixture of antcin C epimers (40.9 mg; flow rate: 2 ml/min; R_t 10.8 min). The thirteenth fraction (fraction 13, 1.4 g) was divided on silica gel column (3.5 cm × 20 cm) with CH_2Cl_2–MeOH (15:1) to yield

seven fractions. Fraction 13-2 (307.3 mg) was chromatographed by preparative TLC which is eluted twice with CH_2Cl_2–MeOH (15:1) to yield five fractions. Fraction 13-2-2 (40.2 mg) was separated with reverse-phase HPLC (RI detector; Hypersil ODS, 250 mm × 10 mm; ACN–H_2O, 60:40) furnishing the isolation of dehydrosulphurenic acid (**9**) (7.0 mg; flow rate: 2 ml/min; R_t 22.1 min). Fraction 13-5 (107.5 mg) was purified using reverse-phase HPLC (RI detector; Hypersil ODS, 250 mm × 10 mm; ACN–H_2O, 70:30) yielding a mixture of zhankuic acid C epimers (26.0 mg; flow rate: 2 ml/min; R_t 10.6 min). The fifteenth fraction (fraction 15, 245.7 mg) was separated into four fractions using reverse-phase solid phase extraction column (Discovery DSC-18, 10 g) with a gradient solvent mixture of H_2O–MeOH (100:0, 70:30, 50:50, 0:100) obtaining four fractions. Fraction 15-2 (126.0 mg) was further chromatographed using reverse-phase HPLC (254 nm; Hypersil ODS, 250 mm × 10 mm; ACN–H_2O: 35:65 at 0 min, 45:55 at 20 min, 100:0 at 25 min) to obtain a mixture of antcin K epimers (10.3 mg; flow rate: 3 ml/min; R_t 14.2 min).

2.5. Purification of ergostane stereo-isomeric pairs

We developed a highly efficient reverse phase HPLC system to separate the major ergostane stereo-isomeric pairs. Antcin K was chromatographed with HPLC (254 nm; Hypersil ODS, 250 mm × 10 mm; ACN–H_2O: 35:65 at 0 min, 45:55 at 20 min, 100:0 at 25 min) to yield compounds **1** (flow rate: 4.7 ml/min; R_t 13.4 min) and **2** (flow rate: 4.7 ml/min; R_t 14.0 min), respectively. The separation of other ergostane stereo-isomeric pairs was achieved utilizing acidic mobile phase. In this mobile phase system, solvent A was acetonitrile and solvent B was water containing 0.05% acetic acid. Antcin C was divided using HPLC system (254 nm; Cosmosil 5C-18-MS-II, 250 mm × 10 mm; solvent A–B, 50:50) to offer compounds **3** (flow rate: 3 ml/min; R_t 26.8 min) and **4** (flow rate: 3 ml/min; R_t 29.3 min), respectively. Zhankuic acid C was separated with HPLC system (254 nm; Cosmosil 5C-18-MS-II, 250 mm × 10 mm; solvent A–B, 50:50) to yield compounds **5** (flow rate: 3 ml/min; R_t 31.1 min) and **6** (flow rate: 3 ml/min; R_t 32.7 min), respectively. Zhankuic acid A was chromatographed by HPLC system (254 nm; Cosmosil 5C-18-MS-II, 250 mm × 10 mm; solvent A–B, 50:50) to offer compounds **7** (flow rate: 3 ml/min; R_t 41.9 min) and **8** (flow rate: 3 ml/min; R_t 43.3 min), respectively.

2.6. Synthesis of (R)- and (S)-1-(9-anthryl)-2,2,2-trifluoroethanonyl [(R)- and (S)-AT] esters of compounds **2**–**8**

The isolated compounds reacted with (R)- and (S)-1-(9-anthryl)-2,2,2-trifluoroethanonyl yielding chiral ester, and the absolute configuration of the isolated compounds was achieved through determining the configuration of the formed ester. The isolated quantity of compound **1** was insufficient for chemical modification and its configuration was achieved by comparing it with the configuration of its isomeric pair (compound **2**). The synthesis of chiral esters of the isolated compounds was done utilizing the same method and preparation of compound **7** chiral ester is presented here as an example (for the full synthetic procedures of other isolated compounds please see Supplementary data).

(R)-AT-ester of **7** was prepared as follows. Compound **7** (6.42 mg, 0.014 mmol) and (1R)-1-(9-anthryl)-2,2,2-trifluoroethanol (Sigma–Aldrich Corp., St. Louis, USA) (3.53 mg, 0.014 mmol) were dissolved in tetrahydrofuran (THF) (Sigma–Aldrich Corp., St. Louis, USA) and than were added to a solution of 1-ethyl-3-(3-dimethylaminopropyl)carbodiimide (EDCI) (TCI, Portland, USA) (7.61 mg, 0.042 mmol), triethylamine (Et$_3$N) (Sigma–Aldrich Corp., St. Louis, USA) (3.69 μl, 0.028 mmol) and 4-(dimethylamino)pyridine (DMAP) (Sigma–Aldrich Corp., St. Louis,

USA) (2.43 mg, 0.021 mmol) in CH_2Cl_2. The mixture was stirred at room temperature for 12 h. The reaction mixture was concentrated under reduced pressure and then partitioned with CH_2Cl_2 and H_2O. The organic layer was then evaporated, and the residue was purified using preparative TLC (CH_2Cl_2) to yield (R)-AT-ester of **7** (3.43 mg, 33.75% yield). (S)-AT-ester of **7** was prepared as follows. The procedure was similar to that described for (R)-AT-ester of **7**. Starting from compound **7** (11.15 mg, 0.024 mmol), (1S)-1-(9-anthryl)-2,2,2-trifluoroethanol (Sigma–Aldrich Corp., St. Louis, USA) (6.57 mg, 0.024 mmol), EDCI (13.68 mg, 0.024 mmol), Et$_3$N (6.63 μl, 0.072 mmol), and DMAP (4.36 mg, 0.036 mmol), (S)-AT-ester of **7** (9.01 mg, 51.71% yield) was obtained.

2.7. HPLC analysis method for FEA

Sample analysis was carried out on a LC-10A VP HPLC system (Shimadzu Inc., Tokyo, Japan) consisting of a quaternary pump (LC-10AT), an on-line degasser (DGU-14A), an autosampler (SIL-10AD), a photodiode-array detector (SPD-M10A) and Class VP for data collection. Liquid chromatography was performed using a Cosmosil 5C-18-MS-II column (5 μm, 250 mm × 4.6 mm I.D.) supplied by Nacalai Tesque Inc., Kyoto, Japan. The sample injection volume was 20 μl. The mobile phase was a mixture of acetonitrile (ACN, A) and water (B) containing 0.1% (v/v) acetic acid. A gradient program was used as follows: the initial elution condition was A–B (45:55, v/v), linearly changed to A–B (50:50, v/v) at 30 min, A–B (55:45, v/v) at 35 min, A–B (60:40, v/v) at 45 min, A–B (70:30, v/v) from 45 min to 55 min, A–B (85:15, v/v) at 60 min. Over the next 40 min, the percentage of mobile phase A increased linearly to 100%. The mobile phase was filtered through a 0.22 μm Millipore filter and degassed before use. The flow rate was set at 1.0 ml/min, the column temperature was maintained at room temperature, and detection wavelengths were set at 254 nm and 270 nm. Ethyl acetate fraction (FEA) was obtained from EEAC using a Type 1 fractionation method. From the FEA dry extract, 1 mg was dissolved in 1 ml of methanol and filtered through a 0.45 μm membrane filter prior to loading into the HPLC column. HPLC samples of compounds **1**–**8** pure isolated isomers were prepared in a similar way.

2.8. LC–ESIMS method for FEA

The instrumentation and chromatographic conditions of HPLC for LC–MS were the same as the described in Section 2.7, except the injection volume was set at 10 μl. Identification of FEA was carried out using a Thermo Finnigan LC–MS system (Thermo Finnigan, San Jose, USA) consisting of a Spectra System P 4000 pump, a Spectra System AS 3000 autosampler with injection volume set to 10 μl and a Surveyor MSQ quadrupole mass spectrometer equipped with an electrospray ionization LC–MS interface (ESI). The LC effluent was introduced into the ESI source using a post-column splitting ratio of 2:1. Ultra high-purity nitrogen (N_2) was used as the nebulising gas. ESI was applied in the positive and negative ionization modes and the capillary was held at a potential of 3.0 kV. The cone voltage was set at 40 V and the ionization source was set to a temperature of 550 °C. We used dwell times of 1 s. For each analysis in the full scan mode, mass range was set at m/z 100–1000, enabling the identification purposes.

2.9. Cytotoxicity assays

Human acute lymphoblastic leukemia cells (CCRF-CEM and Molt 4) and human promyelocytic leukemia cells (HL 60) were obtained from the American Type Culture Collection. All cell lines were cultured on RPMI-1640 medium supplemented with 10% (v/v) FBS (fetal bovine serum), 100 U/ml penicillin and 100 μg/ml

streptomycin at 37 °C in a humidified atmosphere of 5% CO_2 and 95% air. Cell viability was measured by MTT (3-(4,5-dimethylthiazol-2-yl)-2,5-diphenyltetrazolium bromide) colorimetric method [9]. In brief, freshly trypsinized cell suspensions were seeded in 96-well microtiter plates at densities of 5000–10,000 cells per well and the test compounds were added from DMSO stock solutions (the final concentration of DMSO in culture medium was 0.2%). After 3 days in culture, the attached cells were incubated with MTT (0.5 µg/ml, 4 h) and subsequently solubilized in DMSO. The absorbance was measured at 550 nm using a microplate reader. The calculated IC_{50} was the concentration of the tested agent that reduced cell growth by 50% under the experimental conditions. The results represented the mean of three separate experiments, each performed in triplicate.

3. Results and discussion

3.1. Anti-proliferative effect of AC fractions obtained using a variety of sample preparation methods

Several preparation methods have been developed over the past few years by different research groups for offering AC extracts. We summarised the extraction and partition methods published in the previous papers [1,2,10,14–17]. It was stated in publications that these extraction methods were designed to yield the maximum possible amount of extracts for use in future applications. Developing a high yield process is especially desirable because of the high price of the raw materials (wild fruiting bodies of AC) [3]. In the current study we confirmed the reproducibility of our reported fractionation method to obtain FEA active fraction [9]. According to our previous preparation method, EEAC was sequentially extracted with *n*-hexane, ethyl acetate, and ethanol to obtain three different fractions, FNH, FEA, and FET (Type 1). Other partition methods reported by other research groups can be divided into three methods, labelled here as Types 2–4 (see Fig. S1; Section 2.3) [2,10,14,15]. In Type 2, EEAC was partitioned between EtOAc and H_2O according to the method published by Chen et al. and Hsu et al. [10,15], yielding both an ethyl acetate fraction (FEA-EEAC) and a water fraction (FW1-EEAC). In Type 3, EEAC was partitioned between $CHCl_3$ and H_2O, according to the report by Cherng et al. [14], to yield chloroform (FCl3-EEAC) and water (FW2-EEAC) fractions. In Type 4, CH_2Cl_2 (FCl2-EEAC) and H_2O (FW3-EEAC) fractions were obtained by liquid–liquid partition from EEAC according to method published by Shen et al. [2].

All fractions and EEAC were subjected to a cytotoxic assay against HL 60 cell line (Fig. S1). In all cases, the results showed that organic fractions with lower polarity (FNH, FEA, FEA-EEAC, FCl3-EEAC, and FCl2-EEAC) were active, whereas the highly polar fractions (FET, FW1-EEAC, FW2-EEAC, and FW3-EEAC) were inactive. In Type 1, FEA exhibited the best activity and demonstrated good repeatability for concentrating the cytotoxic components from EEAC. Interestingly the antiproliferative activity of the ethyl acetate active fraction (FEA) prepared by food science acceptable fraction method (Type 1) was more potent (104.10 µg/ml) than FEA-EEAC (156.47 µg/ml) prepared by Type 2. Although the anti-proliferative activity of fractions (FCl3-EEAC and FCl2-EEAC) was comparable to FEA, the use of chlorine-containing organic solvents, such as CH_2Cl_2 and $CHCl_3$, limits their application in pharmaceutical related products. Based on these findings, the previously established methods were not ideal preparation procedures [2,14,16]. Encouraged by the high antiproliferative activity of FEA and its benign fractionation procedures, we decided to shed light on the chemical composition and the pharmacological activity of FEA.

3.2. Chemical profile of FEA major components

HPLC analyses were applied to trace the complexity of the chemical profile of FEA and provided the guidance for further chemical isolation (Figs. S2 and S3). Based on our experience, the separation of FEA components using normal phase chromatography or reverse phase HPLC with $MeOH:H_2O$ solvent system was not ideal. After testing several mobile phase systems with reverse phase HPLC, we found that the using gradient mobile phase of acetonitrile with acidic water (0.1% acetic acid in water) served to separate FEA constituents. The HPLC traces at 254 nm revealed the presence of ten major peaks, labelled numerically (Fig. S3). Upon shifting to a longer UV wave length (270 nm), peaks 9 and 10 did not appear (Fig. S3), suggesting a different conjugation pattern from peaks 1 to 8. Moreover, we observed that the retention times for peak pairs 1 and 2, 3 and 4, 5 and 6, as well as 7 and 8 are very close and single peak of each pair cannot be entirely separated using different chromatographic designs. This phenomenon suggests that each peak pair represents an isomeric-pair of compounds.

Triterpenoids and steroids from natural sources displayed no or weak UV absorption; however, ergostane and lanostane triterpenes from AC exhibited a UV absorption maxima within the range from 230 to 270 nm, due to the conjugated functionalities in their skeleton at C-7, C-8, C-9, and C-11 [1,16]. The major constituents of AC triterpenoid are zhankuic acids derivatives having chiral center at C-25. Zhankuic acids were isolated previously as a mixture of stereo-isomeric pairs [10]. According to literature findings and FEA HPLC fingerprint, it suggested that peaks 1–8 should be four pairs of zhankuic acid derivatives. In order to identify the components of FEA by HPLC, we attempted to isolate the compounds that corresponded to the major HPLC peaks (Figs. S2 and S3). The FEA was separated by normal phase fresh column chromatography using gradient mixtures of *n*-hexane–EtOAc–MeOH as eluents. According to the TLC results, seventeen fractions were obtained. The collected seventeen fractions were analyzed by analytical scale HPLC and the fractions containing constituents in the same polarity region corresponding to peaks 1–10 of FEA were further chromatographed (Fig. S3). Fraction 4, which was enriched with peak 10, was separated by Sephadex LH-20, silica gel columns and further purified by RP-HPLC, yielding compound **10**. After comparing its physical and spectroscopic data to those reported in literatures, compound **10** was identified as dehydroeburicoic acid [2]. Zhankuic acid A isomeric pair [10] was obtained by separation from fraction 6, enriched with peaks 7 and 8. The other three zhankuic acid derivatives, antcin C [10], zhankuic acid C [14], and antcin K [2] were obtained from fractions 10, 13, and 15, respectively, using similar methods. Dehydrosulphurenic acid (**9**) [2,16], corresponding to peak 9, was obtained from fraction 13 together with zhankuic acid C and then further purified with column chromatography.

In previous isolation processes [10,14,16,17], these ergostane and lanostane triterpenes were reported to be purified with a normal phase open column and/or preparative TLC. Based on our experience testing previously reported isolation methods, these methods could not lead to the isolation of pure isomers. For example, zhankuic acid A, one of the major ergostane constituents, showed only one spot on normal phase TLC, nevertheless, other impurities can be observed in reverse phase TLC and HPLC (Fig. S4). Similar findings were observed in the isolation of dehydroeburicoic acid, belonging to lanostane triterpenes (Fig. S5). To overcome these difficulties we used our developed reverse phase HPLC with acetonitrile–0.05% acetic acid in H_2O to separate the closely related isomeric pairs of steroidal AC triterpenes.

Identification of the ten peaks was achieved by comparing their retention time and ultraviolet absorption with isolated compounds (Fig. 1). The areas of these labelled peaks accounted for 78.57% and 85.07% of the total area of all the peaks at 254 nm and 270 nm,
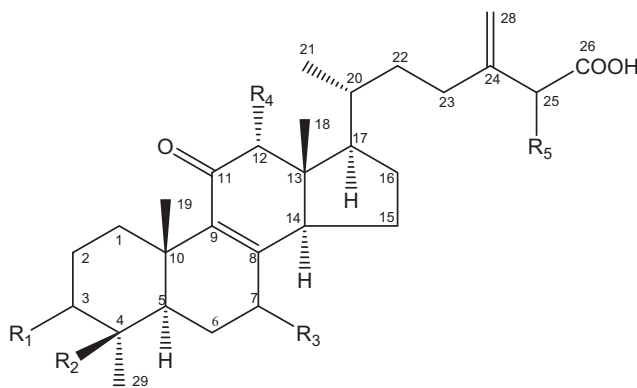
	R$_1$	R$_2$	R$_3$	R$_4$	R$_5$	peak no.	separation from
1	β-OH	OH	α-OH	H	α-CH$_3$	1	antcin K
2	β-OH	OH	α-OH	H	β-CH$_3$	2	
3	=O	H	α-OH	H	α-CH$_3$	3	antcin C
4	=O	H	α-OH	H	β-CH$_3$	4	
5	β-OH	H	=O	OH	β-CH$_3$	5	zhankuic acid C
6	β-OH	H	=O	OH	α-CH$_3$	6	
7	=O	H	=O	H	α-CH$_3$	7	zhankuic acid A
8	=O	H	=O	H	β-CH$_3$	8	

	R	peak no.
9	OH	9
10	H	10

Fig. 1. Chemical structures of compounds **1**–**10**.

respectively (Fig. S3). Under our HPLC optimized conditions (Fig. 2A and B), a series of peak pairs corresponded to zhankuic acid isomeric pairs were observed in the obtained chromatograms. Peak intensities of 1 and 2 (antcin K) as well as peaks 3 and 4 (antcin C) decreased at 270 nm due to less conjugation compared to peaks 5 and 6 (zhankuic acid C) as well as peaks 7 and 8 (zhankuic acid A). Peaks 9 and 10 were identified as dehydrosulphurenic acid (**9**) and dehydroeburicoic acid (**10**), respectively, which posses a single conjugated system in the lanostane skeleton showing no UV absorption at 270 nm. Comparing peak areas and heights of FEA respective constituents at 254 and 270 nm, indicated that FEA is mainly composed of the following major triterpenoids, antcin K, antcin C, zhankuic acid C, dehydrosulphurenic acid, zhankuic acid A, and dehydroeburicoic acid. Among the major triterpenoids, zhankuic acid A,

corresponding to peaks 7 and 8, accounted the majority of peaks area and height.

3.3. Purification and structure elucidation of ergostane stereo-isomeric pairs

Analysing the separated peaks by NMR, pointed out that our developed HPLC system was able to separate zhankuic acids stereo-isomeric pairs for the first time. Purification and structural elucidation of zhankuic acid A isomeric pair, the major component in FEA, are illustrated here as an example. The recycle chromatography system in the reverse phase HPLC (254 nm; Hypersil ODS, 250 mm × 10 mm; ACN–H$_2$O, 55:45; flow rate: 4.3 ml/min) was used for purifying zhankuic acid A stereo-isomeric pair. Through
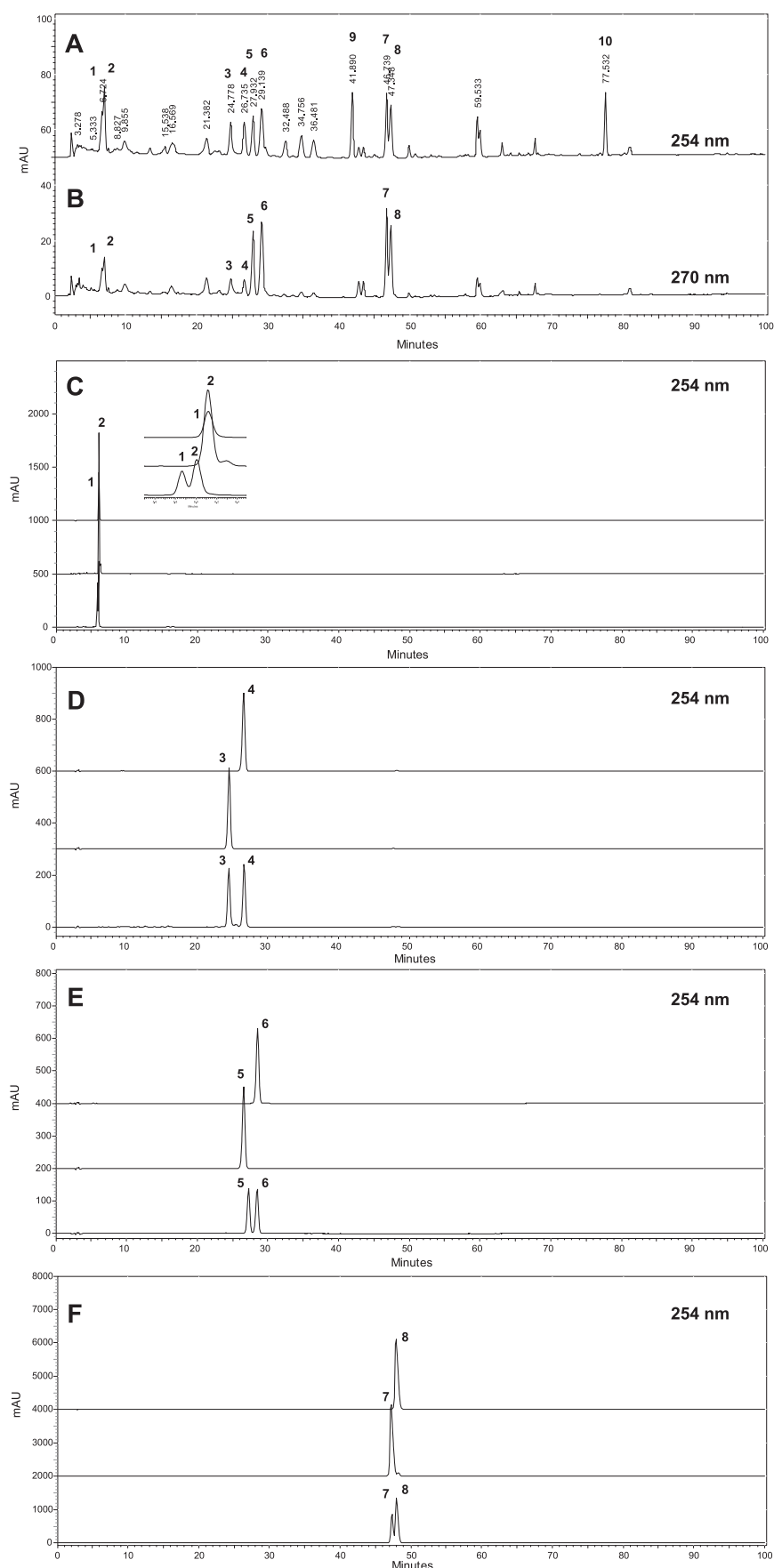
Fig. 2. HPLC chromatogram of the ethyl acetate fraction obtained using Type 1 process (FEA). Isolated compounds **1**–**8** are shown for comparison.

eight successive recycles, compounds **7** and **8** were separated and collected at the retention time of 416.2 and 446.5 min (Fig. S6). After several trials, we were able to separate compound **7** (R_t 41.9 min) and **8** (R_t 43.3 min) utilizing our developed HPLC system (254 nm; Cosmosil 5C-18-MS-II, 250 mm × 10 mm; 1:1 ACN:0.05% acetic acid in H_2O, flow rate: 3.0 ml/min) (see Fig. S7; Section 2.5). By comparing to the original recycle chromatography method, the application of the acidic solvent system decreased the retention time of the separated compounds ten folds. The other ergostane stereo-isomeric pairs were purified using similar HPLC system with slight modification of the mobile phase composition. Also antcin K, antcin C, and zhankuic acid C isomeric pairs were separated yielding compounds **1**–**6**, respectively (Figs. 1 and 2C–F).

The stereoconfiguration of the isolated compounds was determined based on NMR analysis and chemical modification through reacting the isolated compounds with chiral alcohol. Determination of the stereoconfiguration of the isomeric pair **7** and **8** is presented here as an example. The ^{1}H NMR spectrum of zhankuic acid A (in pyridine-D5, 600 MHz) exhibited two overlapped secondary methyl signals at δ_H 1.521 (3H-27, d, J = 7.2 Hz) and δ_H 1.528 (3H-27, d, J = 7.2 Hz), indicating the presence of two stereoisomers with different configuration at C-25 chiral center (Fig. S8A). The overlapped methyl signals cannot be clearly detected using lower frequencies NMR machine (e.g. 200 MHz and 400 MHz). Using 600 MHz NMR, two pairs of partially overlapped signals of the terminal olefinic protons (H_2-28) were also observed (Fig. S8A). The ^{13}C NMR spectrum of zhankuic acid A (in pyridine-D5, 150 MHz) clearly showed the isomeric pair patterns at δ_C 34.242 and 34.342 (CH_2-22), 31.575 and 31.766 (CH_2-23), 46.558 and 46.793 (CH-25), as well as 17.003 and 17.179 (CH_3-27), representing carbon signals close to C-25 on the 24-exo-methylene-26-oic acid side chain (Fig. S9A). On the other hand identical carbons of the isomeric pairs separated by more than 3 carbon atoms from C-25 showed slight difference in the chemical shift such as signals at δ_C 27.960 and 27.997 (CH_2-16), 53.937 and 53.986 (CH-17), 35.847 and 35.885 (CH-20), together with 18.519 and 18.564 (CH_3-21) (Fig. S9A). In an identical NMR experiment (pyridine-D5, 600 MHz), the ^{1}H and ^{13}C NMR spectra of the isomeric pair (**7** and **8**) showed only single signal pattern compared to the double signal pattern observed in zhankuic acid A spectra (Figs. S8B, S8C, S9B, and S9C). Assignments of the ^{1}H and ^{13}C signals of compounds **7** and **8** were performed by extended 2D NMR methods. Due to the high similarity of ^{1}H and ^{13}C signals of compounds **7** and **8**, the spectral data are presented in three significant figures after the decimal point (Tables 1 and 2). The NOE correlations in **7** and **8** were too similar to recognize the stereo chemical difference. To determine the absolute configuration of the chiral carbon at C-25 (α) to the carboxylic acid, chemical derivatization utilizing chiral pure alcohol was applied [18,19]. Compound **7** was treated separately with chiral derivatizing reagents, (1R)- and (1S)-1-(9-anthryl)-2,2,2-trifluoroethanol [(R)- and (S)-AT] to yield the (R)- and (S)-AT ester derivatives, respectively (Fig. S10A and S10B). The AT esters were formed successfully at C-26 as elucidated from the ^{13}C NMR signals of the ester carbonyl group at δ_C 172.774 [(R)-AT-ester of **7**] and δ_C 172.681 [(S)-AT-ester of **7**]. The calculated differences in chemical shifts [δ of protons in the (R)-AT-ester minus δ of the corresponding protons in the (S)-AT-ester] led to the assignment of the absolute configuration at C-25 in **7** as (S) (Fig. S10C and Table S1). Thus, compound **7** was named as 4α-methylergosta-8,24(28)-dien-3,7,11-trion-25S-26-oic acid. The absolute configuration of **8** at C-25 was assigned as R by using the same method (Table S1), and it was named 4α-methylergosta-8,24(28)-dien-3,7,11-trion-25R-26-oic acid.

After determining the absolute configuration, we tried to measure the optical rotation aiming to complete the spectral profile for the isolated compounds. In a previous report [2], the mixture form of zhankuic acid A was dissolved in methanol to measure its

optical rotation. However, the solubility of **7** (25S) and **8** (25R) was not sufficient in single solvent (methanol or ethanol). The solubility of compounds **7** and **8** improved through using acetone-methanol mixture. Considering compounds solubility and the convenience of collecting physical and spectral data using single solvent, pyridine was used in optical rotation experiment. The optical rotation value of compounds **7** ($[\alpha]_D^{25}$ +32.1, c 0.70, pyridine) and **8** ($[\alpha]_D^{25}$ +9.0, c 0.84, pyridine) were determined.

The structures of compounds **1**–**6** were assigned by the 2D NMR methods (Tables 1 and 2) and the absolute configuration of the chiral center at C-25 was assigned as described for compounds **7** and **8** (Table S1). Compound **3** was assigned as 7β-hydroxy-4α-methylergosta-8,24(28)-dien-3,11-dion-25S-26-oic acid and its optical rotation was $[\alpha]_D^{25}$ +124.8 (c 0.81, pyridine). Compound **4** was assigned as 7β-hydroxy-4α-methylergosta-8,24(28)-dien-3,11-dion-25R-26-oic acid and its optical rotation was $[\alpha]_D^{25}$ +79.9 (c 0.47, pyridine). Compounds **5** and **6** were assigned as 3α,12α-dihydroxy-4α-methylergosta-8,24(28)-dien-7,11-dion-25R-26-oic acid and 3α,12α-dihydroxy-4α-methylergosta-8,24(28)-dien-7,11-dion-25S-26-oic acid, respectively. The optical rotation data of **5** and **6** were $[\alpha]_D^{25}$ +82.0 (c 0.64, pyridine) and $[\alpha]_D^{25}$ +110.6 (c 0.70, pyridine), respectively. Compounds **1** and **2** showed $[\alpha]_D^{25}$ +61.0 (c 0.42, pyridine) and $[\alpha]_D^{25}$ +71.8 (c 0.27, pyridine), respectively. From the results of chemical derivatization, **2** was assigned as 3α,4β,7β-trihydroxy-4α-methylergosta-8,24(28)-dien-11-on-25R-26-oic acid. Unfortunately, the separated quantity of compound **1** was insufficient for chemical modification. In order to assign compound **1** absolute configuration we depended on the general trend observed in determining the stereoconfiguration of the isolated isomeric pairs. It was noticed that in each isomeric pair, if the chiral center at C-25 is assigned as (S) the other isomer chiral center is assigned as (R). Based on this finding and by knowing the absolute configuration of the chiral center in compound **2** as (R), the chiral center at C-25 in compound **1** was estimated as (S). Compound **1** was assigned as 3α,4β,7β-trihydroxy-4α-methylergosta-8,24(28)-dien-11-on-25S-26-oic acid. It is clear that with respect to optical rotation values of the pure isomers, all (S) isomers possessed higher optical rotation values compared to the (R) isomers except for compounds **1** and **2**.

3.4. HPLC method optimization and relative percentage evaluation of FEA

The HPLC conditions for the active ethyl acetate fraction were further optimized after isolating the major triterpenes as standards from FEA (Fig. 2). Because the skeleton of these triterpenes contained a carboxylic acid moiety, symmetrical sharp peaks were easily obtained in the HPLC chromatogram using acidic mobile phase with a relatively low pH value. Due to the acidic properties of these AC triterpenes, three types of 0.1% organic acids, including trifluoroacetic acid (pH 2.2), acetic acid (pH 3.3) and formic acid (pH 2.8) were screened as additive to the mobile phase. The use of acidic additive in the separation of acidic constituents usually results in symmetrical well resolved peaks. We studied the relationship between peak area and retention time for the major peaks after adding organic acid into the aqueous phase. The results showed that retention times of the major peaks in these three different acidic systems were nearly identical. However, the best results in terms of maximum peak area of the major triterpenoids were obtained using the formic and acetic acidic systems. Although both 0.1% formic and acetic acids produced similar results, the latter was selected. The use of acetic acid provided more stable baseline and improved the shape of the desired peaks in the HPLC fingerprints. The maximum absorbance (λ_{max}) of ergostane and lanostane triterpenes was detected at 254 nm and 270 nm, respectively (Fig. 2A and B).

Table 1
^{1}H NMR data[a] for compounds **1–8** (C$_5$D$_5$N, δ in ppm, J in Hz).

Proton	1	2	3	4	5	6	7	8
1a	2.110 m	2.108 m	1.416 m	1.436 m	1.957 m	1.946 m	1.437 m	1.422 m
1b	3.148 dt (13.2, 3.0)	3.149 dt (13.2, 3.6)	3.232 qd (6.0, 2.4)	3.231 qd (6.6, 2.4)	2.737 dt (12.0, 3.6)	2.734 dt (13.2, 3.0)	3.178 qd (6.6, 3.0)	3.178 qd (6.6, 2.4)
2a	1.965 m	1.975 m	2.390 m	2.389 m	1.855 m	1.857 m	2.406 m	2.406 m
2b	2.771 m	2.778 m	2.548 m	2.537 m	1.855 m	1.857 m	2.588 m	2.570 m
3	β 4.092 s	β 4.094 s			β 3.877 s	β 3.874 br s		
4			β 2.374 m	β 2.373 m	β 1.692 m	β 1.699 m	β 2.464 m	β 2.458 m
5	α 2.202 m	α 2.201 m	α 1.416 m	α 1.414 m	α 2.596 m	α 2.592 m	α 1.886 m	α 1.880 m
6a	2.461 m	2.466 m	1.823 m	1.822 m	2.448 m	2.448 m	2.584 m	2.570 m
6b	2.749 m	2.750 m	2.374 m	2.373 m	2.611 m	2.613 m	2.584 m	2.570 m
7	α 4.650 t (8.4)	α 4.651 br t	α 4.524 t (7.8)	α 4.527 td (8.4, 1.2)				
12a	2.476 m	2.462 m	2.473 d (13.8)	2.477 d (13.8)	β 4.505 s	β 4.500 s	2.503 m	2.503 m
12b	3.000 d (13.2)	3.000 d (13.8)	3.000 d (13.8)	3.000 d (13.8)			3.019 d (13.8)	3.018 d (13.8)
14	α 2.666 m	α 2.674 m	α 2.755 ddd (12.0, 6.6, 1.2)	α 2.763 ddd (12.6, 7.2, 1.8)	α 3.567 dd (13.2, 7.8)	α 3.559 dd (13.2, 7.8)	α 2.742 m	α 2.745 m
15a	2.120 m	2.128 m	2.113 m	2.116 m	1.674 m	1.677 m	1.547 m	1.552 m
15b	2.546 m	2.541 m	2.548 m	2.537 m	2.858 m	2.854 m	2.753 m	2.734 m
16a	1.328 m	1.360 m	1.336 m	1.337 m	1.327 m	1.315 m	1.240 m	1.242 m
16b	1.965 m	1.952 m	1.947 m	1.924 m	1.978 m	1.982 m	1.915 m	1.906 m
17	α 1.441 m	α 1.436 m	α 1.416 m	α 1.424 m	α 2.302 m	α 2.300 m	α 1.390 m	α 1.382 m
18	0.929 s	0.925 s	0.893 s	0.891 s	0.821 s	0.819 s	0.707 s	0.703 s
19	2.099 s	2.098 s	1.604 s	1.602 s	1.547 s	1.547 s	1.611 s	1.609 s
20	β 1.405 m	β 1.417 m	β 1.336 m	β 1.335 m	β 1.490 m	β 1.478 m	β 1.381 m	β 1.390 m
21	0.908 d (6.0)	0.909 d (6.0)	0.911 d (6.0)	0.913 d (6.0)	1.077 d (6.6)	1.075 d (6.6)	0.895 d (5.4)	0.892 d (6.0)
22a	1.328 m	1.297 m	1.354 m	1.313 m	1.346 m	1.389 m	1.314 m	1.272 m
22b	1.740 m	1.789 m	1.737 td (12.0, 5.4)	1.775 m	1.806 m	1.767 m	1.697 td (11.4, 5.4)	1.738 td (12.0, 3.6)
23a	2.237 m	2.238 m	2.236 m	2.235 m	2.236 m	2.233 m	2.211 m	2.223 m
23b	2.498 m	2.439 m	2.484 m	2.431 m	2.423 m	2.474 m	2.448 m	2.406 m
25	3.485 br q	3.491 q (7.2)	3.487 br q (6.6)	3.483 q (6.6)	3.457 q (7.2)	3.452 q (7.2)	3.464 br q (7.2)	3.480 br q (6.6)
27	1.534 d (6.6)	1.530 d (7.2)	1.530 d (6.6)	1.522 d (7.2)	1.496 d (7.2)	1.504 d (6.6)	1.524 d (7.2)	1.529 d (6.6)
28a	5.076 s	5.083 s	5.089 s	5.085 s	5.059 s	5.073 s	5.069 s	5.060 s
28b	5.234 s	5.256 s	5.242 s	5.256 s	5.234 s	5.226 s	5.231 s	5.248 s
29	1.763 s	1.765 s	1.132 d (6.6)	1.132 d (6.6)	1.052 d (6.6)	1.050 d (7.2)	1.039 d (6.6)	1.039 d (6.6)

[a] Assignments were confirmed by coupling constants, ^{1}H–^{1}H COSY, NOESY, HMQC, and HMBC analysis.

Table 2
^{13}C NMR data[a] for compounds **1–8** (C$_5$D$_5$N, δ in ppm).

Carbon	1	2	3	4	5	6	7	8
1	29.687	29.687	36.163	36.160	28.583	28.575	34.947	34.936
2	26.786	26.785	38.123	38.121	30.155	30.148	37.771	37.767
3	74.711	74.711	211.368	211.359	69.308	69.301	209.898	209.909
4	73.957	73.957	44.069	44.074	35.324	35.316	43.925	43.918
5	43.498	43.498	48.629	48.634	41.605	41.602	48.914	48.896
6	30.199	30.199	33.504	33.509	38.685	38.677	39.208	39.201
7	70.805	70.805	69.311	69.319	202.004	201.993	200.778	200.789
8	154.299	154.292	155.860	155.856	144.406	144.395	145.504	145.504
9	143.939	143.939	140.862	140.873	153.160	153.145	151.957	151.953
10	38.755	38.751	37.391	37.396	38.980	38.976	38.630	38.618
11	201.504	201.504	201.318	201.317	203.938	203.927	202.679	202.701
12	58.817	58.817	58.454	58.470	80.956	80.941	57.474	57.470
13	47.942	47.938	47.882	47.891	50.240	50.225	47.238	47.234
14	53.768	53.772	53.577	53.597	42.707	42.692	49.471	49.463
15	25.486	25.490	25.362	25.371	24.617	24.598	25.297	25.301
16	28.298	28.234	28.227	28.183	27.351	27.377	28.027	27.979
17	54.855	54.877	54.645	54.699	46.079	46.027	54.001	54.016
18	12.493	12.493	12.470	12.480	11.815	11.796	12.092	12.092
19	20.956	20.956	17.643	17.648	16.457	16.449	16.249	16.241
20	36.242	36.271	36.114	36.160	35.974	35.891	35.881	35.959
21	18.614	18.655	18.603	18.657	18.141	18.070	18.549	18.601
22	34.419	34.509	34.359	34.472	34.640	34.491	34.253	34.383
23	31.999	31.764	31.860	31.675	31.843	32.052	31.855	31.657
24	150.833	150.707	150.601	150.616	150.830	150.490	150.642	150.116
25	47.068	47.005	46.720	46.923	47.095	46.602	47.006	47.518
26	177.842	177.237	177.371	177.154	177.479	177.113	177.770	178.124
27	17.165	17.255	17.086	17.234	17.290	17.058	17.138	17.425
28	110.003	110.186	110.280	110.302	110.145	110.291	110.127	109.888
29	28.059	28.059	11.888	11.893	16.394	16.393	11.558	11.551

[a] Assignments were confirmed by coupling constants, ^{1}H–^{1}H COSY, NOESY, HMQC, and HMBC analysis.

Considering the absorbance of these two type triterpenes, 254 nm was chosen as the detection wavelength. Accordingly, detection wavelength, acid concentration, and injection volume were set at 254 nm, 0.1% acetic acid, and 20 μl. The chromatogram was analyzed by using the software 'Class VP', and the percentage of all peaks with mean chromatogram were calculated by the same software based on the peak area. In addition, the relative peak area (RPA) of each characteristic peak (peaks 1–10) was calculated in comparison to the reference peak (peak 9) offering a semi-quantitative determination of the chemical composition of FEA.

In a simulative median chromatogram of FEA, it had ten well-resolved 'characteristic peaks', including eight ergostane triterpenes (peaks 1–8) and two lanostane triterpenes (peaks 9 and 10). Among them, peak 9, which appeared in the middle of the chromatogram with a maximum area, was considered as the internal reference peak. The RPA data of the ten characteristic peaks in FEA were 0.532 (compound **1**, peak 1, R_t 6.724), 0.781 (compound **2**, peak 2, R_t 7.004), 0.669 (compound **3**, peak 3, R_t 24.778), 0.623 (compound **4**, peak 4, R_t 26.735), 0.771 (compound **5**, peak 5, R_t 27.932), 0.996 (compound **6**, peak 6, R_t 29.139), 1.046 (compound **7**, peak 7, R_t 46.739), 0.862 (compound **8**, peak 8, R_t 47.348), 1.000 (compound **9**, peak 9, R_t 41.890), and 0.701 (compound **10**, peak 10, R_t 77.532), individually. The absolute stereoconfiguration at C-25 was not the decisive factor for the elution order in HPLC experiments. In the reverse phase HPLC analysis of antcin K and zhankuic acid C pure isomeric forms, peaks 1 and 5 corresponding to (R) isomers were eluted first followed by peaks 2 and 6 corresponding to (S) isomers. However an opposite trend was observed in the separating of pure isomeric forms of antcin C and zhankuic acid A. In both cases the (S) isomers were eluted first.

3.5. LC–ESI-MS analysis of FEA

In order to further identify the ergostane stereo-isomeric pairs in FEA, we employed HPLC-PDA/MS. Identification was accomplished by using on-line DAD, ESI-MS techniques, and co-elution with compounds **1–10**. At the beginning, both positive and negative ion modes were used in an attempt to ionize compounds **1–10**. It was found that the positive mode resulted in a larger number of ions compared to the negative mode. Therefore, ESI in the positive mode was selected for the follow-up analysis. Moreover, the MS peak intensity was compared at three different ionization source temperatures (350 °C, 450 °C and 550 °C). The MS results indicated that peak intensity obtained under ionization source temperature of 550 °C was over two fold higher than those at 450 °C or 350 °C. Therefore, 550 °C was selected as the suitable ionization source temperature. The total ion current (TIC) chromatogram in the positive mode is shown in Fig. S11. By comparing FEA and compounds **1–8** in the on-line ESI-MS spectra, the four major stereo-isomeric pairs of ergostane triterpenes (antcin K, antcin C, zhankuic acid C, and zhankuic acid A) were detected, corresponding to peak pairs of 1 and 2, 3 and 4, 5 and 6, as well as 7 and 8, respectively. The m/z data in the HPLC-ESI/MS spectra for these four major peak pairs (peaks 1–8) are shown in Table S2. The mass spectra of each isomer were similar to the mass spectra of the other isomer in the same pair as 1 and 2, 3 and 4, 5 and 6, 7 and 8. Fragments of these four major peak pairs were observed at $[M+H-18]^+$ or $[M+H-15]^+$, corresponding to the loss of hydroxyl or methyl groups. Furthermore, the fragment ion $[M+H-44]^+$, corresponding to the loss of $-COO^-$, was detected indicated the existence of carboxylic group in the structures. This is the first reported identification of these novel paired triterpene stereo-isomers in AC using HPLC and LC–MS. It was observed that lanostane triterpenes, dehydrosulphurenic acid and dehydroeburicoic acid, corresponding to peaks 9 and 10, disappeared in the TIC chromatogram. The absence of peaks 9 and 10 indicated that the corresponding compounds cannot be easily

ionized or their ions are unstable under the processes of electron spray ionization. To the best of our knowledge this is the first report showing differences in mass spectroscopic results between lanostane and ergostane triterpenes of AC.

3.6. Fractionation procedures for concentrating zhankuic acids from wild fruiting bodies of A. camphorata

We developed highly efficient fractionation procedures to concentrate zhankuic acids in FEA. On the basis of LC analysis, it was confirmed that zhankuic acid A and other zhankuic acid derivatives are the major components of FEA. The ^{1}H NMR spectrum of zhankuic acid A as a standard, proved also that the process developed in the current study was capable of concentrating zhankuic acids in FEA. The same result was observed in the isolation process of FEA (the ratio of zhankuic acid A weight to FEA was approximately 1:5). In order to study the difference in chemical composition between FEA and other fractions (FNH and FET) obtained using Type 1, ^{1}H NMR experiments were conducted. Several deuterated solvents such as $CDCl_3$, CD_3OD, D_2O, and pyridine-D5 were tested and considered for NMR measurements. After evaluating compounds solubility and analysing NMR data of the tested samples, pyridine-D5 was chosen as the deuterated solvent for our experiments. ^{1}H NMR spectra of EEAC, FNH, FEA, FET, and zhankuic acid A were measured under identical conditions (10 mg/0.75 ml, 400 MHz), and plotted for comparison (Fig. 3). The characteristic ^{1}H NMR signals of zhankuic acid A showed two tertiary methyl signals [δ_H 0.70 (H_3-18) and 1.61 (H_3-19) (each 3H, s)], three secondary methyl signals [δ_H 0.89 (3H-21, d, J = 5.6 Hz), 1.03 (3H-29, d, J = 6.4 Hz), and 1.52 (3H-27, d, J = 7.2 Hz)], and terminal olefinic protons (H_2-28) in a 24-exo-methylene-26-oic acid side-chain [δ_H 5.08 (1H, br s) and 5.24 (1H, br s)]. ^{1}H NMR spectra of EEAC and FEA clearly exhibited these distinguishable signals. Moreover, the signals of methine protons [δ_H 3.01 (1H-12, d, J = 13.6 Hz), 3.17 (1H-1, ddd, J = 13.3, 6.8, 2.4 Hz), and 3.48 (1H-25, q, J = 7.2 Hz)] of zhankuic acid A were also detected in ^{1}H-NMR spectra of EEAC and FEA. However, the specific signals mentioned above were not observed at all in the ^{1}H NMR spectra of FNH and FET. Therefore, it can be concluded that the major active component, zhankuic acid A, of the ethanolic extract of wild fruiting bodies of *A. camphorata* (EEAC) is concentrated in the ethyl acetate fraction (FEA) by the method presented in this study. On the basis HPLC and NMR analysis, FEA is unmistakably defined as the active triterpenoids-rich fraction.

3.7. Cytotoxic screening of ergostane stereo-isomeric pairs on leukemia cancer cell lines

Previous studies revealed that triterpenes from AC possessed anti-inflammatory activity in neutrophils [20] and cytotoxicity against leukemia, colon, liver, breast and lung cancer cells [21]. However, the relationship between the stereochemistry and bioactivity of 25-(R) and 25-(S) ergostane stereo-isomers has never been reported. In our continuing research for cytotoxic metabolites from FEA, compounds **1–8** and their mixture forms (antcin K, antcin C, zhankuic acid C, and zhankuic acid A) were subjected to an anti-proliferation assay against a panel of cancer cell lines, including two human acute lymphoblastic leukemia cells (CCRF-CEM and Molt 4) and one human promyelocytic leukemia cells (HL 60) (Table 3). Results showed that derivatives with the 3-carbonyl functional group (**3**, **4**, **7**, **8**, antcin C, and zhankuic acid A) exhibited better cytotoxicity with IC_{50} values ranging from 16.44 to 77.04 μg/ml. Comparatively, compounds with a hydroxyl group at C-3 were less active (IC_{50} > 80 μg/ml) suggesting the presence of carbonyl group is important for cytotoxic activity. Moreover the presence of other hydroxyl groups in rings A (C-4), B (C-7), C (C-12) did not have a
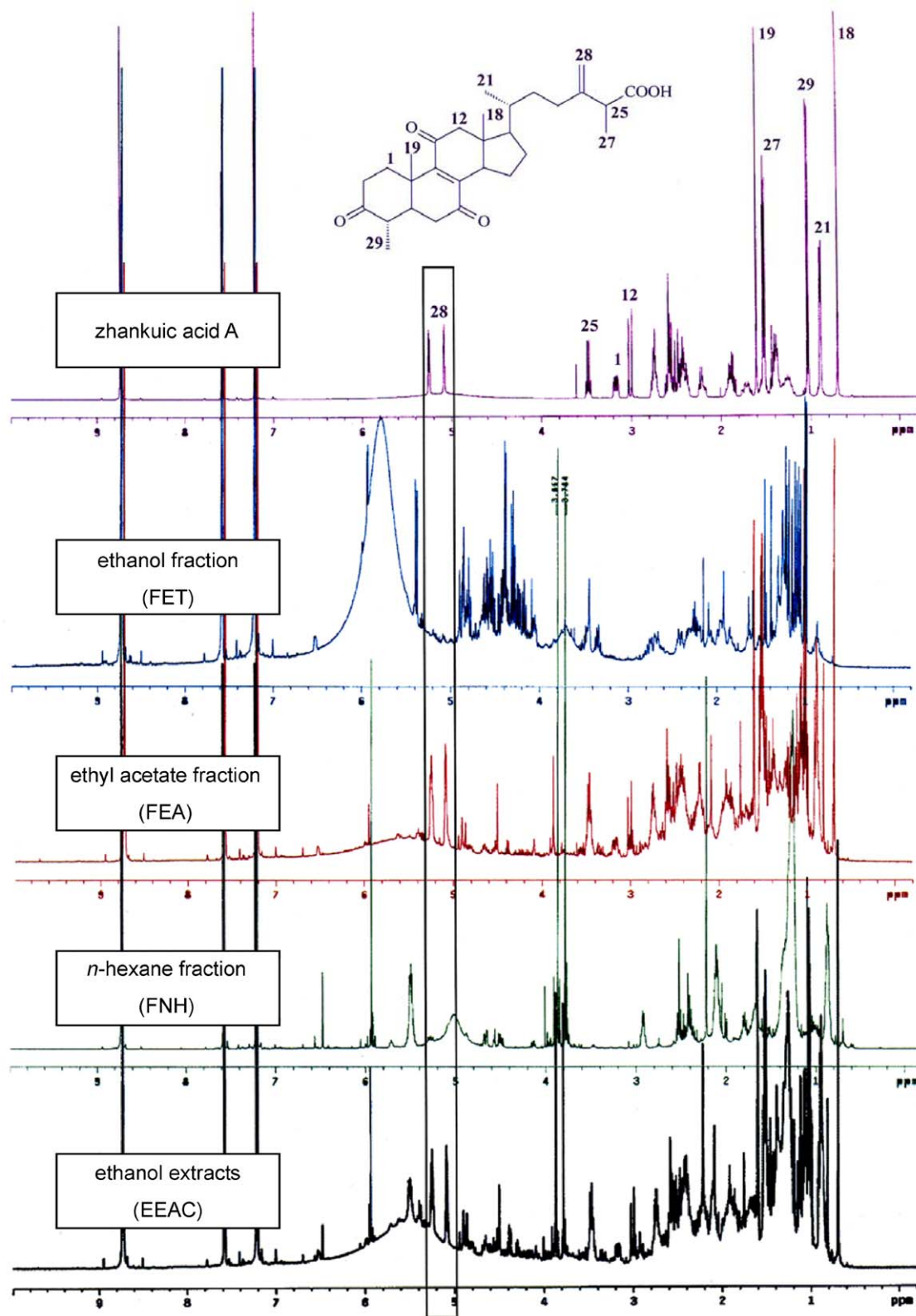
Fig. 3. ¹H NMR profiles of zhankuic acid A, FNH (n-hexane fraction), FEA (ethyl acetate fraction), FET (ethanol fraction), and EEAC (ethanol extract) separated using Type 1 process.

significant effect on cytotoxicity. To understand the effect of stereo-configuration of the isolated compounds on their cytotoxic activity, the activity of the isolated pure isomers and their mixture forms on leukemia cell lines was evaluated. Compounds 7 and 8 showed higher inhibitory potency than their mixture form, zhankuic acid

A, in all cancer cell lines. On the other hand compounds 3 and 4 isolated from antcin C lost their cytotoxicity (IC$_{50}$ > 80 μg/ml) against HL 60 cells. In the Molt 4 cell line, the 25R forms (4 and 8) were more active than the related 25S forms (3 and 7). Similar results in the HL 60 cell line were observed with compounds 7 and 8. However,

Table 3
Cytotoxicity of zhankuic acids on leukemia cancer cell lines.

Compound	IC_{50} (μg/ml)[a]		
	CCRF-CEM[b]	Molt 4[b]	HL 60[c]
1	>80	>80	>80
2	>80	>80	>80
3	30.68 ± 5.30	77.04 ± 2.78	>80
4	27.94 ± 6.44	54.28 ± 1.96	>80
5	>80	>80	>80
6	>80	>80	>80
7	21.99 ± 7.91	42.16 ± 2.33	54.67 ± 8.14
8	22.90 ± 7.60	16.44 ± 3.77	23.32 ± 1.60
Antcin K	>80	>80	>80
Antcin C	28.82 ± 6.79	55.02 ± 3.34	47.02 ± 4.45
Zhankuic acid C	>80	>80	>80
Zhankuic acid A	47.04 ± 6.191	53.23 ± 3.88	69.98 ± 18.98

[a] Data are expressed as mean ± SD (n = 3).
[b] Human acute lymphoblastic leukemia cells.
[c] Human promyelocytic leukemia cells.

the 25R forms (**4** and **8**) and 25S forms (**3** and **7**) exhibited nearly equal potency against CCRF-CEM cells. Based on these findings, a clear correlation between the stereoconfiguration of AC ergostane triterpenes and their cytotoxic activity cannot be defined.

4. Conclusions

We developed a convenient fractionation procedure for concentrating the anti-proliferative triterpenoids from AC fruiting bodies. The chemical profile of this triterpenoids-rich fraction was illustrated by HPLC, NMR, and HPLC-PDA/MS. Triterpenes (FEA) were the major constituents of AC fruiting bodies, accounting for about 22% of the original crude material total weight and nearly 20% of the total FEA weight was zhankuic acid A. Using a combination of extraction, fractionation, and HPLC, an effective analysis and preparation procedure of AC major triterpenes was established. The method we developed is feasible for comprehensive quality evaluation of AC fruiting bodies and its related products.

Since the first isolation of zhankuic acids in 1995 [10], the separation of their pure isomers has been always an unresolved issue. For the first time we report the separation of zhankuic acid derivatives in a pure isomeric form and the determination of their cytotoxic activity on different cancer cell lines.

In the current study we investigated also the effect of difference in stereoconfiguration at C-25 of the isolated triterpenes on the elution order in HPLC experiments, optical rotation values and cytotoxic activity. The biofunction and pharmacological mechanism of pure and individual zhankuic acid isomers are under investigation in our laboratory.

Appendix A. Supplementary data

Supplementary data associated with this article can be found, in the online version, at doi:10.1016/j.jpba.2011.09.007.

References

[1] Z.H. Ao, Z.H. Xu, Z.M. Lu, H.Y. Xu, X.M. Zhang, W.F. Dou, Niuchangchih (*Antrodia camphorata*) and its potential in treating liver diseases, J. Ethnopharmacol. 121 (2009) 194–212.
[2] C.C. Shen, Y.C. Kuo, R.L. Huang, L.C. Lin, M.J. Don, T.T. Chang, C.J. Chou, New ergostane and lanostane from *Antrodia camphorata*, J. Chin. Med. 14 (2003) 247–258.
[3] M.C. Lu, S.L. Hwang, F.R. Chang, Y.H. Chen, T.T. Chang, C.S. Hung, C.L. Wang, Y.H. Chu, S.H. Pan, Y.C. Wu, Immunostimulatory effect of *Antrodia camphorata* extract on functional maturation of dendritic cells, Food Chem. 113 (2009) 1049–1057.
[4] M. Geethangili, Y.M. Tzeng, Review of pharmacological effects of *Antrodia camphorata* and its bioactive compounds, Evid. Based Complement Altern. Med. 2011 (2009) 1–17.
[5] Y.C. Wu, M.C. Lu, F.R. Chang, Y.C. Du, T.Y. Wu, Ethanol extract of *Antrodia camphorata* for inducing apoptosis and preparation method thereof, United States Patent, US 2010/0210869 A1, August 19 (2010).
[6] Y.C. Chen, H.O. Ho, C.H. Su, M.T. Sheu, Anticancer effects of *Taiwanofungus camphoratus* extracts, isolated compounds and its combinational use, J. Exp. Clin. Med. 2 (2010) 274–281.
[7] Y.Y. Chan, C.S. Chang, L.H. Chien, T.F. Wu, Apoptotic effects of a high performance liquid chromatography (HPLC) fraction of *Antrodia camphorata* mycelia are mediated by down-regulation of the expressions of four tumor-related genes in human non-small cell lung carcinoma A549 cell, J. Ethnopharmacol. 127 (2010) 652–661.
[8] Y.H. Kuo, B.F. Lin, Compounds from *Antrodia camphorata*, United States Patent, US 7932285 B2, April 26 (2011).
[9] M.C. Lu, Y.C. Du, J.J. Chuu, S.L. Hwang, P.C. Hsieh, C.S. Hung, F.R. Chang, Y.C. Wu, Active extracts of wild fruiting bodies of *Antrodia camphorata* (EEAC) induce leukemia HL 60 cells apoptosis partially through histone hypoacetylation and synergistically promote anticancer effect of trichostatin A, Arch. Toxicol. 83 (2009) 121–129.
[10] C.H. Chen, S.W. Yang, Y.C. Shen, New steroid acids from *Antrodia cinnamomea*, a fungal parasite of *Cinnamomum micranthum*, J. Nat. Prod. 58 (1995) 1655–1661.
[11] E. Majid, K.B. Male, Y.M. Tzeng, J.O. Omamogho, J.D. Glennon, J.H. Luong, Cyclodextrin-modified capillary electrophoresis for achiral and chiral separation of ergostane and lanostane compounds extracted from the fruiting body of *Antrodia camphorata*, Electrophoresis 30 (2009) 1967–1975.
[12] J.B. Bartlett, K. Dredge, A.G. Dalgleish, The evolution of thalidomide and its IMiD derivatives as anticancer agents, Nat. Rev. Cancer 4 (2004) 314–322.
[13] C. Goosen, T.J. Laing, J.d. Plessis, T.C. Goosen, G.L. Flynn, Physicochemical characterization and solubility analysis of thalidomide and its N-alkyl analogs, Pharm. Res. 19 (2002) 13–19.
[14] I.H. Cherng, H.C. Chiang, M.C. Cheng, Y. Wang, Three new triterpenoids from *Antrodia cinnamomea*, J. Nat. Prod. 58 (1995) 365–371.
[15] Y.L. Hsu, Y.C. Kuo, P.L. Kuo, L.T. Ng, Y.H. Kuo, C.C. Lin, Apoptotic effects of extract from *Antrodia camphorata* fruiting bodies in human hepatocellular carcinoma cell lines, Cancer Lett. 221 (2005) 77–89.
[16] K.B. Male, Y.K. Rao, Y.M. Tzeng, J. Montes, A. Kamen, J.H. Luong, Probing inhibitory effects of *Antrodia camphorata* isolates using insect cell-based impedance spectroscopy: inhibition vs chemical structure, Chem. Res. Toxicol. 21 (2008) 2127–2133.
[17] S.W. Yang, Y.C. Shen, C.H. Chen, Steroids and triterpenoids of *Antrodia cinnamomea* – a fungus parasitic on *Cinnamomum micranthum*, Phytochemistry 41 (1996) 1389–1392.
[18] J.M. Seco, E. Quiñoá, R. Riguera, The assignment of absolute configuration by NMR, Chem. Rev. 104 (2004) 17–117.
[19] L. Muñoz, M.P. Bosch, G. Rosell, A. Guerrero, Asymmetric synthesis of (R)- and (S)-4-methyloctanoic acids. A new route to chiral fatty acids with remote stereocenters, Tetrahedron: Asymmetr. 20 (2009) 420–424.
[20] Y.C. Shen, Y.H. Wang, Y.C. Chou, C.F. Chen, L.C. Lin, T.T. Chang, J.H. Tien, C.J. Chou, Evaluation of the anti-inflammatory activity of zhankuic acids isolated from the fruiting bodies of *Antrodia camphorata*, Planta Med. 70 (2004) 310–314.
[21] C.T. Yeh, Y.K. Rao, C.J. Yao, C.F. Yeh, C.H. Li, S.E. Chuang, J.H. Luong, G.M. Lai, Y.M. Tzeng, Cytotoxic triterpenes from *Antrodia camphorata* and their mode of action in HT-29 human colon cancer cells, Cancer Lett. 285 (2009) 73–79.

Simple and rapid simultaneous profiling of minor components of honey by size exclusion chromatography (SEC) coupled to ultraviolet diode array detection (UV-DAD), combined with chemometric methods

Giangiacomo Beretta [a,*], Paola Fermo [b], Roberto Maffei Facino [a]

[a] *Department of Pharmaceutical Sciences "Pietro Pratesi", Faculty of Pharmacy, University of Milan, Via Mangiagalli 25, 20133 Milan, Italy*
[b] *Department of Chemistry, Faculty of Pharmacy, University of Milan, Via Venezian 21, 20133 Milan, Italy*

ABSTRACT

This paper discusses the importance of profiling UV-responsive components, properly integrated with chemometric techniques, in detecting indicative parameters for quality control of honey. The minor components in honeys of different botanical and geographical origins were investigated by size SEC-UV-DAD. We diluted honey with mobile phase before injection into the chromatographic apparatus and a single chromatographic run gave a fast profile of high- (proteins and enzymes), intermediate- (e.g. terpenoid glycosides in lime tree honey) and low-molecular-weight components (secondary metabolites, e.g. kynurenic acid in chestnut honey).

The analysis of a total number of 32 honey samples from different regions (Italy, Western Balkan countries, Brazil, Cameroon, Kenya) and of different botanical origins (herbal flower and arboreal flower nectars/honeydews) showed peculiar and characteristic distribution of these markers, which were basically related to their floral origin.

Chemometric examination carried out using principal component analysis (PCA) and hierarchical cluster analysis (HCA) of the chromatograms (RT vs. absorption) detected four main clusters in which the groups of (i) chestnut honeys, (ii) honeys from rain forests and (iii) counterfeit/adulterated honeys were clearly separated from the main group of flower nectar honeys.

The method is fast, requiring minimal sample handling, and the chromatographic data can be analyzed by multivariate statistical techniques to obtain descriptive information about the honey's quality and composition.

© 2011 Elsevier B.V. All rights reserved.

1. Introduction

Honey is a natural food of great interest for its high nutritional value and therapeutic and medicinal properties [1]. Apitherapy (the medicinal use of honeybee products) has recently gained attention for preventive medicine in several conditions and diseases as well as for promoting health and well-being [2].

Because of its sweetness, color and flavor, honey is also often used in place of sugar and as an ingredient or natural preservative in many manufactured foods. It can prevent oxidative reactions in foods (e.g. lipid oxidation in meat [3] and enzymatic browning of fruits and vegetables [4]). The composition and properties of a particular honey sample depend strongly on the type of flowers the bees visited, on the climatic conditions in which the plants grow and on the beekeeper's contribution [5,6].

From the chemical point of view, honey is a highly complex, concentrated mixture of sugars with a large pool of minor constituents of different molecular weights (MW) and chemical nature embedded. Many of these components are thought to be responsible for its beneficial properties, from high-MW components (proteins) excreted by honey bees into honey (e.g. glucose oxidase, invertase, saccharase, diastase and catalase) [1,7], to peculiar and particularly abundant plant secondary metabolites (e.g. kynurenic acid (KA) in chestnut honey [8–11] or cyclohexa-1,3-diene-1-carboxylic acid (CDCA) in lime tree honey [11,12]), and/or an array of minor compounds (phenolic acid derivatives such as ferulic acid, caffeic acid and coumaric acid and its esters, and flavonoid aglycones) deriving from the original composition of the nectars and sugar-rich materials on which honey bees feed to produce honey [13–15].

Further to our previous investigations on honey quality, botanical and geographical origins [8,11], here we describe a fast, cheap method for simultaneous screening of honey's minor organic components, from high to low MW (300 kDa to 100 Da) using size exclusion chromatography (SEC) coupled to ultraviolet diode array detection (UV-DAD). The chromatographic findings were analyzed

Table 1
Botanical and geographical origins of the honey samples analyzed by SEC-UV-DAD chromatography.

Sample no.	Lab code	Botanical origin	Geographical origin	Honey bee species
1	ALB01	Acacia (Robinia pseudoacacia)	Albania	Apis mellifera carnica/macedonica
2	ALB02	Multiflora	Albania	Apis mellifera carnica/macedonica
3	ALB03	Multiflora	Albania	Apis mellifera carnica/macedonica
4	ALB04	Acacia (Robinia pseudoacacia)	Albania	Apis mellifera carnica/macedonica
5	ALB05	Unknown	Albania	Apis mellifera carnica/macedonica
6	ALB06	Multiflora	Albania	Apis mellifera carnica/macedonica
7	ALB07	Honeydew (Pine)	Albania	Apis mellifera carnica/macedonica
8	ALB08	Chestnut (Castanea sativa)	Albania	Apis mellifera carnica/macedonica
9	ALB09	Acacia	Albania	Apis mellifera carnica/macedonica
10	SRB01	Acacia (Robinia pseudoacacia)	Serbia	Apis mellifera carnica
11	BRA02	Sweet orange (Laranjeira, Citrus sinensis)	Brazil	Apis mellifera scutellata
12	CAM04	Rainforest	Cameroon	Apis mellifera adansonii
13	CAM05	Rainforest	Cameroon	Apis mellifera adansonii
14	CAM34	Rainforest	Cameroon	Apis mellifera adansonii
15	CAM35	Rainforest	Cameroon	Apis mellifera adansonii
16	CRO01	Mountain	Croatia	Apis mellifera carnica
17	CRO02	Chestnut (Castanea sativa)	Croatia	Apis mellifera carnica
18	IT01	Chestnut (Castanea sativa)	Italy	Apis mellifera ligustica
19	IT02	Acacia (Robinia pseudoacacia)	Italy	Apis mellifera ligustica
20	IT03	Multiflora	Italy	Apis mellifera ligustica
21	IT04	Mountain	Italy	Apis mellifera ligustica
22	IT05	Chestnut (Castanea sativa)	Italy	Apis mellifera ligustica
23	IT30	Dog Rose (Rosa canina)	Italy	Apis mellifera ligustica
24	KEN01	Mango (Mangifera indica)	Kenya	Apis mellifera adansonii
25	SRB02	Acacia (Robinia pseudoacacia)	Serbia	Apis mellifera carnica
26	KOS02	Multiflora	Kosovo	Apis mellifera carnica
27	KOS03	Chestnut (Castanea sativa)	Kosovo	Apis mellifera carnica
28	KOS05	Acacia (Robinia pseudoacacia)	Kosovo	Apis mellifera carnica
29	MAK01	Meadow	Macedonia	Apis mellifera macedonica
30	MAK02	Multiflora	Macedonia	Apis mellifera macedonica
31	SLO01	Honeydew (Fir)	Slovenia	Apis mellifera carnica
32	SLO02	Chestnut (Castanea sativa)	Slovenia	Apis mellifera carnica

using multivariate chemometric techniques, principal component analysis (PCA) and hierarchical cluster analysis (HCA) to distinguish the different honeys on the basis of the distribution/profiles of their minor components. This approach enabled us (i) to simultaneously profile honey proteins, and some known/unknown molecular species with intermediate and low MW, (ii) to distinguish the components associated with flower nectar/honeydew from those very likely coming from the honey bee, and (iii) to distinguish authentic honeys from counterfeit/adulterated ones. We applied the method to honey samples from different regions (Italy, Western Balkan countries, Brazil, Cameroon, Kenya) and botanical origins (herbal and arboreal flowers nectars and honeydews).

2. Experimental

2.1. Reagents and materials

Sodium chloride, monosodium dihydrogen phosphate and disodium monohydrogen phosphate were from Sigma–Aldrich–Fluka (Milan, Italy). Water for the preparation of solutions and running buffers was purified by a Milli-Q apparatus (Millipore, Milford, MA, USA). Honey samples of different botanical origins (multiflora, acacia, chestnut, dog rose, mango, and honeydew) were obtained during the years 2009/2010 from local markets or beekeepers in Italy, Kosovo, Cameroon, Kenya and Brazil, authenticated and processed with the procedures previously described [16].

2.2. Experimental procedure

Native honey (1 g), was dissolved in mobile phase (10 mL final volume) and 10 μL of the clear solution obtained after centrifugation (10,000 × g) to remove solid particles (pollens, debris, etc.) were analyzed by SEC-UV-DAD. Chromatographic runs were done using a Varian LC-940 analytical/semipreparative HPLC system (Varian, Turin, Italy) equipped with a binary pump system, an autosampler, a fraction collector, a UV-DAD detector operating (200–400 nm) at $\lambda_1 = 220$ nm and $\lambda_2 = 280$ nm and a scale-up module. Analytical separations were done on a TSKgel G2000 SWXL column (300 mm × 7.8 mm and 250 mm × 21.2 mm, Tosoh Bioscience, Japan). The solvent system was NaCl (8.5 g/L)/NaH$_2$PO$_4$ (2 g/L)/Na$_2$HPO$_4$ (1 g/L) (pH 6.7), flow rate 1.2 mL/min. Analyses were done from 0 to 20 min of the chromatographic run to ensure that analytes with the lowest MW were eluted.

The SEC-UV-DAD data indicated that the chromatographic reproducibility was highly satisfactory with the average relative standard deviations (RSD) of the peak retention times (RT) less than 0.3%, and those of the peak heights less than 2% (interday, $n = 4$ independent experiments carried out on $n = 4$ different samples in $n = 4$ different days: IT01, KOS06, BRA02, CAM34). For the calculations where considered peaks with relative maximal absorbance higher than the 30% of the most intense peak of the chromatogram (100%). The good reproducibility meant the subsequent multivariate statistical analysis was reliable.

2.3. MW calibration

The MW of known and unknown substances was estimated by comparing their RT with those of standards with MW in the range 190–390,000 Da. KA, MW 189 Da; 3-PKA, MW 258 Da; NADP, MW 741 Da; GSSG, MW 612 Da; diastase, MW 35 kDa (Aspergillus oryzae); glucose oxidase, MW 72,000; catalase, MW 230 kDa (bovine liver); invertase, MW = 270 kDa (Saccharomyces cerevisiae); catalase MW = 323 kDa (Aspergillus niger). The relationship between RT and the $\log_{10}$(MW) was linear in two different time regions: RT 4–8 min ($\log_{10}$MW $-0.51 \times$ RT + 7.86) and RT 8–18 min ($\log_{10}$MW $-0.07 \times$ RT + 3.51).
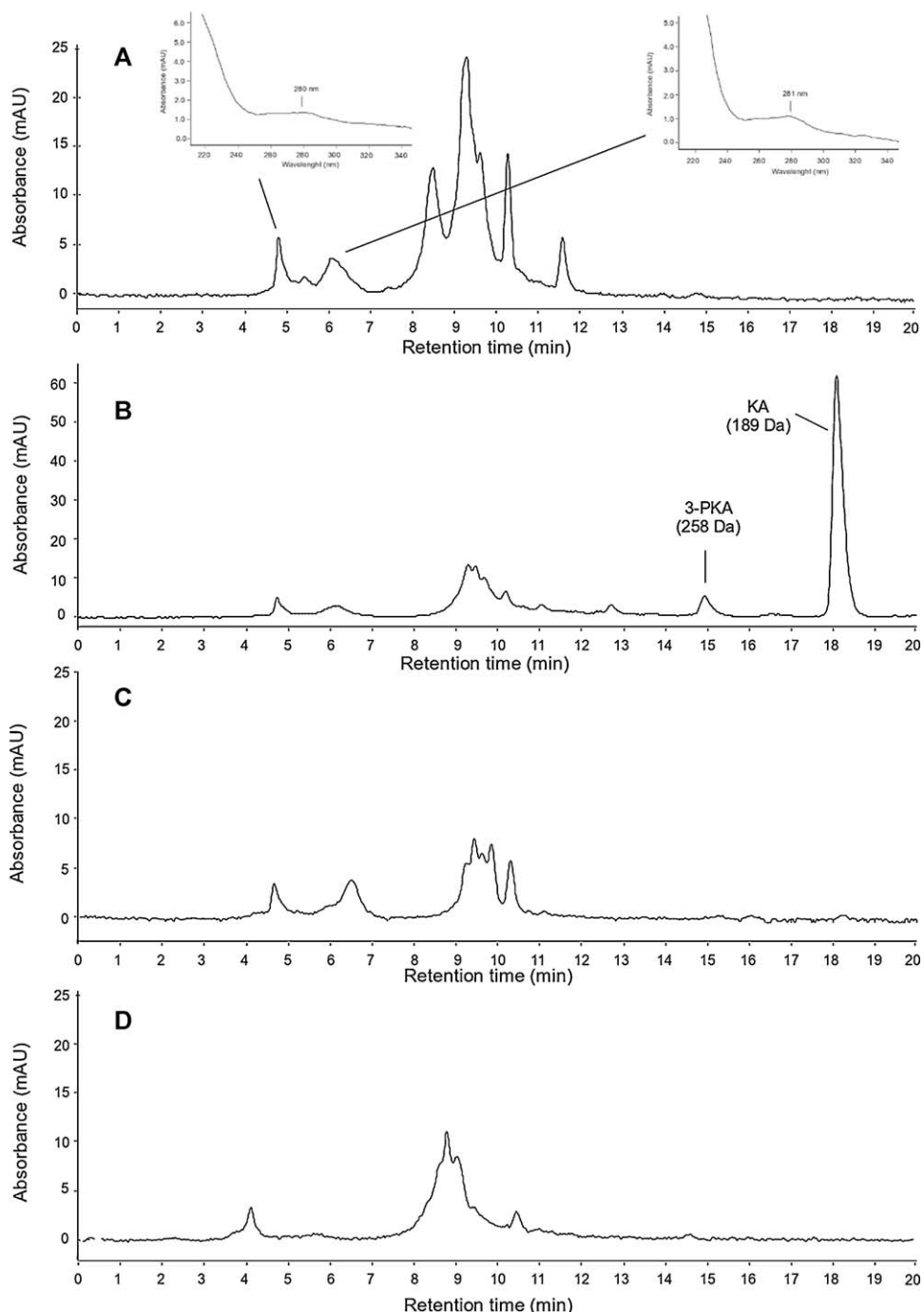
Fig. 1. Representative SEC-UV-DAD chromatograms of (A) mountain flowers, (B) chestnut, (C) mango and (D) laranjeira honeys. Representative UV-DAD spectra of proteins are shown in the insets of Panel A.

2.4. Multivariate analysis

We constructed a data matrix with rows for the different honey samples (objects) and columns showing the cumulative absorbance calculated every 18 s (variables or features). The SEC-UV-DAD data were exported from the Galaxy station of the HPLC equipment in the form of text files with the UV absorbance data and RT lists were exported in a 32 × 33 matrix for HCA and PCA. The first part of the chromatogram (0–4 min) gave no information on the composition of the honey, so we removed it before statistical analysis. Before PCA and HCA the data were mean-centered (i.e. for each chromatogram the mean cumulative absorbance was subtracted from each

sub-cumulative absorbance: see above). The data matrix was built with an OpenOffice Spreadsheet for Linux (v. 3.2.1), and all computations were done with R-commander GUI for R (v. 1.5–6) [17].

3. Results and discussion

3.1. Profiling honey minor components by SEC-UV-DAD

In the first part of this study we investigated the potential of the SEC technique coupled to UV-DAD detection for rapid simultaneous profiling of the minor components in 32 honey samples of different botanical and geographical origins (Table 1).
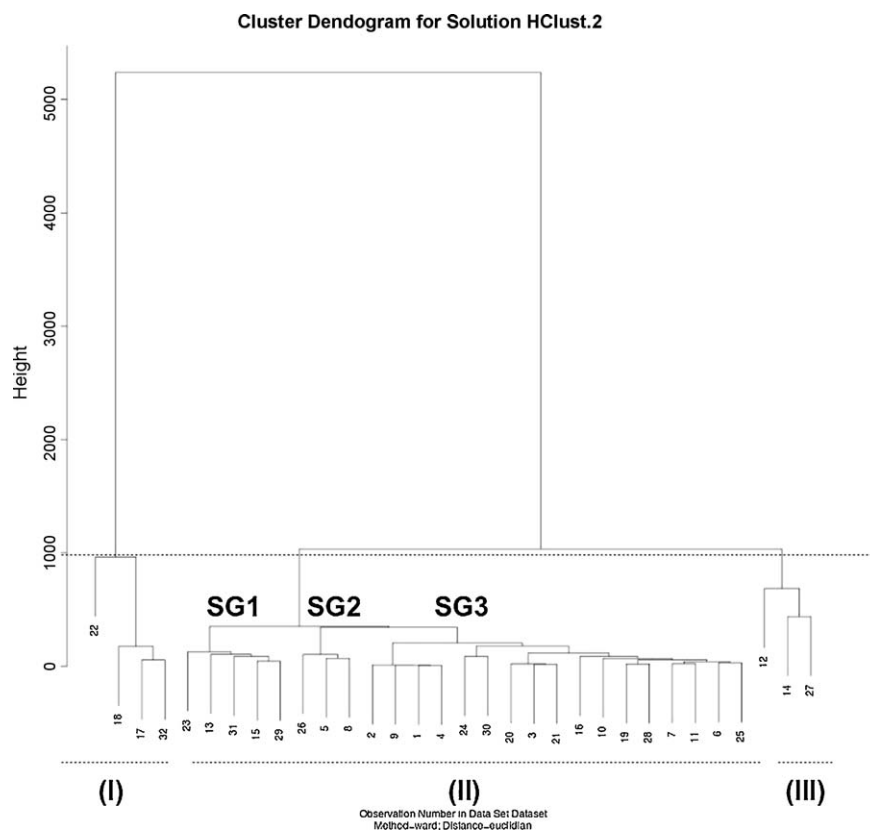
Fig. 2. Dendrogram from HCA.

Honeys were diluted with the chromatographic mobile phase (1 g/10 mL) since with this procedure no precipitate forms after centrifugation, whereas proteins and other insoluble components precipitate when this step is carried out with acidic water [11,18] or methanol [11]. This might be because of the high ionic strength of the mobile phase, which keeps in solution the protein pool constituted by the enzymes (glucose oxidase, invertase, saccharase, diastase and catalase) in honey resulting from their incorporation by bees into the nectars and the sugar-rich materials collected for honey production [7].

Fig. 1 reports representative chromatographic profiles (λ_{max} 220 nm) of honeys from chestnut (22, IT05, Fig. 1A), forest multiflora (26, KOS02, Fig. 1B), mango (22, KEN01, Fig. 1C) and laranjeira (11, BRA02, Fig. 1D). Diluted honey injected into the SEC-UV-DAD system resulted in the separation of several peak envelopes which dropped in different RT regions of the chromatogram. Substantial amounts of chemical species of high and intermediate MW were detected in all the honeys, while only chestnut honeys contained low-MW metabolites (MW < 300 Da).

3.1.1. Region A

RT 4.5–5.2 min, 5.3–7.0 min. On the basis of their RT and UV spectra (secondary maxima at λ_{max} = 270–280 nm, data not shown), we attributed these peaks to proteins with MW in the range of 300–100 kDa and 100–50 kDa respectively, which show a good match with the MWs of the honey bee enzymes mentioned [7]. These peaks were present with different intensities in the chromatographic profiles of almost all honeys (the lowest in samples 1, 2, 4 and 9 from Albania and the highest in 12 from the rainforest of southern Cameroon). This finding provides preliminary but substantial evidence that the protein content of honey may be influenced by its floral type and/or its geographical origin (Table 1).

3.1.2. Region B

RT 8.4–11.8 min. All honeys showed several peaks generated by species with intermediate MWs (approximately 30 kDa to 500 Da) with different UV-DAD profiles. The differences seemed mainly related to components from different botanical sources. To the best of our knowledge most of the UV profiles of these peaks were not attributable to any of the substances previously identified in honey and further work is currently in progress to clarify their structure. Only in linden honey (not shown) there was a clearly recognizable peak generated by the 1-O-gentiobiosyl ester (GBE) of the monoterpene cyclohexa-1,3-diene-1-carboxylic acid (CDCA, $MW_{CDCA-GBE}$ 506 Da, which has already been characterized as a typical component of linden and chestnut honey) [11,12].

3.1.3. Region C

RT 12–20 min. This region was poorly populated. In agreement with previous findings, only chestnut honeys (n = 6) gave detectable peaks (Fig. 1C) with different intensities, attributed to KA (MW = 189, RT = 18 min) and its 3-2′-pyrrolidinyl derivative (3-PKA, MW = 258 Da, RT = 12 min) [8,11,19].

3.2. Multivariate analyses of SEC-UV-DAD data

3.2.1. HCA

HCA was applied to the SEC-UV-DAD chromatogram data and the dendrogram in Fig. 2 shows the results. At the arbitrary distance d = 950, the samples were separated into three main clusters: samples 17, 18, 22, 32 (chestnut honeys) in cluster IA, samples 12, 14 (rainforest honeys from Cameroon), 27 in cluster IIIA and all the others in cluster IIA. The remaining 25 samples were all clustered together, and further divided into subgroups SG1, SG2 and SG3 when the distance threshold was reduced to d = 250.
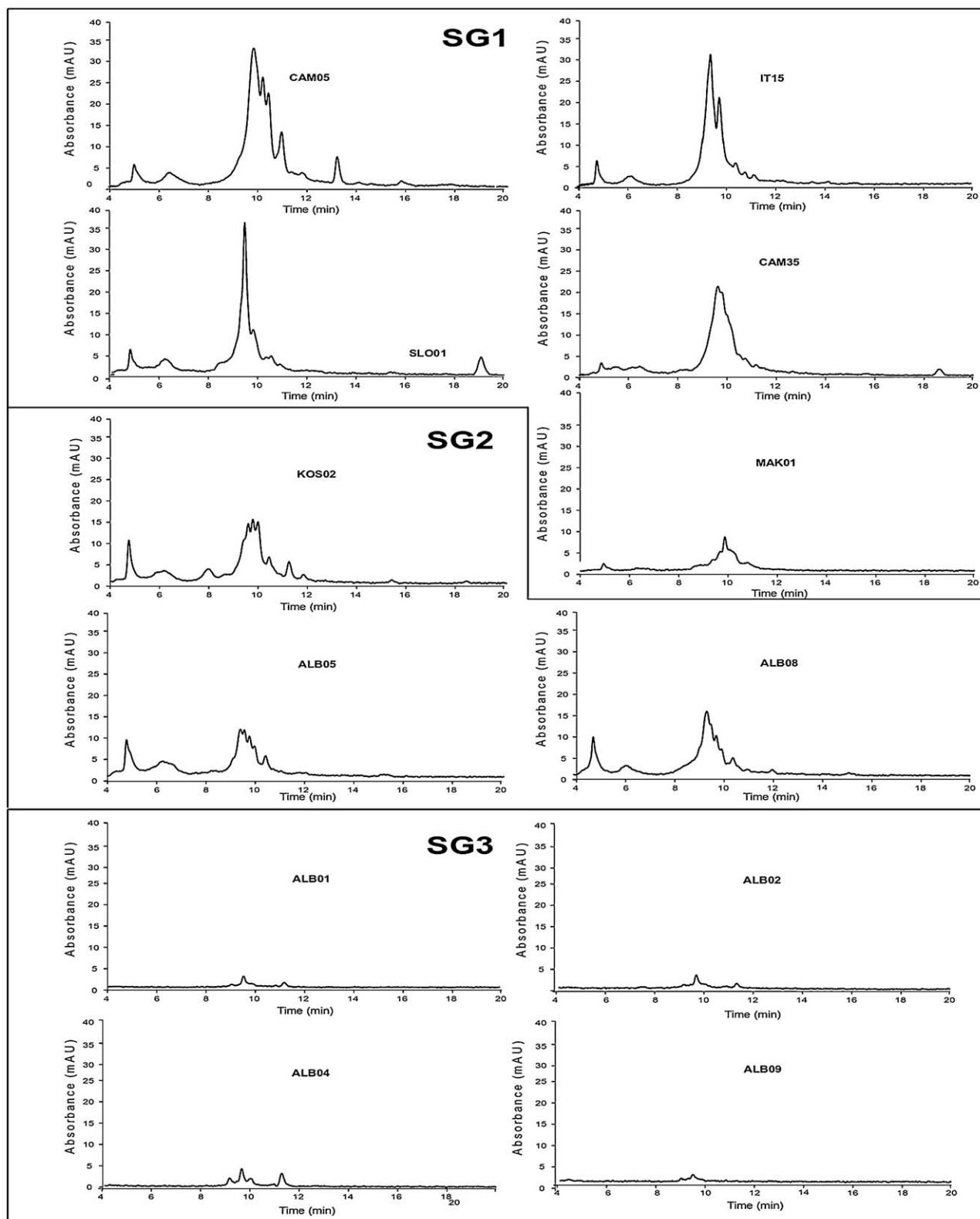
Fig. 3. SEC-DAD chromatograms ($\lambda = 220$ nm) of the honeys classified in clusters SG1 (upper panel), SG2 (middle panel) and SG3 (lower panel).

Fig. 3 shows the chromatographic profiles of the honeys in these subgroups. SG1 grouped samples 13 and 15 from Cameroon, the Italian dog rose honey 23, meadow 29 from Macedonia and chest-nut 31 from Slovenia (Fig. 3, upper panel). All these samples had heterogeneous chromatographic profiles in the RT range 8–12 min corresponding to molecular species with MW between 10 kDa and 400 Da. Honeys 5, 8, and 26 in cluster SG2 were all of multifloral origin with a homogeneous chromatographic profile (Fig. 3, middle panel). Finally, cluster SG3 grouped samples 1, 2, 4 and 9 (Fig. 3, lower panel).
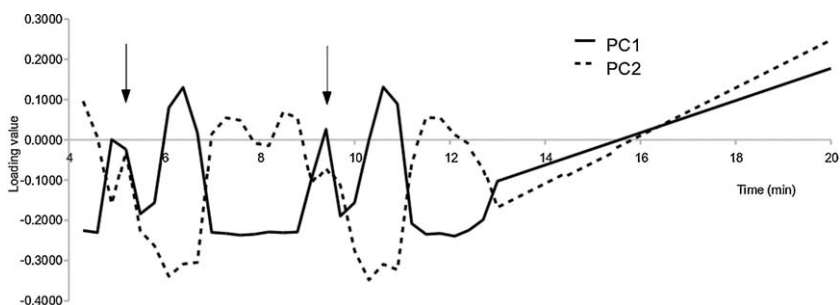
Fig. 4. RT Loadings of PC1 and PC2.

3.2.2. PCA

The loadings for the variables (e.g. the cumulative absorbance of the species within each 0.3-min RT interval, Fig. 4) in the first two PC show that the molecular species in the RT ranges from 4.30 to 5.50 min (350–100 kDa), 5.80–7.00 min (75–20 kDa), and 9.70–11.20 min (650–400 Da) were the dominant features in the PC1, which accounted for 54.7% of the total data variance; the species in the RT ranges 6.10–10.30 min and 10.90–13.00 min dominated PC2, accounting for 22.8% of the total data variance. In the RT range 4–14 min, the highest loading values in PC1, centered approximately at RT 6.4 min and RT 10.6 min, were paralleled by the lowest loadings for the same RT in PC2. The opposite situation was observed for the highest loadings in PC2 at 7.0–9.0 min and 11–13 min, which were matched by the highest loadings in PC1, confirming the orthogonality of PC1 and PC2. Only in the RT range of 4.9–5.2 min and to a lesser extent around 9.2 min the two first PC showed a parallel trend of variation of their loading values, indicating that the molecular species eluting at these RT are present in all honeys (very likely due to the honey bee metabolism) and thus are not useful for differentiation.

In the scores plot of PC1 and PC2 (cumulative variance 77.5%; Fig. 5) there were four clusters of honey samples. From left to right, moving from lower (negative) to higher (positive) PC1 values, the first to separate were four honeys from Albania (samples 1, 2, 4 and 9), followed by most of the others, clustered close to the graph origin, and by chestnut honeys and two samples from Cameroon

(CAM04 and CAM34) at positive PC1 values. Moving along PC2 from the bottom to the top, chestnut honeys were further separated in the right upper part (cluster A), while those from Cameroon (particularly CAM04) were shifted toward the lower right (cluster B).

4. Discussion

Previous studies investigated the composition of different classes of minor components of honey using different analytical techniques (HPLC and capillary electrophoresis (CE) [20,21], gas-chromatography (GC) [21], NMR [22–24], HPLC–MS [25], MALDI-MS [26] or immunoblotting [27,28]) to gain useful information about the composition in volatile and non-volatile species (flavonoids and phenolic acids and proteins). However, these studies suffered several limitations due to the selectivity of the technique used to determine a single analyte or a single class of analytes, which lead to the loss of analytes or of different classes of analytes resulting from the sample processing and preparation. These studies focused closely on identifying single specific target compounds or molecular species as markers of a honey's floral/geographical origin, and the results are expressed in terms of the presence/absence or mean concentrations of these markers, so important correlations between these different classes of compounds and other markers are lost.

In this context, our procedure gave information about the semi-quantitative distribution of UV-absorbing species from high to low MW (with no interference from sugars) on the same sample, with a short analysis time (20 min), and no loss of UV-DAD-sensitive water-soluble analytes. In addition, as already done by other authors working on the physico-chemical parameters of honey [29], proteins [26], amino acids [30], minerals [31] and heavy metals [32], we checked the results by multivariate statistical analysis for any latent structures in the distribution of minor components in honey that might explain the differences reflecting the botanical and geographical origin, climatic conditions and the bees' metabolic activity.

Both chemometric techniques (PCA and HCA) indicated a clear separation of the honey samples in four classes/clusters. This appeared to be based on (i) the relative total amounts of the minor components (independently from their MW) and (ii) their MW/dependent relative abundance.

In PCA, the four Albanian samples with the lowest total AUC, labeled as acacia and multiflora honeys (cluster A, Fig. 5) were tightly grouped on the left of the scores plot. These were easily recognized as counterfeit/adulterated products. Their SEC-UV-DAD profiles indicated that they contained none – or very little – of the proteins found in all the other honeys, specific enzymes incorporated directly by the bees (the proteins from flower pollen are virtually negligible [27,28]) to hydrolyze oligosaccharides and polysaccharides to glucose and fructose, or of the species with MW between 10 kDa and 300 kDa (Fig. 1).
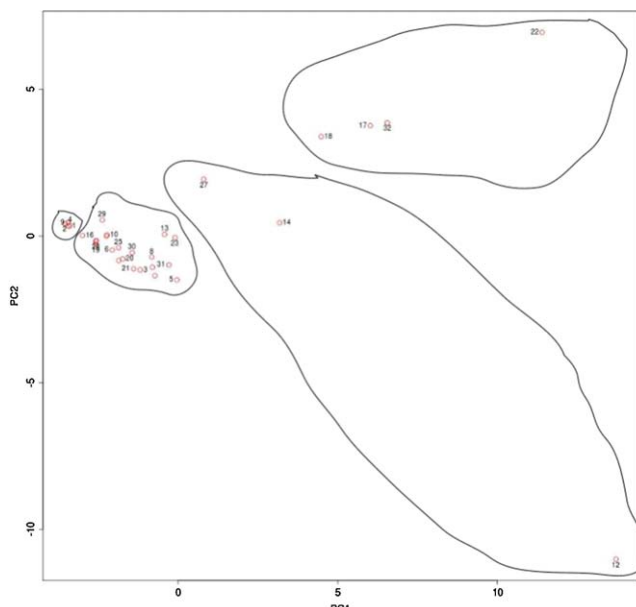
Fig. 5. First two principal components in PCA of honeys (n = 32) of different geographic and botanical origins (see Table 1).

By contrast, the clear separation of the chromatographic profiles of chestnut honeys and the two rainforest honeys was due to (i) the intense peak of the low-MW species kynurenic acid, the typical marker of chestnut nectar (only samples 8 and 27 did not enter this cluster, due to mislabeling of the first and the lower content of this metabolite in the second) [8–10], and (ii) the high AUC of the peaks generated by the proteins in the samples from Cameroon.

In addition, the loadings of PC1 and PC2 indicated that all the honeys (with the exception of counterfeits samples ALB01, ALB02, ALB04 and ALB09) contained proteins in the RT range between 4.9 and 5.2 min, independently from their geographical and botanical origin (and to a lesser extent around 9.2 min), suggesting that their presence was influenced only by the different metabolisms in the species of *Apis mellifera* involved in this study (*A. mellifera ligustica*, *A. mellifera carnica*, *A. mellifera macedonica*, *A. mellifera scutellata*); the distribution of all the other components may be affected by other factors, such as the phytochemical composition of the nectar(s) and/or honeydew collected for honey production.

5. Conclusions

These findings indicate that SEC-UV-DAD is a powerful analytical technique for profiling honey minor components from low to high MWs. The method is fast, requires only minimal sample handling and the chromatographic data can be analyzed by multivariate statistical techniques to obtain descriptive information about the honey's quality and composition. It (i) promptly separated counterfeit from authentic honeys, and (ii) highlighted the qualitative and quantitative differences in composition between honey varieties from flower nectars and those from arboreal species and/or honeydew. In addition, it indicated a striking difference in the phytochemical profile of tropical honeys compared to honeys from western countries. Further analytical work is needed to clarify the origins of these differences which may basically derive (i) from the different composition of the honey bee's feed (nectar, honeydew, propolis and pollens) available in different regions and (ii) from the different bee species involved in producing the honey.

References

[1] S. Bogdanov, T. Jurendic, R. Sieber, P. Gallmann, Honey for nutrition and health: a review, J. Am. Coll. Nutr. 27 (2008) 677–689.

[2] K. Inoue, S. Murayama, F. Seshimi, K. Takeba, Y. Yoshimura, H. Nakazawa, Identification of phenolic compound in manuka honey as specific superoxide anion radical scavenger using electron spin resonance (ESR) and liquid chromatography with coulometric array detection, J. Sci. Food Agric. 85 (2005) 872–878.

[3] T. Nagai, R. Inoue, N. Kanamori, N. Suzuki, T. Nagashima, Characterization of honey from different floral sources. Its functional properties and effects of honey species on storage of meat, Food Chem. 97 (2006) 256–262.

[4] E. Ibñez, A. Cifuentes, New analytical techniques in food science, Crit. Rev. Food Sci. Nutr. 41 (2000) 413–450.

[5] H.M. Abu-Tarbousch, H.A. Al-Kahtani, M.S. El-Sarrage, Floral-type identification and quality evaluation of some honey types, Food Chem. 46 (1993) 13–17.

[6] C. Perez-Arquillue, P. Conchello, A. Arino, T. Juan, A. Herresa, Quality evaluation of Spanish rosemary (*Rosmarinus officinalis*) honey, Food Chem. 51 (1994) 207–210.

[7] J. Roderick, The contribution of catalase and other natural products to the antibacterial activity of honey: a review, Food Chem. 71 (2000) 235–239.

[8] G. Beretta, E. Caneva, R. Maffei Facino, Kynurenic acid in honey from arboreal plants: MS and NMR evidence, Planta Med. 73 (2007) 1592–1595.

[9] M.P. Turski, M. Turska, W. Zgrajka, D. Kuc, W.A. Turski, Presence of kynurenic acid in food and honeybee products, Amino acids 36 (2008) 75–80.

[10] J.A. Donarski, S.A. Jones, M. Harrison, M. Driffield, A.J. Charlton, Identification of botanical biomarkers found in Corsican honey, Food Chem. 118 (2010) 987–994.

[11] G. Beretta, R. Artali, E. Caneva, S. Orlandini, M. Centini, R. Maffei Facino, Quinoline alkaloids in honey: further analytical (HPLC-DAD-ESI-MS, multidimensional diffusion-ordered NMR spectroscopy), theoretical and chemometric studies, J. Pharm. Biomed. Anal. 50 (2009) 432–439.

[12] E. Frérot, A. Velluz, E. Decorzant, R. Naef, From linden flower to linden honey. Part 2: glycosidic precursors of cyclohexa-1,3-diene-1-carboxylic acids, Chem. Biodivers. 3 (2006) 94–100.

[13] P. Cabras, A. Angioni, C. Tuberoso, I. Floris, F. Reniero, C. Guillou, S. Ghelli, Homogentisic acid: a phenolic acid as a marker of strawberry-tree (*Arbutus unedo*) honey, J. Agric. Food Chem. 47 (1999) 4064–4077.

[14] I. Martos, F. Ferreres, F.A. Tomás-Barberán, Identification of flavonoid markers for the botanical origin of eucalyptus honey, J. Agric. Food Chem. 48 (2000) 1498–1502.

[15] M.I. Gil, F. Ferreres, A. Ortiz, E. Subra, F.A. Tomas-Barberan, Plant phenolic metabolites and floral origin of rosemary honey, J. Agric. Food Chem. 43 (1995) 2833–2838.

[16] G. Beretta, P. Granata, M. Ferrero, M. Orioli, R. Maffei Facino, Standardization of antioxidant properties of honey by a combination of spectrophotometric/fluorimetric assays and chemometrics, Anal. Chim. Acta 533 (2005) 185–191.

[17] J. Fox, The R-commander. A basic statistics graphical user interface to R, J. Stat. Softw. 14 (2005) 1–42.

[18] N. Gheldof, X-H. Wang, N.J. Engeseth, Identification and quantification of antioxidant components of honeys from various floral sources, J. Agric. Food. Chem. 50 (2002) 5870–5877.

[19] G. Beretta, G. Vistoli, E. Caneva, C. Anselmi, R. Maffei Facino, Structure elucidation and NMR assignments of two new pyrrolidinyl quinoline alkaloids from chestnut honey, Magn. Reson. Chem. 47 (2009) 456–459.

[20] K. Pyrzynska, M. Biesaga, Analysis of phenolic acids and flavonoids in honey, Trends Anal. Chem. 28 (2009) 893–902.

[21] A.M. Gómez-Caravaca, M. Gómez-Romero, D. Arráez-Román, A. Segura-Carretero, A. Fernández-Gutiérrez, Advances in the analysis of phenolic compounds in products derived from bee, J. Pharm. Biomed. Anal. 41 (2006) 1220–1234.

[22] E. Schievano, E. Peggion, S. Mammi, ^{1}H nuclear magnetic resonance spectra of chloroform extracts of honey for chemometric determination of its botanical origin, J. Agric. Food Chem. 58 (2010) 57–65.

[23] F. Rastrelli, E. Schievano, A. Bagno, S. Mammi, NMR quantification of trace components in complex matrices with band-selective excitation with adiabatic pulses, Magn. Reson. Chem. 47 (2009) 868–872.

[24] P. Sandusky, D. Raftery, Use of selective TOCSY NMR experiments for quantifying minor components in complex mixtures: application to the metabonomics of amino acids in honey, Anal. Chem. 77 (2005) 2455–2463.

[25] C.I. Tuberoso, E. Bifulco, P. Caboni, F. Cottiglia, P. Cabras, I. Floris, Floral markers of strawberry tree (*Arbutus unedo* L.) honey, J. Agric. Food Chem. 58 (2010) 384–389.

[26] J. Wang, M.M. Kliks, W. Qu, S. Jun, G. Shi, Q.X. Li, Rapid determination of the geographical origin of honey based on protein fingerprinting and barcoding using MALDI TOF MS, J. Agric. Food Chem. 57 (2009) 10081–10088.

[27] M.V. Baroni, G.A. Chiabrando, C. Costa, D.A. Wunderlin, Assessment of the floral origin of honey by SDS-page immunoblot techniques, J. Agric. Food Chem. 50 (2002) 1362–1367.

[28] L. Bauer, A. Kohlich, R. Hirschwehr, U. Siemann, H. Ebner, O. Scheiner, D. Kraft, C. Ebner, Food allergy to honey: pollen or bee products? Characterization of allergenic proteins in honey by means of immunoblotting, J. Allergy Clin. Immunol. 97 (1996) 65–73.

[29] B. López, M.J. Latorre, M.I. Fernández, M.A. García, S. García, C. Herrero, Chemometric classification of honeys according to their type based on quality control data, Food Chem. 55 (1996) 281–287.

[30] I. Hermosín, R.M. Chicón, M.D. Cabezudo, Free amino acid composition and botanical origin of honey, Food Chem. 83 (2003) 263–268.

[31] M-J. Nozal Nalda, J.L. Bernal Yagüe, J.C. Diego Calva, M.T. Martín Gómez, Classifying honeys from the Soria Province of Spain via multivariate analysis, Anal. Bioanal. Chem. 382 (2005) 311–319.

[32] J.C. Rodríguez García, R.I. Rodríguez, R.M. Peña Crecente, J.B. García, S.G. Martín, C.H. Latorre, Preliminary chemometric study on the use of honey as an environmental marker in Galicia (Northwestern Spain), J. Agric. Food Chem. 54 (2006) 7206–7212.

Size exclusion chromatography with evaporative light scattering detection as a method for speciation analysis of polydimethylsiloxanes. III. Identification and determination of dimeticone and simeticone in pharmaceutical formulations

Krystyna Mojsiewicz-Pieńkowska*

Medical University of Gdańsk, Faculty of Pharmacy, Department of Physical Chemistry, 80-416 Gdańsk, Al. Gen. Hallera 107, Poland

ABSTRACT

The pharmaceutical industry is one of the more important sectors for the use of polydimethylsiloxanes (PDMS), which belong to the organosilicon polymers. In drugs for internal use, they are used as an active pharmaceutical ingredient (API) called dimeticone or simeticone. Due to their specific chemical nature, PDMS can have different degrees of polymerization, which determine the molecular weight and viscosity. The Pharmacopoeial monographs for dimeticone and simeticone, only give the permitted polymerization and viscosity range. It is, however, essential to know also the degree of polymerization or the specific molecular weight of PDMS that are present in pharmaceutical formulations. In the literature there is information about the impact of particle size, and thus molecular weight, on the toxicity, absorption and migration in living organisms. This study focused on the use of a developed method – the exclusion chromatography with evaporative light scattering detector (SEC-ELSD) – for identification and determination of dimeticone and simeticone in various pharmaceutical formulations. The method had a high degree of specificity and was suitable for speciation analysis of these polymers. So far the developed method has not been used in the control of medicinal products containing dimeticone or simeticone.

© 2011 Elsevier B.V. All rights reserved.

1. Introduction

The interest in polydimethylsiloxanes (PDMS) is related to their common use in various fields. Products where these polymers are in direct contact with humans are pharmaceuticals, medical supplies (e.g., implants, medical materials, ocular endotamponades, the silanized surfaces of, e.g. syringes, drains, catheters), food (functional additive E-900), and cosmetics, as well as in the environment (e.g. water, soil) [1–17]. PDMS are high-molecular compounds belonging to a group of organosilicon polymers that can have either a linear or a cyclic structure. They belong to polysiloxanes which are commonly referred to as silicones. Polysiloxanes can be represented by the general formula – $[R_2Si–O]$ –, where R is usually one of the following groups: methyl, ethyl, propyl, phenyl, fluoroalkyl, vinyl, or aminoalkyl. Polysiloxanes can be liquids, resins, rubbers or elastomers depending on the type of functional groups, structure, and degree of polymerization or cross-linking. When PDMS are liquids, the R represents a methyl group [18,19].

The pharmaceutical industry is one of the most important sectors for the use of polydimethylsiloxanes. In medicinal products

for internal use they may serve as the active pharmaceutical ingredient (API), the excipient or as the matrix in the drug delivery system [1–4,12]. As an active substance they are called dimeticone or simeticone, and there are various forms of pharmaceutical formulations, e.g. capsules, drops, chewable tablets, emulsions, suspensions, and granules. Simeticone is a mixture of dimeticone with 4–7% silicon dioxide [1,2,20–22]. These polymers act in an anti-flatulence, anti-foaming and protective manner. For this reason, preparations containing dimeticone or simeticone are used against flatulence, colic, in preparation for medical diagnosis and as alternatives for: irritable bowel syndrome, gastric ulcer, pancreatic insufficiency, and heartburn. It is important to note that pharmaceutical preparations containing dimeticone or simeticone are used for both adults and infants (especially for problems like flatulence) [1,2].

In medicinal products that are intended for internal use, only the linear polydimethylsiloxanes are allowed. PDMS with this structure differ in the degree of polymerization and molecular size, and therefore have different molecular weights (Table 1) [8,23–25]. This in turn determines the viscosity, which is the basis for the Pharmacopoeias regulations regarding which applications that are allowed (Table 2) [20–22].

However, no Pharmacopoeia specifies the viscosity of the PDMS that can be used for manufacturing medicinal products. Only in the European [21] and the British [22] Pharmacopoeia, is there a note

---

* Tel.: +48 58 349 31 56; fax: +48 58 349 31 52.
  E-mail address: kpienk@gumed.edu.pl

Table 1
Dependence of molecular weight and viscosity PDMS on the degree of polymerization.

Degree of polymerization number n	Molecular weight [Da]	Viscosity [cSt]	Type of polymer
2	237	1	
8	770	5	Low molecular weight
15	1250	10	
25	2000	20	
50	3500	50	
80	6000	100	
125	9500	200	
160	12 000	300	Middle molecular weight
190	13 600	350	
400	30 000	1000	
650	48 000	5000	
800	60 000	10 000	
1230	91 000	30 000	
1500	116 500	60 000	High molecular weight
1870	139 000	100 000	

that PDMS molecules with a viscosity below 50 cSt may only be used in pharmaceutical formulations intended for external use.

The rules for the use of PDMS as a functional additive (E-900) in food products are much more specific. In 1979, at their eighteenth meeting, the joint FAO/WHO Expert Committee on Food Additives (JECFA) established the Acceptable Daily Intake (ADI) of PDMS at 0–1.5 mg/kg body weight. At the twenty-third meeting in 1980, the JECFA Committee reviewed the ADI and stated that this applied only to PDMS with the number of repeated subunits $-[(CH_3)_2SiO]$ in the range $n = 200$–300, which corresponds to a molecular weight between 15 000 and 22 000 Da. This decision was taken after concerns that polymers with lower molecular weight might be more readily absorbed in organisms. Generally the normative of values for PDMS was associated with the results of toxicological studies. In 1990, at the thirty-seventh meeting, the Committee further revised the specifications for PDMS saying that the ADI only applies to PDMS with $n = 90$–410, corresponding to molecular weights of 6800–30 000 Da and viscosities between 100 and 1500 cSt. The toxicological properties were not re-evaluated at that time, but the WHO and FAO later initiated a toxicological study of PDMS. That report was presented at the sixty-ninth meeting of JECFA in 2009, and contained research results for PDMS with a viscosity of 10 and 350 cSt, which corresponds to a molecular weight in the range of 1250–13 600 Da. The study showed that oral administration of PDMS to rats resulted in ocular lesions (e.g. corneal opacities and granulomatous inflammation), but probably very little absorption. In 2009, it was decided to temporarily reduce the ADI from 0 to 1.5 mg/kg bw to 0–0.8 mg/kg bw, while investigating the repeatability of the toxicological study [26–28].

A literature review (covering the years 1948–2010) regarding toxicity aspects of silicone, including PDMS, showed that there is no unambiguous answer to the question: "Are silicones non-toxic and safe for living organisms?" The results in the literature are often contradictory. With this in mind, it is worrying that in certain pharmaceutical preparations, which are used not only for adults but also for children, the viscosity of the dimeticone or simeticone used is unknown. However, there is a possibility that there may be a linear PDMS, but unallowable the degree of polymerization. Data presented in the literature indicates that linear PDMS with a low molecular weight (i.e. low viscosity) and cyclic PDMS can be toxic to living organisms. It is also shown that the degree of polymerization for linear PDMS, which influences the molecular weight and viscosity, has a direct effect on the toxicity, absorption and migration in living organisms [29–36].

However, few studies have focused on the identification and determination of simeticone or dimeticone in pharmaceutical preparations. In 1989, a paper by Anderson and colleagues was published, in which the authors used size exclusion chromatography with a refractometric detector to determine PDMS in emulsions [37]. The authors believed that the IR method, despite being the most commonly used method to determine polydimethylsiloxanes, is not suitable for analysis of oral suspensions or emulsions. They believed that the background originating from the matrix adversely affects the measurement of the PDMS. In 1999, Torrado and colleagues [38] used infrared spectroscopy Fourier transform (FTIR), as currently prescribed in the Pharmacopoeias, to identify dimeticone in tablets and capsules. For extracts from tablets and capsules they obtained spectra that were similar to the standard PDMS spectrum, with the exception of one preparation. This case, however, was not specifically commented on by the authors. They concluded that FTIR spectroscopy is useful for determination of dimeticone in pharmaceutical formulations. In 2002, Moore and others used liquid chromatography in reversed phase with evaporative light scattering detection (RP-HPLC-ELSD). They obtained a single peak but noted the asymmetric shape, and suggested that this could be due to the fact that PDMS is not a single compound, but a mixture of oligomers. However, they did not determine the molecular weight or the viscosity of the identified PDMS. The authors claimed that the IR method described in the Pharmacopoeia is not satisfactory for determination of PDMS in pharmaceutical preparations, which contain multiple components. Specifically, they noted the existence of interactions with magnesium hydroxide and aluminum on PDMS. When determining PDMS with IR, the results were variable and generally overestimated the content [39]. In 2003, Jia and colleagues analyzed trace amounts of PDMS in tablets, where they occurred as impurities of devices. The study used atomic emission spectrometry with inductively coupled plasma (ICP-AES) [40].

It is worth noting that the IR method is recommended by the Pharmacopoeias for identify and quantitative analysis simeticone or dimeticone contained in drugs [20–22]. It involves identification of the bands of valence (stretching) and deformation (bending) vibrations CH$_3$, Si–CH$_3$ and Si–O groups, which have fixed positions in the spectrum, regardless of the molecular weight of the PDMS. Thus, these bands appear not only for the PDMS that are approved for use in medicinal products, but also for PDMS with a viscosity

Table 2
Characteristic of dimeticonum and simeticonum according to various Pharmacopoeias.

Pharmacopoeia	Degree of polymerization (n)	Viscosity [cSt]	Comment
European Pharmacopoeia Ph.Eur. 6.0 (2007)	20–400	Dimeticone: 20–1300 Simeticone: 20–1300	Dimeticones with nominal viscosity of 50 cSt or lower are intended for external use only.
British Pharmacopoeia BP (2007)	20–400	Dimeticone: 20–1300 Simeticone: 20–1300	Dimeticones with nominal viscosity of 50 cSt or lower are intended for external use only.
The United States Pharmacopoeia USP 32 (2009)	No information	Dimeticone: 20–30 000 Simethicone: no information	–

below 50 cSt and for other organosilicon compounds containing the same groups. The IR and FTIR methods are therefore not specific for these polymers.

Most of the methods used in the publications listed above were selective but not specific for PDMS, and researchers have not turned attention to the problems with speciation analysis of PDMS present in various forms of pharmaceutical preparations (as dimeticone or simeticone). Therefore, the aim of this study was to use size exclusion chromatography with evaporative light scattering detection (SEC-ELSD) [7,8] for identification and determination of linear poly-dimethylsiloxanes, with different degree of polymerization (hence molecular weight and viscosity), in various pharmaceutical preparations. The SEC-ELSD method has not previously been used for control of medicines containing PDMS in various matrices. The present work is the third in a cycle which describes this method [7,41].

2. Experimental

2.1. Instrument and chromatographic conditions

All details about the SEC-ELSD chromatographic system has been described in [7]. An evaporative light scattering detector, manufactured by BBT Automatyka Sp. z o. o. Polska (model 030195), was used for the method development. The TSK – GEL GMH$_{HR}$-M column with polystyrene–divinylobenzen packing (5 μm particle size, 300 mm × 7.8 mm) used in this method is manufactured by Tosoh Biosep company and distributed by Sigma–Aldrich (Poznan, Poland). Data acquisition, analysis and reporting were done using the Eurochrom 2000 (Knauer Germany) chromatography software. In this study, the following optimal conditions were used: temperature in the drift tube 50 °C; temperature in the detection cell – 50 °C; pressure of the carrier gas (for nebulisation) 140 kPa; flow rate of the mobile phase (chloroform) 1 ml/min.

2.2. Materials and analytical chemicals

All the solvents used were of analytical grade. Chloroform was purchased from Sigma–Aldrich (Poznan, Poland), hydrochloric acid from POCH (Gliwice, Poland), and certified polystyrene standards from Sigma–Aldrich (Poznań, Poland). Three standard mixtures with four standards polystyrene in each vial were used, with molecular weights at peak maximum (M_p) ranging from 376 to 2 570 000 Da. The polystyrene standards are characterized as M_w and M_n and have a low polydispersity index (PDI = M_w/M_n) 1.02–1.11. Polydimethylsiloxane (PDMS) standard of viscosity 350 cSt was from Sigma–Aldrich (Poznań, Poland) and Simethicone, the USP reference standard, was purchased from Dow Corning Corporation. Syringe filters (25 mm, PET-polyester, pore size 0.45 μm) from Macherey-Nagel (Bioanalytic, Poland).

2.3. Formulation

Polydimethylsiloxanes, as an Active Pharmaceutical Ingredient (API), exist in different pharmaceutical formulations. Qualitative and quantitative analyses were carried out on various forms of selected medicinal product for internal use, such as capsules, granules, suspensions, emulsions, and chewable tablets (Table 3).

2.4. Preparation of samples

The procedures for preparing samples for analysis were partly based on the monographs contained in various Pharmacopoeias such as the American (USP 32 2009) [20], the British (BP 2007) [21] and the European (EP 6.0 2007) [22]. The Pharmacopoeias do not include detailed monographs describing the exact way of analysing specific formulations. Only the U.S. Pharmacopoeia [20] contains monographs describing the identification and quantitative analysis of capsules, tablets, suspensions, and emulsions using infrared (IR or FTIR) spectroscopy. However, by comparing all the monographs included in the Pharmacopoeias a common strategy for the analysis of dimeticone or simethicone can be identified.

The sample preparation was based on chloroform extraction of the active substance. The selection of this organic solvent was linked to its role as a mobile phase in the size exclusion chromatography. The quantities of the pharmaceutical formulations were selected so that the concentration of PDMS in the sample after extraction would be in the range of 0.1–1.0%. To the extent possible, care was taken to ensure that the concentration levels were similar for all the pharmaceutical formulations, i.e. between 0.4% and 0.7%. For each medicinal product, seven independent samples were prepared, and the different preparation steps are described in Table 4.

3. Results and discussion

The medicinal products differed among themselves the formulations, the matrix, the expiration date and the content of PDMS. Therefore, the purpose of the study was not only identification and quantitative studies but also to (i) compare the identity of dimeticone or simeticone when present in various forms of a drug from the same manufacturer, (ii) the effect of the matrix on the chromatograms, (iii) compare the identity of dimeticone used by different manufacturers, (iv) assess the impact of the expiration date on changes in the dimeticone, and (v) to assess the effect of HCl to recovery PDMS, as this is an important step when preparing samples for the analysis.

Optimization of the methods and choice of the experimental parameters were described in detail in part I of these publication series [7]. The validation parameters were determined in accordance with guidelines from the International Commission of Harmonization (International Conference on Harmonization, ICH), the World Health Organization (WHO), the Food and Drug Organization, and recommendations in the United States [20] and European Pharmacopoeia [21], and are presented in the part II of the series of publications [41]. In this publication [41] was showed the values of parameters of validation and acceptance criteria defined for the evaluation of usefulness of the SEC-ELSD method as a tool for speciation analysis of the polydimethylsiloxanes used in pharmaceutical industry. Moreover, the maximum errors for determining of molecular weights PDMS and quantitative analysis were showed.

Dimeticone and simeticone were identified based on differences in retention times and molecular weights. To determine the molecular weights at peak maximum (M_p), a calibration curve as a calibration column TSK-GEL GMH$_{HR}$-M filled with polystyrene–divinylobenzen was used together with certified polystyrene standards with molecular weights M_p between 376 and 2 570 000 Da. On the basis of accuracy and trueness [41], it may be concluded that polystyrene standards can use to calibration column for determining molecular weight PDMS. The hydrodynamic volumes for polystyrene and polydimethylsiloxane are similar and, therefore, the molecular weights of polydimethylsiloxane are equivalent to the polystyrene.

The calibration curve was determined from the relationship between the logarithm of the molecular weight at peak maximum and the retention time (Eq. (1)):

$$y = -0.8336x + 10.704 \tag{1}$$

where x is the retention time (t_r) [min], and y the logarithm of the molecular weight at peak maximum (log M_p) [Da]. The coefficient of determination for the column was high, $R^2 = 0.9938$.

Table 3
Characteristics of selected pharmaceutical formulations containing dimeticone or simethiconeused in this study.

Trade name Producer	Dosage form	Content API[a]	Composition
Esputicon *Synteza* *Polska*	Drops	980 mg/1 g	Dimeticone Silicon dioxide 20 mg
	Capsules	50 mg/caps.	Dimeticone
	Granule	150 mg/5 g	Dimeticone Fumed silica Aromatic sugar to 5 g
Infacol*Pharmax LimitedWielka Brytania*	Suspensions	40 mg/ml	Simethicone[b] Sodium saccharin Hydroxypropylmethylcellulose Methyl hydroxybenzoate Propyl hydroxybenzoate Orange flavor Purified water
Bobotic *Medana PharmaTerpol Polska*	Emulsion	66.66 mg/ml	Simethicone, Sodium saccharin 2.5 mg Methyl hydroxybenzoate 1.5 mg Propyl hydroxybenzoate 0.5 mg, Sodium carboxymethylcellulose Citric acid Raspberry flavor Purified water to 1 ml
Espumisan *Berlin Chemie* *Niemcy*	Emulsion	40 mg/ml (20 drops)	Simethicone Hydroxypropylcellulose Sorbic acid Sodium cyclamate Sodium saccharin Banana flavor Purified water
	Emulsion	40 mg/5 ml	Simethicone Methyl 4-hydroxybenzoate Polisorbate 80 Sodium cyclamate Sodium saccharin Sodium carboxymethyl cellulose Silicon dioxide flavor
Manti Gastop *US Pharmacia USA*	Chewable tablets	125 mg/tabl.	Simethicone Lactose anhydrous Sorbitol Tricalcium phosphate Sodium stearate Mint flavor

[a] API – Active Pharmaceutical Ingredient.
[b] Simeticone – dimeticone + SiO_2.

For the quantitative analyses, the peak area was used as the mode for peak evaluation. In previous studies in detail the issues linear ELSD detector response was discussed [41–43]. The concentration of dimeticone was calculated from a rectilinear regression equation obtained from measurements of 10 PDMS solutions with a viscosity of 350 cSt at concentrations ranging from 0.1 to 1.0%, with $R^2 = 0.9958$ (Eq. (2)):

$$y = 66.647x + 1.6844 \tag{2}$$

where x is the concentration [%], and y the peak area [mV min].

A rectilinear regression equation obtained from measurements of 10 Simeticone USP standard solutions in the concentration range 0.1–1.0% ($R^2 = 0.9979$) was used for determination of simeticone in medical preparations (Eq. (3)):

$$y = 66.458x - 0.6244 \tag{3}$$

where x is the concentration [%], and y the peak area [mV min].

Table 5 summarizes the results from analyses of pharmaceutical preparations with different matrices, different manufacturers, but a valid expiration date. The results are averages of seven independently prepared samples with three independent measurements of

Table 4
Procedures for preparation of medicinal products samples for analysis of dimeticone and simethicone with size exclusion chromatography with evaporative light scattering detection.

Dosage form	Amount used for sample preparation	Steps in sample preparation
Drops	0.2 g	1. Accurate transfer of a suitable amount of the pharmaceutical formulation to Erlenmeyer flasks (volume 100 ml);
Granule	of micronized granules	2. Addition of 50 ml dilute hydrochloric acid (2:5)
Suspension	4.6 ml	3. Addition of 25 ml chloroform;
Emulsion (dosage form – ml)	25.0 ml (Espumisan)	4. Extraction for 10 min;
Emulsion (dosage form – drops)	4.6 ml (Espumisan)	5. Separation of the layers;
	2.7 ml (Bobotic)	6. Transfer of about 5 ml extract to a vial
Capsule	3	7. Filtration with syringe filters;
Chewable tablet	2	8. Injection of sample to the chromatographic system

Table 5
The results for analysis of dimeticone or simeticone in pharmaceutical formulations using SEC-ELSD.

Trade name	Analysis				
	Qualitative		Quantitative		
	Retention time mean values [min]	Molecular weight M_p [Da]	Peak area mean values [mV min]	Content dimeticone or simeticone	
	RSD [%] $n = 7$		RSD [%] $n = 7$	Declared	Measured recovery [%]
Esputicon (capsules)	8.08 0.54	9301	29.47 1.46	50 mg/caps.	51.77 mg/caps. 103.50
Esputicon (drops)	8.08 0.59	9301	41.57 1.09	980 mg/g	1114.7 mg/g 113.8
Esputicon (granule)	8.06 0.79	9683	27.23 2.16	30 mg/1 g	28.55 mg/g 95.17
Infacol (suspension)	8.09 0.85	9124	32.02 2.06	40 mg/ml	39.78 mg/ml 99.45
Bobotic (emulsion)	8.05 1.09	9852	35.52 1.76	66.66 mg/ml	75.04 mg/ml 112.57
Espumisan (emulsion-drops)	7.91 0.55	12 889	32.67 1.53	40 mg/ml	40.57 mg/ml 101.43
	9.35 0.56	813	3.03[a] 4.79		4.45 mg/ml[a] 11.13
Espumisan (emulsion-ml)	7.97 0.72	11 487	36.16 2.09	40 mg/5 ml	41.94 mg/5 ml 104.85
Manti Gastop (chewable tablets)	7.81 0.68	15 617	49.68 1.49	125 mg/tabl.	140.99 mg/tabl. 112.79

[a] Estimated value due to the lack of sufficient separation of peaks.

each. Table 6 shows a comparison of the analytical results for pharmaceutical preparations with a valid expiry date and those that had expired, as well as the influence of hydrochloric acid on the recovery of PDMS samples.

No difference in the polydimethylsiloxane identity could be detected between two different types of pharmaceutical formulations from the same manufacturer, which confirmed that it was the same active substance (Fig. 1). The results also confirmed that there was no significant matrix effect.

The identity of dimeticone used by different manufacturers was also compared, and it could be concluded that the dimeticone present in Esputicon, Infacol and Bobotic did not differ significantly (Table 5). Only dimeticone in the Manti Gastop tablets had a molecular weight that differed from the others (Fig. 2).

The identification of simeticone and dimeticone showed that in general the active substance in the selected formulations was characterized by a molecular weight M_p of 9124–15 617 Da, which corresponds to a viscosity of about 140–440 cSt. In all cases, except the Espumisan emulsion for drop dosage, both the simeticone and the dimeticone identity complied with the characteristics given in the Pharmacopoeias (Table 2) for PDMS used as the active substance in medicines for internal use. Only in the Espumisan emulsion administered as droplets, polymers with an illegal molecular weight were found, as there was an additional peak in the chromatogram with a retention time 9.35 min, which corresponds to a molecular weight of 813 Da (Table 5, Fig. 3).There were two possible reasons for the additional peak in the chromatogram of the Espumisan extract:

Table 6
The results for SEC-ELSD analysis of dimeticone or simeticone in pharmaceutical formulations valid with expiry date and that had expired, and the influence of HCl addition on the recovery in Bobotic emulsions.

Trade name	Analysis				
	Qualitative		Quantitative		
	Retention time mean values [min]	Molecular weight M_p [Da]	Peak area mean values [mV min]	Content dimeticone lub simeticone	
	RSD [%] $n = 7$		RSD [%] $n = 7$	Declared	Measured recovery [%]
Esputicon (capsules) exp. dat. 2011	8.08 0.54	9301	29.47 1.46	50 mg/caps.	51.77 mg/caps. 103.50
Esputicon (capsules) exp. dat. 2006	8.07 0.87	9481	27.89 1.62	50 mg/caps.	48.82 mg/caps. 97.64
Espumisan (emulsion-drops) exp. dat. 2011	7.91 0.55	12 889	32.67 1.53	40 mg/ml	40.57 mg/ml 101.43
	9.35 0.56	813	3.03[a] 4.79		4.45 mg/ml* 11.13
Espumisan (emulsion-drops) exp. dat. 2007	7.92 0.75	12 644	31.58 1.43	40 mg/ml	39.24 mg/ml 98.10
	9.34 0.81	828	3.27[a] 3.73		4.75 mg/ml[a] 11.88
Bobotic (emulsion) with HCl	8.05 1.09	9852	35.52 1.76	66.66 mg/ml	75.04 mg/ml 112.57
Bobotic (emulsion) without HCl	8.04 1.67	10 042	13.05 1.97	66.66 mg/ml	28.34 mg/ml 42.51

[a] Estimated value due to the lack of sufficient separation of peaks.
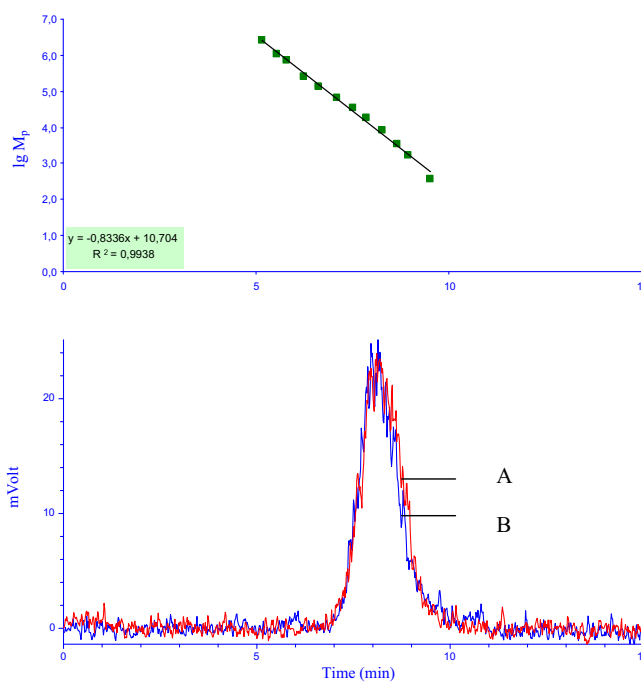
**Fig. 1.** SEC-ELSD chromatograms of Esputicon as granules (A) and capsules (B) extracts and calibration curve of column.
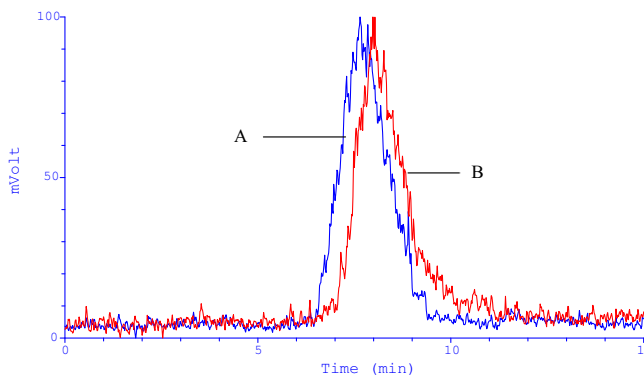
Fig. 2. SEC-ELSD chromatogram of a Manti Gastop chewable tablets extract (A), and of an Infacol suspension extract (B).
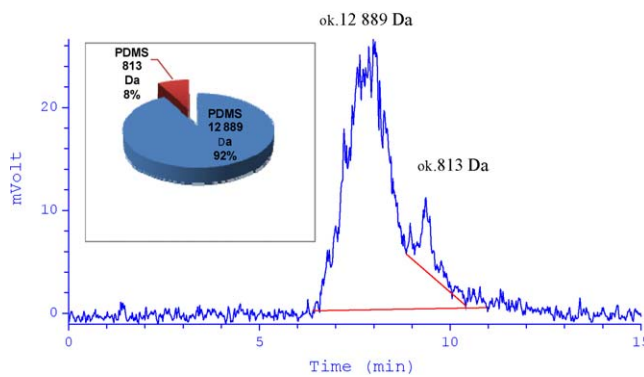

Fig. 3. SEC-ELSD chromatogram of an extract of the Espumisan emulsion in drops as a dosage form, and the proportion (%) of each PDMS polymer type in the medical formulation.

Table 7
Solubility and molecular weights of the excipients in the Espumisan emulsion in drops as a dosage form.

Excipients	Solubility	Molecular weight [Da]
Hydroxypropylmethylcellulose	Cold water Anhydrous ethanol Methanol Propylene glycol	64 000–92 000
Sorbic acid	Ethanol Diethyl ether Water (poorly)	112.1
Sodium cyclamate	Water	201.22
Sodium saccharin	Water	215
Banana flavor	Water (poorly) Ethanol Diethyl ether Acetic acid (glacial) Benzene Chloroform	130.2

1. extraction of a matrix component (tr = 9.35 min, molecular weight 813 Da) in addition to the active substance (tr = 7.91 min, molecular weight 12 889 Da), or
2. the active substance (simeticone) was present as a mixture of polymers with different molecular weights, and thus viscosity.

Matrix constituents and their molecular weight and solubility are given in Table 7 [21,44]. It was concluded that the reason could no be extraction of sorbic acid, sodium cyclamate, sodium saccharin and hydroxypropyl since they are not soluble in chloroform. Banana flavoring is an ester of isoamyl alcohol (isoamyl acetate) with acetic acid and can be dissolved in chloroform, but its molecular weight does not correspond with the second peak in the chromatogram.

Thus, it appears that a mixture of polymers has been used to manufacture the active ingredient (simeticone), and that the additional fraction of PDMS has a too low molecular weight to comply with the recommendations in the European and British Pharmacopoeia [21,22].

The study also included the effect of storage time on changes in dimeticone. The analytical results for Espumisan emulsion drops showed that there was no significant difference in retention time between the formulations, and hence that the storage time had little effect on the active ingredient (Fig. 4).

Pharmacopoeial monographs do not contain information on which, dimeticone molecular weights that are allowed in pharmaceutical preparations intended for oral use, but only the limits with respect to viscosity. Therefore, the chromatograms of an extract from Manti chewable tablets, and the Gastop Simeticone USP standard was compared (Fig. 5).
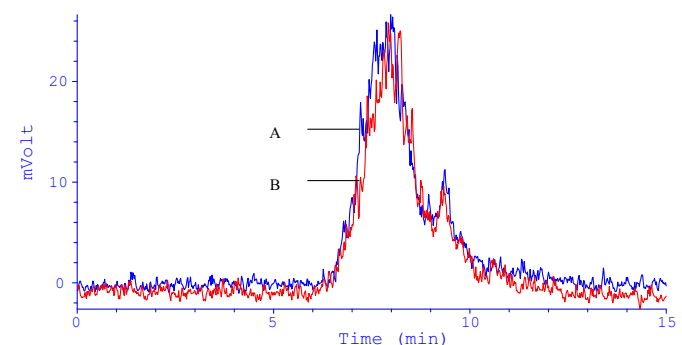
Fig. 4. SEC-ELSD chromatogram of extracts of an Espumisan emulsion with a valid expiry date (A), and one with a date that had expired (B).
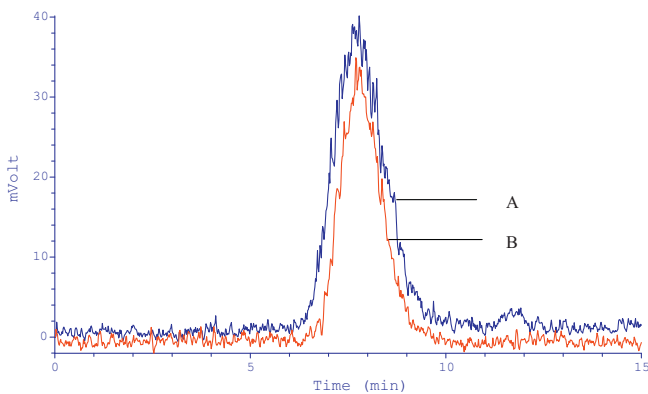
Fig. 5. SEC-ELSD chromatogram of a Manti Gastop chewable tablets extract (A) and the Simeticone USP reference standard (B).
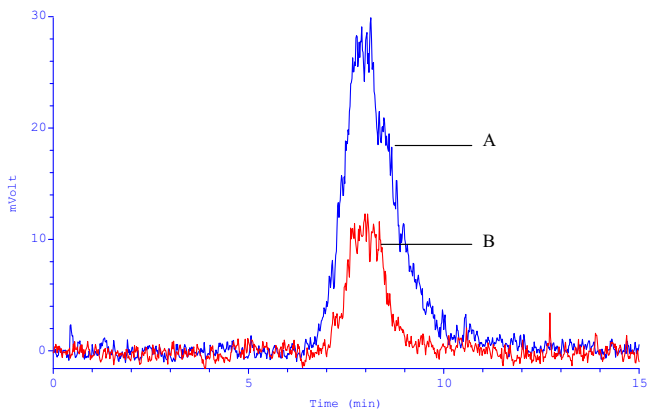
Fig. 6. Chromatograms obtained with SEC-ELSD when extracting PDMS from the medicinal product Bobotic with (A) and without (B) diluted HCl.

An important part of the study was to determine the content of dimeticone or simeticone in selected drugs and compare with the values declared by the manufacturer. The results indicated that the real content of the active ingredient was between 95.2 and 114% of the amount declared (Table 5).

The quantitative analysis was also used to evaluate the effect of adding diluted HCl in the sample preparation procedure. This was analyzed using the Bobotic emulsion with drops dosage as an example, as the matrix of this product contained many different compounds. When excluding HCl, the content of PDMS was about 2.5 times lower than when extracting this preparation in an acidic environment (Table 6, Fig. 6). The reason could be the presence of a complex matrix, which may adsorb simeticone and dimeticone and prevent a complete extraction. Addition of hydrochloric acid probably decreased the effect adsorption polymer as an effect of interactions PDMS with excipients, vastly increasing the efficiency of extraction. Hence, it can be concluded that addition of diluted (2:3) HCl is an essential step when preparing samples for SEC-ELSD analysis of pharmaceutical formulations.

4. Conclusion

For control of medicinal products, analytical methods with a high degree of specificity should be used. This is particularly relevant for polydimethylsiloxanes as they differ in the degree of polymerization, which determines the molecular weight and viscosity. They can be divided into low-molecular, medium-molecular and high-molecular polymers. Because the polydimethylsiloxanes are not specific compounds, there is a need for analytical methods

that can be used for speciation analysis. The patients should be informed about which polydimethylsiloxane (dimeticonum or simeticonum) that occurs in a pharmaceutical formulations, particularly the viscosity of the polymers. The exclusion chromatography with evaporative laser scattering detector method (SEC-ELSD) has proved useful for the identification of these polymers in various forms of pharmaceutical formulations, and the method meets the requirement on degree of specificity. This method can also be used for quantitative studies. The need to find new and innovative analytical methods should be linked not only to reports from toxicity studies, but also to the need for reliable routine controls to ensure the safety of medicinal products.

References

[1] S.C. Sweetman (Ed.), Martindale 36, Complete Drug Reference, 2009, p. 1849.
[2] S.C. Sweetman (Ed.), Martindale 36, The Complete Drug Reference, 2009, pp. 1594–1595.
[3] R.K. Subedi, S.Y. Oh, M.K. Chun, H.K. Choi, Recent advances in transdermal drug delivery, Arch. Pharmacol. Res. 33 (3) (2010) 339–351.
[4] H. Maeda, T. Sugie, A. Sano, H. Kawasami, Y. Kurosami, Study on accelerated evaluation system for release profiles of covered-rod type silicone formulation using indomethacin as a model drug, J. Control. Release 94 (2004) 337–349.
[5] S. Bondurant, V. Ernster, R. Herdman, Safety of Silicone Breast Implants, The National Academy of Sciences, Washington, 2000.
[6] J. Intra, J.M. Glasgow, H.Q. Mai, A.K. Salem, Pulsatile release of biomolecules from polydimethylsiloxane (PDMS) chips with hydrolytically degradable seals, J. Control. Release 127 (2008) 280–287.
[7] K. Mojsiewicz-Pieńkowska, Size exclusion chromatography with evaporative light scattering detection as a method for speciation analysis of polydimethylsiloxanes. I: influence of selected factors on the signal intensity of the detector, J. Pharm. Biomed. Anal. 53 (3) (2010) 503–509.
[8] K. Mojsiewicz-Pieńkowska, Size-exclusion chromatography with evaporative light scattering detection: Method for determination of polydimethylsiloxanes. II. Application of TSK-GEL H$_{HR}$ GMH$_{HR}$-M column to determine and separate molecular weight of linear polydimethylsiloxanes, J. Chromatogr. B 865 (2008) 7–12.
[9] E. Van den Kerckhove, K. Stappaerts, W. Boeckx, B. Van den Hof, S. Monstrey, A. Van der Kelen, et al., Silicones in the rehabilitation of burns: a review and overview, Burns 27 (2001) 205–214.
[10] A. Colas, J. Curtis, Silicone biomaterials: history and chemistry, in: B.D. Ratner, A.S. Hoffman, F.J. Schoen, J.E. Lemons (Eds.), Biomaterials Science, 2nd ed., Elsevier/Academic Press, New York, 2004, p. 80 (Chapter 2.3).
[11] J. Curtis, A. Colas, Medical applications of silicones, in: B.D. Ratner, A.S. Hoffman, F.J. Schoen, J.E. Lemons (Eds.), Biomaterials Science, 2nd ed., Elsevier/Academic Press, New York, 2004, p. 698 (Chapter 7.19).
[12] A. Colas, Silicones in Pharmaceutical Applications, Dow Corning Corp, 2001.
[13] L.W. Luria, The role of medical grade silicones in surgery and its topical applications, Oper. Tech. Plastic Reconst. Surg. 9 (2003) 67–74.
[14] V. Rajendra, Y. Chen, M.A. Brook, Structured hydrophilic domains on silicone elastomers, Polym. Chem. 1 (2010) 312–320.
[15] S. Varaprath, D.H. Stutts, G.E. Kozerski, A primer on the analytical aspects of silicones at trace levels-challenges and artifacts – a review, Silicon Chem. 3 (2006) 79–102.
[16] Y. Horii, K. Kannan, Survey of organosilicone compounds, including cyclic and linear siloxanes, in personal-care and household products, Arch. Environ. Contam. Toxicol. 55 (2008) 701–710.
[17] M.R. Rosen (Ed.), Delivery System Handbook for Personal Care and Cosmetic Products. Technology, Applications, and Formulations, William Andrew, Inc., United States, 2005.
[18] N.J. Fendinger, R.G. Lehmann, E.M. Mikaich, Polydimethylosiloxane, in: G. Chandra (Ed.), The Handbook of Environmental Chemistry, Organosilicon Materials, vol. 3, Spinger-Verlag, Berlin, Heidelberg, 1997, pp. 182–223.
[19] M.A. Brook, Silicon in Organic, Organometallic and Polymer Chemistry, John Wiley & Sons Ltd., Chichester, 2000.
[20] US Pharmacopeia 32, United States Pharmacopeal Convention, Rockville, MD, 2009.
[21] European Pharmacopeia 6.0, 2007.
[22] British Pharmacopeia, 2007.
[23] http://www.sigmaaldrich.com/etc/medialib/docs/Aldrich/General_Information/viscosity.Par.0001.File.tmp/viscosity.pdf.
[24] A.C.M. Kuo, Polydimethylsiloxanes in Polymer Data Handbook, Oxford University Press, Inc., 1999.
[25] http://www.gelest.com/pdf/siliconefluids.pdf.
[26] WHO technical series, Evaluation of certain food additives, Sixty-ninth report of the Joint FAO/WHO Expert Committee on Food Additives, World Health Organisation, Geneva, 2009.
[27] Evaluations of the Joint FAO/WHO Expert Committee on Food Additives (JECFA), http://apps.who.int/ipsc/database/evaluations/PrintPreview.aspx?chemID=2755.

[28] Safety evaluation of certain food additives/prepared by the sixty-ninth meeting of the Joint FAO/WHO Expert Committee on Food Additives (JECFA), World Health Organization, 2009.

[29] G. Gaubitz, C. Jackisch, W. Domschke, W. Heindel, Silicone breast implants: correlation between implant ruptures, magnetic resonance spectroscopically estimated silicone presence in the liver, antibody status and clinical symptoms, Rheumatology 41 (2002) 129–135.

[30] S. Bondurant, V. Ernster, R. Herdman (Eds.), Safety of Silicone Breast Implants, National Academy Press, Washinghton, 2000.

[31] J.C. Salamone (Ed.), Polymeric Materials Encyclopedia, vol. 1, CRC Press, 1996.

[32] D. Flassbeck, B. Pfleiderer, R. Grümping, A.V. Hirner, Determination of low molecular weight silicones in plasma and blood of women after exposure to silicone breast implants by GC/MS, Anal. Chem. 73 (2001) 606–611.

[33] C. Sanchez-Brrunete, E. Miguel, B. Albero, J.L. Tadeo, Determination of cyclic and linear siloxanes in soil samples by ultrasonic-assisted extraction and gas chromatography–mass spectrometry, J. Chromatogr. A 1217 (2010) 7024–7030.

[34] A. Papp, J. Toth, T. Kerényi, M. Jackel, I. Suveges, Silicone oil in the subarachnoidal space—A possible route to the brain? Pathol. Res. Pract. 200 (2004) 247–252.

[35] S.J. Lugowski, D.C. Smith, H. Bonek, J. Lugowski, W. Peters, J. Semple, Analysis of silicon in human tissues with special reference to silicone breast implants, J. Trace Elem. Med. Biol. 14 (2000) 31–42.

[36] D. Flassbeck, B. Pfleiderer, P. Klemens, K.G. Heumann, E. Eltze, A.V. Hirner, Determination of siloxanes, silicon, and platinum in tissues of women with silicone gel-filled implants, Anal. Bioanal. Chem. 375 (2003) 356–362.

[37] S. Anderson, U. Hedsten, S. Jacobsson, Quantitation of polydimethylsiloxane in pharmaceutical formulations by gel pereation chromatography, J. Chromatogr. 477 (1989) 474–476.

[38] G. Torrado, A. Garcia-Arieta, F. de los Rios, J.C. Menendez, S. Torrado, Quantitative determination of dimethicone in commercial tablets and capsules by Fourier transform infrared spectroscopy and antifoaming activity test, J. Pharm. Biomed. Anal. 19 (1999) 285–292.

[39] D.E. Moore, T.X. Liu, W.G. Miao, A. Edwards, R. Elliss, A RP-LC method with evaporative light scattering detection for the assay of simethicone in pharmaceutical formulations, J. Pharm. Biomed. Anal. 30 (2002) 273–278.

[40] X. Jia, T. Wang, X. Bu, J. Wu, Isolation and analysis of trace level of silicone oil in pharmaceutical bulk drug substance by ICP-AES, Microchem. J. 75 (2003) 103–107.

[41] K. Mojsiewicz-Pieńkowska, Size exclusion chromatography with evaporative light scattering detection as a method for speciation analysis of polydimethylsiloxanes. II: validation of the method for analysis of pharmaceutical formulations, J. Pharm. Biomed. Anal. 56 (4) (2011) 851–858.

[42] K. Mojsiewicz-Pieńkowska, Size-exclusion chromatography with evaporative light scattering detection: Method for determination of polydimethylsiloxanes. I. Testing dependence of molecular weight of polydimethylsiloxanes and injected mass upon the detector signal, J. Chromatogr. B 865 (2008) 1–6.

[43] K. Mojsiewicz-Pieńkowska, On the issue of characteristic evaporative light scattering detector response, Crit. Rev. Anal. Chem. 39 (2009) 89–94.

[44] L. Zhu, R.A. Seburg, E.W. Tsai, Determination of surface-bound hydroxypropylcellulose (HPC) on drug particles in colloidal dispersions using size exclusion chromatography: a comparison of ELS and RI detection, J. Pharm. Biomed. Anal. 40 (5) (2006) 1089–1096.

Journal of Pharmaceutical and Biomedical Analysis